

## REFERENCES

1. Shammas NW. Epidemiology, classification, and modifiable risk factors of peripheral arterial disease. *Vasc Health Risk Manag.* 2007;3:229–234.
2. McKenna M, Wolfson S, Kuller L. The ratio of ankle and arm arterial pressure as an independent predictor of mortality. *Atherosclerosis.* 1991;87:119–128.
3. Newman AB, Sutton-Tyrrell K, Vogt MT, Kuller LH. Morbidity and mortality in hypertensive adults with a low ankle/arm blood pressure index. *JAMA.* 1993;270:487–489.
4. Strandness Jr DE, Schultz RD, Sumner DS, Rushmer RF. Ultrasonic flow detection. A useful technic in the evaluation of peripheral vascular disease. *Am J Surg.* 1967;113:311–320.
5. Bascom PA, Johnston KW, Cobbold RS, Ojha M. Defining the limitations of measurements from Doppler spectral recordings. *J Vasc Surg.* 1996;24:34–44; discussion 44–45.
6. Thiele BLHK, Greene FM, et al. Pulsed Doppler waveform patterns produced by smooth stenosis in the dog thoracic aorta. In: Taylor DMSA, ed. *Blood Flow: Theory and Practice.* San Diego, CA: Academic Press; 1983:85–104.
7. Yao ST, Hobbs JT, Irvine WT. Ankle systolic pressure measurements in arterial disease affecting the lower extremities. *Br J Surg.* 1969;56:676–679.
8. Aboyans V, Criqui MH, Abraham P, et al. Measurement and interpretation of the ankle-brachial index: a scientific statement from the American Heart Association. *Circulation.* 2012;126:2890–2909.
9. Korhonen P, Aarnio P. Borderline peripheral arterial disease. *Int J Angiol.* 2008;17:175–177.
10. Dachun X, Jue L, Liling Z, et al. Sensitivity and specificity of the ankle-brachial index to diagnose peripheral artery disease: a structured review. *Vasc Med.* 2010;15:361–369.
11. 2011 ACCF/AHA Focused Update of the Guideline for the Management of Patients With Peripheral Artery Disease (Updating the 2005 Guideline): A Report of the American College of Cardiology Foundation/American Heart Association Task Force on Practice Guidelines. *Catheter Cardiovasc Interv.* 2012;79(4):501–531.
12. McDermott MM, Criqui MH, Liu K, et al. Lower ankle/brachial index, as calculated by averaging the dorsalis pedis and posterior tibial arterial pressures, and association with leg functioning in peripheral arterial disease. *J Vasc Surg.* 2000;32:1164–1171.
13. Stevens DL, Bisno AL, Chambers HF, et al. Practice guidelines for the diagnosis and management of skin and soft-tissue infections. *Clin Infect Dis.* 2005;41:1373–1406.
14. Beckman JA, Higgins CO, Gerhard-Herman M. Automated oscillometric determination of the ankle-brachial index provides accuracy necessary for office practice. *Hypertension.* 2006;47:35–38.
15. Turnipseed WD. Clinical review of patients treated for atypical claudication: a 28-year experience. *J Vasc Surg.* 2004;40:79–85.
16. Turnipseed WD, Pozniak M. Popliteal entrapment as a result of neurovascular compression by the soleus and plantaris muscles. *J Vasc Surg.* 1992;15:285–293; discussion 293–294.
17. Jelnes R, Gaardsting O, Hougaard Jensen K, et al. Fate in intermittent claudication: outcome and risk factors. *Br Med J (Clin Res Ed).* 1986;293:1137–1140.
18. Aquino R, Johnnides C, Makaroun M, et al. Natural history of claudication: long-term serial follow-up study of 1244 claudicants. *J Vasc Surg.* 2001;34:962–970.
19. Feringa HH, Karagiannis SE, Schouten O, et al. Prognostic significance of declining ankle-brachial index values in patients with suspected or known peripheral arterial disease. *Eur J Vasc Endovasc Surg.* 2007;34:206–213.
20. Suominen V, Uurto I, Saarinen J, et al. PAD as a risk factor for mortality among patients with elevated ABI—a clinical study. *Eur J Vasc Endovasc Surg.* 2010;39:316–322.
21. Thatipelli MR, Pellikka PA, McBane RD, et al. Prognostic value of ankle-brachial index and dobutamine stress echocardiography for cardiovascular morbidity and all-cause mortality in patients with peripheral arterial disease. *J Vasc Surg.* 2007;46:62–70.
22. Kusunose K, Sato M, Yamada H, et al. Prognostic implications of non-invasive vascular function tests in high-risk atherosclerosis patients. *Circ J.* 2016;80:1034–1040.
23. Diehm C, Allenberg JR, Pittrow D, et al. Mortality and vascular morbidity in older adults with asymptomatic versus symptomatic peripheral artery disease. *Circulation.* 2009;120:2053–2061.
24. American Diabetes A. Standards of medical care in diabetes-2015 abridged for primary care providers. *Clin Diabetes.* 2015;33:97–111.
25. Alahdab F, Wang AT, Elraiyah TA, et al. A systematic review for the screening for peripheral arterial disease in asymptomatic patients. *J Vasc Surg.* 2015;61:42S–53S.
26. Lin JS, Olson CM, Johnson ES, Whitlock EP. The ankle-brachial index for peripheral artery disease screening and cardiovascular disease prediction among asymptomatic adults: a systematic evidence review for the U.S. Preventive Services Task Force. *Ann Intern Med.* 2013;159:333–341.
27. Rodondi N, Auer R, de Bosset Sulzer V, Ghali WA, Cornuz J. Atherosclerosis screening by noninvasive imaging for cardiovascular prevention: a systematic review. *J Gen Intern Med.* 2012;27:220–231.
28. American College of Cardiology Foundation, American College of Radiology, American Institute of Ultrasound in Medicine, et al. ACCF/ACR/AIUM/ASE/ASN/ICAVL/SCAI/SCCT/SIR/SVM/VS 2012 appropriate use criteria for peripheral vascular ultrasound and physiological testing part I: arterial ultrasound and physiological testing: a report of the American College of Cardiology Foundation Appropriate Use Criteria Task Force, American College of Radiology, American Institute of Ultrasound in Medicine, American Society of Echocardiography, American Society of Nephrology, Intersocietal Commission for the Accreditation of Vascular Laboratories, Society for Cardiovascular Angiography and Interventions, Society of Cardiovascular Computed Tomography, Society for Interventional Radiology, Society for Vascular Medicine, and Society for Vascular Surgery. *J Vasc Surg.* 2012;56:e17–e51.
29. Hirsch AT, Allison MA, Gomes AS, et al. A call to action: women and peripheral artery disease: a scientific statement from the American Heart Association. *Circulation.* 2012;125(11):1449–1472.
30. Pickering TG, Hall JE, Appel LJ, et al. Recommendations for blood pressure measurement in humans: an AHA scientific statement from the Council on High Blood Pressure Research Professional and Public Education Subcommittee. *J Clin Hypertens (Greenwich).* 2005;7:102–109.
31. AbuRahma AF, Adams E, AbuRahma J, et al. Critical analysis and limitations of resting ankle-brachial index in the diagnosis of symptomatic peripheral arterial disease: role of diabetes mellitus and chronic kidney disease. *J Vasc Surg.* 2020;71:937–945.
32. Boren CH, Towne JB, Bernhard VM, Salles-Cunha S. Profundopopliteal collateral index. A guide to successful profundaplasty. *Arch Surg.* 1980;115:1366–1372.
33. Mawatari K, Muto Y, Komori K, et al. Value of the profundopopliteal collateral index for selecting between an in-flow and sequential arterial reconstruction in patients with multisegment arterial occlusive disease. *J Cardiovasc Surg (Torino).* 2000;41:79–82.
34. Gale SS, Scissons RP, Salles-Cunha SX, et al. Lower extremity arterial evaluation: are segmental arterial blood pressures worthwhile? *J Vasc Surg.* 1998;27:831–838; discussion 838–839.
35. Hoyer C, Sandermann J, Paludan JP, et al. Diagnostic accuracy of laser Doppler flowmetry versus strain gauge plethysmography for segmental pressure measurement. *J Vasc Surg.* 2013;58:1563–1570.
36. Ramsey DE, Manke DA, Sumner DS. Toe blood pressure. A valuable adjunct to ankle pressure measurement for assessing peripheral arterial disease. *J Cardiovasc Surg (Torino).* 1983;24:43–48.
37. Abraham P, Bickert S, Vielle B, et al. Pressure measurements at rest and after heavy exercise to detect moderate arterial lesions in athletes. *J Vasc Surg.* 2001;33:721–727.
38. Corretti MC, Anderson TJ, Benjamin EJ, et al. Guidelines for the ultrasound assessment of endothelial-dependent flow-mediated vasodilation of the brachial artery: a report of the International Brachial Artery Reactivity Task Force. *J Am Coll Cardiol.* 2002;39:257–265.
39. McMahon CG. Correlation of penile duplex ultrasonography, PBI, DICC and angiography in the diagnosis of impotence. *Int J Impot Res.* 1998;10:153–158.

40. Strandness Jr DE, Bell JW. Peripheral vascular disease: diagnosis and objective evaluation using a mercury strain gauge. *Ann Surg.* 1965;161:4–35.
41. Raines JK, Darling RC, Buth J, et al. Vascular laboratory criteria for the management of peripheral vascular disease of the lower extremities. *Surgery.* 1976;79:21–29.
42. Raines JK. The pulse volume recorder in peripheral arterial disease. In: Bernstein EF, ed. *Noninvasive Diagnostic Techniques in Vascular Disease.* St. Louis, MO: CV Mosby; 1985:513–544.
43. Rutherford RB, Lowenstein DH, Klein MF. Combining segmental systolic pressures and plethysmography to diagnose arterial occlusive disease of the legs. *Am J Surg.* 1979;138:211–218.
44. Elgendi M. On the analysis of fingertip photoplethysmogram signals. *Curr Cardiol Rev.* 2012;8:14–25.
45. Allen J, Howell K. Microvascular imaging: techniques and opportunities for clinical physiological measurements. *Physiol Meas.* 2014;35:R91–R141.
46. Abularrage CJ, Sidawy AN, Aidinian G, et al. Evaluation of the microcirculation in vascular disease. *J Vasc Surg.* 2005;42:574–581.
47. Rich K. Transcutaneous oxygen measurements: implications for nursing. *J Vasc Nurs.* 2001;19(55–59); quiz 60–61.
48. Quigley FG, Faris IB. Transcutaneous oxygen tension measurements in the assessment of limb ischaemia. *Clin Physiol.* 1991;11:315–320.
49. Rich K. Effects of leg and body position on transcutaneous oxygen measurements in healthy subjects and subjects with peripheral artery disease after lower-extremity arterial revascularization: a pilot study. *J Vasc Nurs.* 2002;20:125–135; quiz 136–137.
50. Moosa HH, Peitzman AB, Makaroun MS, et al. Transcutaneous oxygen measurements in lower extremity ischemia: effects of position, oxygen inhalation, and arterial reconstruction. *Surgery.* 1988;103:193–198.
51. Harward TR, Volny J, Golbranson F, et al. Oxygen inhalation-induced transcutaneous PO<sub>2</sub> changes as a predictor of amputation level. *J Vasc Surg.* 1985;2:220–227.
52. Humeau A, Steenbergen W, Nilsson H, Stromberg T. Laser Doppler perfusion monitoring and imaging: novel approaches. *Med Biol Eng Comput.* 2007;45:421–435.
53. Castronovo Jr JJ, Adera HM, Smiell JM, Price RM. Skin perfusion pressure measurement is valuable in the diagnosis of critical limb ischemia. *J Vasc Surg.* 1997;26:629–637.
54. Yamada T, Ohta T, Ishibashi H, et al. Clinical reliability and utility of skin perfusion pressure measurement in ischemic limbs—comparison with other noninvasive diagnostic methods. *J Vasc Surg.* 2008;47:318–323.

# Vascular Laboratory: Arterial Duplex Scanning

PATRICK A. STONE and ROSS M. CLARK

## INSTRUMENTATION AND BASIC CONCEPTS 254

Blood Flow Imaging Techniques 254

*Color Doppler Imaging* 255

*Power Doppler Imaging* 255

*B-Flow Imaging* 255

Pulsed Doppler Spectral Analysis 256

Measurements 256

Artifacts and Errors 256

Duplex Velocity Spectral Classification of Arterial Stenosis 257

## PATIENT TESTING 258

Peripheral Arteries 258

*Indications* 258

*Technique* 258

*Interpretation* 259

*Diagnostic Accuracy* 259

Iliac Arteries 260

*Interpretation* 260

DIRECT IMAGING CRITERIA 260

INDIRECT IMAGING CRITERIA 260

*Accuracy* 260

DIRECT IMAGING 260

INDIRECT IMAGING 260

Femoral-Popliteal and Tibial Arteries 260

*Limitations* 261

## DUPLEX SURVEILLANCE 261

Bypass Graft and Endovascular Intervention Surveillance 261

*Vein Grafts* 261

TECHNIQUE 261

INTERPRETATION 262

RESULTS 262

*Prosthetic Grafts* 263

Peripheral Endovascular Interventions 263

*Threshold Criteria* 263

*Femoropopliteal Interventions* 263

*Tibial Therapies* 264

*Iliac Interventions* 264

Duplex ultrasound (DUS) is an integral component of diagnostic testing for the evaluation and management of arterial disease. This technology, which combines the acquisition of blood flow (pulsed Doppler spectral analysis) and anatomic (B-mode and color Doppler imaging) information, was developed under the guidance of D. Eugene Strandness, Jr., at the University of Washington in the 1970s.<sup>1</sup> The initial clinical application of arterial duplex scanning assessed the extracranial carotid artery bifurcation for the presence and extent of atherosclerotic plaque and developed velocity criteria to estimate internal carotid artery (ICA) stenosis on the basis of correlations with angiographic measurements.<sup>2</sup> Commercial duplex scanners became available by the 1980s, and the clinical use of DUS rapidly expanded into peripheral arterial, visceral arterial, and peripheral venous applications. The development of

real-time, color-encoded Doppler imaging was an important technologic advance that simplified patient testing, enhanced diagnostic accuracy, and led to additional clinical applications in the areas of screening for arterial disease, intraoperative assessment, and surveillance after arterial intervention.

Modern DUS systems provide high-resolution B-mode ultrasound imaging of tissue and vessel anatomy, including three-dimensional vessel reconstruction and evaluation of atherosclerotic plaque morphology. Detailed assessment of blood flow characteristics can be made in real time by one of several techniques, color Doppler imaging, power Doppler imaging, B-flow imaging, or pulsed Doppler spectral analysis.

Test interpretation is based on both imaging and Doppler findings with classification ranging from normal to clinically relevant disease categories. Duplex testing is noninvasive and

cost-effective and thus suitable for serial examination; because it not only permits the identification of disease, but also reveals its natural history, including progression, regression, and response to intervention. In many patients, duplex testing can establish a definitive diagnosis and can allow interventions, such as carotid endarterectomy or peripheral artery angioplasty, to be based solely on the B-mode imaging and velocity spectral changes recorded from diseased arterial segments. In the upper and lower limbs, duplex testing should be performed in conjunction with indirect physiologic testing (measurement of systolic blood pressure, pulse volume plethysmography) to assess arterial hemodynamics (see Ch. 21, Vascular Laboratory: Arterial Physiologic Assessment). When peripheral arterial disease is identified, DUS can be used to map the site or sites of occlusive or aneurysmal lesions, analogous to contrast-enhanced arteriography. Arterial duplex test interpretation combined with the patient's clinical history and physical examination is often sufficient to counsel the patient on the advisability of intervention and whether it can be treated by an endovascular or conventional open surgical procedure.

The reliability of arterial duplex testing depends on several factors, including the expertise of the examiner (vascular technologist, physician) and the knowledge and experience of the interpreting physician. Testing performed and interpreted in an accredited vascular laboratory has sufficient diagnostic accuracy for clinicians to rely on the final interpretation provided and often avoid performing more invasive, expensive diagnostic testing, such as computed tomography, magnetic resonance imaging, or catheter-based contrast-enhanced angiography, to confirm disease severity (see Ch. 18, Noninvasive Vascular Laboratory Quality Assurance and Accreditation).

## INSTRUMENTATION AND BASIC CONCEPTS

DUS systems use transducers fabricated from piezoelectric crystals to convert electrical activity to mechanical energy (ultrasound) and vice versa, thereby allowing the same device to transmit and receive ultrasound signals to and from the patient to produce images of tissue anatomy as well as to characterize blood flow. Transducers consist of multiple elements that enable focusing of the ultrasound beam, steering of the beam, and resolution sufficient for detailed tissue imaging at depths of less than 1 cm to more than 20 cm. To perform detailed arterial mapping, DUS instrumentation for carotid and peripheral testing should be equipped with linear array transducers with frequencies ranging from 5 to 12 MHz. For visceral artery or abdominal imaging and transcranial Doppler (TCD) examination, lower frequency transducers are needed because of the higher tissue attenuation; typically, 2.5- or 3.5-MHz curved linear or phased array transducers are appropriate. Newer generation transducers have an ultrawide bandwidth that enables harmonic imaging, with its increased resolution and freedom from artifacts, and dynamic frequency tuning for improving image quality at greater tissue depths. Moreover, the development of two-dimensional transducer arrays enables the beam

to be focused at a specific depth and steered, which facilitates the use of three-dimensional imaging.

A duplex B-mode, or brightness mode, ultrasound image is displayed as gray-scale pixels reflecting the amplitude and position of returning ultrasound echoes. By processing up to 200 or more separate ultrasound beam signals retrieved from the transducer array, a scan converter organizes both horizontal and vertical pixels to yield a two-dimensional view of the tissue being scanned. Optimal arterial anatomic imaging is achieved when the transducer scan lines (beam) are directed perpendicular to the vessel wall. A 90-degree imaging angle is best used for measuring vessel diameter, identifying intima-media thickening, and assessing atherosclerotic plaque composition. Transmit power and receiver gain should be adjusted to produce a gray-scale image with the best tissue signal-to-noise ratio so that subtle differences can be perceived by the human eye. The examiner can modify image appearance by adjustment of the instrument's time gain compensation, which is designed to correct for the effects of increasing attenuation with depth. When duplex arterial imaging is performed, the left side of the image should be oriented toward the patient's head.

There are two types of Doppler ultrasound displays. In one form, a color-flow Doppler image shows the flow velocity distribution over a wide area displayed as a color-encoded map superimposed on the gray-scale B-mode tissue image. The second type, often referred to as spectral Doppler, shows the time-varying flow velocity distribution at a selected sample volume. Spectral Doppler provides quantitative information on the peak velocity within the sample volume, whereas color-flow Doppler provides semiquantitative information on the distribution of velocities over an entire region.

To obtain reliable information from spectral Doppler, it is best to use scan line angles (i.e., Doppler angles) of 60 degrees or less relative to the transducer insonation beam and arterial wall (Fig. 22.1). Assignment of the Doppler angle is controlled by the examiner. Because calculation of blood flow velocity is determined by the Doppler equation, which is proportional to the cosine of the Doppler angle, recording velocity spectra at large Doppler angles results in reduced Doppler frequency shift and thereby increases flow velocity error as a result of uncertainty in knowing the true Doppler angle. For example, an error in Doppler angle assignment such as 5 degrees higher than the recommended 60 degrees (i.e., at 65 degrees) will result in a 15% measurement error in flow velocity, whereas if a 55-degree angle was assigned, an 8% error results. The velocity measurement error caused by incorrect or imprecise assignment of the Doppler angle by the examiner is a common duplex testing inaccuracy that can result in overestimation or underestimation of the severity of the stenosis when disease classification is based on peak systolic velocity (PSV) or end-diastolic velocity (EDV) criteria. When pulsed Doppler flow signals are recorded, the instrument sample volume should be sized to encompass less than a third of the flow lumen and should be positioned in the center stream of flow.

### Blood Flow Imaging Techniques

Blood flow detection can be performed with one of three imaging techniques: color Doppler, power Doppler, and B-flow.

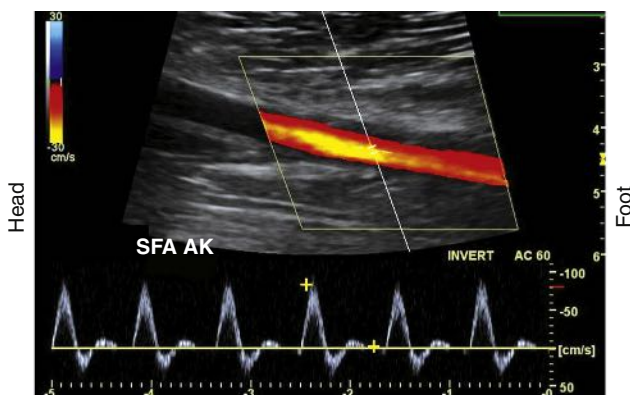


**Figure 22.1** Color duplex image with velocity spectra of normal superficial femoral artery (SFA) flow recorded from the above-knee segment (AK) with a 60-degree Doppler beam angle. Note that the pulsed Doppler sample volume is positioned in the center stream of flow, where color-flow pixels indicate the highest flow velocity.

### Color Doppler Imaging

Color Doppler imaging refers to pixel encoding of blood flow based on a color bar that depicts both flow direction (toward and away from the transducer) and mean velocity (MV). The examiner adjusts the velocity scale, color priority, and saturation of the color bar as well as instrument color gain to show the appearance of normal, laminar arterial flow as homogeneous regions varying in color-coded pixels during the pulse cycle. To set the color gain correctly, the examiner should increase the gain until a noise speckle appears within the flow region and then reduce it slightly. This technique will optimize the display of weak or lower velocity blood flow signals, such as those adjacent to the artery wall. Excessive color gain causes color-coded flow pixels to bleed into or beyond the artery wall, thus making the flow lumen appear larger than it is. Interpretation of real-time color Doppler flow is based on the color bar settings (peak MV, baseline, wall filter, and color assignment of flow toward or away from the transducer). In tortuous vessels, blood flow is color-coded according to its direction relative to the transducer scan lines. When blood flow velocity exceeds the mean peak velocity threshold of the color bar, color aliasing occurs, because the sampling rate as defined by the pulse repetition frequency is no longer sufficient (the Nyquist limit). With aliasing, blood flow is erroneously encoded as the “wrap-around” color shown in the color bar, and the color image display will show flow in the opposite direction. Increasing the pulse repetition frequency and increasing the Doppler angle are two techniques that can be used to reduce the color-flow “aliasing” artifact.

Arterial stenosis is recognized by color Doppler imaging as a reduction in the color-encoded flow lumen, imaging of a high-velocity flow region with color bar aliasing, and development of a mosaic flow pattern in the lumen signifying turbulent flow. At the site of a high-grade (>75% diameter reduction) stenosis, real-time color Doppler flow will appear as a whitened, color-desaturated “flow jet” with mosaic color flow extending for several vessel diameters downstream corresponding to post-stenotic turbulence (Fig. 22.2). A tissue bruit may appear as low-velocity flow signals outside the artery lumen and is caused

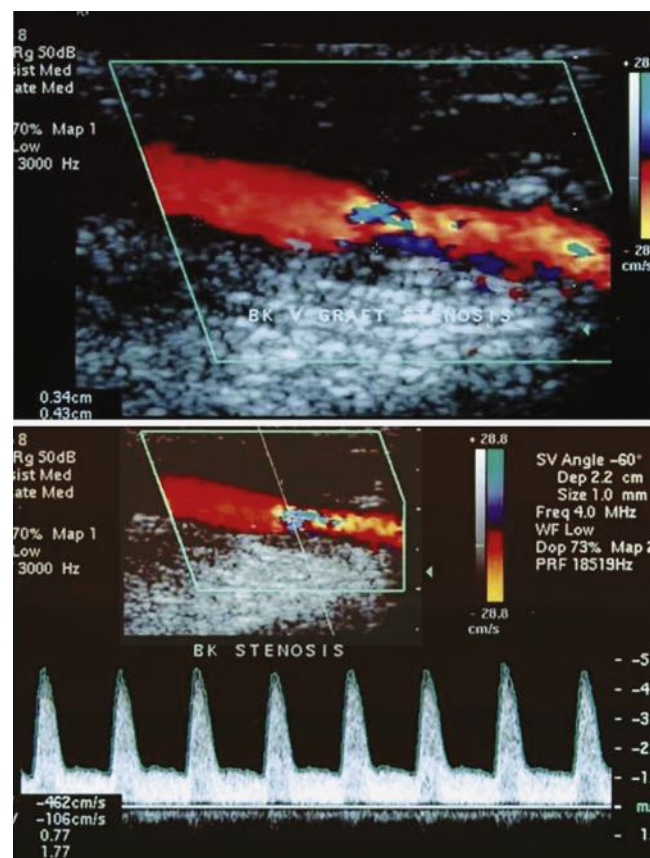


**Figure 22.2** Color duplex image and velocity spectra of an arterial vein bypass graft stenosis. *Top image*, Color aliasing occurs at the stenosis when mean velocity is greater than 28 cm/s and extends for several vessel diameters downstream. *Bottom image*, Velocity spectra recording at the stenosis “flow jet” indicates a peak velocity of 426 cm/s and spectral broadening of highly disturbed, turbulent flow.

by vibration of the arterial wall. The presence of persistence of color, color bar aliasing, and changes in flow lumen diameter on color Doppler imaging is indicative of abnormal flow patterns produced by stenosis. The examiner should then carefully interrogate this diseased arterial segment with pulsed Doppler spectral analysis to measure changes in flow velocity, which are then used to estimate the severity of the stenosis.

### Power Doppler Imaging

Power Doppler imaging is a technique in which the display of blood flow is based on the amplitude of the backscattered Doppler signal; it increases the sensitivity of flow detection three to five times with respect to color Doppler imaging. This imaging mode is termed “color angio” and is used by the technologist for imaging of small-diameter vessels, detection of slow flow, assessment of residual lumen diameter at a stenosis, and detection of “trickle” flow associated with high-grade stenosis. Flow direction is not evident with the power Doppler imaging option, and the flow signal is less dependent on the Doppler angle.

### B-Flow Imaging

B-flow imaging shows blood flow in gray scale; that is, flowing blood and the surrounding structures are depicted in shades of gray. The imaging technique is a visual depiction

of flow hemodynamics and should not be confused with color Doppler imaging, because no velocity information is provided. B-flow imaging relies on the amplification of weak echoes from moving red blood cells and is most useful during arterial imaging to show boundary layer flow adjacent to the vessel wall and traversing atherosclerotic plaque. B-flow imaging can demonstrate the complex flow patterns seen at bypass graft anastomoses and arteriovenous fistulae and within dialysis access conduits where color Doppler artifacts can obscure flow patterns.

## Pulsed Doppler Spectral Analysis

Pulsed Doppler velocity spectra recorded from a normal artery have a narrow range of velocities throughout the pulse cycle, which indicates that red blood cells are moving at a similar speed and direction in a nondisturbed, or laminar, flow pattern. If the “sample volume” of the pulsed Doppler is too large relative to the diameter of the artery or positioned adjacent to the arterial wall, low-velocity flow signals will be displayed as “broadening” or increased width of the velocity spectra.

Spectral broadening in the pulsed Doppler signal can also indicate “disturbed” flow or flow turbulence when it is recorded center-stream at bifurcations, regions of abrupt diameter change, and sites of stenosis. The “normal” appearance of arterial duplex flow varies with the artery being studied (peripheral, carotid, renal, or mesenteric) but should demonstrate rapid flow acceleration in systole, narrow spectral width, and varied diastolic flow corresponding to the vascular resistance of the arterial bed.

The velocity spectrum of a normal peripheral (aorta, iliac, extremity, external carotid) artery is triphasic or multiphasic (see Fig. 22.1) and consists of high outflow resistance with a systolic flow component, early diastolic flow reversal, and late diastolic forward flow. Low-resistance arterial flow, such as in the internal carotid, vertebral, renal, celiac, splenic, and hepatic arteries, is characterized by continuous flow throughout the pulse cycle with only a single (systolic) phasic flow component producing a monophasic pulsed Doppler spectral waveform. Changes in flow resistance of the microcirculation are primarily reflected as an increase or decrease in diastolic flow velocity.

## Measurements

The pulsed Doppler spectral parameters of acceleration time, pulsatility index (PI), resistive index (RI), and maximum spectral velocity measured at peak systole (PSV) and end-diastole (EDV) constitute the primary criteria used for test interpretation. The PSV measurement is reproducible and thus the most common velocity spectral parameter used for the interpretation of normal arterial flow and critical limb ischemia and for the grading of arterial stenosis. The EDV measurement is used in conjunction with PSV for evaluating high-grade stenosis (>70% diameter reduction; see Table 22.1).

The RI is calculated by subtracting EDV from PSV and then dividing by PSV. It is used clinically to assess the renal and cerebral circulations for abnormal peripheral resistance. Normal values are less than 0.7, and levels higher than 0.85 are

**TABLE 22.1** Velocity Spectra Waveform Parameters Used for Interpretation of Duplex Tests

Testing Area	PSV	EDV	RI	AT	PI	Mean Flow Velocity
Carotid duplex	X	X	X	X		
Transcranial Doppler	X		X		X	X
Peripheral duplex	X	X		X	X	
Duplex draft surveillance	X	X	X	X	X	
Renal duplex	X		X		X	
Mesenteric duplex	X	X	X	X	X	

AT, systolic acceleration time; EDV, end-diastolic velocity; PI, pulsatility index; PSV, peak systolic velocity; RI, resistive index.

associated with increased vascular bed resistance and decreased end-organ perfusion.

The PI is calculated by dividing the peak-to-peak velocity spectral shift by the average (mean) velocity. The PI of normal peripheral arteries is greater than 4.0 (femoral artery, >6; popliteal artery, >8). PI values lower than 4 may reflect proximal inflow or occlusive disease, and change in PI or spectral waveform damping is diagnostic of multilevel occlusive disease. Division of distal artery PI by proximal artery PI calculates the “damping factor;” a normal value is 0.9 or higher, and a value of less than 0.9 is diagnostic of occlusive disease.

The systolic acceleration time during systole can also be used to diagnose occlusive disease proximal to the pulsed Doppler recording site. A normal value is less than 133 ms. As systolic acceleration time increases to longer than 200 ms, the spectral waveform develops a rounded upslope configuration, termed tardus-parvus, because of the prolonged time to PSV. Diagnostic accuracy of the systolic acceleration time is influenced by cardiac conditions (cardiomyopathy, aortic valve disease), but downstream occlusive disease has minimal influence on diagnostic sensitivity.

## Artifacts and Errors

Artifacts and errors in ultrasound measurement can limit the effectiveness of the evaluation and create inaccurate results. Various artifacts include mirror image artifacts, shadowing from overlying vessel calcification, inaccuracy due to refraction, and aliasing. Most errors can be attributed to the technologist, because studies using flow models have found that adjustment of Doppler angle, sample volume placement, and Doppler gain were the most significant sources of error in PSV measurement.

Spectral Doppler aliasing is the most common artifact and, similar to color Doppler aliasing, is recognized by a “characteristic” signal wraparound in the spectral display. Adjustment of the velocity scale (i.e., pulse repetition frequency) to above the Nyquist limit or a reduction in the baseline level can shift the spectrum downward and eliminate the artifact. Shadowing from overlying calcification impedes adequate visualization of underlying vessel anatomy with B-mode imaging and

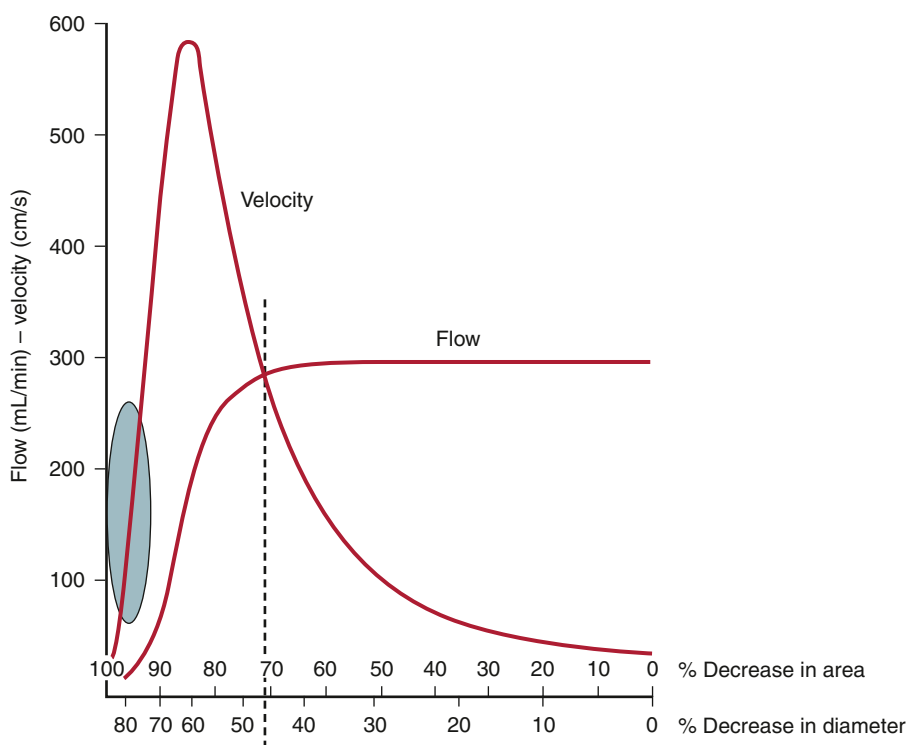


**Figure 22.3** Correlation of percent diameter reduction with increases in blood flow velocity (cm/s) and reduction in volume flow (mL/min) in arteries. Note that a high-grade (>95%) diameter-reducing stenosis causes volume flow to decrease toward zero, whereas the velocity within the stenosis may be minimally elevated.

interferes with accurate velocity measurement. Mirror image artifacts, created when a tissue structure is reproduced at an incorrect location, occur when a strongly reflecting surface is further reflected by other strongly reflecting surfaces.<sup>3</sup> Refraction can cause misregistration of the image and the Doppler sample volume and occurs when an ultrasound beam passes through mediums with different propagation speeds. Crosstalk, found only in Doppler evaluation, creates a mirror image where identical spectra appear above and below the baseline. It is usually caused by an excessive receiver gain setting or an incident angle near 90 degrees. Ghosting occurs when low-velocity motion from pulsating vessel walls produces small Doppler shifts that can cause color flashing into the surrounding anatomy; it can be fixed with wall filters.

Variability of diagnostic criteria between laboratories stems from methods for defining the percentage of stenosis, different machines, and differences in technique.<sup>3</sup> Factors such as gender and physiologic condition of the patient can also affect the outcomes of DUS evaluations. Studies have found that carotid PSV measurements in women average 10% higher than in men.<sup>4</sup> Congestive heart failure, dysrhythmias, and artificial support measures (ventilators, intraaortic balloon pumps, or pacemakers) can alter cardiac output, which in turn can affect PSV measurements. Regarding technologist error, the largest source is error in accurately aligning the cursor of the sample volume. Even small errors in angle measurement can result in significant errors in velocity measurement and severity of the stenosis.<sup>3</sup> Sample volume assumes that flow is parallel to the walls; however, flow is not usually parallel in tortuous vessels

or beyond an asymmetrical stenosis, and these situations can make correct sample volume positioning and true velocity readings difficult. Finally, the most accurate measurement of PSV at a stenosis is within the narrowest portion of the stenosis, and reproducible measurements can be best obtained only if the sample volume is placed at or very near this area.

### Duplex Velocity Spectral Classification of Arterial Stenosis

A significant or “critical” arterial stenosis is a lesion that is associated with a resting systolic pressure gradient of more than 15 mm Hg and reduces volume flow. In the peripheral arterial circulation, this correlates with a 50% or greater diameter reduction stenosis or greater than 75% reduction in cross-sectional area. A significant stenosis produces losses in blood energy primarily as a result of losses in inertial energy caused by the development of turbulent flow; such losses are much greater than the friction energy losses predicted by Poiseuille law.

By measuring changes in velocity proximal to and across an arterial stenosis, duplex testing can noninvasively estimate its hemodynamic significance and predict reductions in diameter within specified ranges (e.g., 0%–49% diameter reduction, ≥50%, 50%–79%, ≥80%). The relationship between the increase in flow velocity and the reduction in diameter by stenosis is nonlinear, especially with stenoses greater than 50% diameter reduction (Fig. 22.3). The DUS characteristics of greater than 50% diameter reduction arterial stenosis include elevated PSV in comparison to adjacent normal segment, a

color Doppler mosaic flow pattern, and pulsed Doppler spectral broadening of highly disturbed flow (i.e., post-stenotic turbulence with simultaneous forward and retrograde velocity spectra during systole).

The ratio of PSV ( $V_r$ ) across a stenosis is a useful parameter for grading the severity of a stenosis; a  $V_r$  value higher than 2 indicates a greater than 50% diameter reduction, and a value higher than 4 correlates with greater than 70% diameter reduction. Typically, a pressure-reducing (peak systolic pressure >20 to 30 mm Hg) and flow-reducing arterial stenosis is associated with a  $V_r$  above 3.5, a PSV higher than 250 to 300 cm/s, and an elevation in EDV of 40 cm/s or more. Downstream of a “significant” pressure-reducing arterial stenosis, the spectral waveform should appear damped and monophasic with prolongation of the acceleration time and a decrease in PSV to below normal levels. As stenosis severity increases beyond greater than 90% diameter reduction, volume flow through the stenosis tends toward zero, which can produce PSV at the stenosis in a minimally elevated range (100–200 cm/s) and low-velocity (<10 cm/s) trickle flow downstream. The atherosclerotic plaque associated with greater than 50% stenosis is typically irregular and may be calcified, which produces an acoustic shadow on the image and makes measurements of residual artery diameter or reduction in cross-sectional area too inaccurate on transverse imaging to classify the severity of an arterial stenosis. Correlation studies between duplex testing and angiographic measurements have found that PSV and  $V_r$  are the best predictors of the severity of a stenosis when it is expressed as percentage diameter reduction.

Validation studies comparing duplex interpretation of stenosis severity with angiographic measurements have reported different threshold PSVs for lesions with greater than 50% diameter reduction.<sup>5–20</sup> PSV measurement variation is in the ±15% range, similar to other biologic measurements. This variation is related to the type of ultrasound system used and differences in Doppler angle assessment and sample volume positioning by the examiner. This limitation of duplex scanning can be minimized by reporting stenosis (i.e., diameter reduction) within a specified range (e.g., 0%–49%, 50%–75%, and 76%–99%). In each clinical application, it is recommended that the vascular laboratory conduct ongoing quality assurance studies to confirm the diagnostic accuracy of stenosis interpretation in their laboratory in comparison to angiographic reports.

## PATIENT TESTING

Arterial duplex scanning can be performed as a portable bedside or vascular laboratory examination. Scanning should be conducted on a height-adjustable table or stretcher with the patient in a supine position. The bed and room environment should provide a comfortable, quiet atmosphere for patient examination, a warm room temperature (75–77°F) to avoid vasoconstriction of the extremities, and sufficient space to permit bilateral body access for ultrasound scanning. The typical examination time ranges from 30 to 60 minutes. Patients should refrain from tobacco use for at least 1 hour before the examination, and if abdominal scanning or visceral artery

testing is planned, the patient should have fasted for 4 hours, and the examination should be performed in the morning to minimize accumulation of intestinal gas. Assessment of visceral artery flow before and after a test meal may be required for the evaluation of patients with symptoms of mesenteric ischemia.

## Peripheral Arteries

Vascular specialists should be familiar with the spectrum of testing available as well as the information provided in conjunction with other hemodynamic tests. The duplex testing performed in the vascular laboratory is an extension of clinical assessment and is used to verify the presence and extent of disease. Numerous studies have analyzed the role of DUS, computed tomography, or MRA for preoperative assessment in efforts to limit the need for digital subtraction arteriography. In contemporary vascular practices, imaging with contrast-based modalities is generally limited to interventional procedures. This is because less invasive alternative imaging techniques can usually determine whether interventional treatment is possible without the performance of diagnostic arteriography. In patients with peripheral arterial disease, duplex imaging can determine disease location and length of lesions and help guide interventions.

### Indications

DUS evaluation is beneficial for the following: patients with suspected symptomatic, chronic peripheral arterial disease<sup>5–10</sup>; patients with suspected acute limb ischemia; patients with pedal infection without a palpable pulse; patients with atheroembolic or thromboembolic disease states; and patients who require surveillance after revascularization procedures.

### Technique

The extent of duplex arterial mapping should be individualized to the indication for peripheral arterial testing. Screening for aneurysm and imaging to identify tibial artery calcification are appropriate indications for testing in selected patients. Evaluation of patients with symptoms of claudication or other signs of peripheral arterial disease can localize sites of occlusive disease. Arterial scanning proceeds from proximal to distal, with notation of artery diameter, wall and plaque morphology, thrombus accumulation, and velocity spectral waveform. It can include both upper and lower extremities.

Abdominal imaging is optimally performed after fasting to minimize intestinal gas artifact. Lower limb testing should include imaging (3- to 5-MHz phased, curvilinear, or linear array transducer) of the abdominal aorta and iliac arteries for aneurysm and occlusive disease and the common femoral arteries for the presence of normal (i.e., triphasic) velocity spectra. Multiple scan windows are used to image the aorta at the level of the renal arteries, proceeding to the tibial arteries at the ankle. From the inguinal ligament distally, a 5- to 7-MHz linear array transducer is used to map the arterial tree. PSV and EDV should be reported in the arteries evaluated, with ratios of PSV compared with a more proximal segment of designated healthy vessel.

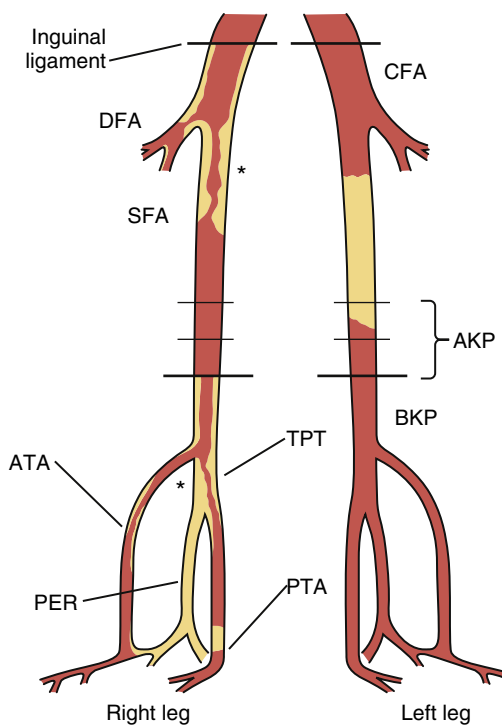


**Figure 22.4** Schematic of the Lower Limb Arteries for Recording of Arterial Duplex Map Findings. Occlusion is denoted by a filled-in lumen and stenosis by an asterisk\* at the lesion. *AKP*, above-knee popliteal; *ATA*, anterior tibial artery; *BKP*, below-knee popliteal; *CFA*, common femoral artery; *DFA*, deep femoral artery; *PER*, peroneal artery; *PTA*, posterior tibial artery; *SFA*, superficial femoral artery; *TPT*, tibioperoneal trunk.

The findings on duplex mapping should be recorded in a schematic of the extremity arterial tree, analogous to an arteriogram, with notation of the site or sites of aneurysm or occlusive disease, and measurements of velocity spectra at nondiseased arterial segments (common femoral, superficial femoral, popliteal, and tibial arteries) and at sites of stenosis (Fig. 22.4). Standardized values for arterial diameter and PSV in the lower limb arteries have been reported for healthy subjects under resting conditions (Table 22.2).<sup>5-9</sup> Duplex mapping allows classification of atherosclerotic occlusive disease in the aortoiliac, femoral–popliteal, and popliteal–tibial arterial segments based on Trans-Atlantic Inter-Society Consensus (TASC) guidelines for grading of lesions from A through D according to lesion length and morphology.<sup>10</sup>

### Interpretation

Duplex-derived data to estimate severity of stenosis of the lower extremity have not undergone a consensus recommendation process. Velocity-based criteria have been recommended by Cossman et al.<sup>11</sup> since 1989 (Table 22.3).

The PSV/EDV ratio should be calculated from an adjacent segment of a nonstenotic artery. Although the PI can aid in grading severity of stenosis, this value is not routinely independently used. The classic progression of deterioration of ankle–brachial index (ABI), decreasing PSV, and decreasing PI is depicted in Figure 22.5.

**TABLE 22.2** Artery Diameters and Peak Systolic Velocities in Healthy Subjects

Artery	Diameter (cm)*	Velocity (cm/s)*
Infrarenal aorta	2 ± 0.2	55 ± 12
Common iliac	1.5 ± 0.18	70 ± 18
External iliac	0.8 ± 0.13	115 ± 21
Common femoral	0.8 ± 0.14	114 ± 24
Superior femoral	0.6 ± 11	90 ± 14
Popliteal	0.5 ± 0.1	68 ± 14
Tibial arteries	0.3 ± 0.4	55 ± 10

\*Values are means ± standard deviation.

**TABLE 22.3** Duplex Classification of Peripheral Artery Occlusive Disease

Stenosis Category	Peak Systolic Velocity (cm/s)	Velocity Ratio ( $V_r$ )	Distal Artery Spectral Waveform
Normal	<150	<1.5	Triphasic, normal PSV
30%–49%	150–200	1.5–2	Triphasic, normal PSV
50%–75%	200–400	2–4	Monophasic, reduced PSV
>75%	>400	>4	Damped, monophasic, reduced PSV
Occlusion	No flow; length of occlusion estimated by distance from exit and reentry collaterals		Damped, monophasic, reduced PSV

PSV, peak systolic velocity.

Classification of peripheral arterial stenosis is based on duplex-derived criteria, similar to carotid duplex testing (e.g., PSV, EDV, and PSV ratio across a stenosis identified by color Doppler imaging) (Fig. 22.6) (Table 22.3). A doubling or step-up in PSV to more than 150 cm/s ( $V_r > 2$ ) indicates 50% or greater diameter reduction stenosis. Duplex criteria for a critical flow-limiting stenosis include loss of the triphasic waveform, spectral broadening with an increase in velocity (PSV >200 cm/s, EDV >0 cm/s), and  $V_r$  greater than 3 across the stenosis. Higher degrees of stenosis (>75%) are associated with an EDV higher than 100 cm/s and a  $V_r$  above 4.<sup>12</sup>

### Diagnostic Accuracy

A prospective comparison of DUS to contrast-enhanced MRA was performed including 152 patients, with conventional digital subtraction angiography as the “gold standard.” A PSV ratio of more than 2.5 was used to define a significant stenosis. Duplex had sensitivity, specificity, and overall accuracy of 76%, 93%, and 89%, respectively, whereas MRA had a sensitivity of 84%, a specificity of 97%, and an overall accuracy of 94%, with statistically significant improvements in MRA sensitivity ( $P = 0.002$ ) and specificity ( $P = 0.03$ ).<sup>13</sup> Collins et al.<sup>14</sup> performed a systematic review of the literature comparing

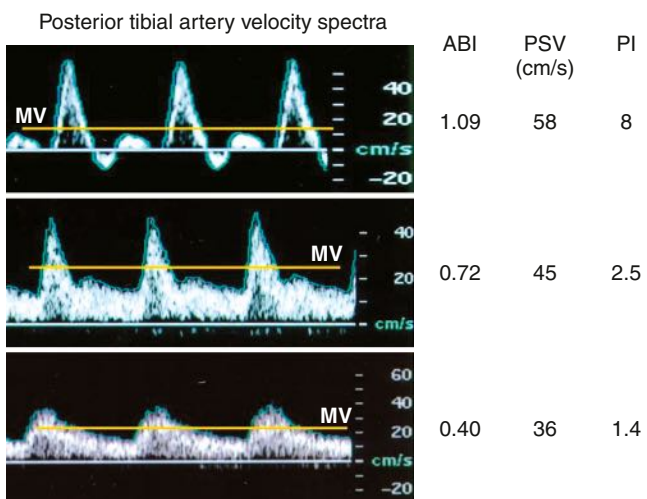


**Figure 22.5** Velocity spectra, ankle-brachial index (ABI), and pulsatility index (PI) recorded from the posterior tibial artery of limbs with normal (ABI  $>0.9$ , PI  $>4$ ), moderate (ABI = 0.5–0.8), and severe (ABI  $<0.5$ , PI  $<1.5$ ) limb ischemia. MV, mean velocity; PSV, peak systolic velocity.

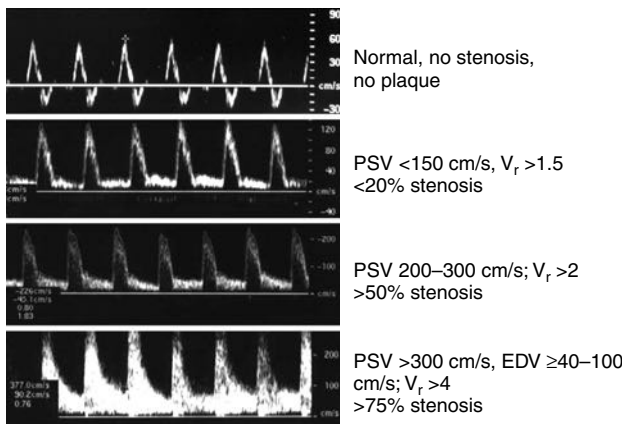


**Figure 22.6** Duplex categories of peripheral artery stenosis based on velocity spectral waveform interpretation. EDV, end-diastolic velocity; PSV, peak systolic velocity.

the three different imaging modalities. In detecting a greater than 50% stenosis, contrast-enhanced MRA demonstrated a median sensitivity and specificity of 95% and 97%, respectively; CTA showed a sensitivity and specificity of 91% and 91%, respectively; and DUS showed a sensitivity and specificity of 88% and 96%, respectively. For detection of occlusions, contrast-enhanced MRA was more sensitive and specific than CTA or DUS.

Excellent agreement between DUS and CTA has also been demonstrated for segments of the lower extremity arterial tree treated by percutaneous procedures. Langenberger and colleagues<sup>15</sup> reported a high degree of correlation between DUS and CTA when used to interrogate the superficial femoral artery after both balloon angioplasty and stent placement with correlation coefficients of  $r = 0.94$  and  $r = 0.71$ , respectively. Overall, the two modalities were found to have a correlation coefficient of  $r = 0.85$  in SFA segments treated by endovascular means.

## Iliac Arteries

The iliac arteries can be evaluated either by direct assessment via interrogation of the iliac artery or by indirect measures of common femoral artery waveform and velocity assessment. Direct assessment requires lower frequency abdominal probes and is limited by body habitus as well as by other factors (e.g., tortuosity, deep vessels) compared with indirect assessment of the femoral arteries.

### Interpretation

#### Direct imaging criteria

Direct imaging criteria for iliac artery stenosis include the following: for greater than 50% stenosis: PSV higher than 200 cm/s or PSV ratio of 2.5 or more; for greater than 75% stenosis: PSV ratio above 5.0 and EDV higher than 40 cm/s. PSV of 400 cm/s or more is suggestive of greater than 75% stenosis.<sup>16</sup>

#### Indirect imaging criteria

Reduced velocities in the common femoral artery (<45 cm/s) with an associated monophasic waveform pattern are nearly 90% accurate in identifying a proximal iliac artery lesion without direct iliac artery evaluation. In addition, Shaalan et al.<sup>17</sup> did not find any statistical difference in velocities of the common femoral artery by gender or in the presence of significant ipsilateral superficial femoral artery or contralateral iliac artery disease.

### Accuracy

The accuracy of DUS for detection of iliac artery disease is as follows.

#### Direct imaging

For greater than 50% stenosis (PSV >200 cm/s): 95% sensitivity, 55% specificity, 68% PPV, 91% NPV, and 75% accuracy; for greater than 75% stenosis (EDV >40 cm/s): 70% sensitivity, 90% specificity, 64% PPV, 92% NPV, and 86% accuracy; for greater than 75% (with V<sub>r</sub> >5.0): 65% sensitivity, 91% specificity, 65% PPV, 91% NPV, and 86% accuracy.<sup>16</sup>

#### Indirect imaging

An abnormal common femoral artery waveform contour (monophasic or biphasic) differentiated ipsilateral iliac artery stenosis of less than 50% from stenosis of greater than 50%, with 95% sensitivity, 89% specificity, 89% PPV, 95% NPV, and 92% accuracy. In differentiating between groups with greater than 50% stenosis and occlusion of the ipsilateral iliac artery, the specificity, PPV, and accuracy for PSV lower than 45 cm/s combined with a common femoral artery monophasic waveform are 97%, 92%, and 88%, respectively (Fig. 22.7).<sup>17</sup>

## Femoral–Popliteal and Tibial Arteries

Studies, including a prospective blinded comparative study, have demonstrated good agreement in the femoral–popliteal segment between DUS and digital subtraction angiography

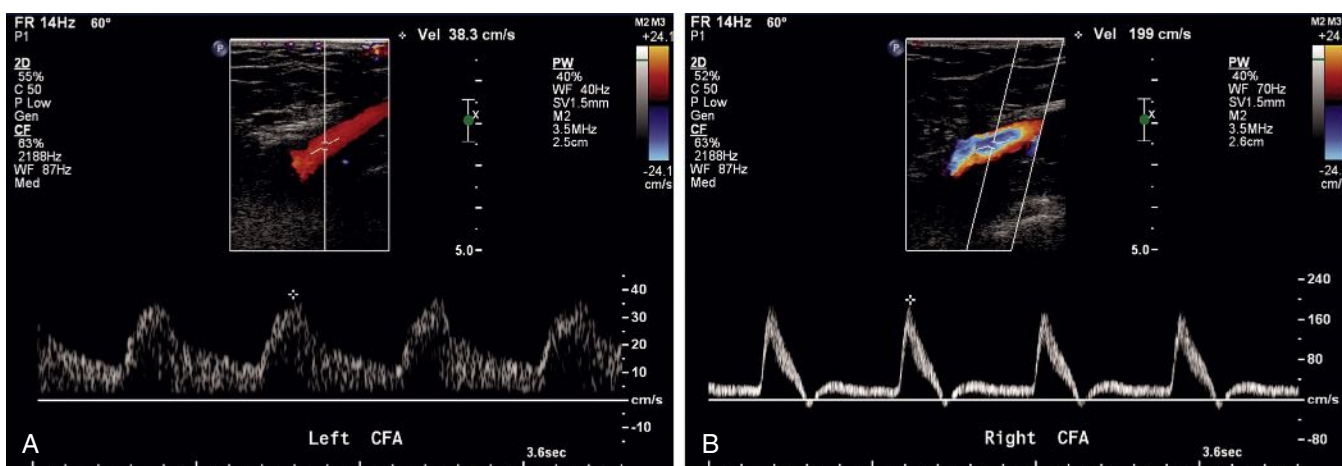


**Figure 22.7** Indirect Imaging of Iliac Arteries. (A) Common femoral artery (CFA) with damped low-velocity waveform. (B) Common femoral artery triphasic waveform for comparison.

with use of a Vr of more than 2 for defining a greater than 50% stenosis by DUS. Agreement was better in the supragenicular than in the infragenicular segments.<sup>18</sup> In a comparison of the agreement with digital subtraction angiography, specific areas had poor correlation: profunda femoral artery, tibioperoneal trunk, peroneal artery, and crural arteries. In addition, a report has recommended the combined use of a PSV higher than 200 cm/s and a Vr above 2 to predict a greater than 70% femoropopliteal stenosis.<sup>19</sup>

The sensitivity and specificity of DUS in the femoral–popliteal arteries depend on criteria used to determine the degree of stenosis. With use of a Vr above 2.4 in detecting a greater than 50% stenosis in the femoral artery, the sensitivity, specificity, PPV, and NPV were 81%, 93%, 84%, and 91%.<sup>17</sup> A combined Vr above 2.0 and a PSV higher than 200 cm/s was associated with a sensitivity, specificity, PPV, and NPV of 79%, 99%, 99%, and 85% in detecting a greater than 70% stenosis.<sup>19</sup>

In the tibial arteries, the largest series reporting the accuracy of DUS in detecting 50% stenosis found a sensitivity of 88%, specificity of 75%, PPV of 83%, and NPV of 81% in 1690 infrageniculate segments correlated with conventional angiography (see Table 22.3).<sup>20</sup>

### Limitations

For the aortoiliac disease segment, body habitus is the main limitation. For infrainguinal stenosis, the major limitation of accuracy is the presence of a proximal stenosis, which can falsely decrease distal velocities. Consequently, the velocity ratio may more accurately identify focal areas of stenosis. DUS may signify a high-grade stenosis instead of occlusion if a collateral vessel is visualized therefore falsely demonstrating flow adjacent to an occluded vessel. Incomplete vessel imaging may occur as a result of poor patient cooperation or acoustic shadowing caused by plaque calcification. Arterial segments difficult to image include the proximal external iliac artery, internal iliac origin, and tibioperoneal trunk. Calcific changes in the tibial arteries can decrease the accuracy of velocities.

The presence of an intraluminal stent has been suggested by some to render the observed PSV falsely elevated due to changes in vessel compliance compared to the adjacent artery. This hypothesis, however, may be refuted by recent *in vitro* work suggesting similar duplex profiles for vessels with and without self-expanding stents.<sup>21</sup>

## DUPLEX SURVEILLANCE

### Bypass Graft and Endovascular Intervention Surveillance

#### Vein Grafts

A surveillance program after lower limb vein bypass grafting is recommended, but the extent of testing, including routine duplex testing, remains controversial.<sup>22</sup> Current recommendations include a baseline examination within 30 days of surgery, if it is not performed intraoperatively, subsequent examinations at 6-month intervals, and then annually after the first year for vein grafts.<sup>23</sup> However, an opposing view by TASC II recommended surveillance with physical examination and ABI only.<sup>10</sup> The latest recommendations for duplex surveillance of infrainguinal vein grafting reported improved efficacy of duplex surveillance with rigorous imaging for high-risk bypasses.<sup>22</sup> When it is conducted appropriately, a graft surveillance program should result in a graft failure rate of less than 3% annually. It can be anticipated with DUS surveillance that approximately 20% of infrainguinal vein bypasses will have either a residual operative stenosis or developing graft stenosis within 1 year of reconstruction.

#### Technique

Similar to native infrainguinal arterial examination, B-mode, color-flow, and pulsed Doppler imaging should be performed of the inflow, conduit, and outflow vessels. B-mode imaging can often identify early technical issues (i.e., retained valves or sclerotic vein segments). Pulsed Doppler with waveform analysis should be mapped of the lower limb with PSV, EDV, and

**TABLE 22.4** Risk Stratification for Vein Graft Occlusion by Duplex Criteria

Category	High-Velocity Criteria, Peak Systolic Velocity	Velocity Ratio (V <sub>r</sub> )	Low-Velocity Criteria, Graft Flow Velocity	Change in ABI
I: Highest risk* (>70% stenosis with low graft flow)	>300 cm/s	>3.5	<45 cm/s or staccato graft flow	>0.15
II: High risk* (>70% stenosis without change or normal graft flow)	>300 cm/s	>3.5	>45 cm/s	<0.15
III: Moderate risk† (50%–70% stenosis with normal graft flow)	180–300 cm/s	>2.0	>45 cm/s	<0.15
IV: Low risk (normal bypass or <50% stenosis with normal graft flow)	<180 cm/s	<2.0	>45 cm/s	<0.15

ABI, ankle-brachial index.

\*Likelihood of progression of stenosis or graft thrombosis within 3 to 6 months is 40% to 50%.

†Of early (<3 months) lesions, 20% to 30% regress, 10% to 20% remain stable, and 40% to 50% progress to greater than 70% stenosis.

V<sub>r</sub> recorded. Specifics of the stenosis should also be recorded: diameter of the vein in transverse imaging above and below the stenosis, including length of stenosis in centimeters and anatomic location.

### Interpretation

A combination of ABI, PSV, and V<sub>r</sub> has been used to stratify patients into risk of subsequent vein graft failure. A PSV higher than 180 cm/s with associated V<sub>r</sub> of 2.0 and no change in ABI correlates well with a 50% stenosis. A critical vein graft stenosis with impending failure has a PSV higher than 300 cm/s, a V<sub>r</sub> of more than 3.5, and a decrease in ABI by 0.15 or more. Refer to Table 22.4 for risk stratification of failure.

Vein graft lesions with the duplex-derived velocity spectra of a high-grade stenosis (PSV >300 cm/s, EDV >20 cm/s, V<sub>r</sub> across the stenosis > 3.5) correlate with a greater than 70% diameter reduction stenosis and should be repaired (see Fig. 22.2). In a prospective study, application of these threshold criteria identified all grafts at risk for thrombosis, and only one lesion with high-velocity criteria regressed. Multiple investigators have observed an approximately 25% incidence of graft thrombosis in stenotic bypasses when a policy of no intervention was followed.<sup>22</sup>

The risk for graft thrombosis is predicted by using the combination of high- and low-velocity duplex criteria and decreases in ABI (Table 22.4). In the highest risk group (category I), the development of a pressure-reducing stenosis produces low flow in the graft, which will result in thrombosis if it is decreased below the “thrombotic threshold velocity.” Prompt repair of category I lesions is recommended, whereas category II lesions can be scheduled for elective repair within 1 to 2 weeks. A category III stenosis (PSV of 180–300 cm/s, V<sub>r</sub> <3.5) does not reduce pressure or flow in the resting limb. Serial scans at 4- to 6-week intervals are recommended to determine hemodynamic progression of these lesions. An important feature of a “graft-threatening” stenosis is its propensity to progress in severity, to reduce graft flow, and to form surface thrombus, which are events that can precipitate thrombosis. By use of serial duplex scans, a category III stenosis that does not progress can be distinguished from a progressive lesion that needs to be

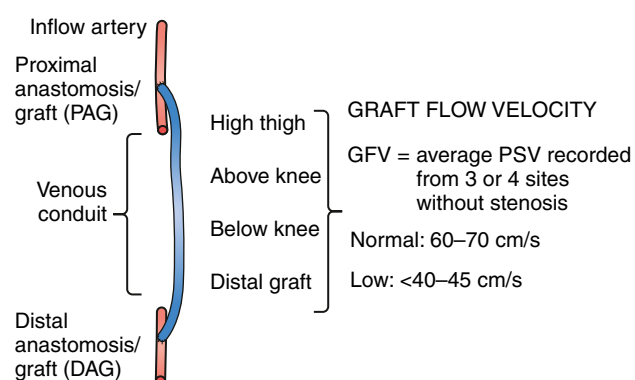


**Figure 22.8** Schematic of a lower limb bypass graft indicating the duplex recording site and calculation of mean graft velocity (MGV). PSV, peak systolic velocity.

repaired. The majority (approximately 80%) of bypass grafts will have no stenosis identified (i.e., category I scan). For these patients, surveillance at 6-month intervals is recommended. In patients with category I scans, a graft flow velocity lower than 40 cm/s indicates a “low-flow” bypass that is at increased risk for thrombosis by the concept of the thrombotic threshold velocity, which is lower in autogenous vein than in prosthetic bypasses. Prescribing an anticoagulation regimen of warfarin to maintain the prothrombin time at an international normalized ratio of 1.6 to 2 and antiplatelet therapy (aspirin, 81 mg/day, or clopidogrel bisulfate, 75 mg/day) may reduce the incidence of low-flow vein bypasses.<sup>22</sup> Patients who are at high risk for development of vein graft stenosis<sup>22</sup> include those with abnormal results on baseline testing (PSV, 180–300 cm/s; V<sub>r</sub>, 2–3.5), multisegment venous conduit, repeated bypass grafting, and need for warfarin therapy (Fig. 22.8).

### Results

Contemporary results of DUS surveillance of autogenous bypass grafts are favorable, with rates of primary assisted patency well in excess of 80% at 1 year. Jongsma et al.<sup>23</sup> reported the outcome of 69 infrainguinal bypass grafts found to be at risk of occlusion by DUS criteria (PSV >300 cm/s; V<sub>r</sub> 3.5). Most grafts were afflicted by a single area of stenosis with approximately

**TABLE 22.5** Summary of Proposed Duplex Criteria for Evaluating Endovascular Reconstructions

Paper	Duplex Criteria	Estimated Stenosis	Arterial Segment	Reconstruction Type
Baril et al. (2009) <sup>33</sup>	PSV >190 cm/s, Vr >1.5 PSV >275 cm/s, Vr >3.5	≥50% ≥80%	SFA	PTA + BMS
Shrikhande et al. (2011) <sup>38</sup>	PSV >223 cm/s, Vr >2.5	≥70%	SFA, Popliteal	PTA ± BMS
Troutman et al. (2014) <sup>39</sup>	PSV >300 cm/s, Vr >3, PSV <50 cm/s	N/A*	Iliac, SFA, Popliteal	Covered Stent Graft
Jones et al. (2015) <sup>40</sup>	Vr >2.5	N/A†	SFA, Popliteal	PTA ± BMS
Gao et al. (2016) <sup>41</sup>	PSV <63 cm/s distal to SFA stent	≥50%	SFA	PTA + BMS

\*Authors evaluated duplex criteria associated with stent graft failure rather than discrete stenosis.

†Authors evaluated duplex criteria associated with the development of recurrent lower extremity symptoms.

BMS, bare metal stent; PTA, percutaneous transluminal angioplasty; SFA, superficial femoral artery.

half occurring at the distal anastomosis. Lesions were treated by percutaneous transluminal balloon angioplasty (PTA) with 91% achieving technical success. Forty-two percent of the bypass grafts in their series required a second PTA, most often at the same site initially treated.

Conversely, Fisker et al. also recognized a significant need for graft-preserving interventions following *in situ* infrainguinal bypass but noted that most of these were triggered by clinical examination and symptomatology, rather than by DUS alone.<sup>24</sup> The authors question the cost-effectiveness of routine surveillance and determined that 60 asymptomatic grafts must be scanned to detect one significant stenosis in their series.

Despite successful DUS surveillance programs instituted by individual centers, the results of randomized trials comparing clinical examination and ABI with and without DUS have yielded mixed results. A recent meta-analysis failed to demonstrate a benefit of DUS on primary, primary-assisted or secondary patency but the authors note that this conclusion was based on low-quality evidence.<sup>25</sup> Guidelines promulgated by the Society for Vascular Surgery (SVS)<sup>26</sup> regard DUS after autogenous infrainguinal bypass as reasonable due to its low cost and risks and potential to detect intervenable lesions, especially within the first two years following initial graft creation.

### Prosthetic Grafts

Although it is not supported by the TASC II recommendations, Mohler et al.,<sup>27</sup> in a consensus document, support the surveillance of prosthetic reconstructions at baseline and at 6-month intervals, similar to vein reconstructions. This sentiment is echoed by recent SVS recommendations which recommend clinical examination and ABI with or without the addition of DUS.<sup>26</sup> Duplex criteria were recommended by Stone et al.<sup>28</sup> for patients after femoral–femoral bypass grafting, with a PSV higher than 300 cm/s in the inflow iliac artery and midgraft velocity lower than 60 cm/s predictive of graft failure. When duplex-directed intervention was performed, assisted patency at 5 years was 88%. Patency appeared to be improved in comparison to most reports in the literature of patency without surveillance.

Duplex surveillance of prosthetic grafts does not appear to detect correctable lesions as in vein bypass grafts. Surveillance appears to serve more as a predictor of graft

thrombosis by the detection of midgraft velocities below 45 cm/s. It has been shown that prosthetic grafts with low velocity benefit from warfarin to improve patency, which may justify surveillance. Brumberg et al.<sup>29</sup> recommended the use of warfarin if the mean graft velocity was below 60 cm/s to reduce the incidence of polytetrafluoroethylene bypass graft thrombosis.

### Peripheral Endovascular Interventions

Current guidelines recommend routine surveillance of peripheral arteries after percutaneous interventions.<sup>27</sup> Recently, the role of duplex examination after percutaneous peripheral interventions has been reported more commonly in the literature. DUS has emerged as a viable tool for guiding the potential need for remedial angiography to maximize patency of endovascular reconstructions.

#### Threshold Criteria

A number of authors have suggested empirically derived threshold criteria which correspond to angiographically proven intervenable lesions following percutaneous procedures. Table 22.5 summarizes DUS criteria utilized by contemporary authors. Taken together, these data suggest that a combination of PSV and Vr coupled with clinical evaluation probably offers the best sensitivity and specificity for restenosis after PTA or the development of in-stent restenosis. Broadly, suggested threshold criteria for repeated angiography included a PSV above 250–300 cm/s and a Vr of 2.5–3.0.<sup>30–41</sup>

#### Femoropopliteal Interventions

There is a growing body of evidence suggesting the benefit of routine surveillance of endovascular treatments applied to the femoropopliteal segment. Zheng et al.<sup>30</sup> followed 116 limbs after stent placement in the SFA and popliteal arteries and reported 100% primary-assisted patency at 18 months when DUS criteria (PSV >300 cm/s, Vr >3.0, PSV <45 cm/s within stented segment) were applied to recommend remedial intervention. Of the limbs screened as “abnormal” but not intervened upon, 70% went on to experience stent occlusion within approximately 6 months, on average.

Post-procedural DUS has also demonstrated value in interventions performed for chronic limb threatening ischemia (CLTI). Humphries et al.<sup>31</sup> reported outcomes after infrainguinal therapies in 113 patients and identified residual stenosis missed on completion angiogram in 56% of those undergoing early DUS. Unfavorable DUS (PSV >180 cm/s, Vr >2.0) within 30 days of index intervention was associated with a 20% rate of limb loss compared to 5% for those without concerning DUS findings.

Conversely, Qato et al.<sup>34</sup> examined 402 asymptomatic patients with femoropopliteal stents placed originally for claudication and found a very low rate of progression of in-stent restenosis (ISR) discovered by DUS with approximately two-thirds demonstrating stable ISR of >50% (Vr >2.0) over a mean follow-up of 34 months. The remaining one-third went on to develop high-grade ISR (>75%, PSV >400 cm/s, Vr >4.0) with a mean time to progression of 20.5 months. The authors suggest that given the extremely low rate of limb loss among those with lower degrees of ISR (1.6% in their series), asymptomatic patients may be safely observed without adverse consequence.

The utility of routine surveillance after endovascular therapy in the femoropopliteal segment has not yet been fully borne out and would benefit from additional high-quality data specifically examining primary-assisted patency as well as patient-centered outcomes of these reconstructions in the setting of regimented post-procedure DUS use.

### Tibial Therapies

Though DUS of the tibial arteries can be technically challenging, follow-up of transcatheter tibial interventions has been utilized successfully. The University of Pittsburgh group has reported on their outcomes following tibial interventions for limb salvage in the setting of chronic limb-threatening ischemia (CLTI)<sup>35,36</sup> including DUS criteria for detecting tibial restenosis (PSV >300 cm/s, Vr >3.0). The authors describe a

33%–59% primary patency rate and 50%–70% primary-assisted patency rate at 1 year with reintervention primarily driven by clinical symptoms and failure of wound healing.

### Iliac Interventions

DUS after iliac artery interventions may serve only a limited role. Back et al.<sup>32</sup> evaluated 67 patients with a mean follow-up of 1 year, finding a 4% stent thrombosis and only 20% of patients with potentially failing stents. Similarly, Al Samaraee et al.<sup>37</sup> reported only 6% of surveilled iliac stents met criteria for intervention, with the majority of ultimately failed iliac stents requiring urgent treatment having a “normal” recent surveillance duplex. The authors discourage DUS for iliac endovascular reconstructions citing inefficient resource allocation.

## SELECTED KEY REFERENCES

- AbuRahma AF, ed. *Noninvasive Vascular Diagnosis: A Practical Guide to Therapy*. 4th ed. New York: Springer; 2017.  
*Latest comprehensive text on noninvasive vascular testing and its clinical implications.*
- Miele FR, ed. *Essentials of Ultrasound Physics*. Forney: TX: Miele Enterprises; 2008.  
*An advanced review of the physics and instrumentation relevant to arterial duplex scanning.*
- Pellerito JS, Polak JF, eds. *Introduction to Vascular Ultrasonography*. 6th ed. Philadelphia: Elsevier Saunders; 2012.  
*An introductory textbook for vascular technologists that provides background physics, hemodynamics, and testing procedures for duplex scanning.*
- Zierler RE. *Strandness's Duplex Scanning in Vascular Disorders*. 4th ed. Philadelphia: Lippincott Williams & Wilkins; 2010.  
*Thorough updated text in the application of duplex ultrasound in vascular disease.*

A complete reference list can be found online at [www.expertconsult.com](http://www.expertconsult.com).

## REFERENCES

1. Brott TG, Halperin JL, Abbasa S, et al. 2011 ASA/ACCF/AHA/AANN/AANS/ACR/ASNR/CNS/SAIP/SCAI/SIR/SNIS/SVM/SVS guideline on the management of patients with extracranial carotid and vertebral artery disease. *Circulation*. 2011;124:489–532.
2. Blackshear WM, Phillips DJ, Chikos PM, et al. Carotid artery velocity patterns in normal and stenotic vessels. *Stroke*. 1980;11:67–71.
3. Johnston KW. Errors and artifacts of carotid ultrasound evaluation. In: AbuRahma AF, Bandyk DF, eds. *Noninvasive Vascular Diagnosis: A Practical Guide to Therapy*. 3rd ed. New York: Springer; 2013.
4. Comerota AJ, Salles-Cunha SX, Daoud Y, et al. Gender differences in blood velocities across carotid stenoses. *J Vasc Surg*. 2004;40:939–944.
5. Kohler TR, Nance DR, Cramer MM, et al. Duplex scanning for diagnosis of aortoiliac and femoropopliteal disease: a prospective study. *Circulation*. 1987;76:1074–1080.
6. Cossman DV, Ellison JE, Wagner WH, et al. Comparison of contrast arteriography to arterial mapping with color-flow duplex imaging in the lower extremities. *J Vasc Surg*. 1989;10:522–529.
7. Grassbaugh JA, Nelson PR, Rzucidlo EM, et al. Blinded comparison of preoperative duplex ultrasound scanning and contrast arteriography for planning revascularization at the level of the tibia. *J Vasc Surg*. 2003;37:1186–1190.
8. Proia RR, Walsh DB, Nelson PR, et al. Early results of infragenicular revascularization based solely on duplex arteriography. *J Vasc Surg*. 2001;33:1165–1170.
9. Moneta GL, Yeager RA, Antonovic R, et al. Accuracy of lower extremity arterial duplex mapping. *J Vasc Surg*. 1992;15:275–284.
10. Norgren L, Hiatt WR, Dormandy JA, et al. TASC II Working Group: inter-society consensus for the management of peripheral arterial disease (TASC II). *J Vasc Surg*. 2007;45:S5–S67.
11. Cossman DV, Ellison JE, Wagner WH, et al. Comparison of contrast arteriography to arterial mapping with color-flow duplex imaging in the lower extremities. *J Vasc Surg*. 1989;10:522–528; discussion 528–529.
12. Armstrong PA, Bandyk DF. Duplex scanning for lower extremity arterial disease. In: AbuRahma AF, Bandyk DF, eds. *Noninvasive Vascular Diagnosis: A Practical Guide to Therapy*. 2nd ed. New York: Springer; 2007.
13. Leiner T, Kessels AG, Nelemans PJ, et al. Peripheral arterial disease: comparison of color duplex and US and contrast enhanced MR angiography for diagnosis. *Radiology*. 2005;235:699–708.
14. Collins R, Burch J, Cranny G, et al. Duplex ultrasound, magnetic resonance angiography, and computed tomography angiography for the diagnosis and assessment of symptomatic, lower limb peripheral disease: systematic review. *BMJ*. 2007;334:1257.
15. Langenberger H, Schillinger M, Plank C, et al. Agreement of duplex ultrasonography vs. computed tomography angiography for evaluation of native and in-stent SFA re-stenosis—Findings from a randomized controlled trial. *Euro J Radiol*. 2012;81:2265–2269.
16. de Smet AA, Ermers EJ, Kitslaar PJ. Duplex velocity characteristics of aortoiliac stenoses. *J Vasc Surg*. 1996;23:628–636.
17. Shaalan WE, French-Sherry E, Castilla M, et al. Reliability of common femoral artery hemodynamics in assessing the severity of aortoiliac inflow disease. *J Vasc Surgery*. 2003;37:960–969.
18. Eiberg JP, Rasmussen JB, Hansen MA, et al. Duplex ultrasound scanning of peripheral arterial disease in the lower limb. *Eur J Vasc Endovasc Surg*. 2010;40:507–512.
19. Schlager O, Francesconi M, Haumer M, et al. Duplex sonography vs. angiography for assessment of femoropopliteal arterial disease in a “real world setting. *J Endovasc Ther*. 2007;14:452–459.
20. Khan SZ, Khan MA, Bradley B, et al. Utility of duplex ultrasound in detecting and grading de novo femoropopliteal lesions. *J Vasc Surg*. 2011;54:1067–1073.
21. Kuppler C, Christie J, Newton W, et al. Stent effects on duplex velocity estimates. *J Surg Res*. 2013;183:457–461.
22. Tinder CH, Chavanpun JP, Bandyk DF, et al. Efficacy of duplex ultrasound surveillance after infrainguinal vein bypass may be enhanced by identification of characteristics predictive of graft stenosis development. *J Vasc Surg*. 2008;48:613.
23. Jongsma H, Bekken J, van Buchem F, et al. Secondary interventions in patients with autologous infrainguinal bypass grafts strongly improve patency rates. *J Vasc Surg*. 2016;63:385–390.
24. Fisker L, Eiberg J, Sillesen H, et al. The role of routine ultrasound surveillance after in situ infrainguinal peripheral vein bypass for critical limb-threatening ischemia. *Ann Vasc Surg*. 2020;66:529–536.
25. Dabrh A, Mohammed K, Farah W, et al. Systematic review and meta-analysis of duplex ultrasound surveillance for infrainguinal vein bypass grafts. *J Vasc Surg*. 2017;66:1885–1891.
26. Zierler E, Jordan W, Lal B, et al. The Society for Vascular Surgery practice guidelines on follow-up after vascular surgery arterial procedures. *J Vasc Surg*. 2018;68:256–284.
27. Mohler ER, Gornik HL, Gerhard-Herman M, et al. ACCF/ACR/AIUM/ASE/ASN/ICAVL/SCAI/SCCT/SIR/SVM/SVS 2012 appropriate use criteria for peripheral vascular ultrasound and physiological testing part 1: arterial ultrasound and physiological testing. *J Am Coll Cardiol*. 2012;60:242–276.
28. Stone PA, Armstrong PA, Bandyk DF, et al. Duplex ultrasound criteria for femoral-femoral bypass revision. *J Vasc Surg*. 2006;44:496–502.
29. Brumberg SR, Back MR, Armstrong PA, et al. The relative importance of graft surveillance and warfarin therapy in infrainguinal prosthetic bypass failure. *J Vasc Surg*. 2007;46:1160–1166.
30. Zheng H, Calligaro K, Jang J, et al. Duplex ultrasound for diagnosis of failing stents placed for lower extremity arterial occlusive disease. *Ann Vasc Surg*. 2020;63:269–274.
31. Humphries M, Pevec W, Laird J, et al. Early duplex scanning after infrainguinal endovascular therapy. *J Vasc Surg*. 2011;53:353–358.
32. Back MR, Novontney M, Roth SM, et al. Utility of duplex surveillance following iliac artery angioplasty and primary stenting. *J Endovasc Ther*. 2001;8:629–637.
33. Baril DT, Rhee RY, Kim J, et al. Duplex criteria for determination of in-stent restenosis after angioplasty and stenting of the superficial femoral artery. *J Vasc Surg*. 2009;49:133–139.
34. Qato K, Conway A, Mondry L, et al. Management of isolated femoropopliteal in-stent restenosis. *J Vasc Surg*. 2018;68:807–810.
35. Fernandez N, McEnaney R, Marone L, et al. Predictors of failure and success of tibial interventions for critical limb ischemia. *J Vasc Surg*. 2010;52:834–842.
36. Saqib N, Domenick N, Cho J, et al. Predictors and outcomes of restenosis following tibial artery endovascular interventions for critical limb ischemia. *J Vasc Surg*. 2013;57:692–699.
37. Al Samaraee A, McCallum I, Cairns T, et al. The results of high-frequency duplex surveillance after iliac artery stenting in a single center. *Vasc and Endovasc Surg*. 2011;45:246–254.
38. Shrikhande G, Graham A, Aparajita R, et al. Determining criteria for predicting stenosis with ultrasound duplex after endovascular intervention in infrainguinal lesions. *Ann Vasc Surg*. 2011;25:454–460.
39. Troutman D, Madden N, Dougherty M, Calligaro K. Duplex ultrasound diagnosis of failing stent grafts placed for occlusive disease. *J Vasc Surg*. 2014;60:1580–1584.
40. Jones D, Graham A, Connolly P, et al. Restenosis and symptom recurrence after endovascular therapy for claudication: Does duplex ultrasound correlate with recurrent claudication? *Vascular*. 2015;23:47–54.
41. Gao M, Zhao X, Tao Y, et al. Incidence and predictors of in-stent restenosis in the superficial femoral artery: Evaluation of long-term outcomes by color duplex ultrasound. *Ultrasound Med Biol*. 2016;42:717–726.

# Techniques to Assess Tissue Perfusion in Peripheral Arterial Occlusive Disease

KIRSTEN F. MA, SIMONE F. KLEISS, and JEAN-PAUL P.M. DE VRIES

## INTRODUCTION 265

### INVASIVE TECHNIQUES TO ASSESS TISSUE PERFUSION 267

Two-Dimensional Perfusion Angiography 267

Computed Tomography Perfusion Imaging 268

Contrast-Enhanced Ultrasound 268

Magnetic Resonance Perfusion Imaging (ASL, BOLD, DCE, IVIM) 274

Near-Infrared Fluorescence Imaging with Indocyanine Green 274

Single Photon Emission Computed Tomography/Computed Tomography 274

### NONINVASIVE TECHNIQUES TO ASSESS TISSUE PERFUSION 274

### Hyperspectral Imaging 274

Laser Doppler Perfusion Imaging and Laser Speckle Contrast Imaging Techniques 275

Micro-Lightguide Spectrophotometry 275

Near-Infrared Spectroscopy 276

Skin Perfusion Pressure 276

Transcutaneous Partial Pressure of Oxygen 276

Thermal Imaging 276

### CLINICAL IMPLICATIONS 277

### FUTURE DIRECTIONS 277

### CONCLUSIONS 277

## INTRODUCTION

Determination of lower limb tissue perfusion in patients with peripheral arterial occlusive disease (PAD) or critical limb-threatening ischemia (CLTI) can be challenging. In addition to the clinical examination, additional diagnostic tools, such as the ankle–brachial index (ABI), toe blood pressure, Doppler ultrasound, computed tomography (CT) angiography, magnetic resonance (MR) angiography, and digital subtraction angiography (DSA), are widely used.<sup>1,2</sup> However, these imaging techniques focus on the pre- and post-procedural blood flow in the macrovasculature and are not able to determine tissue perfusion or oxygenation of the microvasculature. However, impaired tissue perfusion is a major cause of rest pain, nonhealing ulcers, and infection,<sup>3</sup> especially in patients with concomitant comorbidities such as diabetes mellitus or renal insufficiency. With local measurement of tissue oxygenation in peri-wound areas, healing potential and cause of the ulcer (arterial, venous, or a combination) may be determined more accurately.

Another role for tissue perfusion assessment is in the guidance of treatment of patients with PAD and CLTI. Currently, a completion angiography is performed at the end of an endovascular revascularization procedure to determine the technical success, which is mainly judged on the patency of the femoro-crural arteries and pedal circulation. A technically successful revascularization procedure of the major arteries, however, does not always lead to a clinically successful outcome, such as relief of rest pain and wound healing. Local tissue perfusion measurements may be a better predictor of successful revascularization and may guide the interventionalist during revascularization procedures, especially in multi-level obstructive disease in the femoro-crural arteries.

Several techniques have been introduced that enable tissue perfusion measurements, but most of these have not been broadly implemented in clinical practice so far. In this chapter we provide an overview of the currently available techniques to date using tissue perfusion techniques in vascular patients. An overview of the characteristics, indications, and pros and cons of each technique is summarized in Table 23.1.

**TABLE 23.1**

Overview of Characteristics, Indications, and Pros and Cons of Invasive and Noninvasive Techniques to Assess Lower Limb Tissue Perfusion

Type of Measurements	Application of Technique	Diagnostic Accuracy	Benefits	Limitations
<b>Two-dimensional (2D) perfusion angiography</b>				
<b>Tissue perfusion measurements of a ROI in the lower extremity with DSA and post-processing software</b>	Post-processing of DSA at the start and end of the revascularization procedure	Diagnostic accuracy and predictive value are unknown	No extra ionizing radiation or contrast agents except DSA runs Per-procedural data relevant to the technical success of the procedure	Invasive technique Motion artifacts
<b>Computed tomography (CT) perfusion imaging</b>				
<b>Tissue perfusion measurements of a ROI of the lower extremity with CT and post-processing software during revascularization or follow-up</b>	CT perfusion imaging at baseline and/or after revascularization	Diagnostic accuracy and predictive value are unknown	High spatial resolution Easily accessible Short acquisition time Quantitative and qualitative analysis of perfusion in the limbs and feet	Invasive technique Ionizing radiation Motion artifacts
<b>Contrast-enhanced ultrasound (CEUS)</b>				
<b>Perfusion measurements of skeletal muscles of the lower extremity with microbubble contrast agents</b>	CEUS imaging at baseline and/or after revascularization Used in addition to Doppler or duplex ultrasound	Diagnostic accuracy and predictive value are unknown	No ionizing radiation Real-time visualization of muscle perfusion Easily accessible	Invasive technique Operator dependent No stand-alone technique Limited transit time of microbubble agents Motion and bone artifacts
<b>Magnetic resonance (MR) perfusion imaging (ASL, BOLD, DCE, IVIM)</b>				
<b>Perfusion measurements of skeletal muscles of the lower extremity with different MR imaging techniques, such as ASL, BOLD, DCE, and IVIM</b>	Measurements at baseline and/or after revascularization	Diagnostic accuracy and predictive value are unknown	No ionizing radiation Possibility to use without contrast agents	Invasive technique High costs Time consuming Not suitable in case of claustrophobia
<b>Near-infrared fluorescence (NIRF) imaging with indocyanine green</b>				
<b>Skin perfusion measurements of the lower extremity with intravenous indocyanine green contrast agents</b>	NIRF imaging at the start and end of the revascularization procedure	Sensitivity of 67%–100% and specificity of 72%–100% <sup>4</sup> Predictive value is unknown	No ionizing radiation Intraoperative and real-time visualization relevant to the technical success of revascularization	Invasive technique Expensive imaging cameras Low penetration depth
<b>SPECT/CT imaging</b>				
<b>Perfusion measurements of skeletal muscles of the lower extremity with radionuclide imaging</b>	Measurements performed pre- and/or post-intervention	A cutoff value for high perfusion is 5.35 muscle-to-background ratio with an AUC of 0.92 based on MAE <sup>5</sup>	High image quality	Invasive technique Ionizing radiation High costs Use of radioactive isotopes
<b>Hyperspectral imaging (HSI)</b>				
<b>Skin perfusion measurements with visible light spectroscopy based on oxy- and deoxyhemoglobin concentration</b>	Measurements pre- and/or post-intervention Monitoring of wound healing	Sensitivity of 80%, specificity of 74%, and positive predictive value of 90% for diabetic foot ulcer healing <sup>6</sup>	Non-invasive technique Fast Handheld Contact free	Low penetration depth
<b>Laser Doppler and laser speckle contrast perfusion techniques (LDPI and LSCI)</b>				

*Continued*

**TABLE 23.1**

Overview of Characteristics, Indications, and Pros and Cons of Invasive and Noninvasive Techniques to Assess Lower Limb Tissue Perfusion—cont'd

Type of Measurements	Application of Technique	Diagnostic Accuracy	Benefits	Limitations
<b>Skin perfusion measurements using coherent laser light that interferes with the movement of red blood cells in the tissue</b>	Measurements pre- and/or post-intervention	LDPI: Diagnostic accuracy and predictive value are unknown LSCI: Sensitivity of 92.3%, specificity of 75.0%, and positive predictive value of 80.0% for venous ulcer healing <sup>7</sup>	Noninvasive technique No ionizing radiation Short acquisition time	Small measurement area Low penetration depth Measurements are affected by temperature and administration of vasoactive medication
<b>Micro-lightguide spectrophotometry (<math>O_2C</math>)</b>				
<b>Flow measurements of the skin using a combination of laser Doppler flowmetry and spectroscopy</b>	Application at a fixed time pre- and post-intervention or continuously during the intervention	Diagnostic accuracy and predictive value are unknown	Noninvasive technique Fast Real-time visualization	Small measurement area Variable penetration depth
<b>Near-infrared spectroscopy (NIRS)</b>				
<b>Muscle oxygen saturation measured with red and near-infrared light using the absorption spectra of oxy- and deoxyhemoglobin in the lower limb</b>	Measurements pre- and/or post-intervention or continuously during intervention	Diagnostic accuracy and predictive value are unknown	Noninvasive technique Easily applicable at different locations of the lower limbs and feet	Differences in commercially available NIRS systems Artifacts due to adipose tissue
<b>Skin perfusion pressure (SPP)</b>				
<b>Tissue perfusion measurements of the skin with a laser probe incorporated in a pressure cuff</b>	Measurements pre- and/or post-intervention to predict wound healing or amputation	Sensitivity of 79.9% and specificity of 78.2% at a cutoff value of 30 mmHg for wound healing <sup>8</sup>	Noninvasive technique Fast	Cuff placement sometimes difficult and painful Motion artifacts
<b>Transcutaneous partial pressure of oxygen (<math>TcPO_2</math>)</b>				
<b>Measurements of partial pressure of oxygen of the skin with a heated sensor-containing electrode</b>	Measurements pre- and/or post-intervention to predict wound healing or amputation	A cutoff value <40 mmHg is associated with a 24% increased risk of wound complications after amputation <sup>9</sup>	Noninvasive technique Low costs	Time consuming Small measurement area Measurements affected by tissue edema, hair, increased oxygen consumption
<b>Thermal imaging</b>				
<b>Measurement of skin temperature</b>	Measurement pre and/or post-intervention	A decrease of 2°C in temperature had a sensitivity of 100% and specificity of 89% for failure of graft patency after bypass surgery <sup>10</sup>	Noninvasive technique Contact free Fast	Influence of external factors (e.g., surrounding temperature) on skin temperature

ASL, arterial spin labeling; AUC, the area under the receiver-operator-curve; BOLD, blood oxygenation level-dependent; DCE, dynamic contrast enhanced; DSA, digital subtraction angiography; IVIM, intra-voxel incoherent motion; MAE, major adverse event; ROI, region of interest; SPECT, single photon emission computed tomography.

## INVASIVE TECHNIQUES TO ASSESS TISSUE PERFUSION

### Two-Dimensional Perfusion Angiography

Two-dimensional (2D) perfusion angiography is a technique to determine perfusion of the lower limb and foot using digital

subtraction angiography (DSA). These DSA images are analyzed with post-processing software, which can be performed on different workstations during revascularization procedures or post-intervention.<sup>11–14</sup> The post-processing software converts the DSA images to color-coded images based on the change in pixel density over time.<sup>12</sup> A time density curve (TDC) of contrast volume flow in the leg can be extracted to determine tissue

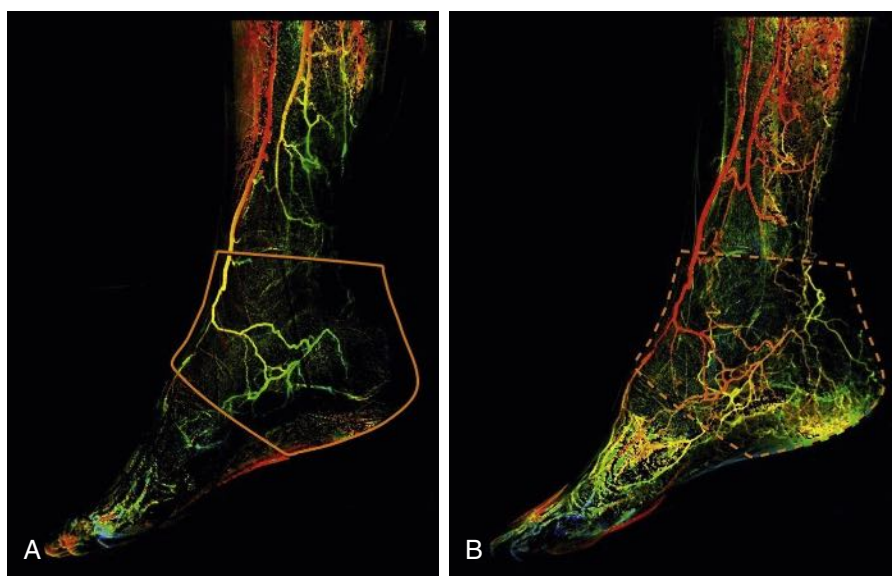


**Figure 23.1** 2D perfusion angiography of a patient undergoing revascularization (A) prior to revascularization, and (B) post-revascularization.

perfusion. After that, a region of interest (ROI) of the feet can be manually selected in the images. A couple of parameters can be derived from the software representing the in- and outflow of contrast in the microcirculation over time.<sup>15,16</sup> An example of the images created with 2D perfusion angiography is shown in Figure 23.1.

This technique has been explored in several prospective cohort studies in patients with PAD<sup>12,13,16,17</sup> and retrospectively<sup>11,14,18,19</sup> with the purpose to determine its feasibility. Different parameters can be used to determine the hemodynamic changes and improvement in tissue perfusion over time.<sup>12,15,16,18</sup> In three studies, 2D perfusion angiography parameters were significantly correlated with ABI, toe-brachial index, or skin perfusion pressure (SPP).<sup>16,18,19</sup> The main outcomes of three prospective cohort studies and one retrospective study are summarized in Table 23.2.

This technique has some limitations, however. It relies on DSA and cannot be used for regular follow-up to monitor disease progression or ulcer healing. Besides, motion artifacts occur in up to 10% of patients.<sup>12</sup> Standardization of the DSA protocol and region of interest (ROI) placement before and after endovascular treatment (EVT) is extremely important to capture any change in perfusion parameters. 2D perfusion angiography is an invasive technique, and at the moment, no validity or accuracy is determined.<sup>20</sup> One of the ongoing studies to determine repeatability and inter- and intra-observer reliability of 2D perfusion angiography is the REPEAT study (see Key reference: Ipema et al.).

### Computed Tomography Perfusion Imaging

Unlike 2D perfusion angiography, volumetric CT perfusion protocols consist of both CT angiography and CT perfusion imaging. With post-processing analysis, the changes in tissue perfusion parameters after intravenous injection of an contrast

medium can be calculated.<sup>21–23</sup> During post-processing, an ROI is selected, and a time-attenuation curve or TDC can be obtained. Perfusion parameters can be extracted based on the contrast density values. In most studies, CT perfusion imaging is performed before and within a pre-defined time interval after revascularization with a maximal follow-up time of 7 days.<sup>21–25</sup> Moreover, CT perfusion has been shown to be feasible and reproducible in lower limb tissue perfusion detection, and changes in perfusion parameters are determined before and after EVT.<sup>22,26</sup> Sah et al.<sup>26</sup> performed the largest study to date and included 35 patients who underwent CT perfusion imaging combined with ABI and duplex ultrasound measurements before EVT. The results of these studies are summarized in Table 23.2.

The main benefit of CT perfusion imaging is the provision of a quantitative and qualitative analysis of the perfusion in the limbs and feet. Compared with MR imaging (MRI) perfusion, CT perfusion imaging provides a higher spatial resolution, is easily accessible, less expensive, and requires a shorter image acquisition time.<sup>25</sup> However, CT perfusion, like 2D perfusion angiography, is sensitive to motion artifacts, especially in PAD patients with pain. In addition, it is an invasive technique that involves radiation exposure.

### Contrast-Enhanced Ultrasound

Standard duplex ultrasound enables detection of stenosis or occlusions in the feeding arteries of the lower extremity.<sup>27</sup> Contrast-Enhanced Ultrasound (CEUS) uses intravenously administered microbubbles to assess the microvascular blood flow. Microbubbles traverse the microcirculation and compress and expand under influence of an ultrasound wave. The ultrasound signal is amplified, and the microbubbles can be distinguished easily from blood.<sup>28,29</sup> After intravenous administration, the desired skeletal muscle can be imaged with the ultrasound transducer, and time to peak (TTP) intensity and

**TABLE 23.2** Recent Publications for Tissue Perfusion Imaging Techniques

Study [year]	Number of subjects	Study design	Measurement protocol	Main outcomes
<b>Two-dimensional (2D) perfusion angiography</b>				
Ikeoka (2020) <sup>16</sup>	33 patients with CLTI	Prospective cohort study	DSA at the start and end of the intervention with 2D angiography and SPP. The ROI was placed distally to the ankle and included the arterial foot arch.	Only the AT was significantly shortened after EVT in rest and during hyperemia. Only hyperemic AT was significantly correlated with the mean SPP both before and after EVT.
Ng (2019) <sup>18</sup>	47 patients with CLTI	Retrospective study	DSA at the start and end of the intervention with 2D perfusion angiography. Results were compared with ABI and TBI before and after EVT. An ROI was placed on the main run-off the pedal artery of the foot. ABI and TBI measurements were also performed.	Washout phase parameters showed a significant reduction in time required for contrast to decay to a specified percentage after peak. Percentages of contrast decay at specified time intervals after peak were increased significantly. The percentage of contrast decay 4 s after peak demonstrated the highest correlation coefficient with improvement in ABI or TBI.
Pärsson (2020) <sup>15</sup>	37 patients with CLTI	Prospective cohort study	DSA at the start and end of the intervention with 2D angiography. The ROI was placed between the tibio-talar joint and the midtarsal region, including part of the calcaneus.	A significant reduction in contrast AT and TTP was shown. A significant increased WiR was observed.
Reekers (2016) <sup>12</sup>	68 patients with CLTI	Prospective cohort study	DSA at the start and end of the intervention with 2D perfusion angiography. ROI was placed not lower than the middle cuneiform bone.	In most patients, perfusion angiography showed an increase in volume flow, an increase in both AUC and maximal PD, in the foot after successful angioplasty of the below-the-knee arteries.
<b>CT perfusion imaging</b>				
Cindil (2020) <sup>25</sup>	16 patients with CLTI	Prospective cohort study	CT perfusion imaging 1 to 3 days before and within 1 week after EVT. The TAC was obtained by placing a ROI on the posterior or anterior tibial artery at the ankle level of the untreated limb. The ROIs for analysis were placed on the dermis and muscle area of the sole of the foot and at the abductor hallucis muscle of both feet.	The post-treatment BF and BV showed a statistically significant increase in the dermal ROI. The percentage change of BF and BV showed statistical correlations with ABI increase. Intra-observer agreement values showed excellent agreement.
Gao (2019) <sup>22</sup>	19 patients with CLTI	Prospective cohort study	Preoperative and postoperative (within 3 days after EVT) CT perfusion scans in supine position. The TDC was obtained by placing a ROI within the transverse section of the dorsal or plantar artery. The ROIs for tissue perfusion analysis were performed at several locations of the foot.	In the treated limb, the mean value of the BF and the average MSI significantly increased, and the average MTT, TTP, IRFT <sub>0</sub> and T <sub>max</sub> were significantly shortened. No statistical difference was found for BV and PS.
Sah (2019) <sup>26</sup>	35 patients with PAD	Prospective cohort study	CT perfusion scan immediately before EVT. Hemodynamic assessment was done with different noninvasive techniques such as ABI. The ROI for TAC was drawn onto the popliteal artery. The ROI for tissue perfusion analysis was manually selected around the calf muscles on every slice and adapted to their confines.	BV of the symptomatic limb was significantly different among ABI groups (ABI ≥0.70; 0.60–0.69; ≤0.59), with higher BV in patients with lower ABI. In the asymptomatic limb, there was no significant difference of BV among the ABI groups.
<b>Contrast-enhanced ultrasound (CEUS)</b>				
Duerschmied (2010) <sup>33</sup>	34 patients with PAD	Prospective cohort study	CEUS before and directly after revascularization and at 3 and 5 months of follow-up. The ROI was the area between the proximal and medial third of gastrocnemius and soleus muscle. ABI, PVR, and improvement in clinical stage (Fontaine) were also recorded. Patients were divided in an EVT and a bypass group.	In the EVT group, median TTP was significantly shortened after the intervention. At follow-up, median TTP decreased slightly in this group. In the bypass group, median TTP decreased significantly directly after and decreased slightly up to 3 to 5 months after surgery. No significant correlation between ABI and TTP was found.

**TABLE 23.2** Recent Publications for Tissue Perfusion Imaging Techniques

Study [year]	Number of subjects	Study design	Measurement protocol	Main outcomes
Kundi (2017) <sup>32</sup>	13 patients with PAD and 8 healthy controls	Prospective cohort study	CEUS before and after treadmill exercise. ROI was the greatest circumference of the calf.	PP and TTP were significantly different between PAD patients and healthy controls after exercise but not in rest. Significant change in PP and TTP within controls before and after exercise but not in patients.
Meneses (2018) <sup>31</sup>	12 patients with PAD and 12 healthy controls	Prospective cohort study	CEUS before and after cuff occlusion and plantar flexion exercise. ROI was the medial gastrocnemius muscle of the largest leg circumference.	There were no significant differences between PAD patients and healthy controls at rest. Post-occlusion perfusion was lower in patients than in controls. Post-exercise perfusion was not different, but BV was higher in patients compared with controls.
<b>MR perfusion imaging (ASL, BOLD, DCE, IVIM)*</b>				
Bakermans (2020) <sup>43</sup>	15 patients with PAD and 18 healthy controls	Prospective cohort study	BOLD MR imaging in supine position. Analysis was performed in the transverse plane outlining the gastrocnemius and soleus muscle. Measurements were done at baseline and after hyperemia, including ABI measurements	The relative amplitude of hyperemic perfusion response was significantly higher in PAD patients compared with healthy controls and showed a strong correlation with the ABI for both groups combined.
Galanakis (2020) <sup>42</sup>	10 patients with CLTI	Prospective cohort study	DCE-MRI perfusion imaging of the affected foot before and within 1 month after EVT. Follow-up included clinical examination, ABI, and DUS at 1, 3, 6, and 12 months. Multiple ROIs were placed in the sagittal plane around the entire foot, on the dermis and muscle tissue. Inter-observer reliability was calculated.	After PTA, perfusion parameters increased significantly. There was no significant correlation between perfusion parameters and ABI. Inter-observer reliability was excellent, with ICCs ranging from 0.91 to 0.95.
Grözinger (2014) <sup>41</sup>	10 patients with PAD	Prospective cohort study	PCASL MRI before and after revascularization. Measurements were done at baseline and after hyperemia (cuff occlusion). ROIs were placed in the transverse plane in the dorsal flexor compartment, the soleus muscle, and in the anterior compartment, the tibialis anterior muscle. ABI and pain-free walking distance were analyzed before and after PTA.	Hyperemic perfusion increased in the soleus muscle and increased significantly in the tibialis anterior muscle. Time to peak perfusion decreased in the soleus muscle and significantly in the tibialis anterior. A similar pattern was detected for the time of hyperemia. The mean ABI significantly increased. Pain-free walking improved in 8 patients.
Suo (2018) <sup>39</sup>	14 patients PAD or CLTI and 10 healthy controls	Prospective cohort study	ASL, BOLD, and IVIM cardiovascular MRI after 15 min of rest. Analyses were performed in the axial plane in the middle of the calf for the anterior and lateral compartment and the soleus and gastrocnemius muscle.	BOLD perfusion T2* values were significantly lower in patients with PAD compared with age-matched healthy controls. T2* was significantly lower in patients with CLTI compared with claudicant patients.
<b>NIRF imaging with ICG</b>				
Colvard (2016) <sup>44</sup>	93 patients with CLTI	Prospective cohort study	NIRF imaging with ICG before and immediately after revascularization. Plantar surface of the foot was measured. Measurements were compared with ABI, improvement of walking distance, and decrease in patient-reported claudication symptoms.	Mean ingress, egress, and peak perfusion of the plantar side of the foot increased significantly. Patients with clinically successful outcomes showed significant improvements in ABI, ingress, egress, and peak perfusion. The overall change in ABI significantly correlated with postoperative changes in ingress and peak perfusion.
Seinturier (2020) <sup>48</sup>	29 patients with PAD or suspected CLTI	Prospective cohort study	NIRF imaging with ICG of both feet consecutively, 15 min between two ICG administrations. ROI was determined for the whole foot and sub-areas. TBP measurement was performed as a reference.	No correlation between TBP and NIRF ICG parameters. In CLTI there was a correlation between the amplitude of ICG intensity on the forefoot and TBP. NIRF ICG parameters did not show any prognostic value for amputation, revascularization, or death.

Settembre (2017) <sup>47</sup>	101 patients with CLTI	Prospective cohort study	NIRF imaging with ICG before and immediately after revascularization. The dorsum of the foot was measured. ABI and TBP measurements were also performed.	The mean ingress and mean ingress rate increased significantly.
<b>SPECT/CT imaging</b>				
Alvelo (2018) <sup>52</sup>	42 patients with CLTI and 9 healthy controls	Prospective cohort study	SPECT/CT imaging was performed after an 8-hr fast and 15 min after injection of $^{99m}\text{Tc}$ -tetrofosmin at the ankle and foot. In 8 healthy subjects and 6 patients, imaging was repeated 45 min after the tracer injection. Angiosomes of the foot were segmented.	Perfusion was significantly lower in patients with CLTI compared with healthy controls. Perfusion correlated with ABI for all participants but not for patients with CLTI alone. ICC showed excellent agreement of repeated measurements in both groups.
Hashimoto (2017) <sup>5</sup>	38 patients with suspected PAD	Retrospective study	SPECT/CT imaging was performed 15 min after injection of $^{99m}\text{Tc}$ -tetrofosmin of the lower legs and feet. 3D VOI were selected from toes to knees. Data analysis was repeated to determine intra- and inter-operator reproducibility.	Patients with low perfusion had significantly more MAEs within 1 year. A multivariate analysis identified low perfusion as an independent prognostic factor for MAE. Linear regression analysis showed excellent reproducibility.
<b>Hyperspectral imaging (HSI)</b>				
Chiang (2017) <sup>55</sup>	150 patients with PAD and 20 healthy controls	Prospective cohort study	HSI was performed over the head of the first metatarsal on the plantar side in supine position. $\text{TcPO}_2$ measurements were performed afterward.	Oxyhemoglobin and oxygen saturation correlated significantly with the severity of disease. Deoxyhemoglobin and oxygen saturation correlated significantly with $\text{TcPO}_2$ . Intra- and inter-operator reliability was excellent.
Grambow (2019) <sup>56</sup>	24 PAD, 25 patients without PAD, and 25 healthy controls	Prospective cohort study	HSI was performed at the plantar angiosome of the foot with patients in prone position.	HSI analysis revealed significantly reduced values for tissue oxygenation in patients with PAD. Tissue oxygenation did not correlate strongly or significantly with ABI.
<b>Laser Doppler (LDPI) and laser speckle contrast-based perfusion imaging (LSCI)</b>				
Humeau-Heurtier (2017) <sup>60</sup>	34 patients with PAD and 14 healthy controls	Prospective cohort study	LSCI was performed at the lower anterior part of the leg. $\text{TcPO}_2$ measurements were also performed.	The LSCI values of patients were significantly different compared with controls. LSCI significantly correlated with $\text{TcPO}_2$ .
Kikuchi (2019) <sup>62</sup>	31 patients with CLTI and 23 non-PAD controls	Prospective cohort study	LSCI before and immediately and 3 and 7 days after revascularization. ROI at the plantar side of the foot.	The LSCI value of the medial and lateral plantar surface was significantly increased immediately after the procedure and reached a maximum on day 7 after revascularization. The LSCI value was significantly lower for PAD limbs compared with non-PAD controls.
Pawlaczyk-Gabriel (2014) <sup>61</sup>	216 patients with PAD and CLTI and 27 healthy controls	Prospective cohort study	LDPI was performed after 15-min rest, during thermal stimulation, and post-ischemic hyperemia, at the dorsum of the foot between second and third metatarsal. $\text{TcPO}_2$ was also performed.	Skin blood flow was significantly lower in patients than in controls during thermal stimulation. Skin blood flow was significantly different between CLTI and controls and CLTI and claudicant patients. No significant differences in skin blood flow between patients and controls in rest.
<b>Micro-lightguide spectrophotometry (<math>\text{O}_2\text{C}</math>)</b>				
Gyldenløve (2019) <sup>64</sup>	28 patients with PAD	Prospective cohort study	$\text{O}_2\text{C}$ measurements before and after treadmill test and before and after 12 weeks of exercise therapy. Measurements in supine position after 3 min of rest. ROI was the first toe of the index limb and contralateral limb.	Neither oxygen saturation nor flow was affected after a 12-week exercise program. Significant decrease after treadmill test for $\text{sO}_2$ , at the start and at 12 weeks of follow-up.
Rother (2017) <sup>65</sup>	30 patients with CLTI	Prospective cohort study	$\text{O}_2\text{C}$ measurements continuously during EVT. Three measurement points were defined: dorsal and plantar side of the foot, and lateral side of the ankle. A control probe was placed on the contralateral leg. ABI measurements were also performed.	The mean $\text{sO}_2$ showed a significant improvement after EVT. The overall flow parameter increased significantly after EVT.

Continued

**TABLE 23.2** Recent Publications for Tissue Perfusion Imaging Techniques—cont'd.

Study [year]	Number of subjects	Study design	Measurement protocol	Main outcomes
<b>Near-infrared spectroscopy (NIRS)</b>				
Boezeman (2016) <sup>67</sup>	14 patients with CLTI	Prospective cohort study	Measurements were performed during EVT and 4 weeks later. In patients with arterial ulcers, the probe was placed 2 cm next to it, with a reference probe on the contralateral side. In patients without ulcers, the probes were placed on the dorsum of the feet. ABI and TBI values were also measured.	The mean StO <sub>2</sub> increased significantly after 4 weeks. The mean StO <sub>2</sub> was not significantly different directly before and after revascularization. ABI and TBI values showed no significant correlation with StO <sub>2</sub> values.
Boezeman, Boersma (2016) <sup>69</sup>	61 patients with CLTI and 30 age-matched control patients without PAD	Prospective cohort study	NIRS measurements before EVT at 4 spots: proximal vastus lateralis, distal vastus lateralis, proximal gastrocnemius lateralis, and distal gastrocnemius lateralis. The biceps were used as the reference spot.	Single rSO <sub>2</sub> was significantly lower for every measurement location between PAD and controls. The rSO <sub>2</sub> limb-to-arm ratios were significantly lower in PAD compared with controls at the proximal and distal gastrocnemius lateralis but not at the distal vastus lateralis.
Fuglestad (2020) <sup>72</sup>	40 patients with PAD and 10 healthy controls	Prospective cohort study	NIRS measurements continuously at baseline, after 1 minute of exercise, and during recovery period with a wireless, continuous-wave near-infrared spectrophotometer. The NIRS device was placed over the bilateral gastrocnemius muscle.	Baseline values were comparable between PAD patients and healthy controls. Patients with PAD reached minimum StO <sub>2</sub> significantly earlier than healthy controls. Change in StO <sub>2</sub> was significantly higher in patients with PAD at 1 min of exercise and at exercise minimum.
Khurana (2013) <sup>71</sup>	84 patients with PAD	Prospective cohort study	NIRS measurements using a continuous-wave spectrometer before, during, and after treadmill-walking test until pain caused patients to stop. The medial gastrocnemius muscle was used as the ROI. ABI and ankle systolic blood pressure (SBP) were measured before and 1 min after the treadmill test.	Patients were divided into two groups: SBP <50 mmHg post-exercise and SBP ≥50 mmHg. There were no differences in the decline in calf muscle StO <sub>2</sub> to a minimum value or in the time to reach minimum StO <sub>2</sub> . No significant correlation was found between StO <sub>2</sub> and ABI.
<b>Skin perfusion pressure (SPP)</b>				
Ikeoka (2020) <sup>16</sup>	33 patients with CLTI	Prospective cohort study	SPP on the dorsal and plantar side of the foot before and after EVT.	Dorsal and plantar SPP increased significantly after EVT.
Kimura (2019) <sup>76</sup>	76 patients with wounds	Prospective cohort study	Patients were classified according to the Society for Vascular Surgery WIFL classification, and SPP was performed after 15 min of rest.	Sensitivity of WIFL classification increased by using SPP, from 65% to 80%. Cutoff values for ischemia grade would be 0, >45 mmHg; 1, 44–35 mmHg; 2, 25–34 mmHg; 3, <25 mmHg.
Okamoto (2015) <sup>78</sup>	156 patients with CLTI	Prospective multicenter cohort	SPP was performed after EVT.	Mean pre- and post-EVT SPP was 28 and 46 mmHg, respectively, and correlated significantly with the 1-year amputation-free survival rate, MAEs, and wound healing.
Suzuki (2017) <sup>77</sup>	998 patients with wounds	Retrospective study	Patients who presented with a wound received SPP on the initial visit.	Patients with a SPP <30 mmHg had a significantly longer wound closure time, 235 days compared with 52 days in patients with SPP >50 mmHg.
<b>Transcutaneous partial pressure of oxygen (TcPO<sub>2</sub>)</b>				
Andrews (2013) <sup>89</sup>	307 patients undergoing partial foot amputation	Retrospective, observational study	TcPO <sub>2</sub> was measured at two locations on the dorsum of the foot. Measurements were performed in rest and with the leg elevated or depended.	Sensitivity and specificity of 71% at a cutoff value of 38 mmHg for wound healing after 3 months.
Faglia (2007) <sup>90</sup>	564 patients with DM and CLTI	Retrospective study	TcPO <sub>2</sub> measurements before and after treatment of the ischemic leg on the dorsum of the foot. TcPO <sub>2</sub> was measured for 30 min.	A TcPO <sub>2</sub> of <34 mmHg indicates a need for revascularization. The risk of amputation is <1% with a TcPO <sub>2</sub> >50 mmHg.

De Graaff (2003) <sup>91</sup>	96 patients with suspected CLTI	Randomized controlled trial	Patients randomized for the new diagnostic strategy received $TcPO_2$ measurements at the first metatarsal at 44°C. A threshold of <35 mmHg was an indication for intervention.	The use of $TcPO_2$ did not lead to better patient outcome or reduction of interventions in patients with an uncertain diagnosis of CLTI.
Salaun (2019) <sup>88</sup>	455 patients with CLTI	Prospective cohort study	$TcPO_2$ was performed on the first inter-metatarsal space on the forefoot. Sensor heated to 44°C, determined after 15 min.	The amputation rate was twice as high for patients with a $TcPO_2$ of <10 mmHg compared with patients with $TcPO_2$ >30 mmHg. Sensitivity of 65% and specificity of 58% for $TcPO_2$ at 11 mmHg regarding amputation risk. $TcPO_2$ performed before revascularization could not predict the outcome of the procedure.
<b>Thermal imaging</b>				
Al Shakarchi (2019) <sup>10</sup>	25 patients with PAD	Prospective cohort study	Thermal imaging before and after bypass surgery. Pre- and 2 hours and 21 days postoperatively. Images were taken of the dorsal and plantar side of the feet.	The temperature increased postoperatively and was significantly associated with bypass patency. A decrease of 2°C had a sensitivity of 100% and specificity of 89%, a positive predictive value of 75%, and a negative predictive value of 100% for failure of graft patency.
Ilo (2020) <sup>98</sup>	40 patients with PAD	Prospective cohort study	Thermal imaging before and after revascularization. Pre- and 1 month postoperatively. Images were taken after 15–20 min of rest of the dorsal and plantar side of the feet.	The mean temperature increased significantly on the plantar side and on the dorsal side postoperatively. The difference between the vascularized and contralateral foot decreased significantly after treatment.
Wallace (2018) <sup>97</sup>	23 patients with PAD	Prospective cohort study	Thermal imaging of the hands and feet, and the temperature ratio between foot and hand was determined (tABI). Conventional ABI measurements were performed.	There was a strong and significant correlation between the temperature ratio and ABI. Bland–Altman analysis showed excellent agreement between tABI and ABI.

\*Outcome parameters of MRI perfusion imaging differ between BOLD, ASL, DCE and IVIM. ABI, ankle–brachial index; ASL, arterial spin labelling; AT, arrival time; AUC, area under the curve; BF, blood flow; BOLD, blood oxygenation level dependent; BV, blood volume; CLTI, critical limb threatening ischemia; DCE, dynamic contrast enhanced; DSA, digital subtraction angiography; DUS, Doppler ultrasound; EVT, endovascular treatment; ICG, indocyanine green; IRFt0, impulse response function; IVIM, intra-voxel incoherent motion; MAE, major adverse events; MSI, mean slope of increase; MTT, mean transit time; PAD, peripheral arterial disease; PCASL, pseudo continuous arterial spin labeling; PD, peak density; PP, peak perfusion; PS, permeability surface; PTA, percutaneous angioplasty; PVR, pulse volume recording; ROI, region of interest; rSO2, hemoglobin oxygen saturation; SBP, systolic blood pressure; sO2, oxygen saturation; StO2, oxygen saturation; T2\*, T2 relaxation time; tABI, temperature ankle–brachial index; TAC, time attenuation curve; TBI, toe–brachial index; TBP, toe blood pressure; TDC, time density curve; Tmax, time to peak; TTP, time to peak; VOI, volume of interest; WiFi classification, wound, ischemia, foot infection; WiR, wash in rate.

peak perfusion can be determined. The diagnostic accuracy for CEUS measurements of muscle perfusion has not been determined.

A meta-analysis of patients with PAD compared with healthy individuals showed that CEUS was able to differentiate between these groups based on the TTP intensity.<sup>30</sup> However, no correlation was found between CEUS and ABI.<sup>30</sup> More recent studies using CEUS for muscle perfusion found no differences between PAD patients and healthy controls at rest, but significant differences in perfusion were observed after exercise or induced ischemia between these groups.<sup>31,32</sup> Limited data are available regarding determination of the change in tissue perfusion after revascularization. Up to now, Duerschmied et al.<sup>33</sup> have suggested that a change in tissue perfusion can be detected directly after revascularization but not during follow-up. Results of the studies are summarized in Table 23.2. Limitations of the technique are its invasiveness, heterogeneity in measurement protocols, its operator dependency,<sup>34</sup> and the lack of correlation between CEUS and conventional diagnostics.<sup>30</sup>

## Magnetic Resonance Perfusion Imaging (ASL, BOLD, DCE, IVIM)

MRI can be used for detection of stenotic lesions without the image being substantially affected by calcification. For MR perfusion imaging, different techniques are used, such as arterial spin labeling (ASL), blood oxygenation level dependent (BOLD) imaging, intra-voxel incoherent motion (IVIM), and dynamic contrast-enhanced MRI (DCE-MRI).<sup>35–37</sup> The working mechanism of ASL, BOLD, and IVIM MRI has been described in more detail in several studies.<sup>34–36,38,39</sup> The advantage of ASL, BOLD, and IVIM MRI techniques is that they do not require exogenous contrast agents.

Versluis et al.<sup>37</sup> showed a moderate to good reproducibility for DCE-MRI and BOLD MRI in 10 patients and controls, which was confirmed by Jiji et al.<sup>40</sup> for DCE-MRI measurements on different days in 11 patients and 16 controls. Grözinger et al.<sup>41</sup> performed ASL MRI and Galanakis et al.<sup>42</sup> performed DCE-MRI before and after EVT and showed significant increases in perfusion parameters. Suo et al.<sup>39</sup> integrated ASL, BOLD, and IVIM MRI and compared these techniques between patients with PAD and age-matched healthy volunteers. These findings were recently confirmed in a study using BOLD imaging.<sup>43</sup> The results of these small prospective studies are summarized in Table 23.2.

MR BOLD imaging seems the most reliable method to measure tissue perfusion in rest in PAD patients.<sup>36,39</sup> The application of this technique might be suitable as a supplement in the diagnosis of patients with calcified arteries and contraindications for the use of contrast agents. Disadvantages of MRI perfusion imaging are the high costs, risk of claustrophobia, and time-consuming measurements.

## Near-Infrared Fluorescence Imaging with Indocyanine Green

NIRF imaging with ICG assesses tissue perfusion in different tissues, including the skin of the legs and the feet.<sup>44</sup> ICG ( $t_{1/2}$

= 2.5–3 minutes) is administered intravenously, and tissue perfusion can be visualized at different phases, including arterial inflow phase, local perfusion of capillaries in the skin, and the venous outflow phase. Most NIRF imaging systems consist of a charge-coupled device camera with a laser source and a monitor, which detect perfusion by change in intensity. The penetration depth of ICGA starts at millimeters and is limited to a maximum of 1 cm.<sup>45</sup> The most often used technology in PAD patients is SPY Fluorescence Imaging Technology (Stryker), which has a penetration depth of up to 5 mm.<sup>44,46</sup>

The technique has been used for diagnosis of PAD, with a sensitivity of 67% to 100% and a specificity of 72% to 100%.<sup>4</sup> NIRF imaging with ICG can also be used to evaluate treatment success after revascularization procedures. The findings of two prospective cohort studies with 100 included patients, respectively, showed a significant increase after revascularization.<sup>44,47</sup> More recently, Seinturier et al.<sup>48</sup> could not replicate the prognostic value of NIRF imaging with ICG for clinical outcomes of patients with PAD. The results are summarized in Table 23.2.

The most important limitation of NIRF imaging in PAD is its penetration depth of only 3 to 5 mm.<sup>34,49</sup> Therefore, changes in subcutaneous and muscle microcirculation are not detected. Another limitation preventing this technique to be broadly applied in PAD patients is the heterogeneity in imaging devices and the protocols used in the currently available literature.<sup>4,50</sup>

## Single Photon Emission Computed Tomography/Computed Tomography

When perfusion imaging of the lower extremity is performed with this technique, first, SPECT/CT imaging is performed after the intravenous injection of a radiotracer, and then low-dose CT images are captured. These CT attenuation images are used to segment the ROI in the lower limb and foot. From these images, the (decrease in) intensity values can be determined. The use of SPECT/CT for perfusion imaging of the lower extremity has been investigated with different kinds of radiotracers, such as  $^{99m}\text{Tc}$ -tetrofosmin or  $^{99m}\text{Tc}$ -sestamibi.<sup>51</sup>

Reported experience on this imaging technique is scarce. Reproducibility was determined for intra- and inter-observer variability showing excellent agreement for assessment of tissue perfusion in each angiosome region, but this is based on one retrospective cohort study and one prospective cohort study, both with small sample sizes.<sup>5,52</sup> Results are described in Table 23.2. Limitations of the technique are its invasive character, high costs, and use of ionizing radiation.

## NONINVASIVE TECHNIQUES TO ASSESS TISSUE PERfusion

### Hyperspectral Imaging

Hyperspectral imaging (HSI) uses visible light spectroscopy to determine tissue oxygenation of the skin. Several wavelengths of visible light are used to determine the concentration

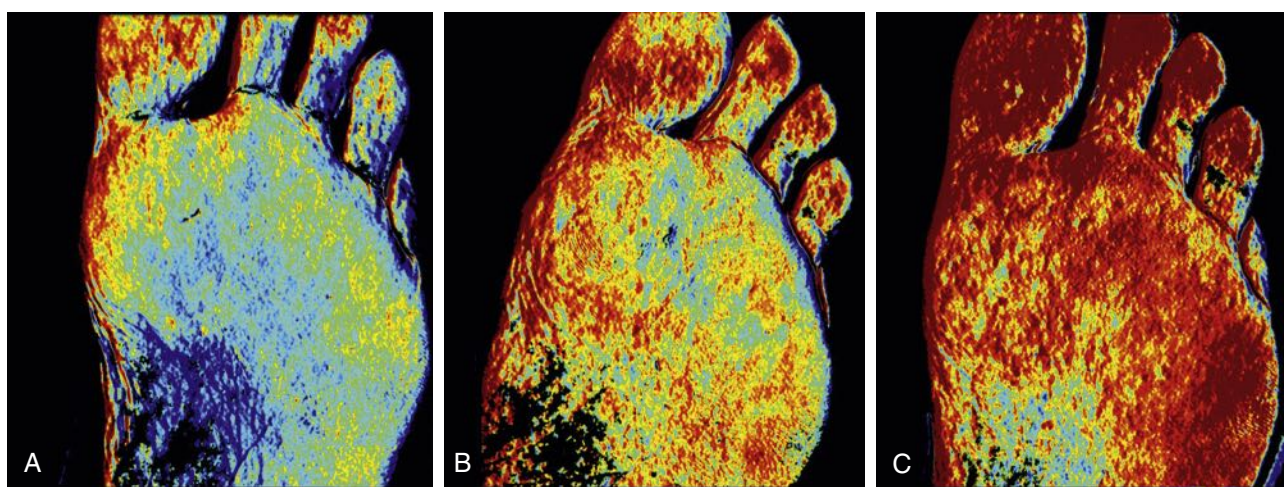


**Figure 23.2** Hyperspectral imaging of increasing oxyhemoglobin concentration measured at the plantar side of a foot (A) directly after revascularization, (B) 1 day after, and (C) 7 days after revascularization.

of oxyhemoglobin and deoxyhemoglobin with a penetration depth of 1 to 2 mm. A concentration can be calculated based on the known absorption spectra of these tissue chromophores. These measurements are presented in a color-coded image of the skin.<sup>53,54</sup> An example of these hyperspectral images is shown in Figure 23.2.

The use of HSI has been investigated in patients with diabetes mellitus (DM) and PAD.<sup>54</sup> The largest prospective study on HSI was performed in 150 patients with PAD<sup>55</sup> and more recently in 24 patients with a newer HSI system.<sup>56</sup> Both showed lower oxygenation in patients with PAD compared with controls. The results are described in Table 23.2.

The main advantage of this technique is the fast image acquisition, with a handheld camera that even enables home monitoring. In studies of diabetic foot ulceration, HSI was a good predictor of wound healing.<sup>6</sup> Unfortunately, the studies have been performed with different camera systems. Another limitation of the technique is the minimal penetration depth.

### Laser Doppler Perfusion Imaging and Laser Speckle Contrast Imaging Techniques

Laser speckle-based perfusion imaging techniques, such as laser speckle contrast imaging (LSCI), and laser Doppler perfusion imaging (LDPI) are relatively new. The basic components consist of a low-powered laser diode, a diffuser, a digital camera, and processing software.<sup>57</sup> Both techniques are non-invasive and illuminate tissue with a coherent laser light, and are based on the dynamic speckle pattern to measure blood flow or microcirculation in tissue. They differ, however, in data acquisition and data processing.<sup>53</sup> The penetration depth of LDPI depends highly on the wavelength (633–785 nm) that is used and can vary from 1 mm to 2 mm.<sup>53,58,59</sup> The penetration depth of LSCI is limited to a few millimeters, depending on the system used. When a wavelength of 785 nm is used, a penetration of only 0.1 mm to 0.5 mm can be reached.<sup>53,60</sup> LSCI has a sensitivity of 92.3%, a specificity of

75.0%, a positive predictive value of 80.0%, and a negative predictive value of 75.0% for predicting wound healing in venous ulcers.<sup>7</sup>

Three prospective cohort studies investigated LDPI and LSCI measurements in PAD patients and healthy controls. Pawlaczyk-Gabriel et al.<sup>61</sup> and Humeau-Heurtier et al.<sup>60</sup> studied LDPI and LSCI and determined a significant difference between the groups, and the results are described in Table 23.2. More recently Kikuchi et al.<sup>62</sup> performed LSCI before revascularization and up to 7 days after the procedure, and showed a significant increase. The results of these studies are described in Table 23.2.

Both techniques are noninvasive and have a short acquisition time, which can create time-dependent blood flow images.<sup>62</sup> Disadvantages are the sensitivity to motion artifacts, a low penetration depth, sensitivity for temperature, and administration of vasoactive medication.<sup>34</sup>

### Micro-Lightguide Spectrophotometry

O<sub>2</sub>C or “oxygen to see” spectrophotometry is a combined technique of laser Doppler flowmetry (LDF) and spectroscopy. It combines white light (500–800 nm) and laser light (830 nm) to illuminate tissue.<sup>63</sup> Spectroscopy is used to measure the relative amount of hemoglobin in the detected skin volume. Together, the overall flow can be measured, and the following parameters can be extracted: oxygen saturation (sO<sub>2</sub>), relative hemoglobin amount, and blood flow velocity.<sup>63–65</sup> Because of the different types of probes that can be used, depending on the distance between illumination and the detection point, the penetration depth of O<sub>2</sub>C ranges from 2 to 8 mm.<sup>64</sup> Diagnostic accuracy is still unknown; however, low saturation has been shown to be predictive of low toe blood pressures.<sup>63</sup> The use of O<sub>2</sub>C to determine treatment results has been studied in small prospective cohorts by Gyldenløve et al.<sup>64</sup> and Rother et al.<sup>65</sup> Results of these studies are summarized in Table 23.2. The technique is limited by the low and variable penetration depth and by the small measurement area.<sup>66</sup>

## Near-Infrared Spectroscopy

Near-infrared spectroscopy (NIRS) measures the tissue oxygen saturation ( $\text{StO}_2$ ) or hemoglobin oxygen saturation ( $\text{rSO}_2$ ), which was first described in 1977.<sup>67</sup> It uses wavelengths of red and near-infrared light (700–1000 nm) to illuminate the tissue of interest.<sup>68</sup> NIRS can determine muscle oxygenation because it has a penetration depth of approximately 15 to 20 mm.<sup>67,69</sup> Specificity and sensitivity values of NIRS regarding PAD patients were described in a systematic review by Boezeman et al.<sup>70</sup> for different parameters. The use of NIRS was investigated to determine the effect of exercise on muscle perfusion by Khurana et al.<sup>71</sup> and more recently by Fuglestad et al.<sup>72</sup> Other applications of NIRS are to distinguish differences in tissue perfusion between PAD patients and healthy controls and to evaluate a change in tissue perfusion after EVT. The results of these relatively small prospective cohort studies are described in Table 23.2.

NIRS is easily applicable at different spots of the legs or feet.<sup>69</sup> Several commercially available NIRS systems have been reported in the literature, with the use of several different protocols.<sup>73,74</sup> As a result of the differences in algorithms, operational assumptions, and wavelengths of light, comparison between the NIRS systems is difficult.<sup>68</sup> NIRS measures the saturation of muscle tissue, which is sensitive for both oxygen delivery and oxygen demand.<sup>75</sup> Inflow and extraction of oxygen both increase during exercise, and it is therefore difficult to state whether a decrease in saturation is caused by impaired tissue perfusion. Especially in patients with DM, oxygen saturation could be falsely low due to high metabolic demand.<sup>20</sup>

## Skin Perfusion Pressure

Skin perfusion pressure (SPP) measurements are based on the blood pressure in the microcirculation. A cuff is placed over the tissue of interest and inflated to 150 to 200 mmHg. As the cuff is gradually deflated, the return of blood flow in the microcirculation is detected by a laser Doppler probe that is placed between the cuff and the skin. SPP is defined as the pressure (mmHg) applied by the pressure cuff above which the microcirculatory blood flow stops. For SPP measurements, a cutoff value of 30 mmHg was established for prediction of wound healing, with a sensitivity of 79.9% and a specificity of 78.2%.<sup>8</sup> The predictive value of SPP for wound healing was stated in a meta-analysis of Pan et al.<sup>8</sup> and more recently confirmed by other authors.<sup>76,77</sup> Post-procedural SPP values increased significantly and correlated significantly with wound healing and amputation-free survival.<sup>16,78</sup> The results from these studies are described in Table 23.2.

Although aforementioned studies show that SPP has added value for predicting wound healing, the technique is limited by the influence of leg position, motion artifacts, and sometimes by difficult or painful cuff placement.<sup>8,62,79,80</sup>

## Transcutaneous Partial Pressure of Oxygen

Transcutaneous oxygen measurements or transcutaneous partial pressure of oxygen ( $\text{TcPO}_2$ ) was originally developed in 1954 by Leland Clark.<sup>81</sup>  $\text{TcPO}_2$  reflects the quantitative assessment

of the amount of oxygen in mmHg that has diffused from the capillaries, through the epidermis, to a heated electrode. Two different types of  $\text{TcPO}_2$  measurement systems are commercially available, for example, the PeriFlux 6000 (Perimed AB/Radiometer, Järfälla, Sweden), which uses the Clark electrode, or the Precisé 8001 (Medicap, Ulrichstein Germany), which uses an optical electrode system.<sup>82,83</sup> The oxygen tension is measured after reaching equilibrium, which takes approximately 15 minutes for the Clark electrode and 8 minutes for the optical sensor.<sup>9,84</sup>

$\text{TcPO}_2$  has most often been investigated to determine amputation level and to determine the healing potential of ulcers or amputation wounds.  $\text{TcPO}_2$  measurements are included in the American and European guidelines for vascular surgery for the grading of ischemia and the determination of the treatment strategy in CLTI patients.<sup>1,2,85,86</sup> Several cutoff values are stated, such as an oxygen tension of the foot in healthy individuals of at least 55 mmHg.<sup>87</sup> A meta-analysis of 14 studies found a threshold of 40 mmHg was indicative of an increased risk for ulcer or wound healing complications. However, only one study determined a threshold of 20 mmHg as an independent predictor of repeat amputation. Therefore, the independent predictive value could not be precisely determined.<sup>9</sup> Most recently, these results were confirmed by Salaun et al.<sup>88</sup> in 2019 (Table 23.2).

Other large retrospective studies have been performed investigating the predictive value of  $\text{TcPO}_2$ , and the results are described in Table 23.2.<sup>89,90</sup> To evaluate the diagnostic value of  $\text{TcPO}_2$ , De Graaff et al.<sup>91</sup> performed a randomized clinical trial including 96 patients with CLTI and showed no added value of  $\text{TcPO}_2$ . The aforementioned studies are a selection of those with the largest cohorts, the most recently published, and/or highest level of evidence. An evaluation of these results must take into account that study designs differ significantly among studies.<sup>92</sup>

$\text{TcPO}_2$  is a noninvasive, cost-effective technique and serves as a supplement in predicting wound healing in CLTI patients.<sup>93</sup> However, the technique is time consuming, operator dependent, and measurements cover only a small area of tissue and take at least 15 minutes.<sup>20</sup>

## Thermal Imaging

Infrared thermal imaging or thermography is a technique to measure the local temperature of any surface with a camera. The technique is based on the emissive radiation of an object, observed through an infrared thermography camera.<sup>94</sup> Reliability of thermal imaging with different cameras has been studied in patients with DM and in healthy individuals, showing good and excellent agreement.<sup>95,96</sup> The diagnostic accuracy of thermal imaging for failure of graft patency after bypass surgery was determined in a small cohort of 25 patients by Al Shakharchi et al.,<sup>10</sup> and a decrease of 2°C had a sensitivity of 100% and specificity of 89% for graft failure. Local skin temperature determined with thermal imaging was also studied by using a foot-to-hand ratio by Wallace et al.,<sup>97</sup> showing excellent agreement with the ABI. More recently, Ilo et al.<sup>98</sup> measured a significant increase in temperature after revascularization therapy.

The results of these small prospective studies are described in Table 23.2.

The main limitation of this technique is that many conditions can influence the temperature of the skin, such as physical activity, infection, and surrounding temperature, among others. Even in healthy individuals, normal skin temperature can be different between the right and left hand or foot.<sup>94</sup> Furthermore, the relation between skin temperature and long-term clinical outcomes has not been established.

## CLINICAL IMPLICATIONS

Assessment of treatment efficacy and follow-up of disease progression in patients with PAD is still mainly based on techniques that assess the macrovasculature. This is clearly shown in most of the recent publications on EVT of femoro-popliteal and below-the-knee lesions, where the main focus is target lesion revascularization, freedom from binary stenosis, and primary and secondary patency and less on patient-reported outcome measures such as pain relief, ulcer healing, walking distance, and quality of life. The majority of patient-reported outcomes of PAD and CLTI are a direct result of insufficient local and regional tissue perfusion, which is why assessing the microcirculation is highly important, especially for the growing number of patients with multiple morbidities, often with concomitant DM.

An increasing number of techniques to assess the microvasculature have emerged in the last couple of years, and a wide range of studies are described in the literature. However, only two meta-analyses of prospective cohorts have been performed for the predictive value of SPP and TcPO<sub>2</sub> for wound healing.<sup>8,9</sup> These meta-analyses were not able to determine the diagnostic accuracy for the assessment of PAD, but for wound healing only. Besides the meta-analyses, only one randomized clinical trial has been performed for the use of TcPO<sub>2</sub>.<sup>91</sup> The diagnostic value of TcPO<sub>2</sub> to incorporate in a treatment strategy was determined and showed no advantage compared with clinical judgment and conventional diagnostics.

The studies described in this chapter are often based on prospective cohorts with a small number of patients. Moreover, study designs, measurement protocols, equipment used, and technical and clinical outcomes are heterogeneous. To carefully assess the quality of diagnostic studies, a method such as the Quality Assessment of Diagnostic Accuracy Studies (QUADAS-2) should be used. The current limitation of using such a quality assessment method is that all studies should be comparable in study design, patient selection, and reference standard. The fact is that to date, most studies on tissue perfusion measurement techniques are based on a variety of references, such as clinical assessment, CT angiography imaging, ABI, or TcPO<sub>2</sub> measurements, which have not been proven to be reliable gold standards. Therefore, a reliable quality assessment score of available literature could not be used in this chapter.

Previously, Ma et al.<sup>36</sup> and Wermelink et al.<sup>99</sup> provided a systematic review of current available techniques to determine

tissue perfusion in PAD and performed both a quality and bias assessment of the studies with the QUADAS-2 method. Results showed a substantial heterogeneity in different aspects, such as inclusion and selection criteria, the diagnosis and severity of PAD, and vascular risk factors and comorbidities. Both reviews stated that it seems to be too early to appoint one of the described perfusion techniques as a reference standard.

## FUTURE DIRECTIONS

Some perfusion techniques might not have been mentioned in this overview of techniques. Optoacoustic or photoacoustic imaging, for example, is a new imaging technique that has been investigated to visualize microvascularization of cancer tumors. However its application for peripheral perfusion measurements is still limited to healthy volunteers.<sup>100</sup> The same applies for techniques such as measurements of mitochondrial oxygen uptake in the skin,<sup>101</sup> combined laser Doppler and diffuse reflectance spectroscopy imaging,<sup>102</sup> and radiolabeled water (<sup>15</sup>O-H<sub>2</sub>O) positron emission tomography imaging.<sup>103</sup>

Ideally, a technique to measure tissue perfusion should be able to answer a couple of questions regarding the fate of the lower extremity in patients with PAD and CLTI. Accurate assessment before treatment should be able to determine whether the toes or feet are still salvageable, which should result in reducing the amount of unnecessary interventions. Besides that, if treatment of the leg is indicated, tissue perfusion measurements should guide the interventionalist in a successful treatment decision. Additionally, the measurements should indicate whether ulcerations or surgical wounds have the potential of healing. In case of revascularization therapy, a technique should provide perioperative and real-time information on the local increase in tissue perfusion in the lower leg or foot. When real-time visualization is possible, these measurements can guide during revascularization procedures.

After treatment, tissue perfusion measurements are essential to monitor the treatment result or disease progression within the hospital and in-home setting. To provide the answers to all of these questions, the ideal tissue perfusion technique should have the following requirements: the technique should be non-invasive, cost-efficient, with relatively fast acquisition, and usable during the entire peri-procedural process.

## CONCLUSIONS

This chapter has described several innovative tissue perfusion techniques; however, the level of evidence is still low, and it seems too early to designate one of the techniques as a new gold standard for perfusion measurements. In addition, there are techniques that are only just on the market or which are not yet commercially available. Considering the particularly large number of PAD and CLTI patients who will be treated worldwide in the coming years, and with the associated health and social costs, it is a global and joined effort to develop peri-procedural tissue perfusion monitoring in such a manner that it can be incorporated as a standard tool within the diagnostic armamentarium of the vascular specialists.

## SELECTED KEY REFERENCES

Arsenault KA, Al-Otaibi A, Devereaux PJ, et al. The use of transcutaneous oximetry to predict healing complications of lower limb amputations: A systematic review and meta-analysis. *Eur J Vasc Endovasc Surg.* 2012;43(3):329–336.

*A meta-analysis including 14 prospective cohorts to determine the diagnostic accuracy of  $TcPO_2$  for wound healing after amputation.*

Bajwa A, Wesolowski R, Patel A, et al. Assessment of tissue perfusion in the lower limb current methods and techniques under development. *Circ Cardiovasc Imaging.* 2014;7(5):836–843.

*A narrative review of tissue perfusion techniques in the lower extremity for the application of patients with PAD.*

Ipema J, Heinen SGH, Janssens AJB, et al. Repeatability, and intra-observer and interobserver agreement of two dimensional perfusion angiography in patients with chronic limb threatening ischaemia. *Eur J Vasc Endovasc Surg.* 2021;61(6):980–987.

*This is the first study to test the reliability of 2D perfusion angiography in patients with chronic limb threatening ischaemia.*

Ma KF, Kleiss SF, Schuurmann RCL, et al. A systematic review of diagnostic techniques to determine tissue perfusion in patients with peripheral arterial disease. *Expert Rev Med Devices.* 2019;16(8):697–710.

*A systematic review of tissue perfusion techniques in the lower extremity of patients with PAD compared with healthy controls.*

Pan X, You C, Chen G, et al. Skin perfusion pressure for the prediction of wound healing in critical limb ischemia: A meta-analysis. *Arch Med Sci.* 2018;14(3):481–487.

*A meta-analysis including five prospective cohorts to determine the diagnostic accuracy of SPP for wound healing.*

Rogers RK, Montero-Baker M, Biswas M, et al. Assessment of foot perfusion: Overview of modalities, review of evidence, and identification of evidence gaps. *Vasc Med.* 2020;25(3):235–245.

*A narrative review of tissue perfusion techniques in the lower extremity in patients with PAD, with a focus on the evidence for clinical application.*

A complete reference list can be found online at [www.expertconsult.com](http://www.expertconsult.com).

## REFERENCES

1. Aboyans V, Ricco JB, Bartelink MLE, et al. 2017 ESC Guidelines on the Diagnosis and Treatment of Peripheral Arterial Diseases, in collaboration with the European Society for Vascular Surgery (ESVS). *Eur Heart J.* 2018;39(9):763–816.
2. Gerhard-Herman MD, Gornik HL, Barrett C, et al. 2016 AHA/ACC Guideline on the Management of Patients with Lower Extremity Peripheral Artery Disease: Executive Summary: A Report of the American College of Cardiology/American Heart Association Task Force on Clinical Practice Guidelines. *Circulation.* 2017;135(12):e686–e725.
3. Norgren L, Hiatt WR, Dormandy JA, et al. Inter-Society Consensus for the Management of Peripheral Arterial Disease (TASC II). *J Vasc Surg.* 2007;45(Suppl S):S5–S7.
4. van den Hoven P, Ooms S, van Manen L, et al. A systematic review of the use of near-infrared fluorescence imaging in patients with peripheral artery disease. *J Vasc Surg.* 2019;70(1):286–297.e1.
5. Hashimoto H, Fukushima Y, Kumita SI, et al. Prognostic value of lower limb perfusion single-photon emission computed tomography-computed tomography in patients with lower limb atherosclerotic peripheral artery disease. *Jpn J Radiol.* 2017;35(2):68–77.
6. Nouvong A, Hoogwerf B, Mohler E, et al. Evaluation of diabetic foot ulcer healing with hyperspectral imaging of oxyhemoglobin and deoxyhemoglobin. *Diabetes Care.* 2009;32(11):2056–2061.
7. van Vuuren TM, Van Zandvoort C, Doganci S, et al. Prediction of venous wound healing with laser speckle imaging. *Phlebology.* 2017;32(10):658–664.
8. Pan X, You C, Chen G, et al. Skin perfusion pressure for the prediction of wound healing in critical limb ischemia: a meta-analysis. *Arch Med Sci.* 2018;14(3):481–487.
9. Arseneault KA, Al-Otaibi A, Devereaux PJ, et al. The use of transcutaneous oximetry to predict healing complications of lower limb amputations: a systematic review and meta-analysis. *Eur J Vasc Endovasc Surg.* 2012;43(3):329–336.
10. Al Shakarchi J, Inston N, Dabare D, et al. Pilot study on the use of infrared thermal imaging to predict infrainguinal bypass outcome in the immediate post-operative period. *Vascular.* 2019;27(6):663–667.
11. Murray T, Rodt T, Lee MJ. Two-dimensional perfusion angiography of the foot: technical considerations and initial analysis. *J Endovasc Ther.* 2016;23(1):58–64.
12. Reekers JA, Koelemay MJW, Marquering HA, et al. Functional imaging of the foot with perfusion angiography in critical limb ischemia. *Cardiovasc Interv Radiol.* 2016;39(2):183–189.
13. Jens S, Marquering HA, Koelemay MJW, et al. Perfusion angiography of the foot in patients with critical limb ischemia: description of the technique. *Cardiovasc Interv Radiol.* 2015;38(1):201–205.
14. Hinrichs JB, Murray T, Akin M, et al. Evaluation of a novel 2D perfusion angiography technique independent of pump injections for assessment of interventional treatment of peripheral vascular disease. *Int J Cardiovasc Imaging.* 2017;33(3):295–301.
15. Pärsson HN, Lundin N, Lindgren H. 2D perfusion-angiography during endovascular intervention for critical limb threatening ischemia – a feasibility study. *JRSM Cardiovasc Dis.* 2020;9:204800402091539.
16. Ikeoka K, Watanabe T, Shinoda Y, et al. Below-the-ankle arrival time as a novel limb tissue perfusion index: two-dimensional perfusion angiography evaluation. *J Endovasc Ther.* 2020;27(2):198–204.
17. Kim AH, Shevitz AJ, Morrow KL, et al. Characterizing tissue perfusion after lower extremity intervention using two-dimensional color-coded digital subtraction angiography. *J Vasc Surg.* 2017;66(5):1464–1472.
18. Ng JJ, Papadimas E, Dharmaraj RB. Assessment of flow after lower extremity endovascular revascularisation: a feasibility study using time attenuation curve analysis of digital subtraction angiography. *EJVES Short Rep.* 2019;45:1–6.
19. Lou WS, Su HB, Huang KY, et al. Evaluation of distal hemodynamic changes of lower extremity after endovascular treatment: correlation between measurements of color-coded quantitative digital subtraction angiography and ankle-brachial index. *J Vasc Interv Radiol.* 2016;27(6):852–858.
20. Rogers RK, Montero-Baker M, Biswas M, et al. Assessment of foot perfusion: overview of modalities, review of evidence, and identification of evidence gaps. *Vasc Med.* 2020;25(3):235–245.
21. Galanakis N, Maris TG, Kontopodis N, et al. CT foot perfusion examination for evaluation of percutaneous transluminal angioplasty outcome in patients with critical limb ischemia: a feasibility study. *J Vasc Interv Radiol.* 2019;30(4):560–568.
22. Li M, Li Z, Gao P, et al. Quantitative evaluation of postintervention foot blood supply in patients with peripheral artery disease by computed tomography perfusion. *J Vasc Surg.* 2020;72(3):1035–1042.
23. Iezzi R, Santoro M, Dattesi R, et al. Foot CT perfusion in patients with peripheral arterial occlusive disease (PAD): a feasibility study. *Eur J Radiol.* 2013;82(9):455–464.
24. Hur S, Jae HJ, Jang Y, et al. Quantitative assessment of foot blood flow by using dynamic volume perfusion CT technique: A feasibility study. *Radiology.* 2016;279(1):195–206.
25. Cindil E, Erbas G, Akkan K, et al. Dynamic volume perfusion CT of the foot in critical limb ischemia: response to percutaneous revascularization. *Am J Roentgenol.* 2020;214(6):1398–1408.
26. Sah BR, Veit-Haibach P, Strobel K, et al. CT-perfusion in peripheral arterial disease – Correlation with angiographic and hemodynamic parameters. *PLoS One.* 2019;14(9):1–15.
27. Sultan S, Tawfick W, Hynes N. Ten-year technical and clinical outcomes in TransAtlantic Inter-Society Consensus II infrainguinal C/D lesions using duplex ultrasound arterial mapping as the sole imaging modality for critical lower limb ischemia. *J Vasc Surg.* 2013;57(4):1038–1045.
28. Bredahl K, Mestre XM, Coll RV, et al. Contrast-enhanced ultrasound in vascular surgery: review and update. *Ann Vasc Surg.* 2017;45:287–293.
29. Mestre XM, Coll RV, Villegas AR, et al. Role of contrast-enhanced ultrasound arterial mapping in surgical planning for patients with critical limb ischemia. *Ultrasound Med Biol.* 2015;41(6):1570–1576.
30. Hou XX, Chu GH, Yu Y. Prospects of contrast-enhanced ultrasonography for the diagnosis of peripheral arterial disease: a meta-analysis. *J Ultrasound Med.* 2018;37(5):1081–1090.
31. Meneses AL, Nam MCY, Bailey TG, et al. Leg blood flow and skeletal muscle microvascular perfusion responses to submaximal exercise in peripheral arterial disease. *Am J Physiol Heart Circ Physiol.* 2018;315(5):H1425–H1433.
32. Kundi R, Prior SJ, Addison O, Lu M, Ryan AS, Lal BK. Contrast-Enhanced Ultrasound Reveals Exercise-Induced Perfusion Deficits in Claudicants. *J Vasc Endovasc Surg.* 2017;02(01):1–16.
33. Duerschmied D, Maletzki P, Freund G, et al. Success of arterial revascularization determined by contrast ultrasound muscle perfusion imaging. *J Vasc Surg.* 2010;52(6):1531–1536.
34. Bajwa A, Wesolowski R, Patel A, et al. Assessment of tissue perfusion in the lower limb current methods and techniques under development. *Circ Cardiovasc Imaging.* 2014;7(5):836–843.
35. Englund EK, Langham MC. Quantitative and dynamic MRI measures of peripheral vascular function. *Front Physiol.* 2020;11(February):1–9.
36. Ma KF, Kleiss SF, Schuurmann RCL, et al. A systematic review of diagnostic techniques to determine tissue perfusion in patients with peripheral arterial disease. *Expert Rev Med Devices.* 2019;16(8):697–710.
37. Versluis B, Backes WH, van Eupen MGA, et al. Magnetic resonance imaging in peripheral arterial disease. *Invest Radiol.* 2011;46(1):11–24.
38. Partovi S, Karimi S, Jacobi B, et al. Clinical implications of skeletal muscle blood-oxygenation-level-dependent (BOLD) MRI. *MAGMA.* 2012;25(4):251–261.
39. Suo S, Zhang L, Tang H, et al. Evaluation of skeletal muscle microvascular perfusion of lower extremities by cardiovascular magnetic resonance arterial spin labeling, blood oxygenation level-dependent, and intravoxel incoherent motion techniques. *J Cardiovasc Magn Reson.* 2018;20(1):1–14.
40. Jiji RS, Pollak AW, Epstein FH, et al. Reproducibility of rest and exercise stress contrast-enhanced calf perfusion magnetic resonance imaging in peripheral arterial disease. *J Cardiovasc Magn Reson.* 2013;15(1):1–7.
41. Grözinger G, Pohmann R, Schick F, et al. Perfusion measurements of the calf in patients with peripheral arterial occlusive disease before and after percutaneous transluminal angioplasty using mr arterial spin labeling. *J Magn Reson Imaging.* 2014;40(4):980–987.

42. Galanakis N, Maris TG, Kontopodis N, et al. The role of dynamic contrast-enhanced MRI in evaluation of percutaneous transluminal angioplasty outcome in patients with critical limb ischemia. *Eur J Radiol.* 2020;129(March):109081.
43. Bakermans AJ, Wessel CH, Zheng KH, et al. Dynamic magnetic resonance measurements of calf muscle oxygenation and energy metabolism in peripheral artery disease. *J Magn Reson Imaging.* 2020;51(1):98–107.
44. Colvard B, Itoga NK, Hitchner E, et al. SPY technology as an adjunctive measure for lower extremity perfusion. *J Vasc Surg.* 2016;64(1):195–201.
45. Vahrmeijer AL, Hutmeyer M, Van Der Vorst JR, et al. Image-guided cancer surgery using near-infrared fluorescence. *Nat Rev Clin Oncol.* 2013;10(9):507–518.
46. Braun JD, Trinidad-Hernandez M, Perry D, et al. Early quantitative evaluation of indocyanine green angiography in patients with critical limb ischemia. *J Vasc Surg.* 2013;57(5):1213–1218.
47. Settembre N, Kauhanen P, Albäck A, et al. Quality control of the foot revascularization using indocyanine green fluorescence imaging. *World J Surg.* 2017;41(7):1919–1926.
48. Seinturier C, Blaise S, Tiffet T, et al. Fluorescence angiography compared to toe blood pressure in the evaluation of severe limb ischemia. *Vasa.* 2020;49(3):230–234.
49. Zimmermann A, Roenneberg C, Reeps C, et al. The determination of tissue perfusion and collateralization in peripheral arterial disease with indocyanine green fluorescence angiography. *Clin Hemorheol Microcirc.* 2012;50(3):157–166.
50. DSouza AV, Lin H, Henderson ER, et al. Review of fluorescence guided surgery systems: identification of key performance capabilities beyond indocyanine green imaging. *J Biomed Opt.* 2016;21(8):080901.
51. Khor YM, Dorbala S. SPECT/CT quantification of lower limb perfusion: The next frontier in radionuclide perfusion imaging? *J Nucl Cardiol.* 2020;27(6):1934–1938.
52. Alvelo JL, Papademetris X, Mena-Hurtado C, et al. Radiotracer imaging allows for noninvasive detection and quantification of abnormalities in angiosome foot perfusion in diabetic patients with critical limb ischemia and nonhealing wounds. *Circ Cardiovasc Imaging.* 2018;11(5):e006932.
53. Mennes OA, van Netten JJ, Slart RHJ, Steenbergen W. Novel optical techniques for imaging microcirculation in the diabetic foot. *Curr Pharm Des.* 2018;24(12):1304–1316.
54. Kleiss SF, Ma KF, Schuurmann RC, et al. Hyperspectral imaging for noninvasive tissue perfusion measurements of the lower leg: Review of literature and introduction of a standardized measurement protocol with a portable system. *J Cardiovasc Surg (Torino).* 2019;60(6):652–661.
55. Chiang N, Jain JK, Sleigh J, et al. Evaluation of hyperspectral imaging technology in patients with peripheral vascular disease. *J Vasc Surg.* 2017;66(4):1192–1201.
56. Grambow E, Dau M, Sandkuhler NA, et al. Evaluation of peripheral artery disease with the TIVITA® Tissue hyperspectral imaging camera system. *Clin Hemorheol Microcirc.* 2019;73(1):3–17.
57. Heeman W, Steenbergen W, van Dam GM, et al. Clinical applications of laser speckle contrast imaging: a review. *J Biomed Opt.* 2019;24(08):1.
58. Briers JD. Laser Doppler, speckle and related techniques for blood perfusion mapping and imaging. *Physiol Meas.* 2001;22(4):R35–66.
59. Humeau-Heurtier A, Guerreschi E, Abraham P, et al. Relevance of laser Doppler and laser speckle techniques for assessing vascular function: State of the art and future trends. *IEEE Trans Biomed Eng.* 2013;60(3):659–666.
60. Humeau-Heurtier A, Abraham P, Henni S. Bi-dimensional variational mode decomposition of laser speckle contrast imaging data: A clinical approach to critical limb ischemia? *Comput Biol Med.* 2017;86:107–112.
61. Pawlaczek-Gabriel K, Gabriel M, Krasiński Z, et al. Influence of low and moderate grade leg ischaemia on the skin microcirculation parameters in peripheral arterial occlusive disease patients. *Acta Angiol.* 2014;20(4):133–140.
62. Kikuchi S, Miyake K, Tada Y, et al. Laser speckle flowgraphy can also be used to show dynamic changes in the blood flow of the skin of the foot after surgical revascularization. *Vascular.* 2019;27(3):242–251.
63. Jørgensen LP, Schroeder TV. Micro-lightguide spectrophotometry for tissue perfusion in ischemic limbs. *J Vasc Surg.* 2012;56(3):746–752.
64. Gyldenlove T, Jørgensen LP, Schroeder TV. Micro-lightguide spectrophotometry (O2C) for lower limb perfusion: Effects of exercise walking in claudicants. *Int J Angiol.* 2019;28(3):161–166.
65. Rother U, Krenz K, Lang W, et al. Immediate changes of angiosome perfusion during tibial angioplasty. *J Vasc Surg.* 2017;65(2):422–430.
66. Marcoccia A, Klein-Weigel PF, Gschwandtner ME, et al. Microcirculatory assessment of vascular diseases. *Vasa.* 2020;49(3):175–186.
67. Boezeman RPE, Beex BP, van den Heuvel DAF, et al. Monitoring of foot oxygenation with near-infrared spectroscopy in patients with critical limb ischemia undergoing percutaneous transluminal angioplasty: a pilot study. *Eur J Vasc Endovasc Surg.* 2016;52(5):650–656.
68. Simonson SG, Piantadosi CA. Near-infrared spectroscopy. *Crit Care Clin.* 1996;12(4):1019–1029.
69. Boezeman RPE, Boersma D, Wille J, et al. The significance of regional hemoglobin oxygen saturation values and limb-to-arm ratios of near-infrared spectroscopy to detect critical limb ischemia. *Vascular.* 2016;24(5):492–500.
70. Boezeman RPE, Moll FL, Ünlü Ç, de Vries JPPM. Systematic review of clinical applications of monitoring muscle tissue oxygenation with near-infrared spectroscopy in vascular disease. *Microvasc Res.* 2016;104:11–22.
71. Khurana A, Stoner JA, Whitsett TL, et al. Clinical significance of ankle systolic blood pressure following exercise in assessing calf muscle tissue ischemia in peripheral artery disease. *Angiology.* 2013;64(5):364–370.
72. Fuglestad MA, Hernandez H, Gao Y, et al. A low-cost, wireless near-infrared spectroscopy device detects the presence of lower extremity atherosclerosis as measured by computed tomographic angiography and characterizes walking impairment in peripheral artery disease. *J Vasc Surg.* 2020;71(3):946–957.
73. Malagoni AM, Felisatti M, Mandini S, et al. Resting muscle oxygen consumption by near-infrared spectroscopy in peripheral arterial disease: A parameter to be considered in a clinical setting? *Angiology.* 2010;61(6):530–536.
74. Vardi M, Nini A. Near-infrared spectroscopy for evaluation of peripheral vascular disease. a systematic review of literature. *Eur J Vasc Endovasc Surg.* 2008;35(1):68–74.
75. Miller AJ, Luck JC, Kim DJK, et al. Blood pressure and leg deoxygenation are exaggerated during treadmill walking in patients with peripheral artery disease. *J Appl Physiol.* 2017;123(5):1160–1165.
76. Kimura T, Watanabe Y, Tokuoka S, et al. Utility of skin perfusion pressure values with the Society for Vascular Surgery Wound, Ischemia, and foot Infection classification system. *J Vasc Surg.* 2019;70(4):1308–1317.
77. Suzuki K, Birnbaum Z, Lockhart R. Skin perfusion pressure and wound closure time in lower extremity wounds. *J Am Coll Clin Wound Spec.* 2017;9(1-3):14–18.
78. Okamoto S, Iida O, Nakamura M, et al. Postprocedural skin perfusion pressure correlates with clinical outcomes 1 year after endovascular therapy for patients with critical limb ischemia. *Angiology.* 2015;66(9):862–866.
79. Misra S, Shishehbor MH, Takahashi EA, et al. Perfusion Assessment in Critical Limb Ischemia: Principles for Understanding and the Development of Evidence and Evaluation of Devices: A Scientific Statement from the American Heart Association. *Circulation.* 2019;140(12):E657–E672.
80. Lo T, Sample R, Moore P, Gold P. Prediction of wound healing outcome using skin perfusion pressure and transcutaneous oximetry: a single-center experience in 100 patients. *Wounds.* 2009;21(11):310–316.
81. Severinghaus JW. The invention and development of blood gas analysis apparatus. *Anesthesiology.* 2002;97(1):253–256.

82. Geis S, Schreml S, Lamby P, et al. Postoperative assessment of free skin flap viability by transcutaneous pO<sub>2</sub> measurement using dynamic phosphorescence imaging. *Clin Hemorheol Microcirc.* 2009;43(1–2):11–18.
83. Rother U, Lang W. Noninvasive measurements of tissue perfusion in critical limb ischemia. *Gefasschirurgie.* 2018;23(March):8–12.
84. Urban M, Fouasson-Chailloux A, et al. Comparison of two devices for measuring exercise transcutaneous oxygen pressures in patients with claudication. *Vasa.* 2015;44(5):355–362.
85. Mills JL, Conte MS, Armstrong DG, et al. The society for vascular surgery lower extremity threatened limb classification system: Risk stratification based on Wound, Ischemia, and foot Infection (WFIf). *J Vasc Surg.* 2014;59(1):220–234.e2.
86. Cerqueira LO, Junior EGD, Barros ALS, et al. WFIf Classification - The Society for Vascular Surgery lower extremity threatened limb classification system: a literature review. *J Vasc Bras.* 2020;19:1–9.
87. Cina C, Katsamouris A, Megerman J, et al. Utility of transcutaneous oxygen tension measurements in peripheral arterial occlusive disease. *J Vasc Surg.* 1984;1(2):362–371.
88. Salaun P, Desormais I, Lapébie FX, et al. Comparison of ankle pressure, systolic toe pressure, and transcutaneous oxygen pressure to predict major amputation after 1 year in the COPART cohort. *Angiology.* 2019;70(3):229–236.
89. Andrews KL, Dib MY, Shives TC, et al. Noninvasive arterial studies including transcutaneous oxygen pressure measurements with the limbs elevated or dependent to predict healing after partial foot amputation. *Am J Phys Med Rehabil.* 2013;92(5):385–392.
90. Faglia E, Clerici G, Caminiti M, et al. Predictive values of transcutaneous oxygen tension for above-the-ankle amputation in diabetic patients with critical limb ischemia. *Eur J Vasc Endovasc Surg.* 2007;33(6):731–736.
91. de Graaff JC, Ubbink DT, Legemate DA, et al. Evaluation of toe pressure and transcutaneous oxygen measurements in management of chronic critical leg ischemia: a diagnostic randomized clinical trial. *J Vasc Surg.* 2003;38(3):528–534.
92. Leenstra B, Wijnand J, Verhoeven B, et al. Applicability of transcutaneous oxygen tension measurement in the assessment of chronic limb-threatening ischemia. *Angiology.* 2020;71(3):208–216.
93. Sumpio BJ, Miller SM, Benitez E, et al. Limb salvage of the diabetic foot. *Limb Salvage Diabet Foot.* 2019:243–257.
94. Lahiri BB, Bagavathiappan S, Jayakumar T, et al. Medical applications of infrared thermography: a review. *Infrared Phys Technol.* 2012;55(4):221–235.
95. Silva NCM, Castro HA, Carvalho LC, et al. Reliability of infrared thermography images in the analysis of the plantar surface temperature in diabetes mellitus. *J Chiropr Med.* 2018;17(1):30–35.
96. Petrova NL, Whittam A, MacDonald A, et al. Reliability of a novel thermal imaging system for temperature assessment of healthy feet. *J Foot Ankle Res.* 2018;11(1):1–6.
97. Wallace GA, Singh N, Quiroga E, et al. The use of smart phone thermal imaging for assessment of peripheral perfusion in vascular patients. *Ann Vasc Surg.* 2018;47:157–161.
98. Ilo A, Romsi P, Pokela M, et al. Infrared thermography follow-up after lower limb revascularization. *J Diabetes Sci Technol.* 2021;15:807–815.
99. Wermelink B., Ma K.F., Haalboom M., et al. A systematic review and critical appraisal of peri-procedural tissue perfusion techniques and their clinical value in patients with peripheral arterial disease. *Eur J Vasc Endovasc Surg.* 2021;62(6):896–908.
100. Karlas A, Kallmayer M, Fasoula NA, et al. Multispectral optoacoustic tomography of muscle perfusion and oxygenation under arterial and venous occlusion: A human pilot study. *J Biophotonics.* 2020;13(6):1–9.
101. Ubbink R, Bettink MAW, Janse R, et al. A monitor for Cellular Oxygen METabolism (COMET): monitoring tissue oxygenation at the mitochondrial level. *J Clin Monit Comput.* 2017;31(6):1143–1150.
102. Jonasson H, Fredriksson I, Bergstrand S, et al. In vivo characterization of light scattering properties of human skin in the 475- to 850-nm wavelength range in a Swedish cohort. *J Biomed Opt.* 2018;23(12):1.
103. Gliemann L, Mortensen SP, Hellsten Y. Methods for the determination of skeletal muscle blood flow: development, strengths and limitations. *Eur J Appl Physiol.* 2018;118(6):1081–1094.

# Vascular Laboratory: Venous Physiologic Assessment

JOANN LOHR and DEVIN S. ZARKOWSKY

Based on a previous edition chapter by Brajash K. Lal and Shahab Toursavadkohi

## AMBULATORY VENOUS PRESSURE 279

- Technique 280
- Interpretation 280
- Accuracy 280
- Limitations 281
- PLETHYSMOGRAPHY 281**
- Strain-Gauge Plethysmography 282
- Impedance Plethysmography 282

## Photoplethysmography 282

- Foot Volume Plethysmography 282
- Air Plethysmography 282
- Technique and Interpretation 282
- Accuracy 284
- Limitations 284

## RELIABILITY OF VENOUS TESTING 284

Venous pathophysiology in the lower extremity manifests as a spectrum of disorders (see Section 23, Chronic Venous Disorders). Reporting standards published first in 1994 and revised in 2004 recognized pathophysiologic assessment as a key feature in assessing patients with chronic venous disease (CVD) properly, as well communicating results to the venous care community.<sup>1,2</sup> The 2014 joint Society for Vascular Surgery/American Venous Forum clinical practice guideline on venous leg ulcer (VLU) management recommends all patients with this most severe CVD sequela be classified according to their Clinical class, Etiology, Anatomy and Pathophysiology (CEAP).<sup>3</sup> Figure 24.1 demonstrates common clinical and anatomic features associated with CVD. Patients with less severe CVD manifestations benefit from whole limb venous physiologic evaluation as well. Categorizing the pathology is critical to directing the patient's clinical course, as well as establishing treatment success and failure.

Duplex ultrasonography is often the first-line diagnostic tool applied in CVD. Grayscale B-mode combined with Doppler insonation allows direct, real-time visualization of vein segments to detect flow limitation or valvular reflux. Color flow duplex is an accurate, noninvasive, easily repeated test (see Ch. 25, Vascular Laboratory: Venous Duplex Scanning). Anatomic information obtained from B-mode imaging reveals structural pathology from the iliac bifurcation distally, depending on patient body habitus, while Doppler waveform analysis

with provocative maneuvers provides insight on flow characteristics. The latter evaluation is reported as "reflux time." Venous duplex scanning provides further details on this assessment. Reflux time is a surrogate for pathophysiology with different values accepted to correlate with obstruction, valvular incompetence or a combination of both depending on the anatomic location. Danielsson et al. demonstrated duplex-calculated reflux time did not correlate with CEAP classification, while a more thorough physiologic evaluation with plethysmography did.<sup>4</sup> Another concept that has fallen out of favor, valve closure time, has similarly been suggested not to correlate with disease severity.<sup>5</sup>

Consequently, complete clinical evaluation in CVD patients necessitates applying physiologic noninvasive testing in addition to duplex scanning. Several techniques exist and are employed with varying frequency dependent on local practice patterns. This chapter describes each technique's application and interpretation, as well as limitations.

## AMBULATORY VENOUS PRESSURE

The first reported venous pressure measurement in a walking subject was reported in 1936.<sup>6</sup> Pollack and Wood are largely credited with standardizing the recording method<sup>7</sup> and identifying the contribution of defective vein valves to alterations in venous ankle pressures.<sup>8</sup> Several contributors defined the



**Figure 24.1** (A) Varicose veins associated with reflux. (B) CVI patient with ulceration. (C) Vein valves visible on an ascending venogram. (D) May-Thurner syndrome with cross-pelvic collaterals in a prone patient treated for a left common iliac artery aneurysm. (E) Free floating thrombus in the iliofemoral vein segment. (F) Chronically occluded common femoral vein.

relationship between vein and lower leg muscle over the next two decades, resulting in the unicameral model.<sup>9–11</sup> Essentially, calf muscle contraction propels blood heart-ward through the deep and superficial venous systems, creating a pressure drop below the knee, termed “calf diastole.”

### Technique

Classically, the dorsal foot vein (DFV) is accessed percutaneously with the patient at rest and a baseline, or standing leg, pressure recorded by a transducer. Patients then perform 10 tiptoe stands; the resultant pressure changes are graphed against time. That pressure recorded after the last exercise – generally the nadir – is the ambulatory venous pressure (AVP). Calf diastole is the time required to achieve 90% baseline pressure, also called venous refill time (VRT or VFT).

A recent study of 76 limbs in 38 normal patients suggested a subtle revision to the unicameral model.<sup>12</sup> The polycameral model considers the deep and superficial lower leg compartments, as well as the dorsal foot, as separate physiologic units. Great saphenous vein (GSV) and DFV AVP were noted to be different, suggesting AVP monitoring via the DFV does not accurately reflect pressure changes in the GSV.

### Interpretation

Figure 24.2A depicts a normal subject’s venous pressure-time curve during AVP monitoring.

A normal AVP results in a minimum 50% decrease in venous pressure relative to baseline, while calf diastole lasts a minimum of 20 seconds. Pathophysiology associated with CVD introduces multiple alterations to the normal tracing (Fig. 24.2B). Valvular insufficiency in superficial or deep veins leads to a shorter duration for calf diastole. Obstruction would result in a pressure increase from baseline. Combined disease incorporates both an increased exercise pressure and decreased calf diastole time.

These parameters correlate with CEAP class, particularly increasing AVP.<sup>13</sup> Deep venous insufficiency produces higher AVPs than does superficial insufficiency, while combined deep vein incompetence and iliofemoral obstruction produced the highest AVP values.

### Accuracy

The polycameral model suggests perforators draining from the superficial to deep vein system during calf diastole results in AVP discrepancies when monitored via the GSV versus the

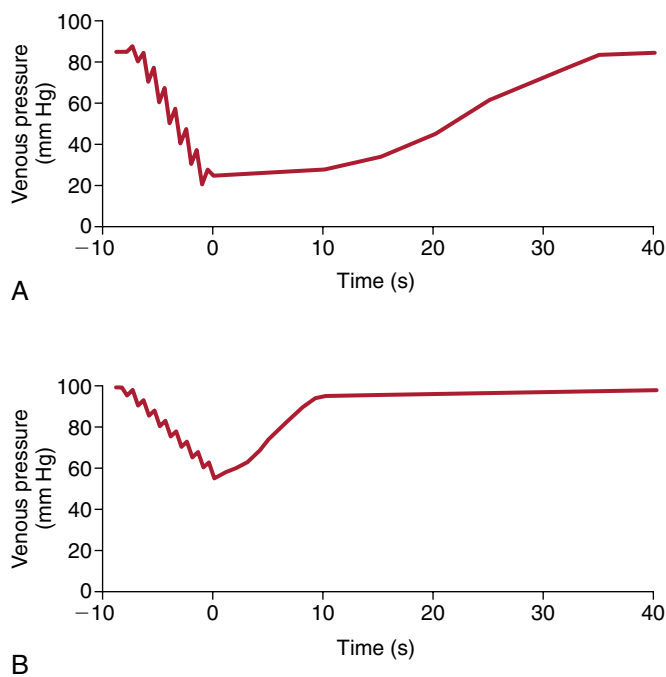


**Figure 24.2** (A) Tracing of ambulatory venous pressure (AVP) in a normal subject. Note the rapid fall in pressure during 10 calf contractions, indicative of good venous outflow and calf muscle pump function. Also note the slow rise to baseline pressure on completion of the calf contractions, indicative of absence of venous reflux. (B) Tracing of AVP in a patient with chronic venous insufficiency. Note the higher baseline pressure, slow fall in pressure with tiptoe maneuvers, and high pressure on completion of the contractions, indicative of venous outflow obstruction and poor calf muscle pump function. Also note the rapid rise to baseline on completion of the calf contractions, indicative of severe venous reflux.

DFV,<sup>12</sup> perhaps explaining the significant proportion – up to 25% – of patients with ulcers despite normal AVP values.<sup>14</sup> A phlebotomy tourniquet application during monitoring interrupts the contribution from superficial venous insufficiency. Correction to normal AVP and calf diastole times suggests superficial disease, while continued abnormal values suggests deep system pathology.<sup>15</sup> Column interruption duration (CID) reflects the interval from calf blood ejection to flow re-appearance by Duplex, providing the opportunity to evaluate both deep and superficial vein valves independently and provide a more accurate estimate of their individual contributions to whole limb CVD.<sup>12</sup>

Venous hypertension may result from venous obstruction, or calf muscle pump dysfunction, in addition to valvular incompetence. Deficiencies in calf muscle pump function may occur without anatomic CVI. Araki et al. demonstrated no difference in the degree of valvular incompetence determined by duplex between patients with active or healed venous ulcers and those with no prior ulceration.<sup>16</sup> Decrease in EF and increase in RVF was observed in C6 patients compared with C4 and C5. These findings suggest that venous ulceration might be aggravated by the combination of valvular incompetence and poor calf muscle pump function.<sup>16</sup> In addition, ankle range of motion was decreased in C4–6 limbs when compared to normal limbs;

similar deterioration was observed at higher CEAP classes.<sup>17</sup> A normal EF, >60%, was associated with a low incidence of ulceration in the presence of reflux and an abnormal EF, whereas an EF <40%, was found in limbs with active ulceration and minimal reflux.<sup>18</sup>

## Limitations

Conceptual evolution from the unicameral model to the polycameral model of CVD remains controversial and unvalidated. The ability to quantify the contribution superficial, deep, and foot vein incompetence promises to supplant AVP as the physiologic CVD gold standard. Duplex imaging would also eliminate the need to access the DFV, which can be challenging in patients with extensive ulceration or skin changes often present in CVD.

Quantitative assessment of venous disease by AVP has been thought of as the “standard” to which other modalities should be compared. Nicolaides and Zukowskii demonstrated that AVP reflects global hemodynamics within an extremity, while correlating linearly with clinical disease severity.<sup>19</sup> Unfortunately, AVP cannot reliably localize hemodynamic abnormalities beyond the deep and superficial systems, nor differentiate obstruction from reflux. Since AVP requires cannulating a foot vein, patients often prefer noninvasive testing methods that produce comparable data.

## PLETHYSMOGRAPHY

During the cardiac cycle, blood flow through an extremity produces a measurable change in volume.<sup>20,21</sup> Tissue volume remains essentially constant, affording the opportunity to assess arterial inflow with pulse-volume recording<sup>22</sup> (see Ch. 21, Vascular Laboratory: Arterial Physiologic Assessment), and venous outflow with multiple modalities. Venous plethysmography assists in quantifying physiologic obstruction and venous reflux. The tools described herein describe hemodynamic disease severity, which should theoretically change with treatment of the underlying condition.

Blood pressure cuff occlusion of the deep and superficial veins is preferred to provocative maneuvers during plethysmography testing, as reproducibility is improved. Supine positioning ensures a patient’s lower extremity veins are not fully engorged when the test period begins, allowing the occlusion cuff to artificially increase the blood volume present in the leg over time. The patient’s knees are bent slightly to facilitate popliteal vein outflow with legs raised off the table. A monitor is applied and the blood pressure cuff inflated above venous pressure to about 30–50 mm Hg. Once the volume measure reported by the monitor stabilizes for 2–3 seconds, the blood pressure cuff is deflated. Figure 24.3A depicts normal volume-time values; note the rapid return to baseline limb volume, suggesting unobstructed venous outflow (VO).

Outflow obstruction results in a longer time to baseline (Fig. 24.3B). Calf venous volume (VV) is the other important parameter derived from the volume-time curve plateau.

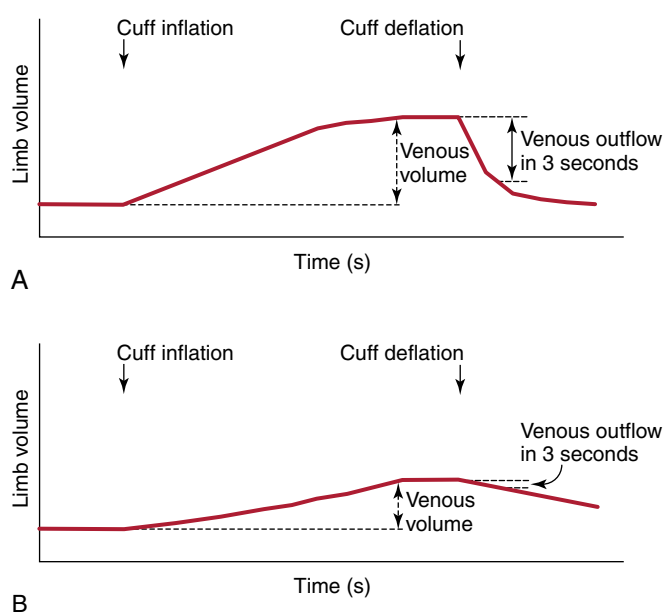


**Figure 24.3** (A) Representative plethysmographic tracing in a normal subject during inflation and deflation of proximal thigh occlusive cuff. (B) Representative plethysmographic tracing in a patient with chronic venous insufficiency. Note the significantly reduced venous outflow recorded during the 3 seconds after cuff deflation (3-second venous outflow), indicative of severe venous outflow obstruction. The slope of the outflow curve (maximum venous outflow) is also reduced in comparison with the normal tracing in A.

### Strain-Gauge Plethysmography

Strain-gauge plethysmography (SPG) measures calf volume changes by generating an electrical current as a mercury-filled Silastic tube stretches and relaxes with changes in lower leg circumference. Venous outflow obstruction is reflected by an increased VO time, as the Silastic tube requires a longer period to relax back to baseline stretch. Femoral–popliteal DVT was historically the clinical condition of interest with SPG demonstrating a 90% sensitivity above the knee, however only 66% below the knee sensitivity has led to Duplex ultrasound as the modality of choice.<sup>23</sup> A Swedish group employed computerized SPG to assess venous claudication patients prior to intervening on associated iliofemoral obstruction, finding severe symptoms correlated with reduced outflow over the 4 seconds following cuff deflation.<sup>24</sup> The authors have yet to comment on whether this finding correlated with symptom resolution following treatment.

### Impedance Plethysmography

Impedance plethysmography (IPG) measures capacitance of the calf as a function of the change in electrical resistance. A voltage-generating electrode placed on the lower leg produces a current detected by a sensor at a different location. Variations as the extremity volume changes are reflected by a change in resistance. IPG demonstrates a wide sensitivity range for DVT based on clinical scenario and anatomic location.<sup>25</sup> Duplex ultrasonography has replaced IPG in DVT diagnosis. There has been renewed interest in IPG utilizing redesigned sensors and acquisition equipment,<sup>26</sup> as a therapeutic for venous

insufficiency,<sup>27</sup> and a way to determine central venous pressure.<sup>27</sup> However, these efforts are in their nascent stages and not yet commercially available.

### Photoplethysmography

Photoplethysmography (PPG) measures the rapidity of refill with dependency using a photosensor. Photoelectrodes applied to the lower leg skin produce infrared light and detect variations in absorbance by hemoglobin circulating through underlying capillaries, allowing the sensory equipment to report changes in extremity blood volume over time. PPG was introduced in 1983 as a noninvasive means of estimating AVP.<sup>28</sup> Subsequent validation studies demonstrated a 92%–100% sensitivity for reflux and 60%–88% specificity.<sup>29,30</sup> Specificity associated with PPG decreases in the presence of edema, varicose veins, phlebitis, and arterial disease. Test reproducibility is further affected by room lighting, as well as patient positioning and participation.<sup>31</sup>

New wearable technologies are repurposing PPG to monitor other medical conditions. In combination with IPG, PPG can detect blood pressure without an occlusive cuff.<sup>32,33</sup> Heart rhythms are also readily monitored.<sup>34,35</sup> As PPG technology continues to evolve, there is an opportunity to refine the venous disease applications.

### Foot Volume Plethysmography

Foot volume plethysmography (FPG) has been employed in Europe to directly measure below-ankle venous hemodynamics.<sup>36</sup> This technique has been applied to venous pathophysiology, but remains a niche tool.<sup>37,38</sup>

### Air Plethysmography

Air plethysmography (APG) measures volume displacement as a change in pressure exerted by the calf on an air-filled chamber. As a technique to quantify multiple CVI parameters, including venous reflux, outflow obstruction, and calf muscle pump function, APG is a flexible, precise diagnostic tool without the shortcomings of the other described plethysmography methods. Allan introduced the concept of limb volume changes captured by a recording cuff in 1964.<sup>39</sup> Christopoulos et al. reported on this technique in 1987, incorporating computer-based instrumentation, and the application has remained similar since that time.<sup>40</sup>

### Technique and Interpretation

A polyvinyl chloride cuff extending from knee to ankle is applied to the patient's lower leg and inflated to 6 mm Hg (Fig. 24.4).

The patient is placed in a supine position with their leg elevated at 45 degrees for 5 minutes to allow the venous system to drain, as well as the leg and air chamber to equilibrate with room temperature, 22–24°C. A calibration curve is generated by injecting 200 mL of water in 50 mL increments with a temperature of 37°C.

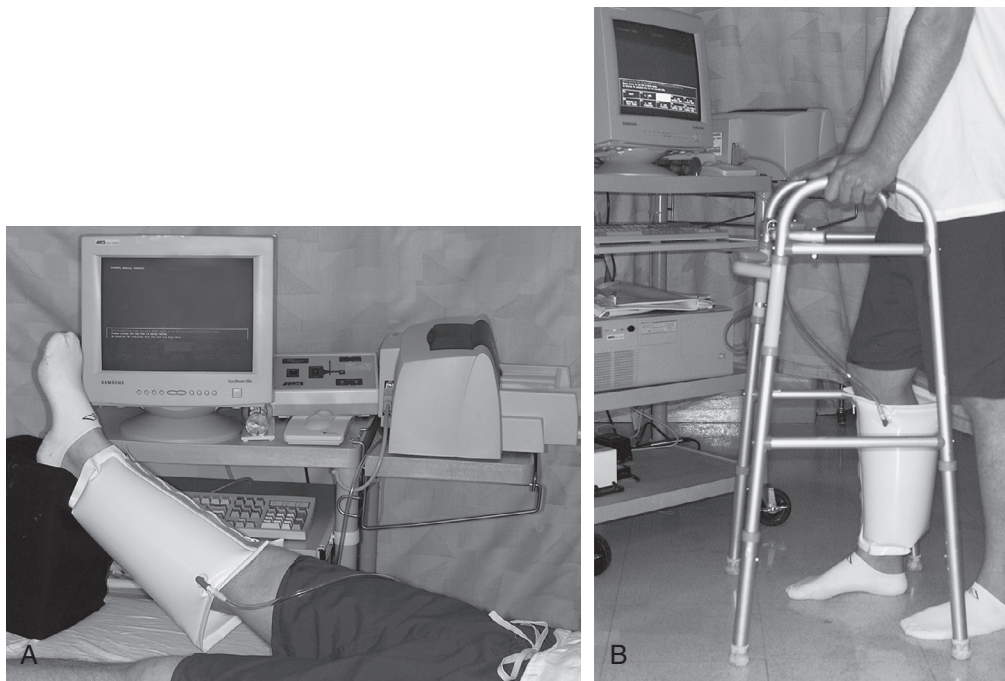


**Figure 24.4** (A) Recording of baseline leg volume at the onset of air plethysmography (APG) testing with the patient supine and the leg elevated to minimize venous volume. Note the APG cuff over the leg. (B) Patient demonstrating a tiptoe maneuver during APG and the use of a walker to allow the limb under examination to remain relaxed.

Next, the patient stands with their weight on the non-monitored foot, allowing the veins in the monitored leg to passively fill. A walker is helpful for the patient's balance, allowing the non-monitored foot to accept bodyweight while the monitored foot remains passive. The plateau pressure value is the venous volume (VV). The time to 90% of the plateau pressure value is the venous filling time (VFT90). Venous filling index (VFI) is calculated by dividing 90%VV by VFT90; this value reflects the extremity's average filling rate in mL/s (Fig. 24.5).

Evaluating calf pump function by APG involves determining the lower extremity ejection fraction (EF) and the residual volume (RVF). The patient then stands on both feet and performs one tiptoe maneuver, ejecting blood from the calf; the measured volume change is the ejection volume (EV). A re-equilibration period allows venous filling to plateau. Following 10 tiptoe maneuvers at a rate of 1 per second, the volume of blood remaining in the lower leg is the residual volume (RV). Ejection fraction (EF) is calculated by dividing EV/VV. Residual volume fraction (RVF) – another indicator of calf muscle pump function – is the dividend of RV/VV; a normal value is <35%. Both EF and RVF correlate with the clinical severity of venous disease,<sup>41,42</sup> and RVF correlates reasonably well with AVP,<sup>43</sup> providing a noninvasive alternative to dorsal foot vein catheterization.

To determine the relative contribution of the deep and superficial systems, this testing protocol is repeated with an occlusive cuff around the thigh; in this way, venous outflow (VO) may also be measured. With the occlusive cuff inflated to 80 mm Hg and the patient supine, the lower extremity is allowed to fill with blood and equilibrate at a plateau VV. The cuff is then deflated and VO recorded. Venous outflow over 1 second divided by plateau venous volume yields the outflow fraction ( $OF_1 = VO_1/VV$ ).<sup>44</sup> Normal limbs demonstrate  $OF_1 > 38\%$ , while  $< 28\%$  indicates severe obstruction.<sup>45</sup> Figure 24.6 depicts the relative changes in affected and unaffected extremity hemodynamics 3 years after a femoropopliteal DVT.<sup>46</sup>

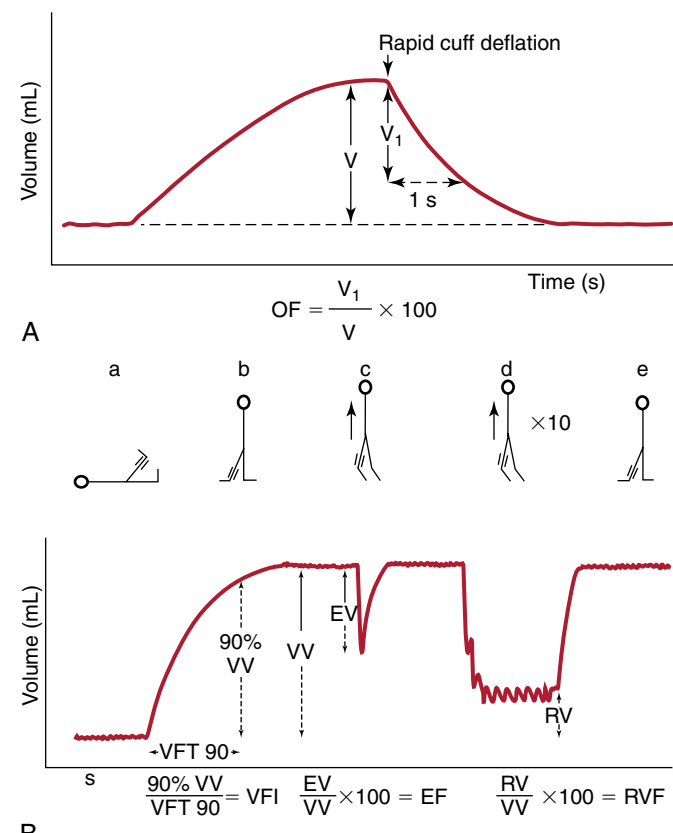


**Figure 24.5** (A) Typical outflow fraction tracing obtained with air plethysmography (APG). After venous congestion is created with a thigh occlusion cuff, rapid deflation allows venous emptying. The outflow fraction (OF) is obtained by dividing the amount of venous volume emptied in 1 second ( $V_1$ ) by the venous volume (V) and multiplying by 100. (B) APG data obtained from tracings. The figures along the top indicate the patient's position and maneuvers performed during the recording. EF, ejection fraction; EV, ejected volume; RV, residual volume; RVF, residual volume fraction; VFI, venous filling index; VFT, venous filling time; VV, venous volume. (Redrawn from Christopoulos DG, Nicolaides AN, Szendro G, et al. Air plethysmography and the effect of elastic compression on venous hemodynamics of the leg. *J Vasc Surg*. 1987;5:148–159.)

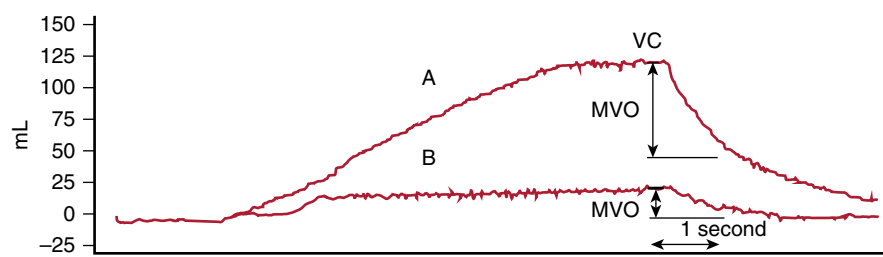


**Figure 24.6** APG associated with (A) unaffected limb and (B) limb 3 years after femoropopliteal DVT. (Redrawn from Gloviczki P, Dalsing MC. *Handbook of venous disorders: guidelines of the American Venous Forum*, 3rd ed. London: Hodder Arnold; 2009.<sup>46</sup>)

**TABLE 24.1**

Prevalence of the Sequelae of Venous Disease in Relation to Venous Filling Index in 134 Limbs with Venous Disease Studied with Air Plethysmography

VFI (mL/s)	Swelling (%)	Skin Changes (%)	Ulceration (%)
<3	0	0	0
3–5	12	19	0
5–10	46	61	46
>10	76	76	58

VFI, venous filling index.

A recently validated parameter, venous drainage index (VDI), quantifies change in calf volume as measured by APG on raising a leg from dependent to elevated.<sup>49</sup> Deriving VDI involves measuring the venous blood volume drained (VDV) from the leg over time; the VDV at 90% plateau drainage is employed in the calculation and the result expressed in mL/s. Lattimer et al. reported on 21 patients fitted with a thigh cuff inflated to multiple increasing pressures, finding VDI correlates with varying degrees of venous stenosis induced by cuff compression (Spearman  $r = -0.69$ ,  $P < 0.001$ ).

Extremities without venous disease exhibit VFIs <3 mL/s, while increasing volume flows correlate with progressively more severe CVD manifestations (Table 24.1<sup>47</sup> and see Fig. 24.2<sup>48</sup>).

Figure 24.7<sup>49</sup> from the Lattimer validation study depicts the relationship between venous drainage index (VDI) and obstruction pressure (Fig. 24.7A), as well as the blood volume retained in the limb with increasing obstruction to outflow (Fig. 24.7B). This test demonstrates a noninvasive method to reliably quantify obstructive venous pathophysiology. A follow-up study examining CEAP-based clinical parameters before and after treatment would provide further evidence on VDI's value.

### Accuracy

Plethysmographic tests tend to produce consistent information. Figure 24.8 demonstrates the concordance between SPG, IPG, and APG.<sup>50</sup>

Raju et al. reported pre- and post-stenting APG results on 551 patients treated for venous obstruction.<sup>51</sup> They suggest statistically significant changes in EV, VV, RVF and EF, however the median values for each parameter differ by small amounts and carry wide confidence intervals, rendering extrapolation to individual patients' results challenging. This difficulty has been encountered by other groups.<sup>52,53</sup> With further dissemination, VDI may prove a valuable APG-derived parameter that provides more intuitive metrics to guide and assess venous interventions.

Regarding VFI, multiple studies have shown a correlation with CEAP class and reflux, with values less than 2 mL/s correlating with resolution of disease.<sup>54,55</sup>

### Limitations

Mobility impairment, ulcerations, musculoskeletal disabilities, and calf size all limit APG's applicability. Decreased ankle flexion, either from wounds or musculoskeletal dysfunction, prevents activation of the calf muscle pump on tiptoe maneuver. Wounds also may prevent the monitoring cuff from being placed and inflated comfortably. Lymphedema, however, should not be considered a barrier to proper APG evaluation.<sup>56</sup>

Ambulatory venous pressure measurements reflect the global hemodynamics within an extremity and show a linear relationship with clinical disease severity. However, APG cannot reliably localize the hemodynamic abnormalities beyond the superficial or deep systems, or differentiate obstruction from reflux. This noninvasive test is generally well-tolerated by patients and may therefore be repeated frequently, adding not only hemodynamic information to duplex evaluation, but also additional data regarding calf muscle pump function.

## RELIABILITY OF VENOUS TESTING

Venous testing reliability has always been subject to changes in ambient temperature. Physiologic testing introduces numerous variables, including the patient's ability to stand from supine, perform tiptoe raises, and exert maximal effort. Standardizing variability between tests is challenging for the vascular diagnostician. Christopolous et al. reported variation between these plethysmographic parameters ranging from 2.9% to 9.8%,<sup>40</sup> while Yang et al. found this range to be 7.0% to 27.9% and recommended multiple tests to improve accuracy.<sup>18</sup> Testing deterioration sufficient to produce a category change from normal to abnormal in 20% of subjects has been reported when morning tests were compared with afternoon.<sup>57</sup> Thus, controlling for time of day and technique, as well as incorporating repeat tests may be necessary to produce meaningful results. These physiologic tests may also be applied to the upper extremity.

Correctable anatomic problems (greater saphenous and popliteal vein) have been identified following hemodynamic deterioration through plethysmography.<sup>58</sup> Plethysmography has been used to measure improvement following treatment by both compression and surgery.<sup>57,59</sup> Diagnosis of calf pump failure may be identified even when anatomic disease appears

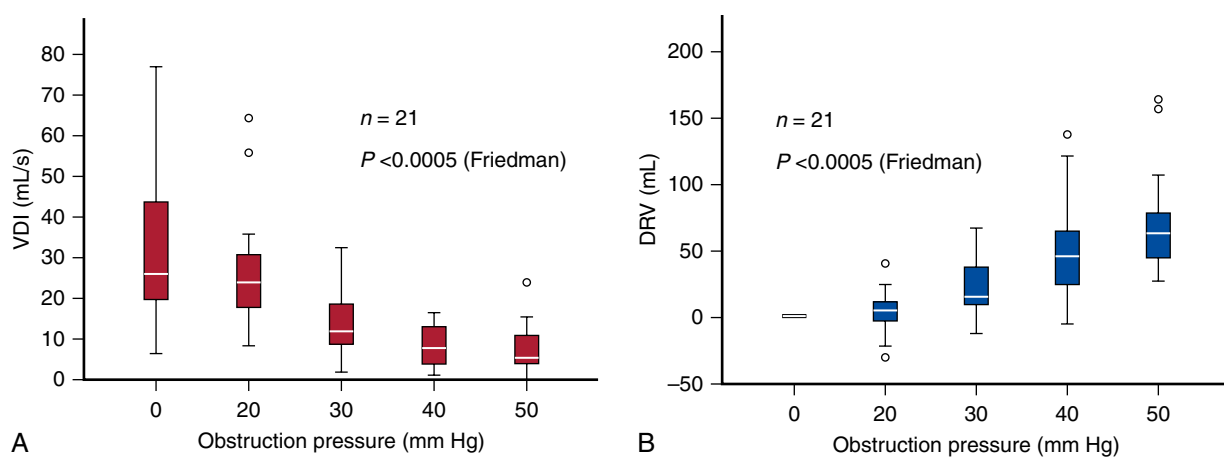


**Figure 24.7** (A) VDI versus increasing obstruction pressure. (B) Residual venous volume in the lower leg with increasing obstruction pressure.<sup>49</sup>

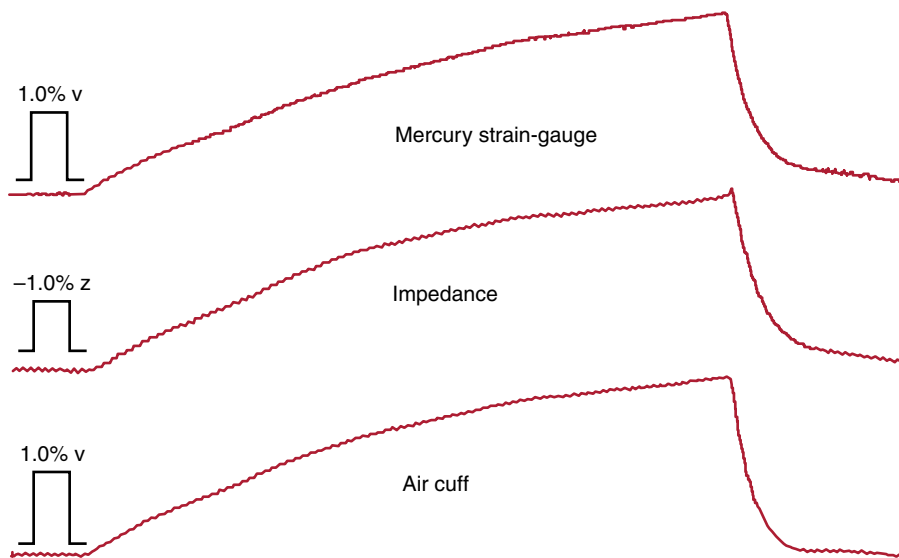


**Figure 24.8** Concordance between plethysmographic tests. (Redrawn from Bernstein EF. *Vascular Diagnosis*, 4th ed. St. Louis: Mosby; 1993.<sup>50</sup>)

mild or inconsequential. Serial examination is facilitated by noninvasive examinations with both duplex and plethysmography. Thus, plethysmography complements clinical evaluation and duplex testing. Integrating each component is essential to advancing our understand of venous disease and CVI patient management.

## SELECTED KEY REFERENCES

Labropoulos N, Giannoukas AD, Nicolaides AN, et al. The role of venous reflux and calf muscle pump function in nonthrombotic chronic venous insufficiency. Correlation with severity of signs and symptoms. *Arch Surg*. 1996;131(4):403–406.

*A study of lower-limb venous hemodynamics in patients with varying grades of chronic venous insufficiency not due to deep vein thrombosis.*

Lattimer CR, Doucet S, Geroulakos G, Kalodiki E. Validation of the novel venous drainage index with stepwise increases in thigh compression pressure in the quantification of venous obstruction. *J Vasc Surg Venous Lymphat Disord*. 2017;5(1):88–95.

*A study to quantify the relationship of novel gravitational venous drainage to increasing venous obstruction.*

Lattimer CR, Rudolph PB, Recke A, et al. Comparison of four haemodynamic tests that quantify superficial venous insufficiency. *Eur J Vasc Endovasc Surg*. 2019;57(4):570–577.

*An assessment of quantitative methods to evaluate superficial venous insufficiency.*

Lurie F, Passman M, Meisner M, et al. The 2020 update of the CEAP classification system and reporting standards. *J Vasc Surg Venous Lymphat Disord*. 2020;8(3):342–352.

*Presentation of the CEAP system and reporting standards.*

Nicolaides AN, Zukowski AJ. The value of dynamic venous pressure measurements. *World J Surg*. 1986;10(6):919–924.

*Overview of the clinical role of venous pressure assessment.*

Nicolaides AN, Hussein MK, Szendro G, et al. The relation of venous ulceration with ambulatory venous pressure measurements. *J Vasc Surg*. 1993;17(2):414–419.

*Presents the physiologic assessment of the patient with venous ulceration.*

Raju S, Walker W, May C. Measurement of ambulatory venous pressure and column interruption duration in normal volunteers. *J Vasc Surg Venous Lymphat Disord*. 2020;8(1):127–136.

*A critical assessment of ambulatory venous pressure measured via the dorsal foot vein and greater saphenous vein.*

A complete reference list can be found online at [www.expertconsult.com](http://www.expertconsult.com).

## REFERENCES

1. Porter JM, Moneta GL. Reporting standards in venous disease: an update. International Consensus Committee on Chronic Venous Disease. *J Vasc Surg.* 1995;21(4):635–645.
2. Eklof B, Rutherford RB, Bergan JJ, et al. Revision of the CEAP classification for chronic venous disorders: consensus statement. *J Vasc Surg.* 2004;40(6):1248–1252.
3. Lurie F, Passman M, Meisner M, et al. The 2020 update of the CEAP classification system and reporting standards. *J Vasc Surg Venous Lymphat Disord.* 2020;8(3):342–352.
4. Danielsson G, Norgren L, Jungbeck C, Peterson K. Global venous function correlates better than duplex derived reflux to clinical class in the evaluation of chronic venous disease. *Int Angiol.* 2003;22(2):177–181.
5. Rodriguez AA, Whitehead CM, McLaughlin RL, et al. Duplex-derived valve closure times fail to correlate with reflux flow volumes in patients with chronic venous insufficiency. *J Vasc Surg.* 1996;23(4):606–610.
6. Smirk FH. First direct measurement of venous pressure at the ankle. *Clin Sci.* 1936;2:317.
7. Pollack AA, Wood EH. Venous pressure in the saphenous vein at the ankle in man during exercise and changes in posture. *J Appl Physiol.* 1949;1:649–662.
8. Pollack AA, Taylor BE, Myers TT, Wood EH. The effect of exercise and body position on the venous pressure at the ankle in patients having venous valvular defects. *J Clin Invest.* 1949;28:559–563.
9. Arnoldi CC. Venous pressure in the leg of healthy human subjects at rest and during muscular exercise in the nearly erect position. *Acta Chir Scand.* 1965;130(6):570–583.
10. Højengård IC, Strup H. Static and dynamic pressures in superficial and deep veins of the lower extremity in man. *Acta Physiol Scand.* 1952;27(1):49–67.
11. Ludbrook J. Functional aspects of the veins of the leg. *Am Heart J.* 1962;64:706–713.
12. Raju S, Walker W, May C. Measurement of ambulatory venous pressure and column interruption duration in normal volunteers. *J Vasc Surg Venous Lymphat Disord.* 2020;8(1):127–136.
13. Nicolaides AN, Hussein MK, Szendro G, et al. The relation of venous ulceration with ambulatory venous pressure measurements. *J Vasc Surg.* 1993;17(2):414–419.
14. Raju S, Fredericks R. Hemodynamic basis of stasis ulceration--a hypothesis. *J Vasc Surg.* 1991;13(4):491–495.
15. Payne SP, London NJ, Newland CJ, et al. Ambulatory venous pressure: correlation with skin condition and role in identifying surgically correctible disease. *Eur J Vasc Endovasc Surg.* 1996;11(2):195–200.
16. Araki CT, Back TL, Padberg FT, et al. The significance of calf muscle pump function in venous ulceration. *J Vasc Surg.* 1994;20(6):872–877; discussion 878–879.
17. Back TL, Padberg Jr FT, Araki CT, Thompson PN, Hobson 2nd RW. Limited range of motion is a significant factor in venous ulceration. *J Vasc Surg.* 1995;22(5):519–523.
18. Yang D, Vandongen YK, Stacey MC. Variability and reliability of air plethysmographic measurements for the evaluation of chronic venous disease. *J Vasc Surg.* 1997;26(4):638–642.
19. Nicolaides AN, Zukowski AJ. The value of dynamic venous pressure measurements. *World J Surg.* 1986;10(6):919–924.
20. Whitney RJ. The measurement of volume changes in human limbs. *J Physiol.* 1953;121(1):1–27.
21. Whitney RJ. The measurement of changes in human limb-volume by means of a mercury-inrubber strain gauge. *J Physiol.* 1949;109(1–2): Proc, 5.
22. Darling RC, Raines JK, Brener BJ, Austen WG. Quantitative segmental pulse volume recorder: a clinical tool. *Surgery.* 1972;72(6):873–877.
23. Barnes RW, Collicott PE, Mozersky DJ, et al. Noninvasive quantitation of maximum venous outflow in acute thrombophlebitis. *Surgery.* 1972;72(6):971–979.
24. Rosfors S, Blomgren L. Venous occlusion plethysmography in patients with post-thrombotic venous claudication. *J Vasc Surg.* 2013;58(3):722–726.
25. Hull RD, Hirsh J, Carter CJ, et al. Diagnostic efficacy of impedance plethysmography for clinically suspected deep-vein thrombosis. A randomized trial. *Ann Intern Med.* 1985;102(1):21–28.
26. Hashim ZQ, Constantinou L, Triantis IF. Modelling dynamically resizeable electrodes (DRE) for targeted transcutaneous measurements in impedance plethysmography. *IEEE Trans Biomed Circuits Syst.* 2020;14(1):104–112.
27. Weyrer S, Weishaupt F, Kleeberg C, et al. Development of an adaptive multi-sensor to prevent venous stasis. *Sensors (Basel).* 2016;16(4):428.
28. Norris CS, Beyrau A, Barnes RW. Quantitative photoplethysmography in chronic venous insufficiency: a new method of noninvasive estimation of ambulatory venous pressure. *Surgery.* 1983;94(5):758–764.
29. Garcia-Serrano A, Elefterion A, Ginestet MC, Boccalon H. [Diagnostic value and significance of photoplethysmography in venous insufficiency]. *Phlebologie.* 1989;42(3):503–518.
30. Bays RA, Healy DA, Atnip RG, et al. Validation of air plethysmography, photoplethysmography, and duplex ultrasonography in the evaluation of severe venous stasis. *J Vasc Surg.* 1994;20(5):721–727.
31. Nicolaides AN, Miles C. Photoplethysmography in the assessment of venous insufficiency. *J Vasc Surg.* 1987;5(3):405–412.
32. Rachim VP, Chung WY. Compressive sensing of cuff-less biosensor for energy-efficient blood pressure monitoring. *Conf Proc IEEE Eng Med Biol Soc.* 2019;2019:7072–7075.
33. Chandrasekhar A, Yavarimanesh M, Natarajan K, et al. PPG sensor contact pressure should be taken into account for cuff-less blood pressure measurement. *IEEE Trans Biomed Eng.* 2020;67(11):3134–3140.
34. Hochstadt A, Havakuk O, Chorin E, et al. Continuous heart rhythm monitoring using mobile photoplethysmography in ambulatory patients. *J Electrocardiol.* 2020;60:138–141.
35. Verbrugge FH, Proesmans T, Vijgen J, et al. Atrial fibrillation screening with photo-plethysmography through a smartphone camera. *Europace.* 2019;21(8):1167–1175.
36. Diebschlag W. [A simple apparatus for the determination of foot volume and its changes]. *Z Gesamte Exp Med.* 1970;152(3):179–186.
37. Amoore JN, van Oudenhoove LB, Immelman E, Jeffery P. The assessment of the post-thrombotic limb by foot volumetry and pedal venous pressure. *J Med Eng Technol.* 1983;7(4):180–185.
38. Danielsson G, Jungbeck C, Peterson K, Norgren L. Venous function after restoring valve competence of the great saphenous vein. *J Endovasc Ther.* 2003;10(2):350–355.
39. Allan JC. Volume changes in the lower limb in response to postural alterations and muscular exercise. *S Afr J Surg.* 1964;2:75–90.
40. Christopoulos DG, Nicolaides AN, Szendro G, et al. Air-plethysmography and the effect of elastic compression on venous hemodynamics of the leg. *J Vasc Surg.* 1987;5(1):148–159.
41. Labropoulos N, Giannoukas AD, Nicolaides AN, et al. The role of venous reflux and calf muscle pump function in nonthrombotic chronic venous insufficiency. Correlation with severity of signs and symptoms. *Arch Surg.* 1996;131(4):403–406.
42. Christopoulos D, Nicolaides AN, Cook A, et al. Pathogenesis of venous ulceration in relation to the calf muscle pump function. *Surgery.* 1989;106(5):829–835.
43. Welkie JF, Comerota AJ, Kerr RP, et al. The hemodynamics of venous ulceration. *Ann Vasc Surg.* 1992;6(1):1–4.
44. Nicolaides AN. Cardiovascular Disease Educational and Research Trust; European Society of Vascular Surgery, et al. Investigation of chronic venous insufficiency: A consensus statement (France, March 5–9, 1997). *Circulation.* 2000;102(20):E126–E163.
45. Kalodiki E, Calahoras LS, Delis KT, et al. Air plethysmography: the answer in detecting past deep venous thrombosis. *J Vasc Surg.* 2001;33(4):715–720.
46. Gloviczki P, Dalsing MC. In: *Handbook of Venous Disorders: Guidelines of the American Venous Forum.* 3rd ed. London: Hodder Arnold; 2009.

47. Christopoulos D, Nicolaides AN, Szendro G. Venous reflux: quantification and correlation with the clinical severity of chronic venous disease. *Br J Surg.* 1988;75(4):352–356.
48. Criado E, Farber MA, Marston WA, et al. The role of air plethysmography in the diagnosis of chronic venous insufficiency. *J Vasc Surg.* 1998;27(4):660–670.
49. Lattimer CR, Doucet S, Geroulakos G, Kalodiki E. Validation of the novel venous drainage index with stepwise increases in thigh compression pressure in the quantification of venous obstruction. *J Vasc Surg Venous Lymphat Disord.* 2017;5(1):88–95.
50. Bernstein EF. In: *Vascular Diagnosis.* 4th ed. St. Louis: Mosby; 1993.
51. Raju S, Kirk O, Davis M, Olivier J. Hemodynamics of “critical” venous stenosis and stent treatment. *J Vasc Surg Venous Lymphat Disord.* 2014;2(1):52–59.
52. Kurstjens RL, de Wolf MA, Alsadah SA, et al. The value of hemodynamic measurements by air plethysmography in diagnosing venous obstruction of the lower limb. *J Vasc Surg Venous Lymphat Disord.* 2016;4(3):313–319.
53. Kurstjens RL, Catarinella FS, Lam YL, et al. The inability of venous occlusion air plethysmography to identify patients who will benefit from stenting of deep venous obstruction. *Phlebology.* 2018;33(7):483–491.
54. Lattimer CR, Rudolphi PB, Recke A, et al. Comparison of four haemodynamic tests that quantify superficial venous insufficiency. *Eur J Vasc Endovasc Surg.* 2019;57(4):570–577.
55. Owens LV, Farber MA, Young ML, et al. The value of air plethysmography in predicting clinical outcome after surgical treatment of chronic venous insufficiency. *J Vasc Surg.* 2000;32(5):961–968.
56. Suehiro K, Morikage N, Ueda K, et al. Venous hemodynamics assessed with air plethysmography in legs with lymphedema. *Vasc Med.* 2018;23(2):139–142.
57. Katz ML, Comerota AJ, Kerr RP, Caputo GC. Variability of venous-hemodynamics with daily activity. *J Vasc Surg.* 1994;19(2):361–365.
58. Bradbury AW, Stonebridge PA, Callam MJ, et al. Foot volumetry and duplex ultrasonography after saphenous and subfascial perforating vein ligation for recurrent venous ulceration. *Br J Surg.* 1993;80(7):845–848.
59. Padberg Jr FT. Surgical intervention in venous ulceration. *Cardiovasc Surg.* 1999;7(1):83–90.

# Vascular Laboratory: Venous Duplex Scanning

DAVID L. DAWSON

INTRODUCTION	286
NORMAL B-MODE IMAGING FINDINGS	289
NORMAL FLOW PATTERNS IN VEINS	289
DIAGNOSIS OF DEEP VENOUS THROMBOSIS	290
CALF VEIN THROMBOSIS	291
ILIAC VEINS AND INFERIOR VENA CAVA	292
DIAGNOSIS OF UPPER EXTREMITY DEEP VENOUS THROMBOSIS	294
LIMITED OR POINT-OF-CARE ULTRASOUND EXAMINATIONS	294
DETERMINATION OF THROMBUS AGE	295

NOVEL ULTRASOUND TECHNIQUES:	
ELASTOGRAPHY	297
DETERMINING THE DURATION OF THERAPY FOR ACUTE DVT	298
DIAGNOSIS OF RECURRENT THROMBOSIS	298
SUPERFICIAL VEINS	299
VEIN MAPPING	299
EVALUATION FOR CHRONIC VENOUS DISEASE: VENOUS INSUFFICIENCY	300
PERFORATING VEINS	304
CHAPTER ALGORITHM	305

## INTRODUCTION

Duplex scanning is readily available, noninvasive, and inexpensive. It is the primary means for diagnosis of deep vein thrombosis (DVT) and chronic venous insufficiency (CVI)<sup>1–4</sup> (see Ch. 148, Acute Lower Extremity Deep Venous Thrombosis: Presentation, Diagnosis, and Medical Treatment; and Ch. 156, Chronic Venous Disorders: Postthrombotic Syndrome, Natural History, Pathophysiology, and Etiology). There are limitations, however. The accuracy and reliability of venous duplex scanning still depend on the thoroughness of the examination, the skill of the technologist performing the study, and the competence of the interpreting physician.

The use of Doppler ultrasound for the evaluation of lower extremity veins was pioneered in the 1960s.<sup>5,6</sup> In 1968, David Sumner, Dennis Baker, and D. Eugene Strandness described use of an ultrasonic flow detector to assess venous flow patterns.<sup>7</sup> In 1972, Strandness and Sumner published their observations on the use of Doppler ultrasound for the diagnosis of venous thrombosis.<sup>8</sup> Steven Talbot, a vascular technologist, published his description of the use of B-mode (2-D grayscale) imaging for the diagnosis of deep vein thrombosis (DVT) in 1982.<sup>9,10</sup>

Early validation studies that compared venous ultrasonography to venography identified limitations of B-mode imaging when it was used as a sole modality. Imaging of deeper structures was limited. Moderate probe compression did not collapse some normal vein segments (e.g., femoral vein at the level of the adductor hiatus) and vein compressibility could also be limited by obesity, edema, or tenderness. It was soon recognized that the accuracy of the examination was improved by combining imaging and Doppler-derived information about the presence and nature of venous flow in the interrogated segments.<sup>11,12</sup> Within a few years, duplex scanning became the primary diagnostic modality for diagnosis of venous disorders, not just a screening method.

In the modern era, the primacy of duplex scanning for diagnosis is no longer in question. Now, vascular laboratories have a greater focus on how to optimize examination efficiency (tailoring study protocols for individual patients), improving reporting, and reducing variation.

Variation is reduced by exam standardization and by the use of appropriate study procedures and interpretation criteria. The Intersocietal Accreditation Commission (IAC) accredits imaging facilities specific to vascular testing. Accreditation recognizes facilities that provide quality vascular testing

**TABLE 25.1** Vascular Laboratory Standards for Peripheral Venous Testing

<b>Indications:</b> Peripheral venous testing must be performed for appropriate clinical indications	<ul style="list-style-type: none"> <li>Testing indication must be documented</li> </ul>
<b>Equipment:</b> Equipment must provide accurate data	<ul style="list-style-type: none"> <li>Imaging equipment: duplex ultrasound with color flow Doppler, with <ul style="list-style-type: none"> <li>imaging frequencies appropriate for the structures evaluated</li> <li>Doppler frequencies appropriate for the vessels evaluated</li> <li>range-gated spectral Doppler with ability to adjust the depth and position of the range gate in the area of interest</li> <li>Doppler angle which is measurable and adjustable</li> <li>visual display and permanent recording of images</li> <li>visual display, audible output, and permanent recording of Doppler waveforms and corresponding images</li> </ul> </li> <li>Equipment quality control: equipment used for diagnostic testing must be maintained in good operating condition</li> </ul>
<b>Protocols:</b> There must be a written protocol for each examination, including:	<ul style="list-style-type: none"> <li>equipment to be used</li> <li>proper technique</li> <li>Anatomic extent of a complete examination, generally includes entire course of the accessible portion of each vessel</li> <li>variations in technique following vascular interventions, including dialysis access</li> <li>variations in technique and documentation for limited exams</li> <li>routine documentation and additional documentation that must be acquired to describe abnormalities</li> <li>description of how color Doppler or other flow imaging modes (e.g., power Doppler) are used to supplement grayscale imaging and spectral Doppler measurements</li> </ul>
<b>Techniques:</b> Appropriate techniques to document their severity, location, extent and (whenever possible) etiology	<ul style="list-style-type: none"> <li>Elements of proper technique include: <ul style="list-style-type: none"> <li>performance of an examination according to a specific written protocol</li> <li>proper patient positioning <ul style="list-style-type: none"> <li>for assessing reflux: standing, sitting or reverse Trendelenburg (at least 15 degrees)</li> </ul> </li> <li>patient preparation</li> <li>appropriate equipment and transducer selection</li> <li>appropriate transducer positioning</li> <li>identification of vessels by imaging and Doppler</li> <li>proper sample volume size and positioning</li> <li>optimization of equipment gain and display settings</li> <li>proper vein diameter measurements: <ul style="list-style-type: none"> <li>acquired with the limb in a dependent position</li> <li>measured anterior wall to posterior wall</li> <li>no external pressure is applied to the vein during measurement</li> </ul> </li> <li>transverse grayscale imaging without and with transducer compressions</li> <li>provocative maneuvers are used to test for reflux in lower extremity vein <ul style="list-style-type: none"> <li>the limb must be examined in a dependent position; standing is preferred</li> <li>manual distal compression or automated rapid cuff inflation/deflation devices should be used to elicit reflux in deep and superficial veins</li> <li>Valsalva maneuvers may be substituted for distal compression when examining the common femoral vein and the saphenofemoral junction</li> </ul> </li> </ul> </li> </ul>
<b>Documentation</b>	<ul style="list-style-type: none"> <li>grayscale images</li> <li>color Doppler images</li> <li>Doppler waveforms</li> <li>velocity measurements</li> <li>vein diameter</li> <li>valve closure time, reflux duration</li> <li>abnormalities will require additional images and waveforms that demonstrate the severity, location, extent, and etiology</li> <li>areas of suspected obstruction must include representative Doppler waveforms recorded at and distal to the obstruction</li> <li>superficial reflux must be traced to its source (e.g., saphenous junctions, great, small, anterior accessory saphenous vein, perforating vein, pelvic origin varicose veins), with reflux duration time documented</li> </ul>

(Modified from: Intersocietal Accreditation Commission - Vascular Testing. IAC Standards and Guidelines for Vascular Testing Accreditation. Section 4B: Peripheral Venous Testing 2020. <https://www.intersocietal.org/vascular/standards/IACVascularTestingStandards2020.pdf>)

services by compliance with relevant standards. It also serves as an educational tool to improve overall quality. IAC accreditation standards are regularly updated; they represent a consensus on what constitutes an appropriate vascular laboratory examination.<sup>13</sup> These standards include appropriate training and credentials of technologists and interpreting physicians,

and the use of established, consistent examination protocols (**Tables 25.1 and 25.2**). Maintaining accreditation requires that facilities implement quality improvement programs that focus on consistency and appropriateness of testing and reporting (see **Ch. 18**, Noninvasive Vascular Laboratory Quality Assurance and Accreditation).

**TABLE 25.2** Components of Venous Duplex Scans: Peripheral Venous Documentation

<b>Lower Extremity Venous Duplex for Thrombosis and Patency</b>	<ul style="list-style-type: none"> <li>• Transverse grayscale images without and with transducer compression, including:           <ul style="list-style-type: none"> <li>◦ common femoral vein</li> <li>◦ saphenofemoral junction</li> <li>◦ proximal femoral vein</li> <li>◦ mid femoral vein</li> <li>◦ distal femoral vein</li> <li>◦ popliteal vein</li> <li>◦ posterior tibial veins</li> <li>◦ peroneal veins</li> <li>◦ additional images to document areas of suspected thrombus</li> </ul> </li> <li>• Spectral Doppler waveforms demonstrating spontaneous venous flow, phasicity and/or flow augmentation, including:           <ul style="list-style-type: none"> <li>◦ right and left common femoral veins</li> <li>◦ popliteal vein</li> <li>◦ additional waveforms, as appropriate</li> <li>◦ abnormalities require additional images, waveforms and velocity measurements</li> </ul> </li> </ul>
<b>Lower Extremity Venous Duplex for Reflux</b>	<ul style="list-style-type: none"> <li>• Transverse grayscale images without and with transducer compression, including:           <ul style="list-style-type: none"> <li>◦ common femoral vein</li> <li>◦ saphenofemoral junction</li> <li>◦ mid femoral vein</li> <li>◦ great saphenous vein</li> <li>◦ popliteal vein</li> <li>◦ small saphenous vein</li> </ul> </li> <li>• Spectral Doppler waveforms with the leg in a dependent position, demonstrating baseline flow and response to distal augmentation; if reflux is present, duration of retrograde flow is measured with calipers:           <ul style="list-style-type: none"> <li>◦ common femoral vein</li> <li>◦ saphenofemoral junction</li> <li>◦ great saphenous vein</li> <li>◦ mid femoral vein</li> <li>◦ popliteal vein</li> <li>◦ small saphenous vein</li> </ul> </li> <li>• Transverse grayscale images without and with transducer compression, including:           <ul style="list-style-type: none"> <li>◦ saphenofemoral junction</li> <li>◦ great saphenous vein at proximal thigh</li> <li>◦ great saphenous vein at knee</li> <li>◦ small saphenous vein (at saphenopopliteal junction)</li> </ul> </li> </ul>
<b>Upper Extremity Venous Duplex for Thrombosis and Patency</b>	<ul style="list-style-type: none"> <li>• Transverse grayscale images without and with transducer compression, including:           <ul style="list-style-type: none"> <li>◦ internal jugular vein</li> <li>◦ subclavian vein</li> <li>◦ axillary vein</li> <li>◦ brachial vein(s)</li> <li>◦ basilic vein</li> <li>◦ cephalic vein</li> <li>◦ additional images to document areas of suspected thrombus</li> <li>◦ brachiocephalic vein should be imaged, if possible, but compression maneuvers are not used for intrathoracic veins</li> </ul> </li> <li>• Spectral Doppler waveforms demonstrating spontaneous venous flow, phasicity and/or flow augmentation, including:           <ul style="list-style-type: none"> <li>◦ internal jugular vein</li> <li>◦ right and left subclavian veins</li> <li>◦ axillary vein</li> <li>◦ additional waveforms (e.g., brachiocephalic veins), as appropriate</li> </ul> </li> </ul>
<b>Vein Mapping</b>	<ul style="list-style-type: none"> <li>• assessment of the veins required by the facility protocol</li> <li>• vein patency and size</li> </ul>
<b>Venous Stents</b>	<ul style="list-style-type: none"> <li>• Spectral Doppler waveforms with color Doppler images, including:           <ul style="list-style-type: none"> <li>◦ proximal stent</li> <li>◦ mid stent</li> <li>◦ distal stent</li> <li>◦ native vessel adjacent to the proximal end of the stent</li> <li>◦ native vessel adjacent to distal end of the stent</li> </ul> </li> </ul>

(Modified from: Intersocietal Accreditation Commission – Vascular Testing. IAC Standards and Guidelines for Vascular Testing Accreditation. Section 4B: Peripheral Venous Testing Peripheral Venous Testing 2020 <https://www.intersocietal.org/vascular/standards/IACVascularTestingStandards2020.pdf>)

## NORMAL B-MODE IMAGING FINDINGS

Venous duplex scanning may be performed with most ultrasound systems. Transducer selection depends on the depth of the veins to be scanned. A 5- to 10-MHz linear array transducer is sufficient for a most extremity venous examinations, but a 3- to 5-MHz curved linear transducer may be needed to evaluate deeply located vessels, such as the inferior vena cava and iliac veins, or to evaluate obese or edematous extremities. High-frequency transducers may be used for mapping or guiding access to superficial veins.

Blood is not an effective reflector of ultrasound. Thus, with conventional B-mode imaging the lumen of normal vein is typically anechoic (black). The interface between blood and the vein wall is echogenic (bright), especially when specular reflections are created when the ultrasound angle of incidence is close to 90 degrees. The wall of a vein appears thinner than the wall of the adjacent artery. Flowing blood may sometimes be seen within veins, especially when a high-frequency transducer is used to examine a vein that is close to the skin surface. This may be most apparent when slow flow conditions result

in red blood cell aggregation with rouleaux formation, creating greater echogenicity.<sup>14</sup>

Extremity veins may vary in size and profile. With hypovolemia, veins may appear ovoid or collapsed. Because of the normally low pressure in veins, they are easily collapsed with extrinsic compression. (Of note, normal arteries may also be compressible if sufficient probe pressure is applied.) When venous pressure is high (heart failure, more central obstruction, etc.), veins may be distended. Extremity veins may appear collapsed when the limb is elevated above the phlebostatic axis (level of the right atrium) and they will be full and dilated when the limb is dependent. Lower extremity examinations are typically done with some reverse-Trendelenburg (foot down) positioning to make the veins easier to identify.

## NORMAL FLOW PATTERNS IN VEINS

Color flow Doppler and pulsed Doppler spectral waveform analysis are used to evaluate venous flow characteristics (Fig. 25.1). Terms for describing Doppler waveforms have been standardized.<sup>15</sup> Venous waveforms are described by major key descriptors (flow direction, flow pattern, and spontaneity).

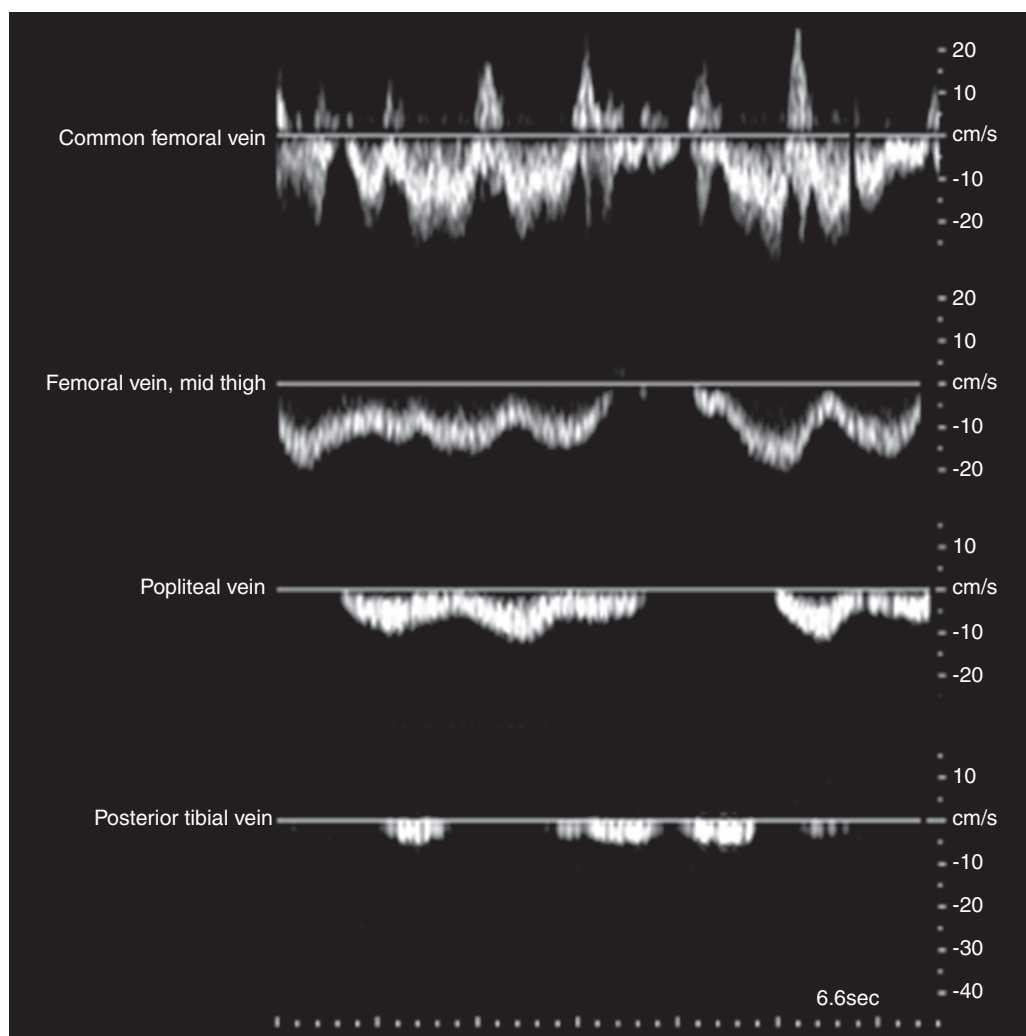


**Figure 25.1** Normal flow in the lower extremity veins is spontaneous (occurring without calf pump function or other augmentation maneuvers) and phasic with respiration. Flow patterns differ at proximal and distal locations, with less spontaneous flow observed in the smaller veins in the distal limb. The presence or absence of thrombus within an imaged vein can be confirmed with probe compression. (Image from Dawson DL, Gray HM. Acute lower extremity deep vein thrombosis. In: Zierler RE, Dawson DL (Eds). *Strandness's Duplex Scanning in Vascular Disorders*, 5th ed. Philadelphia: Wolters Kluwer; 2016:235, Figure 19.8.)

Additional modifier terms for venous waveforms include augmentation (normal, reduced, or absent), reflux, and fistula flow patterns.

In the arterial system, pumping action of the heart is the primary driving force for blood flow, but in the low-pressure venous system antegrade movement of venous blood flow is substantially affected by other factors. Normal venous flow is **phasic** with respiratory movements (respirophasic). During inspiration, the diaphragm moves downward and intraabdominal pressure is increased. This decreases venous return from the lower extremities. Flow increases during expiration. In the upper extremity veins, respiratory phasicity has a different pattern. Intrathoracic pressure is decreased during inspiration; antegrade flow in upper extremity veins is increased. The cardiac cycle has greater effects on venous flow patterns in more central veins.

**Spontaneous** antegrade venous flow is seen under resting conditions, but flow velocity is dramatically augmented with voluntary muscle contraction or by manual compression by the examiner. Muscle contraction transiently increases compartment pressures, compresses deep veins and venous sinuses within the muscles, and thereby functions as a peripheral pumping mechanism in the circulation. Venous obstruction interferes with the flow **augmentation** produced by compression or other provocative maneuvers.

## DIAGNOSIS OF DEEP VENOUS THROMBOSIS

Direct ultrasound visualization of thrombus within a vein is the most obvious finding associated with deep vein thrombosis (DVT). Deep veins that are acutely occluded by thrombosis are often distended, appearing round and larger than the adjacent artery. Thrombus echogenicity increases as the clot organizes, making it easier to detect with B-mode imaging over time. Acute thrombus may be adherent to the vein wall, or it may be loosely attached and mobile, a “free floating thrombus” or “thrombus tail.”

B-mode imaging alone has limited sensitivity. Fresh thrombus may be hypoechoic. It can also be difficult to recognize

intraluminal thrombus if the imaging quality is suboptimal, as can be the case with an uncooperative patient, greater imaging depth (obesity), failure to optimize imaging settings, or other technical factors.

For better detection of thrombus in the lumen, venous scanning is done with compression maneuvers (Fig. 25.2). Pressure is manually applied with the imaging probe. Normal vein walls collapse with modest compression. Vein walls will not coapt when there is thrombus in the lumen, though soft thrombus may deform with firm pressure. Partial compressibility may be seen with non-obstructive acute thrombosis or as recanalization of an occluded segment occurs over time.

It is therefore recommended that B-mode imaging not be used as a stand-alone modality for DVT diagnosis. Imaging of deeper structures can be limited and some normal venous segments may not collapse with probe pressure (e.g., femoral vein at the level of the adductor hiatus). Venous compressibility can also be limited by obesity, edema, or tenderness. Calf veins may be difficult to visualize. Duplex scanning, the combination of imaging and Doppler-derived information about the presence and nature of venous flow, improves the accuracy of the examination<sup>11</sup> (Fig. 25.3). The addition of flow information makes it possible to identify veins that are not well demonstrated with B-mode alone and to determine patency. Color flow Doppler helps confirm patency of venous segments that were incompletely evaluated with B-mode imaging. It can help to distinguish between occluding and non-occluding thrombus and identify anechoic thrombus by visualization of flow around it. The color velocity scale (pulse repetition frequency or PRF) should be at a low setting to detect low velocity venous flow.

The diagnostic accuracy of duplex ultrasound scanning is good enough that it has replaced contrast venography as the definitive diagnostic test for DVT, except in limited situations. A systematic review found 100 publications from 1966 to 2004 that compared ultrasound to venography in patients with suspected DVT. Meta-analyses of data from these studies confirmed that the best results were obtained with examinations that combined B-mode, pulsed Doppler, and color Doppler imaging.<sup>16</sup> The pooled sensitivity was 96% for proximal

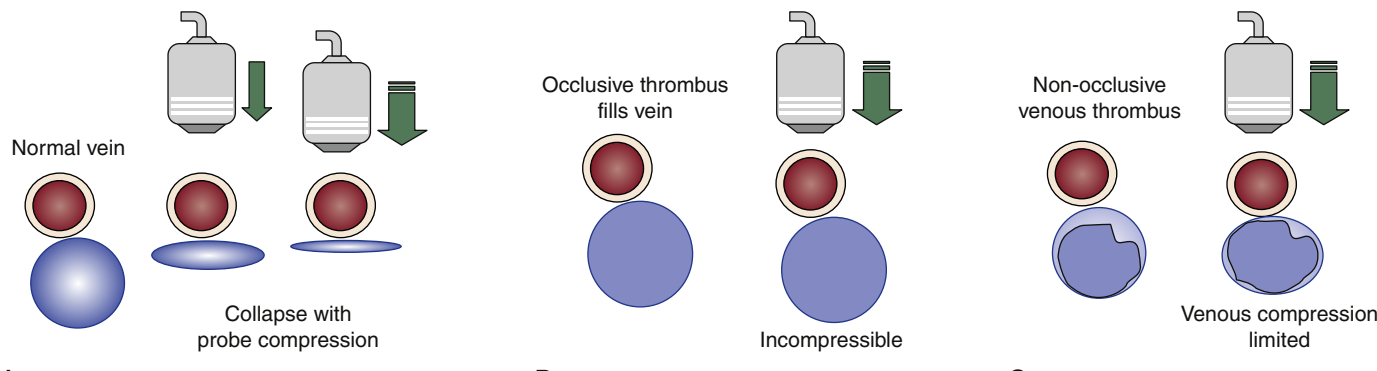


**Figure 25.2** The presence or absence of thrombus within an imaged vein can be confirmed with probe compression. (Adapted from Dawson DL, Gray HM. Acute lower extremity deep vein thrombosis. In: Zierler RE, Dawson DL (Eds). *Strandness's Duplex Scanning in Vascular Disorders*, 5th ed. Philadelphia: Wolters Kluwer; 2016:233, Figure 19.2.)

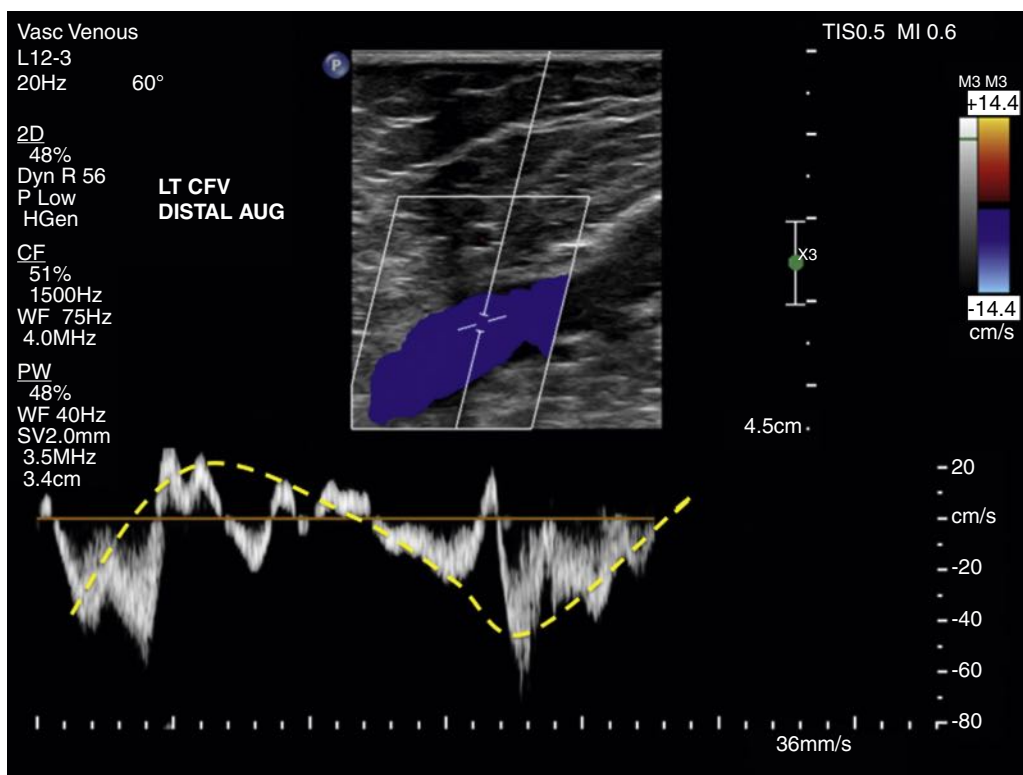


**Figure 25.3** Color Doppler image of a normal common femoral vein. There is complete color filling of the vein lumen. The flow velocity waveform demonstrates spontaneous flow that is phasic with respiration (highlighted by dashed yellow line). Cardiac effects are also seen in the waveform.

limb DVT, 75% for distal DVT and a pooled specificity of 94%. Sensitivity was found to be higher in the more recently published studies, in cohorts with higher pre-test probability of DVT and more proximal DVT, and was lower in cohorts that reported interpretation by a radiologist. Specificity was higher in cohorts that excluded patients with known prior DVT.

Imaging techniques and provocative maneuvers need to be used in combination to correctly distinguish normal flow variations from DVT (Fig. 25.4). The presence of intraluminal echoes from rouleaux formation can be distinguished from thrombus by the disruption of the echogenic erythrocyte aggregates by flow augmentation and by vein wall collapse with compression. The absence of spontaneous flow (pulsed Doppler or color Doppler) may be normal in the distal limb or it may be the result of more central obstruction. Augmentation maneuvers (calf pump, manual distal compression) will demonstrate flow.

Despite the cost-effectiveness of using pretest probability scoring and D-dimer testing in the outpatient setting to determine the need for imaging, duplex scanning continues to be used primarily as a stand-alone testing modality.<sup>17</sup> This may be due to the availability of ultrasound in most settings (see Ch. 146, Acute Deep Venous Thrombosis: Epidemiology and Natural History).

## CALF VEIN THROMBOSIS

All lower extremity deep veins should be examined as part of a complete DVT examination, including infrapopliteal

veins: peroneal, posterior tibial, soleal, and gastrocnemius veins. Isolated distal deep vein thromboses are common in patients with acute DVT and often occur as an isolated finding.<sup>18,19</sup> The peroneal and posterior tibial veins are involved in the majority of cases. Anterior tibial vein thrombi are less common.

Duplex scanning can reliably evaluate for calf vein DVT, but there are some differences in examination technique and interpretation. Spontaneous flow is not always detected, but there will be Doppler-detectable flow with augmentation by distal manual compression. Calf veins may be difficult to visualize with B-mode imaging, especially in the obese or those with significant edema. Detection of venous flow with color Doppler, with or without augmentation maneuvers, can confirm calf vein patency (Fig. 25.5).

Isolated calf vein thrombi rarely cause clinically relevant pulmonary emboli (PE), but patients with calf vein DVT are at risk for progression to involve the femoropopliteal veins. Symptomatic calf vein DVT is associated with progression or recurrent thrombosis in 15%–20% of patients within three months.<sup>20,21</sup> Calf vein DVT is a marker for increased thromboembolic risk, for which anticoagulation may be indicated.<sup>22</sup> Few patients with calf vein DVT are at high risk for progression or PE.<sup>23</sup> Risk is higher when thrombus is isolated to calf veins,<sup>24–26</sup> if the DVT was a second or subsequent venous thromboembolism (VTE) episode, in patients with recent orthopedic procedures, in patients with malignancy, and in those who are immobile.<sup>27–29</sup>

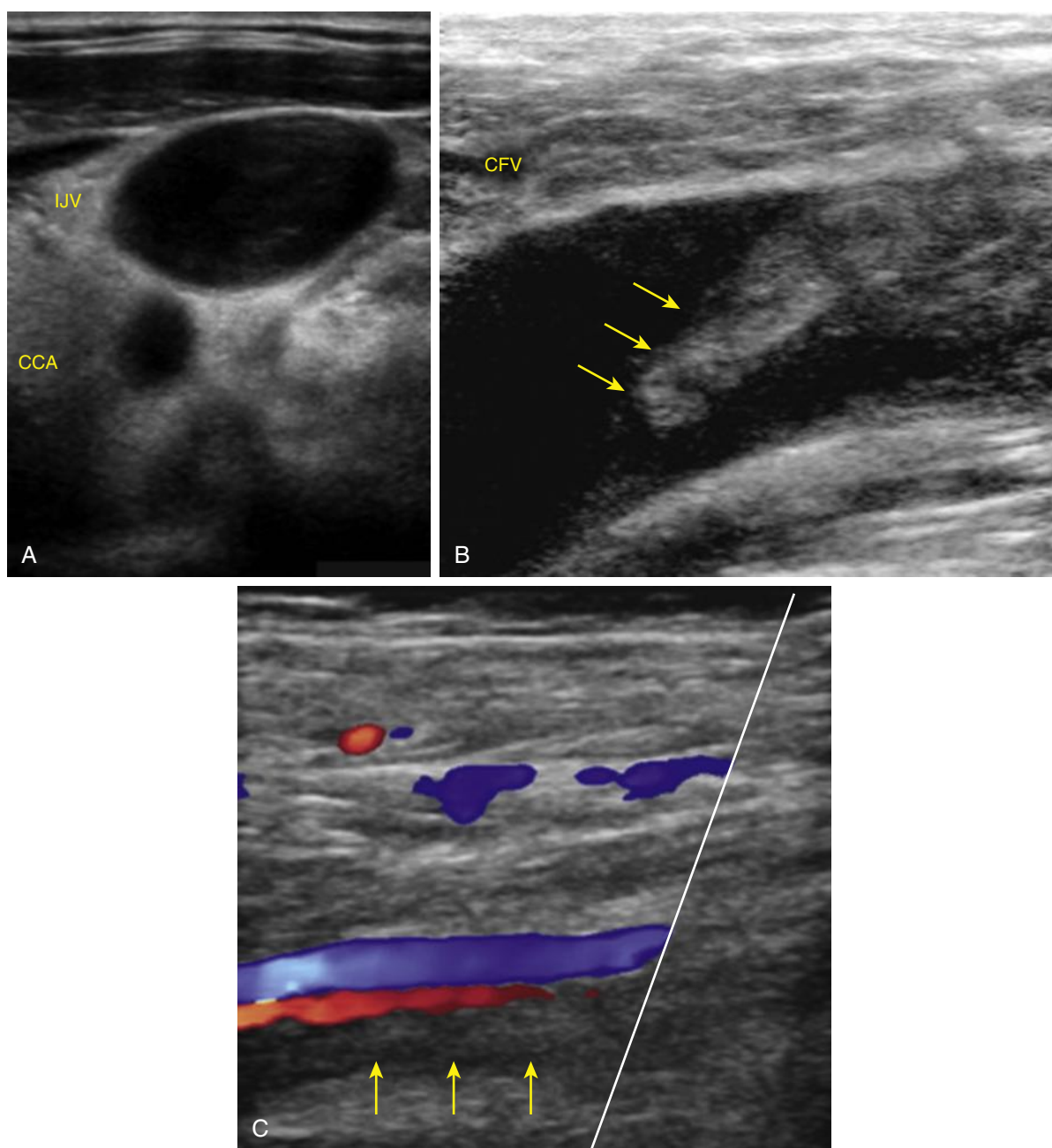


**Figure 25.4** Examples of Acute Deep Vein Thrombosis. (A) Dilated internal jugular vein with hypoechoic lumen. (B) Intraluminal thrombus in the common femoral vein with a “free floating tail” extending cephalad. (C) Absence of color filling in one of two peroneal veins.

When anticoagulation is not used to treat acute, isolated calf vein thrombi, follow-up duplex scanning over at least 2 weeks is recommended to evaluate for progression.<sup>30</sup>

Thrombosis of intramuscular veins, those within the gastrocnemius or soleus muscles, can be associated with localized calf tenderness. In rare cases, there can be propagation and subsequent pulmonary embolism, but isolated muscular calf vein thrombosis, has a low risk of extension. If extension is not observed within two weeks, it is very unlikely.<sup>30–33</sup> Patients with muscular calf vein thrombosis, with only transient risk factors, do not require anticoagulation, but they should be re-evaluated with duplex scanning

1 week after diagnosis to confirm thrombus resolution or absence of progression.<sup>34</sup>

## ILIAC VEINS AND INFERIOR VENA CAVA

The inferior vena cava (IVC) and iliac veins, like other intraabdominal and retroperitoneal vessels, can be difficult to evaluate due to overlying abdominal bowel gas and the decreased resolution of ultrasound when evaluating deeper structures. When possible, patients should fast for 6 hours prior to the

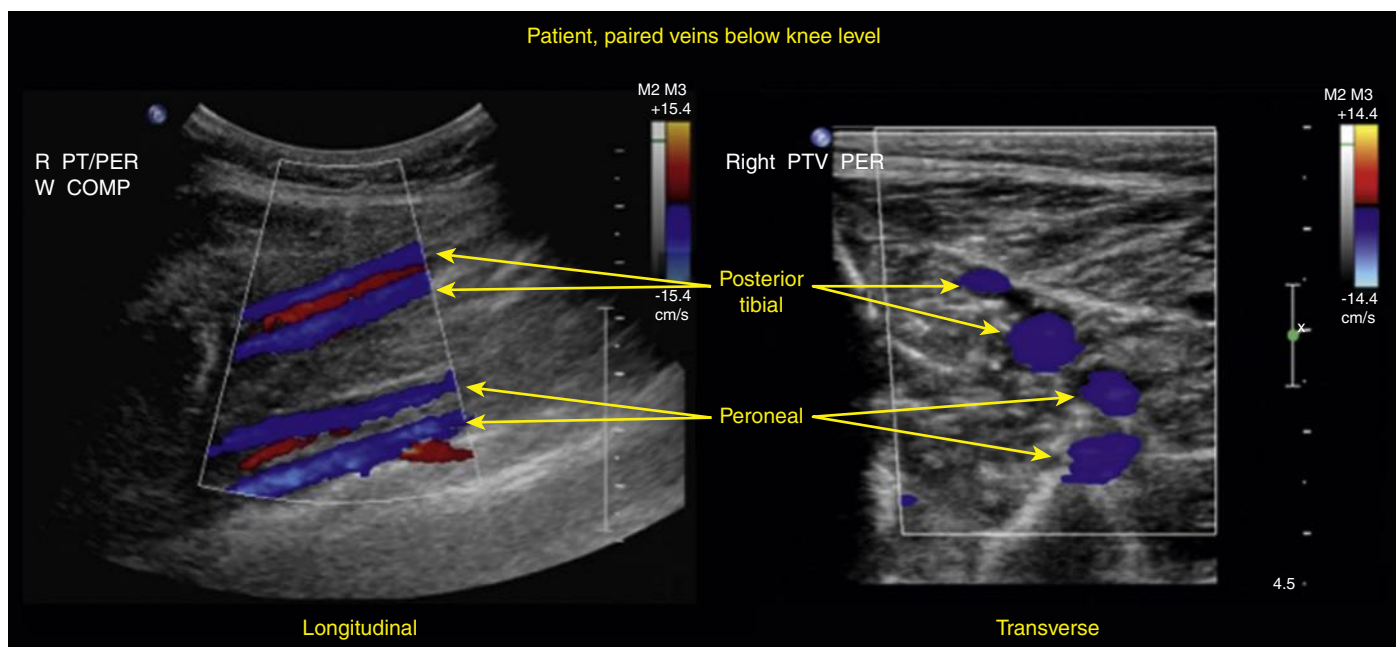


**Figure 25.5** Imaging of the posterior tibial and peroneal veins: left, longitudinal view; right, transverse view. Color flow imaging can confirm patency of the posterior tibial and peroneal veins. This can help to rule out calf DVT when vein wall coaptation with compression maneuvers is difficult to demonstrate. (Image from Dawson DL, Gray HM. Acute lower extremity deep vein thrombosis. In: Zierler RE, Dawson DL (Eds). *Strandness's Duplex Scanning in Vascular Disorders*, 5th edition. Philadelphia: Wolters Kluwer; 2016:240, Figure 19.17.)

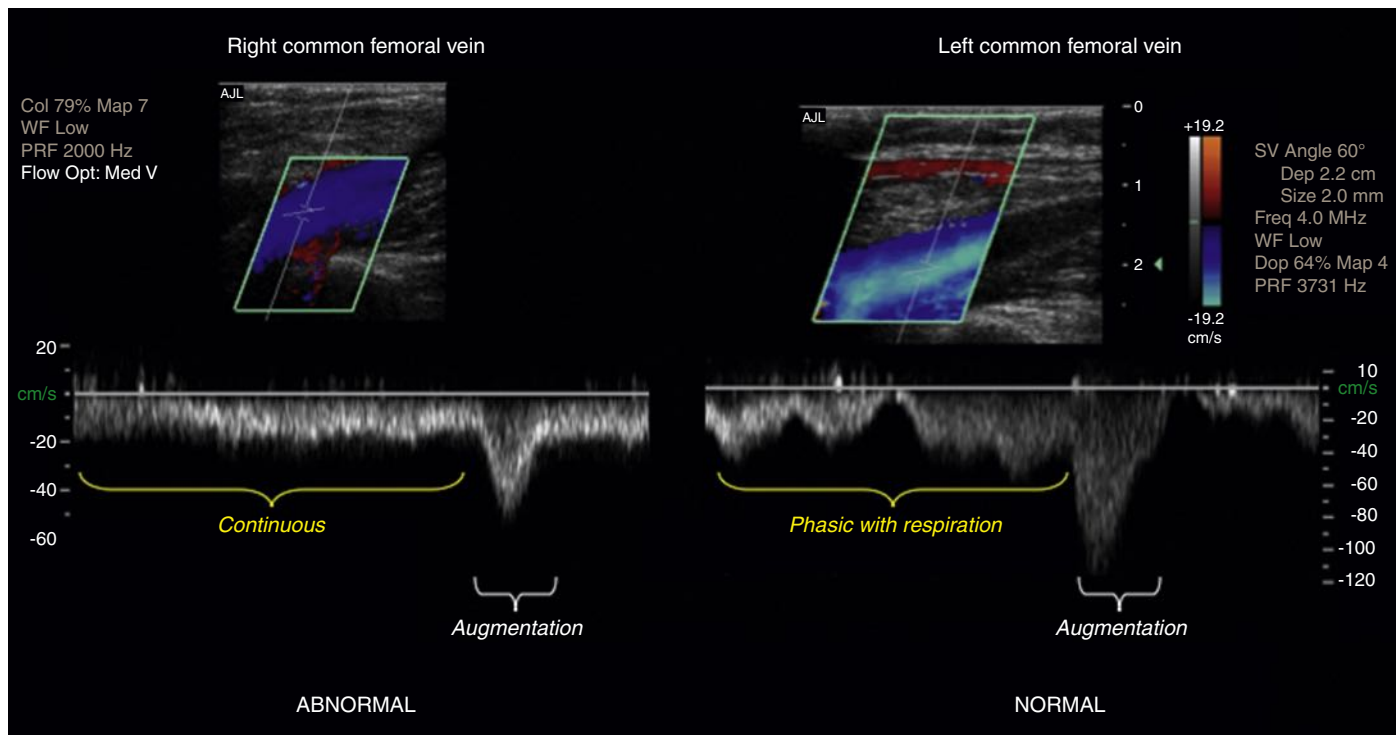


**Figure 25.6** Continuous venous flow (loss of normal respiratory phasic variation) indicates venous outflow obstruction. This indirect finding does not distinguish occlusion, non-occlusive thrombosis, chronic narrowing, or extrinsic compression. When seen in one common femoral vein, as shown, it indicates iliac vein obstruction. (Image from Dawson DL, Gray HM. Acute lower extremity deep vein thrombosis. In: Zierler RE, Dawson DL (Eds). *Strandness's Duplex Scanning in Vascular Disorders*, 5th edition. Philadelphia: Wolters Kluwer; 2016:233, Figure 19.2.)

examination to help reduce bowel gas. B-mode imaging and transverse probe compression maneuvers are seldom effective when evaluating abdominal or pelvic veins. Therefore, color flow and Doppler spectral waveforms are the primary

modalities for evaluation of the IVC and iliac veins. Color scale and gain settings are adjusted for the depth.

IVC flow should be spontaneous and phasic throughout. Greater pulsatility is seen in the inferior vena cava due to its

proximity to the heart. Absence of detectable flow by pulsed Doppler and color Doppler imaging suggests IVC occlusion or thrombosis.

External iliac and common iliac veins can be evaluated from the inguinal ligament to the level of the IVC. Augmentation of flow is produced with thigh compressions. Internal iliac veins are identified at their confluence with the external iliac veins. Complete or partial absence of color flow within the iliac veins may indicate intraluminal thrombus. Absence of spontaneous flow or lack of respiratory phasicity (continuous flow) may indicate a more central venous obstruction. Comparison of venous flow characteristics to the contralateral side may show indirect findings that indicate common iliac vein obstruction or compression (Fig. 25.6). Continuous venous waveforms with elevated flow velocities may be seen with venous stenosis.

Abnormal flow patterns in lower extremity veins may reflect abnormal (central) cardiovascular abnormalities. Heart failure or tricuspid valve regurgitation can increase venous flow variations with each cardiac cycle.

## DIAGNOSIS OF UPPER EXTREMITY DEEP VENOUS THROMBOSIS

Compared to the lower extremities, the upper extremities are less frequently affected by venous thrombosis.<sup>35–37</sup> Upper extremity DVT usually develops secondary to an identified inciting factor, such as the presence of central venous catheters (Fig. 25.7), pacemaker wires, or malignancy<sup>36,38</sup> (see Ch. 150, Acute Upper Extremity and Catheter-Related Venous Thrombosis). Primary upper extremity venous thrombosis, when it does occur, is most commonly due to extrinsic compression at the level of the thoracic outlet (Paget–Schroetter syndrome)<sup>36,38–43</sup> (see Ch. 126, Thoracic Outlet Syndrome: Venous).

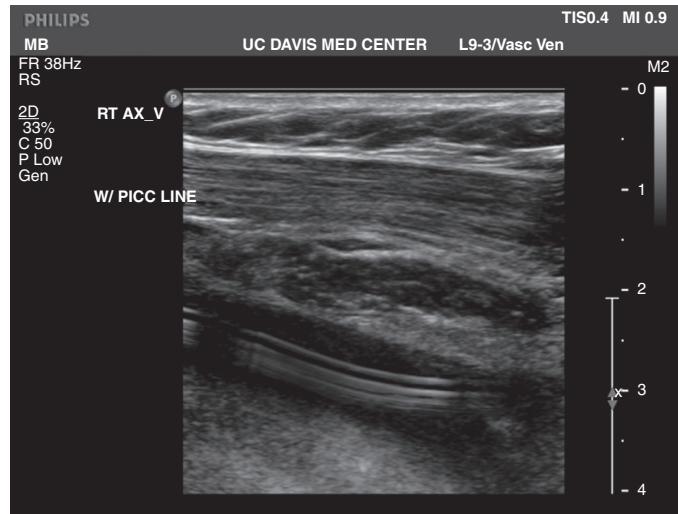


**Figure 25.7** Intraluminal foreign bodies can be visualized with B-mode grayscale ultrasound imaging. In this example, the echogenic walls of a catheter are seen within the anechoic lumen of the axillary vein. The echogenicity of the catheter produces the reverberation artifact, seen here. Upper extremity venous thrombosis is often associated with the presence of an indwelling catheter.

Catheter venography may be performed for diagnosis or as part of an intervention to treat upper extremity or central venous thrombosis or stenosis, but duplex scanning is the primary diagnostic modality in clinical practice.

Upper extremity venous duplex scanning, compared to lower extremity studies, has both similarities and differences. Venous incompressibility is similarly used in upper extremity examinations as a sign of vein thrombosis, but compression techniques are not practical for evaluation of veins under the clavicle or more centrally. The presence or absence of Doppler detectable flow can be used to assess for patency, but anatomic features limit direct B-mode imaging of the central venous outflow from the upper extremities (brachiocephalic veins and superior vena cava). Greater pulsatility is a normal finding in central veins or proximal upper extremity veins (Fig. 25.8). Indirect findings, such as asymmetry of venous flow velocity waveforms, may suggest the presence of central venous obstruction, but robust collateral formation may develop around chronically occluded segments, limiting the reliability of indirect findings. In some cases, occluded axillo-subclavian venous segments may be incorrectly identified as patent due to prominence of adjacent collateral veins.

A systematic review of diagnostic tests for clinically suspected upper extremity DVT found 84%–97% sensitivity and 93%–96% specificity for venous ultrasound techniques, including compression ultrasonography, Doppler ultrasonography, or combinations of techniques.<sup>44</sup> Methodological limitations, difference between studies, and small sample sizes limited the strength of the evidence.

## LIMITED OR POINT-OF-CARE ULTRASOUND EXAMINATIONS

Point-of-care ultrasound (POCUS) examinations have become more common as ultrasound imaging systems become smaller, less expensive, and more user-friendly. POCUS examinations can be used to evaluate for DVT in outpatient settings, emergency rooms, or inpatient settings.<sup>45</sup> It is anticipated that venous POCUS applications will have increasing importance in clinical practice.

With appropriate training and testing procedures, it appears that diagnosis of femoropopliteal DVT by providers at the point-of-care may approach the accuracy of vascular laboratory professionals.<sup>46</sup> Options include “two-point” compression ultrasound examination that only evaluates the common femoral and popliteal veins; or the “three-point” technique that assesses the common femoral vein at the saphenofemoral junction, the deep and femoral veins in the proximal thigh, and the popliteal vein.<sup>47</sup> Though the limited extent of POCUS examinations reduces exam sensitivity,<sup>48</sup> this shortcoming may not be a major issue when evaluating ambulatory patients who have appropriate follow-up and for whom there is a low suspicion for DVT.<sup>49</sup> The difference may be clinically relevant in high-risk patients, e.g. severely ill hospitalized patients.<sup>48,50</sup>

A systematic review that included meta-analysis including six studies with 2379 patients compared emergency department

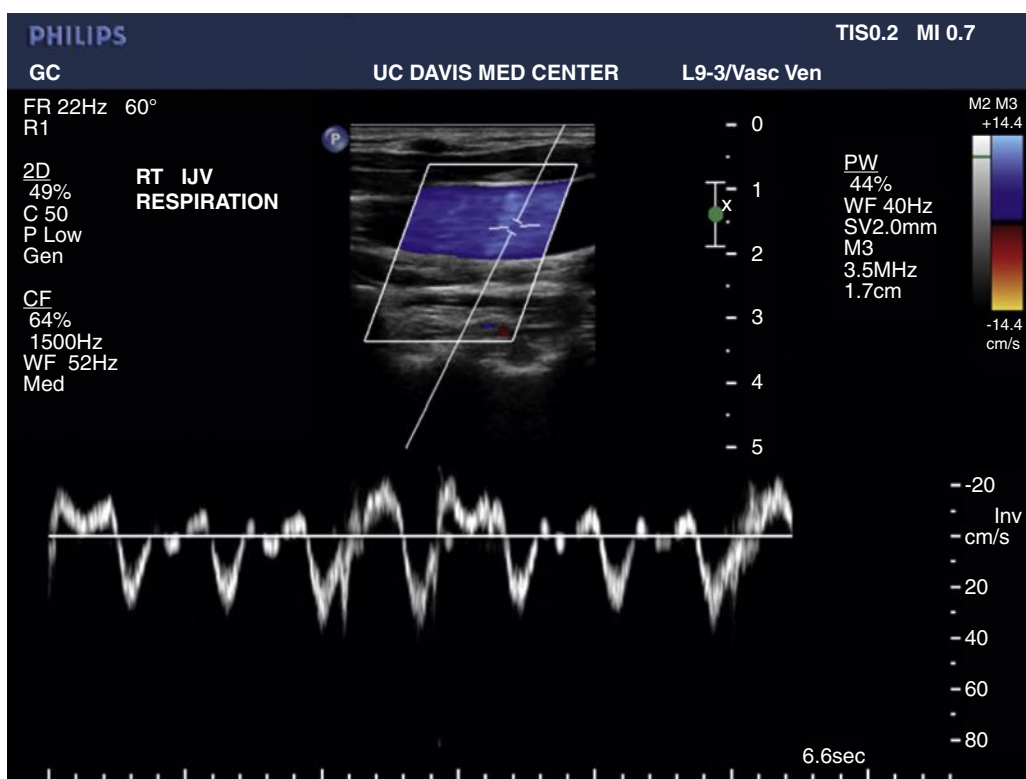


**Figure 25.8** The normal flow pattern in the internal jugular vein, like other veins close to the heart, is more affected by the cardiac cycle than by phasic respiratory variation. Flow reverses in atrial systole.

POCUS examinations to a reference examination (color flow duplex scan performed by a radiology department or vascular laboratory, or to angiography) for the diagnosis of DVT. The prevalence of DVT was high in these studies: 23% (498 in 2379 patients). The weighted mean sensitivity of emergency department POCUS, compared to the reference imaging test, was 96% with a weighted mean specificity of 97%, suggesting that with appropriate patient selection and testing procedures, point-of-care ultrasound can be a useful tool for DVT diagnosis.<sup>51</sup> The differences in the clinical characteristics of patients in various settings will substantially affect the pre-test probability of DVT, and the training and experience of the clinicians performing the examinations will affect the accuracy of the results.

In vascular laboratories, routine bilateral evaluation is not standard in the absence of bilateral symptoms or other indications.<sup>52,53</sup> Unilateral studies are a common and accepted practice, except when a prothrombotic state is suspected, there are systemic symptoms, or there is a suspicion of pulmonary embolism.<sup>54,55</sup> The incidence of unilateral thrombus in an asymptomatic extremity in an otherwise healthy individual approximates 1%.<sup>56</sup>

## DETERMINATION OF THROMBUS AGE

The manifestations and clinical significance of venous thrombus change over time. Acute thrombus in the deep veins is associated with the highest risk of thromboembolism. As the thrombus ages, it becomes less friable, increasingly fibrotic, and more firmly attached to the vein wall. Therefore, embolic risk declines over time. The age and characteristics of venous thrombus also affect the potential for success with thrombolysis

**TABLE 25.3** Ultrasound Features that May Determine Venous Thrombus Age

Feature	Early (Acute Deep Vein Thrombosis)	Late
Thrombus appearance	Hypoechoic, may be mobile or loosely attached to vein wall	Echogenic
Vein lumen size	Larger, distended	Smaller than adjacent artery, irregular
Vein wall	Thin, smooth luminal surface	Thickened, hyperechoic
Compressibility	Slightly deformable, "spongy" (may or may not occlude lumen)	Rigid, incompressible (may be partially recanalized)
Flow	Absent, or abnormal on color Doppler, with filling defects	Varying degree of recanalization
Collateral veins	Absent	Present
Valvular function	Competent (usually)	Incompetent (reflux)

or thrombus extraction procedures. Thrombus age may also affect the clinical manifestations of DVT. Thus, diagnostic assessments need to consider whether identified abnormalities reflect acute or chronic disease. Vascular laboratories are expected to have diagnostic criteria to report the appearance, characteristics and "age" of thrombus.

Typical features of acute DVT and its late sequelae are summarized in Table 25.3. The sonographic appearance of fresh

thrombus is relatively hypoechoic. Acute thrombus may have some deformability that can be demonstrated with probe compression. The vein may be occluded or there may be some residual flow around the thrombus, which may not be firmly attached to the vessel wall. In some cases, there may be a cephalad tail of free-floating thrombus that may be visualized moving in the lumen. As time passes, soft acute thrombus becomes firmer and more echogenic. Fibrin cross-links are formed and thrombus becomes more organized and adherent to the vessel wall. Subsequently, there may be thrombolysis and vein recanalization, or inflammatory changes in the thrombus and vessel wall may lead to fibrosis<sup>57,58</sup> (Figs. 25.9 and 25.10). Thrombus extent in deep veins generally regresses over time after acute DVT, but the rate and extent of thrombus resolution is variable.<sup>59</sup>

Venous thrombosis is appropriately described as “acute” when it first occurs. Various descriptive terms have been applied to venous thrombus as time passes. “Chronic venous thrombosis” has been used in the past to describe the appearance of late intraluminal obstruction after acute DVT, but the term may be inaccurate and confusing. Fibrotic tissue, not thrombus may be the principal content of residual intraluminal material. Abnormal ultrasound findings may persist for months or years after DVT.<sup>60</sup> Some providers mistakenly assume that anticoagulation needs to be prescribed if these findings are reported as “chronic DVT.” In the absence of recurrent thrombosis, however, there is generally no need for anticoagulation. Therefore, *chronic post-thrombotic change* has become the preferred term to describe what is seen months

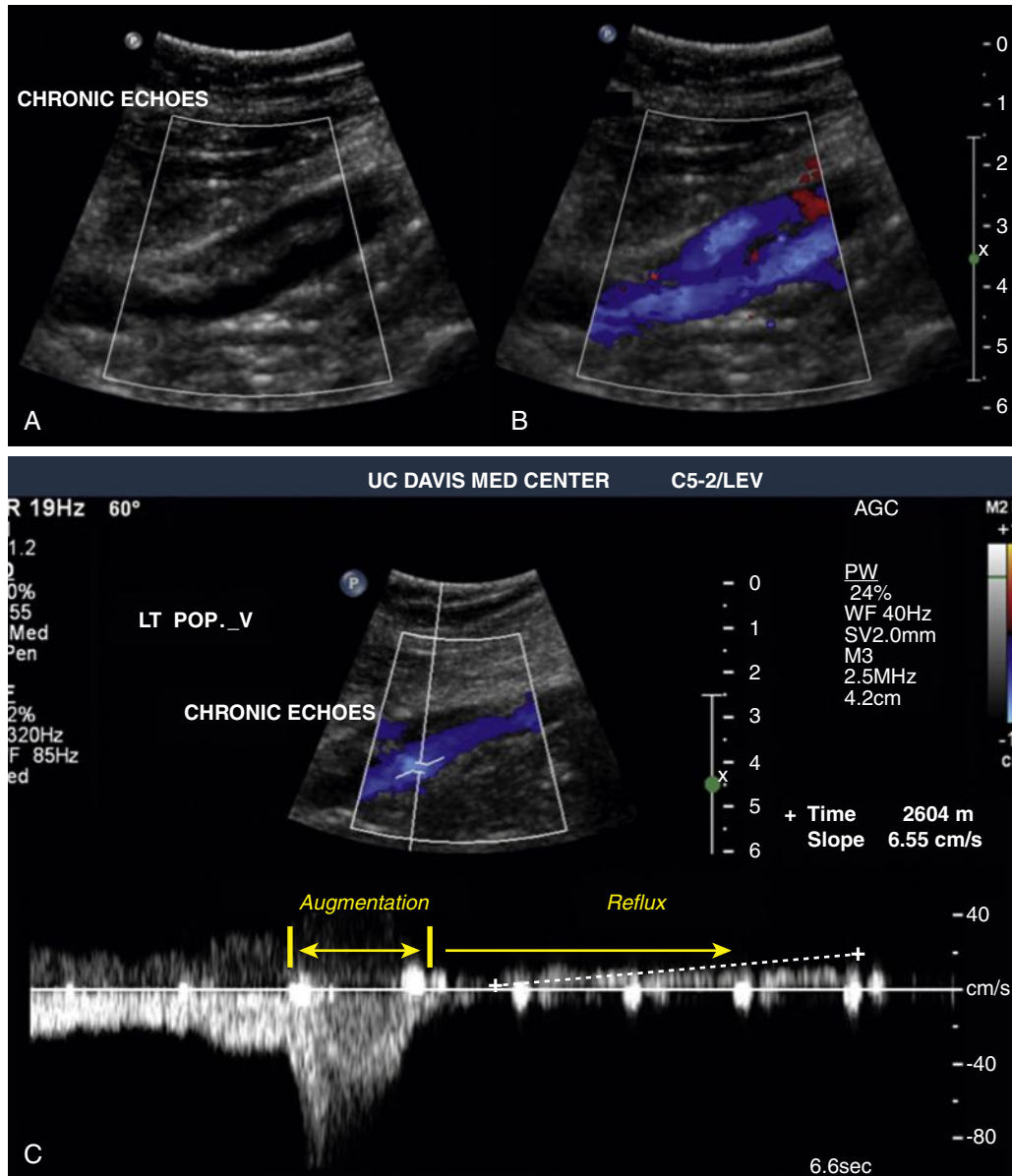


**Figure 25.9** Chronic Post-Thrombotic Changes in the Popliteal Vein. (A) Echogenic material is seen in the lumen. (B) Color flow Doppler shows partial recanalization. (C) Venous reflux indicates valvular incompetence (though retrograde flow is slow in this example from a supine patient).

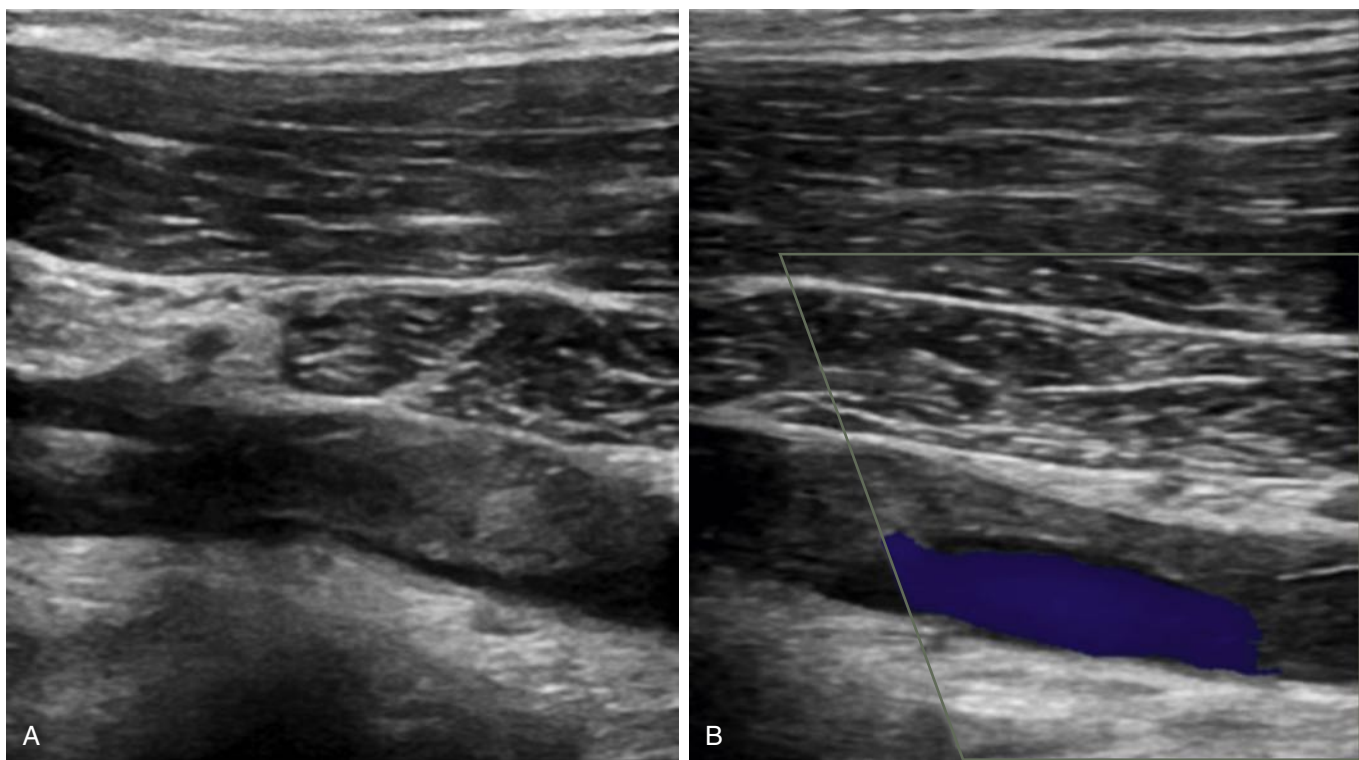


**Figure 25.10** Chronic Post-Thrombotic Changes in the Right Axillary Vein. (A) Echogenic material is seen in the lumen. (B) Color flow Doppler shows partial recanalization.

after an acute DVT. This nomenclature emphasizes the pathophysiology and may reduce misunderstandings about the implications of the diagnosis. Post-thrombotic changes may be associated with a variety of manifestations of chronic venous disease, including swelling, pain, skin change, and secondary varicosities (see Ch. 156, Chronic Venous Disorders: Post-Phlebitic Syndrome, Natural History, Pathophysiology, and Etiology).

The term “subacute venous thrombosis” is nonspecific and its use is no longer recommended. There is no standard definition for the duration of the acute period. There are no verified ultrasound criteria that can be used to determine the age of thrombus in the weeks or months after acute venous thrombosis. Further, the term does not have clinical significance. Clinical information, such as the duration of symptoms, may be considered when results of duplex scanning are reported. For the purposes of ultrasound diagnosis, when the findings are not clearly acute or chronic, the preferred terminology for reporting is *venous thrombosis, indeterminate age*.

Therapeutic decisions consider individual circumstances and risk factors. If DVT is found in an asymptomatic patient without clues from clinical history to help establish when the thrombosis occurred, it may be reasonable to consider anticoagulation, though no randomized trials have evaluated the value of anticoagulation for incidentally found venous thromboembolism. The benefit of anticoagulation may be less than for patients with symptomatic DVT, as the extent of the thrombosis may be less. Clinical assessment of DVT risk is especially important in this setting.

## NOVEL ULTRASOUND TECHNIQUES: ELASTOGRAPHY

Ultrasonic elastography uses ultrasound imaging to measure soft tissue strain to objectively assess the mechanical properties of tissues, such as hardness or stiffness.<sup>61,62</sup> This may be considered a correlate to palpation of tissue to determine its characteristics. Several ultrasonic elastography methods for tissue characterization in research and clinical applications (liver, breast masses, etc.) and elastography has been studied as an additional diagnostic modality for characterization of the chronicity of venous thrombus.<sup>63–66</sup>

Compression elastography (quasistatic elastography or strain imaging) uses ultrasound imaging with and without external probe compression. Areas of interest are compared/evaluated to determine relative deformation. More rigid tissues or thrombi have less deformation.<sup>61,67,68</sup> Tissue strain is determined by relative distortion.

Acoustic Radiation Force Impulse (ARFI) imaging uses energy of the insonated ultrasound to move tissues at microscopic level. ARFI provides a qualitative stiffness value along the axis of the beam. This technique is most widely used for evaluation of hepatic fibrosis, but studies of venous thrombus have used variations of this modality.<sup>64</sup>

In addition to the compression waves that propagate acoustic energy through tissue, there are also shear waves (transverse waves) created by oscillations at right angles to the direction of ultrasound beam. The compressional wave speed through tissue is related to the bulk modulus, while the shear wave speed is

related to the shear modulus. Because variations in tissue characteristics have a greater effect on the shear modulus than the bulk modulus, changes in the shear wave speed indicate structural differences in tissues. Because of this, several advanced imaging modalities use shear waves for tissue characterization. Feasibility studies with shear wave elasticity imaging (SWEI), or shear wave induced resonance elastography (SWIRE), have shown that thrombus elasticity can be quantitatively assessed.<sup>64,69,70</sup>

To date, however, elastography for thrombus characterization has not been standardized or sufficiently validated for their practical use in the vascular laboratory.

## DETERMINING THE DURATION OF THERAPY FOR ACUTE DVT

Benefits and risks of anticoagulant therapy should be considered when choosing the duration of anticoagulation for a first episode of unprovoked venous thromboembolism.<sup>30</sup> Factors affecting risk of recurrence after cessation of treatment include continued presence of provoking risk factor, unprovoked VTE, and active malignancy. If there is a reversible VTE risk factor, the recurrence risk is low if the provoking factor was recent surgery. Isolated calf vein DVT has half the risk of recurrence compared to proximal DVT and PE. On the other hand, a second or subsequent episode of VTE is estimated to have a 50% higher of recurrence risk compared to a first time VTE.<sup>30</sup>

Good data are lacking regarding recurrent VTE risk after stopping anticoagulation in cancer patients, as treatment is generally continued in these high-risk patients because of their high recurrence risk.

Venous ultrasound findings may have some value in predicting recurrence risk. Residual vein thrombosis (RVT) may indicate a continuing prothrombotic state.<sup>71</sup> The Duration of Anticoagulation based on Compression UltraSonography (DACSUS) study found residual thrombus in the proximal veins was associated with an increased risk of recurrent thrombosis after a first episode of DVT. Conversely, absence of RVT identified patients at very low risk for recurrence. A subsequent study similarly found that in the absence of RVT, a short period of DVT treatment may be sufficient. For those with persistent RVT, treatment extended to 2 years substantially reduced, but did not eliminate, the risk of recurrent thrombosis.<sup>72</sup> Among 409 patients with unprovoked DVT, 33% did not have RVT and anticoagulation was stopped after three months, with a recurrent DVT rate of only 1.4%. Patients found to have residual thrombus ( $n = 273$ ) received anticoagulants for an additional 21 months. Anticoagulation was stopped after a total of 24 months and the subjects were again evaluated for residual thrombus. The rate of recurrent thrombotic events in the following year was 1.4% in those with no RVT after extended therapy, but 10.4% in those with persistent RVT.

The Cancer-DACUS study evaluated association of residual vein thrombosis to recurrent VTE in patients with lower extremity DVT and cancer.<sup>73</sup> In cancer patients with a first DVT, treated for 6 months, the overall risk of thrombosis after cessation of anticoagulation was 15% at 1 year. The absence of RVT

identified a subgroup at low risk for recurrent thrombosis, but this study's findings were not considered compelling enough to warrant a change in the guideline for long-term anticoagulation treatment for VTE in patients with cancer.<sup>30</sup>

D-dimer level is another predictor of recurrent thrombosis in patients after an unprovoked first episode of VTE. Recurrence rates were found to be higher for patients with positive d-dimer results compared to those with a normal D-dimer level (3.5% vs. 8.9%).<sup>74</sup> The PROLONG study looked at residual venous obstruction, alone and in combination with D-dimer, to predict risk for recurrence after anticoagulation withdrawal following a first episode of DVT. An elevated D-dimer at one month after anticoagulation withdrawal appeared to be a risk factor for recurrence, while residual venous obstruction at the time of anticoagulation withdrawal was not.<sup>75,76</sup>

## DIAGNOSIS OF RECURRENT THROMBOSIS

The diagnosis of recurrent venous thrombosis can be challenging.<sup>77,78</sup> Previous DVT is a known predictor of risk for venous thrombosis, particularly when the predisposing factor was a non-surgical condition or if no clinical risk factor was identified.<sup>79</sup> Previous DVT is also a cause for symptoms occurring months or years after the acute event.

Patients with prior DVT may undergo venous duplex ultrasound to evaluate newly recognized (or chronic) leg pain or swelling; however, abnormal findings may not be indicative of acute thrombosis. Visualized abnormalities may be residua of prior DVT (chronic post-thrombotic changes), not recurrent DVT. Residual vein incompressibility or other post-thrombotic abnormalities can be found in approximately 80% of DVT patients at 3 months<sup>80,81</sup> and up to 50% at 1 year.<sup>80,82,83</sup>

Distinguishing acute from chronic findings is important, as post-thrombotic syndrome is not treated with anticoagulation (in the absence of recurrent thrombosis or another indication). If venous reflux is demonstrated, post-thrombotic syndrome may fully explain chronic or persistent symptoms.

There can be recurrent acute thrombosis in an abnormal segment ("acute on chronic" DVT) or there may be new acute DVT in a previously normal venous segment. Imaging findings typical of acute thrombosis, in combination with other chronic post-thrombotic changes, suggest the recurrent, acute DVT.

Findings from a single ultrasound imaging study may be insufficient to make the diagnosis of recurrent DVT. Comparison with a prior venous duplex scan is the most reliable means to distinguish new from chronic abnormalities.<sup>84</sup> A study performed after completion of a course of anticoagulation establishes a new baseline for future comparison.<sup>85</sup> This examination can determine the post-treatment status of venous segments previously shown to have acute thrombus, including: whether there is persistent occlusive thrombus, partial recanalization or post-thrombotic change, or if there has been complete recanalization of the segment. If a subsequent examination is abnormal, comparison with the post-treatment baseline study allows the interpreting physician to distinguish

persistent abnormalities from new ones. Late recanalization (9 to 12 months) after DVT may occur; so imaging findings after DVT should not be assumed to be static over time.<sup>86,87</sup>

When a post-treatment study is unavailable for comparison, the clinical, laboratory, and imaging findings should be considered together.<sup>88</sup> Recurrent DVT is more likely when there are new or persistent risk factors (malignancy, acute illness, injury, recent surgery, etc.). A normal d-dimer level is a strong indicator that abnormal venous imaging findings are due to chronic post-thrombotic changes. An elevated d-dimer level is not diagnostically useful, though.<sup>76</sup> d-dimer testing frequently yields false-positive results associated with other conditions (cancer, chronic diseases, advanced age, inflammatory status, infections, etc.).

## SUPERFICIAL VEINS

Patients may be referred to the vascular laboratory when symptoms prompt concern for deep vein thrombosis, but other venous problems, including superficial vein disorders, may also need to be considered.<sup>89,90</sup> Examination of the great saphenous vein at the level of the saphenofemoral junction is a routine part of a lower extremity veins evaluation for DVT, but a more thorough evaluation of the superficial veins is needed when patients report symptoms of localized pain, swelling, erythema, palpable venous cord, or painful varicosities. Imaging of superficial veins is also used to determine suitability of venous segments as conduits for vascular reconstruction.

*Superficial venous thrombosis* (SVT) is the most broadly applicable term to describe thrombotic occlusion of a superficial vein. The term *superficial thrombophlebitis* may be used when clinical findings of inflammation are present (pain, tender vein, palpable venous cord, erythema; see Ch. 151, Superficial Thrombophlebitis and Its Management).

Inflammation is more common with superficial vein thrombosis than with deep vein thrombosis. The term *suppurative thrombophlebitis* is used when there is bacterial infection of a thrombosed vein.

Thrombosis of lower extremity superficial veins is commonly associated with varicose veins, but 5%–10% of patients with superficial venous thrombosis may have non-varicose veins. In this setting, phlebitis may be a marker for hypercoagulable conditions, malignancy, vasculitis, or other systemic disease.<sup>76</sup> The Trouseau sign of malignancy, characterized by recurrent, migratory thrombosis in superficial veins, including uncommon sites such as the torso and upper extremities, is associated with adenocarcinoma, especially of pancreas or lung origin.<sup>91</sup> Inherited (factor V Leiden, prothrombin G20210A mutation, and MTHFR C677T mutation) and acquired thrombophilias are associated with an increased risk of superficial vein phlebitis and thrombosis, as well as an increased risk of thrombus progression to involve the deep veins.<sup>92</sup> Thrombophlebitis of upper extremity superficial veins most commonly occurs as a complication of venipuncture and intravenous catheter use<sup>93</sup> (see Ch. 40, Disorders of Coagulation: Hypercoagulable States).

The ultrasound findings used to diagnose superficial venous thrombosis are similar to those for deep vein thrombosis:

venous distension, incompressibility, intraluminal echogenic material, and the absence of flow. With inflammation, there can also be vein wall thickening, perivascular edema, and tenderness with examination.

It is important to determine the extent of superficial vein thrombus, as progression of thrombosis on serial examinations, or the proximity of the thrombus to the confluence with the deep system (saphenofemoral junction) may help guide therapy. Anticoagulation for SVT reduces the incidence of thrombus extension or recurrence in high risk cases.<sup>92,94</sup> In a single center series of patients with SVT who were not anticoagulated, progression to involve the deep veins was seen in 11%, most commonly through the saphenofemoral junction.<sup>95</sup> Based on observations like these, it has been recommended that great saphenous vein thrombosis in the proximal thigh should be treated with anticoagulation or at least followed by serial duplex ultrasound evaluation.

In a cross-sectional, prospective epidemiologic cohort study of consecutive patients with symptomatic lower extremity superficial venous thrombosis, 10% developed thromboembolic complications at 3 months (pulmonary embolism, 0.5%; DVT, 2.8%; extension of SVT, 3.3%; and recurrent SVT, 1.9%), despite therapeutic anticoagulation of more than 60%.<sup>96</sup> Risk factors for complications at three months were male sex, history of DVT or pulmonary embolism, previous cancer, and absence of varicose veins.

Evaluation of lower extremity superficial veins is an integral component of examinations of patients with chronic venous insufficiency. Varicose axial veins (great saphenous and short saphenous veins) and varicose tributaries are assessed for patency, diameter, and their course. As superficial vein anatomy and patterns of varicose vein development are variable, a worksheet with a diagram to illustrate the sonographer's findings is particularly useful. Prior to procedures to treat varicose veins, the duplex scanning to define the venous segments with reflux and to demonstrate the relationships of varicosities or symptomatic sites to the sources of reflux is needed.

## VEIN MAPPING

An arteriovenous fistula (AVF) for dialysis access is the preferred option for long-term dialysis, but procedures to create AVFs have a considerable failure rate. Preoperative imaging helps determine suitability of superficial veins that might be used for creation of an AVF. Routine preoperative vascular ultrasound improves AVF outcomes in terms of patency and use for dialysis.<sup>97</sup> It can guide the selection of which vein segment to use and which type of procedure to perform. In a randomized, prospective study, addition of ultrasound imaging to the preoperative assessment was found better than physical examination alone, with a significantly lower rate of immediate technical failure and better rates of fistula maturation to usability. Assisted primary patency at 1 year was significantly better for the ultrasound group (80% versus 65%,  $P = 0.012$ ).<sup>98</sup>

When hemodialysis will be needed for management of advanced kidney disease, National Kidney Foundation guidelines recommend that access should be placed distally and in the

**TABLE 25.4**

Characteristic of Superficial Vein Segments to Consider Prior Use as Bypass Conduit (Great Saphenous, Short Saphenous, Cephalic, and Basilic Veins)

	Compressibility	Diameter	Other Factors to be Considered
Findings considered <b>suitable</b> for use as bypass conduit	<ul style="list-style-type: none"> <li>Fully compressible at all levels</li> <li>No intraluminal echoes</li> </ul>	≥0.20 cm	Vein should be of uniform caliber, without tortuosity
Findings considered <b>unsuitable</b> for use as bypass conduit	<ul style="list-style-type: none"> <li>Intraluminal echoes</li> <li>Incompressible</li> <li>Thickened walls</li> </ul>	<0.20 cm	Tortuosity; varicose segments, multiple branches, location superficial to fascia

upper extremities whenever possible, and that options for arteriovenous fistula (AVF) placement should be considered first.<sup>99</sup> Further, patients should be considered for construction of new autologous fistula after dialysis AV access failure. Upper extremity veins 2.5 mm or greater in diameter are sought for AVF creation,<sup>100</sup> though there is not consensus about an absolute threshold. A 2-mm vein may be usable. A larger vein is better.

Ultrasound vein mapping prior to revascularization procedures can assess superficial veins for potential suitability as bypass conduits<sup>101</sup> (Table 25.4). Preoperative vein mapping reduces costs and improves outcomes for patients undergoing infrainguinal bypass surgery.<sup>102,103</sup> Vein mapping in the vascular laboratory or a point-of-care ultrasound examination prior to arteriography provides practical information that can help select between an endovascular intervention or an open surgical approach. For a patient with critical limb ischemia who needs durable revascularization, a bypass with an autologous vein graft might be preferred. However, an endovascular approach might be selected for a patient who does not have sufficient vein to perform a bypass.

Guidelines for lower extremity vein mapping recommend examinations be performed with the patient in reverse Trendelenburg position using a high frequency transducer.<sup>104</sup> For standard vein mapping, the entire length of the great saphenous and small saphenous vein (if indicated) are evaluated with diameter measurements in transverse views. The vein is evaluated for anomalies or anatomic variants and large branches are noted. In addition to measuring diameter, the vein is assessed for evidence of prior thrombosis or phlebitis, checking for compressibility, wall thickening, intraluminal echoes, and sclerotic valve leaflets (Fig. 25.11). It may be helpful to mark the course of the superficial veins to facilitate positioning of skin incisions.

A venous tourniquet is used to dilate the veins for upper extremity vein mapping.<sup>105</sup> An elastic tourniquet is placed at the axilla for upper arm vein mapping and at the antecubital fossa for the forearm. The diameters of the brachial, cephalic, and basilic veins are measured in transverse view, throughout their course.

## EVALUATION FOR CHRONIC VENOUS DISEASE: VENOUS INSUFFICIENCY

The vascular laboratory has an integral role in the evaluation of patients with chronic venous insufficiency.<sup>106–110</sup>

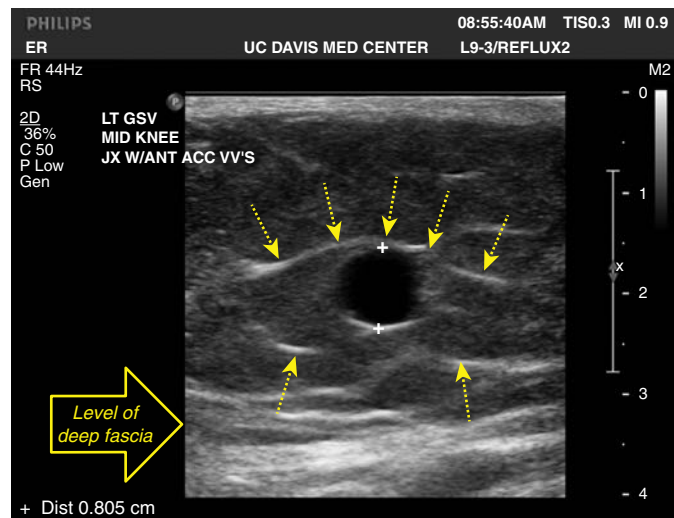


**Figure 25.11** Lower extremity superficial veins are measured with electronic calipers. Measurements are performed with the leg in a dependent position. Superficial veins are distinguished from deep veins by their location between the skin and muscular fascia. A layer of subcutaneous fascia envelops the great saphenous vein (dashed arrows).

The CEAP system (Clinical–Etiology–Anatomy–Pathophysiology) is a descriptive classification (developed in 1993, updated most recently in 2020) that standardizes reporting and clinical documentation of chronic venous disease.<sup>111,112</sup> Diagnostic assessments for chronic venous disorders are organized into levels of testing, which may be included in the reporting of CEAP classification:

**Level I:** office visit, with history and clinical examination, which may include use of a hand-held Doppler.

**Level II:** noninvasive vascular laboratory testing, including duplex color scanning, and plethysmographic methods.

**Level III:** invasive investigations or more complex imaging studies, including ascending and descending venography, venous pressure measurements, computed tomography venous scanning (CTV), or magnetic resonance imaging (MRI).

The Level II assessment with duplex ultrasound scanning allows for objective evaluation of the affected anatomic levels and locations (A), as well as the pathophysiology (P) involved.

The scanning techniques for venous insufficiency testing evolved from the techniques developed for DVT diagnosis, with increased emphasis on the Doppler evaluation of flow patterns.<sup>54,107,113</sup> The limb swelling and pain associated with acute DVT are due to venous obstruction. Chronic venous insufficiency (CVI) is the result of abnormally elevated venous



**Figure 25.12** Examinations to evaluate for reflux (valvular incompetence) in lower extremity veins should be performed with the patient standing. Reflux is elicited with release of a pneumatic cuff while imaging the vein approximately 5 cm about the cuff.

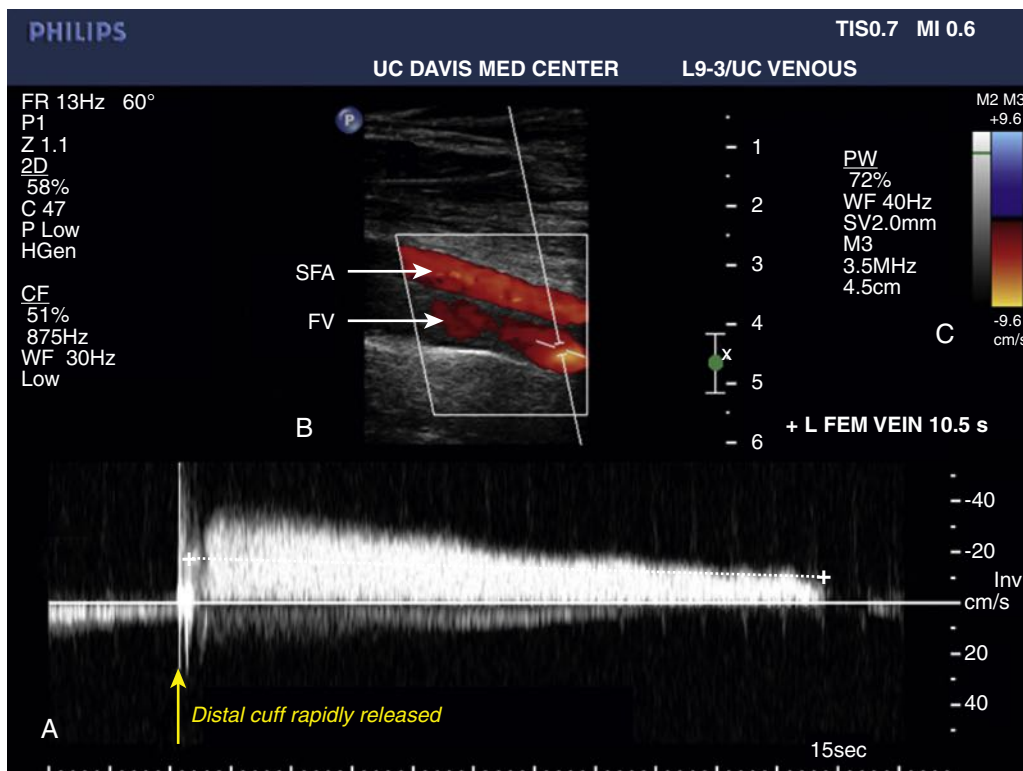


**Figure 25.13** Deep Vein Reflux with Standing Examination. (A) Slow antegrade flow is demonstrated with pulsed Doppler waveform. Rapid reversal of flow (negative values shown above baseline) immediately after release of pneumatic cuff on distal thigh. (B) Color flow image shows the same direction of flow in the superficial femoral artery (SFA) and the adjacent femoral vein (FV). (C) The color map with red colors below the baseline indicates flow vector away from the transducer (cephalad to caudal direction in this example.)

**TABLE 25.5** Avoiding Common Pitfalls in Venous Ultrasound Testing

Potential Error	Situation	Indicated Action	Comment
Failure to diagnose iliac or caval DVT	Femoropopliteal or limited examination	<ul style="list-style-type: none"> <li>Evaluate CFV waveforms for presence of respiratory phasicity, symmetry</li> <li>Consider more central extension of thrombus if DVT seen in CFV</li> </ul>	Perform duplex scan of abdominal and pelvic veins
Failure to diagnose calf vein DVT	Femoropopliteal or limited examination	<ul style="list-style-type: none"> <li>Directly assess posterior tibial and peroneal veins</li> <li>Directly evaluate muscular deep vein (sural and soleal veins)</li> </ul>	Consider assessment of calf veins to be mandatory for patients presenting with calf pain
False-positive DVT diagnosis based on B-mode imaging	Lack of compressibility due to high venous pressure or incompressibility of surrounding tissue (e.g., adductor canal) Imaging may be limited by obesity or edema	<ul style="list-style-type: none"> <li>Include pulsed Doppler and color Doppler assessment of flow</li> <li>Evaluate for augmentation of flow with distal limb compression</li> </ul>	
False-positive diagnosis of recurrent DVT	Prior DVT; residual post-thrombotic changes, including echogenic intraluminal material, obstruction	<ul style="list-style-type: none"> <li>Evaluate for features of chronicity (see Table 25.3)</li> <li>Compare current findings to prior examinations; evaluate for thrombus in previously patent segments</li> <li>Check d-dimer level; low or normal in absence of acute (recurrent) thrombosis; high value lacks diagnostic significance</li> </ul>	Patients with post-thrombotic syndrome present with pain and swelling, which may suggest clinical diagnosis of acute DVT
False-positives or false-negative findings on examination for reflux	Examination performed with patient supine Use of Valsalva maneuver to elicit reflux	<ul style="list-style-type: none"> <li>Evaluate patient in upright position</li> <li>Use release of distal compression to elicit reflux</li> </ul>	Facilitated by use of positioning aids and automated device for cuff inflation and rapid deflation
Venous disease incorrectly excluded	DVT examination protocol is used to evaluate patients referred for chronic limb pain and swelling; findings reported as negative for DVT	<ul style="list-style-type: none"> <li>Evaluate for valvular competence/reflux with upright examination</li> </ul>	Patients with chronic venous insufficiency due to valvular incompetence often have no thrombus or obstruction

Abbreviations: DVT, deep vein thrombosis; CFV, common femoral vein; PE, pulmonary embolism; CT, computed tomography.

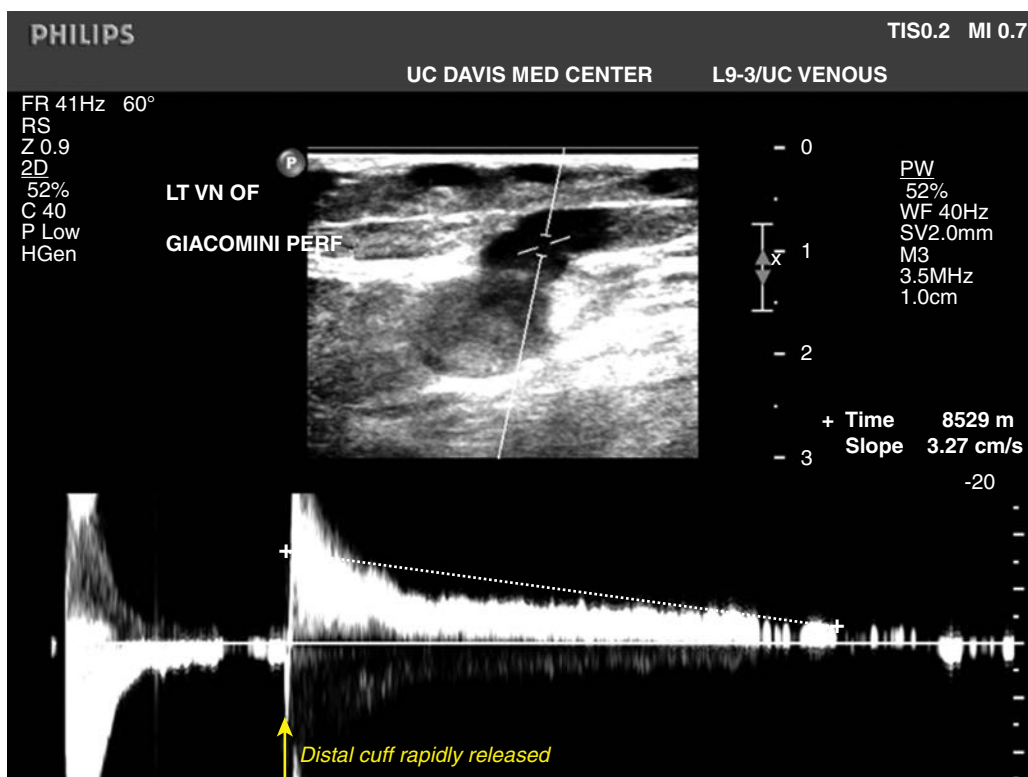


**Figure 25.14** Reflux in an Incompetent Perforating Vein. Rapid reversal of flow (negative values shown above baseline) immediately after release of pneumatic cuff on proximal calf. Though the lumen of the vein deep to the fascia appears echogenic, this is an artifact from high grayscale gain setting. The fascial gap measured 0.52 cm. Large perforators often have incompetent valves.

pressure due to outflow obstruction (similar to acute DVT), pathologic reflux, or a combination of the two. Chronic venous stenosis or occlusion can be the cause of continued symptoms. Venous hypertension due to outflow obstruction worsens when limb blood flow is increased. This is the pathophysiologic mechanism of venous claudication.<sup>114,115</sup>

Incompetence of venous valves is the most common etiology of chronic venous insufficiency.<sup>116</sup> Valvular incompetence can be primary (without an underlying or antecedent disorder) or secondary, where valvular dysfunction is the result prior venous thrombosis or injury.<sup>117</sup> Competent venous valves and muscular pumping of venous blood are needed to move blood from the lower extremities to the central circulation when upright.<sup>118</sup> When valves are incompetent, the musculovenous pump becomes ineffective. Distal limb pressure is not decreased with walking as it should, and ambulatory venous hypertension results.

A duplex scan for CVI directly evaluates for obstruction by examining the appearance and compressibility of the vein, as well as flow patterns, including assessment with provocative maneuvers to augment antegrade flow or to cause retrograde flow. Indirect findings that may indicate more central venous obstruction include asymmetry in flow velocity, lack of respiratory flow variation, or lack of spontaneous flow.

A 4- to 7-MHz linear array transducer is commonly used, though a lower frequency curved array probe may be useful for large or obese patients. A higher-frequency probe is best for

scanning superficial veins. Testing for deep and superficial vein reflux is properly performed with the patient upright, with the lower extremity externally rotated (Fig. 25.12). The heel may be on the ground, with weight-bearing on the opposite limb, or a step may be used to offload the examined side.<sup>108</sup>

Though some venous valves may be visualized with high-resolution B-mode imaging, the functioning of the bicuspid venous valves is determined observing the direction of blood flow. Normally, in the supine position, venous flow is phasic with respiration. Retrograde flow may be physiologic, as valve closure may not occur if the velocity of the retrograde flow is less than 30 cm/s, too slow to close the valve leaflets. In the upright position, vein valves open to allow antegrade flow, then snap shut as forward flow ceases and flow reversal commences.

Venous reflux is defined as retrograde flow of abnormal duration (Fig. 25.13). Venous reflux can be characterized as axial if there is uninterrupted retrograde flow from the groin to the calf. Segmental reflux involves only some segments of the venous system, while other segments retain competent functioning valves.<sup>119</sup>

Techniques to elicit reflux include increasing intraabdominal pressure using a Valsalva maneuver (for the common femoral vein or the saphenofemoral junctions) or by manual compression and release of the limb distal to the point of examination. The preferred method, however, is to use a standardized technique with calibrated inflation and rapid (less than 0.3 seconds)

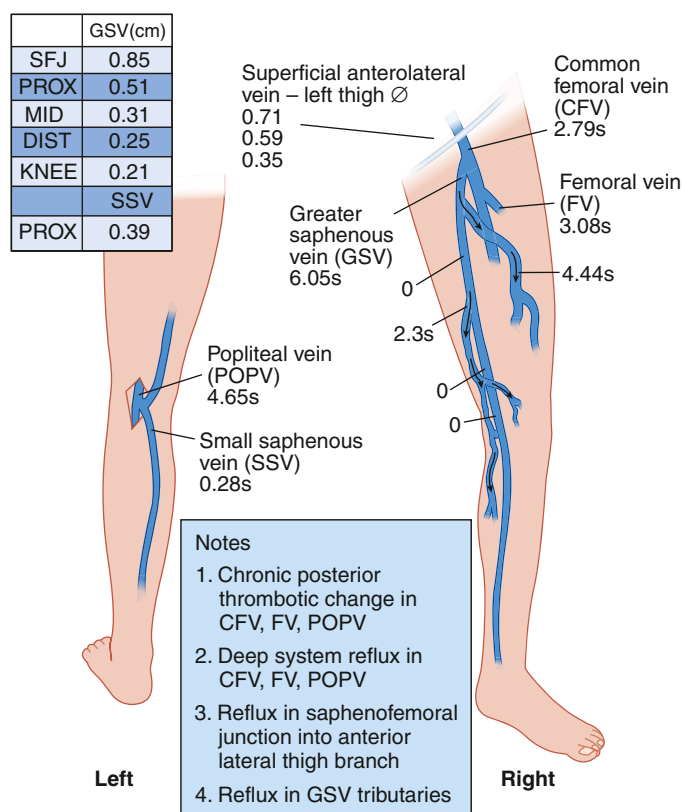


**Figure 25.15** This figure is representative of a drawing by a vascular technologist. Drawings, sketches or other graphics can be invaluable for documentation of the location of incompetent venous tributaries, variant anatomy, location of perforating veins, and other observations. The diameter of deep and superficial vein segments, perforating veins, and varicosities can be recorded. Duration of reflux after provocative maneuvers can be documented. In this example, the patient had post-thrombotic syndrome with chronic post-thrombotic changes and reflux in the deep veins, reflux in the saphenofemoral junction into a saphenous tributary, but not into the great saphenous vein (GSV) in the mid and distal thigh. There is tributary reflux creating branch varicosities, but most of the GSV has competent valves.

deflation of a pneumatic cuff applied distally on the limb.<sup>120</sup> The advantage of the distal cuff deflation technique was emphasized by van Bommelen et al.<sup>121</sup> This technique, when performed in the standing position, initiates retrograde flow of 30 cm/s or greater, the physiologic condition needed to reliably close normal valves. The supine position is not physiologically relevant and should not be used for reflux testing, as both false-positives and false-negatives result.<sup>120,122–124</sup> Modest degrees of reverse Trendelenburg (15 degrees) do not provide the consistency of upright testing.<sup>125</sup>

A prospective study to establish the upper limits of normal for the duration of retrograde flow in lower extremity veins suggested that the cutoff value should be 1.0 seconds for identifying deep vein reflux in the femoral and popliteal veins; the cutoff value to define reflux should be greater than 0.5 seconds in the superficial veins and the deep veins of the calf; and outward flow in perforating veins should be considered abnormal if greater than 350 ms.<sup>126</sup> A multicenter study suggested a 0.5-second threshold for defining reversed venous flow as abnormal could be used for all veins.<sup>127</sup> Use of this standard value may provide diagnostic sensitivity. Diagnostic reports should include the measured reflux time in each examined vein, the patient's position (if not standing, the reason), and the reflux-provoking maneuver used (Table 25.5).

## PERFORATING VEINS

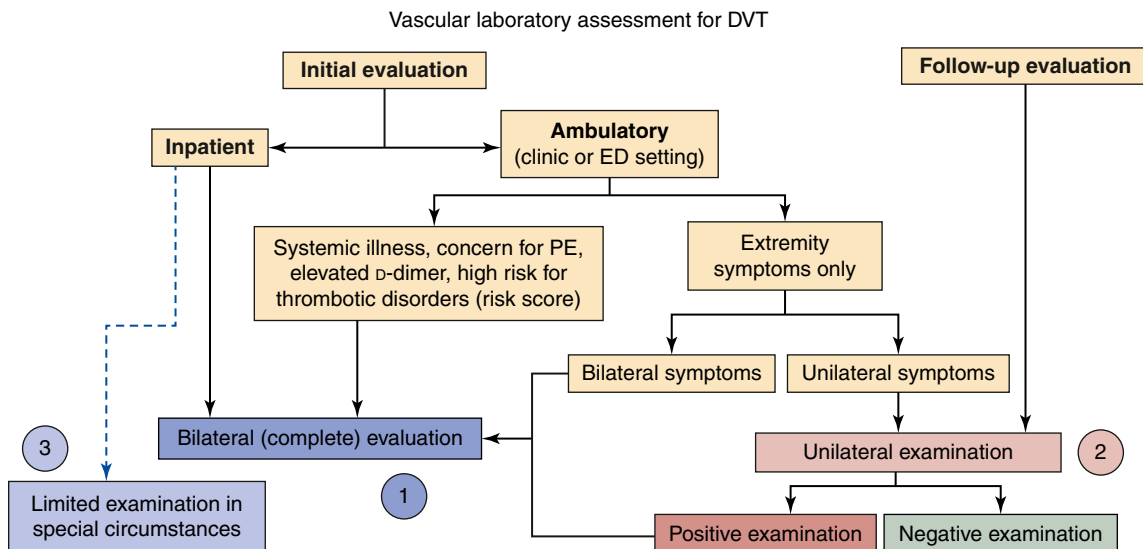
Perforating veins in the lower extremities connect the superficial veins to the deep veins. They pass through the fascia that separates the muscular compartments from the subcutaneous tissue. Normal venous flow is from superficial to deep, but valves are only present in larger perforators. Perforating veins less than 1 mm in size do not have valves.

Scanning of perforators is best done with imaging in the transverse plane, focusing on the boundary between the deep and superficial compartments, looking for the interruptions in the fascia through which the perforating veins pass. Flow in perforating veins may be bidirectional, but reflux is diagnosed when there is net outward (deep to superficial) flow (Fig. 25.14).

Perforating veins may be evaluated selectively, e.g., for patients with advanced disease or when evaluating recurrent varicose veins. The need for treatment of perforating veins in patients with venous insufficiency continues to be debated, but guidelines suggest potential utility for the treatment of pathologic perforating veins, which are defined as those located underneath healed or active ulcers (CEAP class C<sub>5</sub>–C<sub>6</sub>) with reflux (outward flow duration greater than 350 or 500 ms) and vein diameter 3.5 mm or greater.<sup>113</sup> The finding of a perforating vein greater than 3.5 mm is associated with demonstrable perforator reflux in 90% of patients.<sup>128</sup>

Vascular technologists may use notes and drawings to record findings from venous ultrasound examinations. Diagrams can be particularly useful when the findings are to be used for treatment planning (Fig. 25.15).

## CHAPTER ALGORITHM



- For patients with high pre-test probability for DVT, a bilateral venous duplex scan is appropriate.
- For lower risk patients in outpatient settings, a limited (unilateral) examination may be performed to evaluate symptoms of pain and swelling. A complete examination is appropriate when DVT is found.
- In some circumstances, any positive finding may be sufficient to direct treatment. In this situation, laboratory protocols may permit limited examination for personnel (e.g., patient with transmissible infectious disease).

## SELECTED KEY REFERENCES

### Textbooks

Liem TK. Duplex ultrasound for acute venous disease. Chapter 12. In: Gloviczki P, ed. *Handbook of Venous and Lymphatic Disorders: Guidelines of the American Venous Forum*. 4th ed. Boca Raton, FL: CRC Press, Taylor & Francis Group; 2017:141–150.

Malgor RD, Labropoulos N. Duplex ultrasound scanning for chronic venous obstruction and valvular incompetence. Chapter 13. In: Gloviczki P, ed. *Handbook of Venous and Lymphatic Disorders: Guidelines of the American Venous Forum*. 4th ed. Boca Raton, FL: CRC Press, Taylor & Francis Group; 2017:151–164.

*The American Venous Forum (AVF) is a multi-disciplinary, international medical society that promotes research, education, and clinical care for all aspects of venous disease, including diagnosis, pathophysiology, and treatment. The fourth edition of the AVF Handbook of Venous and Lymphatic Disorders serves as an up-to-date reference for vascular surgeons and specialists in vascular medicine.*

Zierler RE, Dawson DL, eds. Section V. Peripheral Venous. In: Zierler RE, Dawson DL, eds. *Strandness's Duplex Scanning in Vascular Disorders*. 5th ed. Philadelphia: Wolters Kluwer; 2016:223–283.

*Dr. D. Eugene Strandness, Jr. first published his textbook on duplex scanning and its applications in 1990. Dr. Strandness died in 2002, just as the third edition was published. Subsequent editions by his former trainees and colleagues expanded and updated the content. The Strandness textbook now includes clinical perspectives, techniques of scanning, and discussions of applications and pitfalls of vascular laboratory tests. The book is intended as a comprehensive text for residents, fellows, and vascular laboratory professionals.*

### Clinical Practice Guidelines and Appropriate Use Criteria

American Institute of Ultrasound in Medicine. American College of Radiology; Society of Radiologists in Ultrasound. Practice guideline for the performance of peripheral venous ultrasound examinations. *J Ultrasound Med*. 2011;30(1):143–150.

*Guideline for venous duplex scanning developed by ultrasonographers and radiologists, with representation from several organizations, including the American Institute of Ultrasound in Medicine (AIUM). The AIUM was established in 1952 as a multidisciplinary organization when uses of ultrasound for medical diagnosis were first being explored.*

Barleben A, Bandyk DF. Interpretation of peripheral venous duplex testing. *Semin Vasc Surg*. 2013;26(2–3):111–119.

*Review of vascular laboratory standards for venous physiologic testing and duplex scanning.*

Cavezzia A, Labropoulos N, Partsch H, et al. Duplex ultrasound investigation of the veins in chronic venous disease of the lower limbs—UIP consensus document. Part II. Anatomy. *Eur J Vasc Endovasc Surg*. 2006;31(3):288–299.

*This paper reports on an initiative of the Union Internationale de Phléologie (UIP) to establish consensus on the methodology for assessment of anatomy of superficial, deep, and perforating veins in the lower limb by ultrasound imaging. The document provides a detailed description for complete ultrasound assessment of the anatomy of the lower extremity veins.*

Coleridge-Smith P, Labropoulos N, Partsch H, et al. Duplex ultrasound investigation of the veins in chronic venous disease of the lower limbs—UIP consensus document. Part I. Basic principles. *Eur J Vasc Endovasc Surg*. 2006 Jan;31(1):83–92.

*This paper reports on an initiative of the Union Internationale de Phléologie (UIP) to establish a consensus on the methods to be used for duplex ultrasound examination, the interpretation and reporting of images and measurements obtained, and recommendations on training vascular laboratory personnel.*

Gloviczki P, Comerota AJ, Dalsing MC, et al. Society for Vascular Surgery; American Venous Forum. The care of patients with varicose veins and associated chronic venous diseases: clinical practice guidelines of the Society for Vascular Surgery and the American Venous Forum. *J Vasc Surg*. 2011;53(5 Suppl):2S–48S.

*Evidence-based practice guidelines for evaluation and treatment of varicose veins and chronic venous diseases, jointly written by representatives of the Society for Vascular Surgery and the American Venous Forum.*

Intersocietal Accreditation Commission – Vascular Testing. IAC Standards and Guidelines for Vascular Testing Accreditation. *Section 4B: Peripheral Venous Testing* 2020. Available at: <https://www.intersocietal.org/vascular/standards/IACVascularTestingStandards2020.pdf>.

*Intersocietal Accreditation Commission – Vascular Testing (previously the Intersocietal Commission for the Accreditation of Vascular Laboratories) has been the primary organization for vascular laboratory accreditation since 1991. IAC standards, developed by subject matter experts in vascular surgery and other specialties, represent standards of practice in non-invasive vascular testing, including venous duplex scanning.*

Lee BB, Nicolaides AN, Myers K, et al. Venous hemodynamic changes in lower limb venous disease: the UIP consensus according to scientific evidence. *Int Angiol.* 2016;35(3):236–352.

*The Union Internationale de Phlébologie (UIP) commissioned a large group from member societies including the European Venous Forum (EVF), American Venous Forum (AVF), American College of Phlebology (ACP) and Cardiovascular Disease Educational and Research Trust (CDERT) to*

*provide a comprehensive review of venous hemodynamic concepts underlying the pathophysiology of lower limb venous disorders. Chapters include: Basic hemodynamic concepts and normal venous physiology; The mechanism and magnitude of hemodynamic changes in acute deep vein thrombosis; Hemodynamic changes that occur with chronic venous disease; and Hemodynamic changes resulting from treatment by compression, drugs, and surgical or endovenous ablation; as well as other topics.*

Masuda E, Ozsvath K, Vossler J, et al. The 2020 appropriate use criteria for chronic lower extremity venous disease of the American Venous Forum, the Society for Vascular Surgery, the American Vein and Lymphatic Society, and the Society of Interventional Radiology. *J Vasc Surg Venous Lymphat Disord.* 2020;8(4):505–525.e4.

*These Appropriate Use Criteria (AUC) statements guide patient care, particularly when high-quality evidence is lacking, to aid clinicians in making day-to-day decisions for common venous interventions.*

A complete reference list can be found online at [www.expertconsult.com](http://www.expertconsult.com).

## REFERENCES

1. Arnason T, Wells PS, Forster AJ. Appropriateness of diagnostic strategies for evaluating suspected venous thromboembolism. *Thromb Haemost.* 2007;97(2):195–201.
2. Desjardins B, Rybicki FJ, Kim HS, et al. ACR Appropriateness Criteria(R) Suspected upper extremity deep vein thrombosis. *J Am Coll Radiol.* 2012;9(9):613–619.
3. Gornik HL, Gerhard-Herman MD, Misra S, et al. ACCF/ACR/AIUM/ASE/IAC/SCAI/SCVS/SIR/SVM/SVS/SVU 2013 appropriate use criteria for peripheral vascular ultrasound and physiological testing part II: testing for venous disease and evaluation of hemodialysis access: a report of the american college of cardiology foundation appropriate use criteria task force. *J Am Coll Cardiol.* 2013;62(7):649–665.
4. Expert Panel on Vascular I, Hanley M, Steigner ML, et al. ACR Appropriateness Criteria(R) Suspected Lower Extremity Deep Vein Thrombosis. *J Am Coll Radiol.* 2018;15(11S):S413–S417.
5. Sigel B, Popky GL, Wagner DK, et al. Comparison of clinical and Doppler ultrasound evaluation of confirmed lower extremity venous disease. *Surgery.* 1968;64(1):332–338.
6. Sigel B. A brief history of Doppler ultrasound in the diagnosis of peripheral vascular disease. *Ultrasound Med Biol.* 1998;24(2):169–176.
7. Sumner DS, Baker DW, Strandness Jr DE. The ultrasonic velocity detector in a clinical study of venous disease. *Arch Surg.* 1968;97(1):75–80.
8. Strandness DE, Sumner DS. Ultrasonic velocity detector in the diagnosis of thrombophlebitis. *Arch Surg.* 1972;104:180–183.
9. Talbot SR. Use of real-time imaging in identifying deep venous obstruction: a preliminary report. *Bruit.* 1982;7:41–42.
10. Talbot SR. B-mode evaluation of peripheral veins. *Semin Ultrasound CT MR.* 1988;9(4):295–319.
11. Killewich LA, Bedford GR, Beach KW, Strandness Jr DE. Diagnosis of deep venous thrombosis. A prospective study comparing duplex scanning to contrast venography. *Circulation.* 1989;79(4):810–814.
12. Cronan JJ. History of venous ultrasound. *J Ultrasound Med.* 2003;22(11):1143–1146.
13. IAC. Vascular Testing I. IAC Standards and Guidelines for Vascular Testing Accreditation. Intersocietal Commission for Accreditation. Updated November 1, 2020. Available at: <http://intersocietal.org/vascular/standards/IACVascularTestingStandards2020.pdf>
14. Sigel B, Coelho JC, Spigos DG, et al. Ultrasonography of blood during stasis and coagulation. *Invest Radiol.* 1981;16(1):71–76.
15. Kim ES, Sharma AM, Scissons R, et al. Interpretation of peripheral arterial and venous Doppler waveforms: A consensus statement from the Society for Vascular Medicine and Society for Vascular Ultrasound. *Vasc Med.* 2020;25(5):484–506.
16. Goodacre S, Sampson F, Thomas S, et al. Systematic review and meta-analysis of the diagnostic accuracy of ultrasonography for deep vein thrombosis. *BMC Med Imaging.* 2005;5:6.
17. Mousa AY, Broce M, De Wit D, et al. Appropriate use of venous imaging and analysis of the D-dimer/clinical probability testing paradigm in the diagnosis and location of deep venous thrombosis. *Ann Vasc Surg.* 2018;50:21–29.
18. Mattos MA, Melendres G, Sumner DS, et al. Prevalence and distribution of calf vein thrombosis in patients with symptomatic deep venous thrombosis: a color-flow duplex study. *J Vasc Surg.* 1996;24(5):738–744.
19. Elmi G, Rinaldi ER, Domanico A, Aluigi L. Calf deep vein thrombosis - clinical relevance, diagnostic approaches and therapeutic options. *Vasa.* 2020;49(5):359–366.
20. Lagerstedt CI, Olsson CG, Fagher BO, et al. Need for long-term anticoagulant treatment in symptomatic calf-vein thrombosis. *Lancet.* 1985;2(8454):515–518.
21. Masuda EM, Kistner RL, Musikasinthorn C, et al. The controversy of managing calf vein thrombosis. *J Vasc Surg.* 2012;55(2):550–561.
22. Hirsh J, Guyatt G, Albers GW, et al. Antithrombotic and thrombolytic therapy: American College of Chest Physicians Evidence-Based Clinical Practice Guidelines (8th Edition). *Chest.* 2008;133(6 Suppl):110S–112S.
23. Righini M, Paris S, Le Gal G, et al. Clinical relevance of distal deep vein thrombosis. Review of literature data. *Thromb Haemost.* 2006;95(1):56–64.
24. Hansson PO, Sorbo J, Eriksson H. Recurrent venous thromboembolism after deep vein thrombosis: incidence and risk factors. *Arch Intern Med.* 2000;160(6):769–774.
25. Pinede L, Ninet J, Duhaut P, et al. Comparison of 3 and 6 months of oral anticoagulant therapy after a first episode of proximal deep vein thrombosis or pulmonary embolism and comparison of 6 and 12 weeks of therapy after isolated calf deep vein thrombosis. *Circulation.* 2001;103(20):2453–2460.
26. Schulman S, Rhedin AS, Lindmarker P, et al. A comparison of six weeks with six months of oral anticoagulant therapy after a first episode of venous thromboembolism. Duration of Anticoagulation Trial Study Group. *N Engl J Med.* 1995;332(25):1661–1665.
27. Singh K, Yakoub D, Giangola P, et al. Early follow-up and treatment recommendations for isolated calf deep venous thrombosis. *J Vasc Surg.* 2012;55(1):136–140.
28. Ridker PM, Goldhaber SZ, Danielson E, et al. Long-term, low-intensity warfarin therapy for the prevention of recurrent venous thromboembolism. *N Engl J Med.* 2003;348(15):1425–1434.
29. Murin S, Romano PS, White RH. Comparison of outcomes after hospitalization for deep venous thrombosis or pulmonary embolism. *Thromb Haemost.* 2002;88(3):407–414.
30. Kearon C, Akl EA, Ornelas J, et al. Antithrombotic Therapy for VTE Disease: CHEST Guideline and Expert Panel Report. *Chest.* 2016;149(2):315–352.
31. Macdonald PS, Kahn SR, Miller N, Obrand D. Short-term natural history of isolated gastrocnemius and soleal vein thrombosis. *J Vasc Surg.* 2003;37(3):523–527.
32. Sales CM, Haq F, Bustami R, Sun F. Management of isolated soleal and gastrocnemius vein thrombosis. *J Vasc Surg.* 2010;52(5):1251–1254.
33. Henry JC, Satiani B. Calf muscle venous thrombosis: a review of the clinical implications and therapy. *Vasc Endovascular Surg.* 2014;48(5–6):396–401.
34. Schwarz T, Buschmann L, Beyer J, et al. Therapy of isolated calf muscle vein thrombosis: a randomized, controlled study. *J Vasc Surg.* 2010;52(5):1246–1250.
35. Bernardi E, Pesavento R, Prandoni P. Upper extremity deep venous thrombosis. *Sem Thromb Hemost.* 2006;32(7):729–736.
36. Flinterman LE, Van Der Meer FJ, Rosendaal FR, Doggen CJ. Current perspective of venous thrombosis in the upper extremity. *J Thromb Haemost.* 2008;6(8):1262–1266.
37. Isma N, Svensson PJ, Gottsater A, Lindblad B. Upper extremity deep venous thrombosis in the population-based Malmo thrombophilia study (MATS). Epidemiology, risk factors, recurrence risk, and mortality. *Thromb Res.* 2010;125(6):e335–338.
38. Klitfod L, Broholm R, Baekgaard N. Deep venous thrombosis of the upper extremity. A review. *Int Angiol.* 2013;32(5):447–452.
39. Coon WW, Willis 3rd PW. Thrombosis of axillary and subclavian veins. *Arch Surg.* 1967;94(5):657–663.
40. Machleder HI. Effort thrombosis of the axillosubclavian vein: a disabling vascular disorder. *Compr Ther.* 1991;17(5):18–24.
41. Prandoni P, Polistena P, Bernardi E, et al. Upper-extremity deep vein thrombosis. Risk factors, diagnosis, and complications. *Arch Intern Med.* 1997;157(1):57–62.
42. Meissner MH. Axillary-subclavian venous thrombosis. *Rev Cardiovasc Med.* 2002;3(Suppl 2):S76–33.
43. Vemuri C, Salehi P, Benarroch-Gampel J, et al. Diagnosis and treatment of effort-induced thrombosis of the axillary subclavian vein due to venous thoracic outlet syndrome. *J Vasc Surg Venous Lymphat Disord.* 2016;4(4):485–500.
44. Di Nisio M, Van Sluis GL, Bossuyt PM, et al. Accuracy of diagnostic tests for clinically suspected upper extremity deep vein thrombosis: a systematic review. *J Thromb Haemost.* 2010;8(4):684–692.

45. Poley RA, Newbigging JL, Sivilotti ML. Estimated effect of an integrated approach to suspected deep venous thrombosis using limited-compression ultrasound. *Acad Emerg Med.* 2014;21(9):971–980.
46. Crisp JG, Lovato LM, Jang TB. Compression ultrasonography of the lower extremity with portable vascular ultrasonography can accurately detect deep venous thrombosis in the emergency department. *Ann Emerg Med.* 2010;56(6):601–610.
47. Lee JH, Lee SH, Yun SJ. Comparison of 2-point and 3-point point-of-care ultrasound techniques for deep vein thrombosis at the emergency department: A meta-analysis. *Medicine (Baltimore).* 2019;98(22):e15791.
48. Caronia J, Sarzynski A, Tofghi B, et al. Resident performed two-point compression ultrasound is inadequate for diagnosis of deep vein thrombosis in the critically III. *J Thromb Thrombolysis.* 2014;37(3):298–302.
49. Sevestre MA, Labarere J, Casez P, et al. Accuracy of complete compression ultrasound in ruling out suspected deep venous thrombosis in the ambulatory setting. A prospective cohort study. *Thromb Haemost.* 2009;102(1):166–172.
50. Zitek T, Baydoun J, Yepez S, et al. Mistakes and pitfalls associated with two-point compression ultrasound for deep vein thrombosis. *West J Emerg Med.* 2016;17(2):201–208.
51. Pomero F, Dentali F, Borretta V, et al. Accuracy of emergency physician-performed ultrasonography in the diagnosis of deep-vein thrombosis: a systematic review and meta-analysis. *Thromb Haemost.* 2013;109(1):137–145.
52. Strothman G, Blebea J, Fowl RJ, Rosenthal G. Contralateral duplex scanning for deep venous thrombosis is unnecessary in patients with symptoms. *J Vasc Surg.* 1995;22(5):543–547.
53. Sheiman RG, Weintraub JL, McArdle CR. Bilateral lower extremity US in the patient with bilateral symptoms of deep venous thrombosis: assessment of need. *Radiology.* 1995;196(2):379–381.
54. Blebea J, Kihara TK, Neumyer MM, et al. A national survey of practice patterns in the noninvasive diagnosis of deep venous thrombosis. *J Vasc Surg.* 1999;29(5):799–804. 806; discussion 804–805.
55. Pennell RC, Mantese VA, Westfall SG. Duplex scan for deep vein thrombosis—defining who needs an examination of the contralateral asymptomatic leg. *J Vasc Surg.* 2008;48(2):413–416.
56. Cronan JJ. Deep venous thrombosis: one leg or both legs? *Radiology.* 1996;200(2):323–324.
57. Henke PK, Varma MR, Moaveni DK, et al. Fibrotic injury after experimental deep vein thrombosis is determined by the mechanism of thrombogenesis. *Thromb Haemost.* 2007;98(5):1045–1055.
58. Meissner MH, Zierler BK, Bergelin RO, et al. Coagulation, fibrinolysis, and recanalization after acute deep venous thrombosis. *J Vasc Surg.* 2002;35(2):278–285.
59. Haenen JH, Wollersheim H, Janssen MC, et al. Evolution of deep venous thrombosis: a 2-year follow-up using duplex ultrasound scan and strain-gauge plethysmography. *J Vasc Surg.* 2001;34(4):649–655.
60. Gaitini D, Kaftori JK, Pery M, Markel A. Late changes in veins after deep venous thrombosis: ultrasonographic findings. *Raf.* 1990;153(1):68–72.
61. Parker KJ, Doyley MM, Rubens DJ. Imaging the elastic properties of tissue: the 20 year perspective. *Phys med biol.* 2011;56(1):R1–R29.
62. Wells PN, Liang HD. Medical ultrasound: imaging of soft tissue strain and elasticity. *J R Soc Interface.* 2011;8(64):1521–1549.
63. Dharmarajah B, Sounderajah V, Rowland SP, et al. Aging techniques for deep vein thrombosis: a systematic review. *Phlebology.* 2015;30(2):77–84.
64. Yi X, Ni C, Li M, et al. Correlation between biological characteristics of thrombus and short-term efficiency of thrombolytic therapy by acoustic radiation force impulse imaging technique. *Int Angiol.* 2017;36(6):574–579.
65. Hoang P, Wallace A, Sugi M, et al. Elastography techniques in the evaluation of deep vein thrombosis. *Cardiovasc Diagn Ther.* 2017;7(Suppl 3):S238–S245.
66. Mumoli N, Mastroiacovo D, Giorgi-Pierfranceschi M, et al. Ultrasound elastography is useful to distinguish acute and chronic deep vein thrombosis. *J Thromb Haemost.* 2018;16(12):2482–2491.
67. Rubin JM, Aglyamov SR, Wakefield TW, et al. Clinical application of sonographic elasticity imaging for aging of deep venous thrombosis: preliminary findings. *J Ultrasound Med.* 2003;22(5):443–448.
68. Rubin JM, Xie H, Kim K, et al. Sonographic elasticity imaging of acute and chronic deep venous thrombosis in humans. *J Ultrasound Med.* 2006;25(9):1179–1186.
69. Sarvazyan AP, Rudenko OV, Swanson SD, et al. Shear wave elasticity imaging: a new ultrasonic technology of medical diagnostics. *Ultrasound Med Biol.* 1998;24(9):1419–1435.
70. Schmitt C, Montagnon E, Henni AH, et al. Shear wave induced resonance elastography of venous thrombi: a proof-of-concept. *IEEE Trans Med Imaging.* 2013;32(3):565–577.
71. Siragusa S, Malato A, Anastasio R, et al. Residual vein thrombosis to establish duration of anticoagulation after a first episode of deep vein thrombosis: the Duration of Anticoagulation based on Compression UltraSonography (DACSUS) study. *Blood.* 2008;112(3):511–515.
72. Siragusa S, Malato A, Saccullo G, et al. Residual vein thrombosis for assessing duration of anticoagulation after unprovoked deep vein thrombosis of the lower limbs: the extended DACUS study. *Am J Hematol.* 2011;86(11):914–917.
73. Napolitano M, Saccullo G, Malato A, et al. Optimal duration of low molecular weight heparin for the treatment of cancer-related deep vein thrombosis: the Cancer-DACSUS Study. *J Clin Oncol.* 2014;32(32):3607–3612.
74. Verhovsek M, Douketis JD, Yi Q, et al. Systematic review: D-dimer to predict recurrent disease after stopping anticoagulant therapy for unprovoked venous thromboembolism. *Ann Intern Med.* 2008;149(7):481–490. W94.
75. Palareti G, Cosmi B, Legnani C, et al. D-dimer testing to determine the duration of anticoagulation therapy. *N Engl J Med.* 2006;355(17):1780–1789.
76. Ageno W, Cosmi B, Ghirarduzzi A, et al. The negative predictive value of D-dimer on the risk of recurrent venous thromboembolism in patients with multiple previous events: a prospective cohort study (the PROLONG PLUS study). *Am J Hematol.* 2012;87(7):713–715.
77. Cronan JJ, Leen V. Recurrent deep venous thrombosis: limitations of US. *Radiology.* 1989;170(3 Pt 1):739–742.
78. Tan M, Mol G, Kees van Rooden J, Huisman MV. The diagnostic management of recurrent deep vein thrombosis and pulmonary embolism. *Semin Respir Crit Care Med.* 2012;33(2):151–155.
79. Baglin T, Luddington R, Brown K, Baglin C. Incidence of recurrent venous thromboembolism in relation to clinical and thrombophilic risk factors: prospective cohort study. *Lancet.* 2003;362(9383):523–526.
80. Prandoni P, Cogo A, Bernardi E, et al. A simple ultrasound approach for detection of recurrent proximal-vein thrombosis. *Circulation.* 1993;88(4 Pt 1):1730–1735.
81. Tan M, Velthuis SI, Westerbeek RE, et al. High percentage of non-diagnostic compression ultrasonography results and the diagnosis of ipsilateral recurrent proximal deep vein thrombosis. *J Thromb Haemost.* 2010;8(4):848–850.
82. Heijboer H, Jongbloets LM, Buller HR, et al. Clinical utility of real-time compression ultrasonography for diagnostic management of patients with recurrent venous thrombosis. *Acta Radiol.* 1992;33(4):297–300.
83. Piovella F, Crippa L, Barone M, et al. Normalization rates of compression ultrasonography in patients with a first episode of deep vein thrombosis of the lower limbs: association with recurrence and new thrombosis. *Haematologica.* 2002;87(5):515–522.
84. Hamadah A, Alwasaidi T, Le Gal G, et al. Baseline imaging after therapy for unprovoked venous thromboembolism: a randomized controlled comparison of baseline imaging for diagnosis of suspected recurrence. *J Thromb Haemost.* 2011;9(12):2406–2410.
85. Liem TK. Duplex ultrasound for acute venous disease. In: Gloviczki P, ed. *Handbook of Venous and Lymphatic Disorders: Guidelines of the American Venous Forum.* 4th ed. CRC Press, Taylor & Francis Group; 2017:141–150.
86. Meissner MH, Manzo RA, Bergelin RO, et al. Deep venous insufficiency: the relationship between lysis and subsequent reflux. *J Vasc Surg.* 1993;18(4):596–605; discussion 606–608.

87. Meissner MH, Caps MT, Zierler BK, et al. Determinants of chronic venous disease after acute deep venous thrombosis. *J Vasc Surg.* 1998;28(5):826–833.
88. Barco S, Konstantinides S, Huisman MV, Klok FA. Diagnosis of recurrent venous thromboembolism. *Thromb Res.* 2018;163:229–235.
89. Nicolaides A, Clark H, Labropoulos N, et al. Quantitation of reflux and outflow obstruction in patients with CVD and correlation with clinical severity. *Int Angiol.* 2014;33(3):275–281.
90. Nicolaides A, Hull RD, Fareed J. Superficial vein thrombosis. *Clin Appl Thromb Hemost.* 2013;19(2):208–213.
91. Varki A. Trouseau's syndrome: multiple definitions and multiple mechanisms. *Blood.* 2007;110(6):1723–1729.
92. Milio G, Siragusa S, Mina C, et al. Superficial venous thrombosis: prevalence of common genetic risk factors and their role on spreading to deep veins. *Thromb Res.* 2008;123(2):194–199.
93. Di Nisio M, Peinemann F, Porreca E, Rutjes AW. Treatment for superficial infusion thrombophlebitis of the upper extremity. *Cochrane Database Syst Rev.* 2015;(11):CD011015.
94. Wichter IM, Di Nisio M, Buller HR, Middeldorp S. Treatment of superficial vein thrombosis to prevent deep vein thrombosis and pulmonary embolism: a systematic review. *Haematologica.* 2005;90(5):672–677.
95. Chengelis DL, Bendick PJ, Glover JL, et al. Progression of superficial venous thrombosis to deep vein thrombosis. *J Vasc Surg.* 1996;24(5):745–749.
96. Decousus H, Quere I, Presles E, et al. Superficial venous thrombosis and venous thromboembolism: a large, prospective epidemiologic study. *Ann Intern Med.* 2010;152(4):218–224.
97. Ferring M, Henderson J, Wilmink A, Smith S. Vascular ultrasound for the pre-operative evaluation prior to arteriovenous fistula formation for haemodialysis: review of the evidence. *Nephrol Dial Transplant.* 2008;23(6):1809–1815.
98. Ferring M, Claridge M, Smith SA, Wilmink T. Routine preoperative vascular ultrasound improves patency and use of arteriovenous fistulas for hemodialysis: a randomized trial. *Clin J Am Soc Nephrol.* 2010;5(12):2236–2244.
99. Vascular Access Work Group. Clinical practice guidelines for vascular access. *Am J Kidney Dis.* 2006;48(Suppl 1):S176–247.
100. Brown PW. Preoperative radiological assessment for vascular access. *Eur J Vasc Endovasc Surg.* 2006;31(1):64–69.
101. Luckraz H, Lowe J, Pugh N, Azzu AA. Pre-operative long saphenous vein mapping predicts vein anatomy and quality leading to improved post-operative leg morbidity. *Interact Cardiovasc Thorac Surg.* 2008;7(2):188–191; discussion 191.
102. Linni K, Mader N, Aspalter M, et al. Ultrasonic vein mapping prior to infrainguinal autogenous bypass grafting reduces postoperative infections and readmissions. *J Vasc Surg.* 2012;56(1):126–132; discussion 132–133.
103. Linni K, Aspalter M, Mader N, et al. Preoperative duplex vein mapping (DVM) reduces costs in patients undergoing infrainguinal bypass surgery: results of a prospective randomised study. *Eur J Vasc Endovasc Surg.* 2012;43(5):561–566.
104. Society for Vascular Ultrasound. Vascular technology professional performance guideline: Lower extremity venous duplex evaluation for insufficiency. Society for Vascular Ultrasound. Available at: [https://higherlogicdownload.s3.amazonaws.com/SVUNET/c9a8d83b-2044-4a4e-b3ec-cd4b2f542939/UploadedImages/14\\_Lower\\_Extemity\\_Venous\\_Insufficiency\\_Evaluation\\_Updated\\_2019\\_.pdf](https://higherlogicdownload.s3.amazonaws.com/SVUNET/c9a8d83b-2044-4a4e-b3ec-cd4b2f542939/UploadedImages/14_Lower_Extemity_Venous_Insufficiency_Evaluation_Updated_2019_.pdf)
105. Society for Vascular Ultrasound. Vascular technology professional performance guideline: Lower extremity vein mapping. Available at: [https://higherlogicdownload.s3.amazonaws.com/SVUNET/c9a8d83b-2044-4a4e-b3ec-cd4b2f542939/UploadedImages/PPG\\_Docs/12\\_Lower\\_Extemity\\_Vein\\_Mapping\\_Updated\\_2019\\_.pdf](https://higherlogicdownload.s3.amazonaws.com/SVUNET/c9a8d83b-2044-4a4e-b3ec-cd4b2f542939/UploadedImages/PPG_Docs/12_Lower_Extemity_Vein_Mapping_Updated_2019_.pdf)
106. Kohler TR, Strandness Jr DE. Noninvasive testing for the evaluation of chronic venous disease. *World J Surg.* 1986;10(6):903–910.
107. Nicolaides AN. Cardiovascular Disease Educational and Research Trust, European Society of Vascular Surgery, et al. Investigation of chronic venous insufficiency: A consensus statement (France, March 5–9, 1997). *Circulation.* 2000;102(20):E126–163.
108. Coleridge-Smith P, Labropoulos N, Partsch H, et al. Duplex ultrasound investigation of the veins in chronic venous disease of the lower limbs—UIP consensus document. Part I. Basic principles. *Eur J Vasc Endovasc Surg.* 2006;31(1):83–92.
109. Cavezzi A, Labropoulos N, Partsch H, et al. Duplex ultrasound investigation of the veins in chronic venous disease of the lower limbs—UIP consensus document. Part II. *Anatomy Vasa.* 2007;36(1):62–71.
110. Matic PA, Vlajinac HD, Marinkovic JM, et al. Chronic venous disease: Correlation between ultrasound findings and the clinical, etiologic, anatomic and pathophysiologic classification. *Phlebology.* 2014;29(8):522–527.
111. Eklof B, Rutherford RB, Bergan JJ, et al. Revision of the CEAP classification for chronic venous disorders: consensus statement. *J Vasc Surg.* 2004;40(6):1248–1252.
112. Lurie F, Passman M, Meisner M, et al. The 2020 update of the CEAP classification system and reporting standards. *J Vasc Surg Venous Lymphat Disord.* 2020;8(3):342–352.
113. Gloviczk P, Comerota AJ, Dalsing MC, et al. The care of patients with varicose veins and associated chronic venous diseases: clinical practice guidelines of the Society for Vascular Surgery and the American Venous Forum. *J Vasc Surg.* 2011;53(5 Suppl):2S–48S.
114. Tripolitis AJ, Milligan EB, Bodily KC, Strandness Jr DE. The physiology of venous claudication. *Am J Surg.* 1980;139(3):447–448.
115. Killewich LA, Martin R, Cramer M, Beach KW, Strandness Jr DE. Pathophysiology of venous claudication. *J Vasc Surg.* 1984;1(4):507–511.
116. Meissner MH, Moneta G, Burnand K, et al. The hemodynamics and diagnosis of venous disease. *J Vasc Surg.* 2007;46(Suppl S):4S–24S.
117. Meissner MH, Eklof B, Smith PC, et al. Secondary chronic venous disorders. *J Vasc Surg.* 2007;46(Suppl S):68S–83S.
118. Labropoulos N, Giannoukas AD, Nicolaides AN, et al. The role of venous reflux and calf muscle pump function in nonthrombotic chronic venous insufficiency. Correlation with severity of signs and symptoms. *Arch Surg.* 1996;131(4):403–406.
119. Eklof B, Perrin M, Delis KT, et al. Updated terminology of chronic venous disorders: the VEIN-TERM transatlantic interdisciplinary consensus document. *J Vasc Surg.* 2009;49(2):498–501.
120. Markel A, Meissner MH, Manzo RA, et al. A comparison of the cuff deflation method with Valsalva's maneuver and limb compression in detecting venous valvular reflux. *Arch Surg.* 1994;129(7):701–705.
121. van Bemmelen PS, Bedford G, Beach K, Strandness DE. Quantitative segmental evaluation of venous valvular reflux with duplex ultrasound scanning. *J Vasc Surg.* 1989;10(4):425–431.
122. Guideline developed in collaboration with the American College of R, Society of Pediatric R, Society of Radiologists in U. AIUM Practice Guideline for the Performance of Peripheral Venous Ultrasound Examinations. *J Ultrasound Med.* 2015;34(8):1–9.
123. Masuda E, Ozsvath K, Vossler J, et al. The 2020 appropriate use criteria for chronic lower extremity venous disease of the American Venous Forum, the Society for Vascular Surgery, the American Vein and Lymphatic Society, and the Society of Interventional Radiology. *J Vasc Surg Venous Lymphat Disord.* 2020;8(4):505–525.e4.
124. Dawson DL. Moving toward consensus for the best method to test for venous reflux in the vascular laboratory. *J Vasc Surg Venous Lymphat Disord.* 2020;8(4):501–502.
125. van Bemmelen PS, Beach K, Bedford G, Strandness Jr DE. The mechanism of venous valve closure. Its relationship to the velocity of reverse flow. *Arch Surg.* 1990;125(5):617–619.
126. Labropoulos N, Tiengson J, Pryor L, et al. Definition of venous reflux in lower-extremity veins. *J Vasc Surg.* 2003;38(4):793–798.
127. Lurie F, Comerota A, Eklof B, et al. Multicenter assessment of venous reflux by duplex ultrasound. *J Vasc Surg.* 2012;55(2):437–445.
128. Sandri JL, Barros FS, Pontes S, et al. Diameter-reflux relationship in perforating veins of patients with varicose veins. *J Vasc Surg.* 1999;30(5):867–874.

# Radiation Safety

AMY B. REED and MELISSA L. KIRKWOOD

TYPES OF RADIATION	308
MEASUREMENT	308
Absorbed Dose	308
Equivalent Dose	308
Effective Dose	308
BIOLOGIC EFFECTS OF RADIATION	308
Deterministic Effects	309
Stochastic Effects	309
EXPOSURE AND RECOMMENDED LIMITS	310
Background Radiation	310
Occupational and Medical Exposure	310
Recommended Dose Limits	310
PRINCIPLES OF RADIATION PROTECTION	311
RADIATION SAFETY: DIAGNOSTIC PROCEDURES	311
RADIATION SAFETY: ENDOVASCULAR PROCEDURES	312
Emission Control	312
Time	312
Distance	313
Barriers	313
Training	313
Technique	313
Monitoring Exposure	313
RADIATION AND THE ENDOVASCULAR SURGEON	314
RADIATION AND PREGNANCY	315
Declaration of Pregnancy	315
Fetal Risk From Radiation	315
Malformations and Mental Retardation	315
Cancer Risk	315
Recommendations for Pregnant Workers	315

Advances in radiation have led to a significant increase in its use for diagnostic, interventional, and therapeutic purposes. With the ever-increasing utilization of endovascular techniques, concern has grown regarding the potential harmful effects of radiation delivered to both the patient and the operator. Although radiation exposure from diagnostic procedures is generally low and comparable to natural background doses, therapeutic use of radiation during endovascular procedures involves a higher level of exposure, which can be harmful if not controlled.<sup>1</sup> Surgeon education on appropriate use of fluoroscopic equipment, shielding, and protection has been shown to be beneficial in decreasing radiation exposure.<sup>2</sup>

Radiation poses risk to workers and patients alike. Many medical specialists operate medical X-ray equipment frequently. Operating room assistants are often not properly educated regarding the potential damaging effects of radiation and may receive little training on how to minimize exposure to themselves or to the patient. Patients may undergo procedures without being properly informed of the risks. These deficiencies can result in unnecessary exposure for both patients and staff.

The concern about radiation exposure is particularly pressing in the field of vascular surgery, where endovascular procedures are mainstays of clinical practice. Percutaneous angioplasty and stenting of peripheral and carotid arteries, as well as endovascular stent-grafts for treating abdominal and thoracic aortic diseases are now first-line treatment options. Advanced techniques such as fenestrated and branched endografts for complex thoracoabdominal aneurysm repair may carry significant radiation exposure to surgeons and their patients due to the steep gantry angles, long procedural time and use of magnification. Computed tomography angiography (CTA) as a primary modality of investigation and follow-up has become widely accepted in the management of atherosclerotic vascular disease as has coronary CT for the purposes of coronary artery calcium scoring. Given the incidence of coronary disease in the vascular surgery patient population, the potential exists for significant radiation exposure over the patient's lifetime.

The principles of radiation safety have been well addressed by a number of national bodies – the International Commission on Radiological Protection (ICRP) and the National Council

on Radiation Protection and Measurements (NCRP). These organizations provide valuable resources and publications that disseminate information and recommendations about radiation exposure and protection. Additionally, each state has its own regulations regarding radiation safety and annual certification that the endovascular specialist should be aware of. This chapter serves to familiarize vascular surgeons with radiation terminology, dosing metrics, radiation-induced injury, and techniques to lower radiation dose to both the patient and the healthcare team.

## TYPES OF RADIATION

Radiation is a form of energy emitted as electromagnetic waves or particles. It can be classified as nonionizing (ultrasound, magnetic resonance, laser, microwaves) or ionizing (X-rays, gamma rays). Nonionizing radiation does not possess the energy to ionize atoms of the absorbing matter. Ionizing radiation consists of alpha and beta particles, neutrons, and energetic photons (ultraviolet and above), which contain sufficiently high energy to interact with atoms and produce biologic injury. The most common forms of ionizing radiation used in medicine are X-rays, gamma rays, beta rays, and electrons.

## MEASUREMENT

The amount of ionization that radiation produces in air, measured in roentgens (R), does not accurately reflect its potential to cause biologic injury. Importantly, the actual damage or biologic effect of radiation depends upon the total energy of radiation absorbed per unit mass, the sensitivity of the organ, and the strength of the radiation. To quantify radiation for the purposes of risk assessment and setting standards and limits, the terms *absorbed dose*, *equivalent dose*, and *effective dose* are commonly used (Table 26.1).

### Absorbed Dose

The absorbed dose is a measure of the amount of energy deposited in a medium by ionizing radiation per unit mass of matter and is equal to the amount of heat generated by the radiation per tissue weight in a specified material. The International System of Units (SI) measure for absorbed dose is the gray (Gy), named after Louis Harold Gray, a British physicist. One gray equals 1 joule (J) of energy absorbed per kilogram (J/kg). Historically, the unit most commonly used was the radiation absorbed dose (rad); 1 Gy = 100 rad. The absorbed dose is not an accurate indicator of biologic effect given that different types of ionizing radiation produce different degrees of tissue damage.

### Equivalent Dose

The equivalent dose, a measure of the radiation dose to tissue, takes into account the different degrees of damage by different types of radiation by introducing a radiation weighting factor ( $W_R$ ). The SI unit of equivalent dose is the sievert (Sv), named after Rolf Sievert, a Swedish physicist. Thus, equivalent dose

**TABLE 26.1** Units of Radiation

Measurement	Unit	Measures	
Radioactivity	Curie	Number of particles/s from 1 g of radium	
Ionizing radiation	Roentgen (R)	Charge/unit mass	1 R = 2.58 × 10 <sup>-4</sup> C/kg
Absorbed dose	Rad Gray (Gy)	1 rad = 0.01 J/kg 1 Gy = 1 J/kg	1 rad = 0.01 Gy 1 Gy = 100 rad
Equivalent dose/ effective dose	Rem Sievert (Sv)	Rem = rad × W Sv = Gy × W	1 rem = 0.01 Sv 1 Sv = 100 rem

W, weighting factor.

= absorbed dose × W<sub>R</sub>. Another unit, the roentgen equivalent man, or rem, is still sometimes used; 1 Sv = 100 rem.

W<sub>R</sub> is calculated based on the type of radiation, using 1 for X-rays and gamma rays and 3–10 for protons and neutrons. The sievert better describes the biologic effect of radiation and is commonly used when risk from ionizing radiation is assessed. It also allows quantification of risk and comparison to other commonly encountered modes of exposure. For fluoroscopic interventions in vascular surgery, the sievert and gray are roughly equal; absorbed dose = equivalent dose.

### Effective Dose

Different tissues and organs have different sensitivity to radiation, therefore the concept of effective dose is introduced to take into account the part of the body irradiated and the volume and time over which the radiation dose is applied. The effective dose, measured in sieverts, is calculated by weighting the equivalent dose by a tissue weighting factor (W<sub>T</sub>). This calculation takes into consideration the distribution of radiation as well as the radiosensitivity of various organs or tissues. To avoid confusion, W<sub>R</sub> and W<sub>T</sub> are sometimes grouped together into one single weighting factor (W).

Effective dose may be evaluated prospectively for planning and optimization of radiation protection, as well as retrospectively for assessment of the radiation-associated risk incurred. It is mainly used as a protective and regulatory quantity and not for epidemiologic study of populations. It does not provide a precise indicator of an individual patient's risk, as there is no consideration of patient age, gender, or other confounding factors.

Because grays and sieverts quantify relatively large amounts of radiation, in medical use, radiation is typically described using milligrays (mGy) or millisieverts (mSv).

## BIOLOGIC EFFECTS OF RADIATION

Ionizing radiation damages living cells, which can then repair themselves, die, or undergo mutation. The effects of radiation on biologic tissue are generally classified as two types: deterministic effects and stochastic effects.

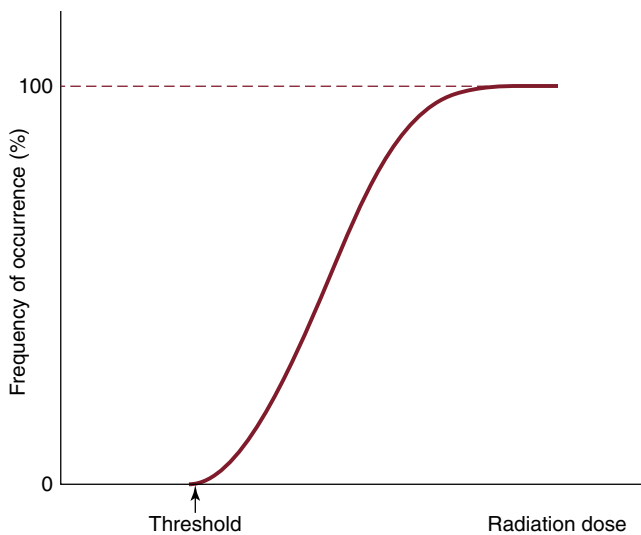


**Figure 26.1** General Dose–Response Curve for the Deterministic Effects of Radiation.

## Deterministic Effects

Deterministic effects of radiation are dose-dependent and result in cell death, impacting hair follicles, skin, subcutaneous tissues, and the lens of the eye. These acute events occur when a threshold level of radiation has been exceeded, and the higher the dose, the greater the injury (Fig. 26.1). The threshold is not absolute and can vary among individuals. Table 26.2 shows some threshold levels of human organs with corresponding deterministic effects. Doses required to produce deterministic effects are often large and exceed 1 to 2 Sv. Symptoms arise when a significant proportion of cells are killed by radiation, and subsequent inflammation or fibrosis may produce additional damage to the organ. Examples of deterministic effects include radiation-induced dermatitis, cataracts, infertility, and organ atrophy or fibrosis (Figs. 26.2 and 26.3). Given increasing concerns about the late manifestation of cataracts from low doses of ionizing radiation, the recommended threshold of the lens is 0.5 Sv.

Whole-body exposure to 10- to 20-Gy of high-energy radiation, delivered at one time, can be fatal to humans. For acute whole-body equivalent doses, 0.5 to 1 Sv may produce light radiation sickness; 1 Sv causes slight blood changes; and 2 to 3 Sv causes nausea, hair loss, and hemorrhage. An acute dose of 3 Sv causes death in 50% of individuals within 30 days, and with doses higher than 6 Sv, survival is unlikely.

## Stochastic Effects

Stochastic, or probabilistic, effects of radiation cause DNA damage to single cells, which results in mutation. This is an all-or-none phenomenon, with the probability of occurrence increasing as the cumulative radiation exposure increases without an established threshold level (Fig. 26.4). The severity of the effect of mutation is unrelated to the dose. Mutations may lead to cancer and heritable genetic defects. Theoretically, stochastic effects can occur even at low doses, but it is assumed that with

**TABLE 26.2**

Deterministic Effects and Threshold Doses of Radiation

Organ	Effects	THRESHOLD EFFECTIVE DOSE (Sv)	
		Single Dose	Multiple Yearly Doses
Gonads	Temporary sterility	0.1	0.4
	Permanent sterility	3–6	2
Eye	Cataracts	0.5	0.2
Bone marrow	Marrow depression	0.5	0.5
Skin	Transient erythema	2	—
	Desquamation	2–10	—
	Temporary hair loss	4	—
	Dermal necrosis	25	—
	Skin atrophy	10	1
Whole body	Acute radiation sickness	1	—

Modified from the International Commission on Radiological Protection guidelines.

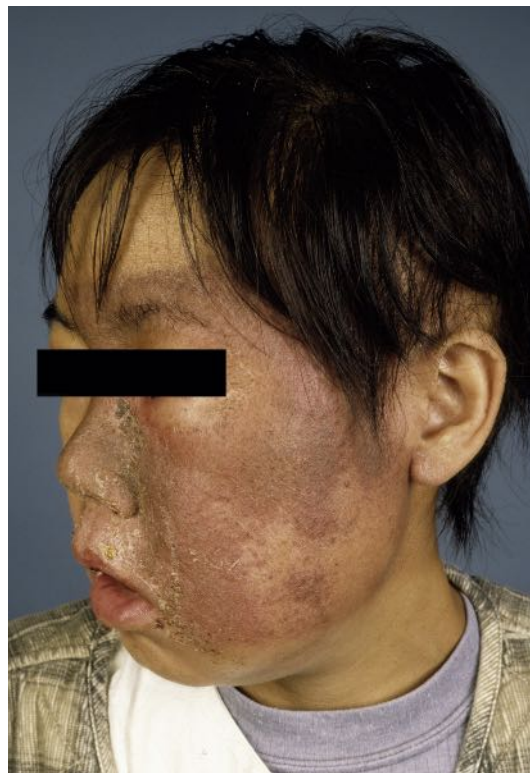


**Figure 26.2** Radiation Dermatitis of the Face.

radiation doses of less than 100 mSv/year, the probability of stochastic effects is very low. At such low doses, it is assumed that the probability of incurring cancer or heritable effects will be directly proportional to the equivalent dose. This is known as the linear-nonthreshold model of incremental risk.

Leukemia and other cancers have been shown to be associated with radiation exposure. It is estimated that the probability



**Figure 26.3** Radiation-Induced Skin Necrosis.

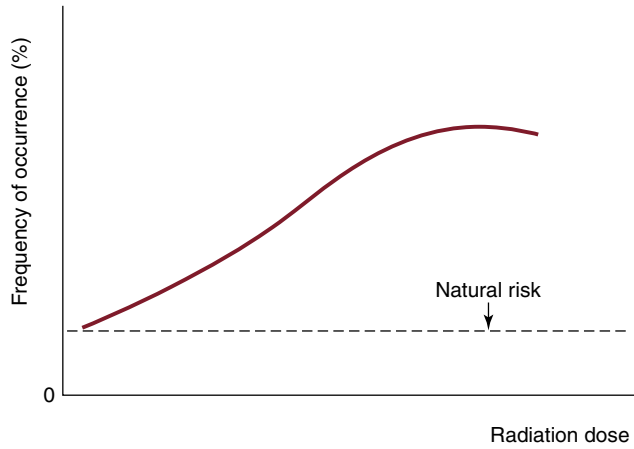


**Figure 26.4** General Dose-Response Curve for the Stochastic Effects of Radiation.

of fatal cancer developing as a result of radiation exposure is 4% per 1 Sv of lifetime dose equivalent (or 0.004% per mSv). For reference, the background risk of spontaneous fatal cancer is approximately 20%. The nominal nonfatal cancer risk has been estimated at 0.8% per sievert. Radiation-induced cancer risks from relatively low-dose exposure are difficult to estimate. A statistically significant increase in cancer risk has not been demonstrated in populations exposed to doses of less than 100 mSv. Studies of atomic bomb survivors showed an increased incidence of leukemia and other tumors of the lung, thyroid, breast, skin, and gastrointestinal tract. There is usually a latent period of 2 to 5 years for the leukemia, 5 years for thyroid cancer, and 10 or more years for other cancers to manifest. The

risk of radiation-induced malignancy with prenatal exposure or for children and adolescents is slightly higher than that seen in adults by a factor of 2 to 3. Fetal effects are discussed in the “Radiation and Pregnancy” section, later in this chapter.

Hereditary effects from radiation exposure have not been observed in humans in studies of the offspring of atomic bomb survivors. Based on extrapolation from animal studies, the ICRP proposed a nominal risk of heritable effects of 0.1% per sievert.

## EXPOSURE AND RECOMMENDED LIMITS

### Background Radiation

We are constantly exposed to radiation through naturally occurring radioactive materials, as well as by cosmic radiation and human activities. The average annual natural background radiation, which varies depending on the geographic location, is around 3 mSv/year in the continental United States. Living at higher altitude is associated with a higher dose. The greatest source of domestic radiation is radon gas (about 2 mSv/year). Radon arises from the decay of radium; it seeps out of the soil and may concentrate in poorly ventilated concrete homes because of its high density. Radon is the second most frequent cause of lung cancer after cigarette smoking. Other manmade radiation sources include building materials, fuel, televisions, smoke detectors, and various fluorescent devices.

### Occupational and Medical Exposure

Approximately 80% of lifetime exposure to radiation for the general public comes from natural sources and the rest from manmade sources such as medical radiographs and CT scans. The total average exposure for Americans is about 3.6 mSv/year. In the United Kingdom, the average yearly dose is about 2.2 mSv. Some of the common occupation-related radiation dosages are addressed in **Table 26.3**. Pilots, who are exposed to solar radiation, are at a higher risk. On average, the amount of cosmic radiation doubles with every 2000-mile increase in altitude; cosmic radiation is strongest at the earth’s poles. Taking a long-haul commercial flight results in about 0.1 mSv of radiation exposure.

The typical doses of common diagnostic radiology examinations are given in **Table 26.4**. These values vary, depending on the machine and manufacturer, study technique, and patient’s body habitus.

### Recommended Dose Limits

The ICRP recommends a dose limit of 1 mSv/year to the general public. For radiation workers, the effective dose limit is 20 mSv/year, averaged over 5 years and not exceeding 50 mSv in any single year. Additional exposure limits for the ocular lens and extremities of workers are defined separately (**Table 26.5**). It is generally believed that for occupational exposure, the risk of health effects is too small to be observed at doses below 50 to 100 mSv/year.

**TABLE 26.3** Background and Occupational Exposure

Occupation	Effective Dose (mSv/year)
Natural background radiation	3
Aircrew (1000 h)	5
Frequent flyer (75,000 miles/200 h)	1
Catheterization laboratory physician	2–60
Catheterization laboratory nurse	8–16

**TABLE 26.4** Typical Effective Dose in Common Diagnostic Procedures

Examination	Effective Dose (mSv)
Chest radiograph (PA)	0.02
Chest radiograph (lateral)	0.04
Skull radiograph	0.03
Pelvic radiograph	0.7
Abdominal radiograph	1.0
Thoracic spine (AP)	0.4
Lumbar spine (AP)	0.7
Mammogram	0.1
Barium swallow	1.5
Barium enema	7.0
CT of the head	2
CT of the thorax	8
CT of the abdomen	10
CT of the pelvis	10
Cardiac CT (calcium score)	2
Coronary angiogram	5–15

AP, anteroposterior; CT, computed tomography; PA, posteroanterior.

## PRINCIPLES OF RADIATION PROTECTION

The ICRP system of protection in medical practice stresses the fundamental principles of justification, optimization, and dose and risk limits. The use of radiation in medicine must be justified – that is, the diagnostic information or therapeutic use should produce more benefit than harm. It is the responsibility of the hospital and medical personnel to ensure that the radiation equipment is properly maintained to deliver the lowest possible dose of radiation and to ensure that safety instructions and protective measures are available and adopted. All procedures involving ionizing radiation should be monitored and the risk limits determined for patients and staff beforehand. A system of reporting and remedial measures should be in place whenever the recommended limit is exceeded. In addition, special operating procedures should be available for high-risk individuals, such as pediatric patients and pregnant patients or workers.

**TABLE 26.5** International Commission on Radiological Protection Safety Dose Limits

	Occupational	Public
Whole-body effective dose	20 mSv/year averaged over 5 years	1 mSv/year
Ocular lens	20 mSv/year	15 mSv/year
Skin	500 mSv/year	50 mSv/year
Extremities	500 mSv/year	—
Pregnant women	1 mSv to the fetus	—

## RADIATION SAFETY: DIAGNOSTIC PROCEDURES

For diagnostic procedures, an alternative imaging modality that does not involve radiation, such as magnetic resonance imaging or ultrasound imaging, should be considered whenever possible. Certain routine radiographs or screening tests, such as chest radiographs on hospital admission and skull radiographs for minor head injuries, are associated with more risk than benefit and therefore should be avoided.

CT has become one of the most commonly used diagnostic tools, largely because of the availability of faster, more powerful machines with multislice capabilities, thus reducing examination time and increasing imaging accuracy. Contrary to common belief, the effective dose of spiral and multislice detector CT scans can be 10% to 30% higher than that for older CT scans, depending on the protocol and machine. In less essential situations, the physician should request lower-dose examinations, wider pitch, and partial rotation instead of large numbers of overlapping scans of extensive body regions. A number of techniques such as automated tube current modulation or attenuation-based kilovoltage selection algorithms can be used to reduce radiation exposure for CT angiograms after endovascular aneurysm repair (EVAR).

Many patients undergo CT angiography and subsequent serial CT scans for follow-up of endovascular aortic procedures. The effective dose of a CT scan of the chest is about 8 mSv, and for the abdomen and pelvis it is about 10 to 20 mSv (see Table 26.4). Repeated examinations of large areas may deliver an effective dose that can approach harmful levels. The excess relative risk of a patient acquiring solid organ malignancy from postoperative CT scans in EVAR surveillance is higher in young patients, women, and those undergoing multiple scans. A policy of switching to standard or contrast-enhanced ultrasound scans for postoperative EVAR surveillance has been shown to be equally effective even for fenestrated grafts, an approach that will further reduce exposure to radiation.<sup>3</sup>

Three-dimensional rotational angiography (DynaCT) has recently found a role in preoperative planning, especially under emergency situations, and also in postoperative identification of endoleaks. The mean dose area product for a DynaCT is in the range of 3500 to 4000  $\mu\text{Gym}^2$ , which is seven to eight times less than the radiation from a standard multidetector CT.<sup>4</sup>

Consideration should be given to the patient as a whole during imaging. Sometimes higher-risk organs may be exposed to unnecessarily high doses even if they are not the targets of the examination. For example, the lens, thyroid, and breast in CT examinations of the head and thorax often receive doses as high as 30 to 40 mSv. The gonads are also at risk during CT scans of the pelvis. This is particularly important for younger patients and females of childbearing age.

Pervading thoughts since the 1950s were to make every effort to shield radiosensitive organs whenever possible – in particular when they are adjacent to but not part of the actual radiographic examination. Radiologists Marsh and Silosky reported in the *American Journal of Roentgenology* in April 2019 that shielding areas of the patient, particularly the thyroid and gonadal regions, had negligible benefits and actually resulted in an increase in radiation exposure overall.<sup>5</sup> Feedback loops used in fluoroscopy for automated brightness control work between the image receptor and the X-ray tube to ensure consistent image quality. If the shielding is in the field of imaging, this feedback loop will actually increase the dose to the patient in an attempt to improve image quality. A similar feedback loop exists in CT imaging. As a result, modern radiographic imaging no longer typically shields the patients, though this continues to evolve given the culture of a lead apron draped over the patient for the last 50 years.

## RADIATION SAFETY: ENDOVASCULAR PROCEDURES

Modern coronary interventional procedures incur an average dose of 0.05 mSv per procedure. Radiation exposure for an operator in modern catheterization laboratories can amount to 5 to 60 mSv/year. The operator's hands are at particular risk. One minute of unprotected screening time leads to 20 mSv of skin dose, and transient skin erythema can result from doses of 2 Sv. Higher doses of radiation can lead to eye damage characterized by cataract formation in the posterior pole of the lens. Chronic exposure will increase the risk of cancer, in particular in the thyroid, brain, and skin.

Although most endovascular procedures are usually performed on older patients in whom the perceived stochastic risks are relatively small, one must always be conscious of the radiation dosage to reduce the probability of deterministic effects to skin, soft tissue, and the eyes. The typical exposure of a patient in a catheterization laboratory with 10 minutes of fluoroscopic time is estimated to be equivalent to 200 to 400 chest radiographs.

In the interventional suite, the operator is responsible for limiting the amount of radiation exposure to themselves, as well as their patients and coworkers. Fluoroscopy should be used intermittently and should never be used unless the operator is viewing the monitor. Only essential personnel should be in the room, and ample warning signs should be displayed at all entrances. All staff not essential to the procedure should leave the room during serial exposure sequences or stand behind a barrier shield. Good practice in minimizing patient exposure will also cut down exposure to the operator and assistant staff.

Radiation equipment should be regularly serviced and inspected by a medical physicist and calibrated at proper intervals. Standard radiation checklists should be used regularly for self-inspection. The radiation dose varies among different machines and room setups. In general, newer machines and fixed systems generate lower energy because of the better quality image intensifier. They also utilize more dose-reducing features such as pulse fluoroscopy and they provide better-quality images, thus further reducing imaging time. Operators should try to familiarize themselves with these safety features to maximize radiation protection.

High dosages during interventional procedures are often due to inappropriate use of imaging or protective equipment or poor technique. It is essential that the operator understand the benefits of proper table manipulation, shielding, collimation and decreasing magnification use. The following are essential practice guidelines to reduce radiation exposure.

### Emission Control

The voltage of the fluoroscopic tube controls the penetration of the beam and contrast, whereas the current determines the number of photons produced by the tube. Most machines have an automatic exposure control based on the feedback from the image receptor. Using higher tube voltage (kVp) and less current (mA) will reduce radiation and will not usually compromise image quality. Lower frame rates should be adopted, and pulsed fluoroscopy instead of continuous fluoroscopy should be used for less critical maneuvers. In pulsed fluoroscopy mode, the X-ray generator emits short bursts of energy, which decreases the exposure time compared with continuous fluoroscopy. Higher dose fluoroscopy modes often increase the pulse rate, thereby increasing radiation dose. A large image intensifier requires less radiation than does a small one. The use of magnification should be limited because magnified views incur two to three times the radiation of a normal view. The use of dual fluoroscopy with live-image digital zooming can provide a magnified appearing view without the associated increase in radiation dose and has been demonstrated to significantly reduce patient and OR staff radiation during fenestrated-branched EVAR.<sup>6</sup> The use of high-level fluoroscopy should be kept to a bare minimum. X-ray field collimation and filters should be used whenever possible. This helps in focusing the beam of radiation by decreasing the field of view, thereby allowing for a clearer image. A large patient will expose the operator to more radiation because of an automatic increase in voltage and current from the machine to obtain a satisfactory image.

### Time

Every effort should be made to minimize fluoroscopy and screening time. A conscientious operator will refrain from continuous activation of the beam-on switch and instead perform intermittent short exposures only when necessary. When the table position must be changed, it should be done before confirming with fluoroscopy. Liberal use of fluoroscopy often accounts for the largest radiation exposure during a procedure.

Safety features are built into modern equipment to alert the operator to excessive use. A timer usually produces an audible warning at the end of a 5-minute interval. Making a habit of noting the total fluoroscopy time and patient absorbed dose at the end of the procedure may increase awareness and motivate improvement in practice.

Digital subtraction angiography is used to acquire images and generate a permanent record, and it requires high-dose rapid-sequence screening. This procedure can result in 10 times more radiation than fluoroscopy and accounts for 60% of total personnel doses. The use of cine fluoroscopic acquisition should be limited and an attempt made by operators to maintain a safe distance by stepping away or leaving the room if possible when activating this function.

## Distance

Personnel should always maintain maximal distance from the X-ray tube and keep the image intensifier as close to the patient and the tube as far away as possible to reduce patient skin dosage. The amount of scatter radiation decreases with the square of the distance from the tube ( $\text{exposure} = 1/d^2$ ); thus, the radiation dose will diminish fourfold if the distance from the operator doubles.

Radiation exposure varies according to the angulation of the tube. The left anterior oblique view exposes the operator, if standing to the right of the patient, to the greatest amount of radiation because the tube is closest to the operator. This view can account for three to five times more radiation than a right anterior oblique view. Steep gantry angulations also increase exposure by increasing the length of the radiation path and the thickness of tissue penetration. Changing the beam angulation during prolonged procedures can help spread out the radiation and reduce the skin dose to a particular area. Mesenteric and renal interventions, alone or in conjunction with endovascular aortic aneurysm repair, require some of the steepest gantry angles. During these cases, it is particularly important to make use of ceiling-mounted plexiglass shields to decrease scatter exposure to the operator.

Maximizing the distance between the radiation source and the patient decreases radiation exposure as a function of the inverse square law. Raising the fluoroscopic table as high as possible, away from the source, decreases the radiation exposure to the patient. Once the table is raised to a comfortable height as high as possible away from the source, the image intensifier should be lowered as close as possible to the patient. A recent study on scatter radiation levels using cadavers showed that operator radiation exposure is lowest with a detector-to-patient distance of <5 cm, a source-to-image distance of <15 cm, and a 10-cm vertical collimation. The assistant's exposure is 23% to 46% of the operator's.<sup>7</sup>

## Barriers

Radiation scatter is not uniform but propagates in isodose curves and decreases exponentially with the distance from the source. The highest scatter exposure is at the table level. A

modern interventional suite should be equipped with tableside lead shields and additional mobile lead shields to reduce scatter. Ceiling-mounted mobile shields are very effective in reducing radiation exposure to the operator, reducing doses to the brain and eye by a factor of 20. The operator should always try to stand behind a barrier for the entire procedure.

Properly worn personal protective equipment is essential. Staff members should wear protective aprons with at least a 0.25-mm lead equivalent; many modern lightweight models provide wraparound designs to maximize frontal protection. A 0.25-mm lead apron will attenuate approximately 96% of the dose, and a 0.5-mm apron, 99%. The front of the apron should be kept toward the X-ray tube at all times. Lead glasses and thyroid shields should always be worn. Protective gloves should be at least a 0.35-mm lead equivalent but are less widely used because of reduced tactile sensitivity and the tendency for operators to place their hands more often in the field. All protective gear should be inspected at least yearly and must be replaced if defective.

Radiation exposure to the brain during endovascular interventions may increase the risk of cerebral neoplasms. Lead equivalent surgical caps have been suggested as a way to effectively reduce exposure to the brain during interventions. Kirkwood et al. noted that use of a lead-equivalent surgical cap attenuated direct X rays from the superficial temporal location but did not protect the majority of exposure due to scatter, thereby rendering the protective caps clinically irrelevant.<sup>8</sup> Good practice habits of time, distance, and shielding consistently remain the most effective techniques in protecting operators from radiation exposure.

## Training

Radiation safety training is an essential part of every vascular surgery training program and is included in the online modules of the Surgical Council on Resident Education (SCORE) curriculum. Trainees are assessed on radiation safety annually on the Vascular Surgery In-Training Examination (VSITE) as well as during the board certification testing process. There exist many high-quality online radiation safety training courses that will satisfy institutional and state requirements. Requirements vary from state to state with regard to demonstrating radiation safety education for initial privileging and subsequent annual safety review and update.

## Technique

The primary operator should possess the necessary endovascular skills to perform the procedure from both a technical and radiation safety standpoint. Even a straightforward endovascular procedure can result in significant radiation exposure if the operator's technique and protection practice are poor.

## Monitoring Exposure

In the work environment, occupational radiation exposure should be routinely monitored for individuals at risk of

exceeding 10% of the annual recommended exposure limit. This is performed using a dosimeter typically worn on the thyroid shield, with a second dosimeter worn at waist level under the apron for pregnant workers. These individual monitoring devices are usually film badge-based, thermoluminescent dosimeters that measure an absolute dose received over a specific period of time. Further investigation is necessary when the cumulative total dose during a year reaches recommended ICRP limits, and temporary withdrawal from radiation work should be enforced.

Compliance with badge dosimeter use can be inconsistent for institutions. Monthly collection and changing out of badges, along with correct positioning on lead garments can be problematic. Bluetooth capability with smart devices has now allowed for easier capture of a provider's exposure and increased efficiency in feedback. Instadose® is an example of this smart technology which is able to capture, measure, transmit, analyze and report radiation dose exposure to the operator on demand. This can be particularly helpful for those who are at risk for increased exposure.

Informed consent and proper recording of patient exposure should be ensured if the anticipated dose of a complicated procedure is high. Discussion should be undertaken with the patient and family immediately after a complicated procedure to inform them of the high use of radiation and possible development of skin reactions or changes. If a patient is exposed to a higher dose of radiation (>3 to 5 Gy), follow-up evaluation with examination of the skin should be arranged within 1 to 2 weeks to determine whether any harmful effects have developed.

## RADIATION AND THE ENDOVASCULAR SURGEON

Endovascular therapy for vascular disease has become more complex, and many hospitals have modern hybrid OR suites installed in lieu of mobile C-arms. Although these fixed units provide much better image quality, operators may become oblivious to total fluoroscopy time and the use of image acquisition and magnification during a more complex case, leading to unnecessary radiation exposure to the patient and members of the OR team.

Multiple studies have evaluated the radiation exposure of vascular surgeons undertaking endovascular procedures. Ho and colleagues conducted a prospective study on an active endovascular practice in an academic unit over a 12-month period.<sup>9</sup> All endovascular procedures were performed with mobile fluoroscopic units in an operating room setting, using tableside barriers, standard 0.5-mm lead aprons, thyroid shields, and protective eyewear. The workload consisted of 149 endovascular procedures, including 30 endovascular aneurysm repairs, 58 diagnostic angiograms, and 61 peripheral angioplasty and stenting procedures. With an average of 500 to 700 minutes of annual fluoroscopy time, the median yearly effective doses that the surgeons received were 0.2 mSv, 0.2 mSv and 1 mSv for the body, eye and hand, respectively. Notably, these amounts are

significantly below ICRP recommended dose limits. The investigators extrapolated that a vascular surgeon would need to perform 2600 endovascular aneurysm repairs or 6500 peripheral interventional procedures annually to reach the dose limit.

Provided that a stringent protection policy is used, the amount of radiation absorbed by vascular surgeons appears to be lower than that absorbed by cardiologists or interventional radiologists, who reportedly receive up to 60 and 10 mSv annually. However, the study also revealed significant individual variations in dosage, probably related to technique and habit. This difference was most notable for doses to the hand, in which case less experienced surgeons accumulated up to 3.3 times the dosage per minute for the same procedure than more experienced surgeons. Regular use of eye protection also reduced eye doses by a factor of 3. Data supporting the protection of the ocular lens with the use of commercially available lead-equivalent eyewear is equivocal. Investigation into the benefits of modified leaded eyewear in the reduction of operator eye radiation dose has been described and was noted to result in a >80% reduction in radiation dose to the operator's left eye in the simulated fluoroscopic intervention and >60% in the clinical fluoroscopic intervention.<sup>10</sup> The functional impact of cataract formation in the vascular interventionalist is of great concern.

A number of studies have focused on the radiation exposure to patients during EVAR, using indirect dose area product (DAP) measurement.<sup>11–15</sup> An estimated average effective dose of 12.4 mSv was reported based on DAP estimation in 111 EVAR cases, and average peak skin dose was 0.69 Gy, with 99% of patients having a peak skin dose of <2 Gy.<sup>11</sup> Significantly higher exposure was reported in patients with a high body mass index (>30),<sup>12</sup> those with complex anatomy,<sup>12</sup> and for those undergoing fenestrated and branched procedures.<sup>14</sup> For a standard EVAR, the average fluoroscopy time is about 20 minutes, with approximately 50% of imaging performed in a magnified view. The incurred entrance skin dose is 0.85 Gy, with a DAP of 60 to 150 Gy cm<sup>2</sup> and a patient effective dose of 8 to 27 mSv. Skin injury is still possible, but it is unlikely at these levels. These dosages can be further decreased by the usage of low-dose and pulse mode, especially for fenestrated and branched grafts, procedures in which mean DAP values of 860 and 1890 Gy cm<sup>2</sup> are to be expected.<sup>12</sup>

Modern imaging systems, which provide multiple high-resolution video screens and give the operator full motorized control of the C-arm, patient position, and imaging mode, have been shown to reduce radiation exposure, operation and screening time, and contrast volume.<sup>16</sup> State-of-the-art equipment now allows for off-table planning, precision of cannulation, and remote control. The use of three-dimensional (3D) navigation software by fusion of preoperative CT with DynaCT images obtained on the table will allow a 3D real-time visualization of catheter position with respect to the target vessels. In complex endograft procedures this reduces radiation exposure and the use of contrast media by facilitating branch cannulation. Also, in development is a robotic system for peripheral vascular interventions, allowing distal 3D catheter tip control by a surgeon from a remote workstation, thus protecting the operator from additional radiation exposure.

## RADIATION AND PREGNANCY

With the increasing use of medical radiation, many women who are pregnant or potentially pregnant will be subject to occupational exposure to ionizing radiation. In most instances, the radiation risk to the fetus is small in comparison to the risk of spontaneous abortion (15%), genetic abnormalities (4%–10%), and malformations (2%–4%) in the general population.

### Declaration of Pregnancy

Under federal law, a pregnant woman can choose to continue to incur occupational radiation exposure at the level allowed for adult workers. However, it is recommended that an occupationally exposed pregnant woman declare pregnancy for the purpose of reducing the risk to the unborn child. Once pregnancy is declared, additional precautions should be adopted to protect the fetus and limit the radiation exposure to recommended levels.

### Fetal Risk From Radiation

Risks to the fetus from radiation depend on the dosage and the stage of pregnancy, the risk being highest during organogenesis in the first trimester and least in the third trimester. For the pregnant patient, whenever possible, diagnostic tests or procedures that involve radiation should be deferred or replaced with safer options. In all cases, the patient should be adequately informed of any chances of radiation exposure as well as the associated risks. Estimated fetal radiation doses for diagnostic tests vary based on the type of procedure and the stage of the pregnancy; doses are generally highest in the later trimesters. A plain anteroposterior radiograph of the pelvis carries a dose of about 1.5 mSv. A lumbar spine anteroposterior radiograph at 3 months of gestation results in about 2 mSv of exposure, however this increases to 9 mSv when performed near term. A CT scan of the head of the mother delivers less than 0.005 mSv to the fetus, but an abdominal CT scan can lead to 8 mSv of fetal exposure.

The major adverse effects on the fetus include abortion, teratogenicity, mental retardation, intrauterine growth retardation, and the induction of cancer. Normal diagnostic procedures would seldom involve sufficient dosage to induce malformations, fetal death, or central nervous system defects, but the threshold may be exceeded with complicated interventional procedures.

### Malformations and Mental Retardation

Based on animal studies, malformations after in utero exposure to doses below 100 mSv are not expected. Central nervous system malformations may appear if a dose threshold of 100 mSv has been exceeded (Table 26.6). Fetal doses of 100 mSv or higher, especially if incurred between 8 and 16 weeks of pregnancy, can be associated with reduction of intelligence and microcephaly. As an example, in victims exposed to in utero radiation during the 1945 atomic bombing of Hiroshima,

**TABLE 26.6**

Probability of Fetal Risk as a Function of Radiation Dose

Fetal Dose (mSv)	Probability of Malformation (%)	Probability of Development of Cancer (%)
1	3	0.3
5	3	0.3
10	3	0.4
50	3	0.6
100	3	0.9

Modified from the International Commission on Radiological Protection guidelines.

the risk of mental retardation has been estimated to be about 0.04% per mSv of exposure, with an estimated loss of 2 to 3 IQ points/mSv.

### Cancer Risk

The main concern with prenatal radiation exposure at lower levels is the risk of cancer. Radiation has been shown to increase the risk of leukemia and cancer in children and the fetus. The threshold exposure associated with childhood cancer induction is not clear. For in utero exposure of 10 mSv, a 1.4-fold increase in leukemia and cancer and 1 excess cancer death per 1700 have been reported.

From studies of atomic bomb survivors and patients receiving radiotherapy, preconception exposure of the gonads to radiation has not been shown to result in a significant increase in the risk of cancer or malformations in children. The risk of serious birth defects was estimated at  $2^{-6}$  per 1-mSv gonadal dose.

### Recommendations for Pregnant Workers

Pregnant healthcare workers may work in a radiation exposure environment as long as it is determined that the cumulative fetal dose can be kept below 1 mSv during the course of pregnancy. Fetal radiation exposure is monitored with an additional dosimeter worn at the waist level underneath the lead apron. With such doses, radiation should have negligible effects on the fetus. Properly sized protection should be worn at all times, although lead aprons may present other health hazards, such as back strain, in pregnant women. Fetal doses approaching 100 mSv pose a small risk of radiation-induced cancer or leukemia, but the risk is minimal in the third trimester. The National Nuclear Commission guideline calls for no more than 5 mSv of equivalent dose exposure during the entire pregnancy, or less than 0.5 mSv/month. If a worker has declared pregnancy while having been exposed to radiation, it should be ensured that any additional dose to the fetus would not exceed 1 mSv during the remainder of the pregnancy.

A unique concern to female vascular surgeons and trainees is radiation exposure during pregnancy. The authors were involved in a multi-institutional study in 2013 aimed to evaluate the dosages recorded on fetal dosimeter badges and compare them to the external badges worn by the same cohort of 81

women.<sup>17</sup> The average fetal dosimeter recording during the pregnancy rounded to zero. Only two women had positive fetal dosimeter recordings; one had a single reading of 3 mrem and the other had a single recording of 7 mrem. No significant difference between maternal exposure prior to, during, and post pregnancy was noted. This documentation of negligible radiation exposure on fetal monitoring suggests that with appropriate safety precautions, heightened concerns during pregnancy may be unfounded.

## SELECTED KEY REFERENCES

- International Commission on Radiological Protection (ICRP) Publication 60. *Recommendations of the International Commission on Radiological Protection*; 1990.
- A concise summary of the principles of radiation protection.*
- International Commission on Radiological Protection (ICRP) Publication 84. *Pregnancy and Medical Radiation*. Oxford: Pergamon Press; 2000.
- Further details on radiation and pregnancy.*
- International Commission on Radiological Protection (ICRP) Publication 103. *Recommendation and Protection Guidelines*.

*A comprehensive update of the current ICRP recommendation and protection guidelines and definitions.*

International Commission on Radiological Protection (ICRP) Publication 117. *Radiological Protection in Fluoroscopically Guided Procedures Performed Outside the Imaging Department*; 2010.

*A modern account on the risks and practice recommendations of operating radiation equipment outside radiology departments.*

Laurier D, Richardson DB, Cardis E, et al. The International Nuclear Workers Study (Inworks): a collaborative epidemiological study to improve knowledge about health effects of protracted low-dose exposure. *Radiat Prot Dosimetry*. 2017;173(1–3):21–25.

*Key reference to INWORKS.*

National Research Council Committee to Assess Health Risks from Exposure to Low Levels of Ionizing Radiation. *Health Risks from Exposure to Low Levels of Ionizing Radiation*. BEIR VII Phase 2. Washington, DC: National Academies Press; 2007. Available at <https://doi.org/10.17226/11340>.

United Nations Scientific Committee on the Effects of Atomic Radiation. Available at <http://www.unscear.org>.

*UNSCEAR report that describes in detail the various source and effects of ionizing radiation.*

A complete reference list can be found online at [www.expertconsult.com](http://www.expertconsult.com).

## REFERENCES

1. Kim KP, et al. Occupational radiation doses to operators performing fluoroscopically guided procedures. *Health Phys.* 2012;103:80–99.
2. Kirkwood ML, et al. Surgeon education decreases radiation dose in complex endovascular procedures and improves patient safety. *J Vasc Surg.* 2013;58(3):715–721.
3. Perini P, et al. Contrast-enhanced ultrasound vs. CT angiography in fenestrated EVAR surveillance: a single-center comparison. *J Endovasc Ther.* 2012;19:648–655.
4. Norton IM, et al. Validation of DynaCT in the morphological assessment of abdominal aortic aneurysm for endovascular repair. *J Endovasc Ther.* 2010;17:183–189.
5. Marsh RM, et al. Patient shielding in diagnostic imaging: discontinuing a legacy practice. *Am J Roent.* 2019;212:755–757.
6. Timaran LI, et al. Dual fluoroscopy with live-image digital zooming significantly reduces patient and operating staff radiation exposure during fenestrated-branched endovascular aortic aneurysm repair. *J Vasc Surg.* 2021;73(2):601–607.
7. Haqqani OP, et al. Minimizing radiation exposure to the vascular surgeon. *J Vasc Surg.* 2012;55:799–805.
8. Kirkwood ML, et al. Radiation brain dose to vascular surgeons during fluoroscopically guided interventions is not effectively reduced by wearing lead equivalent surgical caps. *J Vasc Surg.* 2018;68:567–571.
9. Ho P, et al. Ionizing radiation absorption of vascular surgeons during endovascular procedures. *J Vasc Surg.* 2007;46:455–459.
10. Kirkwood ML, et al. Novel modification to leaded eyewear results in significant operator eye radiation dose reduction. *J Vasc Surg.* 2020;72(6):2139–2144.
11. Walsh C, et al. Measurement and optimization of patient radiation doses in endovascular aneurysm repair. *Eur J Vasc Endovasc Surg.* 2012;43(5):534–539.
12. Maurel B, et al. Evaluation of radiation during EVAR performed on a mobile C-arm. *Eur J Vasc Endovasc Surg.* 2012;43:16–21.
13. Thakor AS, et al. The radiation burden from increasingly complex endovascular aortic aneurysm repair. *Insights Imaging.* 2011;2:699–704.
14. Howells P, et al. Risk of radiation exposure during endovascular aortic repair. *Eur J Vasc Endovasc Surg.* 2012;43:393–397.
15. Kalf-Ezra JA, et al. Endovascular abdominal aortic aneurysm repair: methods of radiological risk reduction. *J Cardiovasc Surg.* 2011;52:769–778.
16. Peach G, et al. Operator-controlled imaging significantly reduces radiation exposure during EVAR. *Eur J Vasc Endovasc Surg.* 2012;44(4):395–398.
17. Chandra V, et al. Monitoring of fetal radiation exposure during pregnancy. *J Vasc Surg.* 2013;58(3):710–714.

# Arteriography

AMIR F. AZARBAL and ROBERT B. McLAFFERTY

## EQUIPMENT 317

- Operating Room Versus Imaging Suite 317
- Fixed-Mount Versus Portable Equipment 318
- Catheters 319
- Contrast Agents 319
  - Iodinated Contrast Agents* 319
  - Carbon Dioxide Arteriography* 319
- Devices for Injection of Contrast Agents 321
  - Power Injection* 321
  - Manual Injection* 321

## TECHNIQUES 322

- Image Processing 322
  - Subtraction Tool and Masking* 322
  - Pixel Shifting* 323
  - View Tracing* 323
  - Roadmapping and Measuring* 323
- Single-Injection Multiple-Linear Field Arteriography 325
  - Stage Technique* 325

## *Stepping Technique* 325

- Limitations of Single-Injection Multiple-Field Arteriography* 326
- Rotational Arteriography** 327
  - Three-Dimensional Fusion Computed Tomography* 327
  - Maximizing Image Quality During Arteriography* 327

## CLINICAL APPLICATIONS 329

## LIMITATIONS AND RISKS 332

- Sources of Error with Arteriography** 332
- Risks from Contrast Agents** 332
  - Systemic Toxicity* 332
  - Cardiac Toxicity* 334
  - Hematologic Toxicity* 334
  - Nephrotoxicity* 334
  - METFORMIN* 335
  - PREVENTION OF CONTRAST-INDUCED NEPHROPATHY** 335
    - Limitations and Risks of CO<sub>2</sub> Contrast* 335
- FUTURE ADVANCES** 335

Despite many advances in the quality and availability of less invasive arterial imaging modalities, arteriography remains the “gold standard.” Alternative modalities, such as duplex arterial mapping, computed tomographic angiography (CTA), and magnetic resonance angiography (MRA), are being used with increasing frequency because of improved image quality and minimal risk.<sup>1–6</sup> For some clinical scenarios, such as duplex surveillance of lower extremity vein bypass grafts, these imaging techniques have supplanted arteriography as the preferred test.<sup>7–9</sup> However, arteriography remains an indispensable tool for the vascular surgeon. A comprehensive understanding of basic to advanced techniques permits a wide array of arteriographic imaging studies to be performed optimally. In addition, a wide breadth of knowledge about arterial anatomy, equipment and materials, potential complications, and sources of interpretation error are required for becoming an expert in performing arteriography.

The goal of this chapter is to impart a broad overview of modern arteriography. Clinical acumen about vascular disease

and operative experience also play important roles in determining how to optimize arteriographic imaging. This chapter provides evidence-based guidance, as well as practical experience, for safe performance of high-quality arteriography.

## **EQUIPMENT**

The task to determine what equipment is needed to perform high-quality arteriography can seem overwhelming. The necessary components can be divided into venue, imaging hardware, catheters, contrast agents, devices for delivery of contrast agents, and digital software used to assist in the processing of arteriographic images. Image processing closely relates to techniques of arteriography and is discussed later in the chapter.

### **Operating Room Versus Imaging Suite**

Depending on facility-specific logistics, angiography can be performed with a portable fluoroscopy unit or in a designated

interventional suite with a fixed imaging unit. Many centers contain “hybrid operating rooms,” featuring a fixed-mount imaging unit combined with all the features of an operating room, a fully equipped endovascular stock (catheters, guide wires, and devices), and a trained staff that is proficient in endovascular and open vascular surgery.

The advantages of an operative-endovascular or hybrid suite are clear. Combined endovascular and open procedures are common. Aortic endograft procedures, common femoral endarterectomy with concomitant retrograde or antegrade stenting and hybrid approaches to acute limb ischemia have evolved into the “standard of care.” Lastly, complications that arise during any endovascular procedure, albeit rare, can be managed by immediate and seamless conversion to open surgery, obviating the need for emergency transport from an interventional suite to the operating room.

### Fixed-Mount Versus Portable Equipment

The two principal types of radiographic imaging units that can provide state-of-the-art arteriography are the fixed-mount unit (Fig. 27.1), and the portable fluoroscopy unit equipped with wheels so that it can be moved from room to room (Fig. 27.2). Each type has the basic components, including a power generator for fluoroscopy, a C-arm with image intensifier, screens for viewing real-time and reference images, and digital image processing software. In experienced hands, both types of imaging units have their advantages and disadvantages. Fixed units, while previously mounted to the ceiling or floor are also now available on a gantry that travels on pre-defined paths using laser guidance in the hybrid OR setting. This allows the unit to be parked in the corner of the room, out of the way, when not needed.

In general, fixed-mount units have more powerful generators that allow more detailed imaging. More power allows greater depth of fluoroscopic penetration and thus the ability to discern finer detail. Depending on the types of imaging units compared, fixed-mount units can provide upward of 10 times the resolution of portable units. Although this greater resolution may not be needed in persons of ideal body weight, increased power for improved penetration is important when arteriography is performed on obese patients. Another distinct advantage of a fixed-mount unit is a larger field of view. Modern fixed-mount units now have flat detector image intensifiers as large as 22 inches (57-cm image projection). This increased size translates into the ability to cover more imaging area during arteriography with less radiation exposure and lower total volume of contrast material. In addition, fixed-mount units have tableside controls that allow precise and easily directed movement of the C-arm and table. This feature is useful during visceral and cerebrovascular arteriography where minute manipulations in C-arm angulation can result in significantly improved arterial visualization.

A portable fluoroscopy unit designed for high-quality arteriography is advantageous by the mere ability to move the equipment from room to room. This may be important in trying to fulfill the needs of different types of vascular surgical



**Figure 27.1** Dedicated fixed-mount imaging suite. (Courtesy Siemens Medical Solutions USA, Inc.)



**Figure 27.2** Mobile C-arm portable unit. (Courtesy Philips Healthcare.)

practices, operating rooms, specialty procedure rooms, and intensive care units. Depending on the setting, portable fluoroscopy units may require only one technician in addition to the vascular surgeon for arteriography to be adequately performed, although a nurse able to monitor the patient when moderate sedation is used is often required as well. Fixed-mount units may require three or four specially trained staff, including a technician who is gowned and gloved with the vascular surgeon, a circulator attending to material needs, a technician coordinating image acquisition and processing, and a certified nurse who is responsible for monitoring the patient and administering medications. Finally, portable units are much less costly than fixed-mount units. Not only are fixed-mount units expensive (ranging from \$1.5 to \$5 million), but construction



**Figure 27.3** Flush catheters in various shapes with multiple side holes, as opposed to end-hole catheters (not pictured), are ideal for power injections.

of such a suite may require major structural modifications to an existing room, which can be a significant additional cost.

## Catheters

The type of catheter used also plays an important role in optimizing the arteriographic image and avoiding injury to the vessel. Intraarterial catheters come in virtually all shapes, sizes, wire compatibilities and lengths. Given this variety, attention should be paid to whether the catheter has just an end hole or multiple side holes in addition to the end hole (Fig. 27.3). The latter, known as a flush catheter, is designed for safe, quick, and even dispersion of contrast material at high injection pressures to image large arteries with high flow. These are typically used for aortoiliac arteriography or venography of the iliac veins or vena cava. End-hole catheters, with their greater variety of shapes and sizes, are often all that can be used after remote arterial access is achieved. Care should be taken whenever a power injection is performed with an end-hole catheter in a medium-sized artery. Problems may include loss of a tenuous catheter crossing because of pressure forcing the catheter out of the arterial lumen, creation of intimal flaps, and arterial rupture. Power injection into very small arteries, such as the vertebral or tibial arteries, should be avoided with any type of catheter. Controlled hand injection with either a manifold or syringe should also be performed gently to avoid injury to these vessels.

## Contrast Agents

The concept of angiographic imaging relies on the presence of an intravascular contrast agent. To maximize vascular anatomic detail, this agent needs to have a radiodensity that is distinct from that of the tissue being imaged. Typical contrast agents have greater radiodensity than surrounding tissue and therefore appear markedly darker on imaging. However, an agent significantly less radiodense than surrounding tissue, such as carbon dioxide ( $\text{CO}_2$ ) gas, can also provide adequate contrast to image intravascular anatomic detail,<sup>10,11</sup> albeit with less quality in some cases. The underlying concept is to provide adequate visual contrast between the intravascular space and the extra-vascular space. Selecting the appropriate contrast agent and adjusting the imaging equipment and technique accordingly are essential for patient safety and imaging quality.

## Iodinated Contrast Agents

Conventional contrast agents are composed of molecular compounds containing iodine. These iodinated agents can be categorized as ionic or nonionic.

Ionic contrast agents dissociate into anions and cations when they are placed in solution, which includes flowing blood. The anion is a benzene ring fully substituted with three iodine atoms. Iodine atoms absorb the X-ray photons and are responsible for contrast visualization, or radiopacity, of the artery visualized. The cation can be sodium, methylglucamine, or a combination thereof. When iodinated contrast agents dissolve, their osmolality doubles because of the presence of two ions. The osmolality of these agents ranges from 1500 to 1700 mOsm, thus making them significantly more hyperosmolar than plasma (285 mOsm).

Nonionic contrast agents have considerably less osmolality. Because dissolution of the benzene compound into two ions is prevented, the osmolality remains half that of ionic contrast agents. However, because the number of iodine atoms remains the same, radiopacity remains comparable to that of conventional ionic agents but with much less ionic charge. Osmolality can be further reduced by a compounding method that creates a *dimeric* ionic contrast agent, whereby two benzene rings are attached to each cation. With this formulation, twice the number of iodine atoms are present with the same level of osmolality (ranging from 320 to 880 mOsm). Doubling of the iodine atoms leads to a greater amount of X-ray photon absorption, and thus comparable arteriographic images are achieved with less volume of contrast material (Table 27.1).

## Carbon Dioxide Arteriography

Another contrast agent with novel properties and applications is  $\text{CO}_2$ .<sup>10,11</sup> Injection of this gas with its decreased radiodensity creates radiographic contrast by transiently displacing blood from the artery being imaged. Improvements in equipment, technology, and image-processing software, coupled with the significant number of vascular patients who have compromised renal function, have led to increased use of  $\text{CO}_2$  arteriography.<sup>11–13</sup> Digital subtraction technology has greatly enhanced anatomic definition and visualization with this contrast agent. However, despite improved techniques, image quality still remains inferior to that of conventional contrast agents.

Many techniques can enhance the quality of  $\text{CO}_2$  arteriography. Because of the image settings developed to enhance visualization of intravascular  $\text{CO}_2$ , the presence of bowel gas can especially degrade image quality in this acquisition mode. Because  $\text{CO}_2$  rapidly displaces blood and then dissolves quickly, frame rates are increased during image acquisition (four to eight frames per second). Modern arteriographic imaging systems now feature prescribed settings that depend on the type of contrast agent and area of the body to be imaged. Further image enhancement can be achieved by selective catheterization and magnified views of smaller-caliber vessels (Fig. 27.4). Contrast injections may be performed rapidly by hand or with a power injector system. They should be spaced 3 to 5 minutes apart to allow complete dissolution before the next injection. Overestimation of the degree of stenosis can occur when one is

**TABLE 27.1** Characteristics of Commonly Used Contrast Agents

Contrast Agent	Manufacturer	Structure	Iodine Content (mg/mL)	Osmolality (mOsm/kg)	Average Wholesale Cost (50 mL)
Hexabrix	Mallinckrodt Medical	Ionic dimer	320	600	\$53.50
Isovue-200	Bracco Diagnostics	Nonionic	200	413	\$53.75
Isovue-300	Bracco Diagnostics	Nonionic	300	524	\$57.49
Isovue-370	Bracco Diagnostics	Nonionic	370	796	\$62.50
Optiray 160	Mallinckrodt Medical	Nonionic	160	355	\$39.60
Optiray 320	Mallinckrodt Medical	Nonionic	320	702	\$57.60
Omnipaque 140	GE Healthcare	Nonionic	140	322	\$38.94
Omnipaque 300	GE Healthcare	Nonionic	300	672	\$54.00
Omnipaque 350	GE Healthcare	Nonionic	350	844	\$58.81
Oxilan 300	Cook Corporation	Nonionic	300	585	\$45.00
Oxilan 350	Cook Corporation	Nonionic	350	695	\$50.00
RenoCal-76	Bracco Diagnostics	Ionic	370	2188	\$24.25
Renografin-60	Bracco Diagnostics	Ionic	292	1549	\$44.13
Ultravist 150	Bayer	Nonionic	150	328	\$19.80
Ultravist 240	Bayer	Nonionic	240	483	\$22.80
Ultravist 300	Bayer	Nonionic	300	607	\$25.20
Ultravist 370	Bayer	Nonionic	370	774	\$28.80
Visipaque 270	GE Healthcare	Nonionic	270	290	\$63.80
Visipaque 320	GE Healthcare	Nonionic	320	290	\$69.48

Modified from *Drug Topics Red Book* 2008. Montvale, NJ: Thompson Healthcare; 2008.

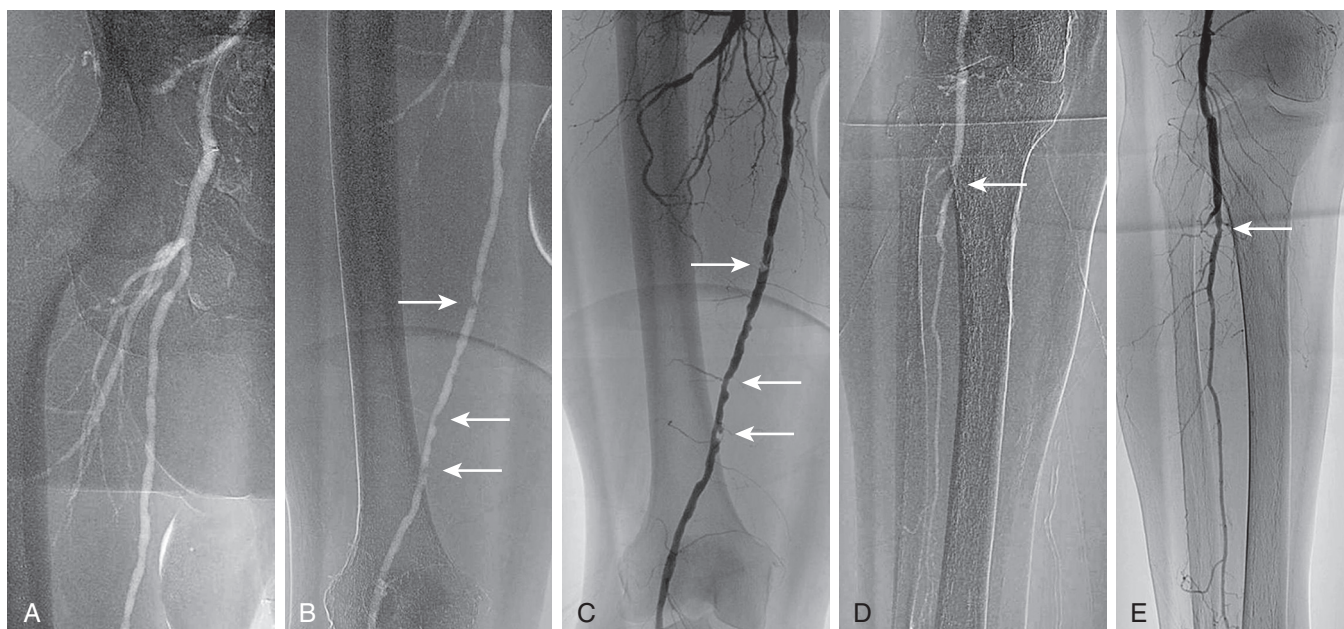


**Figure 27.4** (A) Angiogram of the femoral bifurcation visualized with CO<sub>2</sub> contrast and selective placement of the catheter in the common femoral artery. (B) Opacification of the superficial femoral artery reveals multiple stenoses (arrows). (C) Comparison of the same vessel opacified with iodinated contrast material shows much better characterization of each stenosis (arrows). (D) Distal views show relatively well-visualized popliteal and single-vessel peroneal runoff with CO<sub>2</sub>; significant disease is evident at the proximal peroneal artery (arrow). (E) Again, better characterization with iodinated contrast material reveals only a mild stenosis at the proximal peroneal artery (arrow).

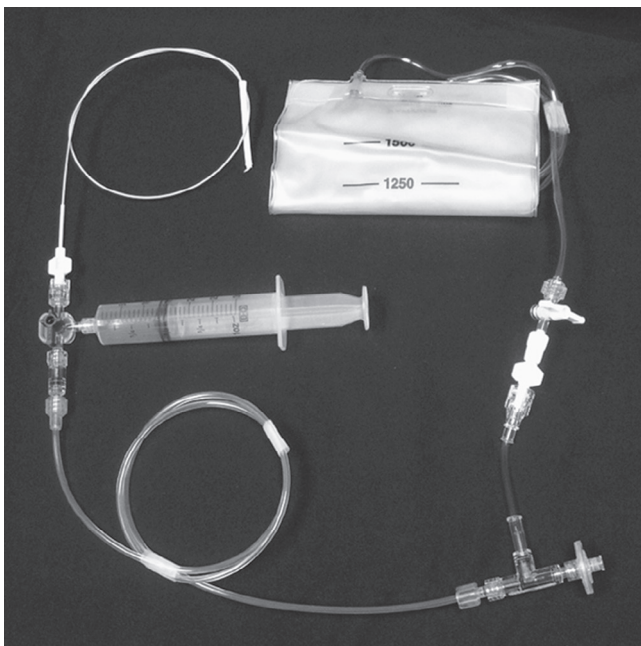


**Figure 27.5** CO<sub>2</sub> System Connected to a Diagnostic Catheter. The delivery system uses a three-way stopcock, check valve, and filter port connected to the gas tank (not shown). A 1500-mL bag is attached to the delivery system with low-pressure tubing and a two-way stopcock. A large Luer-Lok syringe is required for hand injection.

unable to completely fill the diameter of the artery with CO<sub>2</sub>.<sup>14</sup> One technique for facilitating rapid CO<sub>2</sub> injection utilizes a flow switch attached to the Luer-Lok syringe. The flow switch is kept closed during the initial compression of the syringe plunger and then opened with continued compression on the plunger, which allows for more rapid and higher pressure delivery of the CO<sub>2</sub>. For lower extremity arteriography, Trendelenburg positioning or elevation of the extremity to approximately 20 to 30 degrees will slow distal blood flow and promote concentration of the CO<sub>2</sub>, thus slowing the dispersion rate as CO<sub>2</sub> exits the catheter and travels distally.

The CO<sub>2</sub> delivery system includes a 30- to 60-mL Luer-Lok syringe, tubing with a two-way distal stopcock and two one-way check valves, a 1500-mL fixed-volume gas bag, and the CO<sub>2</sub> tank (Fig. 27.5). After assembly of the system, purging of the tubing with three syringe volumes (90 to 180 mL) of gas prevents the possibility of accidental injection of air. Nitrogen gas in ambient air is not soluble and can lead to gas embolization. Once the gas bag is filled with CO<sub>2</sub> directly from the gas reservoir, the syringe is pulled back to be filled with gas from the gas bag. Because of a one-way valve distal to the syringe, only gas from the bag can be withdrawn. Another reversed one-way valve proximal to the syringe forces gas to travel only to the patient on injection.

### Devices for Injection of Contrast Agents

Injection of liquid contrast material can be performed with a power injector or manually. For optimal arteriography, the ability to perform both methods is preferable because both have distinct advantages, depending on which arteries are being imaged.

### Power Injection

Power injectors allow rapid high-pressure injection of contrast material into the catheter. Precise control exists with regard to the pressure setting, measured in pounds per square inch (psi), amount of contrast material injected during a set period, timing of injection in relation to fluoroscopic imaging and catheter position, and rate of rise of the injection. Typically, use of a power injector allows for rapid filling of large arteries at high flow rates. This produces equal distribution of contrast material and hence a higher-quality image. Power injectors can also be used for prolonged injections, generally ranging from 3 to 6 seconds, when the catheter can be placed only in a very proximal position and the target artery is remote. Imaging of the dorsalis pedis and plantar arteries with the catheter placed in the ipsilateral common femoral artery is one such example. When a power injector is used, settings must be adjusted to manipulate pressure and the rate of rise of the injection, depending on the vessels being imaged. Large high-flow arteries require high pressure (800 psi) and rapid rise of the injectate to quickly disperse the contrast agent for a proper image. Smaller arteries, such as the superficial femoral artery, can be traumatized by such settings and require a lower pressure setting (300 to 600 psi) and reduced rate of rise of the injectate. For every power injection, the vascular surgeon will determine what volume of contrast material is to be given during what time. For example, typical aortic arch arteriography may require 20 mL of contrast material per second for a total of 2 seconds. Common jargon in the endovascular suite before such an injection would be “20 for 40,” or 20 mL of contrast material injected per second for a total volume of 40 mL. An advantage of power injection over manual injection is that the proceduralist may distance themselves from the patient and therefore the X-ray source, which may limit the cumulative radiation exposure.

### Manual Injection

Manual injection of contrast material can be performed by use of a simple syringe or a manifold device that allows more precise and rapid loading of contrast material (Fig. 27.6). Manifolds are also equipped with the ability to dilute contrast material with saline, to evacuate air and liquid waste, and to perform real-time intra-arterial pressure measurements. Additionally, devices exist that can be attached to the manifold that will further divert excess contrast and provide real-time use on a monitor.<sup>15</sup>

The ability to perform high-quality arteriography with the use of dilute contrast material should not be underestimated. Contrast agents, many of which are nephrotoxic, should always be used conservatively regardless of renal function. Establishing this habit helps to prevent injury to patients with mild renal disease not yet manifested by abnormal laboratory values. In smaller arteries (e.g., the common carotid artery or tibial arteries), 3 to 4 mL of diluted contrast material (1:1 mixture of contrast material and normal saline) should be sufficient to give a high-quality arteriographic image. The learning curve for maximizing proper use of a manifold is not very steep, and after it is mastered, optimal arteriographic images can be obtained rapidly with minimal volume of contrast material.

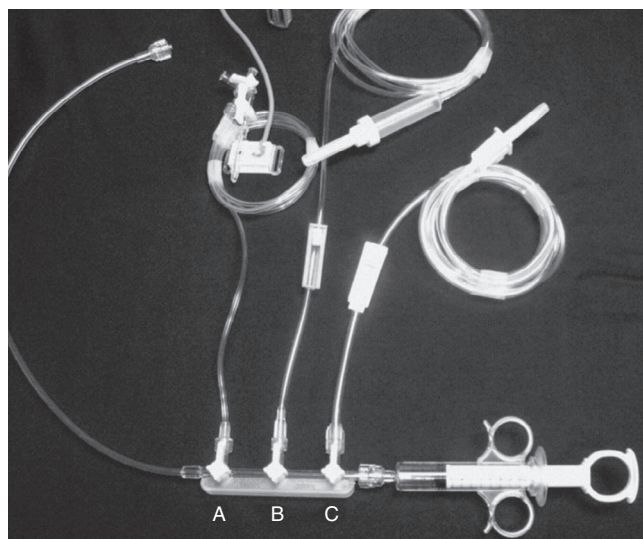


**Figure 27.6** Rapid, Convenient Device for Mixing and Delivery of Contrast Material. The control syringe and manifold allow quick reloading after each injection of contrast agent, with one hand operating the syringe and the other regulating the proportions of contrast material (*C*) and saline (*B*) being drawn up via the stopcocks on the manifold. Between injections, the saline line can be left on flush to keep the catheter irrigated. The third stopcock (*A*) allows continuous monitoring of pressure when it is connected to a transducer.

Typical injection methods, rates, and volumes of contrast agent are detailed in *Table 27.2*.

## TECHNIQUES

Arteriographic imaging in the modern era is synonymous with digital subtraction angiography (DSA). The basic concept behind DSA involves a recording technique by which the captured fluoroscopic image is amplified and digitized. With advanced computer data processing capability, multiple manipulations of the stored data can be performed to optimize image quality.

### Image Processing

Some of the commonly used post-processing capabilities are subtraction, masking, pixel shifting, and view tracing. Other tools, such as roadmapping and unsubtracted image referencing, can assist in guiding wires and catheters during the actual procedure. Not only do these techniques optimize detail of vessel visualization, but their use can also reduce the amount of contrast and radiation utilized.

### Subtraction Tool and Masking

The subtraction tool is the single most effective characteristic of this technology that enhances and improves image quality. This technique subtracts all visible radiodensities on the current image to create a mask image, represented as a blank screen. Once the mask has been established, any motion in the field during the fluoroscopic run will be highlighted as a dynamic image on this blank background. All radiodense tissues subtracted on the mask image will remain subtracted as long as they remain in the same position and alignment as in the

**TABLE 27.2**

Typical Injection Method, Rate, and Volume of Contrast Agent for Various Vascular Regions

Location	Suggested Method	Injection Rate (mL/s)	Total Volume (mL)
Aortic arch	Power injection	20	40
Selective carotid	Hand or power injection	3–5	5–10
Selective vertebral	Hand injection	2–4	2–4
Selective subclavian or brachial	Hand or power injection	5–10	10
Abdominal aorta	Power injection	20	40
Renal or mesenteric	Hand injection	3–5	5–10
Iliac artery	Hand or power injection	10	10
Infringuinal segments	Hand or power injection	5–10	10
Aorta to pedals, stepped run	Power injection	20	90 <sup>a</sup>

<sup>a</sup>Full-strength contrast agent; all others typically performed with a half-strength contrast agent when digital subtraction angiography is used.

mask image. After subtraction is achieved and the mask image is created, the contrast agent is injected and visualized because it is radiodense and moves with blood flow through the vessels of concern. By subtraction of the surrounding tissue and vessel wall from the contrast images, the quality of visualization of intraluminal contrast is greatly enhanced. In an ideal image capture, there is no movement between creation of the mask and flow of the contrast material in through the field of view. This would produce the purest image derived solely from flow of the contrast agent. However, such is often not the case, and unintended motion can greatly compromise imaging. If the mask has been created and the patient then changes position, breathes, or even has bowel peristalsis, this skeletal or visceral motion will be seen on the contrast images because it was not part of the original mask image. Therefore it is essential for the patient to remain very still during image capture. To reduce the likelihood of any movement between masking and contrast filling of the vessels being imaged, timing of contrast injection should be precise and take into account the distance of the injection from the imaging site. When injecting contrast through a catheter remote from the site to be imaged, injection should be performed prior to masking such that contrast enters the imaged field immediately after masking.

Masking can be used beyond the original subtraction maneuver to improve image quality. If a patient moves during an injection, any image prior to contrast appearance or after contrast washout can be used as the mask image to improve image quality and minimize motion artifact. A trial of different mask images is often an effective way of finding the best possible result.

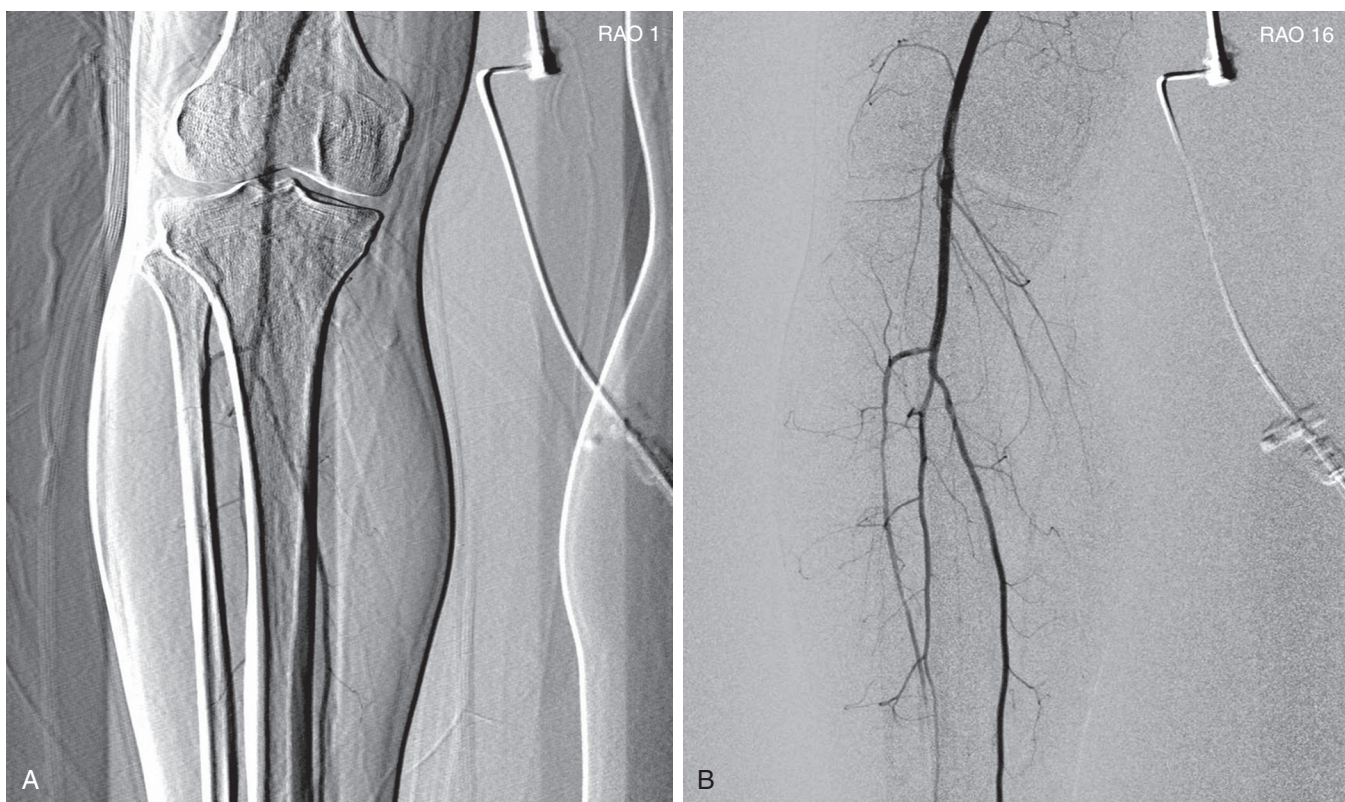


**Figure 27.7** (A) Patient motion during contrast opacification significantly degrading image quality. (B) Pixel shifting during post-processing realigns the mask image with the contrast image and thereby results in optimal visualization of the artery. If the motion occurs before contrast injection as opposed to during it, reassigning the mask image can accomplish a similar result. RAO, right anterior oblique.

### Pixel Shifting

Pixel shifting provides a valuable tool when movement occurs after contrast material has already entered the field of view. Instead of creating a new mask, one can take the existing mask and slide it in a bidirectional plane (vertical, horizontal, or both) to realign the surrounding tissue (Fig. 27.7). This realignment of the existing mask to the patient's current position on the contrast image erases the discrepancy and minimizes the motion artifact. Software programs allow automatic or manual pixel shifting. In the automatic mode the computer will try to realign the mask image to create the best subtracted result for that particular region of the field. In manual mode, the pixel shifting can be performed freehand in real time by sliding the cursor vertically, horizontally, or both until the optimal image is achieved.

### View Tracing

Because arteriography is a dynamic imaging modality, obtaining one static image from a series during injection of contrast material will often fail to provide complete visualization of the target vessel. As the contrast agent opacifies one segment of the blood vessel, a previous segment may already have washed out and a distal segment may not yet have filled with the contrast agent. This property can be ameliorated using view tracing.

View tracing, sometimes referred to as peak opacification, allows consolidation or “stacking” of different time points by

overlaying consecutive static images in a series to provide one cumulative arteriographic image. The first image in which contrast appears may be designated the first image in a view-traced series. Each subsequent image that is stacked over the previous one will show further progression of contrast and further visualization of the vessel distally (Fig. 27.8). However, with each additional view-traced image, any motion artifact will also be superimposed, thereby degrading the image more and more with sequential stacking. To circumvent this problem, each individual static image can first be optimized by pixel shifting to minimize artifact in the final cumulative image.

After broad manipulations with the techniques just discussed, images can be further enhanced by finer adjustments. Image contrast, brightness, edge enhancement, sharpness, and even color of the contrast agent (image invert) can be modified to create a final optimized image. These finalized images can then be stored in the patient database along with the dynamic DSA runs.

### Roadmapping and Measuring

Other useful techniques involving DSA can help with guidance during the actual procedure. Roadmapping allows a previously constructed image of a contrast-filled vessel to be displayed on the working monitor. Real-time fluoroscopic imaging can then be superimposed on the monitor so that the contrast image can be used as a “roadmap” to direct guide wires and catheters.

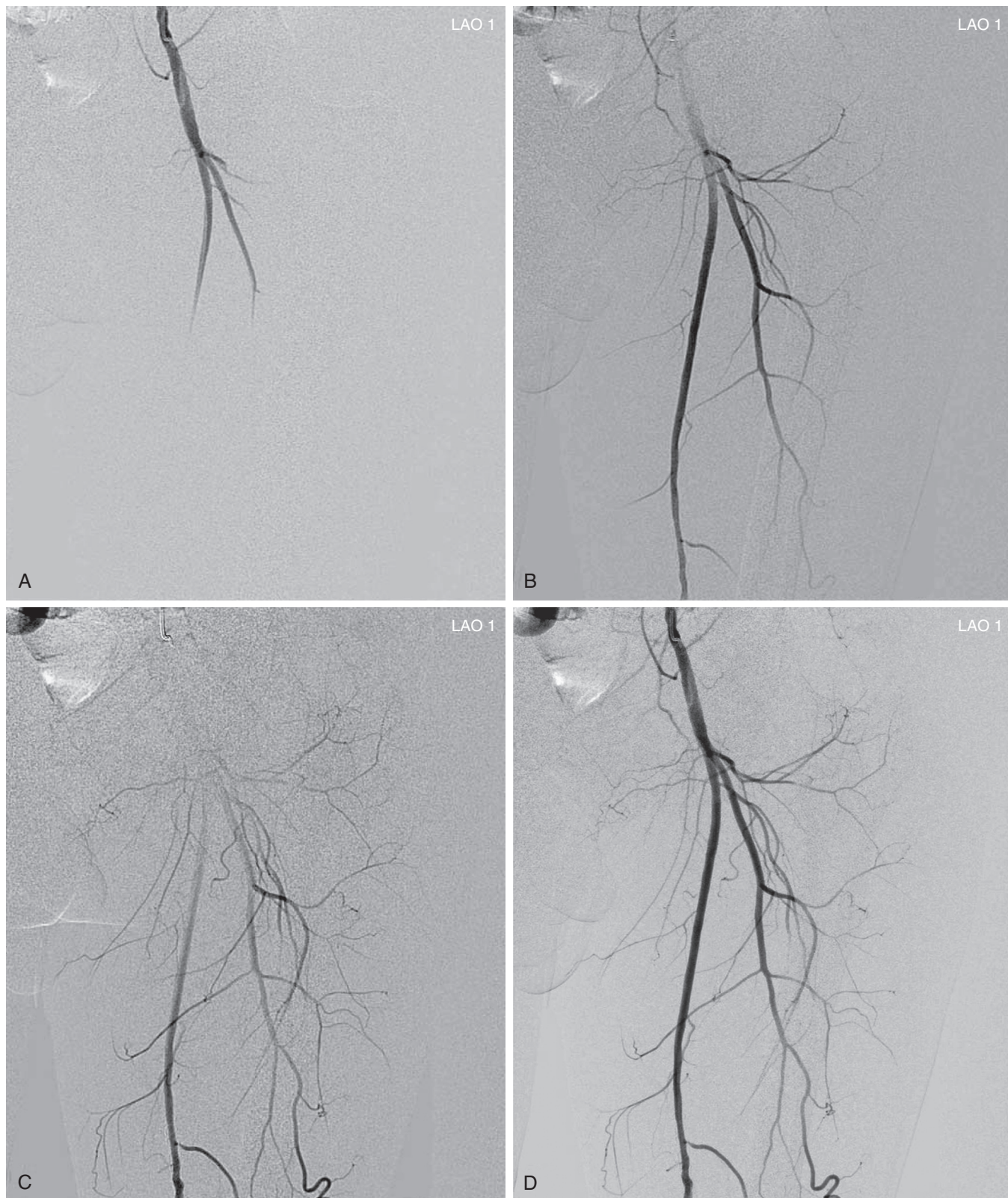


**Figure 27.8** (A) Femoral arteriogram early after injection of contrast material illustrating only proximal opacification of the vessels. (B and C) Progress of contrast opacification through the femoral vessels with improved distal but poor proximal visualization. (D) View tracing allows stacking of sequential images to give a comprehensive view of the vessels with all areas opacified during the different time points of the contrast run. *LAO*, left anterior oblique.

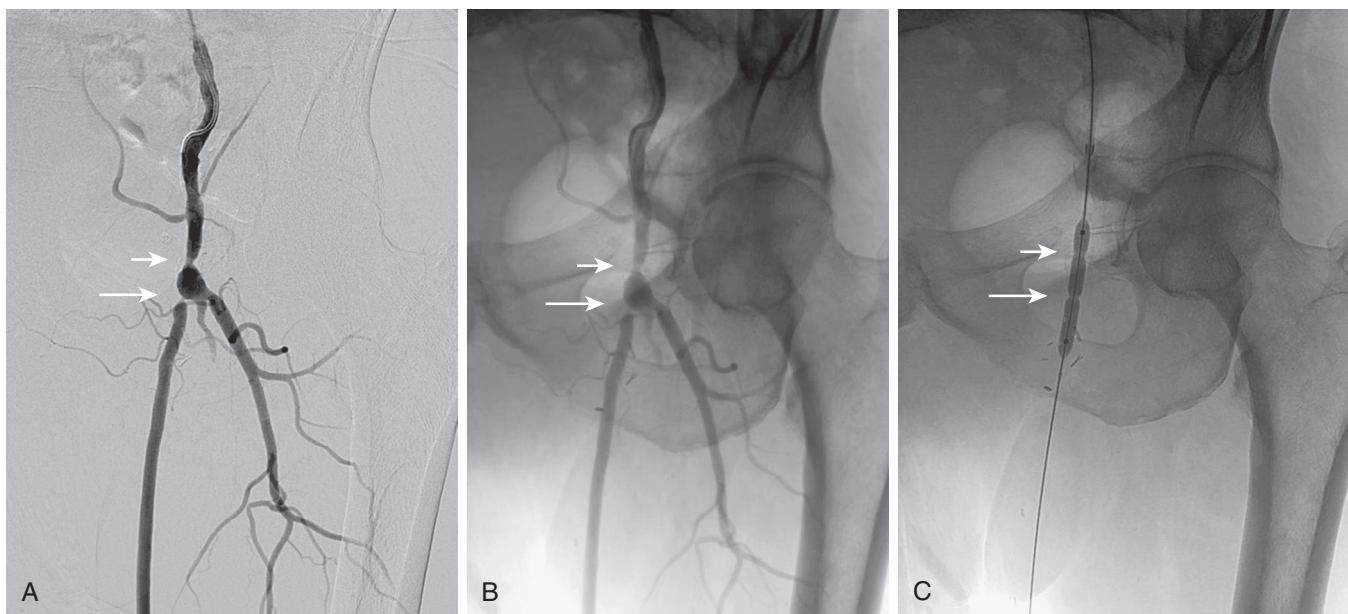


**Figure 27.9** (A) A femoral arteriogram to evaluate a lower extremity bypass graft shows a stenosis at the proximal anastomosis (short arrow) and a second stenosis in the proximal graft (long arrow). (B) Viewing of the same image in an unsubtracted mode allows the use of bone structures, such as the pubic rami and obturator foramen, to serve as reference landmarks. (C) On the unsubtracted reference image, localization and treatment of the target lesions can be performed accurately with guidance from these bone landmarks.

This technique is effective as long as table and patient positions do not change. The roadmap mask is extremely sensitive to motion, and image quality will degrade during use. Another valuable guiding tool during arteriography is the simple use of unsubtracted image referencing. Disabling subtraction from a contrast image allows identification of native tissue reference points, most often bone landmarks, near vessel bifurcations (Fig. 27.9). This image can then be displayed on a reference monitor alongside the working monitor so that the angiographer can manipulate catheters or wires on the basis of these reference points.

Finally, imaging units' software includes measurement tools. These tools can be autocalibrated on the basis of estimated distances from the image intensifier to the center of the patient's body, or they can be manually calibrated by measuring an object with known dimensions, such as a known distance between radiopaque markers on catheters or a known diameter of a sheath or catheter. This allows for more accurate interpretation of stenoses and vessel dimensions than is possible with mere visual estimation or "eyeballing."<sup>16</sup>

### Single-Injection Multiple-Linear Field Arteriography

The technique, which allows imaging of both lower extremities with a single injection of contrast agent, is referred to as single-injection multiple-linear field or bolus chase arteriography. With this method, contrast material is injected into the abdominal aorta and imaging proceeds sequentially down the entire length of both lower extremities. Image intensifiers larger than 15 inches are required to view both extremities in one field with this technique. After a single bolus injection of

contrast agent, imaging must follow the progression of contrast in a dynamic manner.

### Stage Technique

In the stage technique the operator sets the image intensifier at a certain number of sequential positions, or stages, from the lower part of the abdomen to the feet. Four or five stages with some overlap between stages is usually required, depending on the size of the image intensifier. When the imaging process is initiated, the image intensifier starts at the feet and travels proximally from stage to stage to acquire a mask image for each particular position. Once the final mask is obtained in the lower part of the abdomen, a bolus of contrast material is injected and continuous imaging proceeds in a staged manner from the abdominal aorta back down to the feet. In essence, the image intensifier "chases" the bolus of contrast material as it travels distally. On completion, the images can then be viewed at each stage individually and processed in the standard manner (Fig. 27.10). Because the mask images are obtained before the run, the contrast imaging is viewed in subtracted mode, which enhances visualization during the actual run.

### Stepping Technique

In the second technique, referred to as stepping, the image intensifier remains stationary while the fluoroscopic table moves for proper imaging. This method uses a large number of small incremental advancements in position, or steps, as opposed to the smaller number of large position changes in the stage method. The process begins with injection of contrast material into the abdominal aorta as the table is stepped sequentially from the abdomen to the feet. Because the incremental changes in position are smaller than with staging, fluoroscopic imaging

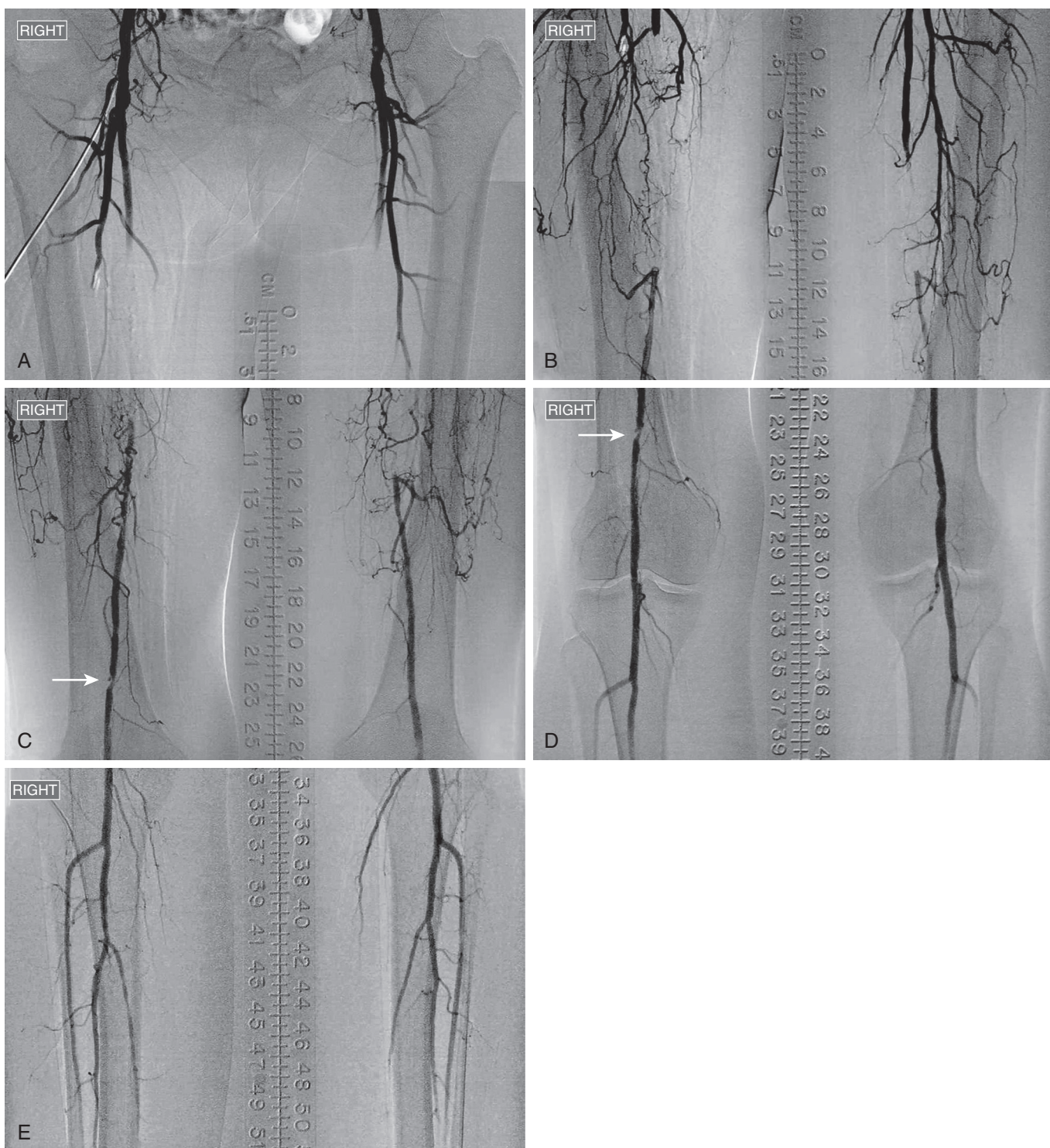


**Figure 27.10** Single-injection multiple-linear field (bolus chase) arteriogram of both lower extremities showing bilateral mid-superficial femoral artery segmental occlusion (**A** and **B**), right popliteal artery stenosis (arrow) (**C** and **D**), and bilateral patent tibioperoneal trunks and three-vessel runoff with posterior tibial artery disease on the right (**E**). Because disease severity appears similar in both lower extremities, there is no discrepancy in contrast transit time between the two; hence imaging appears to have adequate and equal bilateral vessel opacification at each level.

can more precisely follow the progression of contrast material down the extremities. Stepping can be slowed or even stopped by the operator, depending on the rate of travel of the contrast agent. Once the contrast run is completed, the table returns to the original position and automatically proceeds through the same step sequence used to acquire the mask images.

### Limitations of Single-Injection Multiple-Field Arteriography

There are two significant limitations of single-injection multiple-field arteriography. First, as with any DSA imaging, patient movement can significantly compromise image quality. Because the time required to complete this type of study is

considerably longer (often lasting 2 minutes) than a standard single-field run, the possibility of motion artifact is significantly increased. A second limitation occurs in patients with a discrepancy in the severity of arterial occlusive disease between the two extremities. More severe occlusive disease on one side will cause delayed contrast transit time and decreased visualization on that side because the image follows the progression of contrast in the more rapidly filling extremity. In this case, it will be necessary to obtain unilateral images separately. Although this technique of arteriography can be performed for each leg individually, the amount of contrast agent needed to do so must be considered. Typical bolus chase arteriography requires 80 to 100 mL of full-strength contrast material, whereas selective single-field imaging of each extremity can be performed in sequential fashion with a manifold and a diluted contrast agent to provide quality images with significantly less volume of contrast material. In the presence of severe unilateral disease, this is the preferred injection technique.

## Rotational Arteriography

Rotational arteriography involves rotational image capture and incorporates specific computer software to record the fluoroscopic image series in multiple planes. Preset algorithms are then used to convert the data acquisition into a comprehensive three-dimensional (3D) image. The final reconstructed image can be rotated and manipulated to fully visualize the vessel from any angle, thereby addressing the limitations of single-plane arteriography. Figures 27.11 and 27.12 illustrate examples of single-plane and rotational arteriography.

Rotational arteriography is similar to the bolus chase technique in that a single injection of contrast material is administered as images are captured from a series of varying positions. The target vessel is first centered on the fluoroscopic image. As contrast material is injected, the image intensifier rotates between two predetermined points (usually 90 to 213 degrees, depending on the system) and captures a broad spectrum of imaging angles with each frame of acquisition during the rotation. The final reconstructed image can be viewed with or without subtraction, and further “cutting” of surrounding tissue artifact can be performed with post-processing tools (see Fig. 27.12). More recent software even allows roadmapping with 3D imaging for catheter guidance, which has proven useful in the performance of complex aortic endografting and endovascular procedures in the cerebral vasculature.<sup>17</sup>

## Three-Dimensional Fusion Computed Tomography

With the advent of complex aortic endograft procedures, the need to minimize contrast loads and radiation exposure is more critical than ever. Three-dimensional fusion computed tomography (CT) imaging allows for the patient's preoperative CTA to be used as an overlay roadmap image during the procedure. Briefly, the areas of interest, such as the visceral artery origins, are manually marked on the preoperative CTA. Next an intraoperative scan is obtained by performing a rotational imaging spin of the patient. Available commercial software packages align the bony landmarks and aortic calcifications of the preoperative CTA and the intraoperative rotational image, allowing

the preoperative image to overlay the intraoperative image as a roadmap to guide endograft orientation and target vessel cannulation (Fig. 27.13A and B). Use of this imaging technique requires additional training of the surgeon and hybrid room staff but has been shown to reduce procedure times, radiation exposure, and contrast use in fenestrated aortic endograft procedures and coronary angiography.<sup>18,19</sup> More recently, three-dimensional fusion techniques using both CTA and MRA have been adopted in peripheral interventions for occlusive disease, albeit with mixed results in regards to contrast and radiation dose reduction.<sup>20–22</sup> Additional advances under development in the use of fusion imaging include tracking catheter position without the use of fluoroscopy using electromagnetic or fiberoptic tracking, as well as algorithms that can predict vessel deformations.<sup>23,24</sup>

## Maximizing Image Quality During Arteriography

Limiting patient movement is essential to maximize the quality of an arteriographic image. To effectively do so, the angiographer must pay special attention to the patient's comfort and anxiety level. Pain and anxiety can cause a patient to make even subtle position changes that can translate to deleterious artifact on imaging. Explaining each step of the procedure ahead of time can help to alleviate anxiety during imaging. Administration of anxiolytic and narcotic medications before and during the procedure can be a very effective tool to minimize patient motion. For most patients, midazolam (Versed), 1 to 2 mg, and fentanyl, 25 to 50 µg, intravenously is optimal before the start of arteriography procedures. Depending on the patient's condition and tolerance and the length of the procedure, additional small doses can be given as needed. Use of moderate conscious sedation usually requires certification in advanced cardiac life support and also necessitates adequate patient monitoring and the presence of nursing staff during the procedure.

Breathing maneuvers are also important to ensure quality imaging because motion of surrounding tissue secondary to breathing can result in significant image degradation, especially on imaging of the chest, abdomen, or pelvis. Patients should be asked to hold the breath as imaging is initiated, because vessel position can be significantly altered with deep inspiration or expiration. Alternatively, patients can be asked to hold the breath at the midbreath cycle to minimize significant vessel displacement, compared with a deep inspiration, which can cause downward displacement of visceral vessels. When the neck is being imaged, such as the extracranial carotid and vertebral vessels, asking patients to avoid swallowing or talking will likewise prevent significant motion artifact in this area.

Proper positioning of the patient and the imaging equipment is also necessary to maximize information during a study. For example, the legs can be placed closer together during bolus chase angiography to include both of them in the field of view (see Fig. 27.10). Some tables may offer tilt features to increase the capability of patient positioning. However, the majority of positioning relies on adjustment of the image intensifier, including both lateral angular rotation (anteroposterior versus oblique versus lateral views) and craniocaudal angulation.

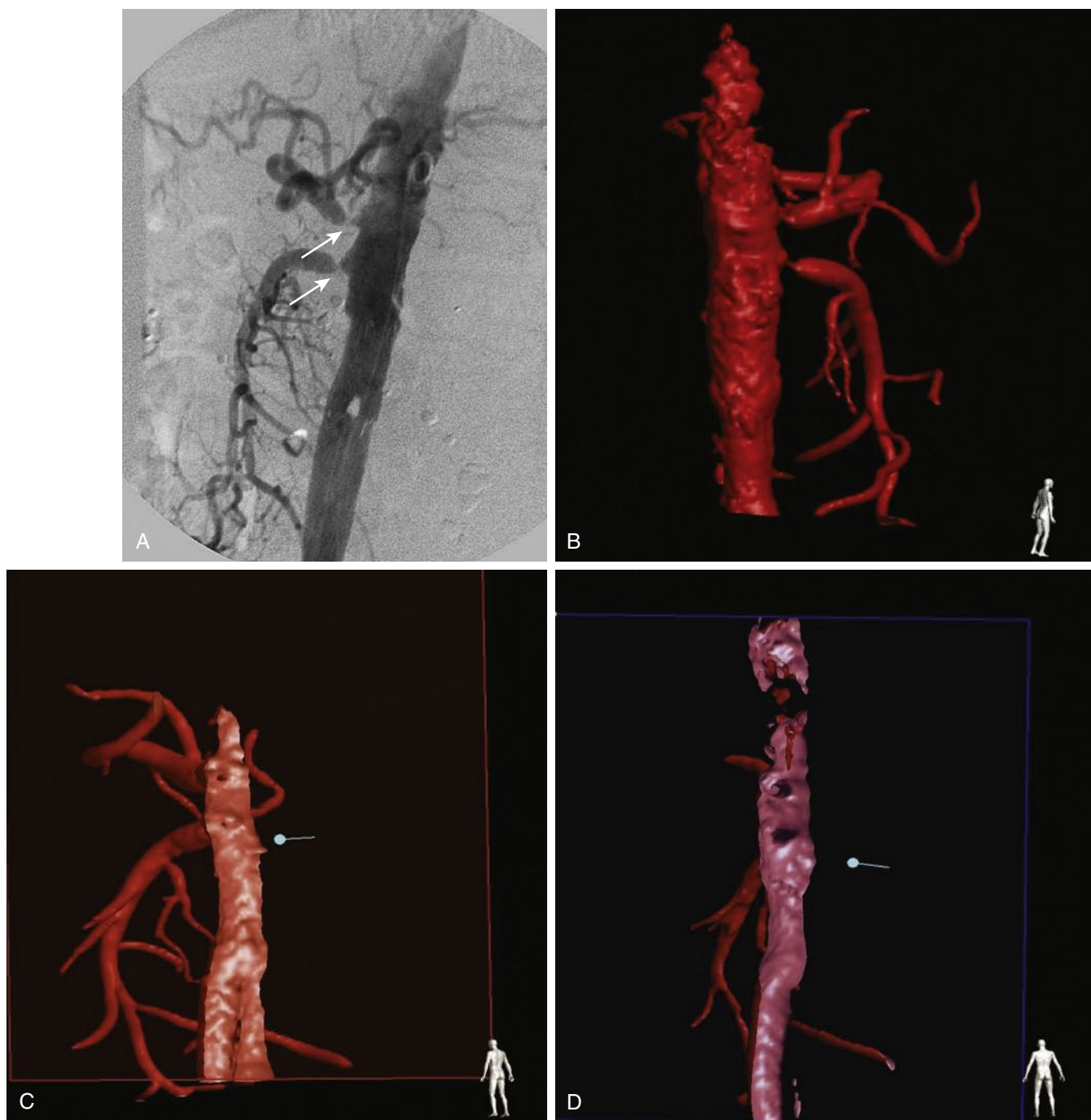


**Figure 27.11** (A) Lateral view arteriogram of the aorta showing proximal celiac and superior mesenteric artery stenoses (arrows). (B) Rotational arteriography with three-dimensional reconstruction allows improved characterization of the lesions and rotating views of the image. The images can also be manipulated to view an intraluminal perspective of the aorta, which reveals significant orificial narrowing of both mesenteric vessels before stenting (C) and improved orificial diameter after stenting (D).

General recommended filming projections for viewing of some commonly imaged arteries are listed in [Table 27.3](#). Depending on the particular vessels being imaged and the patient's individual anatomy, varying degrees of rotation are preferred for optimal visualization ([Figs. 27.14](#) and [27.15](#)).

The maximum size of available image intensifiers has increased significantly in recent years, and current equipment may allow a broad field of view on imaging at maximum

projection. This feature is especially useful in performing abdominal and lower extremity angiography because it allows complete evaluation with less contrast agent and shorter radiation exposure times. However, smaller vessels and subtle lesions may be difficult to characterize at such a wide view. By reduction of the projected image dimension, a magnified view focused on the vessel of interest can be obtained ([Fig. 27.16](#)).

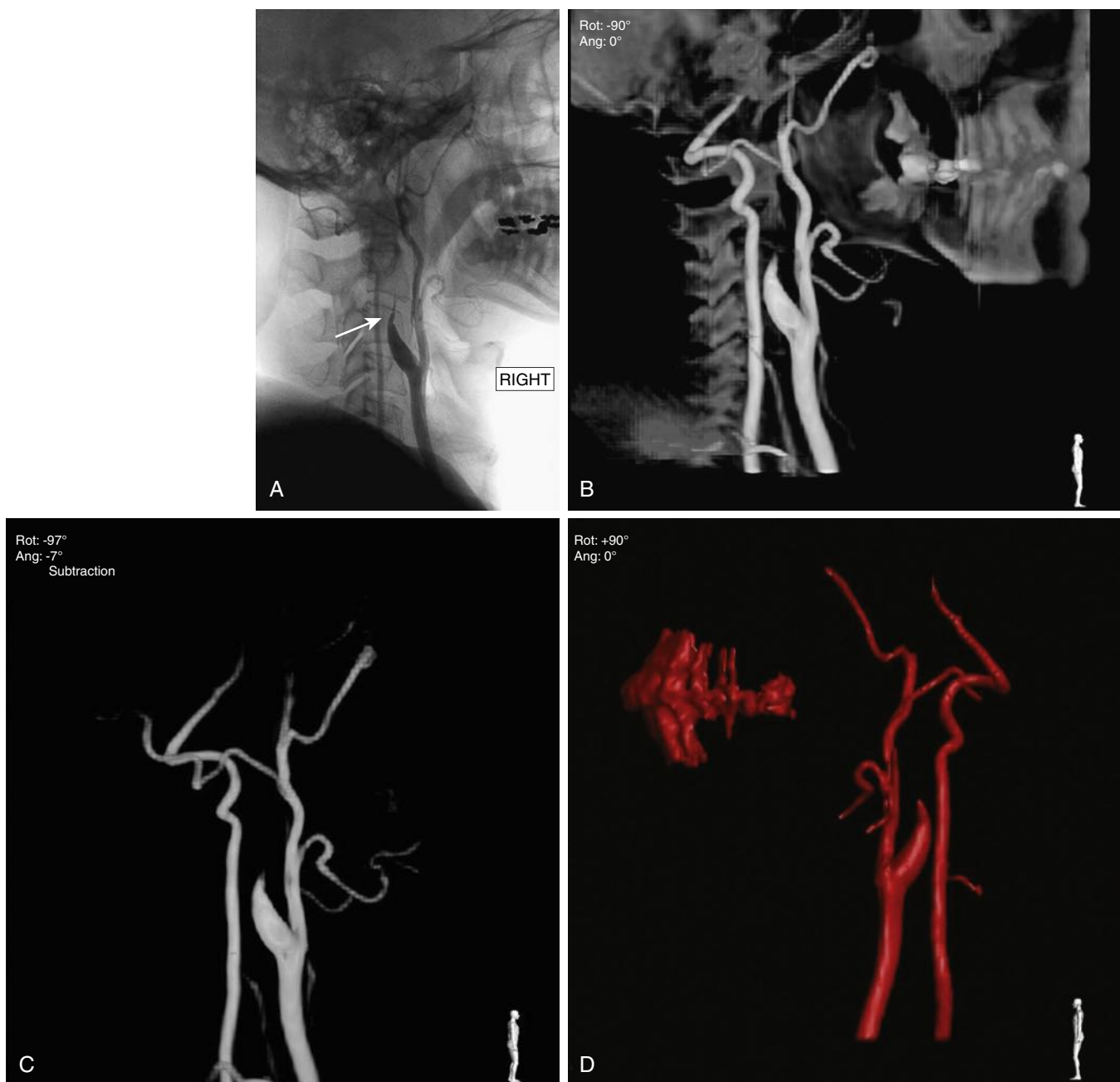


**Figure 27.12** (A) Selective carotid arteriogram showing the typical “tapering” appearance of an internal carotid artery dissection (arrow). (B) Preliminary three-dimensional (3D) reconstructed image from a rotational arteriogram showing the same lesion. (C and D) After color manipulation and “cutting” of surrounding bony tissue, the final 3D image can be rotated for different viewing angles.

## CLINICAL APPLICATIONS

The quality of MRA and CTA has improved immensely during the past 10 years, and in many clinical scenarios, MRA or CTA can become the preferred choice for planning of either endovascular or operative procedures. Nevertheless, arteriography still has a major role as the primary modality to provide a first diagnostic vascular image. Although arteriography remains the criterion standard, variability exists among all three modalities with respect to quality of imaging and useful information that is gained. CTA and MRA continue to improve in ease

of use, accuracy, and speed, but they are still dependent on the physicians and technicians who oversee the production of those images. Therefore variability exists from center to center, which can influence the path that a vascular surgeon will take in obtaining the best vascular images for treatment decisions. Possible variability of MRA and CTA make it all the more important that vascular surgeons be highly adept at performing high-quality arteriography to include such small vascular beds as the foot, hand, viscera, pelvis, and brain.

A thorough history and physical examination have become even more important in an era surrounded by cost consciousness

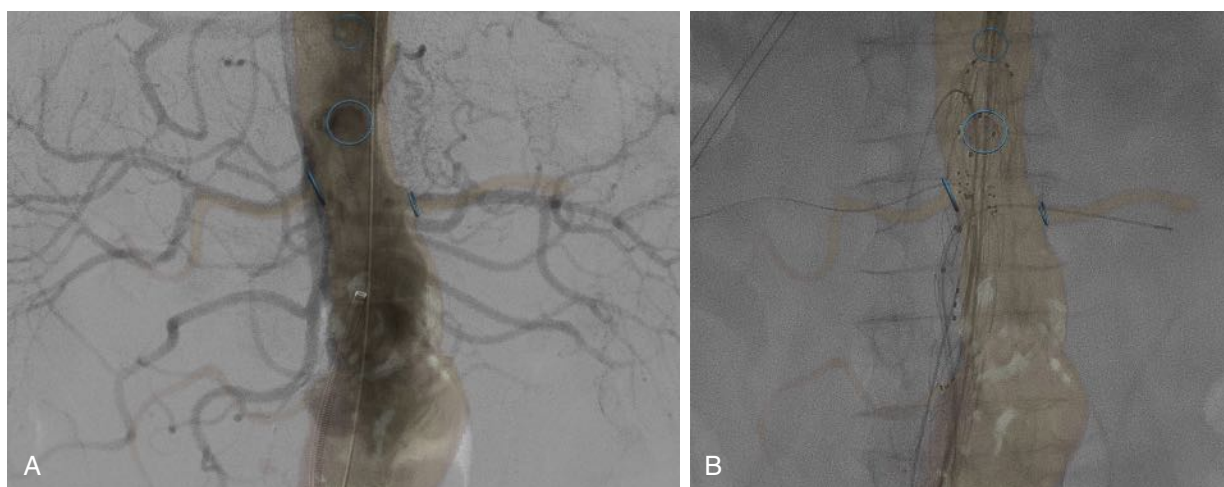


**Figure 27.13** (A) Intraoperative aortogram with overlay of preoperative computed tomography (CT) scan showing good alignment of visceral vessels. (B) Three-dimensional CT scan overlay is used to orient fenestrated aortic endograft and cannulate visceral vessels.

**TABLE 27.3**

Recommended Radiographic Filming Projections for Optimal Branch Separation

Location	Recommended Filming Projection
Aortic arch	30-degree left anterior oblique
Cervical carotids	AP, lateral, and 45-degree ipsilateral anterior oblique
Intracranial carotids	AP and lateral
Verteobasilar system	AP and lateral
Right subclavian	Right anterior oblique
Renal artery origins	AP $\pm$ 10 degrees
Celiac artery and SMA origins	Lateral
Iliac bifurcation	20- to 30-degree contralateral anterior oblique
Femoral bifurcation	20- to 30-degree ipsilateral anterior oblique
Trifurcation and tibial arteries	Anatomic AP (or 20-degree ipsilateral anterior oblique with feet in the neutral supine position)

AP, anteroposterior; SMA, superior mesenteric artery.

and minimization of risks to the patient from unnecessary radiologic evaluation. From a vascular examination perspective, the history and the physical examination in association with routine noninvasive vascular laboratory testing may guide the vascular surgeon directly to primary diagnostic arteriography, particularly if endovascular treatment is anticipated at the time of the diagnostic study. There are several clinical scenarios in which CTA or MRA is indicated before arteriography: when diagnosis of a vascular problem is in question and CTA or MRA can provide a diagnosis that will avoid arteriography; in the diagnosis and treatment of aneurysmal disease; when the route of optimal percutaneous access is uncertain; and when other juxtaposition body imaging information is necessary in

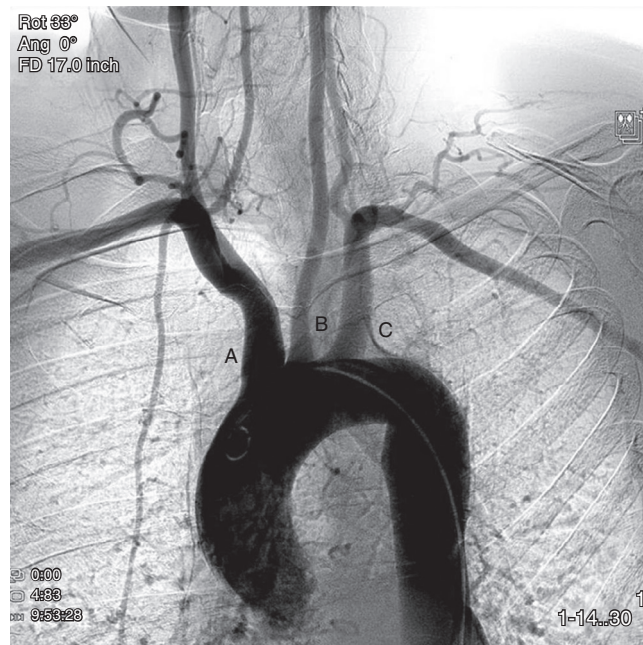


**Figure 27.14** Viewing the aortic arch from an approximately 30-degree left anterior oblique angle splays out the arch anatomy with good visualization of the origins of the innominate (A), left common carotid (B), and left subclavian (C) arteries.

addition to vascular imaging. Arteriography may be accompanied by multiple other intravascular maneuvers. These include monitoring of intra-arterial blood pressures proximal and distal to stenosis to assess hemodynamic significance, therapeutic infusion of a vascular bed with a drug such as a vasodilator, sampling of blood from certain vascular beds and occlusion or embolization treatment of refluxing veins, tumors, or control of hemorrhage.

Studies comparing arteriography with CTA and MRA conflict as to whether the two are equivalent to the criterion standard.<sup>25-34</sup> Some studies have shown benefit of CTA or MRA in clinical decision-making, whereas others have not. Hingorani



**Figure 27.15** (A) An anteroposterior view of an aorto-iliac-femoral arteriogram is the ideal orientation to visualize the aortic bifurcation and bilateral common iliac arteries. Mild stenosis is present in the proximal right common iliac artery, and moderate in-stent restenosis is present in the proximal left common iliac artery (arrows). (B) A 30-degree left anterior oblique view splays out both the right iliac bifurcation (white arrow) and the left femoral bifurcation (black arrow). (C) Alternatively, a right anterior oblique view is ideal for visualizing the left iliac bifurcation (white arrow) and the right femoral bifurcation (black arrow).

et al.<sup>26,28</sup> compared CTA and MRA with contrast arteriography in patients with chronic lower extremity ischemia requiring revascularization. Accuracy of CTA and MRA were poor in femoropopliteal and tibial segments compared with contrast arteriography. In these studies, CTA and MRA could not provide equivalent imaging to ensure the optimal clinical decision for lower extremity revascularization. In contrast, MRA may

have a role in identifying patent tibial target vessels for lower extremity bypass that are not seen on DSA due to very low flows.<sup>31,32</sup> All studies comparing CTA and MRA with DSA for lower extremity arterial occlusive disease are fraught with small numbers of patients and differing methodologies of stenosis criteria and techniques, and the selection of optimal imaging remains somewhat case-, center-, and surgeon-specific.

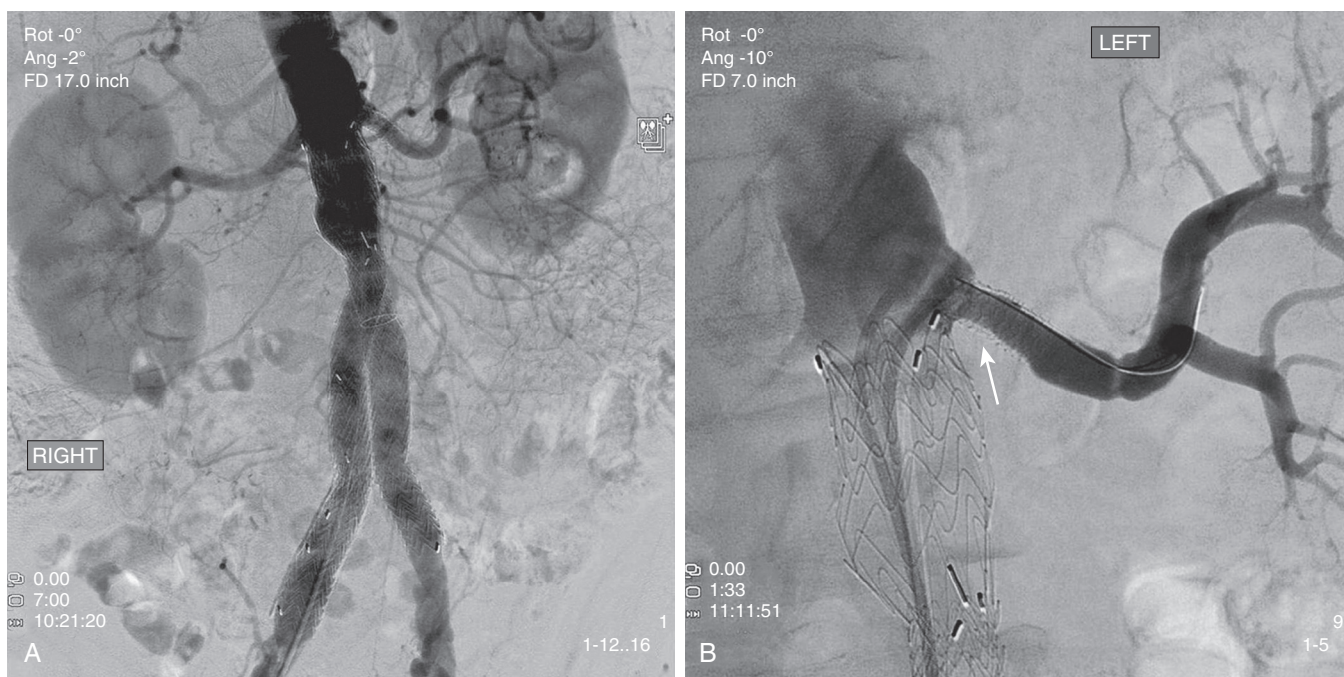


**Figure 27.16** (A) Flush aortic arteriogram showing an adequately sealed aortic endograft and patent left renal artery stent. (B) Adjustment of the image intensifier, or flat detector, from a 17-inch to a 7-inch projection gives a much clearer magnified view of the left renal artery and reveals mild in-stent restenosis (*arrow*).

## LIMITATIONS AND RISKS

### Sources of Error with Arteriography

Motion artifact is the most common source of degradation of image quality and can be devastating to accurate visual interpretation. However, other potential sources of image compromise involve the patient's anatomy. Bone, bowel gas, surgical clips, implanted devices, shrapnel or other foreign bodies, and any other surrounding tissue densities can obscure true anatomic detail of a vessel. This problem is addressed by obtaining images from multiple angles and thereby separating the target vessel from the interfering tissue density. Vital interpretations and interventions are almost never based on a single-plane image. Superimposed contrast columns in overlying arteries can also obscure anatomic detail. This often occurs at vessel bifurcations and in vessels that are angulated in a plane parallel to the angle of view. Because significant occlusive lesions commonly occur at vessel bifurcations, this scenario can adversely affect accurate disease diagnosis and proper management decisions. Recognizing subtle differences in the density of contrast in areas of artery overlap will help to prevent misinterpretation. Again, emphasis should be on changing the angle of view to splay out such a bifurcation and better visualize each individual vessel (Fig. 27.17).

An extremely important concept in angiography is the limitation of expecting a two-dimensional image to accurately represent a 3D structure. Relying solely on single-plane imaging, in an anteroposterior-only view, for example, may lead to underestimation of significant arterial disease in some instances, for example, when posterior plaque is present (Fig. 27.18). In one view, a vessel may appear to have uniform diameter and no

evidence of stenosis; but in an oblique or lateral view, hidden ulceration or a profound stenosis may be evident, a so-called pancake lesion as opposed to a circumferential lesion. This underscores the importance of multiplanar arteriography to improve its accuracy over other imaging modalities.

### Risks from Contrast Agents

#### *Systemic Toxicity*

The toxic side effects of iodinated contrast agents are primarily thought to be due to hyperosmolality. The most common adverse symptoms are nausea, vomiting, and pain in the distribution of the specific arterial bed that is injected. The discomfort seems to become more significant as the osmolality increases,<sup>35</sup> especially when it is greater than 400 to 500 mOsm. Furthermore, nonionic agents tend to cause fewer adverse symptoms than ionic agents do, which is why there has been a significant trend toward formulating lower osmolality, nonionic agents.

Other adverse systemic effects of contrast administration are related to nonspecific reactions involving histamine release. Such reactions are usually treated with antihistamines alone in minor cases, such as urticaria. For more severe reactions, such as laryngeal edema or bronchospasm, treatment starts with inhaled adrenergic medications such as albuterol and, if that is ineffective, intravenous administration of epinephrine. Finally, cardiopulmonary arrest may require full hemodynamic support with vasopressors in addition to mechanical ventilation for respiratory support. It is important to distinguish hemodynamic instability caused by cardiopulmonary collapse from the more common vagally mediated hypotension, which may be due to such causes as anxiety or catheter manipulation and is best treated with intravenous fluid and close observation. In cases of

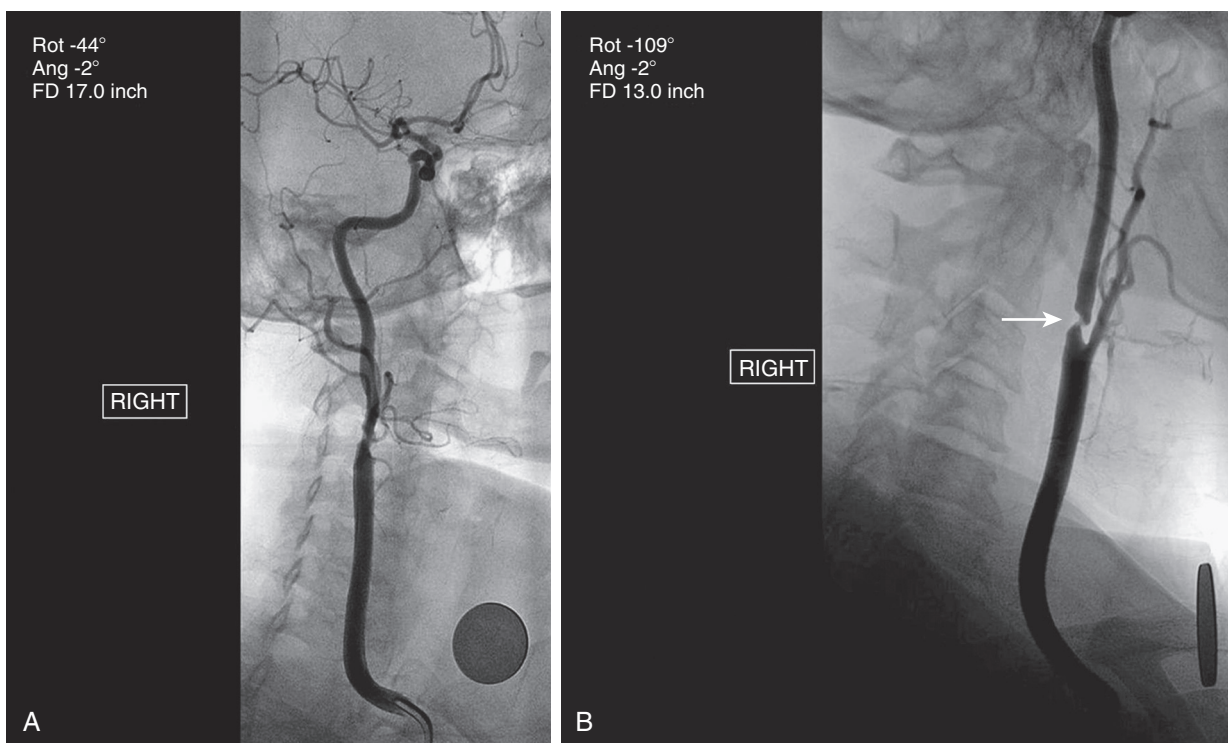


**Figure 27.17** (A) Selective carotid arteriogram showing poor characterization of the carotid bifurcation on an oblique view because of superimposed vessels. (B) Adjustment of the angle of projection opens the bifurcation to clearly visualize the internal and external carotid arteries, revealing a significant proximal internal carotid stenosis (*arrow*) that previously was not apparent.



**Figure 27.18** Selective Carotid Arteriogram Highlighting the Importance of Multiplane Imaging to Unmask Suspicious Posterior Vessel Lesions. (A) An oblique view seems to demonstrate good visualization of the carotid bifurcation with some mild irregularity of the internal carotid artery. (B) Repeated imaging with a lateral projection, however, unveils a high-grade stenosis of the internal carotid artery with an ulcerated posterior plaque (*arrow*).

severe bradycardia and hemodynamic instability, atropine (0.5 to 1.0 mg intravenously) should also be administered. Patients with a history of asthma, other allergies, reactions to contrast media in the past, or anxiety are predisposed to the aforementioned side effects.<sup>36,37</sup>

After a patient has suffered an adverse reaction from exposure to an iodinated contrast agent, it is imperative to minimize this risk in the event of subsequent exposure. Multiple studies have shown corticosteroids to be effective for prophylaxis in these patients.<sup>38–44</sup> Lasser and colleagues demonstrated a significant reduction in reactions related to hyperosmolar agents with the administration of 32 mg of methylprednisolone 12 and 2 hours before injection of the contrast agent. In a similar regimen, these investigators also found that use of a nonionic contrast agent with lower osmolality reduced adverse events from 4.9% in the untreated group to 1.7% in the pretreated group.<sup>39,40</sup> Other studies have shown that premedication with 50 mg of prednisone given at 13, 7, and 1 hour prior to contrast administration, often in conjunction with diphenhydramine, is an effective method of preventing contrast-induced allergic reactions, with breakthrough reactions occurring only 2.1% of the time.<sup>45,46</sup> Katayama and associates found a reduction in adverse reactions from 12.6% to 3.1% with use of ionic, high-osmolality contrast agents, as opposed to nonionic, low-osmolality agents.<sup>47</sup> Steroid premedication should be administered to all patients who have a history of reaction to contrast media or who are otherwise at high risk for such. Some authors assert that despite prophylaxis, albeit at lower doses than described previously, and the use of low-osmolality contrast agents, as many as 10% of patients may still suffer a breakthrough reaction.<sup>48</sup>

### Cardiac Toxicity

Contrast agents can adversely affect cardiac function, particularly during coronary angiography and ventriculography. These physiologic disturbances are spurred by electrolyte imbalances of sodium and calcium in the coronary system caused by passive washout after the injection of contrast material. Even in noncoronary arteriography, some older contrast agents were able to bind calcium and induce arrhythmias by reducing levels of free ionized calcium.<sup>49</sup> The most common hemodynamic effect is a decrease in heart rate and blood pressure, usually temporary and self-limited. However, this can be much more pronounced in patients with severe underlying cardiac dysfunction, aortic stenosis, or direct exposure of the heart to the contrast agent. Use of low-osmolality agents has been shown to reduce the incidence of such adverse hemodynamic effects.<sup>50</sup>

### Hematologic Toxicity

Conventional iodinated contrast agents have been shown to inhibit multiple coagulation factors and antithrombin activity, as well as to exhibit antifibrinolytic properties.<sup>51</sup> The clinical significance of these findings is unclear within circulating blood. However, red blood cells do aggregate when in contact with contrast media.<sup>52</sup> This can present a compromising situation with stasis of blood and contrast material within the catheters and sheaths used for injection. To prevent the

possible introduction of fresh thrombus into the circulation, it is strongly advised that one remain vigilant about frequent flushing of catheters and sheaths with saline. Anticoagulation during endovascular procedures should be considered on a case-by-case basis. In cases in which heparin is administered, measuring activating clotting times and reversing heparin effects with protamine administration on case completion may be beneficial before sheath removal. There is some evidence that use of nonionic contrast agents may reduce these adverse hematologic effects.<sup>53</sup>

### Nephrotoxicity

Contrast-induced nephropathy is perhaps the most commonly cited and studied adverse reaction to iodinated contrast agents and carries with it significant morbidity and mortality. It continues to be the third leading cause of acute renal failure in hospitalized patients.<sup>54,55</sup> The severity of clinical manifestations in these patients ranges from a mild reversible rise in serum creatinine concentration to end-stage renal failure and death. Multiple clinical trials have shown the deleterious effect of iodinated contrast agents on renal function.<sup>56–58</sup> Many risk factors for the development of contrast-induced nephropathy have been identified, of which preexisting renal dysfunction remains the most important.<sup>59</sup> Other risk factors include advanced age,<sup>60</sup> congestive heart failure, dehydration, hyperosmolar states (e.g., multiple myeloma), and severe proteinuria. In such patients the volume of contrast material should be minimized and adequate hydration should be administered. Interestingly, neither the type of contrast agent used nor the total volume infused seems to play a significant role in the development of this complication in patients with normal renal function.<sup>59,61–63</sup> Although administration of contrast agents to patients already suffering from complete renal failure may be done without fear of inducing further nephropathy, these patients are at risk for hyperosmolar volume overload and should be scheduled for dialysis after the angiography procedure.

All iodinated contrast agents are primarily excreted by the kidneys. It was originally thought that the high osmolality and ionization of conventional contrast agents were responsible for contrast-induced nephropathy. However, there is no difference in such occurrence with ionic and nonionic contrast agents.<sup>64</sup> However, there does appear to be reduced risk with the use of low-osmolality contrast agents as opposed to those with high osmolality.<sup>64–66</sup> After infusion, contrast material is filtered by the glomerulus with little or no evidence of tubular reabsorption. The principal site of contrast-induced nephropathy is the renal tubule secondary to transient local ischemia.<sup>67</sup> Because contrast material is filtered without reabsorption, an osmotic gradient is created that results in increased intratubular pressure, afferent arteriolar vasoconstriction, and decreased glomerular filtration rate. This decrease in glomerular filtration rate results in regional tubular ischemia.

The incidence of contrast-induced nephropathy in patients with normal renal function is only 1% to 2%.<sup>66</sup> This risk increases to 10% in patients with creatinine levels of 1.3 to 1.9 mg/dL (115 µmol/L to 168 µmol/L) and to as much as 62% in patients with levels higher than 2 mg/dL (177 µmol/L). The

incidence of contrast-induced nephropathy is high in the diabetic population, although diabetes is not considered an independent risk factor. It is probably an unmasking effect of sub-clinical renal insufficiency, which is common in these patients. Patients with type 1 diabetes are more prone to the development of contrast-induced nephropathy than are patients with type 2 diabetes.<sup>68,69</sup> Moreover, patients with diabetes and renal insufficiency in whom acute contrast-induced renal failure develops are less likely to recover than patients with baseline renal insufficiency alone, and they are at greater risk of permanently requiring dialysis.<sup>68–70</sup>

### Metformin

Diabetic patients taking metformin (*N*-dimethylbiguanide), an oral hypoglycemic agent, require special consideration when receiving iodinated contrast material. Metformin is excreted by the kidneys, and continuing to take this drug in the setting of renal dysfunction can result in lactic acidosis. This is a rare complication resulting from impaired drug clearance in patients in whom nephropathy develops as a result of iodinated contrast material. Despite equivocal evidence that halting metformin prevents metabolic acidosis, there are published guidelines pertaining to the use of contrast material in these patients taking metformin.<sup>71–73</sup> Only low-osmolality contrast agents should be used, and creatinine levels should be checked before and after the procedure. Patients with normal preprocedure and post-procedure renal function should refrain from taking metformin for a period of 48 hours after the procedure. Patients with baseline renal insufficiency that remains stable should refrain from taking the drug for 48 hours before and 48 hours after the procedure. In an emergency setting, patients with renal insufficiency should be well hydrated for 24 hours after the procedure while being monitored for the development of lactic acidosis. Findings can include nausea, vomiting, somnolence, epigastric pain, anorexia, lethargy, diarrhea, thirst, pH less than 7.25, lactic acid level greater than 45 mg/dL (5 mmol/L), anion gap greater than 15 mEq/L (15 mmol/L), and increase in the lactate-to-pyruvate ratio.

### Prevention of contrast-induced nephropathy

Prevention of contrast-induced nephropathy has been the subject of many research trials and studies. Intravenous hydration appears to be the most effective tool,<sup>74,75</sup> with 0.9% saline offering better protection than 0.45% normal saline.<sup>76</sup> Intravenous sodium bicarbonate administered before exposure to contrast material may also significantly reduce renal dysfunction.<sup>77</sup> However, more recent randomized trials have failed to show a benefit to hydration with 0.9% normal saline versus no hydration in patients with eGFR between 30 and 59 mL per min/1.73 m<sup>2</sup>, as well as a difference between hydration with 0.9% saline or sodium bicarbonate.<sup>78,79</sup> Another agent that may offer protection against contrast-induced nephropathy in patients with renal dysfunction is the antioxidant *N*-acetylcysteine<sup>80–84</sup> given at a dose of 600 mg for 2 days before and after the procedure. Tepel and colleagues found that the incidence of contrast-induced nephropathy was reduced from 22% to 2% in patients receiving *N*-acetylcysteine with hydration versus those

receiving hydration alone.<sup>81</sup> Other trials including the large, randomized PRESERVE trial have failed to show a benefit, and therefore the recommendation for routine use remains controversial.<sup>79,85–88</sup> Many other agents have been studied for possible protective effects against contrast-induced nephropathy through the actions of increasing vasodilation, renal perfusion, or diuresis (or any combination of these mechanisms). Such agents include fenoldopam, theophylline, prostaglandin E<sub>1</sub>, endothelin antagonists, calcium channel blockers, dopamine, and diuretics. However, none of these agents can be recommended for the prevention of contrast-induced nephropathy on the basis of current scientific evidence.<sup>57,58,74,89–107</sup> The development of strict protocols with adherence to low dosing of contrast agents has also been shown to further improve results in the prevention of contrast-induced nephropathy. Although many of these protocols have been developed for CT, they are equally applicable to arteriography.<sup>108–110</sup>

### Limitations and Risks of CO<sub>2</sub> Contrast

Because CO<sub>2</sub> gas tends to rise, visualization of vessels with posterior origins may sometimes be difficult in the supine position. A typical example is the left renal artery, which often has a posterolateral takeoff from the aorta. To address this issue, patients can be positioned with the left flank slightly elevated, either by placing a roll under the left side or by tilting the table in that direction if such a feature is available. This will raise the left renal artery above the plane of the catheter and allow better filling with CO<sub>2</sub>. More recent imaging techniques, known as digital variance angiography (DVA), based on principles of kinetic imaging have been shown to increase the quality of CO<sub>2</sub> angiography by decreasing motion artifact. Briefly, DVA creates a more effective mask image than DSA by using an average value of all frames rather than selecting a single image for the mask image.<sup>111</sup>

Complications from CO<sub>2</sub> injection for angiography are extremely uncommon, with only a handful of serious adverse events reported in the literature.<sup>112–116</sup> Most of them were related to mesenteric ischemia secondary to gas trapping. CO<sub>2</sub> dissipates rapidly in the bloodstream, but gas trapping can occur in any vessel and lead to ischemia. The most important consideration when CO<sub>2</sub> is used for intraarterial injection is the potential risk of neurotoxicity. An animal study involving direct injection of CO<sub>2</sub> into the carotid vessels resulted in multiple ischemic infarcts and subsequent neurologic deficits.<sup>117</sup> However, other animal studies found no adverse reactions when CO<sub>2</sub> was injected into the thoracic aorta or carotid vessels.<sup>118,119</sup> Although there is no strong evidence in humans, this potential risk demonstrated in animals has led to the general recommendation to avoid use of CO<sub>2</sub> as a contrast agent when injection is above the diaphragm.

## FUTURE ADVANCES

Arteriography is an essential tool in the practice of vascular surgery, and the outlook of future advances is promising. Arteriography will be integrated with other modalities to create improved images, provide physiologic information, and deliver novel therapies in a targeted manner. The possibilities will

continue to grow as scientists and vascular surgeons alike move to treat standard problems in ways previously thought not possible. A sound education and training in arteriography, with the commitment to modernize as standards of care change, is necessary as vascular surgery continues to evolve.

## SELECTED KEY REFERENCES

Lasser EC, Berry CC, Talner LB, et al. Pretreatment with corticosteroids to alleviate reactions to intravenous contrast material. *N Engl J Med.* 1987;317:845–849.

*Randomized controlled trial showing the benefit of steroid pretreatment in preventing adverse contrast medium-related reactions.*

Nijssen EC, Rennenberg RJ, Nelemans PJ, et al. Prophylactic hydration to protect renal function from intravascular iodinated contrast material in patients at high risk of contrast-induced nephropathy (AMACING): a prospective, randomised, phase 3, controlled, open-label, non-inferiority trial. *Lancet.* 2017;389:1312–1322.

*The AMACING trial demonstrated that prehydration with normal saline infusion did not reduce rates of contrast-induced nephropathy compared to no hydration in patients with eGFR of 30–59 mL per min/1.73 m<sup>2</sup>.*

Parfrey PS, Griffiths SM, Barrett BJ, et al. Contrast material-induced renal failure in patients with diabetes mellitus, renal insufficiency, or both: a prospective controlled study. *N Engl J Med.* 1989;320:143–149.

*Prospective trial showing renal insufficiency as the main risk factor in the development of contrast-induced nephropathy.*

Solomon R, Werner C, Mann D, et al. Effects of saline, mannitol, and furosemide to prevent acute decreases in renal function induced by radiocontrast agents. *N Engl J Med.* 1994;331:1416–1420.

*Important study showing that hydration is more effective than diuresis in preventing contrast-induced nephropathy.*

Tepel M, van der Giet M, Schwarfeld C, et al. Prevention of radiographic-contrast-agent-induced reductions in renal function by acetylcysteine. *N Engl J Med.* 2000;343:180–184.

*This important trial showed a reduction in contrast-induced nephropathy with the administration of N-acetylcysteine (Mucomyst).*

Weisbord SD, Gallagher M, Jneid H, et al. Outcomes after angiography with sodium bicarbonate and acetylcysteine. *N Engl J Med.* 2018;378:603–614.

*The PRESERVE trial demonstrated no advantage for sodium bicarbonate infusion over normal saline and no benefit of acetylcysteine over placebo in reducing contrast-induced nephropathy.*

A complete reference list can be found online at [www.expertconsult.com](http://www.expertconsult.com).

## REFERENCES

1. Mell M, et al. Clinical utility of time-resolved imaging of contrast kinetics (TRICKS) magnetic resonance angiography for infrageniculate arterial occlusive disease. *J Vasc Surg.* 2007;45:543–548.
2. Schläger O, et al. Duplex sonography versus angiography for assessment of femoropopliteal arterial disease in a “real-world” setting. *J Endovasc Ther.* 2007;14:452–459.
3. Gjonnaess E, et al. Gadolinium-enhanced magnetic resonance angiography, colour duplex and digital subtraction angiography of the lower limb arteries from the aorta to the tibio-peroneal trunk in patients with intermittent claudication. *Eur J Endovasc Surg.* 2006;31:53–58.
4. U-King-Im JM, et al. Contrast-enhanced MR angiography for carotid disease. *Neurology.* 2004;62:1282–1290.
5. Nederkoorn PJ, et al. Duplex ultrasound and magnetic resonance angiography compared with digital subtraction angiography in carotid artery stenosis. *Stroke.* 2003;34:1324–1332.
6. Randoux B, et al. Carotid artery stenosis: prospective comparison of CT, three-dimensional gadolinium-enhanced MR, and conventional angiography. *Radiology.* 2001;220:179–185.
7. Mills JL. Infrainguinal vein graft surveillance: how and when. *Semin Vasc Surg.* 2001;14:169–176.
8. Bergamini TM, et al. Intensive surveillance of femoropopliteal-tibial autogenous vein bypass improves long-term graft patency and limb salvage. *Ann Surg.* 1995;221:507–516.
9. Lundell A, et al. Femoropopliteal-crural graft patency is improved by an intensive surveillance program: a prospective randomized study. *J Vasc Surg.* 1995;21:26–34.
10. Weaver FA, et al. Clinical applications of carbon dioxide/digital subtraction angiography. *J Vasc Surg.* 1991;13:266–273.
11. Seeger JM, et al. Carbon dioxide gas as an arterial contrast agent. *Ann Surg.* 1993;217:688–697.
12. Gahlen J, et al. Carbon dioxide angiography for endovascular grafting in high-risk patients with infrarenal abdominal aortic aneurysms. *J Vasc Surg.* 2001;33:646–649.
13. Caridi JG, et al. CO<sub>2</sub> splenoportography: preliminary results. *AJR Am J Roentgenol.* 2003;180:1375–1378.
14. Lang EV, et al. Carbon dioxide angiography: effect of injection parameters on bolus configurations. *J Vasc Interv Radiol.* 1999;10:41–49.
15. Corcione N, et al. Contrast minimization with the new-generation DyeVert Plus system for contrast reduction and real-time monitoring during coronary and peripheral procedures: first experience. *J Invasive Cardiol.* 2017;29(8):259–262.
16. U-King-Im JM, et al. Internal carotid artery stenosis: accuracy of subjective visual impression for evaluation with digital subtraction angiography and contrast-enhanced MR angiography. *Radiology.* 2007;244:213–222.
17. Fierstra J, et al. Amended intraoperative neuronavigation: three-dimensional vascular roadmapping with selective rotational digital subtraction angiography. *World Neurosurg.* 2020;135:183–187.
18. McNally MM, Scali ST, et al. Three-dimensional fusion computed tomography decreases radiation exposure, procedure time, and contrast use during fenestrated endovascular aortic repair. *J Vasc Surg.* 2015;61(2):309–316.
19. Plessis J, Warin Fresse K, et al. Value of image fusion in coronary angiography for the detection of coronary artery bypass grafts. *J Am Heart Assoc.* 2016;5(6):e002233.
20. Stahlberg E, Sieren M, Anton S, et al. Fusion imaging reduces radiation and contrast medium exposure during endovascular revascularization of iliac steno-occlusive disease. *Cardiovasc Intervent Radiol.* 2019;42(11):1635–1643.
21. Schwein A, Chinnadurai P, Shah DJ, et al. Feasibility of three-dimensional magnetic resonance angiography-fluoroscopy image fusion technique in guiding complex endovascular aortic procedures in patients with renal insufficiency. *J Vasc Surg.* 2017;65(5):1440–1452.
22. De Boer SW, Heinen SGH, Goudeketting SR, et al. Novel diagnostic and imaging techniques in endovascular iliac artery procedures. *Expert Rev Cardiovasc Ther.* 2020;10:1080.
23. Abi-Jaoudeh N, Glossop N, Dake M, et al. Electromagnetic navigation for thoracic aortic stent-graft deployment: a pilot study in swine. *J Vasc Interv Radiol.* 2010;21(6):888–895.
24. Schwein A, Kramer B, Chinnadurai P, et al. Electromagnetic tracking of flexible robotic catheters enables “assisted navigation” and brings automation to endovascular navigation in an in vitro study. *J Vasc Surg.* 2018;67(4):1274–1281.
25. Owen AR, et al. Critical lower-limb ischemia: the diagnostic performance of dual-phase injection MR angiography (including high-resolution distal imaging) compared with digital subtraction angiography. *J Vasc Interv Radiol.* 2009;20:165–172.
26. Hingorani A, et al. Comparison of computed tomography angiography to contrast arteriography for patients undergoing evaluation for lower extremity revascularization. *Vasc Endovascular Surg.* 2007;42:115–119.
27. Hingorani A, et al. A comparison of magnetic resonance angiography, contrast arteriography, and duplex arteriography for patients undergoing lower extremity revascularization. *Ann Vasc Surg.* 2004;18:294–301.
28. Hingorani A, et al. Magnetic resonance angiography versus duplex arteriography in patients undergoing lower extremity revascularization: which is the best replacement for contrast arteriography. *J Vasc Surg.* 2004;39:717–722.
29. Lapeyre M, et al. Assessment of critical limb ischemia in patients with diabetes: comparison of MR angiography and digital subtraction angiography. *AJR Am J Roentgenol.* 2005;185:1641–1650.
30. Leiner T, et al. Comparison of contrast-enhanced magnetic resonance angiography and digital subtraction angiography in patients with chronic critical limb ischemia and tissue loss. *Invest Radiol.* 2004;39:435–444.
31. Lundin P, et al. Imaging of aortoiliac arterial disease: duplex ultrasound and MR angiography versus digital subtraction angiography. *Acta Radiol.* 2000;41:125–132.
32. Kreitner K, et al. Diabetes and peripheral arterial occlusive disease: prospective comparison of contrast-enhanced three-dimensional MR angiography with conventional digital subtraction angiography. *AJR Am J Roentgenol.* 2000;174:171–179.
33. Hoch JR, et al. Comparison of treatment plans for lower extremity arterial occlusive disease made with electrocardiography-triggered two-dimensional time-of-flight magnetic resonance angiography and digital subtraction angiography. *Am J Surg.* 1999;178:166–173.
34. Leyendecker JR, et al. The role of infrapopliteal MR angiography in patients undergoing optimal contrast angiography for chronic limb-threatening ischemia. *J Vasc Interv Radiol.* 1998;9:545–551.
35. Smith D, et al. Three new low-osmolality contrast agents: a comparative study of patient discomfort. *AJR Am J Neuroradiol.* 1988;9:137–139.
36. Bettmann MA. Contrast agents. In: Kim D, Orron DE, eds. *Peripheral Vascular Imaging and Intervention.* St. Louis: Mosby-Year Book; 1992.
37. Podrid PJ. Role of higher nervous activity in ventricular arrhythmia and sudden cardiac death: implication for alternative antiarrhythmic therapy. *Ann NY Acad Sci.* 1984;432:296–313.
38. Lasser EC. Pretreatment with corticosteroids to prevent reactions to i.v. contrast material: overview and implications. *AJR Am J Roentgenol.* 1988;150:257–259.
39. Lasser EC, et al. Pretreatment with corticosteroids to prevent adverse reactions to nonionic contrast media. *AJR Am J Roentgenol.* 1994;162:523–526.
40. Lasser EC, et al. Pretreatment with corticosteroids to alleviate reactions to intravenous contrast material. *N Engl J Med.* 1987;317:845–849.
41. Lasser EC, et al. Protective effects of corticosteroids in contrast material anaphylaxis. *Invest Radiol.* 1988;23(suppl 1):S193–S194.
42. Lasser EC, et al. Steroids: theoretical and experimental basis for utilization in prevention of contrast media reactions. *Radiology.* 1977;125:1–9.

43. Greenberger PA, et al. The prevention of immediate generalized reactions to radiocontrast media in high-risk patients. *J Allergy Clin Immunol.* 1991;87:867–872.
44. Greenberger PA, et al. Prophylaxis against repeated radiocontrast media reactions in 857 cases: adverse experience with cimetidine and safety of beta-adrenergic antagonists. *Arch Intern Med.* 1985;145:2197–2200.
45. Greenberger PA, Patterson R, et al. Two pretreatment regimens for high-risk patients receiving radiographic contrast media. *J Allergy Clin Immunol.* 1984;74(4 Pt 1):540–543.
46. Mervak BM, Davenport MS, et al. Rates of breakthrough reactions in inpatients at high risk receiving premedication before contrast-enhanced CT. *AJR Am J Roentgenol.* 2015;205(1):77–84.
47. Katayama H, et al. Adverse reactions to ionic and nonionic contrast media: a report from the Japanese Committee on the Safety of Contrast Media. *Radiology.* 1990;175:621–628.
48. Freed KS, et al. Breakthrough adverse reactions to low-osmolar contrast media after steroid premedication. *AJR Am J Roentgenol.* 2001;176:1389–1392.
49. Morris TW, et al. Work in progress: reduction of calcium activity by radiopaque contrast media. *Radiology.* 1983;148:55–59.
50. Dawson P. Cardiovascular effects of contrast agents. *Am J Cardiol.* 1989;64:2E–9E.
51. Farrehi PM, et al. An analysis of mechanisms underlying the antifibrinolytic properties of radiographic contrast agents. *J Thromb Thrombolysis.* 2001;12:273–281.
52. Kopko PM, et al. Thrombin generation in nonclottable mixtures of blood and nonionic contrast agents. *Radiology.* 1990;174:459–461.
53. Bettmann M. Ionic versus nonionic contrast agents and their effects on blood components: clinical summary and conclusions. *Invest Radiol.* 1988;23(suppl 2):S378–S380.
54. Waybill MM, et al. Contrast media-induced nephrotoxicity: identification of patients at risk and algorithms for prevention. *J Vasc Interv Radiol.* 2001;12:3–9.
55. Agrawal M, et al. Cardiology grand rounds from the University of North Carolina at Chapel Hill: contrast induced nephropathy after angiography. *Am J Med Sci.* 2002;323:252–258.
56. Manske CL, et al. Contrast nephropathy in azotemic diabetic patients undergoing coronary angiography. *Am J Med.* 1990;89:615–620.
57. Stevens MA, et al. A prospective randomized trial of prevention measures in patients at high risk for contrast nephropathy: results of the P.R.I.N.C.E. study. Prevention of Radiocontrast Induced Nephropathy Clinical Evaluation. *J Am Coll Cardiol.* 1999;33:403–411.
58. Weisberg LS, et al. Risk of radiocontrast nephropathy in patients with and without diabetes mellitus. *Kidney Int.* 1994;45:259–265.
59. Parfrey PS, et al. Contrast material-induced renal failure in patients with diabetes mellitus, renal insufficiency, or both: a prospective controlled study. *N Engl J Med.* 1989;320:143–149.
60. Rich MW, et al. Incidence, risk factors, and clinical course of acute renal insufficiency after cardiac catheterization in patients 70 years of age or older: a prospective study. *Arch Intern Med.* 1990;150:1237–1242.
61. Gomes AS, et al. Acute renal dysfunction in high-risk patients after angiography: comparison of ionic and nonionic contrast media. *Radiology.* 1989;170:65–68.
62. Miller DL, et al. Intravascular contrast media: effect of dose on renal function. *Radiology.* 1988;167:607–611.
63. Schwab SJ, et al. Contrast nephrotoxicity: a randomized controlled trial of a nonionic and an ionic radiographic contrast agent. *N Engl J Med.* 1989;320:149–153.
64. Rudnick MR, et al. Nephrotoxicity of ionic and nonionic contrast media in 1196 patients: a randomized trial. The Iohexol Cooperative Study. *Kidney Int.* 1995;47:254–261.
65. Barrett BJ, et al. Metaanalysis of the relative nephrotoxicity of high- and low-osmolality iodinated contrast media. *Radiology.* 1993;188:171–178.
66. Chalmers N, et al. Comparison of ioxilan and iohexol in renal impairment. *Br J Radiol.* 1999;72:701–703.
67. Donadio C, et al. Tubular toxicity is the main renal effect of contrast media. *Ren Fail.* 1996;18:647–656.
68. Harkonen S, et al. Exacerbation of diabetic renal failure following intravenous pyelography. *Am J Med.* 1977;63:939–946.
69. Shieh SD, et al. Low risk of contrast media-induced acute renal failure in nonazotemic type 2 diabetes mellitus. *Kidney Int.* 1982;21:739–743.
70. Weinrauch LA, et al. Coronary angiography and acute renal failure in diabetic azotemic nephropathy. *Ann Intern Med.* 1977;86:56–59.
71. Thomsen HS, et al. Contrast media and the kidney: European Society of Urogenital Radiology (ESUR) guidelines. *Br J Radiol.* 2003;76:513–518.
72. Namazi MH, AlipourParsa S, Roohigilani K, et al. Is it necessary to discontinue metformin in diabetic patients with GFR >60 ml/min per 1.73 m<sup>2</sup> undergoing coronary angiography: A controversy still exists? *Acta Biomed.* 2018;89(2):227–232.
73. Zeller M, Labalette-Bart M, Juliard JM, et al. Metformin and contrast-induced acute kidney injury in diabetic patients treated with primary percutaneous coronary intervention for ST segment elevation myocardial infarction: A multicenter study. *Int J Cardiol.* 2016;220:137–142.
74. Solomon R, et al. Effects of saline, mannitol, and furosemide to prevent acute decreases in renal function induced by radiocontrast agents. *N Engl J Med.* 1994;331:1416–1420.
75. Trivedi HS, et al. A randomized prospective trial to assess the role of saline hydration on the development of contrast nephrotoxicity. *Nephron Clin Pract.* 2003;93:C29–C34.
76. Mueller C, et al. Prevention of contrast media-associated nephropathy: randomized comparison of 2 hydration regimens in 1620 patients undergoing coronary angioplasty. *Arch Intern Med.* 2002;162:329–336.
77. Merten GJ, et al. Prevention of contrast-induced nephropathy with sodium bicarbonate: a randomized controlled trial. *JAMA.* 2004;291:2328–2334.
78. Nijsen EC, Rennenberg RJ, Nelemans PJ, et al. Prophylactic hydration to protect renal function from intravascular iodinated contrast material in patients at high risk of contrast-induced nephropathy (AMACING): a prospective, randomised, phase 3, controlled, open-label, non-inferiority trial. *Lancet.* 2017;389:1312–1322.
79. Weisbord SD, Gallagher M, Jneid H, et al. Outcomes after angiography with sodium bicarbonate and acetylcysteine. *N Engl J Med.* 2018;378:603–614.
80. Briguori C, et al. Acetylcysteine and contrast agent-associated nephrotoxicity. *J Am Coll Cardiol.* 2002;40:298–303.
81. Tepel M, et al. Prevention of radiographic-contrast-agent-induced reductions in renal function by acetylcysteine. *N Engl J Med.* 2000;343:180–184.
82. Kay J, et al. Acetylcysteine for prevention of acute deterioration of renal function following elective coronary angiography and intervention: a randomized controlled trial. *JAMA.* 2003;289:553–558.
83. Diaz-Sandoval LJ, et al. Acetylcysteine to prevent angiography-related renal tissue injury (the APART trial). *Am J Cardiol.* 2002;89:356–358.
84. Shyu KG, et al. Acetylcysteine protects against acute renal damage in patients with abnormal renal function undergoing a coronary procedure. *J Am Coll Cardiol.* 2002;40:1383–1388.
85. Durham JD, et al. A randomized controlled trial of N-acetylcysteine to prevent contrast nephropathy in cardiac angiography. *Kidney Int.* 2002;62:2202–2207.
86. Hoffmann U, et al. The value of N-acetylcysteine in the prevention of radiocontrast agent-induced nephropathy seems questionable. *J Am Soc Nephrol.* 2004;15:407–410.
87. Chong E, Poh KK, et al. Comparison of combination therapy of high-dose oral N-acetylcysteine and intravenous sodium bicarbonate hydration with individual therapies in the reduction of Contrast-induced Nephropathy during Cardiac Catheterisation and Percutaneous Coronary Intervention (CONTRAST): a multi-centre, randomised, controlled trial. *Int J Cardiol.* 2015;201:237–242.
88. Zhao SJ, Zhong ZS, et al. The efficacy of N-acetylcysteine plus sodium bicarbonate in the prevention of contrast-induced nephropathy after cardiac catheterization and percutaneous coronary intervention: a meta-analysis of randomized controlled trials. *Int J Cardiol.* 2016;221:251–259.

89. Weinstein JM, et al. Potential deleterious effect of furosemide in radiocontrast nephropathy. *Nephron*. 1992;62:413–415.
90. Shammas NW, et al. Aminophylline does not protect against radiocontrast nephropathy in patients undergoing percutaneous angiographic procedures. *J Invasive Cardiol*. 2001;13:738–740.
91. Gupta RK, et al. Captopril for prevention of contrast-induced nephropathy in diabetic patients: a randomised study. *Indian Heart J*. 1999;51:521–526.
92. Sketch Jr MH, et al. Prevention of contrast media-induced renal dysfunction with prostaglandin E<sub>1</sub>: a randomized, double-blind, placebo-controlled study. *Am J Ther*. 2001;8:155–162.
93. Huber W, et al. Effectiveness of theophylline prophylaxis of renal impairment after coronary angiography in patients with chronic renal insufficiency. *Am J Cardiol*. 2003;91:1157–1162.
94. Allaqqaband S, et al. Prospective randomized study of N-acetylcysteine, fenoldopam, and saline for prevention of radiocontrast-induced nephropathy. *Catheter Cardiovasc Interv*. 2002;57:279–283.
95. Stone GW, et al. Fenoldopam mesylate for the prevention of contrast-induced nephropathy: a randomized controlled trial. *JAMA*. 2003;290:2284–2291.
96. Erley CM, et al. Prevention of radiocontrast-media induced nephropathy in patients with pre-existing renal insufficiency by hydration in combination with the adenosine antagonist theophylline. *Nephrol Dial Transplant*. 1999;14:1146–1149.
97. Koch JA, et al. Prostaglandin E<sub>1</sub>: a new agent for the prevention of renal dysfunction in high risk patients caused by radiocontrast media? PGE<sub>1</sub> Study Group. *Nephrol Dial Transplant*. 2000;15:43–49.
98. Wang A, et al. Exacerbation of radiocontrast nephrotoxicity by endothelin receptor antagonism. *Kidney Int*. 2000;57:1675–1680.
99. Neumayer HH, et al. Prevention of radiocontrast-media-induced nephrotoxicity by the calcium channel blocker nifedipine: a prospective randomised clinical trial. *Nephrol Dial Transplant*. 1989;4:1030–1036.
100. Carraro M, et al. Dose effect of nifedipine on urinary enzymes and microproteins following non-ionic radiocontrast administration. *Nephrol Dial Transplant*. 1996;11:444–448.
101. Rodicio JL, et al. Calcium antagonists and renal protection. *J Hypertens Suppl*. 1993;11:S49–S53.
102. Spangberg-Viklund B, et al. Does prophylactic treatment with felodipine, a calcium antagonist, prevent low-osmolar contrast-induced renal dysfunction in hydrated diabetic and nondiabetic patients with normal or moderately reduced renal function? *Scand J Urol Nephrol*. 1996;30:63–68.
103. Esnault VL. Radiocontrast media-induced nephrotoxicity in patients with renal failure: rationale for a new double-blind, prospective, randomized trial testing calcium channel antagonists. *Nephrol Dial Transplant*. 2002;17:1362–1364.
104. Hans SS, et al. Effect of dopamine on renal function after arteriography in patients with pre-existing renal insufficiency. *Am Surg*. 1998;64:432–436.
105. Kapoor A, et al. Use of dopamine in prevention of contrast induced acute renal failure—a randomised study. *Int J Cardiol*. 1996;53:233–236.
106. Gare M, et al. The renal effect of low-dose dopamine in high-risk patients undergoing coronary angiography. *J Am Coll Cardiol*. 1999;3:1682–1688.
107. Abizaid AS, et al. Effects of dopamine and aminophylline on contrast-induced acute renal failure after coronary angioplasty in patients with preexisting renal insufficiency. *Am J Cardiol*. 1999;83:260–263. A5.
108. Kidoh M, et al. Low-contrast dose protection protocol for diagnostic computed tomography in patients at high-risk for contrast-induced nephropathy. *J Comput Assist Tomogr*. 2013;37:289–296.
109. Herts BR, et al. Identifying outpatients with renal insufficiency before contrast-enhanced CT by using estimated glomerular filtration rates versus serum creatinine levels. *Radiology*. 2008;248:106–113.
110. Bonsai GJ, et al. Measurement of change in estimated glomerular filtration rate in patients with renal insufficiency after contrast-enhanced computed tomography: a case-control study. *J Comput Assist Tomogr*. 2009;33:455–459.
111. Gyánó M, Gó G, Óriás VI, et al. Kinetic imaging in lower extremity arteriography: comparison to digital subtraction angiography. *Radiology*. 2019;290(1):246–253.
112. Hawkins Jr IF, et al. Modified plastic bag system with O-ring fitting connection for carbon dioxide angiography. *AJR Am J Roentgenol*. 2001;176:229–232.
113. Rundback JH, et al. Livedo reticularis, rhabdomyolysis, massive intestinal infarction, and death after carbon dioxide arteriography. *J Vasc Surg*. 1997;26:337–340.
114. Caridi JG, et al. Carbon dioxide digital subtraction angiography: the practical approach. *Tech Vasc Interv Radiol*. 2001;4:57–65.
115. Huang SG, et al. A prospective study of carbon dioxide digital subtraction versus standard contrast arteriography in the detection of endoleaks in endovascular abdominal aortic aneurysm repairs. *Ann Vasc Surg*. 2013;27:38–44.
116. Chao A, et al. Carbon dioxide digital subtraction angiography-assisted endovascular aortic aneurysm repair in the azotemic patient. *J Vasc Surgery*. 2007;45:451–458.
117. Coffey R, et al. The cerebrovascular effects of intraarterial CO<sub>2</sub> in quantities required for diagnostic imaging. *Radiology*. 1984;151:405–410.
118. Shifrin EG, et al. Cerebral angiography with gaseous carbon dioxide. *J Cardiovasc Surg (Torino)*. 1990;31:603–606.
119. Dimakakos PB, et al. The cerebral effects of carbon dioxide during digital subtraction angiography in the aortic arch and its branches in rabbits. *AJR Am J Neuroradiol*. 1998;19:261–266.

# Venography

CARLOS F. BECHARA

Based on a previous edition chapter by Richard H. Pin, Micheal T. Ayad, and David Gillespie

## BASIC PRINCIPLES 338

## CLINICAL APPLICATIONS 338

### Ascending Venography 338

#### *Deep Venous Thrombosis* 338

##### *Technique* 338

##### *Interpretation* 339

#### *Incompetent Perforating Veins* 339

##### *Technique* 340

##### *Interpretation* 340

#### *Venous Aneurysms and Malformations* 340

##### *Technique* 341

##### *Interpretation* 341

### Descending Venography 342

##### *Technique* 342

##### *Interpretation* 343

## VENOGRAPHY FOR SPECIFIC REGIONS AND CONDITIONS 343

### Iliac Vein Assessment and Inferior Venacavography 343

#### *Technique* 343

#### *Interpretation* 343

### Venography During Treatment of Iliocaval Stenosis 343

#### *Technique* 343

#### *Interpretation* 344

### Diagnostic Venography of Pelvic Congestion Syndrome 344

#### *Technique* 344

#### *Interpretation* 344

## Venography for Varicoceles 345

### *Technique* 345

### *Treatment* 346

## Renal Venography 346

### *Technique* 346

### *Interpretation* 346

## Diagnostic Angiography of Mesenteric or Portal Venous Thrombosis 346

### *Technique* 347

### *Interpretation* 347

## Diagnostic Venography of Budd–Chiari Syndrome 347

### *Technique* 347

### *Interpretation* 348

## Upper Extremity Venography 348

### *Technique* 348

### *Interpretation* 348

## Central Thoracic Venography 348

### *Technique* 349

### *Interpretation* 349

## Pulmonary Arteriography 349

### *Technique* 349

### *Interpretation* 350

## GENERAL LIMITATIONS AND RISKS OF VENOGRAPHY 350

## FUTURE ADVANCES 350

Despite the advances we have made in medical imaging, contrast-enhanced venography has been and is still the “gold standard” for the diagnosis of deep venous thrombosis (DVT) since the early 1970s. Meanwhile, duplex ultrasonography is the most accurate noninvasive testing modality used to diagnose DVT and it is often readily available. Early extremity venography required venous cut-down for access to the deep

venous system, but this technique has evolved such that contrast material is injected percutaneously into a superficial vein in the foot, with a tourniquet applied above the ankle to prevent filling of the superficial veins that often obscure the deep system. As equipment and contrast agents have improved, so has the safety and efficacy of venography in evaluating DVT. Venography remains important in evaluating the ilio-femoral

**BOX 28.1****Current Indications for and Relative Contraindications to Venography****Current indications for venography**

1. Diagnosis of DVT in a patient:
  - a. With a nondiagnostic duplex ultrasound examination or for whom a duplex examination is not technically feasible
  - b. With a high clinical suspicion for DVT but with a negative duplex examination
  - c. When duplex ultrasound is not available
2. As an adjunct during venous intervention (thrombolysis, thrombectomy, angioplasty, and stenting)
3. Evaluation of valvular insufficiency prior to stripping or ligation of superficial varicose veins

DVT, deep venous thrombosis.

Reproduced from ACR-SIR PRACTICE GUIDELINE FOR THE PERFORMANCE OF DIAGNOSTIC INFUSION VENOGRAPHY, revised 2008.

4. Venous mapping prior to or following a surgical interventional procedure
5. Evaluation for venous stenosis or venous hypertension
6. Evaluation for venous malformations
7. Preoperative evaluation for tumor involvement or encasement

**Relative contraindications (including but not limited to)**

1. Evidence of active cellulitis of the extremity to be imaged
2. Iodinated contrast allergy
3. Renal insufficiency in patients who are not on dialysis, particularly those with diabetes or congestive heart failure

or axillo-subclavian veins and integral in the endovascular treatment of DVT. It also remains an effective imaging tool for evaluating venous structures within the thoracic and abdominal cavities. Other modalities are used either as diagnostic (dynamic venography) or adjunctive tools during treatment, such as intravascular ultrasound (IVUS).

## BASIC PRINCIPLES

The two primary techniques of venography that are currently used are ascending and descending venography. Ascending venography is more common and is used to elucidate the presence of DVT in the lower extremity. Descending venography predominantly evaluates incompetent valves in patients with chronic venous insufficiency (CVI). This requires direct access to the deep venous system. The techniques of ascending and descending venography are described in the next section on clinical applications.

## CLINICAL APPLICATIONS

The current indications for venography are detailed in [Box 28.1](#). Despite the availability of less invasive imaging techniques, venography is still considered the gold standard against which all examination modalities are compared to determine the presence of DVT. This is particularly true in instances in which duplex ultrasound is inconclusive or unavailable. Venography also continues to have a higher sensitivity and specificity in detection of infrapopliteal thrombotic disease. Venography is indicated in evaluation of valvular insufficiency and venous malformations, and it has been shown to be helpful in planning adjunctive techniques in the operating room. Relative contraindications to venography are listed in [Box 28.1](#). Other common modalities used in detection of thrombosis and reflux are compared in [Table 28.1](#).

### Ascending Venography

Ascending venography has been used for many indications, including in the evaluation of DVT, incompetent perforating veins, and venous aneurysms and malformations.

### Deep Venous Thrombosis

Clinical examination alone is not a reliable means of diagnosing DVT. The indications for ascending lower extremity venography include a nondiagnostic ultrasound study and a need for improved imaging of calf veins in the setting of high clinical suspicion of DVT.<sup>1</sup> Because of its high diagnostic accuracy, lower extremity venography is useful for evaluation of the presence of deep venous disease in these circumstances. Another indication for venography is delineation of DVT during endovascular intervention, such as thrombolysis, thrombectomy, or angioplasty.

#### Technique

Diagnostic ascending venography requires a 22-gauge catheter, three 20–30-mL syringes, two tourniquets, a tilting fluoroscopic table with footrest, C-arm fluoroscopy, contrast agent, and normal saline. In addition, a 4F micropuncture sheath should be available for direct access to the venous system through the popliteal vein if needed. Ascending venography begins with placement of a catheter in a peripheral vein of the distal extremity. The access device is usually a 22-gauge intravenous catheter inserted into a superficial vein on the dorsum of the foot. When the affected extremity has significant edema, percutaneous catheterization of peripheral veins becomes difficult. In such cases, the use of ultrasound to guide vascular access is helpful. It is important that access for ascending venography not be through the saphenous vein adjacent to the medial malleolus at the ankle because contrast material may preferentially fill the superficial venous system without demonstrating the deep venous system adequately. The likelihood of this problem can be decreased by placing a tourniquet at the ankle and one at the knee, which will drive the contrast material into the deep venous system. However, these tourniquets should be released just before image acquisition to relieve extrinsic compression and to avoid occlusion of the deep veins. The patient is placed on a tilting fluoroscopic table with a footrest to enable near-upright positioning. With the patient initially in a reverse Trendelenburg position, the table is tilted to recumbency as the bolus is tracked. This approach enhances visualization of the large-capacity lower extremity venous anatomy as gravity

**TABLE 28.1** Comparison of Various Modalities for the Detection of Venous Disease

Technique	Pros	Cons
Venography	Good confirmatory test with diagnostic uncertainty and in detection of asymptomatic DVT Good diagnostic ability below the knee Descending venography demonstrates the location of the valve as well as valvular competence or incompetence	Invasive Not as readily available Expensive Potential for patient discomfort Risk of phlebitis Intravenous administration of contrast material Risk of nephrotoxicity Allergic reactions Increased cost Need for adequate intravenous access
Duplex ultrasound	Noninvasive Portable Readily available Absence of ionizing radiation High sensitivity and specificity above the elbow and above the knee	Operator dependent Detection of calf DVT is variable Greater accuracy in detecting DVT in symptomatic versus asymptomatic patients Does not permit accurate localization of the levels of valve stations and specific identification of incompetent segments Difficult to ascertain in those with massive edema, wounds, or obesity
Computed tomography venography	Noninvasive Technically simple Time requirement to ascertain the examination is low High sensitivity and specificity	Contrast agent required Risk of nephrotoxicity Radiation exposure Requires patient participation with breathing techniques Flow artifacts may complicate results
Magnetic resonance venography	Noninvasive Improved image quality	Expensive Long examination requirements Radiation exposure Caution in renal disease Inability to be used in patients with metal-based implanted devices

DVT, deep venous thrombosis.

delays the outflow of contrast material. The contralateral lower extremity is supported with a small platform so that no weight is borne on the extremity being examined. Side grip handles can be placed on the table as needed, depending on the patient's comfort level and security in the semi-upright position.

The examination is begun with the patient in a 40- to 60-degree semi-upright position. The intravenous contrast bolus is followed by radiographic imaging as it flows to the central veins. As the contrast agent ascends, additional filming of the deep and superficial femoral veins is performed. At least two projections are needed in the tibial and popliteal locations. Approximately 50 to 100 mL of contrast material is needed to fill the deep venous system adequately from ankle to groin. Additional contrast material can be injected, as needed, to visualize problem areas. Even with appropriate venous access and the use of tourniquets, adequate opacification of the deep veins of the lower extremities may be difficult because of dilution of the contrast agent and preferential flow from deep to superficial regions, which allows contrast material to escape to the superficial system. In such cases, we place the patient in the prone position, access the popliteal vein under ultrasound guidance, insert a 4F micropuncture sheath, and inject contrast material into the deep venous system. At completion of the examination, the veins are flushed with 50 mL of normal saline to minimize contact of the contrast agent with the venous endothelium and the chance for development of thrombophlebitis. It is important to make sure the

skin over the accessed vein is cleansed appropriately to reduce the risk of infection.

### Interpretation

The classic venographic sign of venous thrombosis is a luminal filling defect with a surrounding rim of contrast (Figs. 28.1–28.3). This appearance of parallel lines of contrast material around the thrombus is referred to as the "tram-track" sign. Other indicators of thromboembolism are an abrupt termination of intravascular contrast or the formation of a meniscus. However, correct and consistent interpretation of lower extremity venography to rule out DVT may be challenging. Intraobserver disagreement about the probable presence or absence of thrombus has been shown to occur in up to 10% of venography cases.<sup>2</sup> The invasive nature of the technique, the exposure to radiation, and the improvement and availability of ultrasound technology have made venography a secondary technique for the detection of acute and chronic venous thrombosis. However, venography does play a primary role in the treatment of DVT, allowing for localization and use of mechanical thrombectomy devices to treat acute venous thrombosis with the use of angioplasty or placement of stents in the setting of chronic venous scarring.

### Incompetent Perforating Veins

The normal outflow from veins of the lower extremity includes pathways from the superficial system to the deep system through



**Figure 28.1** Normal Right Lower Extremity Venogram. (A) Lateral calf projection. (B) Anteroposterior projection of the knee. The anterior tibial veins (small arrow), peroneal veins (short arrow), posterior tibial veins (arrowhead), gastrocnemius veins (open arrow), great saphenous vein (curved arrow), and popliteal vein (long arrow) are indicated.

perforating veins. Perforating veins possess unidirectional valves, which, when competent, prevent reflux of blood from the deep to the superficial veins of the lower extremity. Perforating veins with incompetent valves contribute to the development of venous hypertension in the superficial system, which may result in the formation of varicose veins and/or venous ulceration. Normal perforating veins are small, thin, and smooth. However, refluxing veins are dilated, irregular, and the valves are incompetent. Historically, ascending venography has been a reliable technique for identifying incompetent perforating veins. This invasive technique, although useful, has largely been replaced by color-flow duplex examination of the lower extremity veins.

### Technique

Ascending venography for incompetent perforating veins involves the injection of contrast material into a foot vein with a tight tourniquet around the ankle to occlude the superficial

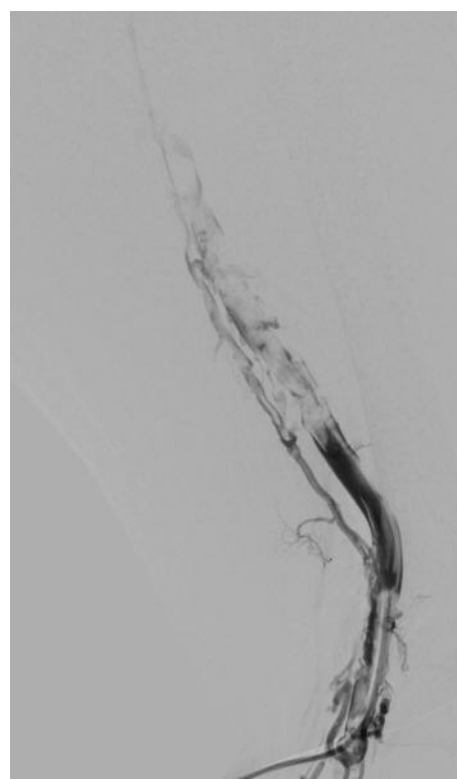


**Figure 28.2** Venogram Demonstrating Acute Thrombus in the Femoropopliteal Vein.

veins such that reverse flow from the deep veins into the superficial veins through the incompetent perforating veins can be seen. A translucent ruler may be used to measure the location of the incompetent perforating vein from the tip of the medial or lateral malleolus. The table is then moved through the horizontal position and into Trendelenburg position, and flow of contrast material is followed under fluoroscopy. Lateral views are especially important in the thigh for accurate localization of a midthigh perforating vein. After a perforating vein is identified, a tourniquet can be used above that level to direct the contrast agent into any incompetent perforating vein.

### Interpretation

Thomas and Bowles compared ascending venography with varicography for identification of incompetent perforating veins.<sup>3</sup> Sixty-one lower extremities of 50 patients were examined with both methods. Incompetent perforating veins of the gastrocnemius muscle and midthigh were more accurately shown with varicography than with ascending venography (Fig. 28.4).

### Venous Aneurysms and Malformations

The most serious complication associated with lower extremity venous aneurysms is the development of thrombus within the aneurysm and subsequent embolization. Pulmonary embolization has been reported to occur frequently in extremity venous aneurysms, most notably in those involving the popliteal vein (Fig. 28.5). Aldridge and coauthors in 1993 reported 24 cases of popliteal venous aneurysm in which all patients had experienced thromboembolic events.<sup>4</sup> Aggressive treatment with immediate anticoagulation and preoperative planning has become

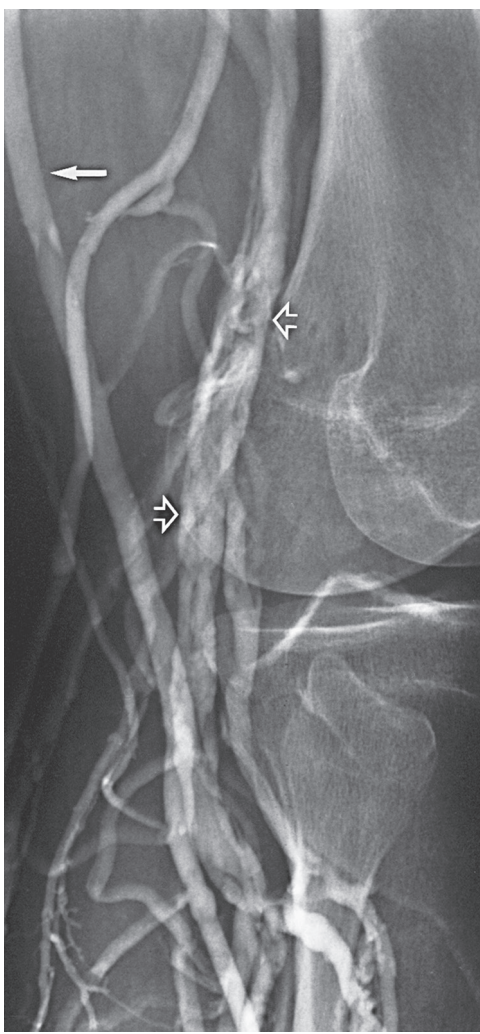


**Figure 28.3** Chronic Popliteal Venous Thrombosis. Note the extensive recanalization of the popliteal vein (open arrows) and relatively large caliber of the great saphenous vein (solid arrow).



**Figure 28.4** Incompetent Medial Calf Perforating Veins. A single-frame image of a videotape shows free flow of contrast material from the posterior tibial vein through the incompetent perforating veins (arrows) into the superficial varicose veins.

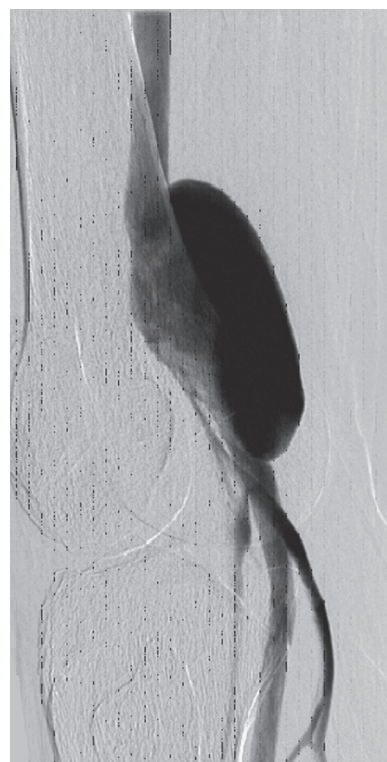


**Figure 28.5** Popliteal Venous Aneurysm. (Courtesy Mitch Cox, MD.)

the standard of care for this reason. Even a recent single center of lower extremity venous aneurysms suggest benefit with surgical treatment of asymptomatic aneurysms.<sup>5</sup> Venography is a useful method for preoperative planning before resection and interposition grafting or lateral suture repair (aneurysmorrhaphy) of these aneurysms.

Venous malformations may take the form of isolated venous lakes or diffuse venous aneurysm formation, such as in Klippel–Trénaunay syndrome (Fig. 28.6). Patients often become symptomatic from mass effect, reflux, or venous thromboembolism. Operative or interventional management may be indicated in symptomatic patients. Most patients do well without treatment or with elastic compression only. Surgical treatment of the vascular malformation in Klippel–Trénaunay syndrome is rarely indicated and continues to be controversial.<sup>6</sup> Preoperative venous imaging with ascending venography or direct puncture varicography is useful for planning treatment.

#### Technique

The technique used is the same as when ascending venography is performed. Direct puncture varicography is most useful for the evaluation of venous malformations (Fig. 28.6). Ultrasound-guided access provides the ability to perform this type of venography. In patients being treated for venous malformations, access can be difficult and painful. In such cases, either general or regional anesthesia may be useful and should be considered.

#### Interpretation

Focal dilation of the deep or superficial venous system is diagnostic of venous aneurysms and malformations. Because of the



**Figure 28.6** Tibial Venous Malformation in a Patient with Klippel–Trénaunay Syndrome. (From Gillespie DL, Villavicencio JL, Gallagher C, et al. Presentation and management of venous aneurysms. *J Vasc Surg*. 1997;26:845–852.)

small number of venous aneurysms included in most series, no single diagnostic method has been reported to be superior. However, most series do report color-flow duplex examination to be valuable in the diagnosis of popliteal venous aneurysms and to provide information on the presence of mural thrombus.<sup>7</sup> Gillespie et al. reported that venous aneurysms were correctly diagnosed in 85% of patients with imaging techniques: phlebography (60%), color-flow duplex scanning (27%), and magnetic resonance imaging (MRI) (10%).<sup>8</sup>

Passive filling of the vascular tree after compressive exsanguination of an extremity, extrinsic occlusion of its arterial supply, and venous drainage has been shown to be a useful technique for evaluation of venous malformations.<sup>9</sup> Closed-system venography was performed in 17 patients, and it correctly identified 11 of 12 surgically confirmed vascular abnormalities. There were no false-positive findings.

## Descending Venography

As with ascending venography, lower extremity descending venography is no longer used as a screening study. It has largely been replaced by color-flow duplex study, which has shown good agreement with descending venography in the grading of deep and superficial vein reflux.<sup>10</sup> However, duplex examination does not always provide accurate localization of the levels of valve stations and incompetent segments. For this reason, descending venography remains the definitive test for identifying incompetent valves in patients with CVI who are candidates for venous valve

**TABLE 28.2** Grades of Venous Reflux

Grade	Description
0	Normal valvular function with no reflux
1	Minimal reflux confined to the upper part of the thigh
2	More extensive reflux, which may reach the lower part of the thigh; a competent valve is present in the popliteal vein, and there is no reflux to the calf level
3	Reflux as above but associated with popliteal valvular incompetence and leakage of contrast material into the calf veins
4	Virtually no valvular competence with immediate and dramatic reflux distally into the calf; this type of reflux often opacifies incompetent calf perforating veins

From Kistner RL, Ferris EB, Randhawa G, Kamida C. A method of performing descending venography. *J Vasc Surg*. 1986;4:464–468; and Herman RJ, Neiman HL, Yao JS, et al. Descending venography: a method of evaluating lower extremity venous valvular function. *Radiology*. 1980;137:63–69.

repair or valve transplantation. Descending venography is used for evaluation of anatomy and function of venous valves in the lower extremities. It shows location of the venous valves and demonstrates competence or incompetence. Kistner<sup>11</sup> and Herman<sup>12</sup> and colleagues developed a classification system used commonly to categorize the severity of deep venous reflux and the functional integrity of the venous valves (Table 28.2).

## Technique

Descending venography requires a tilt table, C-arm fluoroscopy, short 4F or 5F straight catheter with distal side holes, syringes, and contrast agent. It is performed on a tilt table to allow examination in the 40- to 60-degree upright position. Descending venography requires direct catheter access into the deep veins. In most cases, the venous access site is the common femoral vein contralateral to the side of interest. The catheter is advanced to the inferior vena cava (IVC) and then to the iliac vein and common femoral vein of the symptomatic lower extremity. A short 4F or 5F straight catheter with distal side holes is positioned at the junction of the external iliac and common femoral veins. For unilateral examination the catheter is placed from the ipsilateral femoral vein, and for bilateral examination a single femoral vein puncture is used. A transjugular approach may be used to direct the retrograde catheter into both extremities from a single access site. The contralateral lower extremity is supported with a platform, as with ascending venography, so that the extremity being examined will be relaxed and bear no weight. With the catheter tip in the common femoral vein, the table tilted to a 60-degree semi upright position, and the patient bearing weight on a block placed under the nonexamined extremity, contrast material is injected and followed with fluoroscopy as it flows caudad through the incompetent venous valves. A total of 10 mL of contrast material is slowly injected by hand at a rate of 5 mL/s. As the contrast material is injected, the patient breathes normally, after which the patient is instructed to bear down and perform a Valsalva maneuver to enhance evidence of valvular incompetence. Specific areas of interest can be further studied by sequential injections of

contrast to optimize image capture of valve location and function and the extent of reflux.

### Interpretation

Although superficial varicosities are frequently present, they are rarely a prominent feature of symptomatic advanced chronic venous disease.<sup>13</sup> Most patients with symptoms of CVI who undergo venography have reflux into the deep venous system. The two main abnormalities that cause venous valve reflux are postphlebitic and primary valvular incompetence, with the latter being more common.<sup>14</sup> Although venous duplex evaluation is a widely used screening modality for reflux, the use of descending venography provides the degree of detail and specificity that allows selection of candidates for deep venous valve repair or transplantation. These procedures are offered to patients with grade 3 or grade 4 reflux who have recurrent symptoms of venous insufficiency after treatment of superficial varicosities and perforating vein incompetence (Table 28.2).

## VENOGRAPHY FOR SPECIFIC REGIONS AND CONDITIONS

### Iliac Vein Assessment and Inferior Venacavography

IVC anatomy and patency are routinely assessed as part of IVC filter placement. Venography allows assessment of caval anatomy and evaluation for intraluminal thrombus. In addition, there are several anomalies of the IVC, as outlined in previous chapters. Duplicated cava, megacava, and left-sided vena cava are but a few of these anomalies. Although these anomalies are uncommon, it is important to routinely assess with venography before placement of IVC filters to avoid complications caused by either filter misplacement, tilting or leaving the patient vulnerable to pulmonary embolism through alternative pathways.

#### Technique

Access to the venous system is achieved through the internal jugular or common femoral vein. Puncture of a single wall is facilitated by ultrasound guidance, using a micropuncture kit. After access is achieved, a 4 or 5F sheath is placed and proper placement confirmed by free flow of venous blood from the sheath and during femoral access, confirmation by venography that there is no iliac vein thrombus prior to advancing a larger sheath into the vena cava. If placed for lower extremity DVT, access the extremity that is free of DVT. From the groin, a 0.035-inch J wire is passed into the common iliac vein. A 5F pigtail catheter is advanced over the wire into the common iliac vein, and cavography is performed. An alternative method of cavography is to proceed with placement of the IVC filter kit, which consists of a sheath, usually 6.5F to 8F. The IVC filter sheath is advanced over the wire to the level of the common iliac vein, and a cavogram is performed. If access is from the neck, a 0.035-inch J wire is passed through the right atrium to the common iliac vein. Passing the J wire through the right atrium into the IVC can sometimes be a challenge. If simple

manipulation fails, an angled glidewire and angled glide catheter can be useful. After the J wire is in position, an iliocavogram is performed using an injection of 10 mL/s for a total of 20 mL of nonionic contrast agent, either by hand-injection or with low pressure power injection.

#### Interpretation

The iliocavogram is reviewed for the diameter of the vena cava, the anatomic level of the bifurcation, the location of the renal veins, and any other anomalies. Typically, the renal veins will not fill with contrast material and instead will be identified by a characteristic flow pattern of the mixing of blood filled with contrast material and nonopacified blood. Having the patient do a Valsalva maneuver helps identify the renal veins. The confluence of the common iliac veins is usually identified by the spilling over of contrast material into the contralateral side. The IVC filter can then be placed at a level between the lowest renal vein and the common iliac vein junction. IVUS can be helpful in identifying renal vein location as well as thrombus prior to IVC filter placement. This is particularly helpful for bedside filter placements.

Some centers advocate first-order selective venography instead of or as a supplement to nonselective venography. Danetz and coworkers found that when selective venography was used in conjunction with nonselective venography, 23% of patients had either an abnormal finding or aberrant anatomy, and most of these patients required a major change in vena cava filter position.<sup>15</sup>

In consideration for IVC filter retrieval, the surgeon should examine whether the filter has retained thrombus, has penetrated the IVC, migrated, or is angulated. Severely angulated temporary filters with more than 20 degrees of tilt can make endovascular retrieval difficult but not impossible. Filters with retained thrombus should not be percutaneously retrieved unless thrombus can be lysed prior to retrieval.<sup>16</sup> Another option is to anticoagulate the patient for a few months and repeat imaging to see if the thrombus has resolved, then proceed with filter retrieval if that is the case.

### Venography During Treatment of Iliocaval Stenosis

Advances in angioplasty and stent technology have led to routine use of percutaneous treatment for acute and chronic iliocaval occlusion due to thrombosis or external compression (May-Thurner syndrome). Many authors have written on the efficacy of this method of treating lower extremity venous outflow obstruction.<sup>17-40</sup> Investigation of the safety and efficacy of this treatment has led to refinements of the technique. Neglen and Raju have shown that ensuring adequate inflow into the common femoral vein segment is critical to long-term patency.<sup>28-31,41-45</sup> We now have at least two FDA-approved venous stents for use in this scenario.

#### Technique

To facilitate visualization of the confluence of the profunda femoral vein and the femoral vein, it is recommended that

access be obtained at the midthigh or popliteal level.<sup>46</sup> Ultrasound guidance facilitates placement of a 5F sheath into either of these deep veins. Access to the femoral vein is best achieved in the supine position. However, to obtain popliteal venous access, the patient is placed in the prone position. Once venous access has been achieved, a J wire is advanced to the level of the common femoral vein. A catheter is then advanced over this wire, and iliacangiography is performed in the usual fashion using either hand injection or power injection.

### **Interpretation**

Accurate hemodynamic tests for detecting and grading venous outflow stenosis are currently unavailable. Diagnosis and treatment must be based on morphologic findings. Single-plane transfemoral venography is often used as a standard investigation. These studies may show definite obstruction and the development of collaterals. However, findings are often subtle and only suggestive of an underlying obstruction. Subtle findings of significant venous stenosis include widening of the iliac vein, pancaking, “thinning” of the contrast dye, partial intraluminal defects, septae, and pelvic collateral formation.<sup>29</sup> To increase the overall accuracy of detecting iliac vein stenosis, the use of IVUS can complement venography in these circumstances by providing a cross-sectional view of the area of interest and confirming the pathology. IVUS is also crucial in sizing and assessing wall apposition.

## **Diagnostic Venography of Pelvic Congestion Syndrome**

Pelvic venous congestion syndrome is characterized by symptoms of pelvic pain, dysmenorrhea, dysuria, dyspareunia, vulvar and pelvic varices in women, and varicoceles in men.<sup>47</sup> Sources of pelvic venous plexus congestion include ovarian vein reflux, pelvic varices, and hypogastric venous insufficiency. The ovarian veins provide drainage of the parametrium, cervix, mesosalpinx, and pampiniform plexus. Two or three trunks form a single vein at L4, with the right ovarian vein draining directly into the IVC and the left into the left renal vein. These veins have an average diameter of 3.1 mm and possess two or three valves.

In addition to primary valvular incompetence of the ovarian vein valves, pelvic congestion syndrome may also result from obstruction of ovarian vein outflow. This obstruction is most often caused by compression of the left renal vein between the superior mesenteric artery (SMA) and the aorta, also known as nutcracker syndrome. This can also occur in a retroaortic renal vein with compression of the vein between the aorta and spine. Outflow obstruction leads to increased venous pressure and subsequent venodilation, valvular incompetence, and tortuosity of the ovarian vein. The development of numerous pelvic collateral pathways concurrently allows venous drainage around the point of obstruction. Distal obstruction of ovarian vein outflow leads to the development of an elevated pressure gradient between the left renal vein and the vena cava. Normally, there is minimal or no gradient between the left renal vein and the vena cava, so the presence of an elevated gradient is diagnostic of nutcracker syndrome.<sup>48</sup>

Vulvar varices may arise from the lower extremity veins, the pelvic veins, or both. Varicose veins of the lower extremities are a frequent source of venous hypertension resulting in pelvic congestion. Almost half of vulvar varices arise from an incompetent great saphenous vein through the superficial external pudendal or posteromedial tributaries. Less often, they arise from a tributary communicating directly with the common or deep femoral vein. The remaining varices arise from the pelvic veins through branches of the internal iliac, including the internal pudendal vein, the obturator vein, and the inferior gluteal vein. The internal pudendal tributaries communicate with the ovarian vein. Rarely, the veins arise from the round ligament.<sup>49</sup>

### **Technique**

Diagnostic venography of the ovarian vein is achieved with standard catheter-based techniques. After access to the venous system has been achieved, a 4F angled glide catheter is advanced into the vena cava. Selective catheterization of each ovarian vein is then achieved with an angled glidewire and catheter system. After the catheter is placed in the ovarian vein, the angiographic table is tilted into reverse Trendelenburg. Then, after hand injection, the patient is asked to perform a Valsalva maneuver as images are obtained. The diagnosis of nutcracker syndrome is made by determining the retrograde renocaval gradient. To do so, a glide catheter is placed in the distal left renal vein and the pressure transduced. This pressure is compared with the pressure in the vena cava. An elevated renocaval gradient is one clue in making the diagnosis. In addition, contrast-enhanced visualization of the gonadal system and its pelvic and extrapelvic connections should be performed to look for ovarian vein reflux. Intravascular ultrasound can be a useful adjunct in providing a cross-sectional view of the area of extrinsic compression of the left renal vein. Imaging of patients with the clinical and radiologic diagnosis of nutcracker syndrome can be performed in both the supine and prone positions. Placing the patient in the prone position theoretically decreases the renocaval gradient and displaces the SMA forward with the intestinal mass.

### **Interpretation**

The venographic criteria for pelvic congestion syndrome were established by Beard and colleagues in 1984.<sup>50</sup> The criteria for pelvic congestion syndrome include: (1) an ovarian vein diameter of 6 mm or greater; (2) retention of contrast material for longer than 20 seconds; (3) congestion of the pelvic venous plexus or opacification of the ipsilateral or contralateral internal iliac veins; and (4) filling of vulvovaginal and thigh varicosities. Each variable is assigned a value of 1 to 3, depending on the degree of abnormality, and scores higher than 5 indicate pelvic congestion syndrome.<sup>50</sup>

Diagnostic criteria for ovarian vein reflux include a left ovarian vein diameter of 6 mm or greater and retrograde left ovarian vein flow (Fig. 28.7). Valvular incompetence exists in up to 47% of all women. In a study of preoperative aortography in 273 female kidney donors, Belenkay and coworkers found incompetent left ovarian veins during the venous phase

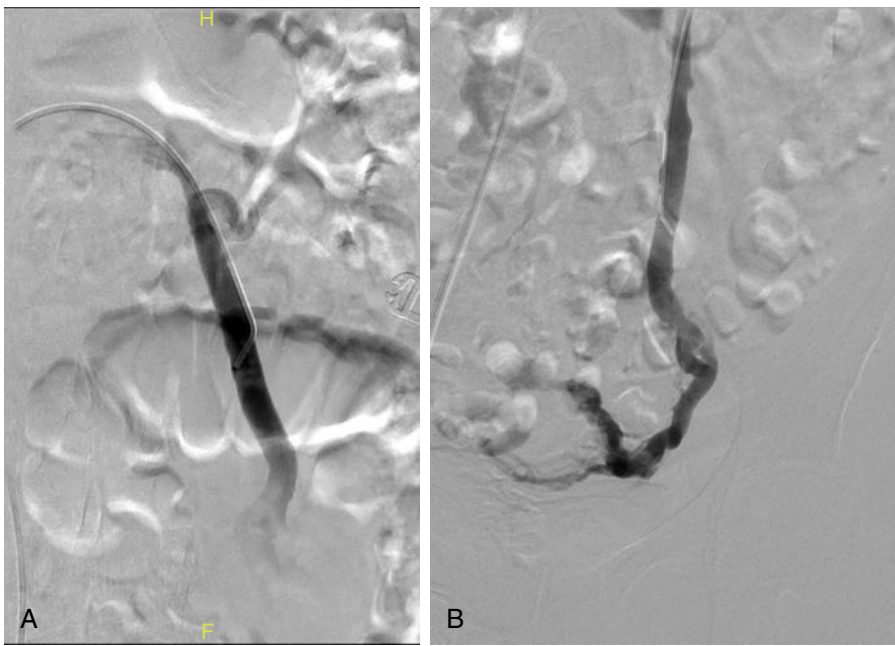


**Figure 28.7** Venogram of large ( $>6$  mm) left ovarian vein (A) with reflux of contrast into pelvic varicosities (B) in a patient with pelvic congestion syndrome resulting from ovarian vein reflux.

of imaging in 27 (9.9%).<sup>51</sup> Fifty-nine percent of these patients had pelvic symptoms. A secondary cause arising from iliac artery or left renal vein compression of the left ovarian vein was noted in 20% of these patients.

Venographic evidence of SMA compression of the renal vein may be seen on an anteroposterior view of midstream venacavography. Further delineation is aided by selective catheterization of the left renal vein to evaluate for proximal compression or “pancaking”. However, definitive documentation requires measurement of the retrograde renocaval gradient and contrast visualization of the gonadal system, as well as of its pelvic and extrapelvic connections. A renocaval gradient greater than 1 mm Hg is consistent with the presence of nutcracker syndrome.<sup>52</sup>

### Venography for Varicoceles

Abnormal distention of the pampiniform venous plexus, the venous drainage from the testicle, results in varicocele formation. Varicocele can be due to absence of testicular vein valves; however, it is generally due to retrograde flow in or impaired drainage of the testicular vein. Veins of the testes, along with tributaries from the epididymis, converge to form the pampiniform plexus. This plexus begins in the scrotum and extends into the spermatic cord and ascends along the cord in front of the ductus deferens. Below the inguinal ring, the pampiniform plexus unites to form three or four veins that enter the abdomen through the inguinal ring that further coalesce to form two gonadal veins. The right gonadal vein drains directly into the infrarenal IVC whereas the left gonadal vein drains into the left renal vein. Collateral pathways for venous drainage of the testis include perirenal, retroperitoneal, and lumbar veins.

Varicocele predominantly occurs on the left, likely due to the indirect drainage of the testicular vein to the IVC via the left renal vein. Bilateral and right-sided varicoceles account for

approximately 10% to 15% of varicoceles.<sup>53</sup> An isolated right-sided varicocele is infrequent, and should prompt an evaluation for obstructive disease like renal tumors or adenopathy.

Patients presenting with varicocele will often report pain and may have a reduced sperm count. Varicoceles have been associated with a time-dependent decrease in size and function of the testes, and contribute to male infertility. Physical examination is the cornerstone in diagnosis – the patient should be examined in the upright position after standing for at least 5 minutes. Visual inspection of the scrotum should occur first, and distention of the spermatic cord is noted. The testicle is palpated before and after Valsalva maneuver, with evaluation for a “bag of worms” or a thickened cord on palpation. Duplex ultrasound scan be performed to confirm the physical examination findings with the presence of two prominent tortuous veins in the pampiniform plexus that measure at least 2 mm in diameter and that increase with the Valsalva maneuver being diagnostic. Other potential imaging modalities include computed tomography (CT) and MRI. However, venography remains the gold standard in diagnosis of varicocele, and reflux of more than 2 seconds is diagnostic.<sup>53</sup> Indications for treatment include an infertile man with a palpable varicocele and an abnormal sperm count, prophylactic repair in adolescent men with a reduction in testicular size, bilateral varicoceles, and impaired spermatogenesis in patients older than 18 years.<sup>53</sup>

### Technique

Access through the femoral vein generally requires a sheath or guiding catheter to stabilize the renal vein access and to allow passage of a catheter into the testicular vein. We obtain a venogram from the midpoint of the renal vein to determine renal vein patency and testicular vein incompetence. Venography with a Valsalva maneuver or a tilt table with the patient placed in the reverse Trendelenburg position is performed of the testicular vein, and retrograde flow and collaterals can be

visualized. Visualizing the entire anatomy of the testicular vein and pampiniform plexus is necessary to evaluate retrograde and collateral flow, as well as aberrant blood supply to the varicocele. During instrumentation, the gonadal vein may spasm, and nitroglycerin may be used. If reflux is not demonstrated with this technique, renal venography with a Valsalva maneuver may be used, or an internal iliac study with an occlusion balloon may be warranted. This technique, described before, is used to determine a right- or left-sided varicocele.

### Treatment

The goal of treatment is to stop the retrograde flow from the gonadal vein or collateral veins to the pampiniform plexus. Occlusion of the testicular vein should extend from just above the inguinal ligament to 5 cm below the convergence of the testicular vein with the left renal vein on the left side. This technique eliminates all collateral and aberrant vessels. Several techniques for occlusion are available: coil embolization, sclerosing agents, and open surgical repair. Coil embolization is commonly used, owing to its painless ease of use. Coils must be sized correctly to at least 10% larger than the diameter of the spermatic vein at the level of deployment. If the coils are undersized, there is a risk of embolization to the pulmonary artery. Other groups, particularly those in Europe, use sclerosants exclusively. In general, if the right side does not have evidence of reflux, it is not routinely treated. Open surgical options for repair involve retroperitoneal or inguinal access to the testicular vein for ligation. The traditional open approach usually requires general anesthesia and a 2- to 3-day hospitalization.

Complications associated with treatment of varicocele include spasm, dissection, and perforation. Venous puncture-associated complications such as hematomas are rare. Thrombo-phlebitis is the most common complication of embolization of the spermatic vein. Patients may present with fever, pain, and scrotal swelling within 24 to 48 hours of intervention. Patients with this complication should undergo an immediate duplex ultrasound examination followed by a repeated study 6 weeks later for evaluation of signs of testicular necrosis, which rarely occurs. Patients may also be treated with a short course of steroids and nonsteroidal anti-inflammatory drugs. Antibiotics may also be prescribed if there is difficulty in differentiating phlebitis from infection. Endovascular treatment for ovarian vein reflux follows similar principles with coil embolization being the most common treatment.

### Renal Venography

The renal veins may be evaluated for anatomic verification or assessment of congenital anomalies or tumor invasion before resection. Renal venography is also useful for the evaluation of suspected renal vein thrombosis in both native and transplanted kidneys. Patients typically have generalized malaise, flank pain, hematuria, and hypertension. Renal vein thrombosis affects men more than women and most often involves the left renal vein.<sup>54</sup> Renal vein thrombosis may arise from four separate causes: (1) thrombus propagating from below to obstruct the IVC and renal veins; (2) caval obstruction or invasion from

malignant neoplasms with compromise of the renal veins; (3) primary renal vein thrombosis, which usually occurs in infants; and (4) renal vein thrombosis secondary to nephritis.<sup>55</sup> Catheter venography may be especially useful in patients with acute renal vein thrombosis because it may be followed by therapeutic intervention consisting of catheter-directed thrombolysis or endovascular thrombectomy.

### Technique

Midstream venacavography results in characteristic flow voids seen at the L2–3 level as a result of mixing of nonopacified renal vein blood with contrast material in the vena cava. However, detailed evaluation of the renal veins is best achieved by selective catheterization. Renal vein selection is easily achieved with standard guidewires and angled catheters. After access to the renal veins has been attained, venography is usually accomplished by hand injections of 5 to 10 mL of dilute contrast material. Improved visualization of the renal veins has been reported with the injection of 10 µg of epinephrine into the renal artery or balloon occlusion of the renal artery, but this is rarely used.<sup>55</sup>

### Interpretation

Although renal venography is a useful technique for demonstrating renal vein anomalies such as a retroaortic left renal vein or circumaortic venous collar, CT and MRI are currently more commonly used. Venographic diagnosis of renal vein thrombosis depends on the demonstration of a persistent filling defect within the renal vein. Acute renal vein thrombosis may be partial or complete. Detection of intraluminal defects showing partial occlusion and no collateral formation is consistent with acute thrombosis. Chronic renal vein thrombosis would appear as main renal vein obstruction with numerous collaterals around the obstruction. The risk for pulmonary embolism during renal venography and treatment has been reported to be low.<sup>54,56</sup>

Definitive exclusion of renal vein thrombosis requires selective catheterization of the renal veins if an initial midstream venacavogram is normal. Martin and Gordon found that only 6 of 15 patients (40%) with documented renal vein thrombosis had caval thrombus, whereas the cava was completely normal in 46%. The authors suggest that inferior venacavography lacks specificity in the diagnosis of renal vein thrombosis when it is associated with primary renal disease and nephrotic syndrome.<sup>55</sup>

### Diagnostic Angiography of Mesenteric or Portal Venous Thrombosis

The signs and symptoms of acute mesenteric or portal venous thrombosis are varied and include vague abdominal pain, nausea, vomiting, melena, bloody diarrhea, and ultimately circulatory collapse.<sup>57</sup> The diagnosis is usually accomplished with CT or MRI but can be made with angiography. High clinical suspicion plus early diagnosis may be lifesaving because it allows systemic anticoagulation or thrombolysis (or both) to be performed.<sup>58</sup>

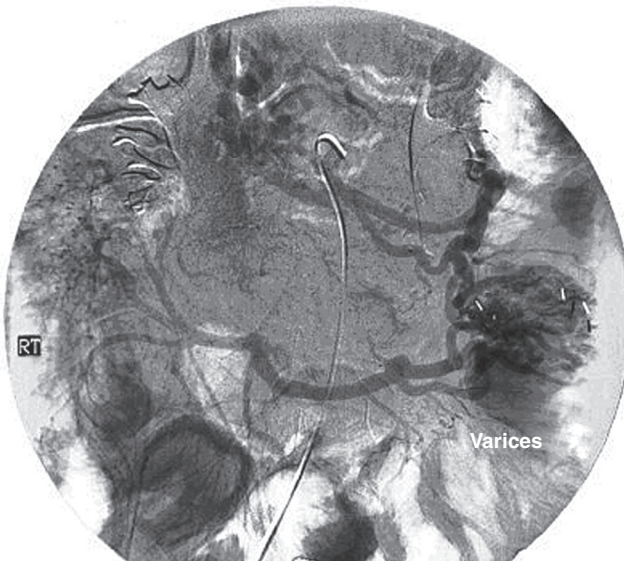


**Figure 28.8** Venous phase of a superior mesenteric arteriogram showing occlusion of the superior mesenteric vein. *RT*, right. (From Ozkan U, Tang SJ, Jutabha R, Jensen DM. Push enteroscopy for recurrent gastrointestinal hemorrhage due to jejunal anastomotic varices: a case report and review of the literature. *Endoscopy*. 2002;34:735.)

### Technique

Visualization of the superior mesenteric veins may be accomplished either indirectly by review of the venous phase of a superior mesenteric arteriogram (Fig. 28.8) or by direct access. Direct access to the superior mesenteric veins can be accomplished through a transjugular–intrahepatic or transhepatic approach and allows percutaneous intervention.

The venous phase of an SMA injection provides visualization of superior mesenteric drainage into the portal venous system. After arterial access is achieved, a reversed catheter like 5F Simmons 1 or SOS catheter is advanced into the aorta. Once the tip is shaped so that it is aimed caudad, the catheter is manipulated into the orifice of the SMA. Hand-injected half-strength contrast dye is helpful in confirming placement of the catheter. Injection of contrast material with a power injector is useful for improving imaging. An injection protocol of 5 mL/s for a total of 10 mL is appropriate. Imaging of the venous phase is accomplished either by delaying acquisition until after injection, which limits radiation exposure, or by continuing to image after the arterial phase has been completed.

The transcutaneous transhepatic approach is a useful direct technique for access to the portal venous system. Under sonographic guidance, the skin is marked at the point where the right portal vein and the right hepatic vein are aligned in one plane with the portal vein closer to the sonography probe. By use of aseptic technique, the right portal vein is punctured with an 18-gauge needle. After imaging, the superior mesenteric vein has been shown to allow thrombolysis, angioplasty, and stenting in a highly select group of patients.<sup>59</sup>

The transjugular intrahepatic approach to portal venography was popularized in the 1960s by Rösch, who modified the technique of liver biopsy and developed the technique of transjugular intrahepatic portosystemic shunting.<sup>60–63</sup> Transjugular

intrahepatic portosystemic shunting is best performed under general anesthesia or intravenous sedation. A 10F introducer sheath is placed through the right internal jugular vein into the IVC. A curved angiographic catheter is then used to select a hepatic vein, and the tip of the sheath is then introduced into the hepatic vein. A 16-gauge, 55-cm Colapinto transjugular needle is passed from the hepatic vein through the liver parenchyma into a portal vein branch. A 0.035-inch Amplatz extroff guide wire is placed into the superior mesenteric vein and the needle exchanged for a 5F angiography catheter. Portal venography is then performed through a multihole diagnostic catheter placed in the portal vein.<sup>64</sup> Postdiagnostic angiographic embolization of the track may be performed.

### Interpretation

The superior mesenteric vein joins with the splenic vein to form the portal vein. In general, noninvasive methods of imaging are used as the initial diagnostic modality in the case of portal or mesenteric vein disease. Indirect visualization of the portomesenteric system can be achieved during mesenteric arteriography by prolonged imaging of the venous phase. However, this method does not provide great detail or access for treatment. Advances in percutaneous technology have led to increased use of the transjugular and transhepatic approaches.<sup>58,59,65</sup> These methods carry increased risk for subcapsular or intraabdominal bleeding complications, especially if they are combined with thrombolytic therapy.

### Diagnostic Venography of Budd–Chiari Syndrome

Normal hepatic venous outflow occurs from the right and left hepatic veins into the retrohepatic vena cava and then into the right atrium. Budd–Chiari syndrome results from thrombosis of hepatic venous outflow, which gives rise to portal hypertension and its sequelae. The liver becomes congested and enlarged, and as the hepatic congestion progresses, hepatic function deteriorates and failure results. For unclear reasons, some patients have mild initial symptoms, whereas others exhibit fulminant hepatic failure and massive hepatic necrosis.<sup>66</sup> Budd–Chiari syndrome can result from various causes, including membranous obstruction of the IVC, pregnancy, oral contraceptive use, tumors, infections, and blood dyscrasias, or it can be idiopathic. The most useful initial test is a color-flow duplex scan of the portal vein, which will establish the diagnosis. This scan should then be followed by venacavography and portal vein venography with portal venous and vena cava pressure measurements, as well as liver biopsy, to help determine further management.<sup>67</sup>

### Technique

The diagnosis of Budd–Chiari syndrome may be confirmed by demonstrating obstruction of hepatic venous outflow, most often by selective catheterization of the right or left hepatic vein. This can easily be accomplished through a transfemoral or transjugular approach. From the groin, a curved catheter, such as a Simmons 1, is placed into the suprahepatic cava and

then used to select the hepatic vein. From the jugular vein, a straight or angled catheter is easily manipulated into the hepatic outflow tract. Hand injection of 5 to 10 mL of contrast material should reveal a characteristic spiderlike appearance of the occluded hepatic venous system.

In some cases, such as membranous obstruction of the vena cava, imaging is best accomplished with venacavography. A pigtail catheter is placed at the level of the distal IVC. Power injection at 15 mL/s for a total volume of 30 mL would be used. The surgeon should look for filling defects in the distal IVC.

### Interpretation

Thrombosis of the hepatic venous outflow tract may be detected by direct catheterization of the hepatic veins. A characteristic spiderlike appearance of the occluded or recanalized hepatic veins is seen. Distal obstruction of the IVC may take the appearance of a weblike band or stenosis.

## Upper Extremity Venography

Upper extremity venography is the procedure of choice for most clinicians in the evaluation of central thoracic veins and for investigation of upper extremity edema. Upper extremity edema can be caused by acute or chronic venous thrombosis, external venous compression by a tumor of the lymph nodes, venous obstruction secondary to fibrosis after radiation therapy or surgery, superior vena cava (SVC) obstruction, and lymphatic obstruction. Although primary axillary–subclavian vein thrombosis is relatively uncommon (<2% of all cases of DVT), the incidence of central venous occlusion is still rising because of the increasing long-term use of central venous catheters and transvenous cardiac pacers (Fig. 28.9).<sup>68,69</sup>

Upper extremity venography is most commonly used in the investigation of arm edema in patients with primary axillary–subclavian venous thrombosis who are candidates for endovascular thrombectomy and/or thrombolytic therapy. The examination shows the extent of thrombosis and guides placement of infusion catheters for the administration of lytic agents. Other common indications are to evaluate patients with suspected central venous occlusion who are not candidates for magnetic resonance angiography (MRA) (e.g., because of a cardiac pacemaker or claustrophobia) and to rule out venous injuries from trauma.

### Technique

Arm venography techniques were initially described in 1971 by Thomas and Andress.<sup>70</sup> The most common method involved accessing the median antecubital vein or a peripheral hand vein and positioning the upper extremity by the side of the patient in 5 to 10 degrees of abduction without the use of tourniquets. Natu and associates modified this technique by abducting the arm 90 degrees, introducing the catheter into a hand vein or forearm vein, and injecting 50 mL of contrast material (Reno-grafin-60) in 5 seconds.<sup>71</sup> If a simultaneous intervention, such as thrombolysis or percutaneous mechanical thrombectomy is contemplated, ultrasound-guided access of the basilic vein in the upper arm is preferred. This site allows for larger sheath

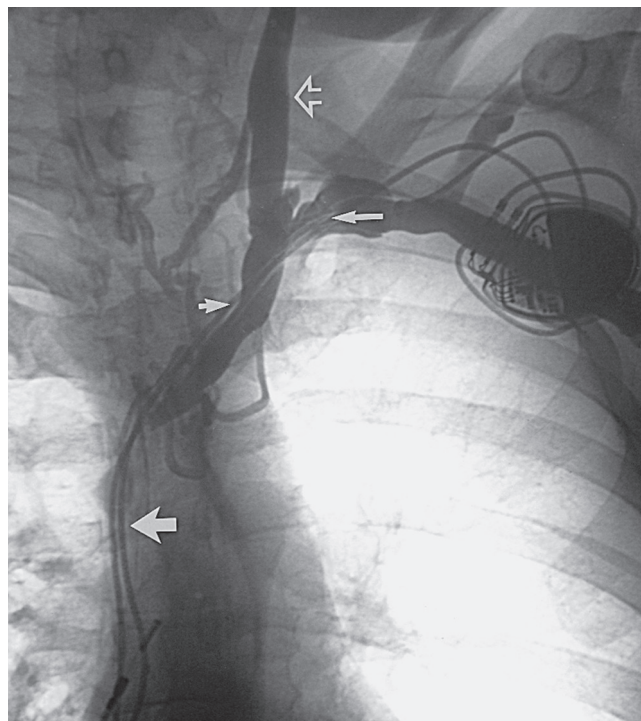


**Figure 28.9** Chronic thrombosis of the superior vena cava, the innominate veins, and the subclavian veins caused by cardiac pacer wires. Chronic subclavian venous thrombosis (long arrow), the innominate vein (short arrow), and the expected location of the superior vena cava (wide arrow) are shown. Note the reflux of contrast material up the left internal jugular vein (open arrow).

placement, as well as a short distance between sheath access site and area of stenosis for improved catheter pushability and control. The arm may be imaged in an adducted position or with less than 90-degree abduction. This can be done with either a hand injection or small volume power injection. The venous system is then reimaged with the arm fully abducted and extended. That position should narrow the thoracic outlet to help diagnose venous thoracic outlet syndrome in patients without axillosubclavian thrombosis.

### Interpretation

Significant findings in subclavian venous thrombosis include nonopacification of the vein with filling of collaterals and visualization of the thrombus within the vein. Stenosis or occlusion of the subclavian vein associated with thoracic outlet syndrome typically occurs as the vein enters the chest at the sternoclavicular junction. This point of impingement is often due to hypertrophy of the subclavius muscle. The stenosis is usually more pronounced with the arm in a provocative maneuver (arm abduction and extension). Large collateral vein formation is seen and allows venous outflow from the arm around the point of obstruction. In patients with pacemaker wires, subclavian vein stenosis will typically occur more distally. Patients with central venous catheters will have stenosis or occlusion from the mid-clavicle, centrally.

## Central Thoracic Venography

Contrast-enhanced venography is considered the diagnostic method of choice for evaluation of SVC obstruction.<sup>72</sup> SVC

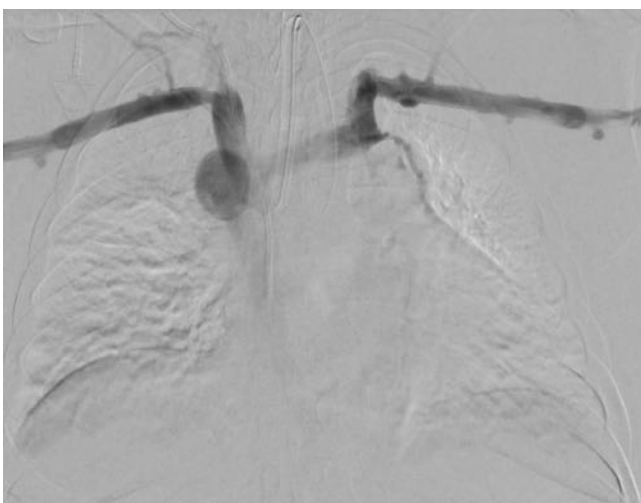


**Figure 28.10** Central venogram by injecting contrast from both upper extremities showing SVC occlusion.

evaluation is necessary in patients with clinical suspicion of SVC or innominate vein obstruction (or both), many times associated with malignancy.<sup>73,74</sup>

### Technique

Sharma and colleagues described their technique for evaluation of the SVC, which involves access in a peripheral vein of each upper extremity and injection of 20 mL of contrast material at a rate of 5 mL/s and a pressure of 150 psi.<sup>75</sup> We perform central thoracic venography similarly by injecting through an intravenous site in the antecubital fossa or forearm with the arm in a neutral position at the patient's side. For each projection needed, 20 to 30 mL of contrast material is injected by hand. Digital images of the mediastinum are obtained at one frame per second until contrast material is seen within the veins, and the frame rate is then increased to three per second. The imaged field should include the upper mediastinum and shoulders for careful evaluation of the site of venous obstruction, collateral channels, and reconstitution of the SVC distal to the obstruction. If central veins are not well opacified with a peripheral IV, then similar to peripheral venography sheath placement can be accomplished percutaneously into the basilic vein with ultrasound guidance. A catheter can then be introduced into the proximal axillary vein, and venography can be performed through a catheter hand injection in closer proximity to the central vein of interest. For better visualization, injecting simultaneously from the right and left side gives a better angiographic image of the central venous pathology (Fig 28.10).

In general, contrast material is injected unilaterally for suspected subclavian vein obstruction and bilaterally for suspected SVC obstruction. This helps to compensate for washout of contrast material in the SVC by nonopacified blood from the opposite innominate vein. Images are acquired at one frame per second, and the duration of injection and acquisition is determined by opacification of the SVC, brachiocephalic veins, and medial third of the subclavian veins. These structures are commonly obscured within the mediastinal shadows on conventional venography.

### Interpretation

Obstruction of the central veins may be associated with either benign or malignant processes. Benign processes are most often related to indwelling catheters for hemodialysis or other infusions. Malignant tumors of the chest may also cause SVC syndrome through external compression or tumor invasion. The existence of large collateral veins arising from the innominate veins and reconstituting in the SVC is indicative of significant obstruction. One may also see less degree of obstruction from extraluminal compression or intraluminal thrombus. Options for treatment of central venous obstruction include operative reconstruction with spiral vein grafts, angioplasty and stenting in select patients, or both.

### Pulmonary Arteriography

In situations in which there is a strong clinical suspicion of pulmonary embolus and computed tomographic angiography (CTA) or MRA is nondiagnostic or the patient has a contraindication to these imaging modalities, pulmonary arteriography should be performed. Pulmonary arteriography is superior to CTA or MRA for identification of small or subtle peripheral or chronic emboli and has the advantage of being able to measure pulmonary arterial pressure.<sup>76</sup> Another indication for pulmonary arteriography is imaging with intent to treat the patient with massive pulmonary embolism through thrombus fragmentation, thrombectomy and thrombolysis.

### Technique

Selective catheter pulmonary arteriography is performed by advancing a pigtail catheter through the right atrium and ventricle. Angulated pigtail catheters such as the Grollman or MONT catheter are preshaped to facilitate advancement from the right ventricle into the pulmonary outflow tract with the guidance of an angled guidewire. Caution should be exercised when the catheter is advanced through the right ventricle because this maneuver can produce transient right bundle branch block. In patients with left bundle branch block, it may cause complete heart block. One should consider the use of a temporary pacemaker in this subset of patients when pulmonary angiography is performed. Another option is to use the Swan-Ganz pulmonary artery catheter to catheterize the pulmonary artery and at the same time obtain pressure measurements to assess pre and post intervention. After the target artery has been selectively catheterized, baseline pulmonary arterial pressure measurements are obtained. The right and left pulmonary artery trunks are normally evaluated separately. Contrast material is injected at 15 to 25 mL/s for a volume of 30 to 50 mL per injection. Fluoroscopy should be set at high frame rates (4–15 frames per second), and patients should be holding their breath during image acquisition. For complete evaluation, frontal and oblique views of each pulmonary artery should be obtained. In patients with pulmonary hypertension, injection of large volumes of contrast material into the pulmonary artery is contraindicated. However, patients with chronic compensated pulmonary hypertension can tolerate pulmonary arteriography without difficulty. A right ventricular end-diastolic pressure of

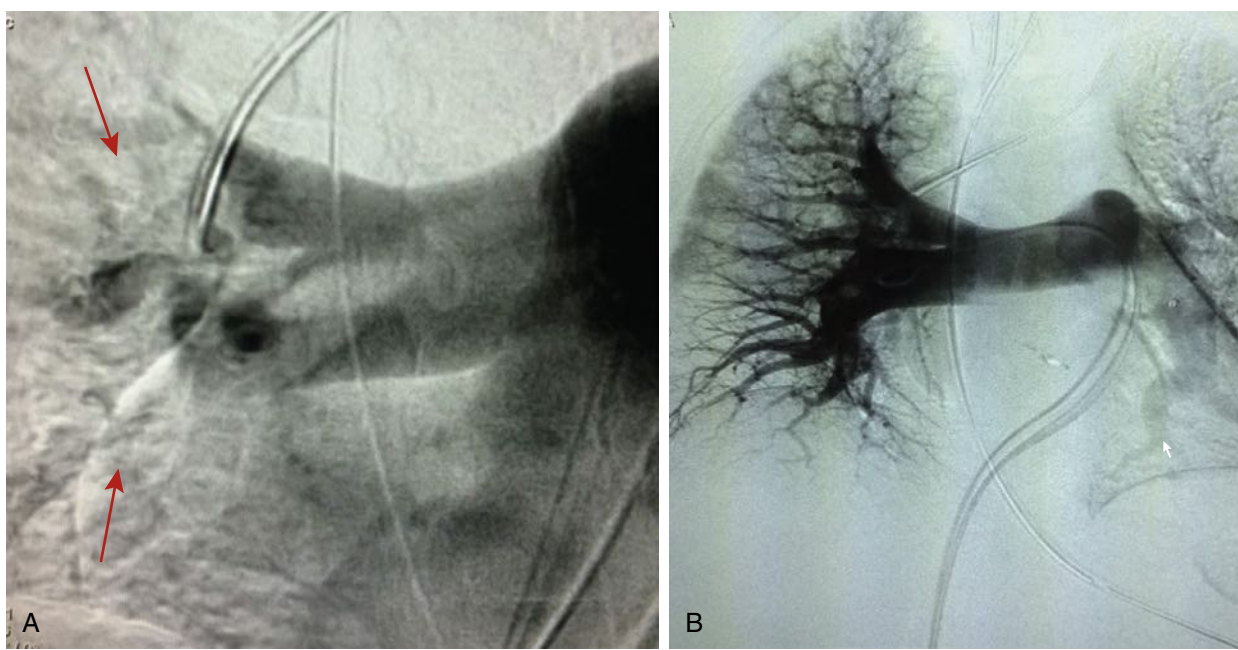


**Figure 28.11** Pulmonary artery arteriograms showing (A) filling defect due pulmonary emboli (arrows) and (B) improvement after thrombolysis.

greater than 20 mm Hg is considered a relative contraindication to high-volume injection of contrast material, and only small amounts should be injected by hand in such cases.

### Interpretation

The classic angiographic sign of acute pulmonary embolism is an intraluminal defect with diminished distal contrast enhancement (Fig. 28.11). Main and segmental pulmonary artery emboli should be easily detectable. Smaller subsegmental pulmonary emboli may be missed with this technique unless digital spot films are obtained. This is often time consuming and less successful. As treatment for massive and submassive pulmonary embolus shifts to percutaneous catheter-directed thrombolysis and mechanical thrombectomy, the use of simultaneous pulmonary angiography will rise despite the widespread use of CT angiogram for its initial diagnosis. Chronic pulmonary emboli are more difficult to detect than acute occlusion and are typically identified as stenosis, webs, or mural thickening consistent with organized thrombus.

## GENERAL LIMITATIONS AND RISKS OF VENOGRAPHY

Although venography is still considered the gold standard in diagnosis of DVT and reflux disease, several limitations and risks accompany its use.

Limitations include the invasive nature of the technique, radiation exposure, differences in intraobserver interpretation of the presence or absence of thrombus, and inability to cannulate the appropriate vein in the setting of extremity edema. Several technical issues, such as incomplete filling of the vein, may lead to a 5% to 15% inadequacy of this study. In instances in which the external or common iliac veins are not well

visualized, access through the common femoral or iliac vein for venography may need to be accomplished.

Risks of venography can range from minor to major and include pain at the site of injection, local infection at the injection site, extravasation of contrast material, contrast-induced allergic reaction, thrombophlebitis, intraabdominal bleeding complications with the transhepatic approach to evaluate mesenteric or portal vein thrombosis, DVT, and pulmonary embolism. Risks specifically associated with pulmonary angiography include transient right bundle branch block. In those with an already present left bundle branch block, complete heart block may ensue.

## FUTURE ADVANCES

It is difficult to ascertain what future role venography will play in the diagnosis of thrombosis or reflux disease. Vascular surgery is a rapidly evolving field, and improvements in less invasive methodologies for diagnosis of disease are evolving. Currently, venography is still the reference by which diagnostic imaging modalities are compared, and its use is preferred in particular instances described earlier in the chapter. As the demand for less invasive diagnostic technology continues, the use of more invasive diagnostic techniques like venography may become more limited. However, the treatment of venous disease is likewise becoming less invasive, shifting from open venous procedures to endovascular techniques. The introduction of intravascular ultrasonography and its utility in venous management had increased the sensitivity and specificity of venography in imaging the venous system, offsetting some of its limitations and yielding more accurate diagnosis and intervention. Venography plays a paramount role in these minimally invasive treatment options, and therefore the knowledge and skill in venography becomes an even greater asset in the vascular surgeon's armamentarium.

## SELECTED KEY REFERENCES

- Baldt MM, Böhler K, Zontsich T, et al. Preoperative imaging of lower extremity varicose veins: color coded duplex sonography or venography. *J Ultrasound Med.* 1996;15:143–154.  
*Lower extremity descending venography is no longer used as a screening study. It has largely been replaced by color duplex sonography, which has shown good agreement with descending venography in the grading of deep and superficial vein reflux.*
- Beard RW, Highman JH, Pearce S, Reginald PW. Diagnosis of pelvic varicosities in women with chronic pelvic pain. *Lancet.* 1984;2:946–949.  
*Established the venographic criteria for diagnosis of pelvic congestion syndrome.*
- Danetz JS, McLafferty RB, Ayerdi J, et al. Selective venography versus non-selective venography before vena cava filter placement: evidence for more, not less. *J Vasc Surg.* 2003;38:928–934.  
*Found that when selective venography was used in conjunction with nonselective venography, 23% of patients had either an abnormal finding or aberrant anatomy, and most of these required a major change in vena cava filter position.*
- Gillespie DL, Villavicencio JL, Gallagher C, et al. Presentation and management of venous aneurysms. *J Vasc Surg.* 1997;26:845–852.  
*Showed that venous aneurysms were correctly diagnosed in 85% of patients by imaging techniques: phlebography (60%), color-flow duplex (27%), and magnetic resonance imaging (10%).*
- Kistner RL, Ferris EB, Randhawa G, Kamida C. A method of performing descending venography. *J Vasc Surg.* 1986;4:464–468.  
*Developed a classification system used commonly to categorize the severity of deep venous reflux and functional integrity of the venous valves.*
- McLachlan MS, Thomson JG, Taylor DW, et al. Observer variation in the interpretation of lower limb venograms. *AJR Am J Roentgenol.* 1979;132:227–229.  
*Showed intraobserver disagreement about the probable presence or absence of thrombus occurring in up to 10% of venographic cases.*
- Neglen P, Raju S. Intravascular ultrasound scan evaluation of the obstructed vein. *J Vasc Surg.* 2002;35:694–700.  
*Showed that subtle findings of significant venous stenosis include widening of the iliac vein, pancaking, “thinning” of the contrast dye, partial intraluminal defects, septa, and transpelvic collateral formation. To increase the overall accuracy of detecting iliac vein stenosis, the use of multiplanar venography is recommended.*
- Patel R, Hanish S, Baril D, et al. Contemporary management of lower extremity venous aneurysms. *J Vasc Surg: Venous and Lym Dis.* 2019;7:860–864.  
Rösch J, Antonovic R, Dotter CT. Transjugular approach to the liver, biliary system, and portal circulation. *Am J Roentgenol Radium Ther Nucl Med.* 1975;125:602–608.  
*Popularized the transjugular intrahepatic approach to portal venography.*
- Thomas ML, Bowles JN. Incompetent perforating veins: comparison of varicography and ascending phlebography. *Radiology.* 1985;154:619–623.  
*Showed that incompetent perforating veins of the gastrocnemius muscle and midthigh were more accurately demonstrated with varicography than with ascending venography.*
- Welch CE, Faxon HH, McGahey CE. The application of phlebography to the therapy of thrombosis and embolism. *Surgery.* 1942;12:162.  
*First to recommended injection of contrast material into a superficial vein in the foot with a tourniquet applied above the ankle to prevent filling of the superficial veins, which often obscured the deep system.*

A complete reference list can be found online at [www.expertconsult.com](http://www.expertconsult.com).

## REFERENCES

1. Wheeler HB, Hirsch J, Wells P, et al. Diagnostic tests for deep vein thrombosis: clinical usefulness depends on probability of disease. *Arch Intern Med.* 1994;154:1921–1928.
2. McLachlan MS, Thomson JG, Taylor DW, et al. Observer variation in the interpretation of lower limb venograms. *AJR Am J Roentgenol.* 1979;132:227–229.
3. Thomas ML, Bowles JN. Incompetent perforating veins: comparison of varicography and ascending phlebography. *Radiology.* 1985;154:619–623.
4. Aldridge SC, Comerota AJ, Katz ML, et al. Popliteal venous aneurysm: report of two cases and review of the world literature. *J Vasc Surg.* 1993;18:708–715.
5. Patel R, Hanish S, Baril D, et al. Contemporary management of lower extremity venous aneurysms. *J Vasc Surg Venous Lymphat Disord.* 2019;7:860–864.
6. Gloviczki P, Stanson AW, Stickler GB, et al. Klippel-Trénaunay syndrome: the risks and benefits of vascular interventions. *Surgery.* 1991;110:469–479.
7. Chahlaoui J, Julien M, Nadeau P, et al. Popliteal venous aneurysm: a source of pulmonary embolism. *AJR Am J Roentgenol.* 1981;136:415–416.
8. Gillespie DL, Villavicencio JL, Gallagher C, et al. Presentation and management of venous aneurysms. *J Vasc Surg.* 1997;26:845–852.
9. Braun SD, Moore Jr AV, Mills SR, et al. Closed-system venography in the evaluation of angiomyxomatous lesions of the extremities. *AJR Am J Roentgenol.* 1983;141:1307–1310.
10. Baldt MM, Bohler K, Zontsich T, et al. Preoperative imaging of lower extremity varicose veins: color coded duplex sonography or venography. *J Ultrasound Med.* 1996;15:143–154.
11. Kistner RL, Ferris EB, Randhawa G, Kamida C. A method of performing descending venography. *J Vasc Surg.* 1986;4:464–468.
12. Herman RJ, Neiman HL, Yao JS, et al. Descending venography: a method of evaluating lower extremity venous valvular function. *Radiology.* 1980;137:63–69.
13. Ju Morano, Raju S. Chronic venous insufficiency: assessment with descending venography. *Radiology.* 1990;174:441–444.
14. Raju S, Fredericks R. Valve reconstruction procedures for nonobstructive venous insufficiency: rationale, techniques, and results in 107 procedures with two- to eight-year follow-up. *J Vasc Surg.* 1988;7:301–310.
15. Danetz JS, McLafferty RB, Ayerdi J, et al. Selective venography versus nonselective venography before vena cava filter placement: evidence for more, not less. *J Vasc Surg.* 2003;38:928–934.
16. Rosenthal D, Wellons ED, Hancock SM, Burkett AB. Retrievability of the Gunther Tulip vena cava filter after dwell times longer than 180 days in patients with multiple trauma. *J Endovasc Ther.* 2007;14:406–410.
17. Broholm R, Baekgaard N, Just SR, Jorgensen M. Endovascular treatment of chronic iliac vein obstruction in patients with venous claudication. *Ugeskr Laeger.* 2007;169:1564–1568.
18. Delis KT, Bjarnason H, Wennberg PW, et al. Successful iliac vein and inferior vena cava stenting ameliorates venous claudication and improves venous outflow, calf muscle pump function, and clinical status in post-thrombotic syndrome. *Ann Surg.* 2007;245:130–139.
19. Elson JD, Becker GJ, Wholey MH, Ehrman KO. Vena caval and central venous stenoses: management with Palmaz balloon-expandable intraluminal stents. *J Vasc Interv Radiol.* 1991;2:215–223.
20. Hartung O, Otero A, Boufi M, et al. Mid-term results of endovascular treatment for symptomatic chronic nonmalignant iliofemoral venous occlusive disease. *J Vasc Surg.* 2005;42:1138–1144.
21. Heniford BT, Senler SO, Olsofska JM, et al. May-Thurner syndrome: management by endovascular surgical techniques. *Ann Vasc Surg.* 1998;12:482–486.
22. Hurst DR, Forauer AR, Bloom JR, et al. Diagnosis and endovascular treatment of iliofemoral compression syndrome. *J Vasc Surg.* 2001;34:106–113.
23. Husmann MJ, Heller G, Kalka C, et al. Stenting of common iliac vein obstructions combined with regional thrombolysis and thrombectomy in acute deep vein thrombosis. *Eur J Vasc Endovasc Surg.* 2007;34:87–91.
24. Knipp BS, Ferguson E, Williams DM, et al. Factors associated with outcome after interventional treatment of symptomatic iliac vein compression syndrome. *J Vasc Surg.* 2007;46:743–749.
25. Kwak HS, Han YM, Lee YS, et al. Stents in common iliac vein obstruction with acute ipsilateral deep venous thrombosis: early and late results. *J Vasc Interv Radiol.* 2005;16:815–822.
26. Mickley V, Schwagierek R, Rilinger N, et al. Left iliac venous thrombosis caused by venous spur: treatment with thrombectomy and stent implantation. *J Vasc Surg.* 1998;28:492–497.
27. Mussa FF, Peden EK, Zhou W, et al. Iliac vein stenting for chronic venous insufficiency. *Tex Heart Inst J.* 2007;34:60–66.
28. Neglen P, Raju S. Balloon dilation and stenting of chronic iliac vein obstruction: technical aspects and early clinical outcome. *J Endovasc Ther.* 2000;7:79–91.
29. Neglen P, Raju S. Proximal lower extremity chronic venous outflow obstruction: recognition and treatment. *Semin Vasc Surg.* 2002;15:57–64.
30. Neglen P, Thrasher TL, Raju S. Venous outflow obstruction: an underestimated contributor to chronic venous disease. *J Vasc Surg.* 2003;38:879–885.
31. Neglen P, Raju S. In-stent recurrent stenosis in stents placed in the lower extremity venous outflow tract. *J Vasc Surg.* 2004;39:181–187.
32. Neglen P, Hollis KC, Raju S. Combined saphenous ablation and iliac stent placement for complex severe chronic venous disease. *J Vasc Surg.* 2006;44:828–833.
33. Neglen P, Hollis KC, Olivier J, Raju S. Stenting of the venous outflow in chronic venous disease: long-term stent-related outcome, clinical, and hemodynamic result. *J Vasc Surg.* 2007;46:979–990.
34. O'Sullivan GJ, Semba CP, Bittner CA, et al. Endovascular management of iliac vein compression (May-Thurner) syndrome. *J Vasc Interv Radiol.* 2000;11:823–836.
35. Raju S, Owen Jr S, Neglen P. Reversal of abnormal lymphoscintigraphy after placement of venous stents for correction of associated venous obstruction. *J Vasc Surg.* 2001;34:779–784.
36. Raju S, Owen Jr S, Neglen P. The clinical impact of iliac venous stents in the management of chronic venous insufficiency. *J Vasc Surg.* 2002;35:8–15.
37. Raju S, Hollis K, Neglen P. Obstructive lesions of the inferior vena cava: clinical features and endovenous treatment. *J Vasc Surg.* 2006;44:820–827.
38. Raju S. Endovenous treatment of patients with iliac-caval venous obstruction. *J Cardiovasc Surg (Torino).* 2008;49:27–33.
39. Sawada S, Fujiwara Y, Koyama T, et al. Application of expandable metallic stents to the venous system. *Acta Radiol.* 1992;33:156–159.
40. Tacke J, Antonucci F, Stuckmann G, et al. [The palliative treatment of venous stenoses in tumor patients with self-expanding vascular prostheses]. *Röfo.* 1994;160:433–440.
41. Raju S, McAllister S, Neglen P. Recanalization of totally occluded iliac and adjacent venous segments. *J Vasc Surg.* 2002;36:903–911.
42. Neglen P, Raju S. Balloon dilation and stenting of chronic iliac vein obstruction: technical aspects and early clinical outcome. *J Endovasc Ther.* 2000;7:79–91.
43. Neglen P, Raju S. Detection of outflow obstruction in chronic venous insufficiency. *J Vasc Surg.* 1993;17:583–589.
44. Ing FF, Fagan TE, Grifka RG, et al. Reconstruction of stenotic or occluded iliofemoral veins and inferior vena cava using intravascular stents: re-establishing access for future cardiac catheterization and cardiac surgery. *J Am Coll Cardiol.* 2001;37:251–257.
45. Chang TC, Zaleski GX, Lin BH, et al. Treatment of inferior vena cava obstruction in hemodialysis patients using Wallstents: early and intermediate results. *AJR Am J Roentgenol.* 1998;171:125–128.
46. Neglen P, Raju S. Detection of outflow obstruction in chronic venous insufficiency. *J Vasc Surg.* 1993;17:583–589.

47. Zerhouni EA, Siegelman SS, Walsh PC, White RI. Elevated pressure in the left renal vein in patients with varicocele: preliminary observations. *J Urol.* 1980;123:512–513.
48. Beinart C, Sniderman KW, Tamura S, et al. Left renal to inferior vena cava pressure relationship in humans. *J Urol.* 1982;127:1070–1071.
49. Hobbs JT. The pelvic congestion syndrome. *Br J Hosp Med.* 1990;43:200–206.
50. Beard RW, Highman JH, Pearce S, Reginald PW. Diagnosis of pelvic varicosities in women with chronic pelvic pain. *Lancet.* 1984;2:946–949.
51. Belenky A, Bartal G, Atar E, et al. Ovarian varices in healthy female kidney donors: incidence, morbidity, and clinical outcome. *AJR Am J Roentgenol.* 2002;179:625–627.
52. Sculertus AH, Villavicencio JL, Gillespie DL. The nutcracker syndrome: its role in the pelvic venous disorders. *J Vasc Surg.* 2001;34:812–819.
53. Bittles MA, Hoffer EK. Gonadal vein embolization: treatment of varicocele and pelvic congestion syndrome. *Semin Intervent Radiol.* 2008;25:261–270.
54. O'Dea MJ, Malek RS, Tucker RM, Fulton RE. Renal vein thrombosis. *J Urol.* 1976;116:410–414.
55. Martin EC, Gordon DH. Selective renal venography in patients with primary renal disease and the nephrotic syndrome. *Cardiovasc Interv Radiol.* 1980;3:175–179.
56. Beckmann CF, Abrams HL. Renal venography: anatomy, technique, applications, analysis of 132 venograms, and a review of the literature. *Cardiovasc Interv Radiol.* 1980;3:45–70.
57. Gertsch P, Matthews J, Lerut J, et al. Acute thrombosis of the splanchnic veins. *Arch Surg.* 1993;128:341–345.
58. Ozkan U, Oguzkurt L, Tercan F, Tokmak N. Percutaneous transhepatic thrombolysis in the treatment of acute portal venous thrombosis. *Diagn Interv Radiol.* 2006;12:105–107.
59. Rosen MP, Sheiman R. Transhepatic mechanical thrombectomy followed by infusion of TPA into the superior mesenteric artery to treat acute mesenteric vein thrombosis. *J Vasc Interv Radiol.* 2000;11:195–198.
60. Rösch J, Hanafee WN, Snow H. Transjugular portal venography and radiologic portacaval shunt: an experimental study. *Radiology.* 1969;92:1112–1114.
61. Rösch J, Hanafee W, Snow H, et al. Transjugular intrahepatic portacaval shunt. An experimental work. *Am J Surg.* 1971;121:588–592.
62. Rösch J, Antonovic R, Dotter CT. Transjugular approach to the liver, biliary system, and portal circulation. *Am J Roentgenol Radium Ther Nucl Med.* 1975;125:602–608.
63. Rösch J, Uchida BT, Barton RE, Keller FS. Coaxial catheter-needle system for transjugular portal vein entrance. *J Vasc Interv Radiol.* 1993;4:145–147.
64. Hebbard GS, Fitt G, Thomson KR, et al. Transjugular intrahepatic portal-systemic shunts (TIPS)—initial experience and clinical outcome. *Aust N Z J Med.* 1994;24:141–148.
65. Ferro C, Rossi UG, Bovio G, et al. Transjugular intrahepatic portosystemic shunt, mechanical aspiration thrombectomy, and direct thrombolysis in the treatment of acute portal and superior mesenteric vein thrombosis. *Cardiovasc Interv Radiol.* 2007;30:1070–1074.
66. Dilawari JB, Bamberg P, Chawla Y, et al. Hepatic outflow obstruction (Budd-Chiari syndrome). Experience with 177 patients and a review of the literature. *Medicine (Baltimore).* 1994;73:21–36.
67. Rosa P, Gillespie DL. Budd-Chiari syndrome: case report and review of the literature. *Vasc Surg.* 2000;34:591–595.
68. Phibbs B, Marriott HJ. Complications of permanent transvenous pacing. *N Engl J Med.* 1985;312:1428–1432.
69. Warden GD, Wilmore DW, Pruitt Jr BA. Central venous thrombosis: a hazard of medical progress. *J Trauma.* 1973;13:620–626.
70. Thomas ML, Andress MR. Axillary phlebography. *Am J Roentgenol Radium Ther Nucl Med.* 1971;113:713–721.
71. Natu SS, Sequeira JC, Weitzman AF. An improved technique for axillary phlebography. *Radiology.* 1982;142:529–530.
72. Shimm DS, Logue GL, Rigsby LC. Evaluating the superior vena cava syndrome. *JAMA.* 1981;245:951–953.
73. Hudson GW. Venography in superior vena caval obstruction. *Radiology.* 1957;68:499–506.
74. Rutherford RB, Hurlbert SN. Primary subclavian-axillary vein thrombosis: consensus and commentary. *Cardiovasc Surg.* 1996;4:420–423.
75. Sharma RP, Keller CE, Shetty PC, Burke MW. Superior vena cava obstruction: evaluation with digital subtraction angiography. *Radiology.* 1986;160:845.
76. Ruiz Y, Caballero P, Caniego JL, et al. Prospective comparison of helical CT with angiography in pulmonary embolism: global and selective vascular territory analysis. Interobserver agreement. *Eur Radiol.* 2003;13:823–829.

# Computed Tomography

JAN D. BLANKENSTEIJN and RUTGER J. LELY

## BASIC PRINCIPLES 352

Types of Scanners 353

Single-Slice Sequential Computed Tomography 353

Spiral (Helical) Computed Tomography 353

Multislice (Multidetector) Computed Tomography 354

Computed Tomography Angiography 354

Acquisition Parameters 354

Pre-scan Parameters 354

kVP and mAs 354

COLLIMATION 355

TABLE FEED AND PITCH 355

PATIENT POSITIONING 355

CONTRAST PROTOCOLS 355

DUAL ENERGY/SOURCE COMPUTED TOMOGRAPHY 355

Post-scan Parameters 355

INCREMENT 355

SLICE WIDTH 355

FIELD OF VIEW 355

WINDOWING 356

RECONSTRUCTION ALGORITHMS: FILTERED BACK PROJECTION AND ITERATIVE RECONSTRUCTION 356

Dynamic Computed Tomography Scanning 356

Electrocardiogram Triggered and Gated Scanning 356

Post-processing 356

Multiplanar Reformatting 356

Measurements 356

Three-Dimensional Reconstruction 358

## CLINICAL APPLICATION 358

Aortic Disease 358

Peripheral Arterial Occlusive Disease 360

Renal and Splanchnic Arterial Disease 360

Venous Disease 360

Vascular Malformations 361

## LIMITATIONS AND RISKS 361

Radiation Dose 361

Contrast-Induced Nephropathy 361

## COMMON ARTIFACTS 361

Partial-Volume Effects 361

Beam-Hardening Artifacts 362

Motion Artifacts 362

Other Common Artifacts 362

## SPECIAL PEDIATRIC CONSIDERATIONS 362

## FUTURE ADVANCES 362

Computed Tomography Versus Duplex Ultrasound and Magnetic Resonance 363

Fusion Imaging 364

Positron Emission Tomography with Computed Tomography 364

Conventional contrast-enhanced arteriography is no longer considered the standard imaging modality for vascular disease.<sup>1–6</sup> As with many technologic advances, however, the process of image creation continues to become more difficult for the average end user to understand. Although the typical vascular surgeon can perform clinical evaluation and can make decisions without an understanding of the basic principles behind computed tomography (CT), these concepts remain important. A better understanding of the imaging process and terminology also aids collaboration between radiologists, radiographers, and the surgeons who use the images to plan interventions. Finally, an understanding of the basic concepts

enhances the ability of the surgeon to understand technologic advances as they become the new standard of care.

## BASIC PRINCIPLES

In the early 1930s, the Dutch radiologist Ziedses des Plantes first devised a technique that reduced the problem of superimposition of structures in basic radiography (X-ray tube and plain film). Physically connecting the X-ray tube and film opposite each other and rotating the combination around a body segment sharpens the image created by the points on the focal plane, whereas the images of points outside the focal plane

are blurred, thereby creating less superimposition artifact. This technique was called “planigraphy” or “tomography,” derived from the Greek words *tomos*, which means “a section” or “a cutting,” and *graphein*, meaning “to write.” Tomography played an important role in diagnostic radiology until the 1970s, when invention of the transverse axial scanning method together with the availability of minicomputers, which allowed computational reconstruction of images, led to the development of so-called computed axial tomography (CAT scan, or later, CT scan).

Two similar methods for transverse axial scanning and image reconstruction were independently invented by Sir Godfrey Newbold Hounsfield in Hayes, United Kingdom, at Elector-Musical Instruments (EMI) Limited Central Research Laboratories, and Allan McLeod Cormack of Tufts University in Massachusetts. A combination of hardware, mathematical algorithms, and computer software resulted in the cross-sectional images. The first so-called EMI scanner was installed in Atkinson Morley’s Hospital, Wimbledon, England, in 1971.<sup>7</sup> In the United States, the first installation was at the Mayo Clinic in Rochester, Minnesota. These machines would acquire two adjacent brain tomographic sections in about 4 minutes and needed about 7 minutes of computation time per picture. This was such a leap forward in imaging technology that Hounsfield and Cormack shared the Nobel Prize in 1980.

Many of the principles used in this first-generation CT scanner are still in use today and provide a framework for understanding the technology. The fundamental unit for this scanning method consists of an emitter and a detector. The emitter produces a thin X-ray beam. The beam is transmitted through the tissue and detected on the other side. The attenuation (the rate of reduction of X-ray energy recorded at the detector) of multiple X-ray beams traversing the same point in the matrix from different angles is collected and an ingenious method applied to calculate backward to the density or CT number that must be present at each location in the matrix.

The resulting CT number is expressed in Hounsfield units (HU). CT numbers range from the extremes of air (-1000 HU) to dense bone (>1000 HU), but fat (-20 to -100 HU), water (0 HU), and muscle and blood (40 to 60 HU) tend to lie in a much narrower range. Differences in factors such as the energy level of the beam and tissue thickness prevent the density in HU from being absolutely uniform from one CT scan to another, but the ranges are similar. When the range of CT numbers for a scan is determined, it can be broken up into smaller ranges for graphic display by a set of gray-scale values. Each gray-scale data point in the matrix is known as a pixel because it represents a “picture element.” When displayed as a whole, this matrix of gray squares becomes an interpretable image.

## Types of Scanners

### Single-Slice Sequential Computed Tomography

A first-generation CT scanner is capable of producing a cross-sectional image with a  $160 \times 160$  matrix. These CT scans were applicable only to parts of the body with limited motion (e.g.,

the head). To obtain useful scans in areas such as the chest and abdomen, subsequent generations of CT scanners were designed to decrease the time required to obtain a complete cross-sectional image.

### Spiral (Helical) Computed Tomography

With development of a so-called slip-ring gantry, the emitter and detector array can rotate continuously in the same direction, and at the same time, the computer can acquire data continuously. If the table moves in a continuous linear motion through the gantry while the X-ray emitter and detector rotate continuously over 360 degrees, data can be acquired in a single sweep over the entire volume of interest. In this technique the emitter traces out a spiral relative to the patient, which is referred to as a spiral CT or helical CT scan.

Spiral or helical CT technology has several important ramifications beyond a simple decrease in scan time. A spiral CT scan collects data over a continuous volume rather than discontinuous slices (Fig. 29.1). The most obvious advantage of acquiring data over a continuous volume is that thin axial slices can be reconstructed from the digital data set at arbitrarily small intervals without additional radiation exposure. Single-slice sequential CT can produce similar overlapping or adjacent axial slices, but the tradeoff is increased scan time and additional radiation exposure. The advantage of sequential scanning, however, is a lower level of reconstruction artifacts because table movement along the z-axis during scanning does not need to be corrected in the acquired data sets. This is the main reason why sequential scanning is often used for brain imaging.

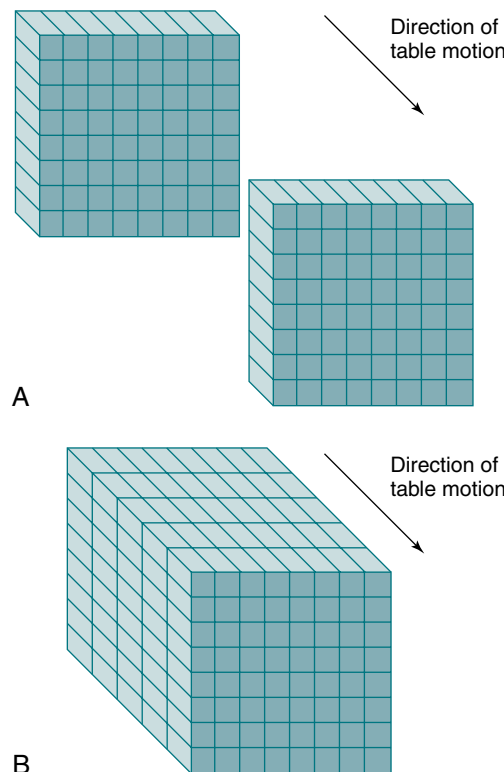


**Figure 29.1** Discontinuous data collection (A) versus continuous data collection (B) for conventional and spiral computed tomography.

## Multislice (Multidetector) Computed Tomography

Multidetector scanners have multiple rows of detectors in craniocaudal direction (z-direction), so that the volume to be scanned can be covered more quickly. Whereas a single-slice detector acquires one slice per rotation, multidetector CT scanners are capable of acquiring multiple separate slices or 1 big volume per rotation. Each slice can be acquired at 1 mm or even smaller with rotation times in the range of 0.2 to 0.3 seconds. Complete imaging of the abdominal vasculature can be accomplished in a fraction of the time required with previous-generation scanners. This diminishes or eliminates many artifacts or compromises that must be dealt with in single-row detector scanners, as discussed subsequently. For this reason, multidetector or multirow scanners have almost completely replaced the earlier-generation single-row scanners.

Advances in hardware and computer software technology have also greatly improved the graphic image display despite the reduction in scan times. A first-generation CT scanner produced a cross-sectional image with a  $160 \times 160$  matrix, but current scanners typically generate a  $512 \times 512$  matrix. Each data point in the matrix is mapped to a gray scale for display, so the size of the matrix and the field of view (FOV) have a direct impact on spatial resolution of the display (the smallest distinguishable element). Data points are displayed as a two-dimensional (2D) picture, and each point in the display matrix is a pixel (picture element). Data points are acquired in three dimensions, however, and each data point in the matrix actually represents a voxel (volume element). The size of the voxel is determined by multiple factors, including FOV (x, y direction) and detector design (x, y, z direction).

## Computed Tomography Angiography

Visualization of vessels on CT is limited by the similar densities of blood and soft tissue. Administration of iodine intravenous contrast material highly overcomes this problem. However, optimal visualization of the vessels (computed tomographic angiography [CTA]) was not possible until the availability of fast spiral CT: faster scan times and increased numbers of detectors will allow a larger part of the body to be imaged as the contrast bolus passes.

Timing of the initiation of image acquisition relative to injection of the contrast agent is crucial for maximizing opacification of vessels in the scanned volume. Various dedicated bolus tracking algorithms have been developed by the CT scanner manufacturers to detect contrast arrival in the vessel of interest in order to start the scan on an appropriate time. These algorithms are all based on a stationary, continuous scan of a single slice in which contrast density is measured in a region of interest (ROI) in a large vessel marked by the operator. When a certain threshold of Hounsfield units is achieved at the region of interest, the spiral CT is initiated.

The iodine concentration, injection rate, and the volume of the contrast bolus are important parameters. Bolus length should be balanced against the length of the volume to be imaged. In the past, a typical CTA study from the celiac axis down to the external iliac arteries would require 120 to 180 mL of 300 mg/mL nonionic contrast.<sup>8,9</sup> For optimal arterial enhancement, fast injection rates are important.

Optimization of scanning and power injector protocols, faster scanning times, and the use of saline push bolus techniques reduced this volume significantly, and often volumes do not exceed 100 mL.

Split-bolus techniques are alternative ways to administer intravenous contrast. These techniques employ multiple phases – for instance, enhancement of venous and arterial structures – in one single scan. This is achieved by splitting the contrast bolus volume into one early bolus of contrast and one late bolus of contrast administration before obtaining the CT scan. This technique decreases ionizing radiation dose since fewer scanning phases are needed per patient.

Another factor that increases contrast enhancement is lowering of beam energy (kVpeak) which increases iodine density on scans.<sup>10</sup>

## Acquisition Parameters

A scan protocol consists of a series of settings of acquisition and contrast parameters, reconstruction parameters, technician and patient instructions, and maneuvers to generate a set of images that is optimal for the specific anatomy and indication for the CT scan. The protocol includes the setting of X-ray emitter parameters (i.e., beam energy expressed in kilovolts peak [kVp] and tube current expressed in milliamper-second [mAs]), rotation time, length of helical exposure, pitch, collimation, patient instructions (i.e., breath-hold), dosage of contrast material, delay, volume and infusion rates, reconstruction interval and reconstruction algorithm, parameters of radiation dose optimization tools, and FOV.

Pre-scan and post-scan parameter settings should be distinguished from each other. Various post-scan settings, such as the reconstruction algorithm or interval, can be applied to the raw image data. This is not true for the pre-scan settings. Obviously, an improper pre-scan setting cannot be corrected after the images have been acquired. Particularly in multislice scanners, proper pre-scan settings are important and have a direct impact on the diagnostic value of the CT scan.

Scan parameter settings are also important for optimization of the scan protocol in relation to the clinical question because this may be the only way to limit the radiation dose delivered by the CT scan.

## Pre-scan Parameters

### kVp and mAs

Tube voltage, measured in kVp, is the value that determines the energy level of the X-ray tube. Higher tube voltage renders better tissue penetration but leads to decreasing relative contrast differences between the various tissues. High kVp settings (120 kV) are recommended to allow sufficient photons to reach the detector elements in obese patients. In children or slim patients, low kVp settings (80 kV, or even lower) should suffice and also produce increased contrast differences.

mAs values describe the tube current time product. The mAs value is linearly related to the duration and amount of radiation. Higher mAs represents more radiation delivered by

the X-ray tube and leads to a decrease in image noise because more photons will reach the detector. However, this decreased noise is achieved at the expense of an increased radiation dose to the patient. kVp and mAs settings are closely linked, and a change in one may dictate a change in the other.

### Collimation

Collimation is a method of reducing the thickness of the X-ray beam. Collimation has a direct impact on spatial resolution in the z-axis and determines the smallest possible slice thickness.

### Table feed and pitch

Pitch (P) is defined as the ratio of table feed (the speed at which the table moves during tube rotation) and collimation. Values above 2 will result in undersampling of the region of interest and might result in artifacts. Values below 1 will result in overlapping scans, which might be beneficial for three-dimensional (3D) reconstructions but will also increase the dose significantly if other scanning parameters are kept constant. For multi-slice CT scanners, pitch calculations are different, depending on whether single collimation of one detector ring or total collimation of the whole detector array is chosen. An asterisk indicates that total collimation of the detector array is being described; for a four-slice scanner, a pitch of 2 corresponds to a P\* of 8.

$$P = \text{TF} / \text{SC}$$

$$P^* = \text{TF} / (\text{N} \times \text{SC})$$

where P = pitch, TF = table feed, N = number of detectors, and SC = single-section collimation.

To give an example for a 64-slice scanner, if pitch is set at 2 and collimation is set at 1 mm, the resulting TF – according to the formula  $P^* = \text{TF}/(\text{N} \times \text{SC})$  – will be 64 mm/s.

Scanning time is the maximum duration of a scan that a certain tube allows while not exceeding the maximum permissible heat capacity. Older scanners are limited to approximately 20 seconds, whereas newer scanners allow scan times of up to 100 seconds.

### Patient positioning

Proper, central positioning of the patient in the gantry can significantly improve image quality and decrease radiation dose. A clear example is raising the arms of the patient when scanning the upper part of the chest (Fig. 29.2).

### Contrast protocols

With the newer scanner types, good timing of the administration of contrast material has become an essential part of the examination. Depending on the indication and parameter settings (pitch), optimization of total volume of contrast, contrast iodine density, volume, and speed of injection is required.

### Dual energy/Source computed tomography

Dual energy/source CT was introduced as a novel technique in 2006. Instead of one X-ray tube, the system was equipped with two X-ray tubes each working at a different kVp. Dual energy/

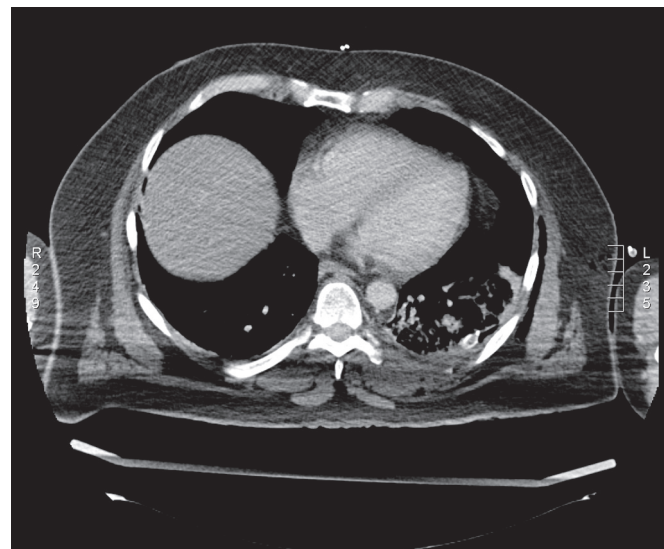


**Figure 29.2** Beam-hardening artifacts caused by the humerus as a consequence of scanning with the patient's arms alongside the upper part of the chest.

source CT has not found broad application for vascular imaging. The use of two different X-ray tubes has inherent hardware design issues and similar advantages might be acquired by smart software algorithms with a single source CT.

### Post-scan Parameters

#### Increment

The increment or reconstruction index defines the spacing of the reconstructed images from the raw data set. One could, for instance, decide to reconstruct only a 1-mm slice every 3 mm. The main advantage would be the fewer number of reconstructed slices than if a 1-mm slice had been reconstructed for every position. If the raw data are saved, it is possible to obtain reconstructed images at different positions retrospectively.

#### Slice width

Slice width or section collimation defines the thickness of the slice. Slices of various thickness ranging from 0.5 to 10 mm can be calculated from the raw data. The minimum slice thickness, however, is defined by the pre-scan collimation setting. The main advantage of a thicker slice is a lower noise level and a significant reduction in the data load.

#### Field of view

As mentioned previously, the size of the display matrix and FOV have a direct impact on axial resolution of the display. By keeping FOV to the minimum necessary, pixel size is decreased. If FOV is 30 cm and the matrix size is  $512 \times 512$ , each pixel in the display of axial slices is 0.6 mm. If FOV is reduced to 20 cm, pixel size is improved to 0.4 mm, but the tradeoff is that a higher radiation dose is required because of an increase in detector noise.

In general, a small FOV is important only when detailed measurements are necessary (e.g., in endovascular surgery, calculation of carotid artery stenosis or intracerebral aneurysms).

In addition, factors such as contrast density, timing of administration of contrast material, window level (WL), and window width (WW) more strongly affect the ability to distinguish different structures and the edges of these structures.

### Windowing

WW sets the number of gray scales displayed, and WL defines the middle gray-scale value of the width. Windowing sets the contrast and the brightness of the image.

### Reconstruction algorithms: filtered back projection and iterative reconstruction

Reconstruction algorithms are used to reconstruct the raw data. Basically during a rotation of the tube, obtained one-dimensional (1D) datasets (raw data) are reconstructed in a 2D data set (back projection). Obtained images in this way are very fuzzy and additional filters need to be applied in order to improve image quality (filtered back projection). Initially, filtered back projection was the algorithm of choice. The algorithm determines the relation between spatial resolution and noise and thus contrast resolution. Changing of parameter settings allows optimization of the images. For instance, if a high spatial resolution (bone or lung pathology) is needed, high-resolution convolution kernels (HR kernels) are applied. This will result in a significant increase in spatial resolution and improved imaging for bone or lung, but at the expense of a significant increase in image noise.

With the increasing computational power of current systems, iterative reconstruction has become the major reconstruction algorithm for clinical practice.

With iterative reconstructions, mathematical calculations of the cone shape of the X-ray beam, the shape of the voxels, focal spot, nature of the X-ray beam, and detectors are all taken into account. By doing this, image noise can be reduced significantly compared to the filtered back projection algorithm (70% to 90%).

The initial iterative reconstruction algorithms were in part based on filtered back projection, but the most recently introduced iterative reconstruction algorithms are fully model based, which means that no filtered back projection is necessary. The major advantage of these algorithms is a substantial decrease in noise and therefore lower radiation doses with an inherent higher noise level can be used, and this will be compensated by the algorithm. The major disadvantage, however, is the high demand on computational power, which, with the ever increasing improvements in computational power, is becoming less of a problem.

### Dynamic Computed Tomography Scanning

With the increased number of detector rings in the new multislice scanners, dynamic CT scanning has become an option.<sup>11</sup> The basic concept is that of obtaining CT images at a fixed location (in other words, without moving the table) during the injection of contrast material. After injection of a contrast agent, imaging at a fixed position with continuous rotation of the CT gantry will provide insight into passage of contrast

material through the arterial, capillary, and venous phases, representing tissue perfusion. The maximum anatomic area covered by this type of imaging is determined by the z length of the detector area. The 256 (or more) slice scanners are better suited for this technique and are currently used predominantly for brain and cardiac perfusion studies.

### Electrocardiogram Triggered and Gated Scanning

Techniques that couple the electrocardiogram (ECG) signal to scan acquisition can be used to obtain images without cardiac pulsation artifacts at the level of the heart, coronaries, and the ascending aorta. Retrospective ECG-gated CT acquisition is a scanning technique in which the ECG is registered during the scan and coupled to the raw data obtained.<sup>12</sup> By partial reconstruction of the images, it is possible to obtain an image at, for instance, 10 different phases of the ECG. The technique is now available on almost all scanners and is most often used for coronary imaging.<sup>13</sup> Because partial reconstructions are used, a major drawback of this technique is that the resulting images are substantially noisier than the full reconstructions. In prospective ECG-gated CT acquisition, the X-ray beams are turned on during preselected phases of the cardiac cycle. The main benefit of this way of sampling is the far lower radiation dose, which, in comparison with retrospective gating, proved to be reduced by 52% to 85%. The main disadvantage is that only preselected phases can be reconstructed.

### Post-processing

#### Multiplanar Reformatting

Reformatting CT data into coronal, sagittal, or other nonaxial planes is often referred to as multiplanar reformatting or multiplanar reconstruction (MPR). A schematic representation of this process is shown in Figure 29.3. The ability of spiral CT to view the data in coronal, sagittal, or arbitrarily defined planes often gives more insight into vascular anatomy than possible with axial views alone.<sup>14</sup>

#### Measurements

Simple axial CT slices often do not cut through planes perpendicular to the vessel, which results in elliptical cross-sections that can make measurements of diameter difficult (Fig. 29.4). Generally, the narrowest diameter of the elliptical cross-section is the “true” arterial diameter, but this is not always the case because the aorta does not always have a simple cylindrical or conical shape.<sup>15</sup> Conventional CT may lead to a slight overestimation of diameter on axial slices, whereas spiral CT slices reconstructed perpendicular to the vessel tend to be more accurate.<sup>3,16</sup> Simply using sagittal or coronal reconstruction is not always adequate because these sections may not be perpendicular to the vessel or may not cut through the center of the vessel over an adequate length. Curvilinear reformats continue to improve, but they make measurements of length difficult and straighten out angles, which may affect an endovascular repair. Spiral CT with 3D reconstruction and CT reformats perpendicular to the vessel lumen eliminate the diameter measurement problems associated with the other techniques (see

**Fig. 29.4.**<sup>3,16</sup> CTA with 3D reconstruction offers several other important benefits that are key for imaging before endovascular surgery. In conjunction with spiral CTA and MPR, 3D

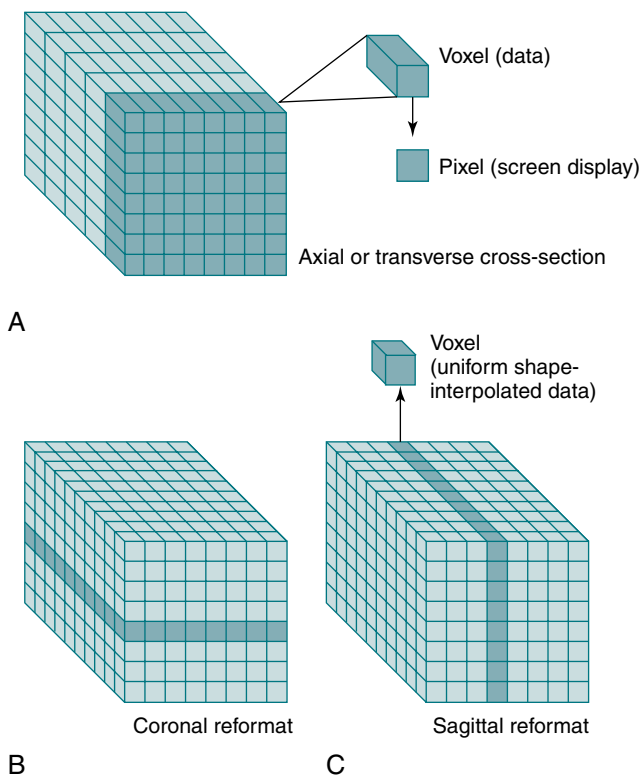


**Figure 29.3** (A–C) Because spiral computed tomography (CT) data are acquired and stored over a continuous volume, they can be used to create axial (A), coronal (B), and sagittal (C) sections. For display purposes, the nonuniform voxel can be interpolated into a cube, but the quality of the data still depends on the length of the original voxel (which is determined by the collimation). Reformating CT data into coronal, sagittal, or other nonaxial planes is often referred to as multiplanar reformatting.

reconstruction speeds assimilation of the CT data and makes the extent of an aneurysm rapidly apparent.<sup>3</sup> More important, specialized measurement software and unique aspects of the 3D reconstruction can eliminate most of the measurement problems associated with conventional techniques.<sup>3,16</sup> Software algorithms can be used to display the centerline of the blood flow channel in the infrarenal aorta and iliac arteries and allow measurements of length along the vessel centerline in tortuous aortic or iliac segments. In some systems, graft paths along a line other than the centerline can also be defined by the user, which is necessary because an endovascular graft may not follow the centerline of the blood flow channel throughout its entire course.

3D reconstructions can be used to calculate the volume of any structure in the 3D model, and data on imaging of tumors and other 3D structures indicate that volume measurements are much more sensitive to changes in size than measurements of maximal diameter.<sup>17–19</sup> Multiple institutions have confirmed that volume measurements are much more sensitive than maximum diameter measurements for the detection of changes in size of abdominal aortic aneurysms (AAAs) after endovascular AAA repair, and it seems that volume is the “gold standard” for early detection and accuracy regarding aneurysm growth or shrinkage.<sup>20–25</sup> Early detection of aneurysm enlargement can be crucial in follow-up of endovascular repair because it indicates that the aneurysm is still at risk for rupture and usually precedes evidence of endoleak or overt rupture.<sup>22,26–28</sup> CT volume measurements may become a standard postoperative test for aneurysm exclusion or risk of rupture either routinely or if the aneurysm is not clearly shrinking.<sup>20–25</sup> These same studies indicate that there may also be a role for early volume measurements within the first 6 months to more clearly identify decreasing aneurysms that may need less frequent imaging or may be able to avoid secondary interventions.

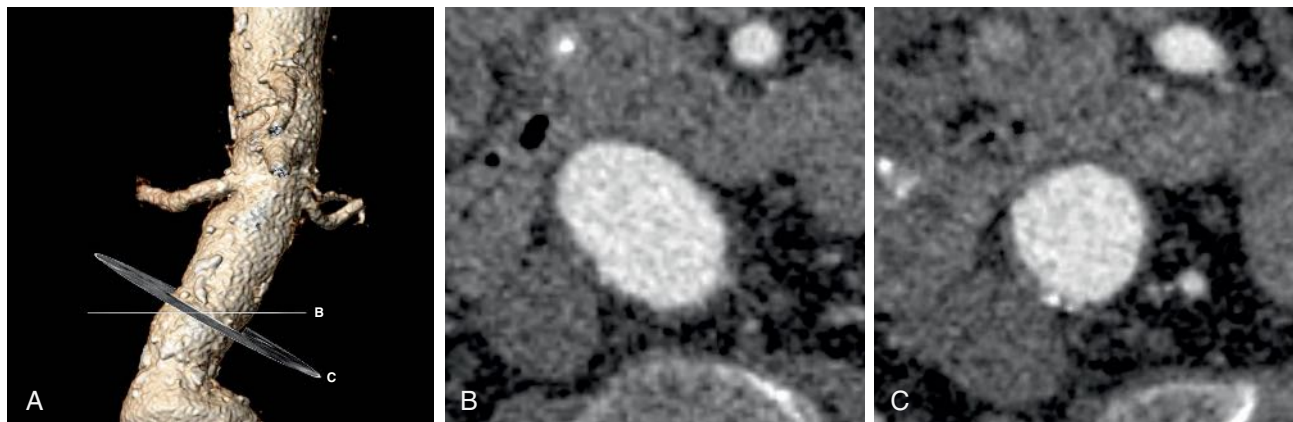


**Figure 29.4** Diameter Measurement Issues and Solutions Using Computed Tomography (CT). (A) Three-dimensional (3D) reconstruction with simultaneous display of CT slices in 3D space. The CT slices shown here are a standard axial reformat and a reformat perpendicular to the aorta. (B) The axial CT slice as shown in (A). The axial slice does not intersect the aortic neck perpendicular to its axis, thereby creating an elliptical cross-section. Although the smaller diameter (minor axis of the ellipse) is usually similar to the true diameter, elliptical cross-sections also occur in noncylindrical vessels and at the margins of aneurysms. Viewing multiple cross-sections in sequence can help with this problem, but evaluation is still difficult. (C) The CT slice reformatted perpendicular to the aorta (shown in A) accurately depicts the essentially circular lumen and provides a diameter measurement without ambiguity. This cross-section of the aorta also provides a more correct impression of thrombus thickness, which is artifactually enhanced on an elliptical cross-section.

Several systems providing all of the aforementioned display and measurement tools (and more) are commercially available or in development.

### Three-Dimensional Reconstruction

The combination of rapid scanning over the volume of interest, new software algorithms, and advances in computer technology has made it possible to create 3D-like reconstructions from spiral CT data. The reconstruction can be limited to individual structures that meet certain parameters, such as density or location within the scan volume. If bony structures are of primary interest, the computer algorithm can select only the elements of the CT (voxels) that are of bone density (i.e., CT numbers representing bone). For vascular structures, CTA produces contrast density within the vessel lumen so that 3D reconstruction of the vessel lumen can be performed. When this type of 3D reconstruction (or 3D model) is created, the density (CT numbers) of vascular contrast and bone may overlap. Bone structures are either included in the model or “cut away” manually or sometimes automatically. Calcium within the vessel wall cannot be cut away easily, however, and is usually included in a reconstruction of the contrast-enhanced vessel lumen. This produces the typical computer-generated 3D reconstruction, which most often is displayed as a shaded surface display (SSD). In an SSD, the exterior of the structure is opaque and shaded to provide an appreciation of depth (Fig. 29.5). The 3D reconstruction can greatly aid in the interpretation of difficult anatomy. Although it lacks the detail of CT scans, morphology within the 3D image is easily recognizable in far less time than it takes to review the CT data. This depiction of 3D relationships is probably most helpful in surgical planning for complicated open procedures or endovascular procedures.<sup>29,30</sup>

One problem with the SSD of 3D models is that the bulk of structures, such as calcified plaque, cannot be fully appreciated because all CT numbers (physical densities) included in the model are given the same opaque color in the display. One method that better displays different physical densities is called the maximum intensity projection (MIP). MIP is a method to produce 2D images in which the voxels with the highest intensity in the chosen plane of projection are shown. Typically, a coronal plane for overview purposes is used (Fig. 29.6). MIP images are relatively familiar to surgeons and interventional radiologists, and they display calcified plaque well. Adequate evaluation of the structure requires many views, however, and even then a heavily calcified vessel may obscure important details regarding the vessel lumen and degree of stenosis.

Another method developed to improve the display of structures with different physical densities involves the SSD of multiple objects simultaneously. In vascular surgery, the most clinically relevant structures are the contrast-enhanced vessel lumen, calcified plaque, noncalcified plaque, and thrombus. Noncalcified atherosclerotic plaque and thrombus have essentially identical CT numbers and cannot be distinguished as separate objects. The latter two structures are distinct from contrast-enhanced blood flow, however, and blood flow can be distinguished from calcified plaque to a reasonable degree. With

proper CT protocols and software algorithms, these structures can be displayed separately on the basis of density. The resulting 3D reconstructions display information that is not available in any other imaging modality (Fig. 29.7). Because the separate elements can be viewed in combination or separately, this type of reconstruction has the advantages of single-object SSD and MIP without most of their disadvantages. This 3D method can display best the extent of an aneurysm (because thrombus is visible), degree of calcification, and lumen narrowing secondary to plaque.

It is important to realize that a 3D SSD is a representation of a real 3D data set, unlike the “fake” 3D created in pictures (or movies) whereby a pair of 2D photographs, each taken from the same point but at a slightly different angle, emulate the physiologic parallax of binocular real 3D vision. Still, this 3D SSD model is displayed in 2D, and real visual depth information is therefore missing. To add the value of depth, several solutions have been proposed. One is the use of sophisticated software programs that add perspective to the 3D CT data (Dextroscope, Bracco AMT, Princeton, CA). The main limitation of this technology is that the observer is required to wear dedicated polarizing glasses to see this effect. With the development of 3D monitors, however, this problem seems to be solved. The end result will be real 3D data sets that can be manipulated, viewed, and analyzed with perspective and that will give the observer an optimal feel for the depth information in the 3D model.

## CLINICAL APPLICATION

The most common noncardiac, nonbrain vascular imaging indications for CTA are aortic disease (aneurysm, dissection, trauma), peripheral arterial occlusive disease, renovascular disease, venous disease, and, rarely, vascular malformations.

### Aortic Disease

In general, CTA has become the primary imaging modality for aortic disease. The excellent spatial resolution and the potential of 3D image reconstruction allow for highly accurate measurements of aortic aneurysms in the preoperative planning of endovascular repair, as well as postoperative follow-up. CTA also allows for imaging of small branches such as the intercostal arteries (important for prevention of spinal cord infarction during thoracic aortic repair) and for tiny contrast enhancements in thrombus (important for identification of endoleak). The CTA acquisition speed of the entire aorta (currently, within 1 minute; in newer scanners, within a few seconds) allows accurate imaging of the aorta in acute cases such as ruptured aneurysm, aortic dissection, and trauma. Endovascular repair of these acute diseases currently relies on acute CTA (Fig. 29.8). ECG gated or triggered CTA aids in detecting or excluding pathology of the ascending aorta.

Apart from the acquisition speed, an important advantage of CTA over MRA in both the acute and elective setting is the ability of CTA to image calcium, for instance, in aortic landing zones of endovascular devices that depend on penetrating

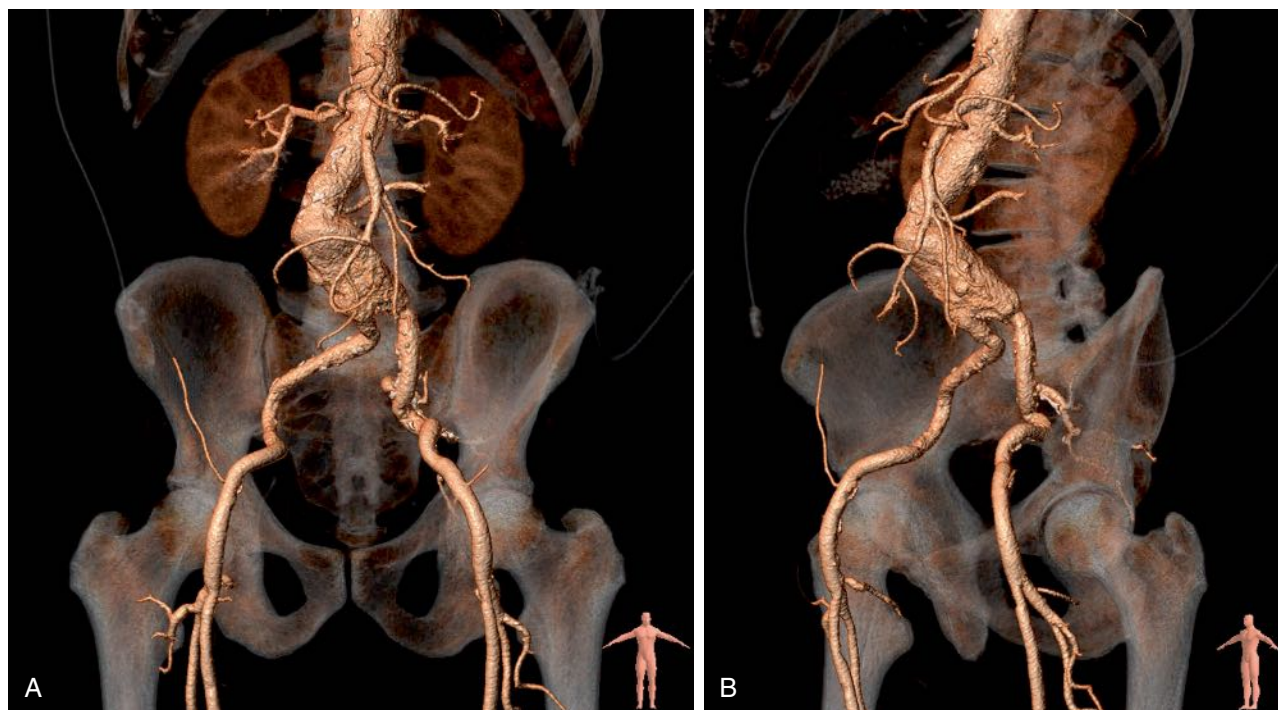


**Figure 29.5** Computer-Generated Shaded Surface Display (SSD) of Computed Tomography Data. The three-dimensional (3D) relationships of the aneurysm and surrounding structures are immediately apparent in these anteroposterior (**A**) and left lateral anterior oblique (**B**) views. In this typical volume-rendered 3D SSD, the threshold for reconstruction is the density of contrast-enhanced blood. Because calcified plaque is denser than contrast-enhanced blood, it is included in the reconstruction. The reconstruction can be rotated interactively, in all planes.



**Figure 29.6** Maximum Intensity Projection (MIP) Image of a Calcified Aortoiliac System. Because this reconstruction represents a two-dimensional projection, the MIP appears to be similar to an arteriogram. Only the structure with maximum intensity is projected, so calcified plaque is displayed prominently. MIP images display calcified plaque well, but this same feature can obscure the residual lumen in locations where the vessel is heavily calcified (note the iliac arteries in particular).

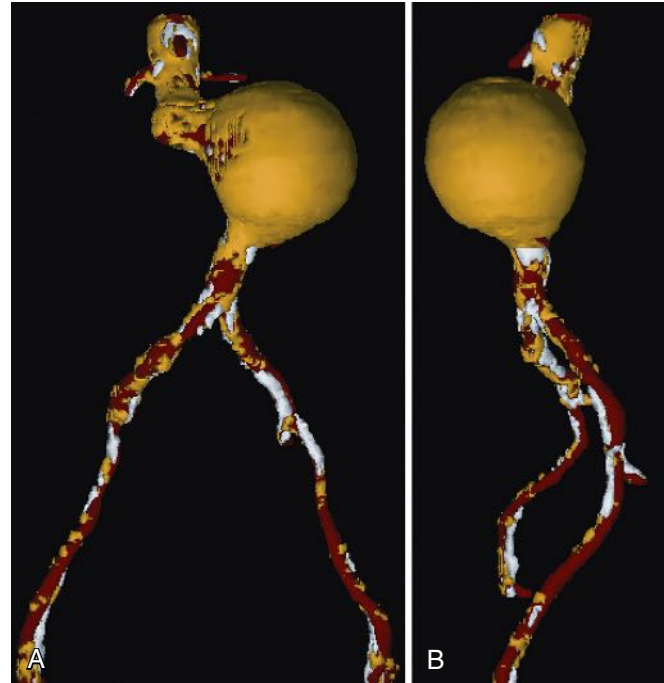


**Figure 29.7** Multiple-object shaded surface display, anteroposterior (**A**) and left lateral (**B**) views of an abdominal aortic aneurysm. Contrast-enhanced blood flow is displayed in red, thrombus and noncalcified plaque in yellow, and calcified plaque in white. In this type of three-dimensional reconstruction, all the components of the aneurysm are seen. The reconstruction can be rotated interactively, in all planes. This type of display is most helpful in determining the true extent of an aneurysm because thrombus is clearly visible.

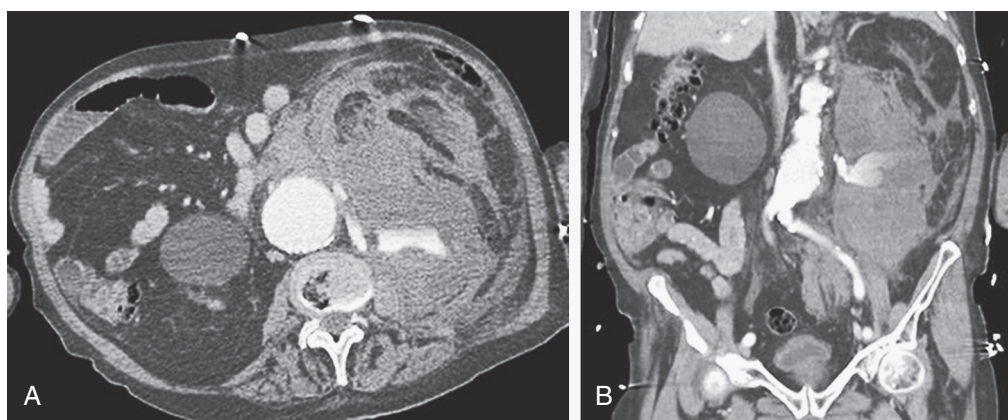


**Figure 29.8** Computed Tomographic Angiography of Ruptured Abdominal Aortic Aneurysm. (A) Axial view. (B) Coronal reconstruction.



**Figure 29.9** Anteroposterior maximum intensity projection (MIP) image of heavily calcified aortoiliac system, after placement of three covered stents in a CERAB-configuration (covered endovascular reconstruction of aortic bifurcation).

hooks and barbs or access arteries that may render endovascular repair difficult or impossible (Fig. 29.9). CTA is preferred over MRA when endovascular devices are in place because metal artifacts are rarely a problem.

### Peripheral Arterial Occlusive Disease

CTA and MRA are both excellent techniques to visualize the peripheral arteries. CTA has the advantage of fast acquisition and reproducibility. On the other hand, the newer MRA techniques do not need the use of contrast material.<sup>31</sup> CTA can be

used to image the arterial tree from the aorta through the pedal vessels in a single contrast-enhanced acquisition run. However, accurate timing of contrast injections is essential. The high resolution of CTA allows for accurate delineation of stenotic segments and planning for open and endovascular intervention. It has been shown to be highly accurate in imaging tibial artery runoff.<sup>32</sup> On the downside, interpretation of CTA images and reconstructions of small arteries (tibial vessels) can be very tedious, particularly the distinction between calcium and contrast. Overestimation of the severity of a calcified stenosis is common.<sup>32</sup> Carotid artery stenosis can be accurately defined by CTA. Although duplex-ultrasound imaging can be impeded by calcified plaques, the accuracy of CTA imaging of the carotid artery is hardly affected by calcium (Fig. 29.10). In addition, it can help differentiate occlusion from high-grade stenosis, and it provides better anatomic reference than duplex. CTA also provides the option of adjacent imaging of the aortic arch and intracranial arteries, which may be of help in the diagnosis and treatment of neurovascular disease.<sup>33</sup>

### Renal and Splanchnic Arterial Disease

CTA and MRA are comparable in sensitivity for the detection of proximal renal and splanchnic artery stenosis. However, if evaluation of more peripheral abnormalities is needed, MRA suffers significantly from respiratory movement of the abdominal organs.

The main benefit of MR for renal splanchnic artery imaging is the fact that contrast-induced renal nephropathy is avoided, although a limiting factor is the rare occurrence of interstitial fibrosis due to gadolinium in patients with renal failure. Valid alternatives include time of flight or comparable MR techniques that allow for flow imaging without the use of gadolinium; however, these techniques provide less optimal imaging quality.

### Venous Disease

Provided that a proper injection protocol with sufficient delay and contrast volume is chosen, CT is able to evaluate a variety of venous pathologies, including mesenteric venous

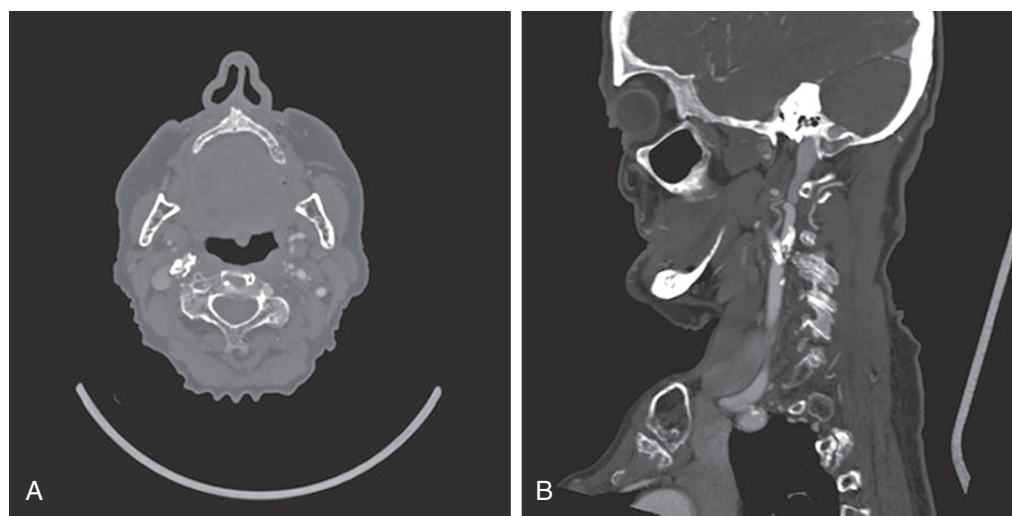


**Figure 29.10** Example of Carotid Artery Computed Tomographic Angiography Imaging. (A) Axial view. (B) Sagittal reconstruction.

thrombosis. For the evaluation and detection of pulmonary emboli, CT has replaced lung perfusion and ventilation studies. However, for peripheral evaluation of venous disease (in legs, iliac veins, subclavian veins), the optimal imaging modality is still duplex ultrasound because this also provides essential flow information. If cross-sectional imaging is required, MRV is an excellent alternative to CT.

### Vascular Malformations

The role of CTA in the evaluation of vascular malformations is limited. Only in cases of high-flow malformations (AVM, AVF) can CTA support a proper diagnosis; the extent and composition of the nidus cannot be adequately evaluated without the use of four-dimensional (4D) imaging. For low-flow malformations there is virtually no role for CT imaging. The limited soft tissue contrast and the extremely low-flow situation make a venous malformation very difficult to characterize with CT. Instead, ultrasound and MRI are the modalities of choice.

## LIMITATIONS AND RISKS

### Radiation Dose

The radiation dose of CT has attracted attention in the recent decade because of the increased frequency of use and recognition of cancer risks.<sup>34</sup> With the development of the new CT technology (spiral and multidetector), the initial hope was that the radiation dose to the patient could be decreased relative to the old single-slice sequential technique. It soon became apparent, however, that this would be true only if the less optimal image quality of the older technique (often 10-mm slices) were still acceptable. However, the advent of CTA, 3D reconstructions, and MPR has led to optimal use of the new technology, often with imaging at the smallest collimation possible to allow use of the advanced post-processing techniques. Furthermore, as image quality improved and the diagnostic value of CT became more apparent, an exponential growth in the number of

CT examinations occurred. As CT rapidly became a major diagnostic instrument, not all physicians ordering CT scans were aware of the long-term carcinogenic potential, particularly in the pediatric group. Additionally, large-scale screening programs for asymptomatic patients based on CT have emerged. The most well known are CT colonography, coronary calcification screening, CT lung screening, and whole-body screening.<sup>34</sup>

Although it is difficult to validate the calculated radiation risk data because they rely heavily on assumptions based on follow-up data from atomic bomb survivors, it is estimated that between 1991 and 1996, 0.4% of all cancers in the United States were attributable to CT studies. As a result of the increased use of CT in the last decade, this figure has increased to 1.5%–2%.<sup>34</sup> Awareness of the potentially harmful side effects of radiation is important and should play an important role in the clinical decision of whether to order a CT scan, particularly in children. In addition, radiation risk should influence the choice of parameter settings and scan protocol.

### Contrast-Induced Nephropathy

Contrast nephropathy has long been considered as an important cause of iatrogenic acute renal failure.<sup>35</sup> This has led to large-scale programs to prevent this entity. During the last years, the debate on less strict criteria for CIN prevention has emerged.<sup>36</sup> However, final conclusions have not yet been drawn. Nephrotoxicity of contrast agents, contrast-induced nephropathy, associated risk factors, prevention, and alternative imaging options are described in detail in Chapter 27 (Arteriography).

## COMMON ARTIFACTS

### Partial-Volume Effects

*Partial volume* refers to a situation in which objects are only partly included within the scan plane. The resulting image simulates a lesion where none exists. A good example of this effect is, for instance, the appearance of a “nonexistent” lung

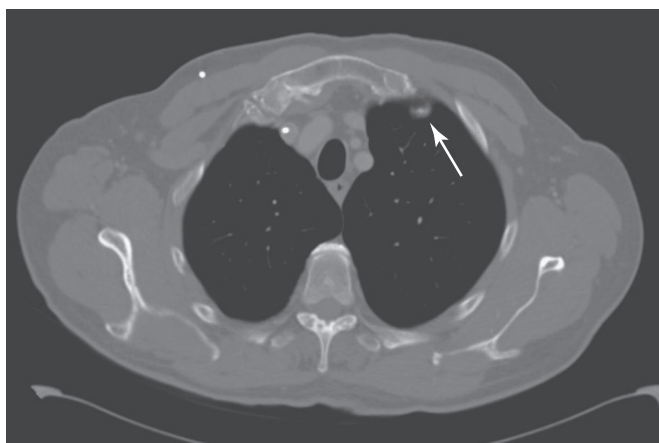


**Figure 29.11** Example of a partial-volume effect, here responsible for the appearance of a nonexistent “lung nodule” adjacent to the anterior attachment of the first rib (arrow).

nodule adjacent to the anterior attachment of the first rib (Fig. 29.11).

### Beam-Hardening Artifacts

Streak artifact or scatter artifact arises from interfaces between materials with large differences in density from the surrounding structures. This artifact is commonly seen with dense materials such as prosthetic hips or metallic stents in endografts. Different materials cause varying levels of artifact. Tantalum and gold stents cause significant beamlike artifacts, whereas platinum has almost no influence on the image. Steel lies in the middle of the spectrum. These artifacts can result in the erroneous interpretation of vessel lumen narrowing – sometimes by 25% to 50%. Tantalum and gold cause few effects on MRI images. Knowledge of the type of stent helps determine the preferable imaging modality.<sup>37,38</sup> Scatter also can occur as a result of dense intravenous contrast material in the subclavian or brachiocephalic veins because dense contrast is often infused rapidly into these veins during the scan. If the aortic arch vessels are the focus of the CT scan, the contrast agent should be infused into the arm opposite the vessel of interest or into the inferior vena cava.

Beam-hardening artifacts can also be seen if both arms are left alongside the body while scanning the chest. To avoid these artifacts, the patient should be positioned with at least one arm, preferably both arms, above the head (see Fig. 29.2), or iterative reconstruction should be used. Another way to reduce this type of artifact is by using metal reducing reconstruction algorithms.

### Motion Artifacts

Different types of motion artifact exist, but the most pronounced is due to movement of the patient during the scan. Other well-known motion artifacts are respiratory and pulsation artifacts. The degree of degradation of the resulting image depends on the degree of movement and ranges from a double contour to double visibility of the body. To avoid respiratory artifacts in dyspneic patients, the general recommendation is to

ask these patients to *not* hold their breath during scanning, because this will often result in a sudden deep inhalation during the scan and subsequent severe motion artifacts and less contrast enhancement. Instead, the patient should be requested to maintain shallow respiration.

### Other Common Artifacts

*Averaging artifact* has already been mentioned with regard to “missing” a small vessel because of surrounding soft tissue, but it can also work in the opposite fashion. In this type of artifact, comparable to partial volume artifacts, the large attenuation from a small piece of calcified plaque within a CT slice “averages” with thrombus-density material to produce a display with an intermediate density – similar to intraluminal contrast. This artifact often occurs within aortic aneurysms and should be suspected when contrast-density material appears with no apparent inflow or outflow vessel and when a piece of calcium or metal is nearby. This type of artifact is reduced by using a small reconstruction interval.

*Stair-step artifact* occurs when the reconstruction interval on a spiral CT scan is too large and a stepped appearance in the vessels is created. This artifact is most likely to occur in vessels oriented away from the z-direction of the scan (e.g., renal or iliac arteries). If such an appearance is noted in a multiplanar reformat, it is difficult to evaluate potential occlusive disease. Some of these artifacts are shown in Figure 29.12.

A number of scanner-related artifacts are also possible. Most are related to scanner malfunction, improper calibration (ring artifacts), tube malfunction, or detector malfunction.

Finally, window and level setting errors affect the ability to visualize contrasting objects. A window setting too narrow will result in a significant increase in visible noise that will degrade the visualization of fine structural details, whereas a window too wide will abolish small differences in contrast.

## SPECIAL PEDIATRIC CONSIDERATIONS

CT scanning should be avoided in the pediatric age group, if at all possible, to avoid the radiation exposure. Alternative imaging techniques, such as ultrasound and MR, can often replace CT. If CT is necessary, strict adherence to the As Low As Reasonable Achievable (ALARA) principle must guide selection of the scan parameters that determine the radiation dose relative to the image quality. A lower image quality can and should be accepted if this is sufficient for a proper diagnosis.

## FUTURE ADVANCES

4D imaging will be incorporated further into clinical practice, and diffusion and perfusion imaging could become an integral part in the evaluation of many organs (e.g., renal transplants). Improved detector designs (with higher-detection quantum efficiency and lower noise levels) combined with noise-reduction iterative algorithms will lower the radiation dose significantly.

Computer-aided diagnostic programs will further expand and be used to assist the clinician in evaluating the huge data sets currently being produced by 256 (or more) slice scanners.

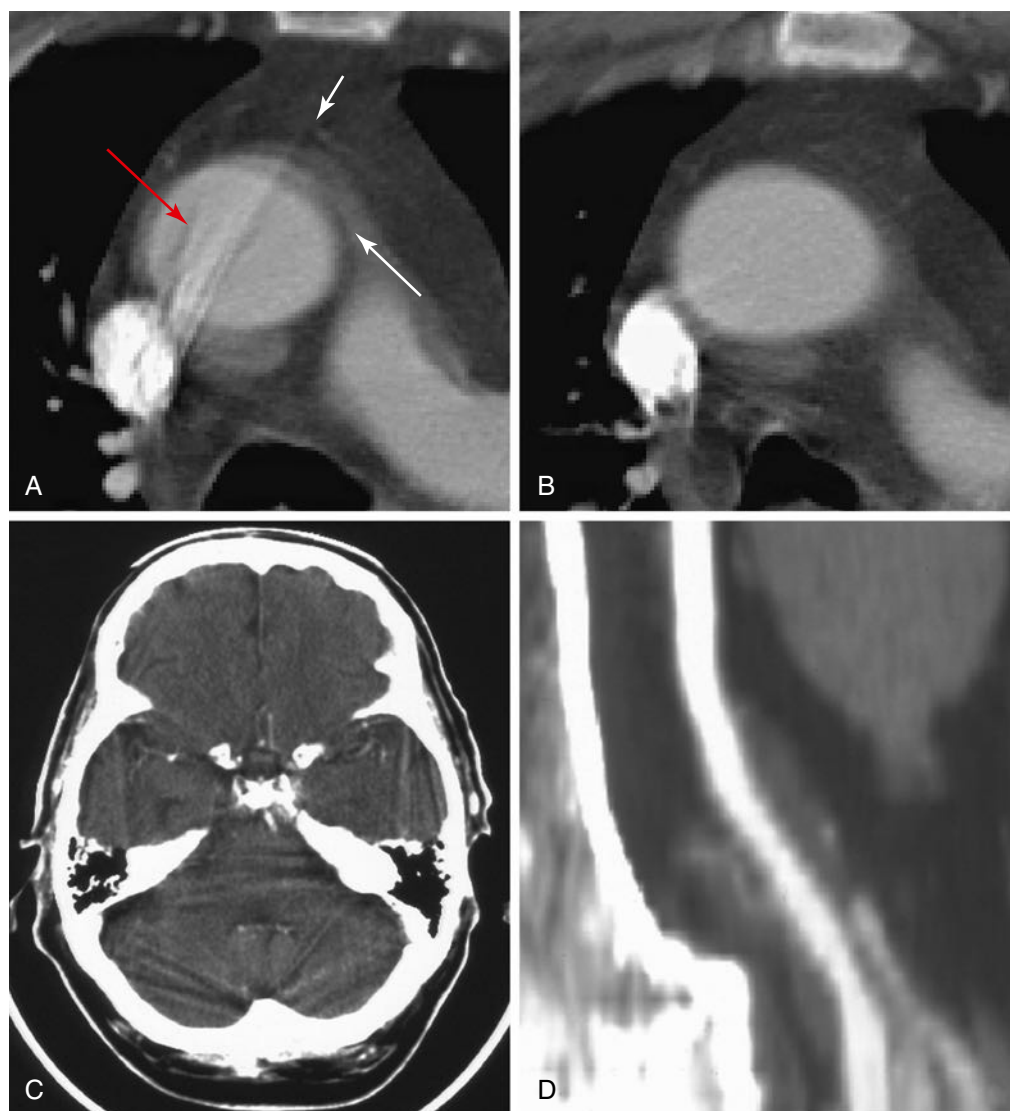


**Figure 29.12** Computed Tomography (CT) Artifacts. (A) Motion artifact in the thoracic aorta creating the impression of an intimal flap or dissection (*long arrow*). The position of these artifacts is usually due to aortic motion from the left anterior to the right posterior position. Streak artifact is also seen arising from dense contrast within the superior vena cava. The longer streak is clearly artifact because it extends beyond the vessel wall (*short arrow*), but the shorter streak could be misinterpreted as an intimal flap (*red arrow*). One clue is the appearance of an obvious streak artifact in the same vessel. Another clue is the interface between structures with large differences in density. Other clues to the true nature of the aorta come from the benign patient history and the immediately adjacent CT slice. (B) The apparent pathology (artifact) shown in A is not present in this immediately adjacent CT slice. (C) An intracranial streak artifact can make it difficult to detect infarcts in locations surrounded by dense bone. Beam-hardening artifact is also common on head CT and occurs when low-energy portions of the X-ray beam are absorbed by thick, dense structures, such as the skull. The residual beam that proceeds through the dense bone has higher energy and may cause a small area of adjacent tissue to appear less dense (darker) than it should be. This can create an artifact resembling an ischemic infarct immediately adjacent to the skull. (D) A stair-step artifact creates a stepped appearance in the vessel (see text). This artifact is unique to spiral or helical CT.

## Computed Tomography Versus Duplex Ultrasound and Magnetic Resonance

Duplex ultrasound is a noninvasive technique and an excellent screening modality in patients with PAOD. However, duplex ultrasound is hampered by the fact that it is operator-dependent and of limited value in patients with heavily calcified arteries or extensive, multilevel disease.

Also, evaluation of the abdominal and pelvic vessels can be quite challenging in the obese patient. In the era of progressive application of endovascular techniques, detailed pre-treatment information is essential, and duplex ultrasound alone frequently fails in that respect because of the previously described limitations. CTA and MRA each have their own pros and cons. CTA is an excellent modality for the evaluation of the aorta in case of endovascular treatment

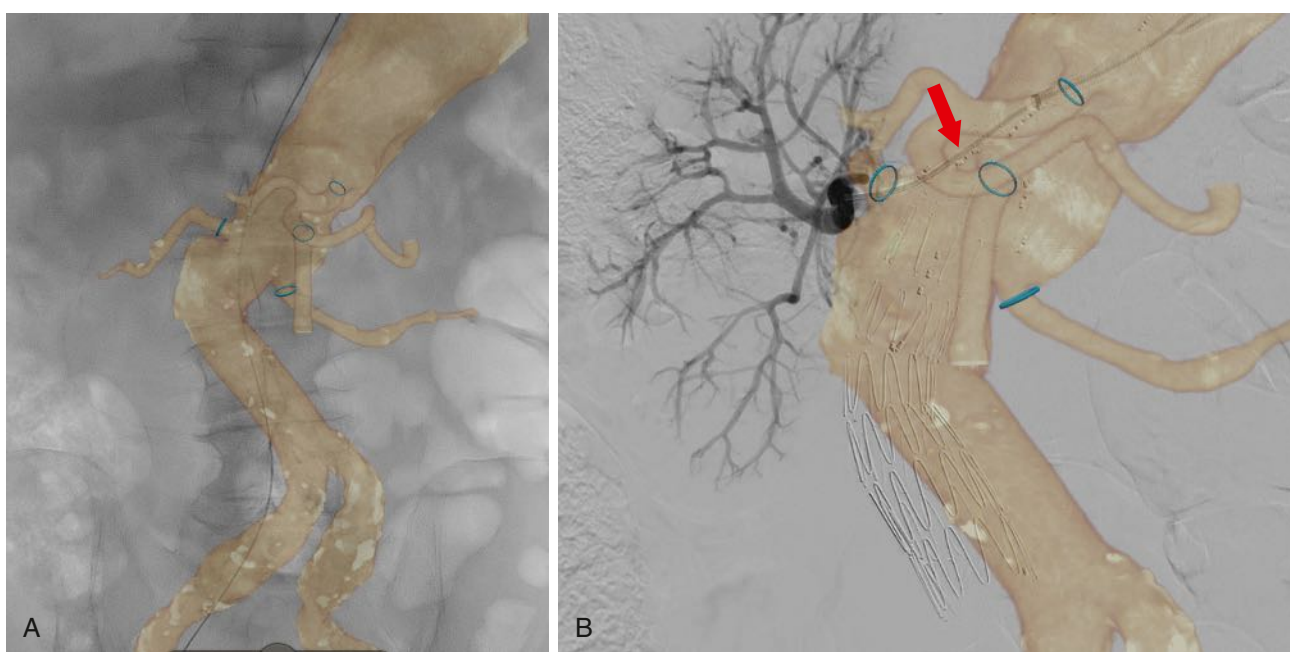


**Figure 29.13** (A) Intraoperative image fusion: plain abdominal fluoroscopy image with stiff guidewire from right common femoral artery into abdominal aorta with a superimposed transparent shaded surface display obtained from segmenting the aortoiliac, splanchnic and renal anatomy in the preprocedural CTA dataset. The guide-wire runs outside the overlay because it straightens the aortic tortuosity (real-time) relative to the preprocedural CTA image. The blue rings indicate the orifices of the relevant branches. (B) Image from a later stage in this procedure, with a branched endograft *in situ*, a catheter passing the right renal artery endograft side branch (arrow) engaging the native proximal right renal artery, and a flush renal angiogram.

and provides detailed and often essential information on calcification in the access arteries and in the wall at the level of landing zones for endografts. MRA is, in this respect, less useful because of its limited ability to visualize calcium. On the other hand, if information about tibial arteries is required, MRA is preferable over CTA because the presence of heavy calcifications in small vessel walls hampers the evaluation of the CTA.

### Fusion Imaging

Although the quality of periprocedural imaging in the operating theater is rapidly improving, detailed preprocedural imaging supported by intraoperative navigation tools is essential to avoid lengthy procedures and high radiation doses. Fusion imaging is an intraoperative tool for three-dimensional (3D) guidance in endovascular aneurysm repair (Fig. 29.13).<sup>39</sup>

The CT overlay technique allows preprocedural CT scans to be projected over the fluoroscopy images when performing an angiogram. For this purpose the preprocedural CT linked with fluoroscopic images using bony landmarks by two two-dimensional (2D) images (acquired at two different angles). This is called 2D-3D registration as opposed to registration using intraoperative cone-beam CT (3D-3D registration). This form of image fusion improves endovascular therapy by reducing: (1) radiation exposure to patients and practitioners; (2) the amount of injected contrast material; and (3) the duration of the procedure.<sup>40</sup>

### Positron Emission Tomography with Computed Tomography

Use of positron emission tomography (PET) in concert with CT combines valuable physiologic information from the PET scanner with anatomic information from CT. In oncology imaging, PET/CT is one of the major evaluation tools for detection of malignancy and inflammation. PET/CT might play a role in vascular imaging for the detection of infected grafts, aortitis and vasculitis. Furthermore, growing evidence indicates that PET/CT may have additional value in identifying inflammatory responses in atherosclerotic plaque, which may allow noninvasive assessment of disease activity.<sup>41,42</sup> In Chapter 31 (Vascular PET/CT and SPECT/CT), vascular nuclear imaging is described in detail.

### ACKNOWLEDGMENT

Leo Schultze Kool, Monique Brink, Gijs Bloemsma, and Maarten Truijers are greatly acknowledged for their help in preparing this chapter.

### SELECTED KEY REFERENCES

- Brenner DJ, Hall DJ. Computed tomography – an increasing source of radiation exposure. *N Engl J Med.* 2007;357:2277–2284.  
*Report on the increasing risk of radiation exposure with the modern CT systems.*
- Hounsfield GN. Computerized transverse axial scanning (tomography). 1. Description of system. *Br J Radiol.* 1973;46:1016–1022.  
*The first description of the CT principle.*

Oudemans-van Straaten HM. Contrast nephropathy, pathophysiology and prevention. *Int J Artif Organs*. 2004;27:1054–1065.

*Good overview on contrast-induced nephropathy.*

Primak AN, McCollough CH, Bruesewitz MR, et al. Relationship between noise, dose, and pitch in cardiac multi-detector row CT. *Radiographics*. 2006;26:1785–1794.

*Excellent overview article describing the relationship between noise, dose, and pitch in multidetector row CT.*

Thomsen HA, Morcos SK. Contrast media and the kidney: European Society of Urogenital Radiology (ESUR) Guidelines. *Br J Radiol*. 2003;76:513–518.

*European Society of Urogenital Radiology Guidelines on the use of contrast media.*

A complete reference list can be found online at [www.expertconsult.com](http://www.expertconsult.com).

## REFERENCES

1. Hingorani A, Ascher E, Marks N. Preprocedural imaging: new options to reduce need for contrast angiography. *Semin Vasc Surg.* 2007;20:15–28.
2. Simoni G, Perrone R, Cittadini Jr G, et al. Helical CT for the study of abdominal aortic aneurysms in patients undergoing conventional surgical repair. *Eur J Vasc Endovasc Surg.* 1996;12:354–358.
3. Wyers MC, Fillinger MF, Schermerhorn ML, et al. Endovascular repair of abdominal aortic aneurysm without preoperative arteriography. *J Vasc Surg.* 2003;38:730–738.
4. Grassbaugh JA, Nelson PR, Rzucidlo EM, et al. Blinded comparison of preoperative duplex ultrasound scanning and contrast arteriography for planning revascularization at the level of the tibia. *J Vasc Surg.* 2003;37:1186–1190.
5. Back MR, Rogers GA, Wilson JS, et al. Magnetic resonance angiography minimizes need for arteriography after inadequate carotid duplex ultrasound scanning. *J Vasc Surg.* 2003;38:422–430.
6. Collins R, Burch J, Cranny G, et al. Duplex ultrasonography, magnetic resonance angiography, and computed tomography angiography for diagnosis and assessment of symptomatic, lower limb peripheral arterial disease: systematic review. *BMJ.* 2007;334:1257.
7. Hounsfield GN. Computerized transverse axial scanning (tomography). 1. Description of system. *Br J Radiol.* 1973;46:1016–1022.
8. Prokop M. CT angiography of the abdominal arteries. *Abdom Imaging.* 1998;23:462–468.
9. Wintersperger BJ, Nikolaou K, Becker CR. Multidetector-row CT angiography of the aorta and visceral arteries. *Semin Ultrasound CT MR.* 2004;25:25–40.
10. Kanematsu M, Goshima S, Kondo H, Bae KT. How should we optimize bolus tracking with multidetector CT of the abdomen? *Radiology.* 2008;246(2):643.
11. Knez A, Becker CR, Leber A, et al. Usefulness of multislice spiral computed tomography angiography for determination of coronary artery stenoses. *Am J Cardiol.* 2001;88:1191–1194.
12. Kachelriess M, Ulzheimer S, Kalender WA. ECG-correlated imaging of the heart with subsecondmultislice spiral CT. *IEEE Trans Med Imaging.* 2000;19:888–901.
13. Roberts WT, Bax JJ, Davies LC. Cardiac CT and CT coronary angiography: technology and application. *Heart.* 2008;94:781–792.
14. Ibukuro K, Charnsangavej C, Chasen MH, et al. Helical CT angiography with multiplanar reformation: techniques and clinical applications. *Radiographics.* 1995;15:671–682.
15. Fillinger MF, Racusin J, Baker RK, et al. Anatomic characteristics of ruptured abdominal aortic aneurysm on conventional CT scans: implications for rupture risk. *J Vasc Surg.* 2004;39:1243–1252.
16. Parker MV, O'Donnell SD, Chang AS, et al. What imaging studies are necessary for abdominal aortic endograft sizing? A prospective blinded study using conventional computed tomography, aortography, and three-dimensional computed tomography. *J Vasc Surg.* 2005;41:199–205.
17. Riccabona M, Nelson TR, Pretorius DH, Davidson TE. In vivo three-dimensional sonographic measurement of organ volume: validation in the urinary bladder. *J Ultrasound Med.* 1996;15:627–632.
18. Wheatley JM, Rosenfield NS, Heller G, et al. Validation of a technique of computer-aided tumor volume determination. *J Surg Res.* 1995;59:621–626.
19. Bargellini I, Cioni R, Petrucci P, et al. Endovascular repair of abdominal aortic aneurysms: analysis of aneurysm volumetric changes at mid-term follow-up. *Cardiovasc Intervent Radiol.* 2005;28:426–433.
20. Wever JJ, Blankenstein JD, Mali WP, Eikelboom BC. Maximal aneurysm diameter follow-up is inadequate after endovascular abdominal aortic aneurysm repair. *Eur J Vasc Endovasc Surg.* 2000;20:177–182.
21. Fillinger MF. New imaging techniques in endovascular surgery. *Surg Clin North Am.* 1999;79:451–475.
22. Lee JT, Aziz IN, Lee JT, et al. Volume regression of abdominal aortic aneurysms and its relation to successful endoluminal exclusion. *J Vasc Surg.* 2003;38:1254–1263.
23. White RA, Donayre CE, Walot I, et al. Computed tomography assessment of abdominal aortic aneurysm morphology after endograft exclusion. *J Vasc Surg.* 2001;33(2 suppl):S1–S10.
24. Prinzen M, Verhoeven EL, Verhagen HJ, Blankenstein JD. Decision-making in follow-up after endovascular aneurysm repair based on diameter and volume measurements: a blinded comparison. *Eur J Vasc Endovasc Surg.* 2003;26:184–187.
25. Pollock JG, Travis SJ, Whitaker SC, et al. Endovascular AAA repair: classification of aneurysm sac volumetric change using spiral computed tomographic angiography. *J Endovasc Ther.* 2002;9:185–193.
26. Torsello GB, Klenk E, Kasprzak B, Umscheid T. Rupture of abdominal aortic aneurysm previously treated by endovascular stentgraft. *J Vasc Surg.* 1998;28:184–187.
27. Lee LK, Faries PL. Assessing the effectiveness of endografts: clinical and experimental perspectives. *J Vasc Surg.* 2007;45(suppl):A123–A130.
28. Balm R, Kaatee R, Blankenstein JD, et al. CT-angiography of abdominal aortic aneurysms after transfemoral endovascular aneurysm management. *Eur J Vasc Endovasc Surg.* 1996;12:182–188.
29. Qanadli SD, Mesurolle B, Coggia M, et al. Abdominal aortic aneurysm: pretherapy assessment with dual-slice helical CT angiography. *AJR Am J Roentgenol.* 2000;174:181–187.
30. Broeders IA, Blankenstein JD. Preoperative imaging of the aortoiliac anatomy in endovascular aneurysm surgery. *Semin Vasc Surg.* 1999;12:306–314.
31. Ouwendijk R, de Vries M, Stijnen T, et al. Multicenter randomized controlled trial of the costs and effects of noninvasive diagnostic imaging in patients with peripheral arterial disease: the DIPAD trial. *AJR Am J Roentgenol.* 2008;190:1349–1357.
32. Anzidei M, Napoli A, Zaccagna F, et al. Diagnostic accuracy of colour Doppler ultrasonography, CT angiography and blood-pool-enhanced MR angiography in assessing carotid stenosis: a comparative study with DSA in 170 patients. *Radiol Med.* 2012;117:54–71.
33. Brenner DJ, Hall DJ. Computed tomography - an increasing source of radiation exposure. *N Engl J Med.* 2007;357:2277–2284.
34. Soma VR, Cavusoglu E, Vidhun R, et al. Contrast-associated nephropathy. *Heart Dis.* 2002;4:372–379.
35. McDonald RJ, McDonald JS, Newhouse JH, Davenport MS. Controversies in contrast material-induced acute kidney injury: closing in on the truth? *Radiology.* 2015;277(3):627–632.
36. Gawenda M, Gossmann A, Kruger K, et al. Comparison of magnetic resonance imaging and computed tomography of 8 aortic stent-graft models. *J Endovasc Ther.* 2004;11:627–634.
37. Siewerssen JH, Moseley DJ, Burch S, et al. Volume CT with a flat-panel detector on a mobile, isocentric C-arm: pre-clinical investigation in guidance of minimally invasive surgery. *Med Phys.* 2005;32:241–254.
38. Ogawa M, Ishino S, Mukai T, et al. (18)F-FDG accumulation in atherosclerotic plaques: immunohistochemical and PET imaging study. *J Nucl Med.* 2004;45:1245–1250.
39. Defawe OD, Hustinx R, Defraigne JO, et al. Distribution of F-18 fluorodeoxyglucose (F-18 FDG) in abdominal aortic aneurysm: high accumulation in macrophages seen on PET imaging and immunohistology. *Clin Nucl Med.* 2005;30:340–341.
40. Wu G, et al. The diagnostic value of non-contrast enhanced quiescent interval single shot (QISS) magnetic resonance angiography at 3T for lower extremity peripheral arterial disease, in comparison to CT angiography. *J Cardiovasc Magn Reson.* 2016;18(1):71.
41. Schulz CJ, et al. Two-dimensional-three-dimensional registration for fusion imaging is noninferior to three-dimensional-three-dimensional registration in infrarenal endovascular aneurysm repair. *J Vasc Surg.* 2019;70(6):2005–2013.
42. Stangenber L, Marc LS, et al. A novel tool for three-dimensional roadmapping reduces radiation exposure and contrast agent dose in complex endovascular interventions. *J Vasc Surg.* 2015;62(2):448–455.

# Magnetic Resonance Imaging and Arteriography

JEFFREY P. CARPENTER, HAROLD LITT, and MAMATHA GOWDA

## BASIC PRINCIPLES 366

- Characteristics of MR Images 367
- Magnetic Resonance Pulse Sequences 367
- Pulse Sequence Parameters 367
- MR Angiography and Venography 367
  - Noncontrast-Enhanced MR Angiography 367
  - Contrast-Enhanced MR Angiography 368
  - Step-Table and Continuous-Table MR Angiography 368
  - Three-Dimensional Image Processing 369
  - Hardware and Software for MR Angiography 370
  - 1.5- vs. 3-TESLA MRI 370
- OTHER HARDWARE AND SOFTWARE 370

## CLINICAL APPLICATIONS OF MR ANGIOGRAPHY 370

- Aortic Vascular Disease 370
- Carotid Vascular Disease 370
- Peripheral Vascular Disease 371
- Renovascular Disease 372
- Mesenteric Vascular Disease 373
- Venous Vascular Disease 373
- Other Applications 373
- LIMITATIONS AND RISKS 375
- Scan Artifacts 375

## Fat Saturation in Chest MR Angiography 375

- Susceptibility Artifact from Concentrated Gadolinium 376
- Susceptibility Metal Artifacts 377
- High Intravascular Signal from Thrombus Containing Methemoglobin 377
- Contraindications to MRI 377
  - Renal Disease and Nephrogenic Systemic Fibrosis 377
  - Pacemakers and Other Implanted Devices 379
  - Vascular Stents, Filters, and Coils 383

## FUTURE ADVANCES 384

- Continuous Moving Table and Time-Resolved MRA 384
- Novel Contrast Agents 385
- Imaging of Blood Flow 386
- Plaque Imaging 386
- Computed Tomographic Angiography vs. Magnetic Resonance Angiography 388
  - Acquisition Speed 388
  - Dynamic Imaging 388
  - Calcification and Other Imaging Artifacts 388
- Radiation Dose and Contrast Concerns 390
- Ease of Use and Convenience 390

## **BASIC PRINCIPLES**

Magnetic resonance imaging (MRI) is performed using a large external magnetic field, magnetic field gradients, and an applied oscillating magnetic field known as the radiofrequency field (RF). The combination of these three applied magnetic fields produces signals from inside tissue that can be used to create MR images.

The details of the external magnetic field, gradients, and RF determine many of the characteristics of MR images. The external magnetic field magnetizes the subject by making the protons align parallel with the external field. The physical characteristics of the protons and the size of the external magnetic field define

the resonance frequency. If the external magnetic field is uniform, all the protons will resonate at the same frequency. Most MRI machines operate at an external field strength of 1.5 or 3 Tesla (T); potential advantages of 3T magnetic resonance angiography (MRA) are discussed later in the chapter. Lower field systems tend to produce images at a slower rate or at a lower resolution than needed for MRA. Recently, 7-Tesla systems have been approved for clinical use in the head and extremities, but they are not currently approved for angiographic imaging.

Magnetic field gradients alter the uniform external magnetic field in a linear fashion in any of three directions. The gradients ramping on and off produce the noise heard when an MR image is being made.

The gradient fields cause protons to resonate at a frequency that is a function of the magnetic field gradient's position, analogous to a radio station's frequency corresponding to a specific position on the dial. The speed and strength of the gradients determine the size of the images and may be a limiting step in imaging speed.

Resonant coils placed either within the bore of the system or adjacent to the region of interest produce the RF. These fields are tuned to match the resonant frequency of the protons inside the patient. The applied RF in combination with the gradients are used to manipulate the protons inside the patient to produce a signal. This signal is detected by a receiver RF coil, also tuned to the resonant frequency of the protons. Once detected, the signal is sent to an amplifier and receiver, where it is digitized and processed with a mathematical algorithm known as a Fourier transform to produce the MR image.

## Characteristics of MR Images

Contrast in MR images depends on characteristics of the object being imaged and specifics of the acquisition process. Images are typically referred to as either T1 weighted or T2 weighted. T2-weighted images display simple fluids such as urine, bile, or cerebrospinal fluid as bright and other tissues as lower signal. T2-weighted imaging is one of the basic sequences for imaging of tumors but is not typically used for angiographic imaging. MRA and MR venography (MRV) are generally performed with T1-weighted image sequences. Objects that are bright on T1-weighted images, including fat, methemoglobin, flow effects, and MRI contrast, will often be bright on MRA sequences.

## Magnetic Resonance Pulse Sequences

An MR pulse sequence is a combination of RF and gradients that are used to create an image. There are many types, but most are variations of spin-echo or gradient-echo sequences. Spin-echo sequences use RF alone to produce the MR signal, whereas gradient-echo sequences use RF and applied gradients. As a rough generalization, spin-echo sequences are used to produce T1- or T2-weighted images while gradient-echo sequences can only create T1-weighted images.

## Pulse Sequence Parameters

The tissue characteristics that determine its MR appearance are the T1 and T2 parameters of the tissue. Some tissues are bright on T1-weighted images whereas others are bright on T2-weighted images. All pulse sequences have fundamental parameters known as echo time (TE) and repetition time (TR) that determine image contrast. T2-weighted images have a longer TE, in the range of 80 ms or greater, and a longer TR, in the range of several seconds. Given the long TE and TR, these sequences are slower and not appropriate for contrast-enhanced MRA. T1-weighted images, however, have a very short TR and TE, with a TE of 1 ms or less and a TR from hundreds of milliseconds to less than 10 ms for MRA sequences.

Fast T1-weighted gradient-echo sequences are used for most contrast-enhanced MRA imaging.

Other parameters include the field of view (FOV) and image matrix. FOV is the size of the imaged region. In a two-dimensional (2D) image, FOV may be  $40 \times 30$  cm with a slice thickness of 5 mm. The resolution of the image in the 5-mm slice depends on the number of pixels within the  $40 \times 30$ -cm region. Most MRA imaging, however, is performed with a three-dimensional (3D) sequence and a FOV specified with three dimensions, such as  $40 \times 30 \times 30$  cm. An image matrix of  $256 \times 192 \times 64$  will result in a voxel (or 3D pixel) size of  $1.56 \times 3.26 \times 4.7$  mm. Post-processing is usually performed to make the last dimension twice as small as specified by the pulse sequence. In this case, yielding a voxel size of  $1.56 \times 3.26 \times 2.35$  mm.

## MR Angiography and Venography

### Noncontrast-Enhanced MR Angiography

Noncontrast-enhanced MRA, such as time-of-flight (TOF) imaging, has largely been supplanted by contrast-enhanced methods.<sup>1–5</sup> However, the risk of nephrogenic systemic fibrosis (NSF) in patients with poor renal function who have received gadolinium-based contrast agents (GBCA)<sup>6,7</sup> (see “Contrast-Enhanced MR Angiography” below for further details) has led to renewed interest in noncontrast techniques.

TOF angiography uses a rapid T1-weighted pulse sequence in sequentially acquired 2D slices or a 3D imaging slab, causing loss of signal within the slice or slab. Fully magnetized protons in vessels flow into the slice or slab, producing higher signal than stationary tissue, resulting in an image in which flowing blood appears much brighter than surrounding tissue. For example, in an axial slice through the mid abdomen, the aorta and inferior vena cava (IVC) as well as the mesenteric arteries and veins would appear bright. To remove either the arteries or veins, a special RF pulse is applied either above or below the slice to eliminate signal from that tissue. If an inferior saturation pulse were used, only the protons flowing into the slab from above (the aorta and mesenteric arteries) would appear bright, while with a superior pulse, only protons flowing from below (inferior vena cava) would appear bright. A series of such images obtained sequentially produces a 2D TOF abdominal MRA.

Additional noncontrast MRA techniques include electrocardiogram (ECG) gated steady-state free precession (SSFP), ECG gated arterial spin labeling (ASL), navigator gated SSFP, and half-Fourier fast spin-echo imaging (HASTE) with flow-spoiled gradients.<sup>8</sup> These use different methods to accentuate signal of flowing blood and attenuate signal from nonmoving structures and tissue with signal characteristics different from blood. The SSFP technique, for example, provides rapid imaging of both large and small vessels, such as the aorta,<sup>9,10</sup> carotids,<sup>11</sup> and renal arteries,<sup>12</sup> without the need for a contrast agent.

Fresh blood imaging (FBI) relies on the signal difference between systolic and diastolic triggered acquisitions. The arterial signal in systole is dark due to spin-dephasing effects of fast arterial flow, whereas venous blood is bright throughout the cardiac cycle because of constant slow flow.<sup>12</sup> By applying

flow-spoiling pulses, arteries can be separated from veins in the peripheral run-off vessels.<sup>13,14</sup> Two alternative approaches using SSFP sequences include flow-sensitive dephasing (FSD) and quiescent-interval single-shot (QISS). QISS MRA is performed using a 2D ECG-gated single-shot SSFP acquisition; initial saturation pulses suppress in-plane background tissues and venous inflow. Advantages of QISS are short acquisition times and ease of use, allowing imaging of fast-flowing vessels



**Figure 30.1** Oblique sagittal noncontrast-enhanced steady-state free precession MR angiogram of the thoracic aorta. The signal from flowing blood appears bright.

such as the aorta and renal arteries, however this technique requires magnetic field homogeneity.<sup>8</sup> Figures 30.1–30.3 show examples of noncontrast MRA acquired using different techniques. Evaluation is ongoing<sup>8</sup>; however, these techniques of image acquisition may replace contrast-enhanced MRA in many circumstances.

### Contrast-Enhanced MR Angiography

MR contrast agents currently approved by the Food and Drug Administration (FDA) include several in which the rare earth element gadolinium is chelated with another substance to avoid release of toxic free gadolinium into the body. These agents shorten the T1 of protons in the vicinity, making them more conspicuous on T1-weighted imaging sequences. There are several important differences between MR contrast and iodinated contrast used for computed tomographic angiography (CTA) or standard angiography. First, as suggested, MRI is designed not to image the agent itself but its effect on protons in the surrounding water. One implication of this is that a very small amount of MR contrast material may be detected by its effect on multiple water molecules, whereas an equivalently small amount of iodinated contrast is simply not detectable directly by CTA or standard angiography. This is one reason that the volume of MR contrast can be much less than that of iodinated contrast used for CTA or angiography. Other advantages of gadolinium-based contrast include decreased nephrotoxicity and a lower incidence of contrast reactions.<sup>15–19</sup>

### Step-Table and Continuous-Table MR Angiography

For imaging a large volume, such as the entire aorta or peripheral arterial runoff, acquisition of the entire volume at once is impractical and may lead to decreased image quality. Image spatial resolution is inversely proportional to the matrix size, and matrix size directly impacts scan duration, so a higher resolution image requires a longer time to acquire. If the FOV

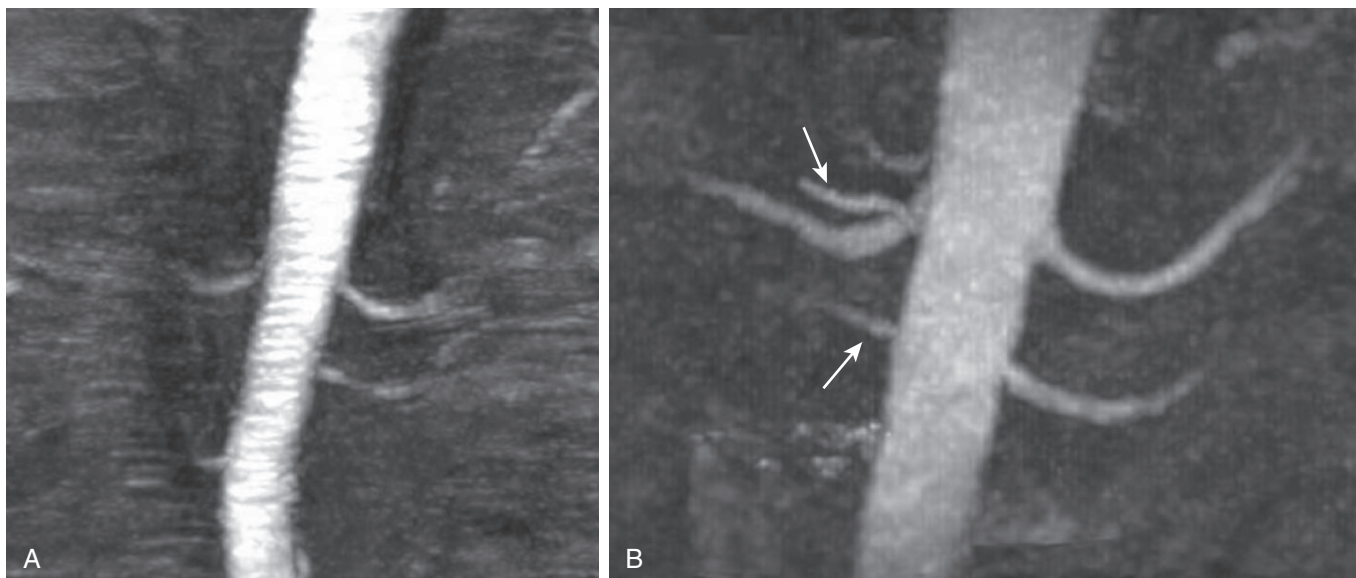


**Figure 30.2** (A) Coronal MIP of time-of-flight MRA of the renal arteries. (B) Coronal MIP of noncontrast MRA acquired with a newer method that uses ECG gating to subtract diastolic from systolic images, leaving only arterial systolic flow. Note markedly improved visualization of accessory right renal arteries compared to TOF technique (arrows).

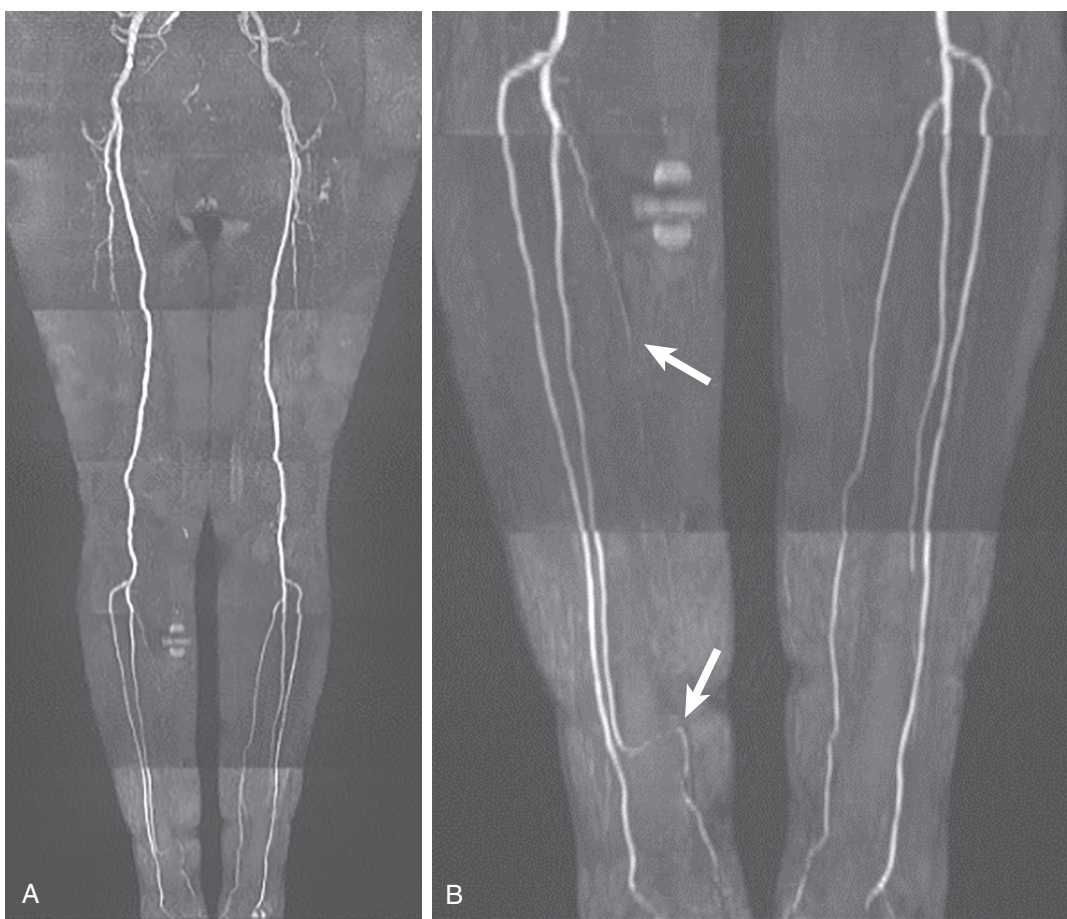


**Figure 30.3** (A) Coronal MRA of the lower extremities acquired using the QISS technique. (B) Zoomed-in view of the calves demonstrates occluded right posterior tibial artery and collaterals around the ankle (*arrows*).

is very large, the acquisition time required to achieve the necessary spatial resolution for visualization of the vessels of interest may be beyond the breath-holding capacity of the patient and can lead to respiratory motion artifact. In addition, intravenously administered contrast will flow from the aortic root to distal vessels in a time dependent on the rate and volume of injection, the patient's cardiac output, and the presence of any proximal occlusive disease; thus, not all portions of the arterial system will enhance optimally at the same time. For these reasons, it is desirable to use a step-table acquisition in which portions of the anatomy of interest are imaged sequentially, with the scanner table moving between stations to place the specific anatomy of interest near the isocenter of the magnet.

A peripheral runoff imaging study may include four step-table stations – abdomen/pelvis, thighs, calves, and feet – each imaged with a coil, FOV, spatial resolution, and orientation optimized to the vascular anatomy in that station. For example, the abdominal and pelvic vessels may best be imaged in the coronal plane with a larger FOV and a large array coil, while smaller pedal vessels would optimally be acquired in an oblique plane oriented along the foot, with a small FOV, high spatial resolution, and smaller coils for an improved signal-to-noise ratio (SNR). Although step-table examinations are generally performed in a proximal-to-distal direction, there may be circumstances in which a “reverse step-table” protocol is

preferable, for example, for a patient with known abdominal aortic pathology in whom there is less suspicion of thoracic aortic disease. In this case, the abdominal aorta could be imaged first, in the coronal plane, followed by the thoracic aorta, imaged in a more advantageous oblique sagittal plane. This would provide higher resolution imaging of both regions, in two shorter breath-holds, than possible with a single large-FOV acquisition, with imaging of the area of interest in a pure arterial phase and perhaps some venous filling for the less critical thoracic portion. Step-table MRA requires additional hardware, including a set of MRI coils for optimal imaging of each anatomic segment and optional software to control the automated table motion. As mentioned before, a disadvantage of the step-table technique may be a longer total acquisition time, which can lead to venous contamination in the later stations.

### Three-Dimensional Image Processing

Contrast-enhanced MRA is performed as a 3D acquisition; the 3D volume can be viewed as a stack of 2D images, but the higher resolution allows multi-planar reformatting (MPR) to create images in multiple orientations that optimize visualization of the anatomy or pathology. Images can be viewed using many types of algorithms to display the 3D data to the best advantage. Because contrast within vessels is designed to have the highest intensity, an algorithm that displays the brightest

voxels, known as maximum intensity projection<sup>20</sup> (MIP), is commonly used for reformatting 3D MR angiograms. Volume rendering (VR) has been demonstrated to be equivalent or superior to MIP for both MRA and CTA of several vascular territories.<sup>21,22</sup>

### **Hardware and Software for MR Angiography**

MRA is performed optimally on a 1.5 or 3T MR system with the fastest and strongest gradients available using multichannel receivers and coils with powerful image reconstruction computer systems. This will result in shorter acquisition times with higher spatial resolution and improved SNR as well as rapid availability of reconstructed images.

#### **1.5- vs. 3-Tesla MRI**

Because the degree of magnetization produced is linearly related to the magnetic field strength, a 3T magnet can increase image signal up to twice as much over the 1.5T magnet. This increased signal can then be traded for decreased imaging time or increased spatial resolution. Although the first applications of 3T use were in brain, spine and musculoskeletal imaging, the entire range of MRI is now being performed at 3T, including breast, body, and cardiac MRI, as well as MRA.<sup>23–26</sup> T1 relaxation times are longer at 3T, which results in increased enhancement using the same amount of gadolinium contrast or the ability to use less contrast to obtain the same degree of enhancement. Preliminary studies have shown improved image quality and accuracy of 3T over 1.5T MRA for imaging of the renal, carotid, and infrapopliteal arteries.<sup>27–29</sup>

One disadvantage of 3T is a fourfold increase in deposition of RF energy, known as the specific absorption rate (SAR). FDA-mandated limits on SAR are encountered more commonly using 3T than 1.5T. Although this is not an important problem for contrast-enhanced MRA, it can be an issue when using noncontrast-enhanced SSFP techniques and in applications such as cardiac MRI. Additional concerns include higher cost for 3T systems and an increase in image artifacts related to magnetic field inhomogeneity.<sup>30</sup> Despite these difficulties, more MRA studies will be performed at 3T as radiology practices switch to this technology given its advantages for general MRI.<sup>31</sup>

#### **Other hardware and software**

Dedicated coils for specific vascular beds are also useful and include at least a neurovascular coil for head and neck MRA and a peripheral angiography coil covering the pelvis to the feet for runoff studies. MRA of the thoracic, abdominal, and pelvic vessels is performed with multiple flexible phased-array coils that can be placed over the anatomy of interest; digital and pedal vessels can be imaged either with small local extremity coils or by placing both extremities in a dedicated head coil that is designed for high-resolution and SNR imaging.

Multichannel coils and RF receivers allow parallel imaging, which refers to a collection of MR acquisition and processing techniques used to accelerate image data acquisition.<sup>32,33</sup> As one of the effects of this acceleration is a loss of signal, parallel imaging is used mostly in high-SNR applications, including

MRA, and most contrast-enhanced MRA examinations done on newer scanners are performed with parallel imaging.<sup>34</sup>

Compressed sensing<sup>35–37</sup> is a mathematical framework that provides reconstruction of data from highly under-sampled measurements in order to gain acceleration of acquisition time. This method is useful in pediatric imaging and where shorter breath-hold sequences are required. Compressed sensing approaches are now available from several manufacturers and will be incorporated into routine MRA protocols in the coming years.

An MR-compatible dual-chamber power injector is needed for rapid administration of contrast, followed by a saline bolus, which can decrease the amount of contrast used. MR-compatible patient monitoring equipment is also useful, especially when imaging hospitalized patients or when sedation is needed. MR-compatible blood pressure cuffs can be useful for reducing venous contamination in extremity MRA. For example, placing cuffs around both thighs while inflating to half to two thirds systemic arterial pressure effectively delays venous return and allows for improved visualization of calf arteries.<sup>38</sup>

Additional software may be needed for step-table and parallel imaging, as well as newer noncontrast-enhanced and contrast-enhanced MRA techniques, so it is important when purchasing MR systems to investigate which sequences are included in the base MR system package and which are optional.

A post-processing workstation with multiplanar reformatting, maximum intensity projection, and volume rendering capability is the minimum necessary for visualization and interpretation of MRA studies. Additional software, such as automated vessel analysis with curved planar reformatting, vessel centerline extraction, automated segmentation, and bone removal, may also be useful for specific applications but is more relevant for CTA than for MRA.

## **CLINICAL APPLICATIONS OF MR ANGIOGRAPHY**

### **Aortic Vascular Disease**

Contrast-enhanced 3D MRA has been used to assess the aorta<sup>39–42</sup> in patients with many different types of disease. Assessment of the aortic arch by contrast-enhanced MRA may be superior to any other technique.<sup>43</sup> Several examples are shown in Figure 30.4. Other diseases that are routinely evaluated by MRA include aortic dissection,<sup>39,43–45</sup> as shown in Figure 30.5, and aneurysms.<sup>39,46</sup> MRA is also used to evaluate patients with other vascular diseases as shown in Figures 30.6 and 30.7, such as connective tissue disorders including Marfan syndrome,<sup>47</sup> and for vascular stent-graft placement planning, as well as for endoleak assessment in those with a nitinol-based stent-graft.<sup>48,49</sup>

### **Carotid Vascular Disease**

MRA has proved to be a very sensitive method for evaluating carotid artery atherosclerosis. For carotid lesions with between 70% and 99% narrowing, MRA has a reported sensitivity of 95% and a specificity of 90%.<sup>50</sup> For all stenoses, MRA

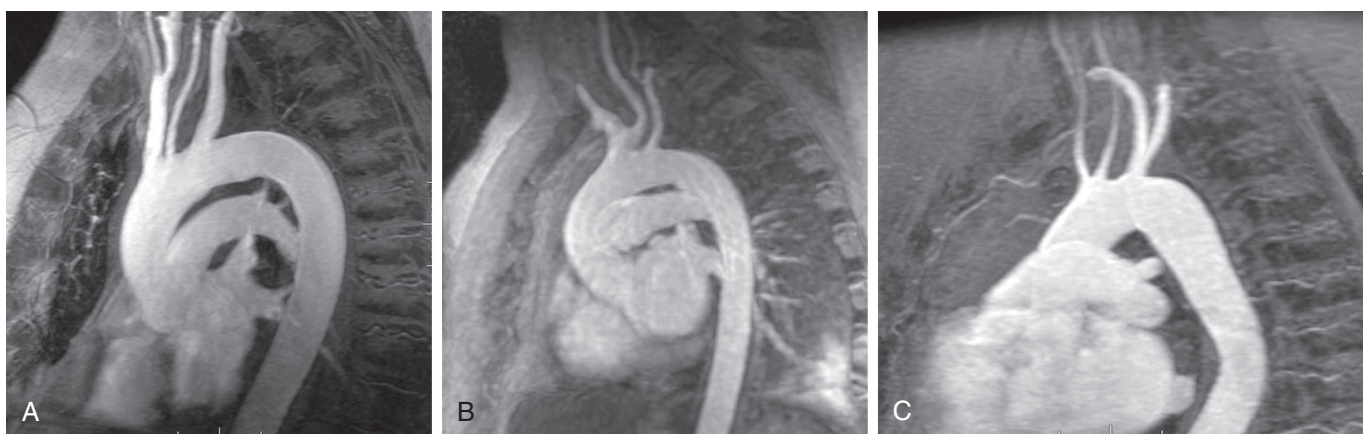


**Figure 30.4** Sagittal oblique reformatted MR angiogram of: (A) normal aortic arch; (B) bovine aortic arch; (C) rare arch anomaly, bicarotid truncus. All four vessels arise separately from the arch – the carotid arteries arise anteriorly and the subclavian arteries arise posteriorly.

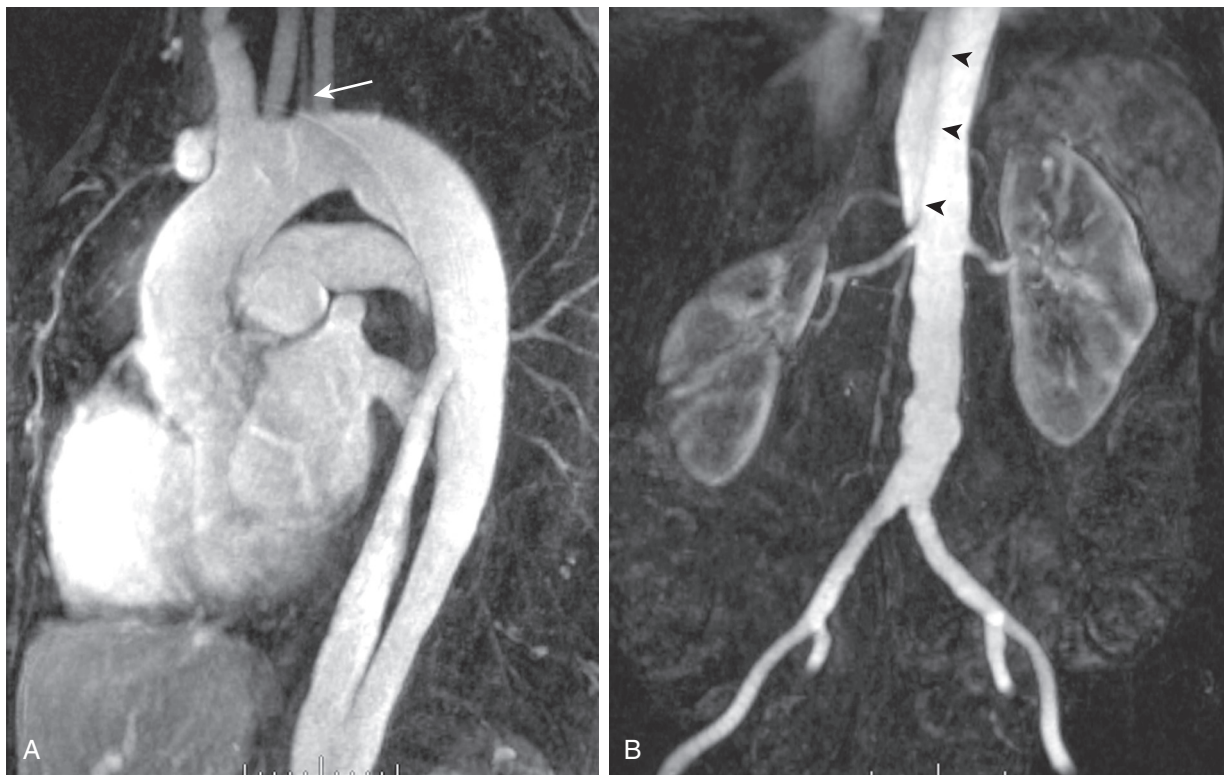


**Figure 30.5** (A) Sagittal oblique reformatted MR angiogram showing a type B dissection. The origin of the intimal flap and filling of the proximal false lumen are seen. A separate origin of the left vertebral artery is seen from the aortic arch (arrow). (B) Coronal 3D MRA obtained during the same examination as the chest-station image by using the step-table technique. The dissection flap (arrowheads) terminates just above the origin of the right renal artery.

has a reported sensitivity of 98% and a specificity of 86%.<sup>51</sup> Figure 30.8 shows MR angiogram of the carotid and vertebral arteries. Several authors conclude that the performance of MRA warrants its use as a tool to plan operative or interventional carotid artery revascularization.<sup>52,53</sup>

### Peripheral Vascular Disease

MRA has become a standard noninvasive method for evaluation of peripheral vascular disease,<sup>54</sup> having been demonstrated

to be effective in the preoperative assessment of patients with peripheral vascular disease,<sup>55–57</sup> including imaging of inflow vessels and evaluation of stenoses, as shown in Figure 30.9. Its sensitivity for detecting hemodynamically significant stenoses is 99.5% with a specificity of 98.8% compared with digital subtraction angiography (DSA).<sup>57</sup> In addition, MRA is effective in imaging suitable target vessels, including vessels not seen by catheter angiography.<sup>58</sup> MRA is also a cost-effective method for evaluation of patients with peripheral vascular disease.

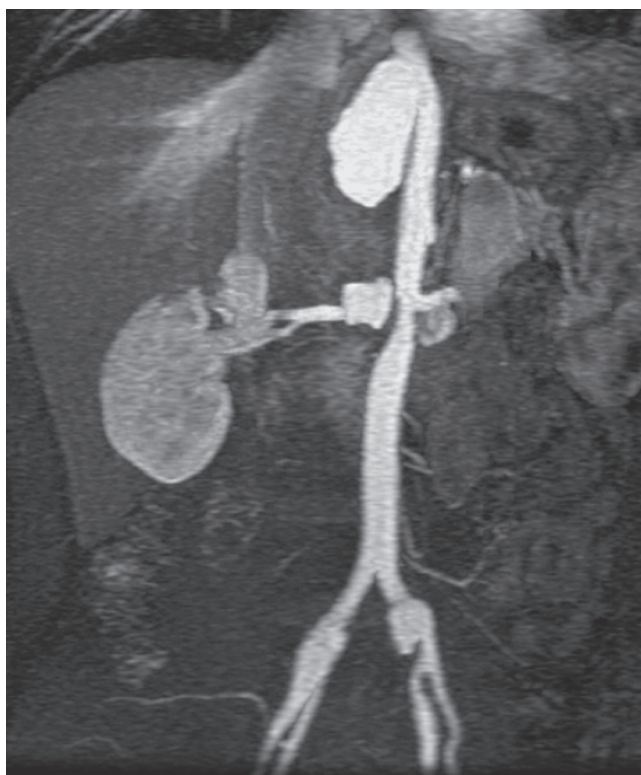


**Figure 30.6** Coronal 3D MR angiogram in a patient with suspected Ehlers-Danlos syndrome. Saccular aneurysms are seen involving the upper abdominal aorta and both renal arteries. An irregular fusiform aneurysm of the left common iliac is also present.

With advancements in technology, MRA evaluation of peripheral vascular disease continues to improve. Step-table techniques have increased the speed and resolution of the examination. This has allowed improved visualization of smaller distal vessels and permitted arterial-phase dedicated imaging of the feet, as shown in [Figure 30.10](#). As mentioned previously, MRA has been shown to be superior to DSA for the evaluation of distal vessels in some cases. In a study of 37 patients, MRA depicted significantly more vascular segments in the foot than did DSA ( $P < 0.0001$ ).<sup>58</sup>

In addition to the value of MRA for diagnosis and pretreatment planning, it may be used for the post-intervention evaluation.<sup>59–61</sup> MRA can be used to assess graft patency and stenosis. [Figure 30.11](#) demonstrates narrowing at the distal anastomosis of a femoral–popliteal artery bypass graft. MRA is also a useful technique for demonstrating complications of graft placement such as pseudoaneurysm formation, as shown in [Figure 30.12](#).

### Renovascular Disease

For the evaluation of renovascular disease, 3D gadolinium-enhanced MRA has become a clinical standard.<sup>62</sup> The most common such disease is atherosclerotic renal artery stenosis. However, MRA has also demonstrated its value for evaluating more subtle renal vascular conditions such as fibromuscular dysplasia, renal artery aneurysms, and accessory renal arteries.<sup>1</sup> Detection of accessory arteries is particularly important for assessment of potential living renal donors.<sup>63,64</sup>

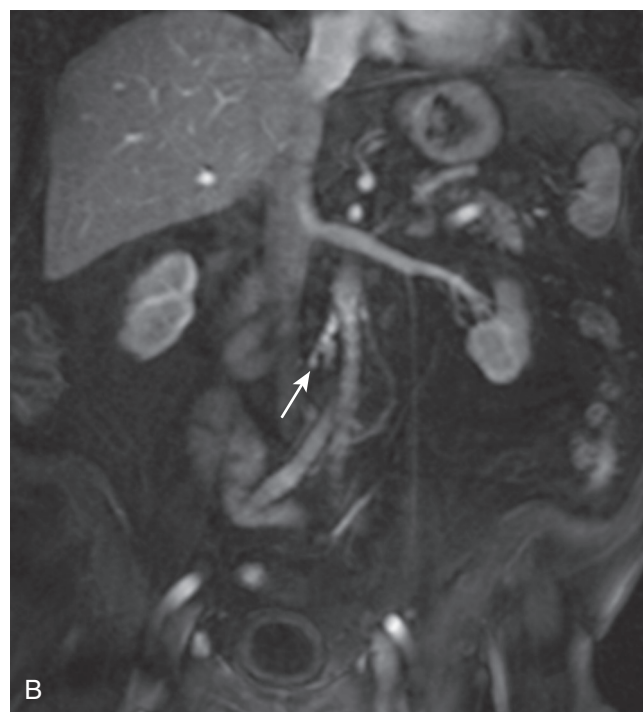
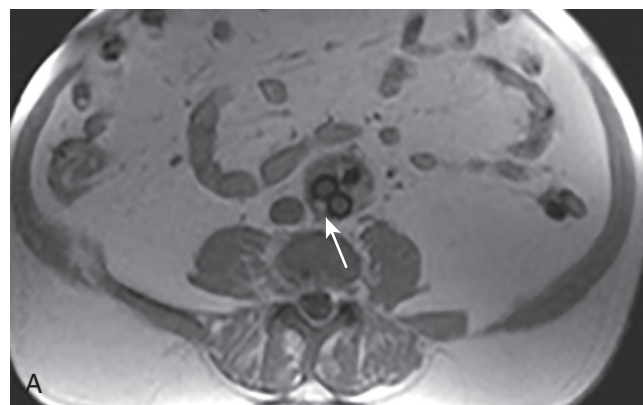


**Figure 30.7** (A) Axial T1-weighted image and (B) coronal MR angiogram images show infrarenal abdominal aortic aneurysm after endograft repair with type Ia endoleak.

Renal artery stenosis is the most common cause of secondary hypertension, and approximately 1% of people with hypertension will have renal artery stenosis.<sup>65</sup> Because renal artery stenosis is so common and potentially curable,<sup>66–69</sup> it is critical that appropriate screening tests exist for those at risk. 3D contrast-enhanced MRA has a sensitivity of 94% and a specificity of 93%.<sup>1</sup> In addition, it has been shown that when MRA is used to plan a renal artery intervention, both the number of pretreatment angiograms and the total amount of contrast are reduced.<sup>68</sup>

As shown in [Figure 30.13](#), the majority of renal artery stenoses are located in the ostial or proximal segments. As methods for 3D contrast-enhanced MRA have improved, diseases that are not typically near the renal artery origin have more commonly been diagnosed by MRA. Such diseases include another curable cause of hypertension, fibromuscular dysplasia,<sup>70</sup> shown in [Figure 30.14](#). Accessory renal arteries occur in nearly 45% of patients, and their diagnosis can be important in

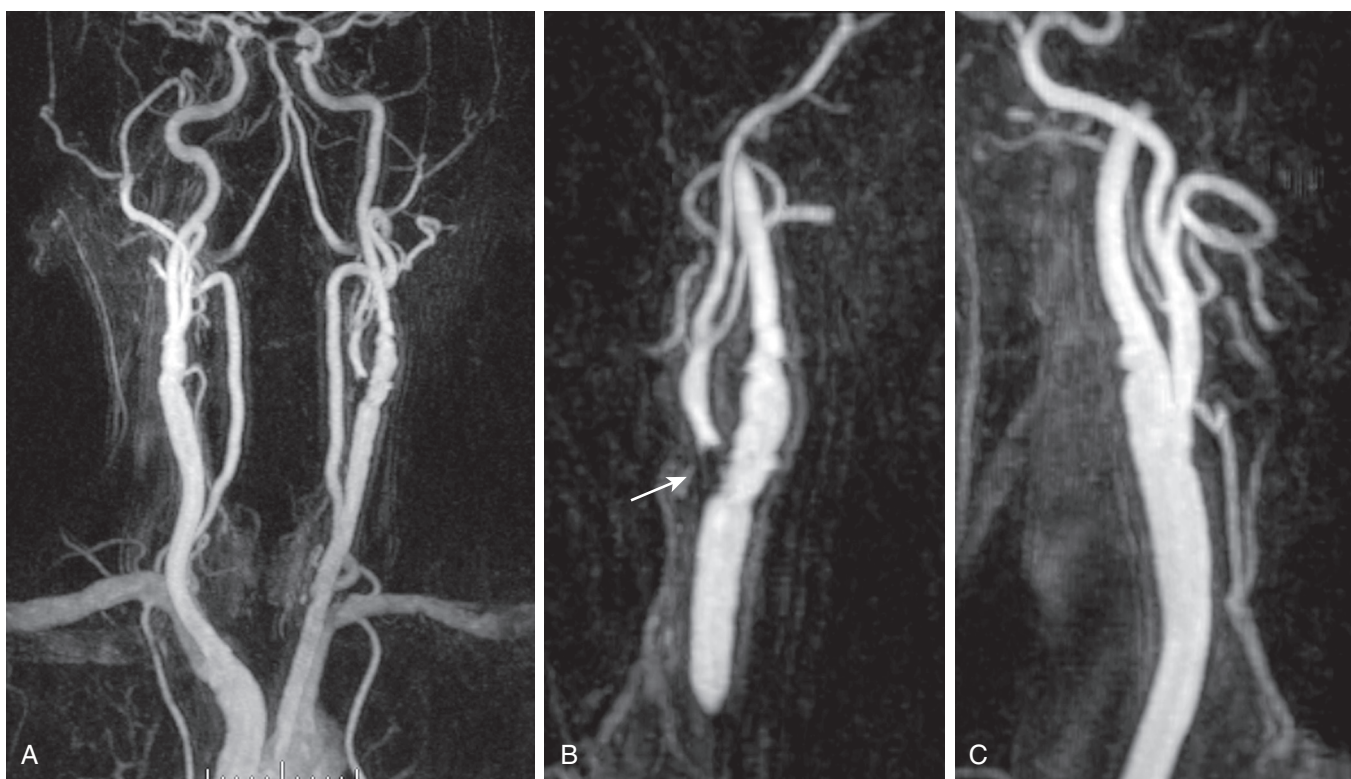


**Figure 30.8** (A) Coronal 3D MR angiogram of the carotid and vertebral arteries. (B) Oblique sagittal reformatted MR angiogram showing high-grade narrowing at the origin of the left external carotid artery (*arrow*) and mild disease of the left internal carotid artery. (C) Oblique sagittal reformatted MR angiogram showing the right carotid bifurcation with mild disease in the proximal right internal carotid artery.

screening candidates for renal donation.<sup>71</sup> Figure 30.15 demonstrates an individual with six total renal arteries.

### Mesenteric Vascular Disease

The most common use of MRA in patients with mesenteric vascular disease is to evaluate those with suspected intestinal angina or chronic mesenteric ischemia.<sup>72,73</sup> MRA is between 95% and 97% accurate for characterizing proximal disease of the superior mesenteric artery<sup>74</sup> in cases of chronic mesenteric ischemia. MRA is also useful to evaluate more complex diseases of the mesenteric vasculature. The median arcuate ligament passes anterior to the descending aorta near the T12 level. During end-expiration the ligament can compress the proximal portion of the celiac axis, which can lead to a false impression of proximal celiac stenosis. MRA can be helpful in demonstrating the effect of the arcuate ligament during a single examination,<sup>75</sup> as shown in Figure 30.16.

In cases of suspected mesenteric venous thrombosis, MRV can be an extremely useful tool and has been suggested to be superior to mesenteric catheter angiography.<sup>76</sup> MRV is particularly successful because of the ease of detecting small amounts of MR contrast. Central injection of MR contrast will be easily visualized in the veins, even after several cycles of circulation. An example of post-contrast 2D MRI is shown in Figure 30.17; the portal vein, splenic vein, superior mesenteric vein, and even inferior mesenteric venous branches occluded with thrombus are clearly depicted.

### Venous Vascular Disease

MRV is a useful technique for evaluating both central<sup>77,78</sup> and deep<sup>79–81</sup> venous structures. Central venous structures, in particular the superior vena cava, can be evaluated with 3D methods with 100% sensitivity for the detection of thrombus when compared with DSA.<sup>78</sup> For pelvic and deep venous structures, it is more common to use 2D TOF angiography.<sup>79,80</sup> In cases of suspected deep venous thrombosis (DVT), this method showed that 20% of patients had pelvic DVT that could not be diagnosed by ultrasound.<sup>81</sup> This same study also demonstrated that in cases of known pulmonary embolism and negative lower extremity Doppler ultrasound, 29% of patients had residual pelvic DVT.

An example of 2D TOF imaging of an IVC thrombus is shown in Figure 30.18 with corresponding 2D post-contrast MR images. Both types of imaging are useful for detecting DVT in the abdomen, pelvis, and lower extremities.

### Other Applications

A large variety of vascular conditions may be evaluated by MRA. The capability of performing the evaluation may depend on the experience of the physicians and technologists performing the study. For example, MRA may be performed to assess patients with suspected thoracic outlet syndrome if the appropriate image sequences can be combined with maneuvers to elicit the symptoms.<sup>82</sup> A case of thoracic outlet syndrome is shown in Figure 30.19, where compression of the subclavian vein is clearly seen when the ipsilateral upper extremity is raised above the head.

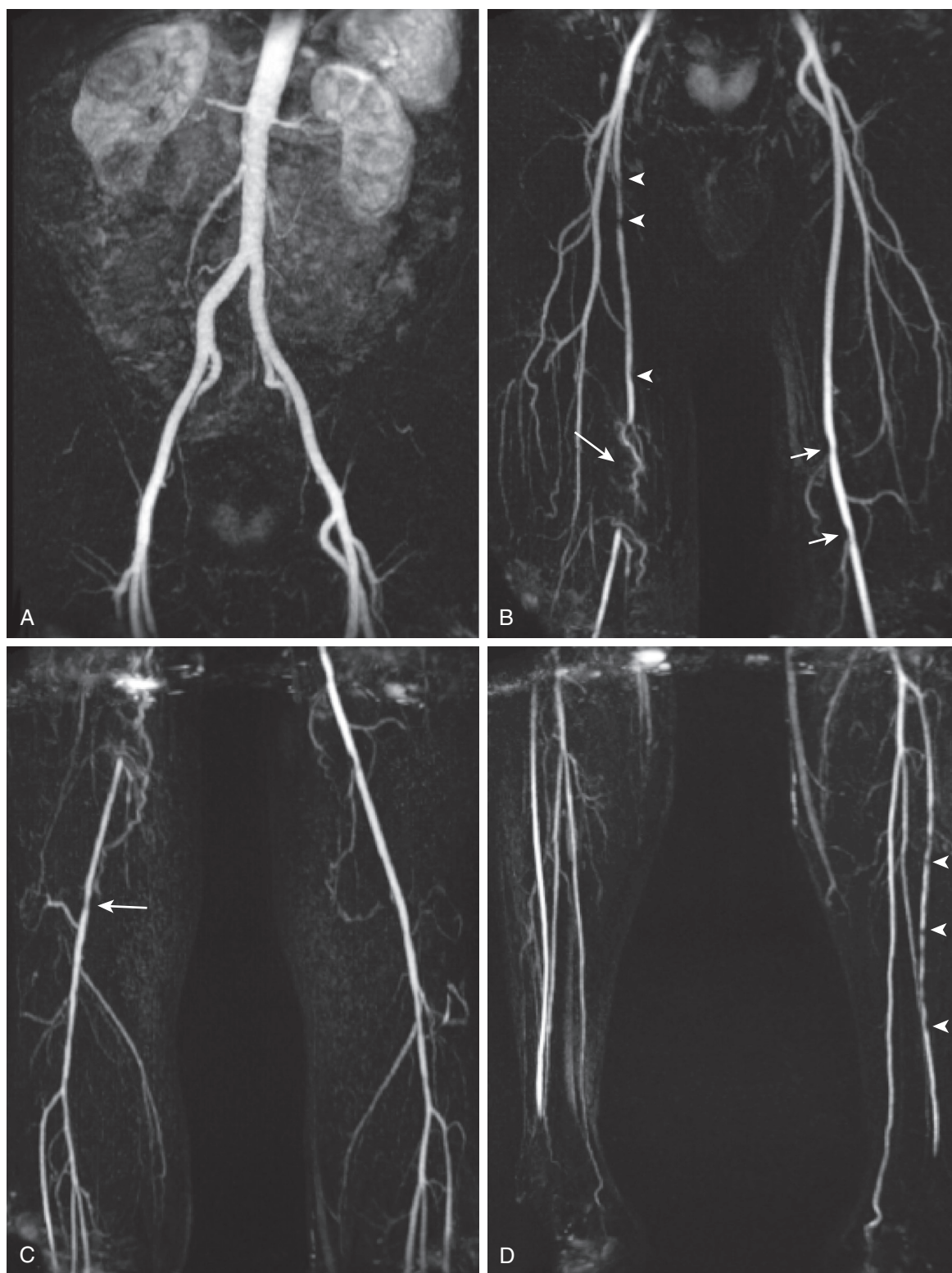


**Figure 30.9** Coronal 3D MRA step-table examination showing (A) normal inflow vessels, and (B) right proximal superficial femoral artery (SFA) stenoses (arrowheads); segmental occlusion of the right distal SFA/popliteal artery (long arrow); and mild left popliteal stenoses (short arrows). (C) Mild right popliteal artery stenosis (arrow) and (D) multiple stenoses of the left anterior tibial artery (arrowheads).

In centers in which transplants are performed, MRA is useful for assessment of potential renal donors,<sup>63,71</sup> as mentioned earlier. In addition, MRA can be useful in the assessment of suspected failure of the arterial or venous anastomoses of the transplant graft.<sup>5,83</sup> Figure 30.20 demonstrates

evaluation of a pancreas transplant graft in the postoperative phase and in a later phase in which graft rejection was occurring.

MRA is also useful to assess less common diseases, for example, to diagnose and assess the response to therapy in cases

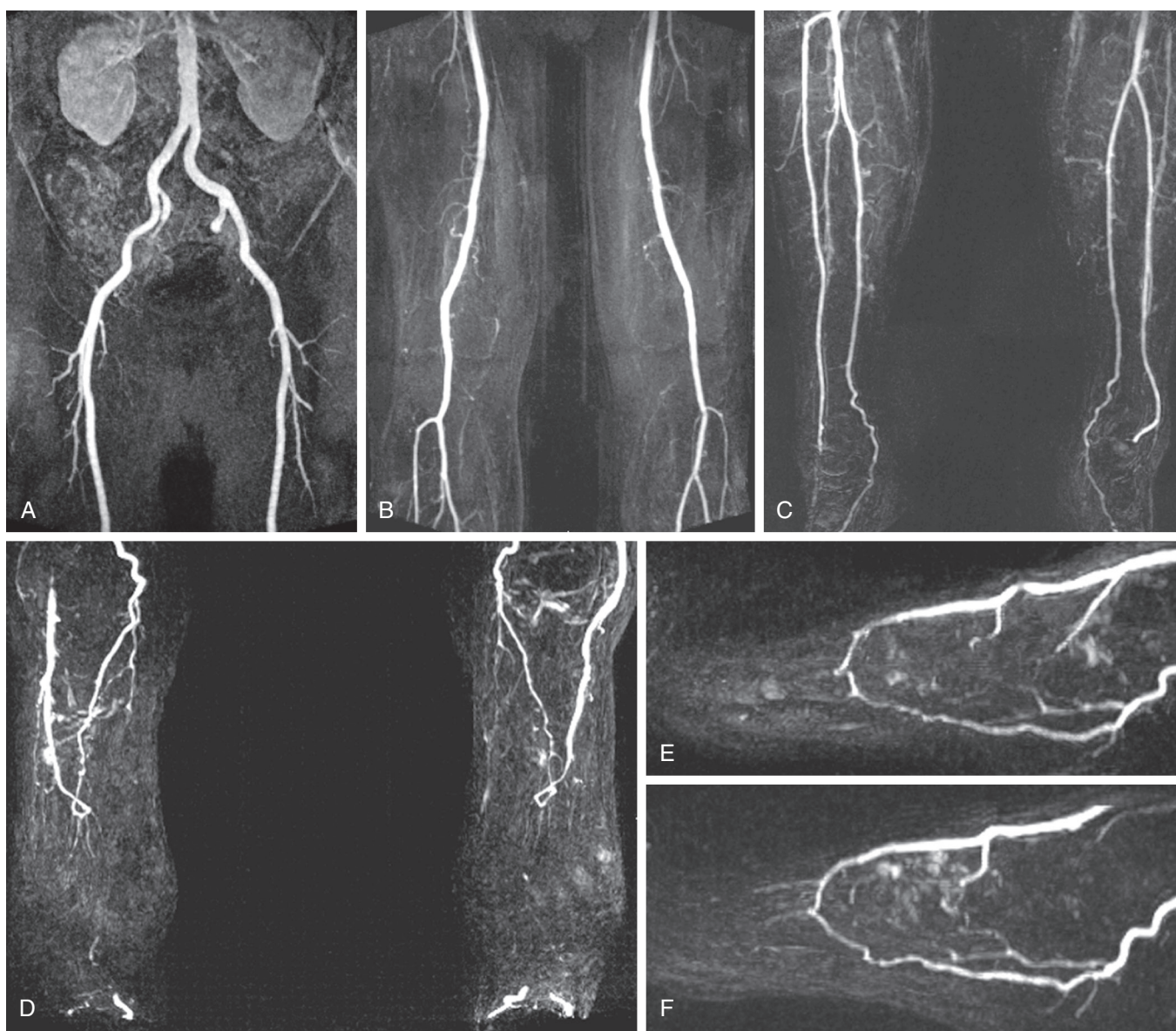


**Figure 30.10** Five-station step-table examination showing: (A) normal inflow vessels to the lower extremities; (B) normal thigh vessels; (C) normal calf vessels; and (D) normal vessels in both feet. The high-resolution 3D data allow reconstruction of each foot in the sagittal plane (E and F), which shows a patent plantar arch in each.

of large- and medium-vessel vasculitis.<sup>84,85</sup> An example of Takayasu arteritis is shown in Figures 30.21 and 30.22. Another example of more esoteric disease that has been assessed by MRA is pulmonary arteriovenous malformations,<sup>86,87</sup> as shown in Figure 30.23. In such cases, MRA has 100% sensitivity for imaging pulmonary arteriovenous malformations greater than 5 mm in size, and all feeding arteries and draining veins are characterized as well.

A newer application of MRA is preoperative evaluation of deep inferior epigastric artery perforators (DIEP) in abdominal flap donor tissue for autologous breast reconstruction, as shown in Figure 30.24. MRA can identify branching pattern, vessel patency, location of largest DIEP at the point of exit from the anterior rectus fascia as well as intramuscular and septocutaneous course.<sup>88</sup>

## LIMITATIONS AND RISKS

### Scan Artifacts

Several common artifacts and pitfalls are associated with MRA. Knowledge of these limitations will allow the user to approach diagnostic MRA with increased confidence that any abnormal findings do represent actual pathology.

### Fat Saturation in Chest MR Angiography

Suppressing the signal from fat may be advantageous in that fat will have high signal on the T1-weighted images used for MRA. However, frequency selective methods of fat suppression used may result in suppression of the water signal instead when vessels are located adjacent to lung.<sup>89</sup> Thus, a vessel that is patent

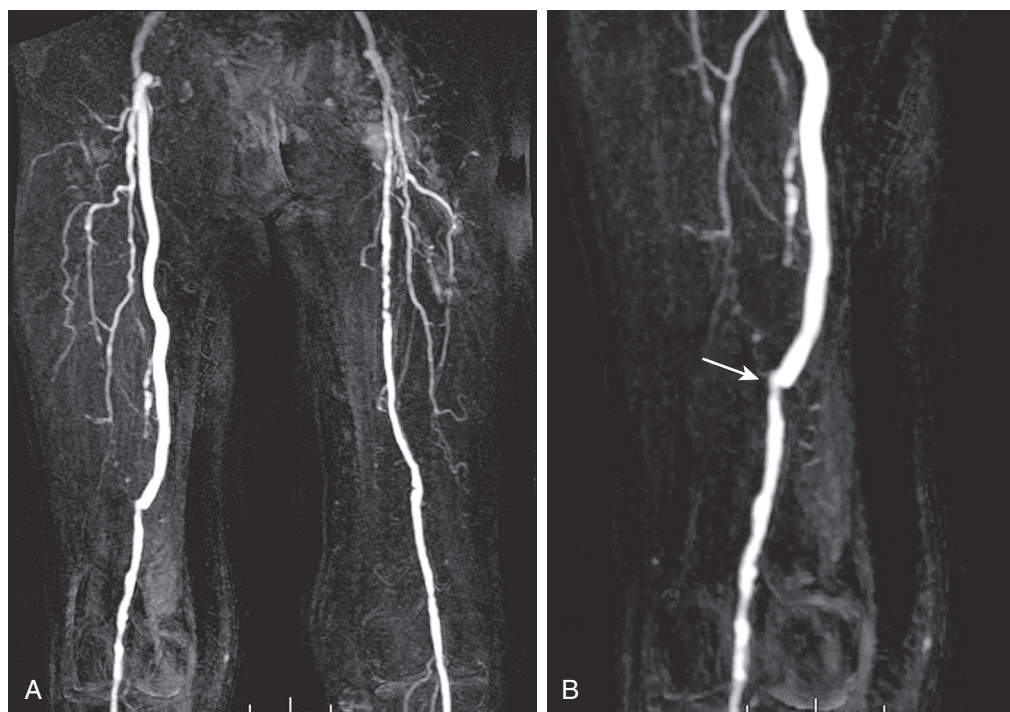


**Figure 30.11** (A) Coronal 3D thigh-station MR angiogram of a femoral–popliteal bypass graft. Note the contralateral disease in the superficial femoral artery. (B) Oblique reformatted image shows narrowing at the distal anastomosis of the bypass graft (arrow).

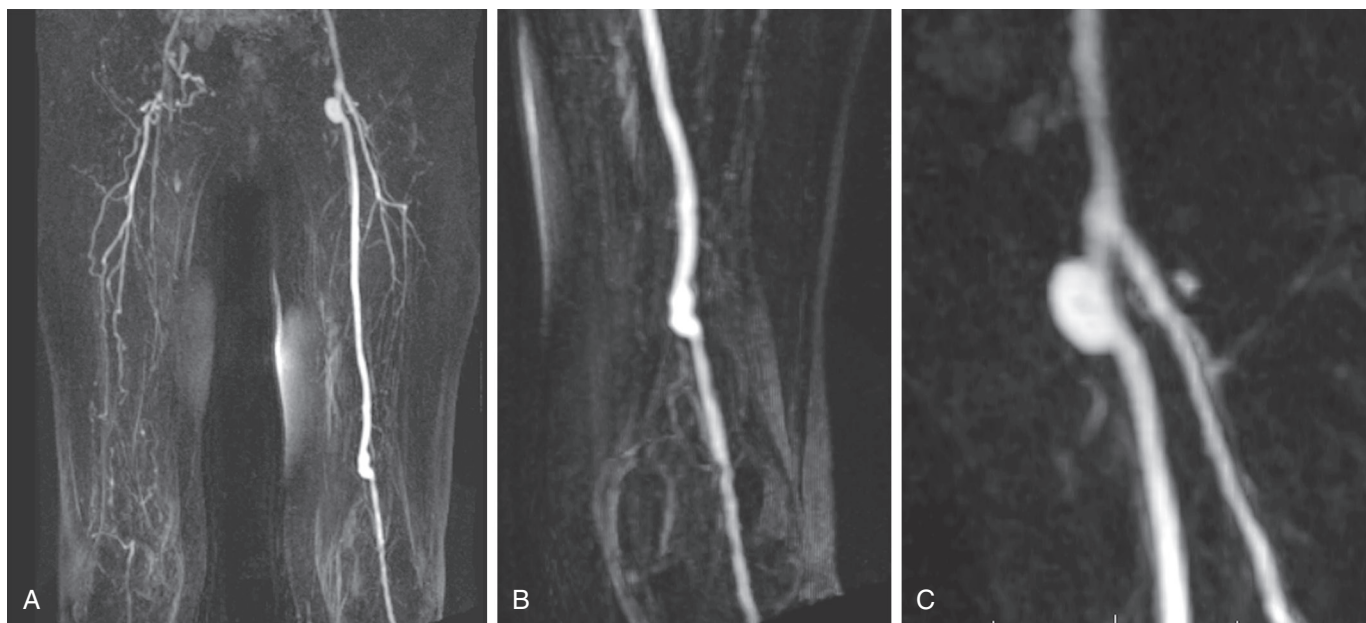


**Figure 30.12** (A) Coronal 3D thigh-station MR angiogram of a left femoral–popliteal bypass graft. Note the contralateral disease in the superficial femoral artery and visualization of multiple collaterals above the right knee. (B) An oblique reformatted image shows the distal region of the bypass graft. (C) Another oblique reformatted image shows a pseudoaneurysm at the origin of the graft.

may appear entirely occluded, or a vessel that is occluded may not be accurately assessed, as shown in Figure 30.25.

#### Susceptibility Artifact from Concentrated Gadolinium

As noted above, MRA contrast contains a chelated form of the rare earth element gadolinium that shortens the T1 of surrounding water. At high concentrations, a T2-shortening effect

that reduces the MR signal also occurs. In effect, at high concentrations, MR contrast behaves like a small piece of metal and produces a susceptibility artifact on the surrounding tissues. These concentrations occur only during the injection of pure contrast and are typically seen in the area of the origin of the great vessels<sup>90</sup> or in the subclavian artery during initial passage of injected contrast through the adjacent vein,<sup>91</sup> as shown in Figure 30.26. If this artifact is suspected to be the cause

of an apparent stenosis, repeating the sequence immediately should demonstrate resolution as contrast in the adjacent vein becomes more dilute.

### Susceptibility Metal Artifacts

Metal produces a large signal void and extensive distortion around the implant in MR imaging. Metal artifact reduction sequences (MARS) reduce metal artifact using several different methods.<sup>92</sup> Multiacquisition with variable resonance image combination (MAVRIC) and slice-encoding metal artifact

correction (SEMAC) are two recently developed metal artifact reduction techniques that significantly reduce susceptibility artifacts near metallic hardware.<sup>93</sup> Metal artifacts also occur in CT imaging, with several techniques including dual energy CT and usage of iterative reconstruction available for artifact reduction.<sup>94</sup>

### High Intravascular Signal from Thrombus Containing Methemoglobin

Clotted blood has varying appearance on MR images, depending on both the redox state of the hemoglobin molecule and the integrity of the red blood cell wall. Clotted blood will pass through a state of either intracellular or extracellular methemoglobin in the subacute phase (1 to 14 days).<sup>95</sup> When the clot contains large amounts of methemoglobin, particularly extracellular methemoglobin, the signal may be high on the T1-weighted images used in MRA. This signal can mimic intravascular contrast, as shown in Figure 30.27. The use of pre-contrast T1-weighted imaging can identify the thrombus, as shown.

### Contraindications to MRI

#### *Renal Disease and Nephrogenic Systemic Fibrosis*

Nephrogenic systemic fibrosis (NSF), previously known as nephrogenic fibrosing dermopathy, is a disease with primarily dermatologic manifestations, although findings in other organs have now been elucidated.<sup>6</sup> NSF is characterized by skin thickening and hyperpigmentation of the extremities and trunk; patients with more severe involvement may have contractures and organ fibrosis, in some cases leading to death. All reported cases to this point have occurred in patients with renal insufficiency, primarily in those with very poor kidney function in the setting of chronic renal failure, although cases have been described



**Figure 30.13** Coronal 3D MR angiogram showing an ostial renal artery plaque (arrow).

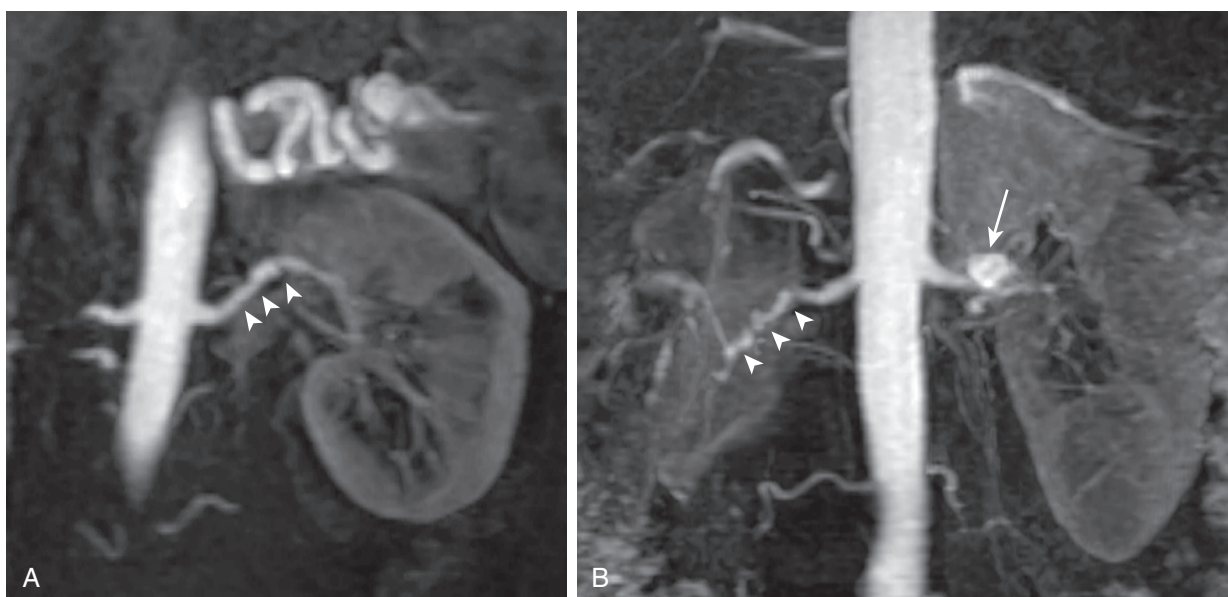


**Figure 30.14** (A) Coronal 3D MR angiogram showing subtle findings associated with fibromuscular dysplasia (arrowheads). Note that the disease is isolated to the distal portion of the main renal artery. (B) Coronal 3D MR angiogram showing right-sided fibromuscular dysplasia (arrowheads) and a left-sided renal artery aneurysm (arrow).

with milder renal dysfunction in acute renal failure. Whereas concomitant liver failure was previously thought to be an additional risk factor, longer term studies have not supported this finding. There is no specific treatment of NSF other than improving renal function, such as through kidney transplantation; steroids and other anti-inflammatory treatments have been used, along with hemodialysis and photopheresis.<sup>96</sup>



**Figure 30.15** Coronal 3D MR angiogram showing two main renal arteries and four accessory renal arteries (arrowheads). Note that the accessory arteries may enter the renal hilum or perforate the cortex.

Although the first cases of NSF were described in 2000,<sup>6</sup> a possible association between NSF and exposure of patients with renal insufficiency to gadolinium-containing contrast agents was not proposed until 2006, when five cases were reported in a cohort of dialysis patients who had undergone MRA.<sup>7</sup> Since that time, approximately 1600 cases have been reported in dialysis and nondialysis patients,<sup>97,98</sup> and several predisposing factors have come to light, including metabolic acidosis, administration of a larger dose of gadolinium contrast agent, repeated contrast-enhanced studies (i.e., the effect may be cumulative), proinflammatory conditions, and recent vascular procedures, including surgery. All but five documented cases of NSF have occurred in patients exposed to gadolinium contrast agents, and thus far, there have been no documented cases of NSF in patients with normal renal function.<sup>96</sup> Whereas gadolinium agents are cleared rapidly by the kidneys in those with normal renal function, residence time may be increased 100-fold in those with markedly impaired renal function. It is currently unknown whether repeated exposure to gadolinium agents could induce NSF even in those with normal renal function.

Gadolinium-based contrast agents (GBCAs) are categorized by their molecular structure (linear or macrocyclic) and type of chelate (ionic or nonionic). Macrocylics have tighter gadolinium binding compared to linear GBCAs. Transmetallation is a process where competing ions such as zinc, copper and iron displace gadolinium from the chelate to a free form of gadolinium, and this process occurs more easily with linear than macrocyclic GBCAs. The American College of Radiology has placed GBCAs into three groups: group I contains one linear



**Figure 30.16** (A) Arterial-phase sagittal 3D MR angiogram at end-expiration showing the impression of the arcuate ligament just proximal to the origin of the left gastric artery. Notice the quality of the evaluation of the proximal superior mesenteric artery as well. (B) Venous-phase sagittal 3D MR angiogram at end-inspiration showing no narrowing of the proximal celiac axis. During the delayed phase there is still sufficient contrast within the aorta and branch vessels for adequate visualization.

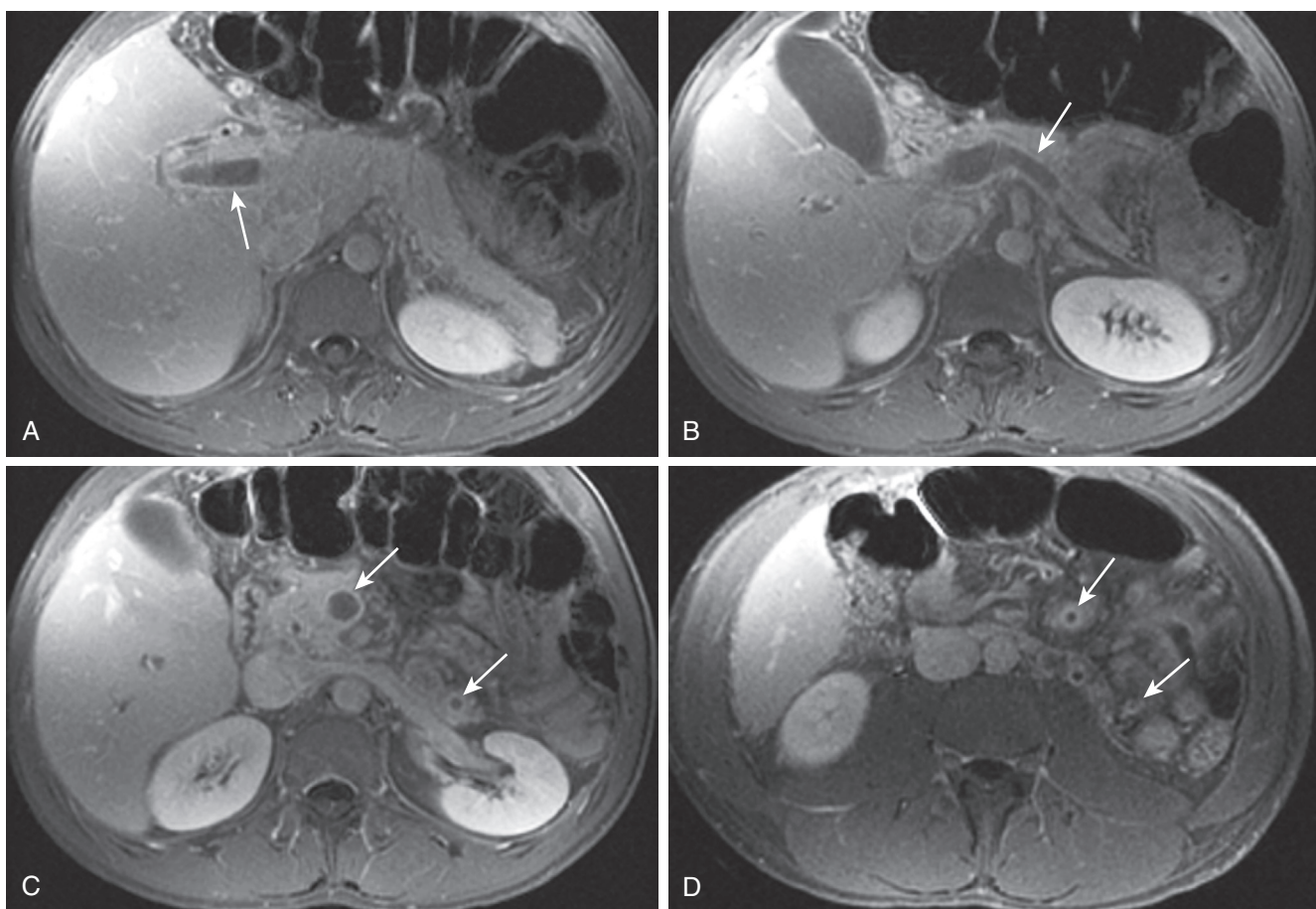


**Figure 30.17** 2D T1-weighted post-contrast MR images showing: (A) portal vein thrombus (*arrow*); (B) splenic vein thrombosis (*arrow*); (C) superior mesenteric vein (SMV) and inferior mesenteric vein (IMV) thrombi (*arrows*); (D) thrombi within small distal branches of the SMV and IMV (*arrows*).

ionic and all available linear nonionic agents and nearly all NSF cases have been associated with administration of group I GBCAs. Group II contains one newer linear ionic agent and three macrocyclic agents and have been associated with a much lower incidence of NSF. A single newer linear ionic agent is contained in group III, for which there is insufficient evidence at present.<sup>99</sup> Based on published systematic review and meta-analysis of 16 unique studies and 4931 patients by Woolen, the risk of NSF from group II GBCA administration in stage 4 or 5 CKD is likely less than 0.07%.<sup>100</sup> This has led to recent recommendations not to deprive patients of needed GBCA enhanced MRI in the presence of severe renal function impairment.<sup>99,101</sup> In such cases, macrocyclic agents should be used at recommended doses, with hemodialysis performed promptly after the MRI in dialysis-dependent patients. Considering angiographic examinations, CTA is an appropriate alternative in dialysis-dependent patients, and noncontrast MRA should be considered for those with stage 4 or 5 CKD not yet on permanent dialysis.

### Pacemakers and Other Implanted Devices

Although MRI is extremely safe, the degree of safety is ensured only by maintaining the appropriate environment around the magnet and by careful screening of patients.<sup>102,103</sup> There are a number of implanted metallic devices that are not safe in or

near an MRI magnet. The more common include implanted pumps or neurostimulators, some cochlear implants, and some intracranial aneurysm clips. Because of the large variety of implanted devices, sources of information regarding which are safe have been developed. Such sources include books,<sup>104</sup> published articles,<sup>105</sup> and websites,<sup>106</sup> and consultation of these resources is highly suggested before considering MRI in a patient with an implanted device. A recent consensus document provides recommendations concerning MR imaging of patients with 10 common implanted devices.<sup>107</sup>

Implanted pacemakers and defibrillators had long been considered absolute contraindications to MRI; however, FDA approved MR conditional devices are now available and several recent reports of large trials have demonstrated that some patients with non-MR conditional pacemakers and defibrillators can be imaged safely under carefully controlled conditions.<sup>108,109</sup> The risks in imaging patients with pacemakers or defibrillators include patient- and device-related complications, although the factor of greatest concern is whether the patient's underlying cardiac rhythm would be able to tolerate the pacemaker's ceasing to function while in the magnet, where immediate treatment may be more difficult. In general, factors that entail greater risk include a pacemaker-dependent patient, pacemaker generator implanted before 2000 (some older models appear to be more susceptible to an electrical reset to default

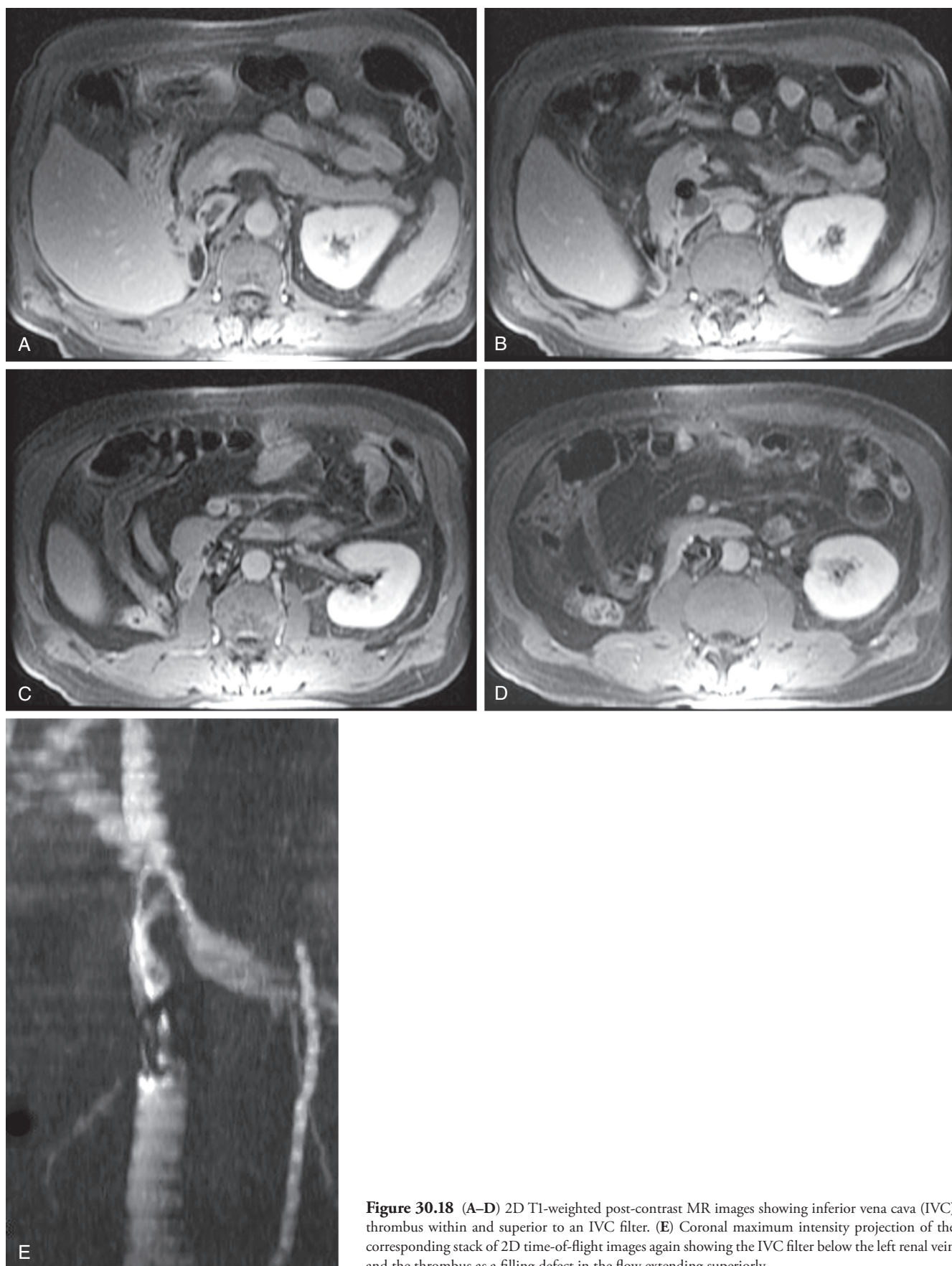


**Figure 30.18** (A–D) 2D T1-weighted post-contrast MR images showing inferior vena cava (IVC) thrombus within and superior to an IVC filter. (E) Coronal maximum intensity projection of the corresponding stack of 2D time-of-flight images again showing the IVC filter below the left renal vein and the thrombus as a filling defect in the flow extending superiorly.



**Figure 30.19** (A) Coronal 3D MR angiogram showing a normal right subclavian vein with the patient's arm lowered. (B) Coronal 3D MR angiogram showing occlusion of the subclavian vein near the junction with the axillary vein with the patient's arm overhead (*arrow*). Note the pooling of very concentrated contrast material in the arm.

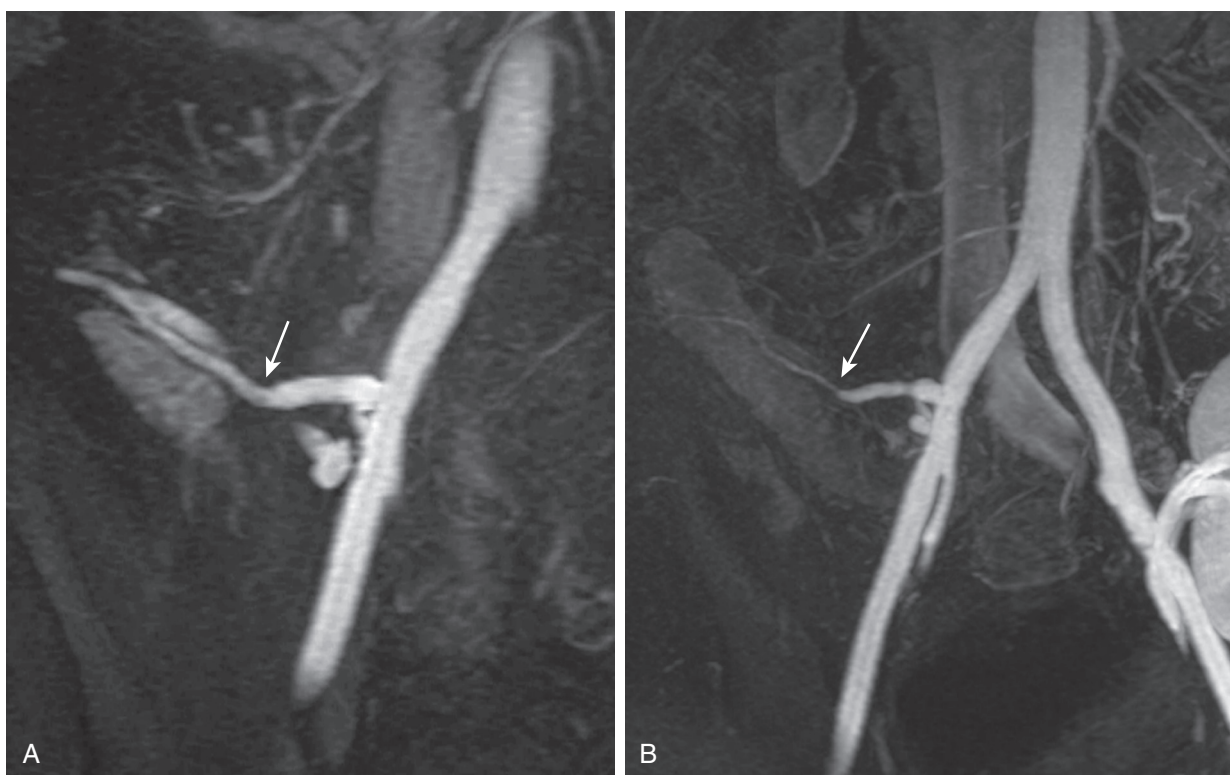


**Figure 30.20** (A) Coronal 3D MR angiogram in a patient with a pancreas transplant showing the anastomosis between the donor external iliac limb of the y-graft and the donor splenic artery feeding the pancreatic body (*arrow*). (B) Coronal 3D MR angiogram performed later during transplant rejection showing narrowing of the donor splenic artery (*arrow*). There is also a renal transplant partially seen in the left hemipelvis.

parameters while in the magnet), presence of an implantable cardioverter-defibrillator (ICD), and inclusion of the pacemaker/ICD generator or leads in the RF field. At our institution, we follow a protocol for nonconditional devices in which the device is interrogated before MRI and pacing parameters altered so that they are less susceptible to interference from the RF and gradient, and an electrophysiologist physician or physician's assistant is present throughout the MRI examination. The ICD's anti-tachycardia therapy capabilities are turned off

during the examination, and thus the device would be unable to respond to episodes of tachycardia that would benefit from shocks. We will perform MRI on patients with pacemakers or defibrillators that are not FDA approved as MRI conditional under the following circumstances:

1. There is a compelling clinical need for the scan, and the information to be gained from the examination has a high likelihood of altering patient management or prognosis.

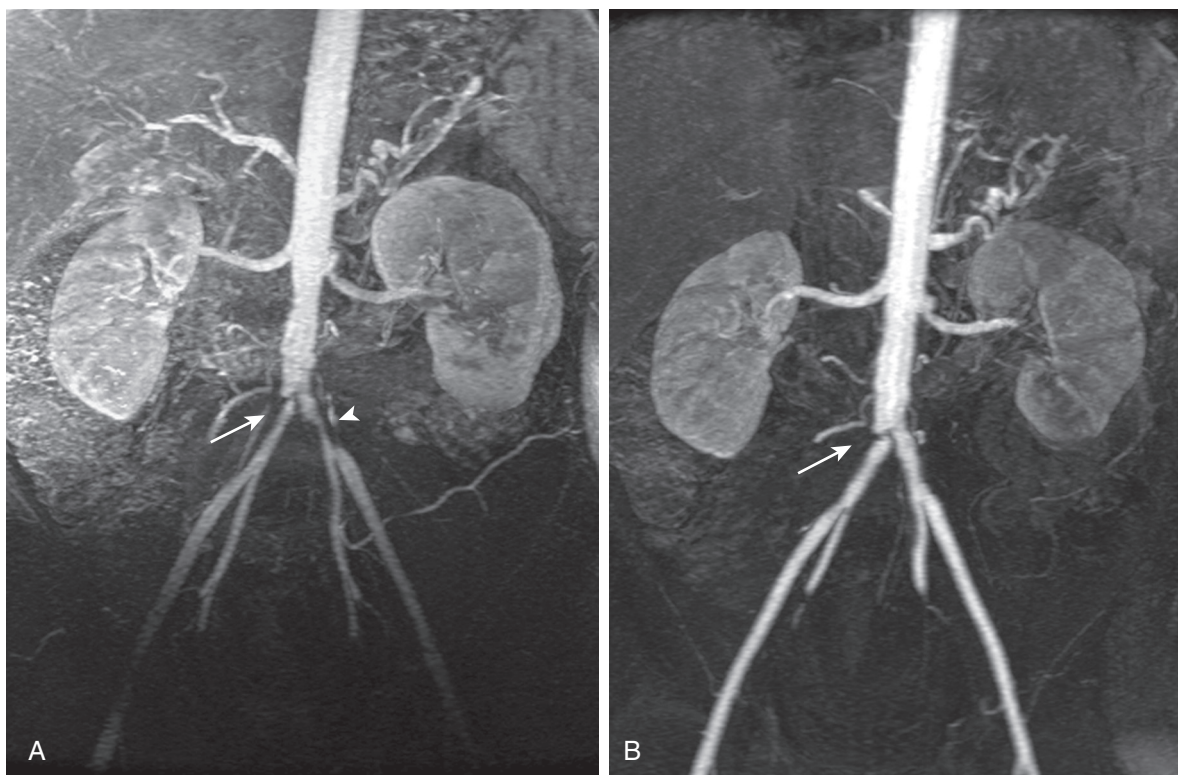


**Figure 30.21** Coronal 3D MR angiogram in a patient with Takayasu arteritis showing (A), narrowing of the proximal common iliac arteries bilaterally (arrow and arrowhead) and (B) complete resolution of the left common iliac narrowing and residual disease (arrow) in the right common iliac after treatment.

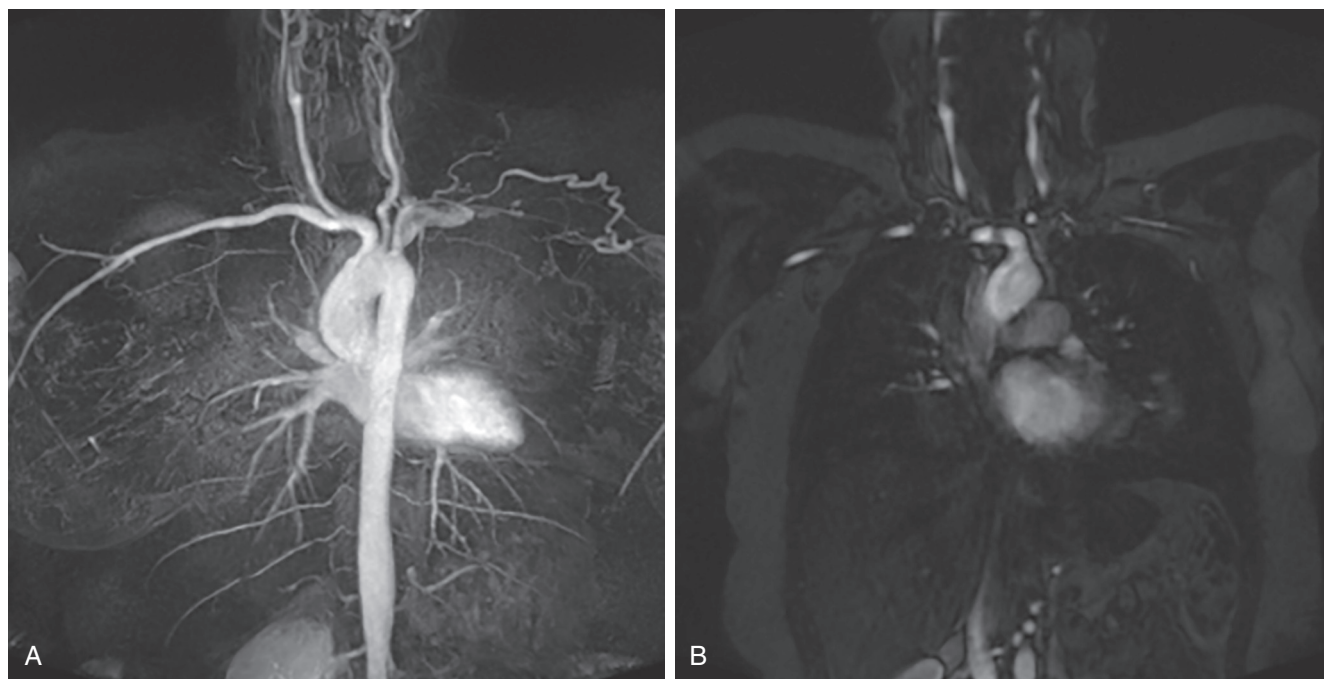


**Figure 30.22** (A) 3D MR MIP coronal image shows collaterals from chronic severe narrowing and occlusion of left subclavian artery in a patient with Takayasu arteritis. (B) MR angiogram shows severe narrowing of left subclavian artery in a patient with Takayasu arteritis.

2. There is no other acceptable imaging alternative.
3. An electrophysiologist concurs that the patient will not be harmed by the temporary modifications to pacemaker/ICD programming just noted.

Given the availability and utility of high-quality CTA, there are very few situations in which these conditions would be met in vascular imaging, and the majority of cases reported in the literature involve neurologic, musculoskeletal, and



**Figure 30.23** Coronal 3D MR angiogram showing a large right-sided pulmonary arteriovenous malformation and several smaller left-sided malformations.

abdominopelvic imaging. However, the recent availability of devices that are approved by the FDA as MRI conditional may mean that MRA of the patients with implanted pacemakers and ICDs will become more routine.

### Vascular Stents, Filters, and Coils

The majority of implantable vascular stents, filters, and coils have been shown to be “MRI safe” or, using newer terminology developed by the American Society for Testing and Materials International, “MRI conditional”<sup>110,106</sup>; that is, they are not subject to significant force when placed inside the magnet and have been demonstrated to pose no known hazards. One exception was the Zenith AAA stent graft system (Cook Inc, Bloomington, IN), which is made of stainless steel and was shown to be subject to significant forces in *in-vitro* testing, and was therefore previously characterized as MR unsafe. This stent has not been systematically studied *in vivo*, however retrospective results have been reported for a small cohort of 11 patients with Zenith stent grafts who underwent a total of 20 MR exams (including 10 of the abdomen, pelvis, or spine) and suffered no ill effects<sup>111</sup> and nonclinical testing at field strengths of up to 3 Tesla demonstrated no significant heating or torquing. Therefore, it is now classified as MR conditional at up to 3 Tesla, beginning immediately after placement.<sup>106</sup>

IVC filters and vascular embolization coils are composed of either nonferromagnetic alloys such as nitinol or weakly ferromagnetic stainless steel. Neither of these materials is subject to significant force when exposed to MRI, and all IVC filters tested are classified as MRI safe or conditional. As with stents, many manufacturers recommend waiting up to 8 weeks after placement of the device before performing MRI because this period is thought to be the amount of time needed for stable incorporation into the vessel wall; however, there are no specific

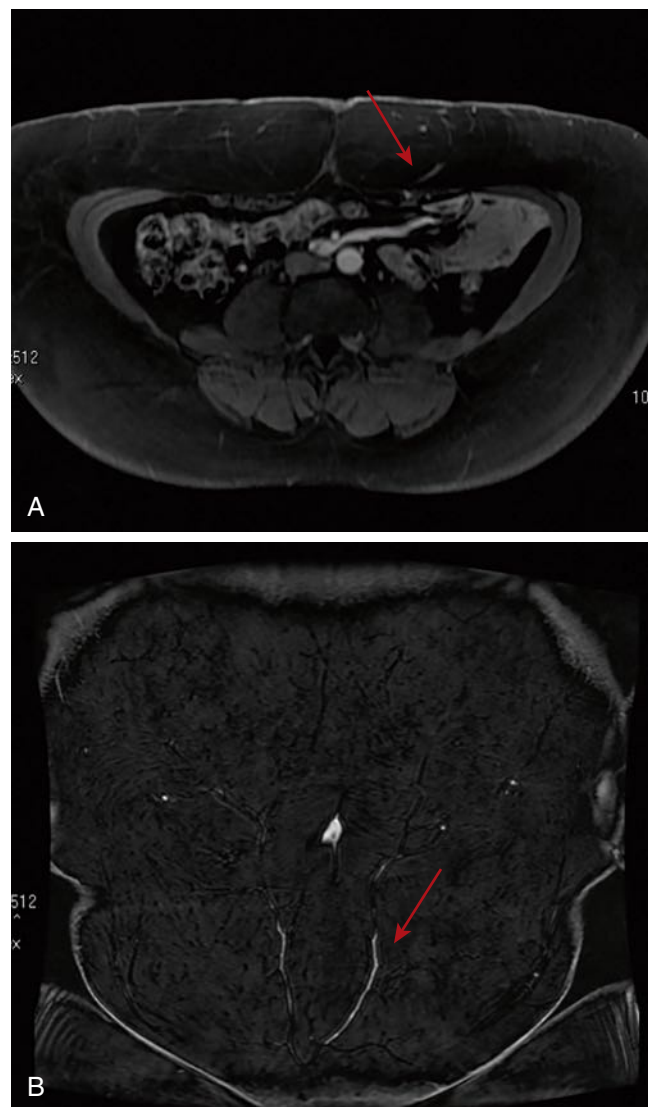


**Figure 30.24** (A) Axial and (B) coronal contrast-enhanced MRA images showing perforators of deep inferior epigastric artery (arrows).

data to justify this policy. Stents, filters, and coils composed of nonferromagnetic material may be safely imaged immediately after placement. For weakly ferromagnetic devices, the decision to perform MRI within 6 to 8 weeks after placement should be accompanied by consideration of the potential risks versus the benefits of the information that the studies will provide.

Although it may be safe to perform MRI on patients with stents, IVC filters, or coils, the presence of such devices may cause severe image artifacts related to distortion of the magnetic field by the metal, thus rendering portions or the entire MR study uninterpretable. Stainless steel devices in particular, as well as platinum and some other materials, will cause large areas of signal void on gradient-echo imaging sequences, the primary type of imaging used for MRA. These artifacts extend beyond the region of the device, and thus, for example, MRI of the right kidney may not be the appropriate examination for someone with a stainless steel IVC filter. Nitinol and other alloys will produce lesser degrees of artifact, and the vessel lumen may be evaluable even inside a stent<sup>48</sup> or adjacent to an IVC

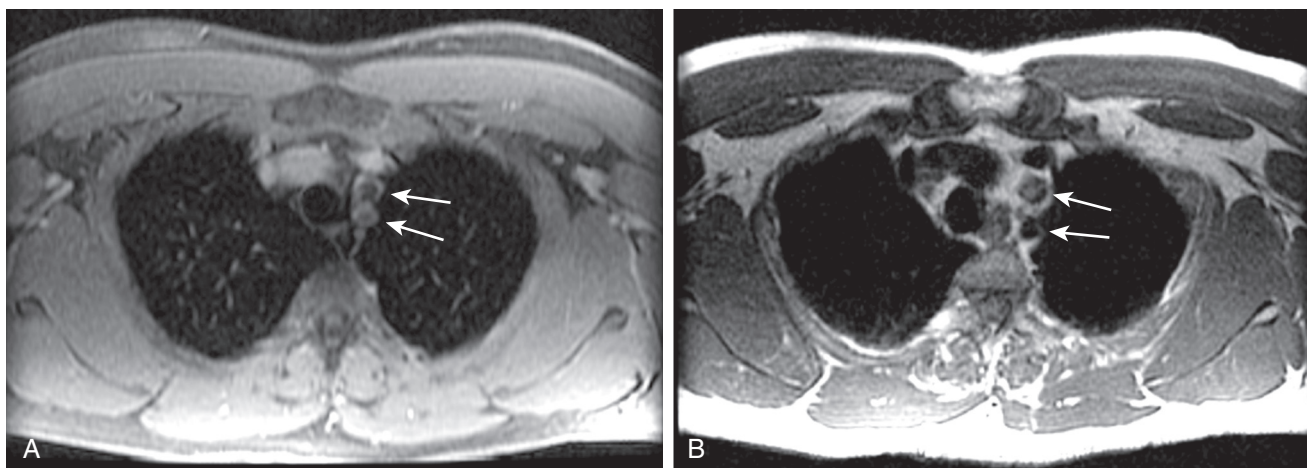


**Figure 30.25** (A) Axial 2D post-contrast fat-saturated T1-weighted image showing no contrast within the left subclavian and left common carotid arteries (arrows) in a patient with a type A dissection. (B) Axial T2-weighted dark blood imaging showing flow void within the left subclavian but signal within the left common carotid arteries (arrows), findings indicative of thrombosis.

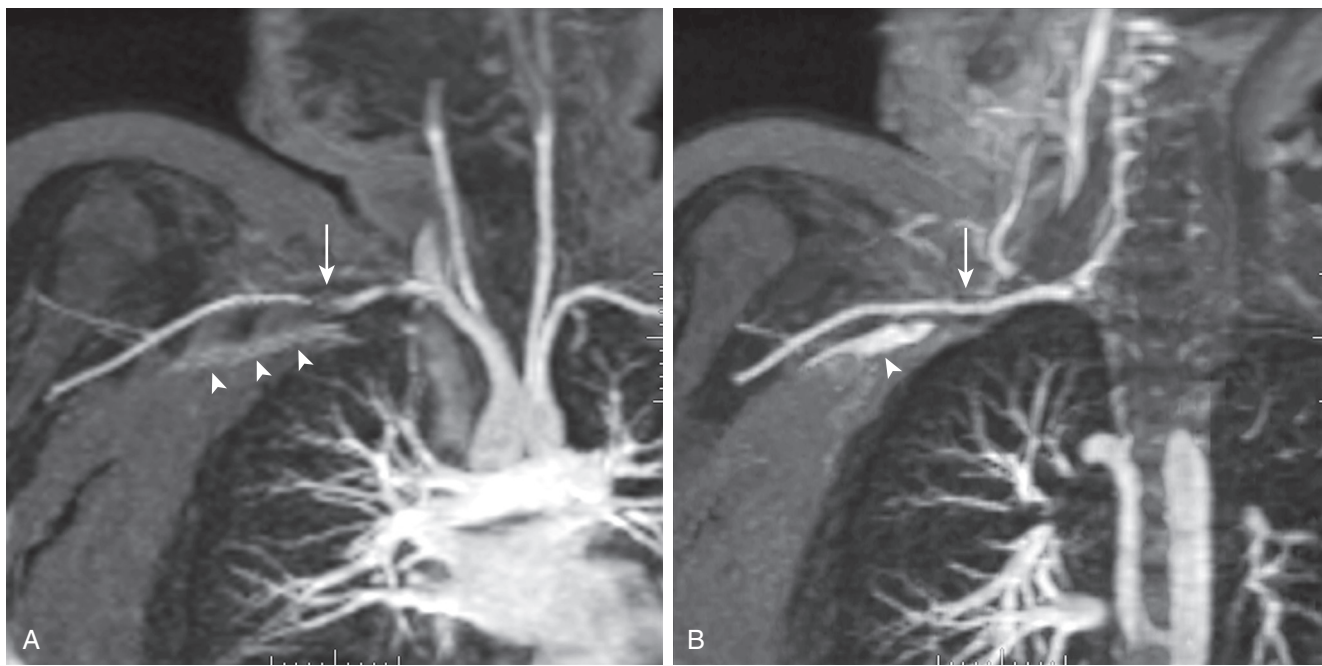


**Figure 30.26** (A) Arterial-phase coronal 3D MR angiogram showing apparent stenosis (arrow) in the right subclavian artery. Note that the signal from the pure contrast in the left subclavian vein (arrowheads) is not as high as the signal from the dilute contrast in the adjacent artery. (B) Delayed-phase 3D MR angiogram showing no stenosis in the subclavian artery (arrow). Note that the signal from the dilute venous contrast is now much higher than that from pure contrast (arrowhead).

filter. Although vessel patency can usually be evaluated, some artifact will still be present, and therefore these images may not reliably demonstrate vessel diameter or the degree of stenosis.

## FUTURE ADVANCES

### Continuous Moving Table and Time-Resolved MRA

One limitation of 3D contrast-enhanced MRA is that signal from the entire volume of data is acquired simultaneously, so

respiratory or other motion at any point during the acquisition may result in artifacts throughout the imaged volume. A solution to this difficulty is continuous moving table MRA, in which, as occurs in helical computed tomography (CT), the table moves throughout the acquisition in a proximal-to-distal direction. As in helical CT, data from only a small volume of tissue are being acquired at any moment, and motion artifacts will affect only the region being acquired at the time of the motion. In addition, continuous moving table techniques may truly permit “bolus chasing” because the speed of table motion can be adjusted to match the transit time of contrast in



**Figure 30.27** (A) Pre-contrast coronal T1-weighted image showing high intravascular signal from a thrombosed femoral bypass graft. The high signal is from methemoglobin in the thrombus. (B) Coronal 3D MR angiogram showing that the signal from the thrombus is as high as signal in the contralateral superficial femoral artery. There are signal voids at the origin and distal anastomosis of the graft, suggesting stenosis, when in fact the entire graft is occluded. (C) Subtraction image of the arterial-phase image minus the pre-contrast image showing only the contrast-enhancing arteries.

the arteries.<sup>112</sup> This technique has shown promising results for peripheral vascular imaging, particularly when combined with parallel imaging techniques to allow decreased scan time and increased resolution, without venous contamination.<sup>113</sup> **Figure 30.28** demonstrates a continuous-table motion MRA runoff obtained at 3T with parallel imaging.

Another limitation of typical contrast-enhanced MRA methods is that they average the appearance of a vessel over a long acquisition time, typically 20 seconds to 2 minutes, thus providing a static view without insight into the dynamic physiology of blood flow. For example, one may not be able to tell whether an artery distal to a high-grade stenosis is filling in an antegrade fashion or retrogradely through collaterals. Long acquisition times may also result in venous contamination if there is rapid transit of contrast through an organ with early venous filling, such as in the kidney. In addition, if two extremities are imaged simultaneously, the optimal imaging time may be different for each if one extremity has early arteriovenous shunting related to cellulitis, varicose veins, or arteriovenous malformations. Time-resolved MRA methods obtain multiple, more rapid acquisitions throughout passage of the contrast from arteries to veins.<sup>114</sup> Typically, time-resolved methods acquire thicker slices than static high-resolution MRA does; some spatial information is sacrificed for improved temporal resolution, but complete 3D data sets are acquired in 2 to 10 seconds instead of 20 to 120 seconds. In this way, images can demonstrate the dynamic flow of contrast into an artery, followed by venous filling. The multiple frames of the resulting time-lapse movie can be viewed to choose the time with optimal arterial filling and minimal venous contamination (Fig. 30.29).

## Novel Contrast Agents

Gd-DTPA and Gd-BOPTA-based contrast agents are extracellular or interstitial contrast agents as they do not enter cells

with intact membranes, however they rapidly equilibrate in the extracellular space after intravascular injection, with predominantly renal clearance, although some hepatic clearance also occurs. This property results in a narrow time window for MRA before the decreased concentration of contrast in the vessels and the increased background tissue signal make further imaging of little value, thus limiting the spatial resolution that can be obtained.

Blood pool contrast agents (BPCAs) remain intravascular for extended periods, which allows longer high-resolution imaging, albeit at a static steady state in which both arteries and veins are filled with contrast. Two principal types of BPCA have been developed – compounds of gadolinium bound to macromolecules and ultrasmall superparamagnetic iron oxide (USPIO) particles<sup>115,116</sup> – both of which may allow up to 1 hour of imaging time. Gadofosveset (Ablavar in the US, Vaso-vist outside the US) binds noncovalently to albumin in plasma and results in an increased degree of enhancement for the same concentration when compared with Gd-DTPA compounds, so a lower dose may be used in imaging (0.03 mmol/kg gadofosveset versus 0.1 mmol/kg Gd-DTPA).<sup>116</sup> One advantage of gadofosveset over some other BPCAs is the ability to obtain a dynamic arterial-phase acquisition in addition to steady-state imaging.

BPCAs have been evaluated for imaging of many vascular territories.<sup>117,118</sup> In most applications, steady-state imaging is performed at isotropic high spatial resolution, from 1 mm to 0.5 mm or less – such high resolution is necessary to be able to distinguish adjacent arteries and veins, both of which are filled with contrast. Imaging of abdominal and thoracic vessels (e.g., the renal arteries) is currently limited by breath-hold length and may not benefit as much from a BPCA, although the non-breath-hold respiratory or navigator-gated techniques currently used for noncontrast-enhanced MRA could be applied in these situations.<sup>119</sup> **Figure 30.30** shows a high resolution axial image



**Figure 30.28** Coronal maximum intensity projection of a continuous-table motion MRA runoff examination acquired at 3T with parallel imaging from the abdomen to the toes in a patient with bilateral iliac stenoses and segmental left superficial femoral artery occlusions. The acquisition time was approximately 90 seconds. Note the lack of venous contamination in the calves and feet.

T1-weighted image obtained through the forearm in a patient with a large vascular malformation more than 5 minutes after administration of a BPCA; contrast remains in both arterial and venous structures. Unfortunately, it was announced in early 2016 that Ablavar would no longer be available for purchase in the USA because of manufacturing difficulties.

Iron-based superparamagnetic nanoparticle MR contrast agents, SPIONS are used in scanning patients who have infection or inflammation. These agents are safe to be used in patients who have chronic renal failure where gadolinium based contrast are contraindicated. SPIONS when injected are phagocytosed by macrophages and show prolonged T2 and T2\* effects on contrast-enhanced MR images in macrophage-infiltrated tissues.<sup>115</sup> Ferumoxytol is one such USPIO agent that is FDA approved for use as an intravenous therapy in

iron deficiency anemia (Fig. 30.31). It has been evaluated as a vascular imaging agent and found applications in the aorta, peripheral vasculature and venous imaging, particularly in patients with renal insufficiency.<sup>116,120,121</sup>

## Imaging of Blood Flow

The above discussion has concentrated on anatomic imaging of blood vessels, using native or exogenous contrast to allow visualization of the vessel lumen. In these techniques, signal within a vessel is relatively independent of flow, although vessels with poor flow may not fill with exogenous contrast or provide enough signal for noncontrast methods. However, MRI can also be used to visualize and measure flow using phase-contrast techniques, in which signal intensity is actually proportional to flow velocity. In cardiac MRI, 2D methods have long been used to measure valvular flow and regurgitation and to calculate shunt fraction, using ECG-gating to acquire velocity maps through the cross-section of a vessel such as the aortic root. The instantaneous flow at each phase of the cardiac cycle is determined by multiplying the average velocity by the area of the cross-section, which is then integrated over the cardiac cycle to provide total flow.<sup>122</sup> The same 2D methods were used in the pre-contrast enhanced MRA era as an alternative to TOF imaging, allowing both anatomic and physiologic characterization of the significance of a stenosis.<sup>123</sup> Generalizing these methods to 3D velocity measurement over time has become possible, with acquisition times dramatically decreased by application of acceleration methods such as parallel imaging and compressed sensing.

Once the complete 4D dataset has been acquired, it can be visualized in a variety of different ways. One popular method creates time-resolved three-dimensional particle traces or path-lines, following the fate of a massless particle released from a specific point over the cardiac cycle. This method has been applied to many different vessels, however the ascending aorta has undergone the most study, allowing visualization and characterization of altered flow dynamics in patients with aneurysms, bicuspid valve, coarctation, and disorders such as Marfan syndrome (Fig. 30.32).<sup>124</sup> While 4D flow has proven useful for generation of hypotheses concerning a variety of pathophysiolgies, whether it will demonstrate value in clinical routine remains to be seen.<sup>125</sup>

## Plaque Imaging

A primary aim of MRA throughout the body is to image arterial stenosis caused by atherosclerotic disease; for this application, the principal advantages of MRI over catheter angiography are its noninvasive character and lack of ionizing radiation. However, stenosis imaging by itself fails to use one of the most powerful capabilities of MRI, soft tissue contrast imaging, which potentially allows visualization of the cause of the arterial stenosis (i.e., atherosclerotic plaque).<sup>126</sup> Several methods are available for imaging plaque, including noncontrast-enhanced techniques, the use of Gd-DTPA and other typical contrast agents, and imaging with contrast agents that concentrate specifically in atherosclerotic plaque.

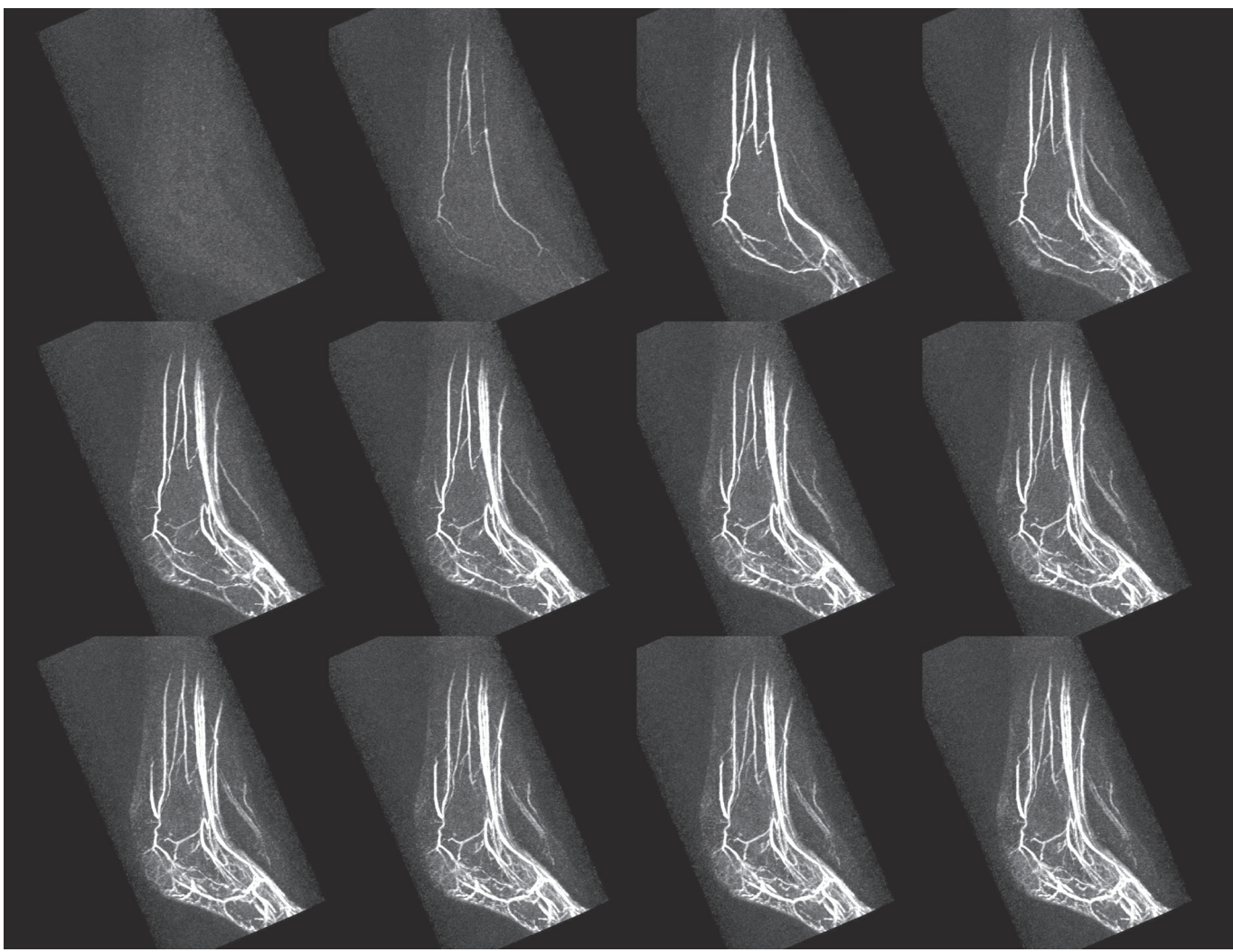


**Figure 30.29** Coronal maximum intensity projection images of successive frames from a time-resolved MRA examination of the feet. Each frame requires approximately 6 to 8 seconds to acquire, and thicker slices are obtained than with a static MR angiogram.

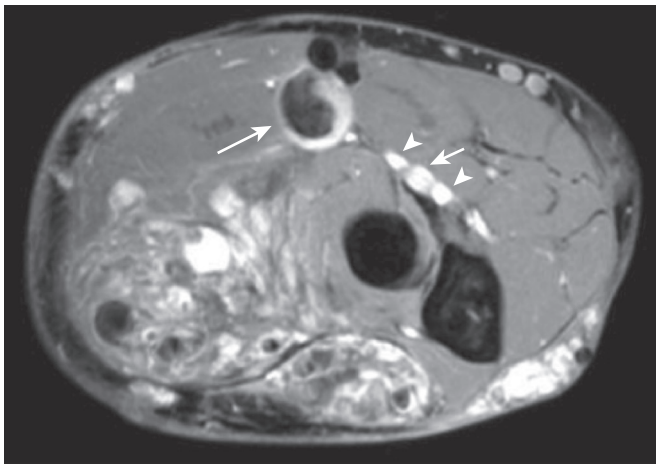


**Figure 30.30** High resolution axial T1-weighted image obtained more than 5 minutes after the administration of a blood pool contrast agent demonstrates contrast filling both arteries and veins (short arrow and arrowheads), and outlining thrombus in an enlarged draining vein (arrow) in a patient with a large forearm vascular malformation.

The carotid bifurcation has been the subject of many investigations of plaque imaging techniques given its superficial location, relative lack of pulsatile motion, high prevalence of atherosclerotic disease, and clinical importance. So-called multispectral imaging, which combines information from sequences with T1, T2, and proton density weighting, has been shown to allow reliable discrimination of the various components of carotid atherosclerotic plaque, including the lipid core and fibrous cap, and distinction between necrotic, calcified, and hemorrhagic plaque.<sup>127,128</sup> Similar techniques have begun to be applied to other vessels, including the aorta<sup>129</sup> and coronary arteries,<sup>130</sup> but imaging of atherosclerotic plaque in these vessels is limited by small diameter or pulsatile motion, or both. Contrast-enhanced imaging has been used to quantify the degree of neovascularity of atherosclerotic plaque, which may be related to vulnerability to or likelihood of rupture.<sup>131,132</sup> In addition to their properties as BPCAs, injected USPIO particles are eventually taken up by macrophages and thus allow



**Figure 30.31** Ferumoxytol-enhanced MRA of the chest and abdomen acquired at least 5 minutes after slow infusion of contrast. Note equal enhancement of systemic and pulmonary arterial as well as systemic and portal venous structures. (Image provided by Peng Hu, Ph.D. University of California, Los Angeles.)

visualization of macrophage-laden plaque, which may be more vulnerable to rupture.<sup>133</sup> One preliminary study has demonstrated increased uptake of gadofosveset, the BPCA described earlier, in inflamed arterial walls adjacent to atherosclerotic plaque.<sup>134</sup> Currently under development are MR molecular imaging agents that specifically bind to components of atherosclerotic plaque or vessel walls, such as integrins.<sup>135</sup> Recent studies have also shown that noninvasive MR angiography allows assessment of presence or absence of greater than 50% coronary artery stenosis with diagnostic accuracy comparable to that of multidetector computer tomography.<sup>136</sup>

### Computed Tomographic Angiography vs. Magnetic Resonance Angiography

The development of multidetector CT technology over the past 20 years has led to a dramatic improvement in the quality and reproducibility of CTA examinations. The latest generation of 64-, 128-, 256-, and 320-slice scanners permit the rapid acquisition of high-resolution data over a large volume, which allows arterial-phase acquisitions at isotropic submillimeter resolution. Although the utility of CTA versus MRA for specific vascular applications will be discussed in later chapters, general advantages and disadvantages of each technique are mentioned here.

#### Acquisition Speed

Despite advances in MRI such as 3T systems and parallel imaging technology, a major advantage of CTA is speed of

acquisition. Newer machines allow scanning of the entire aorta in under 2 seconds, scanning of the chest for evaluation of pulmonary embolism in 1 second, imaging of peripheral runoff from the diaphragm to the toes in less than 10 seconds, and imaging of the coronary arteries in 150 ms. More important than the specific speed of acquisition is the fact that spatial resolution is independent of acquisition time and limited only by detector thickness, focal spot size, and the transit time of contrast down a vessel. outrunning the contrast bolus is a potential complication in CTA,<sup>137</sup> especially in patients with poor cardiac output, large aneurysms with stagnant flow, or proximal occlusive disease. Unlike MRA, there is a cost associated with a repeat scan to allow filling of unopacified vessels, namely, increased radiation dose, although a second scan through the calves will not add much to the overall examination dose given their comparative insensitivity to radiation.<sup>138</sup>

#### Dynamic Imaging

Lack of dependence of spatial resolution on acquisition speed in CT can also be a disadvantage in that it is not possible to trade off these parameters for applications such as time-resolved imaging. As noted earlier, MRA can be performed in a dynamic fashion to provide physiologic information about direction and speed of blood flow, albeit at lower resolution, whereas CTA generally allows only static full-resolution snapshots at one or two time points during the contrast bolus. New wide detector CT systems can image up to 16 cm at each gantry rotation (less than 0.3 seconds), thereby potentially allowing full-resolution dynamic imaging as well. Although this technique has shown some initial promise in neurovascular imaging, where it can also capture brain perfusion, it is not yet clear that the information gained will be worth the substantial penalty in radiation dose engendered by repeated scans.

#### Calcification and Other Imaging Artifacts

MR is limited in its ability to image vascular calcification because it tends to have very low signal on all pulse sequences used for MRA. Although this disadvantage limits the utility of MRI for detection of vascular calcification, it also means that MRA is in general not subject to the artifacts from vascular calcification seen with CTA. Therefore, MRA may be more appropriate for patients with known or a high likelihood of heavily calcified vessels,<sup>139</sup> particularly for distal runoff imaging in diabetics. However, because these patients are also more likely to have renal disease, all options should be carefully considered, including noncontrast-enhanced MRA. Dual energy CT, also known as spectral CT, is a novel technique in which CT data is acquired at two different X-ray energies exploiting the fact that the difference in X-ray attenuation at the two different energies is characteristic of an element, with chemical binding exerting only a small effect. By examining the difference in attenuation for each pixel at the two different energies, one can determine the material in that pixel. Using this method, pixels containing calcium can be separated from those containing iodine, even if their attenuation (in Hounsfield units) is very similar, allowing more accurate subtraction of calcium in bones and vessels from CT angiographic studies.<sup>140</sup> However, while these methods

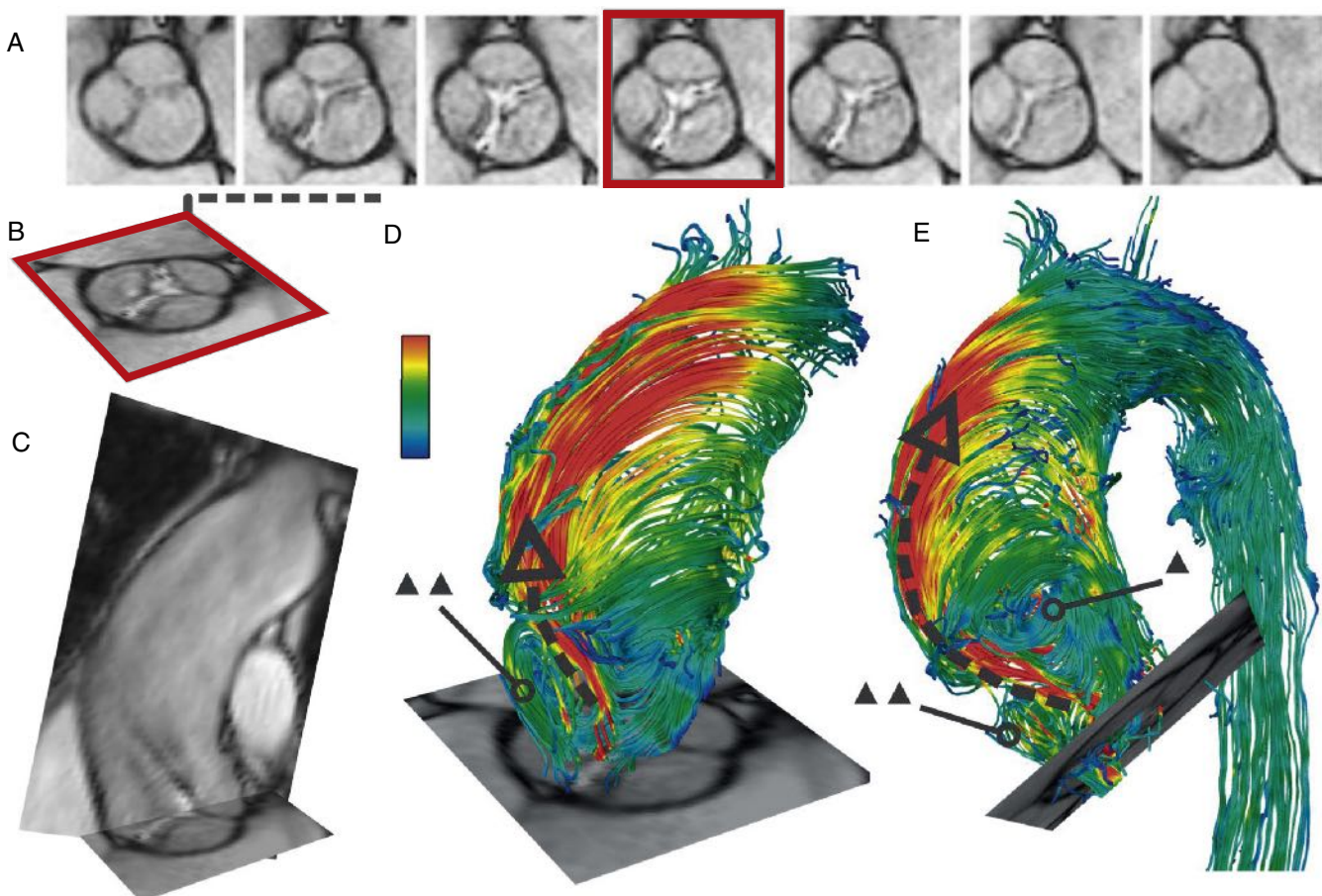


**Figure 30.32** Images obtained from a 4D flow MRA study of a patient with a bicuspid valve including (A,B) cine frames through the valve; (C) oblique sagittal cine frame through the ascending aorta; and (D,E) pathline displays of vortical flow in the dilated ascending aorta; high-velocity flow along the anterior border of the ascending aorta (*large arrow*) and abnormal flow vortices at the aortic root (*arrowheads*).

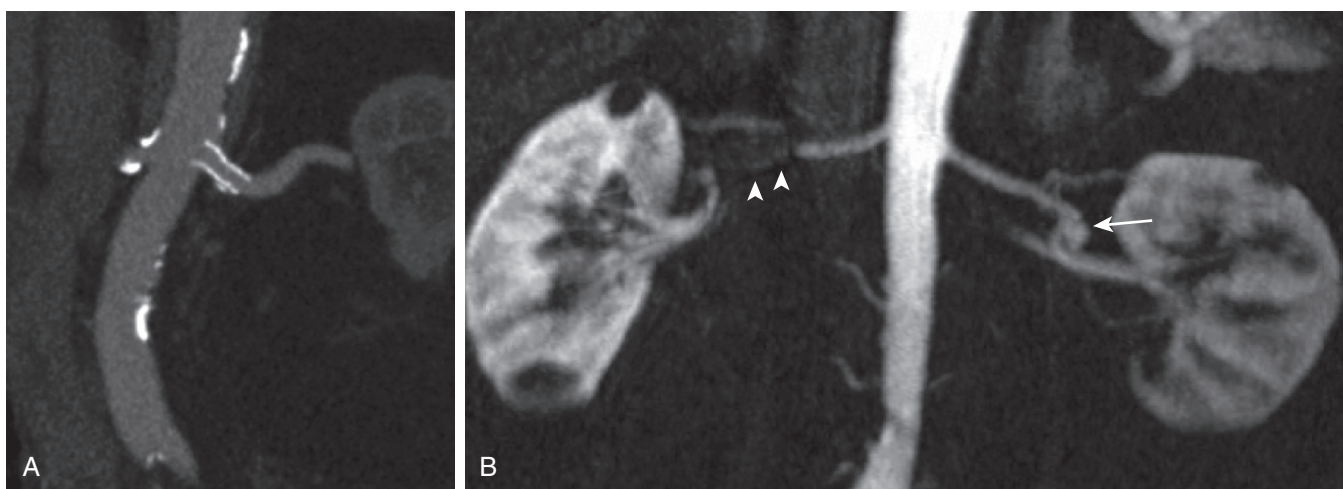


**Figure 30.33** (A) Coronal multiplanar reconstruction (MPR) from a CTA examination demonstrating a patent stent in the left renal artery. (B) Coronal MIP from three-dimensional MRA in a patient with history of previous stent placement for right renal artery aneurysm. Note artifact from the stent obscuring the mid-portion of the renal artery (*arrowheads*); stent patency is inferred from enhancement of right kidney. A left renal artery aneurysm is also present (*arrow*).

may allow improved removal of vascular calcification, they do not decrease the artifacts associated with the calcification, and therefore the degree of stenosis may still be overestimated in a vessel adjacent to a large calcified lesion.

As discussed earlier, MRA may be suboptimal in the presence of vascular stents, filters, or coils, depending on their composition. CTA also is subject to artifacts in these circumstances, though to a lesser degree.<sup>141–144</sup> Figure 30.33 demonstrates

the ability of CT to visualize the stent lumen, as well as the presence of stent artifact on MRA. Specific exceptions include coils containing platinum and stents or other metallic implants made of titanium or gold, all of which can cause severe streak artifacts on CTA.<sup>145,146</sup> Orthopedic hardware can cause artifacts in both modalities, but MRA may provide a better option, depending on the specific device and anatomy being imaged. As noted, CTA is almost always preferred in patients with implanted pacemakers or defibrillators.

### Radiation Dose and Contrast Concerns

With increasing utilization of CT, and of CTA in particular, has come increased concern for the effects of exposure to ionizing radiation. Several high-profile journals and the mainstream media have published reports evaluating the cancer risk engendered by exposure to radiation from CT.<sup>147,148</sup> Although one can disagree with the assumptions behind many of the calculations of cancer risk in these reports, it is clear that repeated CT studies do come with some risk. Therefore, consideration should be given to the use of MRA in radiation-sensitive populations (children, young women, etc.) and in those who will undergo repeated surveillance studies over many years.

As discussed previously, gadolinium contrast agents are not without risk, particularly in patients with renal dysfunction. However, the incidence of CIN is still greater with iodinated contrast (at the doses of each used for clinical imaging), and there is a higher rate of reactions and complications after iodinated contrast agents.<sup>148,149</sup> As stated earlier, contrast-enhanced MRA should not generally be performed in dialysis-dependent patients without a compelling clinical need.

Dual energy CT may provide an opportunity for both radiation and contrast dose reduction in CT angiography. As mentioned above, this technique can be used to determine the material content of an object, e.g., the amount of iodine in a specific pixel. The amount of iodine can then be subtracted, leaving what is called a “virtual noncontrast” or water image. This has two potential benefits: (1) obviating the need for an actual pre-contrast acquisition, for example saving radiation dose in stent-graft follow-up exams<sup>149</sup> and (2) improving the contrast-to-noise ratio (CNR) of contrast enhanced exams, allowing for reductions in iodinated contrast dosage.<sup>150</sup>

### Ease of Use and Convenience

CTA examinations are generally performed much more quickly than MRA, in less than 5 minutes of table time versus 30 minutes or more. This is a result of increased positioning and setup time before data acquisition, increased duration of each acquisition performed during the study, and the increased number of acquisitions per study for MRA vs. CTA. The increased number of acquisitions is related both to the ability to acquire multiple phases during the contrast bolus without a radiation penalty and to the multiple pulse sequences acquired to obtain the different soft tissue contrast (T1 vs. T2) that are available with MRI. Our typical CTA protocol requires four breath-holds (topogram, pre-contrast, arterial phase, and delayed phase), whereas a typical MRA protocol would entail approximately 10 breath-holds (localizers [2], axial T1 in- and out-of-phase imaging [2], axial

T2 in- and out-of-phase imaging [2], pre-contrast imaging [1], arterial- and delayed-phase MRA [2], and post-contrast T1-weighted imaging [1]), which can be completed in less than 15 minutes in most patients. However, CT would still be the recommended initial study for acutely symptomatic vascular disease such as acute aortic syndromes.

Until recently, CTA gantries were larger and more “open” than MR systems; however, the availability of short-bore MRI machines and 64-slice and greater CT has virtually erased that gap, with 70-cm openings and 450-lb or higher table capacity being standard on most CT and MR systems. The presence of the magnetic field does continue to limit the types of monitoring equipment and patient attachments that can be brought into the scan room, as well as ease of access for staff to respond to medical emergencies in the magnet room. Although MR systems tend to be more expensive and less available than CT systems, these differences have also narrowed recently.

MR angiograms tend to be easier to interpret and postprocess than CT angiograms because of the background suppression techniques used in MRA pulse sequences. This allows rapid 3D visualization without the need for the bone removal techniques used in CTA. In addition, there are usually many fewer images in 3D Gd-MRA than in corresponding CTA of the same volume because the MR angiogram can be acquired in the plane that is most advantageous for the specific anatomy, such as oblique sagittal for the aorta, whereas all CT images are acquired axially and then reformatted to the desired orientation.

Both CTA and MRA can provide excellent-quality imaging in almost all clinical circumstances. In the end, the decision concerning whether to perform CTA or MRA may often be most influenced by the local availability of the technology and expertise in performing and interpreting these studies, as well as the experience and comfort of the referring vascular surgeon with the two modalities and the interpreting radiologists.

## SELECTED KEY REFERENCES

- Brenner DJ, Hall EJ. Computed tomography – an increasing source of radiation exposure. *N Engl J Med*. 2007;357:2277–2284.  
*Discussion of theoretical risks of radiation exposure related to CT.*
- Edelman RR, Koktzoglou I. Noncontrast MR angiography: An update. *J Magn Reson Imaging*. 2019;49(2):355–373.  
*Description and comparison of several noncontrast-enhanced MRA techniques.*
- Ersoy H, Rybicki F. MR Angiography of the lower extremities. *AJR Am J Roentgenol*. 2008;190(6):1675–1684.  
*Good overview of current techniques and their performance characteristics.*
- Jahedhar Maralani P, Schieda N, Hecht EM, et al. MRI safety and devices: An update and expert consensus. *J Magn Reson Imaging*. 2020;51(3):657–674.  
*Update concerning MRI in patients with devices and implants, including stents and pacemakers.*
- Rudnick MR, Wahba IM, Leonberg-Yoo AK, Miskulin D, Litt HI. Risks and options with gadolinium-based contrast agents in patients with CKD: a review. *Am J Kidney Dis*. 2021;77(4):517–528.

Review article with advice concerning use of gadolinium contrast agents in patients with renal dysfunction.

Shellock FG. *Reference Manual for Magnetic Resonance Safety, Implants, and Devices: 2020 Edition*. Biomedical Research Publishing Group; 2020.

Reference for advice concerning MRI of patients with implants. Also see [www.mrisafety.com](http://www.mrisafety.com).

Tan KT, van Beek EJ, Brown PW, van Delden OM, Tijssen J, Ramsay LE. Magnetic resonance angiography for the diagnosis of renal artery stenosis: a meta-analysis. *Clin Radiol*. 2002;57:617–624.

Largest meta-analysis of MRA for renal artery stenosis.

A complete reference list can be found online at [www.expertconsult.com](http://www.expertconsult.com).

## REFERENCES

1. Tan KT, van Beek EJ, Brown PW, et al. Magnetic resonance angiography for the diagnosis of renal artery stenosis: a meta-analysis. *Clin Radiol.* 2002;57:617–624.
2. Meaney JF. Magnetic resonance angiography of the peripheral arteries: Current status. *Eur Radiol.* 2003;13:836–852.
3. Hood MN, Ho VB, Foo TK, et al. High-resolution gadolinium-enhanced 3D MRA of the infrapopliteal arteries. Lessons for improving bolus-chase peripheral MRA. *Magn Reson Imaging.* 2002;20:543–549.
4. Sharafuddin MJ, Stolpen AH, Sun S, et al. High-resolution multiphase contrast-enhanced three-dimensional MR angiography compared with two-dimensional time-of-flight MR angiography for the identification of pedal vessels. *J Vasc Interv Radiol.* 2002;13:695–702.
5. Johnson DB, Lerner CA, Prince MR, et al. Gadolinium-enhanced magnetic resonance angiography of renal transplants. *Magn Reson Imaging.* 1997;15:13–20.
6. Cowper SE, Robin HS, Steinberg SM, et al. Scleromyxoedema-like cutaneous diseases in renal dialysis patients. *Lancet.* 2000;356:1000–1001.
7. Grobner T. Gadolinium—a specific trigger for the development of nephrogenic fibrosing dermopathy and nephrogenic systemic fibrosis? *Nephrol Dial Transplant.* 2006;21:1104–1108.
8. Edelman RR, Koktzoglou I. Noncontrast MR angiography: An update. *J Magn Reson Imaging.* 2019;49(2):355–373.
9. François CJ, Tuite D, Deshpande V, et al. Unenhanced MR angiography of the thoracic aorta: initial clinical evaluation. *AJR Am J Roentgenol.* 2008;190:902–906.
10. Knobelsdorff-Brenkenhoff FV, Gruettner H, Ralf F, et al. Comparison of native high-resolution 3D and contrast enhanced MRA for assessing the thoracic aorta. *Eur Heart J Cardiovasc Imaging.* 2014;15(6):651–658.
11. Kramer H, Runge VM, Morelli JN, et al. MRA of the carotid arteries: comparison of unenhanced and contrast enhanced techniques. *Eur Radiol.* 2011;21(8):1667–1676.
12. Angeretti MG, Lumia D, Cani A, et al. Non enhanced MRA of renal arteries: Comparison with contrast enhanced MRA. *Acta Radiol.* 2013;54(7):749–756.
13. Atanasova IP, Kim D, Storey P, et al. Sagittal Fresh Blood Imaging with interleaved acquisition of systolic and diastolic data for improved robustness to motion. *Magn Reson Med.* 2013;69(2):321–328.
14. Miyazaki M, Takai H, Sugiura S, et al. Peripheral MR angiography: separation of arteries from veins with flow-spoiled gradient pulses in electrocardiography-triggered three-dimensional half-Fourier fast spin-echo imaging. *Radiology.* 2003;227:890–896.
15. Spinoza DJ, Angle JF, Hartwell GD, et al. Gadolinium-based contrast agents in angiography and interventional radiology. *Radiol Clin North Am.* 2002;40:693–710.
16. Srodon P, Matson M, Ham R. Contrast nephropathy in lower limb angiography. *Ann R Coll Surg Engl.* 2003;85:187–191.
17. Rieger J, Sitter T, Toepfer M, et al. Gadolinium as an alternative contrast agent for diagnostic and interventional angiographic procedures in patients with impaired renal function. *Nephrol Dial Transplant.* 2002;17:824–828.
18. Freed KS, Leder RA, Alexander C, et al. Breakthrough adverse reactions to low-osmolar contrast media after steroid premedication. *AJR Am J Roentgenol.* 2001;176:1389–1392.
19. Lieberman PL, Seigle RL. Reactions to radiocontrast material. Anaphylactoid events in radiology. *Clin Rev Allergy Immunol.* 1999;17:469–496.
20. Sun Y, Parker DL. Performance analysis of maximum intensity projection algorithm for display of MRA images. *IEEE Trans Med Imaging.* 1999;18:1154–1169.
21. Albert TS, Akahane M, Parienty I, et al. An international multicenter comparison of time-slip unenhanced MRA and contrast enhanced CT angiography for assessing renal artery stenosis: The renal artery contrast free trial. *AJR Am J Roentgenol.* 2015;204(1):182–188.
22. Fink C, Hallscheidt PJ, Hosch WP, et al. Preoperative evaluation of living renal donors: Value of contrast-enhanced 3D MRA and comparison of three rendering algorithms. *Eur Radiol.* 2003;13(4):794–801.
23. Hecht EM, Lee RF, Taouli B, et al. Perspectives on body MR imaging at ultrahigh field. *Magn Reson Imaging Clin N Am.* 2007;15:449–465.
24. DeLano MC, Fisher C. 3T MR imaging of the brain. *Magn Reson Imaging Clin N Am.* 2006;14:77–88.
25. Mosher TJ. Musculoskeletal imaging at 3T: Current techniques and future applications. *Magn Reson Imaging Clin N Am.* 2006;14:63–76.
26. Merkle EM, Dale BM, Paulson EK. Abdominal MR imaging at 3T. *Magn Reson Imaging Clin N Am.* 2006;14:17–26.
27. Michaeli HJ, Attenberger UI, Kramer H, et al. Abdominal and pelvic MR angiography. *Magn Reson Imaging Clin N Am.* 2007;15:301–314.
28. DeMarco JK, Huston 3rd J, Nash AK. Extracranial carotid MR imaging at 3T. *Magn Reson Imaging Clin N Am.* 2006;14:109–121.
29. Diehm N, Kickuth R, Baumgartner I, et al. Magnetic resonance angiography in infrapopliteal arterial disease: prospective comparison of 1.5 and 3 Tesla magnetic resonance imaging. *Invest Radiol.* 2007;42:467–476.
30. Lin W, An H, Chen Y, et al. Practical consideration for 3T imaging. *Magn Reson Imaging Clin N Am.* 2003;11:615–639.
31. Tanenbaum LN. Clinical 3T MR imaging: mastering the challenges. *Magn Reson Imaging Clin N Am.* 2006;14:1–15.
32. Heidemann RM, Ozsarlak O, Parizel PM, et al. A brief review of parallel magnetic resonance imaging. *Eur Radiol.* 2003;13:2323–2337.
33. Larkman DJ, Nunes RG. Parallel magnetic resonance imaging. *Phys Med Biol.* 2007;52:R15–R55.
34. Zenge MO, Vogt FM, Brauck K, et al. High-resolution continuously acquired peripheral MR angiography featuring partial parallel imaging GRAPPA. *Magn Reson Med.* 2006;56:859–865.
35. Tsao J, Boesiger P, Pruessman K. K-tBlast and K-t SENSE: Dynamic MRI with high frame rate exploiting spatio temporal correlations. *Magn Reson Med.* 2003;50:1031–1042.
36. Geethnath S, Reddy R, Konar AS, et al. Compressed sensing: A review. *Crit Rev Biomed Eng.* 2013;4191:213.
37. Jaspan ON, Fleysher R, Lipton ML. Compressed sensing MRI; a review of the clinical literature. *BJR.* 2015;88(1056):20150487.
38. Vogt FM, Ajaj W, Hunold P, et al. Venous compression at high-spatial-resolution three-dimensional MR angiography of peripheral arteries. *Radiology.* 2004;233:913–920.
39. Roberts DA. Magnetic resonance imaging of thoracic aortic aneurysm and dissection. *Semin Roentgenol.* 2001;36:295–308.
40. Carr JC, Finn JP. MR imaging of the thoracic aorta. *Magn Reson Imaging Clin N Am.* 2003;11:135–148.
41. Ho VB, Corse WR. MR angiography of the abdominal aorta and peripheral vessels. *Radiol Clin North Am.* 2003;41:115–144.
42. Vogt FM, Goyen M, Debatin JF. MR angiography of the chest. *Radiol Clin North Am.* 2003;41:29–41.
43. Carpenter JP, Holland GA, Golden MA, et al. Magnetic resonance angiography of the aortic arch. *J Vasc Surg.* 1997;25:145–151.
44. Fernandez GC, Tardaguila FM, Duran D, et al. Dynamic 3-dimensional contrast-enhanced magnetic resonance angiography in acute aortic dissection. *Curr Probl Diagn Radiol.* 2002;31:134–145.
45. Leiner T, Elenbaas TW, Kaandorp DW, et al. Magnetic resonance angiography of an aortic dissection. *Circulation.* 2001;103:E76–E78.
46. Hartnell GG. Imaging of aortic aneurysms and dissection: CT and MRI. *J Thorac Imaging.* 2001;16:35–46.
47. Kawamoto S, Bluemke DA, Traill TA, et al. Thoracoabdominal aorta in Marfan syndrome: MR imaging findings of progression of vasculopathy after surgical repair. *Radiology.* 1997;203:727–732.
48. Cejna M, Loewe C, Schoder M, et al. MR angiography vs CT angiography in the follow-up of nitinol stent grafts in endoluminally treated aortic aneurysms. *Eur Radiol.* 2002;12:2443–2450.
49. Insko EK, Kulzer LM, Fairman RM, et al. MR imaging for the detection of endoleaks in recipients of abdominal aortic stent-grafts with low magnetic susceptibility. *Acad Radiol.* 2003;10:509–513.
50. Nederkoorn PJ, van der Graaf Y, Hunink MG. Duplex ultrasound and magnetic resonance angiography compared with digital subtraction

- angiography in carotid artery stenosis: a systematic review. *Stroke*. 2003;34:1324–1332.
51. Lenhart M, Framme N, Volk M, et al. Time-resolved contrast-enhanced magnetic resonance angiography of the carotid arteries: diagnostic accuracy and inter-observer variability compared with selective catheter angiography. *Invest Radiol*. 2002;37:535–541.
  52. Westwood ME, Kelly S, Berry E, et al. Use of magnetic resonance angiography to select candidates with recently symptomatic carotid stenosis for surgery: Systematic review. *BMJ*. 2002;324:198–222.
  53. Cosottini M, Pingitore A, Puglioli M, et al. Contrast-enhanced three-dimensional magnetic resonance angiography of atherosclerotic internal carotid stenosis as the noninvasive imaging modality in revascularization decision making. *Stroke*. 2003;34:660–664.
  54. Dillavou E, Kahn MB. Peripheral vascular disease. Diagnosing and treating the 3 most common peripheral vasculopathies. *Geriatrics*. 2003;58:37–42.
  55. Sharafuddin MJ, Wroblecka JT, Sun S, et al. Percutaneous vascular intervention based on gadolinium-enhanced MR angiography. *J Vasc Interv Radiol*. 2000;11:739–746.
  56. Wurz C, Davari A, Ackerman H. Diagnostic performance of contrast enhanced – MRA in grading stenosis and therapy planning with TASC II classification. *Vascular*. 2015;23(4):403–410.
  57. Khilnani NM, Winchester PA, Prince MR, et al. Peripheral vascular disease: combined 3D bolus chase and dynamic 2D MR angiography compared with x-ray angiography for treatment planning. *Radiology*. 2002;224:63–74.
  58. Hofmann WJ, Forstner R, Kofler B, et al. Pedal artery imaging—a comparison of selective digital subtraction angiography, contrast enhanced magnetic resonance angiography and duplex ultrasound. *Eur J Vasc Endovasc Surg*. 2002;24:287–292.
  59. Heverhagen JT, Wagner HJ, Bandorski D, et al. Magnetic resonance phase contrast velocity measurement for non-invasive follow up after percutaneous transluminal angioplasty. *Vasa*. 2002;31:235–240.
  60. Heverhagen JT, Kalinowski M, Schwarz U, et al. Quantitative human in vivo evaluation of high resolution MRI for vessel wall morphometry after percutaneous transluminal angioplasty. *Magn Reson Imaging*. 2000;18:985–989.
  61. Couloden RA, Moss H, Graves MJ, et al. High resolution magnetic resonance imaging of atherosclerosis and the response to balloon angioplasty. *Heart*. 2000;83:188–191.
  62. Marcos HB, Choyke PL. Magnetic resonance angiography of the kidney. *Semin Nephrol*. 2000;20:450–455.
  63. Fleury N, Vallee JP, Hadaya K, et al. Magnetic resonance imaging as the sole radiological assessment for living donor nephrectomy. *Urol Int*. 2010;84(1):56–60.
  64. Israel GM, Lee VS, Edye M, et al. Comprehensive MR imaging in the preoperative evaluation of living donor candidates for laparoscopic nephrectomy: initial experience. *Radiology*. 2002;225:427–432.
  65. Derkx FHM, Schalekamp MADH. Renal artery stenosis and hypertension. *Lancet*. 1994;344:237–239.
  66. Andersson M, Jagervall K, Eriksson P, et al. How to measure renal artery stenosis – a retrospective comparison of morphological measurement approaches in relation to hemodynamic significance. *BMC Med Imaging*. 2015;15:42.
  67. Baumgartner I, von Aesch K, Do DD, et al. Stent placement in ostial and nonostial atherosclerotic renal arterial stenoses: a prospective follow-up study. *Radiology*. 2000;216:498–505.
  68. Bush RL, Najibi S, MacDonald MJ, et al. Endovascular revascularization of renal artery stenosis: technical and clinical results. *J Vasc Surg*. 2001;33:1041–1049.
  69. Kaatee R, Beek FJ, Verschuylen EJ, et al. Atherosclerotic renal artery stenosis: ostial or truncal? *Radiology*. 1996;199:637–640.
  70. Willoteaux S, Faivre-Pierret M, Moranne O, et al. Fibromuscular dysplasia of the main renal arteries: comparison of contrast-enhanced MR angiography with digital subtraction angiography. *Radiology*. 2006;241(3):922–929.
  71. Debatin JF, Sostman HD, Knelson M, et al. Renal magnetic resonance angiography in the preoperative detection of supernumerary renal arteries in potential kidney donors. *Invest Radiol*. 1993;28:882–889.
  72. Chow LC, Chan FP, Li KC. A comprehensive approach to MR imaging of mesenteric ischemia. *Abdom Imaging*. 2002;27:507–516.
  73. Cognet F, Salem BD, Dransart M, et al. Chronic mesenteric ischemia: imaging and percutaneous treatment. *Radiographics*. 2002;22:863–879. discussion 879–880.
  74. Carlos RC, Stanley JC, Stafford-Johnson D, et al. Interobserver variability in the evaluation of chronic mesenteric ischemia with gadolinium-enhanced MR angiography. *Acad Radiol*. 2001;8:879–887.
  75. Lee VS, Morgan JN, Tan AG, et al. Celiac artery compression by the median arcuate ligament: a pitfall of end-expiratory MR imaging. *Radiology*. 2003;228:437–442.
  76. Bradbury MS, Kavanagh PV, Bechtold RE, et al. Mesenteric venous thrombosis: diagnosis and noninvasive imaging. *Radiographics*. 2002;22:527–541.
  77. Kroencke TJ, Taupitz M, Arnold R, et al. Three-dimensional gadolinium-enhanced magnetic resonance venography in suspected thrombo-occlusive disease of the central chest veins. *Chest*. 2001;120:1570–1576.
  78. Thornton MJ, Ryan R, Varghese JC, et al. A three-dimensional gadolinium-enhanced MR venography technique for imaging central veins. *AJR Am J Roentgenol*. 1999;173:999–1003.
  79. Stern JB, Abehsara M, Grenet D, et al. Detection of pelvic vein thrombosis by magnetic resonance angiography in patients with acute pulmonary embolism and normal lower limb compression ultrasonography. *Chest*. 2002;122:115–121.
  80. Spritzer CE, Arata MA, Freed KS. Isolated pelvic deep venous thrombosis: relative frequency as detected with MR imaging. *Radiology*. 2001;219:521–525.
  81. Evans AJ, Sostman HD, Witty LA, et al. Detection of deep venous thrombosis: prospective comparison of MR imaging and sonography. *J Magn Reson Imaging*. 1996;6:44–51.
  82. Ersoy H, Steigner ML, Coyner KB, et al. Vascular thoracic outlet syndrome: Protocol design and diagnostic value of contrast enhanced 3D MR angiography and equilibrium phase imaging on 1.5 and 3-T MRI scanners. *AJR Am J Roentgenol*. 2012;198:1180–1187.
  83. Fang YC, Siegelman ES. Complications of renal transplantation: MR findings. *J Comput Assist Tomogr*. 2001;25:836–842.
  84. Atalay MK, Bluemke DA. Magnetic resonance imaging of large vessel vasculitis. *Curr Opin Rheumatol*. 2001;13:41–47.
  85. Papa M, De Cobelli F, Baldissera E, et al. Takayasu Arteritis: Intravascular contrast medium for MR angiography in the evaluation of disease activity. *AJR Am J Roentgenol*. 2012;198:279–284.
  86. Goyen M, Ruehm SG, Jagenburg A, et al. Pulmonary arteriovenous malformation: characterization with time-resolved ultrafast 3D MR angiography. *J Magn Reson Imaging*. 2001;13:458–460.
  87. Maki DD, Siegelman ES, Roberts DA, et al. Pulmonary arteriovenous malformations: three-dimensional gadolinium-enhanced MR angiography—initial experience. *Radiology*. 2001;219:243–246.
  88. Vasile JV, Levine JL. Magnetic resonance angiography in perforator flap breast reconstruction. *Gland Surg*. 2016;5(20):197–211.
  89. Siegelman ES, Charafeddine R, Stolpen AH, et al. Suppression of intravascular signal on fat-saturated contrast-enhanced thoracic MR arteriograms. *Radiology*. 2000;217:115–118.
  90. Tirkes AT, Rosen MA, Siegelman ES. Gadolinium susceptibility artifact causing false positive stenosis isolated to the proximal common carotid artery in 3D dynamic contrast medium enhanced MR angiography of the thorax—a brief review of causes and prevention. *Int J Cardiovasc Imaging*. 2003;19:151–155.
  91. Neimatallah MA, Chenevert TL, Carlos RC, et al. Subclavian MR arteriography: reduction of susceptibility artifact with short echo time and dilute gadopentetate dimeglumine. *Radiology*. 2000;217:581–586.
  92. Olsen RV, Munk PL, Lee MJ, et al. Metal artifact reduction sequence: Early clinical applications. *Radiographics*. 2000;20:699–712.
  93. Choi SJ, Kevin KM, Hargreaves BA, et al. Metal artifact reduction with MAVRIC SL at 3-T MRI in patients with hip arthroplasty. *AJR Am J Roentgenol*. 2015;204(1):140–147.
  94. Yu L, Leng S, McCollough CH. Dual-Energy CT-Based Monochromatic Imaging. *AJR Am J Roentgenol*. 2012;199:S9–S15.

95. Insko EK, Siegelman ES, Stolpen AH. Subacute clot mimicking flow in a thrombosed arterial bypass graft on two-dimensional time-of-flight and three-dimensional contrast-enhanced MRA. *J Magn Reson Imaging*. 2000;11:192–194.
96. Saab G, Abu-Alfa A. Nephrogenic systemic fibrosis—implications for nephrologists. *Eur J Radiol*. 2008;66:208–212.
97. Thomsen HS, Morcos SK, Almén T, et al. Nephrogenic systemic fibrosis and gadolinium-based contrast media: updated ESUR Contrast Medium Safety Committee guidelines. *Eur Radiol*. 2013;23:307–318.
98. Yan I, Krefting I, Gorovets A, et al. Nephrogenic systemic fibrosis and Class Labelling of Gadolinium-based contrast Agents by the Food and Drug Administration. *Radiology*. 2012;265:248–253.
99. Rudnick MR, Wahba IM, Leonberg-Yoo AK, Miskulin D, Litt HI. Risks and options with gadolinium-based contrast agents in patients with CKD: a review. *Am J Kidney Dis*. 2021;77(4):517–528.
100. Woolen SA, Shankar PR, Gagnier JJ, et al. Risk of nephrogenic systemic fibrosis in patients with stage 4 or 5 chronic kidney disease receiving a group II gadolinium-based contrast agent: a systematic review and meta-analysis. *JAMA Intern Med*. 2020;180(2):223–230.
101. Abu-Alfa AK. Use of gadolinium-based contrast agents in kidney disease patients: time for a change. *Am J Kidney Dis*. 2020;76(3):436–439.
102. Dempsey MF, Condon B, Hadley DM. MRI safety review. *Semin Ultrasound CT MR*. 2002;23:392–401.
103. McNeil Jr DG. M.R.I.'s Strong Magnets Cited in Accidents. *The New York Times*, August 19. 2005.
104. Shellock FG. *Reference Manual for Magnetic Resonance Safety, Implants, and Devices: 2020 Edition*. Biomedical Research Publishing Group; 2020.
105. Shellock FG. Magnetic resonance safety update 2002: implants and devices. *J Magn Reson Imaging*. 2002;16:485–496.
106. Shellock FG. [www.MRIsafety.com](http://www.MRIsafety.com).
107. Jabehdar Maralani P, Schieda N, Hecht EM, et al. MRI safety and devices: An update and expert consensus. *J Magn Reson Imaging*. 2020;51(3):657–674.
108. Nazarian S, Hansford R, Rahsepar AA, et al. Safety of magnetic resonance imaging in patients with cardiac devices. *N Engl J Med*. 2017;377(26):2555–2564.
109. Russo RJ, Costa HS, Silva PD, et al. Assessing the Risks Associated with MRI in Patients with a Pacemaker or Defibrillator. *N Engl J Med*. 2017;376(8):755–764.
110. American Society for Testing and Materials (ASTM) International: ASTM F2503-05: Standard Practice for Marking Medical Devices and Other Items for Safety in the Magnetic Resonance Environment. West Conshohocken, PA, ASTM International; 2005. Available at: <http://www.astm.org>.
111. Hiramoto JS, Reilly LM, Schneider DB, et al. The effect of magnetic resonance imaging on stainless-steel Z-stent-based abdominal aortic prosthesis. *J Vasc Surg*. 2007;45:472–474.
112. Kruger DG, Riederer SJ, Grimm RC, et al. Continuously moving table data acquisition method for long FOV contrast-enhanced MRA and whole-body MRI. *Magn Reson Med*. 2002;47:224–231.
113. Zenge MO, Vogt FM, Brauck K, et al. High-resolution continuously acquired peripheral MR angiography featuring partial parallel imaging GRAPPA. *Magn Reson Med*. 2006;56:859–865.
114. Andreisek G, Pfammatter T, Goepfert K, et al. Peripheral arteries in diabetic patients: Standard bolus-chase and time-resolved MR angiography. *Radiology*. 2007;242:610–620.
115. Neuwelt A, Sidhu N, Hu CA, et al. Iron-based supermagnetic nanoparticle contrast agents for MRI of infection and inflammation. *AJR Am J Roentgenol*. 2015;204:302–313.
116. Hope M, Hope T, Zhu C, et al. Vascular Imaging with Ferumoxytol as a contrast agent. *AJR Am J Roentgenol*. 2015;205:366–373.
117. Rapp JH, Wolff SD, Quinn SF, et al. Aortoiliac occlusive disease in patients with known or suspected peripheral vascular disease: safety and efficacy of gadofosveset-enhanced MR angiography—multicenter comparative phase III study. *Radiology*. 2005;236(1):71–78.
118. Leiner T, Schoenberg SO. Current status of renal artery magnetic resonance imaging: theoretical and practical considerations and the potential role of blood-pool contrast agents. *Eur Radiol*. 2007;17(Suppl 2):B13–B17.
119. Maki JH, Wilson GJ, Eubank WB, et al. Navigator-gated MR angiography of the renal arteries: a potential screening tool for renal artery stenosis. *AJR Am J Roentgenol*. 2007;188:540–546.
120. Lehrman ED, Plotnik AN, Hope T, Saloner D. Ferumoxytol-enhanced MRI in the peripheral vasculature. *Clin Radiol*. 2019;74(1):37–50.
121. Shahrouki P, Moriarty JM, Khan SN, et al. High resolution, 3-dimensional Ferumoxytol-enhanced cardiovascular magnetic resonance venography in central venous occlusion. *J Cardiovasc Magn Reson*. 2019;21(1):17.
122. Chai P, Mohiaddin R. How we perform cardiovascular magnetic resonance flow assessment using phase-contrast velocity mapping. *J Cardiovasc Magn Reson*. 2005;7:705–716.
123. Duda SH, Schick F, Teufl F, et al. Phase-contrast MR angiography for detection of arteriosclerotic renal artery stenosis. *Acta Radiol*. 1997;38:287–291.
124. Markl M, Frydrychowicz A, Kozerke S, Hope M, Wieben O. 4D flow MRI. *J Magn Reson Imaging*. 2012;36:1015–1036.
125. Dyverfeldt P, Bissell M, Barker A, et al. 4D flow cardiovascular magnetic resonance consensus statement. *J Cardiovasc Magn Reson*. 2015;17:72.
126. Fayad ZA. MR imaging for the noninvasive assessment of atherosclerotic plaques. *Magn Reson Imaging Clin N Am*. 2003;11:101–113.
127. Yuan C, Mitsumori LM, Ferguson MS, et al. In vivo accuracy of multi-spectral magnetic resonance imaging for identifying lipid-rich necrotic cores and intraplaque hemorrhage in advanced human carotid plaques. *Circulation*. 2001;104:2051–2056.
128. Cai JM, Hatsukami TS, Ferguson MS, et al. Classification of human carotid atherosclerotic lesions with in vivo multicontrast magnetic resonance imaging. *Circulation*. 2002;106:1368–1373.
129. Fayad ZA, Nahar T, Fallon JT, et al. In vivo magnetic resonance evaluation of atherosclerotic plaques in the human thoracic aorta: a comparison with transesophageal echocardiography. *Circulation*. 2000;101:2503–2509.
130. Botnar RM, Stuber M, Kissinger KV, et al. Noninvasive coronary vessel wall and plaque imaging with magnetic resonance imaging. *Circulation*. 2000;102:2582–2587.
131. Wasserman BA, Smith WI, Trout III HH, et al. Carotid artery atherosclerosis: in vivo morphologic characterization with gadolinium-enhanced double-oblique MR imaging initial results. *Radiology*. 2002;223:566–573.
132. Yuan C, Kerwin WS, Ferguson MS, et al. Contrast-enhanced high resolution MRI for atherosclerotic carotid artery tissue characterization. *J Magn Reson Imaging*. 2002;15:62–67.
133. Kooi ME, Cappendijk VC, Cleutjens KB, et al. Accumulation of ultrasmall superparamagnetic particles of iron oxide in human atherosclerotic plaques can be detected by in vivo magnetic resonance imaging. *Circulation*. 2003;107:2453–2458.
134. Maki JH, Wilson GJ, Laufer RB, et al. Apparent vessel wall inflammation detected using MS-325, a blood pool contrast agent. *Proc Int Soc Mag Reson Med*. 2001;9:639.
135. Winter PM, Morawski AM, Caruthers SD, et al. Molecular imaging of angiogenesis in early-stage atherosclerosis with alpha(v)beta3-integrin-targeted nanoparticles. *Circulation*. 2003;108:2270–2274.
136. Makowski MR, Henningsson M, Spuentrup E, et al. Characterization of coronary atherosclerosis by Magnetic Resonance Imaging. *Circulation*. 2013;128:1244–1255.
137. Meyer BC, Oldenburg A, Frericks BB, et al. Quantitative and qualitative evaluation of the influence of different table feeds on visualization of peripheral arteries in CT angiography of aortoiliac and lower extremity arteries. *Eur Radiol*. 2008;18:1546–1555.
138. International Commission on Radiological Protection. *Managing Patient Dose in Computed Tomography, ICRP Publication 87*. Ann ICRP; 2001:30.
139. Liu X, Zhao X, Huang J, et al. Comparison of 3D free-breathing coronary MR angiography and 64-MDCT angiography for detection of

- coronary stenosis in patients with high calcium scores. *AJR Am J Roentgenol.* 2007;189:1326–1332.
140. Schulz B, Kuehling K, Kromen W, et al. Automatic bone removal technique in whole-body dual-energy CT angiography: performance and image quality. *AJR Am J Roentgenol.* 2012;199:W646–650.
141. Amano Y, Ishihara M, Hayashi H, et al. Metallic artifacts of coronary and iliac arteries stents in MR angiography and contrast-enhanced CT. *Clin Imaging.* 1999;23:85–89.
142. Maintz D, Fischbach R, Juergens KU, et al. Multislice CT angiography of the iliac arteries in the presence of various stents: in vitro evaluation of artifacts and lumen visibility. *Invest Radiol.* 2001;36:699–704.
143. Willoteaux S, Negawi Z, Lions C, et al. Observations from multidetector CT imaging of different types of renal artery stents. *J Endovasc Ther.* 2004;11:560–569.
144. Létourneau-Guillon L, Soulez G, Beaudoin G, et al. CT and MR imaging of nitinol stents with radiopaque distal markers. *J Vasc Interv Radiol.* 2004;15:615–624.
145. Sagara Y, Kirosue H, Hori Y, et al. Limitations of three-dimensional reconstructed computerized tomography angiography after clip placement for intracranial aneurysms. *J Neurosurg.* 2005;103:656–661.
146. van der Schaaf I, van Leeuwen M, Vlassenbroek A, et al. Minimizing clip artifacts in multi CT angiography of clipped patients. *AJNR Am J Neuroradiol.* 2006;27:60–66.
147. Brenner DJ, Hall EJ. Computed tomography—an increasing source of radiation exposure. *N Engl J Med.* 2007;357:2277–2284.
148. Einstein AJ, Henzlova MJ, Rajagopalan S. Estimating risk of cancer associated with radiation exposure from 64-slice computed tomography coronary angiography. *JAMA.* 2007;298:317–323.
149. Numburi UD, Schoenhagen P, Flamm SD, et al. Feasibility of dual-energy CT in the arterial phase: Imaging after endovascular aortic repair. *AJR Am J Roentgenol.* 2010;195:486–493.
150. Delesalle MA, Pontana F, Duhamel A, et al. Spectral optimization of chest CT angiography with reduced iodine load: experience in 80 patients evaluated with dual-source, dual-energy CT. *Radiology.* 2013;267(1):256–266.

# Vascular PET/CT and SPECT/CT

ANDOR W.J.M. GLAUDEMANS, ORA ISRAEL, SIMONA BEN-HAIM,  
and RIEMER H.J.A. SLART

<b>BASIC PRINCIPLES</b>	392
Single-Photon Emission Computed Tomography, Positron Emission Tomography, and Hybrid Imaging	392
Most Commonly Used Tracers for Vascular Diseases	393
<sup>18</sup> F-Fluorodeoxyglucose	393
<sup>18</sup> F-Sodium Fluoride	393
Labeled White Blood Cells	393
Other Available Tracers	393
<b>CLINICAL APPLICATIONS</b>	393
Molecular Imaging of Atherosclerosis	393
Fluorodeoxyglucose Uptake in Carotid Plaque	393
Monitoring Treatment with Fluorodeoxyglucose Uptake	394
Fluorodeoxyglucose-Avid Arterial Wall Calcifications	394

<i>Change in Plaque Fluorodeoxyglucose Uptake Over Time</i>	394
<i>Challenges</i>	394
<i>Other Tracers for Plaque Imaging</i>	395
Molecular Imaging of Aortic Pathology	396
<i>Abdominal Aortic Aneurysm</i>	396
<i>Aortic Dissection</i>	396
Molecular Imaging of Large Vessel Vasculitis	398
Molecular Imaging of Vascular Graft Infection	399
<i>Radiolabeled White Blood Cell Imaging</i>	400
<i>Fluorodeoxyglucose Positron Emission Tomography</i>	400
<b>LIMITATIONS AND RISKS</b>	402
<b>FUTURE ADVANCES</b>	403

Conventional radiological imaging modalities for the assessment of blood vessels have focused on size, irregularity of the vascular lumen, and anatomic changes in adjacent structures. The ability of these morphologic imaging techniques to identify physiologic changes such as active inflammatory processes and plaques at risk for rupture is, however, limited. Molecular imaging has the advantage of enabling noninvasive physiologic assessment of these processes with radionuclides, very often early in the course of disease. Such early assessment can lead to subsequent changes in clinical management, potentially affecting patients' outcomes.

The limitations of traditional nuclear medicine techniques, mainly low spatial resolution and lack of anatomic details, have been overcome in the last decade with the introduction of the hybrid single-photon emission computed tomography/computed tomography (SPECT/CT) and positron emission tomography (PET)/CT imaging devices. A large body of evidence has accumulated on the use of molecular tracers for the assessment of vascular inflammation and infection (especially in vascular graft infections and vasculitis), early diagnosis, precise determination of the extent of disease, and assessment of response to therapy.

## BASIC PRINCIPLES

### Single-Photon Emission Computed Tomography, Positron Emission Tomography, and Hybrid Imaging

In nuclear medicine imaging, radiopharmaceuticals are administered to the patient intravenously. Images are obtained from radiation, which is emitted at the location of disease processes in the patient's body. Two main camera systems, the gamma camera and the PET camera, convert this radiation into images.

The gamma camera forms the basis of conventional nuclear medicine and provides two-dimensional imaging of the body. Image contrast of this planar imaging is rather low due to the presence of overlying structures that interfere with the region of interest. This limitation can be overcome by collecting images from different angles around the patient, the so-called SPECT, which leads to better spatial resolution, higher contrast, and improved sensitivity.

PET is an imaging tool based on radionuclides that emit positrons to become stable. For example, decay of the radioisotope fluorine-18 ( $^{18}\text{F}$ ) leads to emission of a positron that collides with an electron after traveling a short distance in tissue, thereby generating a pair of 511-keV annihilating photons (in opposite directions) that can be detected by the PET imaging device. The major advantage of PET over SPECT is that the PET camera system is more effective in detecting photons and provides better spatial resolution (around 3–4 mm). Furthermore, quantification is easier with PET. Uptake of PET radiopharmaceuticals can be quantified by standardized uptake values (SUVs), which measure the tracer uptake within a region of interest in relation to the injected dose and patient's body weight.<sup>1</sup>

However, both modalities provide only very limited morphologic information. Therefore PET as well as SPECT are now combined with CT in a single imaging modality. Hybrid SPECT/CT, PET/CT, and now also emerging PET/magnetic resonance imaging (MRI) improve the sensitivity by anatomic detection of small structures, such as plaques, and may also improve the specificity, confirming active disease in these small lesions.<sup>2</sup> Other advantages of combining radiologic and nuclear medicine techniques in one imaging modality are reduced costs, perfect correlation of pathophysiologic with anatomic information, and the one-stop-shop principle, which is convenient for the patient and reduces waiting time.

## Most Commonly Used Tracers for Vascular Diseases

### $^{18}\text{F}$ -Fluorodeoxyglucose

Fluorodeoxyglucose (FDG) is an analogue of glucose, taken up by and accumulating in cells in proportion to their metabolic activity. The transfer of glucose into cells is facilitated by glucose transporters (GLUTs) and sodium glucose cotransporters (SGLTs). After entering the cell, glucose undergoes phosphorylation by hexokinase, forming glucose-6-phosphate. After its glycolysis by hexose-6-phosphate isomerase, fructose-6 phosphate is formed. In contrast, the analogue 2-deoxy-D-glucose cannot undergo conversion by hexose-6-phosphate isomerase; therefore, FDG becomes trapped in the cytosol. Glucose and FDG have otherwise similar properties, and the rates of phosphorylation *in vivo* are proportional to each other, reflecting the general rates of glucose metabolism.<sup>3</sup>

FDG imaging is today the “gold standard” in the assessment of patients with cancer, for staging tumors, monitoring response to treatment, and diagnosing recurrence. FDG also has an increasing role in infectious and inflammation diseases, since many cells involved in infection and inflammation (activated leukocytes, monocytes, lymphocytes, macrophages, and giant cells) use glucose for their metabolism. This tracer is extensively used in vascular inflammation and infection imaging.

### $^{18}\text{F}$ -Sodium Fluoride

Sodium fluoride (NaF) is mainly used for skeletal imaging, since it has the desirable characteristics of high and rapid bone uptake accompanied by a very rapid blood clearance, which

results in a high bone-to-background ratio.<sup>4</sup> Its use in vascular imaging is, at this time, limited to plaque imaging due to uptake in the calcifications. Since NaF is not physiologically taken up in the myocardium and blood vessels, it could also potentially be a better agent than FDG in assessing the coronary vessels.

### Labeled White Blood Cells

Scintigraphy using autologous white blood cells – also called “leukocyte scintigraphy” – is still considered the gold standard nuclear imaging modality for infections. In using the correct acquisition protocols and interpretation criteria, this technique is highly accurate. Limitations, however, are the needs for a laborious labeling procedure and for imaging at several time points. White blood cell scintigraphy is primarily used in musculoskeletal infections but has also been evaluated in vascular diseases, such as vascular graft infections.

## Other Available Tracers

Besides the already mentioned commonly used tracers, various other radiopharmaceuticals have been developed and tested, most of them in atherosclerosis. SPECT and PET imaging of atherosclerosis takes advantage of the wide array of biologic mechanisms involved in the different stages of atherosclerosis and plaque formation. Tracers have been developed for targeting the atherosclerotic lesion components, such as technetium-99m ( $^{99\text{m}}\text{Tc}$ )-labeled low-density lipoprotein (LDL),  $^{99\text{m}}\text{Tc}$ -labeled oxidized LDL, labeled antibodies against plaques and degradation products, and labeled interleukin-2 to detect activated lymphocytes at the site of a vulnerable plaque. Since an unstable plaque with rupture or erosion of the fibrous cap demonstrates activation of platelets and of the clotting cascade, other studies have focused on labeled platelets and fibrins. Apoptosis has also been demonstrated in macrophages as well as in smooth muscle cells of atherosclerotic plaques and is often observed in the fibrous cap of a ruptured plaque. Therefore,  $^{99\text{m}}\text{Tc}$ -labeled annexin V has also been used for specifically targeting the atherosclerotic plaque. Also matrix metalloproteinases (MMPs), excreted by macrophages and activated by plasmin as part of the inflammatory process in active atherosclerotic lesions, were labeled and tested. Many of the molecular probes developed for plaque imaging are linked with inflammation, a major component of vulnerable plaques. Labeled macrophages, monocytes, and lymphocytes were all used for imaging the inflammatory process. An overview of all the possible radiopharmaceuticals for imaging atherosclerosis can be found in an extensive review.<sup>5</sup>

## CLINICAL APPLICATIONS

### Molecular Imaging of Atherosclerosis

#### Fluorodeoxyglucose Uptake in Carotid Plaque

In patients undergoing FDG PET/CT scans for cancer imaging, increased FDG uptake was reported in the vascular walls of 31% to 59% of patients older than 50 years,<sup>6–9</sup> the uptake

being more evident with advancing age, male sex, and the presence of cardiovascular risk factors such as hypertension and hypercholesterolemia.<sup>7,8,10,11</sup> Rudd et al.<sup>12</sup> were the first to show, in a prospective study in eight patients imaged shortly after a transient ischemic attack (TIA), that FDG uptake was 27% higher in the symptomatic carotid artery than in the asymptomatic contralateral artery. Autoradiography confirmed the location of uptake in macrophages.<sup>12</sup> Coregistration of FDG PET and MRI indicated the presence of increased tracer uptake in arterial plaques in 10 of 12 patients with an embolic event, consistent with clinical symptoms. In addition, 25% of lesions determined to be nonstenotic by magnetic resonance angiography (MRA) in symptomatic patients had increased FDG activity in significantly inflamed plaques.<sup>13</sup> Plaques with unstable features, such as a large lipid core and intraplaque hemorrhage on MRI or echolucency on ultrasound, show higher FDG uptake than more stable lesions.<sup>14–17</sup> Lipid-rich necrotic plaques show higher FDG uptake than collagenous or calcified plaques.<sup>14</sup> In patients with severe carotid stenosis imaged prior to endarterectomy, an excellent correlation of FDG activity was reported with macrophage staining but not with plaque thickness, plaque area, or smooth muscle staining. This confirms that FDG can be used to assess the severity of inflammation in patients with carotid plaques.<sup>18,19</sup> Significantly increased carotid FDG activity had been demonstrated in patients with stroke.<sup>20,21</sup> FDG uptake in carotid vessels correlates with serum levels of C-reactive protein, a marker of systemic inflammation.<sup>22,23</sup> This observation is consistent with the definition of the “vulnerable patient” rather than “vulnerable plaque”: the finding of one vulnerable lesion may increase the likelihood of other vulnerable lesions.<sup>24</sup> FDG activity in vessels was greater in patients with more than one cardiovascular risk factor and known coronary artery disease.<sup>23</sup> In addition, patients with type 2 diabetes mellitus and/or metabolic syndrome also demonstrated increased carotid FDG uptake.<sup>25,26</sup>

### **Monitoring Treatment with Fluorodeoxyglucose Uptake**

Sequential PET/CT studies can be used to monitor the effect of lipid-lowering treatment on FDG uptake in atherosclerotic plaques. Reduced plaque inflammation after treatment with probucol, a lipid-lowering antioxidant, has been shown in an experimental rabbit model.<sup>27</sup> In human studies, high-resolution MRI has demonstrated that more than 12 months of simvastatin treatment is required to show regression of atherosclerotic plaques.<sup>28–30</sup> In a group of 43 patients with cancer who had increased FDG activity in the thoracic aorta or carotid arteries, half of the subjects who were subsequently randomly assigned to treatment with simvastatin showed reduced FDG uptake in the arterial wall as well as a decrease in LDL cholesterol by 30% and an increase in high-density lipoprotein (HDL) cholesterol by 15%. The second half of the study group received dietary management and did not show any change in FDG uptake.<sup>30</sup> On the other hand, dietary and lifestyle modifications in asymptomatic subjects caused a 65% reduction in the number of FDG-positive vascular regions.<sup>31</sup>

### **Fluorodeoxyglucose-Avid Arterial Wall Calcifications**

Co-localization of FDG on PET and arterial calcifications on CT has been previously studied using PET/CT, with FDG-avid arterial wall calcifications observed in 2% to 14% of lesions.<sup>7–9</sup> Findings in the vascular wall of patients more than 50 years of age showed three different patterns: PET-negative and CT-positive, PET- and CT-positive, and PET-positive and CT-negative. Although there were many CT-positive atherosclerotic lesions (in 82%–92% of patients), FDG uptake indicating active inflammation was variable (15%–74%). Lesions with evidence of both past (CT-positive) and current (PET-positive) inflammation were seen in 10% of patients.<sup>8,32</sup> Other researchers have described none or a negative correlation between areas of calcification and FDG uptake.<sup>33</sup> The incongruence between FDG PET and CT findings may represent variations in the stage of the atherosclerotic process. The presence and extent of calcifications on CT define morphologic changes likely consistent with advanced disease, whereas FDG avidity demonstrates transient plaque inflammation, possibly indicating future complications.

### **Change in Plaque Fluorodeoxyglucose Uptake Over Time**

Changes in vascular wall uptake over time in 50 patients with cancer and a mean age of 68 years who had repeat PET/CT scans 8 to 26 months apart were also reported. Changes in the pattern of vascular findings were observed in 48% of FDG-positive sites, compared with 4% of PET-negative foci and 7% of CT-positive lesions (Fig. 31.1).<sup>32</sup> Transient FDG uptake in the arterial wall was found in a group of 205 studies from 50 patients with a mean age of 49 years who underwent at least four PET/CT scans for a mean follow-up of 27 months.<sup>33</sup> The variable FDG uptake in the vascular wall suggests that inflammation may be a transient feature of a dynamic process, whereas calcifications may represent a chronic process or stable atherosclerosis.<sup>32</sup> This observation may have potential future implications for the design of trials for monitoring the response of vascular inflammation to therapeutic interventions.

### **Challenges**

There are a number of challenges in the molecular imaging of vascular plaques. Their small size (most are less than 5 mm in diameter) is close to the resolution limit of SPECT and PET. Also, some arteries are located deep within the body, and in some regions, such as the coronary arteries, imaging is of lower quality because of artifacts related to cardiac and respiratory motion.<sup>6</sup> Most of the radiopharmaceuticals labeled with single-photon emitters have unfavorable imaging properties, including slow blood clearance and a low ratio of target (atherosclerotic plaque) to background (blood pool); they may also demonstrate affinity with nonspecific binding sites. Despite the large variety of probes labeled with single-photon emitters, none is being widely used in the clinical setting to identify vulnerable plaques. More research is needed to identify a suitable probe that will also yield a robust clinical imaging tool.

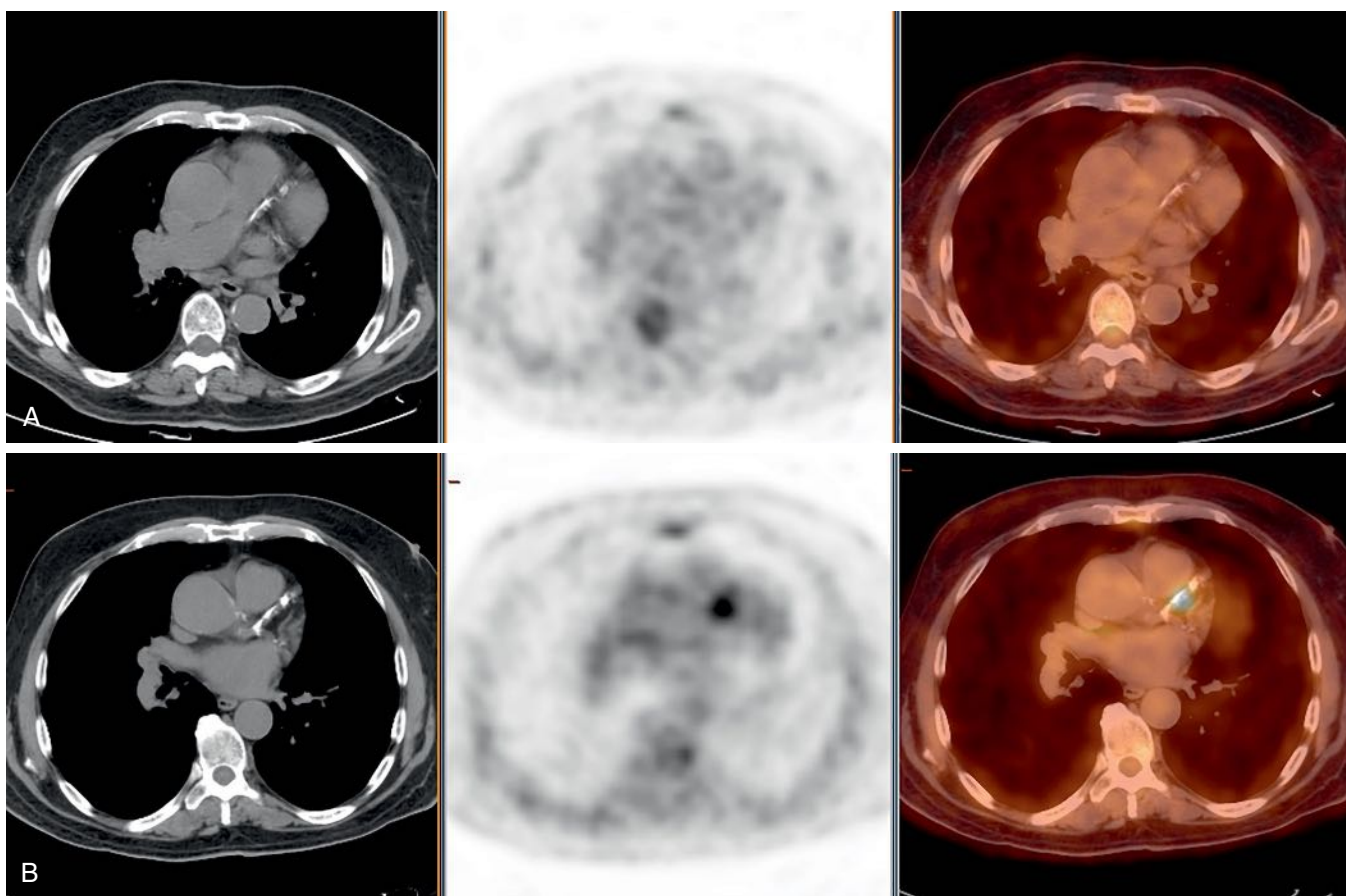


**Figure 31.1** Changing pattern of vascular wall fluorodeoxyglucose (FDG) uptake in a 70-year-old patient referred for routine follow-up after completion of chemotherapy for diffuse large B-cell lymphoma. Whole-body FDG positron emission tomography/computed tomography (PET/CT) images showed no evidence of FDG-avid disease. (A) Selected axial slice shows left anterior descending (LAD) coronary artery calcifications on CT (left) with no focal increased FDG activity on PET (center) or on the fused PET/CT image (right). (B) On follow-up scanning 8 months after the previous study, CT shows that LAD calcifications have progressed (left), and there is also focal FDG activity in the LAD calcifications on the PET (center) scan and localized activity on the fused PET/CT scan (right).

### Other Tracers for Plaque Imaging

The majority of data related to metabolic imaging of atherosclerosis refer to the use of FDG, mainly because of its wide availability and the vast clinical experience with its use accumulated over the last few decades. Because of the limitations of FDG, including the nonspecific nature of its uptake in various types of cells that metabolize glucose as well as the technically challenging imaging of the coronary vessels, other tracers are being sought and evaluated.

Active plaque calcification can contribute to plaque instability<sup>34</sup> and can be assessed with NaF, which can potentially better assess the coronary vessels than FDG owing to the lack of significant physiologic myocardial uptake and its high target-to-background ratio. It has been shown that NaF adsorbs to calcified deposits within plaque with high affinity and is selective and specific.<sup>35</sup> NaF PET/CT imaging can distinguish between areas of macro- and microcalcification. A group of 45 patients with cancer were assessed with FDG, NaF, and CT for the presence of inflammation, active calcium deposition, and calcifications, respectively. Of 105 lesions with NaF uptake, 77% showed calcification on CT and 14% showed increased FDG

activity.<sup>36</sup> It has been hypothesized that in early atherosclerosis, only inflammatory changes and therefore only FDG uptake can be seen, whereas later during the course of this process, there is also active calcification, reflected by uptake of both FDG and NaF. At a late stage, when the density of calcium deposits exceeds a certain threshold, calcifications would also become visible on CT. When calcification and mineralization exceed the inflammatory process, uptake of NaF but not of FDG would be found in calcified lesions seen on CT. At the final stage of dense calcification with no significant calcium turnover, lesions would be seen only on CT.<sup>24</sup>

<sup>99m</sup>Tc-labeled LDL has been shown to accumulate in experimental atherosclerotic plaques in rabbits.<sup>37</sup> In clinical studies, a fourfold greater uptake was found in carotid endarterectomy macrophage-rich specimens than in fibrotic specimens.<sup>38</sup> Owing to slow blood clearance, however, this tracer was not suitable for *in-vivo* imaging. <sup>99m</sup>Tc-labeled oxidized LDL is taken up by macrophages and has a more rapid blood clearance. It was detected at 150% higher levels in 10 of 11 plaques than in normal arterial segments and therefore provides better image quality.<sup>39</sup> Indium-111

( $^{111}\text{In}$ )- or  $^{99\text{m}}\text{Tc}$ -labeled antibodies against plaque and its degradation products, fibrin and platelets, have also been used for the imaging of atherosclerosis in an experimental setting.<sup>40</sup> The  $^{111}\text{In}$ -labeled polyclonal human immunoglobulin (Ig) G contains an Fc unit that binds to macrophage receptors. It showed a poor target-to-background ratio in rabbits, whereas in humans uptake was found in carotid atheromas in 86% of patients, with no correlation with ultrasound findings.<sup>41</sup>

In patients with known cardiovascular events, imaging with  $^{111}\text{In}$ -labeled platelets correlated with plaque burden and ulcerations seen on ultrasound.<sup>42,43</sup> However, blood clearance of labeled platelets is slow, so imaging cannot be performed until 48 hours after the injection. In addition, discontinuation of antiplatelet medication is needed, which cannot be considered in patients with suspected vascular events. Fibrin fragment E1 labeled with  $^{123}\text{iodine}$  and  $^{99\text{m}}\text{Tc}$  can detect thrombi in animals with deep venous thrombosis.<sup>44</sup> This agent clears rapidly from the circulation and has good imaging qualities. At present there are no reports on the use of this tracer in the evaluation of atherosclerosis.

$^{99\text{m}}\text{Tc}$ -labeled annexin V has been used for specific targeting of active atherosclerotic lesions. Uptake of  $^{99\text{m}}\text{Tc}$ -annexin V has been reported in experimental models of aortic lesions<sup>45</sup> as well as in patients with carotid artery disease.<sup>46</sup> The role of this substance to assess apoptosis is limited by the lack of specificity.  $^{99\text{m}}\text{Tc}$ -annexin V binds to phosphatidylserine on platelets within the thrombus, but because thrombosis occurs in vulnerable plaques, this feature represents only a relative limitation for imaging with  $^{99\text{m}}\text{Tc}$ -annexin V.<sup>47</sup>

Lymphocytes constitute at least 20% of infiltrating cells in vulnerable plaques. Therefore the interleukin-2 (IL-2) receptor, being overexpressed on activated T lymphocytes, may represent an attractive biomarker for plaque vulnerability. Radio-labeled IL-2 was therefore tested for imaging the lymphocytic infiltration in carotid plaques.  $^{99\text{m}}\text{Tc}$ -IL-2 was found specific for imaging activated T lymphocytes in the carotid plaque. A significant correlation was found between the number of CD25 $^+$  lymphocytes and the total number of CD25 $^+$  cells in the plaque and the tracer uptake in the plaque.<sup>48</sup>

Preliminary work using  $^{11}\text{C}$ -PK11195, a selective ligand of a translocator protein with 20 times greater density expression on macrophages than on vascular smooth muscle cells, has been reported. This tracer binds to macrophage-rich regions in human carotid plaques,<sup>49</sup> and promising results have been reported in patients with vasculitis.<sup>50</sup>

Other potentially useful tracers include  $^{68}\text{Ga}$ -DOTATATE, which binds to somatostatin receptors subtype 2 expressed by macrophages,<sup>51</sup> and  $^{11}\text{C}$ - or  $^{18}\text{F}$ -labeled choline, which is taken up by macrophages, undergoes phosphorylation and metabolism to phosphatidyl choline, and is incorporated into the cellular membrane.<sup>52,53</sup> In an experimental model,  $^{18}\text{F}$ -labeled choline uptake correlated better than FDG uptake with fat staining and macrophage-positive areas.<sup>53</sup> In patients with cancer,  $^{11}\text{C}$ -labeled choline was not taken up by the normal vascular wall or by calcified vascular wall lesions.<sup>52</sup>

## Molecular Imaging of Aortic Pathology

### Abdominal Aortic Aneurysm

Increased FDG activity has been reported in patients with asymptomatic abdominal aortic aneurysms (AAAs), probably owing to the presence of transmural inflammation and the accumulation of FDG in macrophage aggregates.<sup>54,55</sup> A possible association between increased FDG uptake and AAA expansion and rupture has been suggested.<sup>56</sup> Higher FDG uptake in AAA has been associated with higher wall stress<sup>57</sup> and correlated with instability and macrophage infiltration.<sup>58</sup> Aneurysmal dilatation develops after an inflammatory phase with increased FDG activity.<sup>59</sup> An inverse relationship between FDG uptake and future expansion of the aneurysm, as measured by Doppler ultrasound, was found in 25 patients with AAAs who underwent routine surveillance over a period of 12 months.<sup>60</sup> In patients with asymptomatic AAAs, no increase in FDG uptake was observed in large lesions referred to surgery.<sup>61</sup> A marked reduction in cell density in AAAs correlated with low FDG activity.<sup>61</sup> Increased FDG activity is more frequent in small aneurysms and in lesions with inflammatory changes, which are more often symptomatic and require direct surgical intervention (Fig. 31.2).<sup>58</sup>

### Aortic Dissection

Thoracic aortic dissections are uncommon but are associated with high mortality rates, 10% to 30% within 30 days of diagnosis.<sup>62,63</sup> The disease is mediated by inflammatory changes.<sup>64</sup> In one study, FDG PET/CT was performed in 33 patients with acute aortic syndrome. Increased FDG activity (positive result) was seen in one-third of the patients, 82% of whom showed progression of disease; 55% of patients with negative PET results showed stable disease on follow-up.<sup>65</sup> In another study, FDG uptake in 28 patients with acute or chronic dissection was compared with that in a group of 14 age-matched controls for prediction of adverse outcomes. Patients were followed for up to 6 months after PET/CT. Within a subgroup of eight patients with unfavorable outcomes (death from cardiovascular causes, rupture or progression of aortic dissection, requirement for surgical repair, or cardiovascular events during or after initial hospitalization), FDG uptake was significantly higher in those with acute dissecting aneurysms than in controls. It was also higher at the site of maximum dissection in patients with unfavorable outcomes than in those with favorable outcomes. Multivariate analysis showed that the mean SUV of FDG uptake at the site of maximum dissection independently predicted an unfavorable outcome. The investigators concluded that FDG PET/CT may play a role in predicting the prognosis of patients with type B aortic dissection and may also be useful in selecting patients at high risk for near-term complications requiring early surgery.<sup>66</sup>

More clinical data from larger and longitudinal patient cohorts will establish the role of FDG PET/CT in guiding patient selection for surgery and for follow-up of patients with aortic pathology.

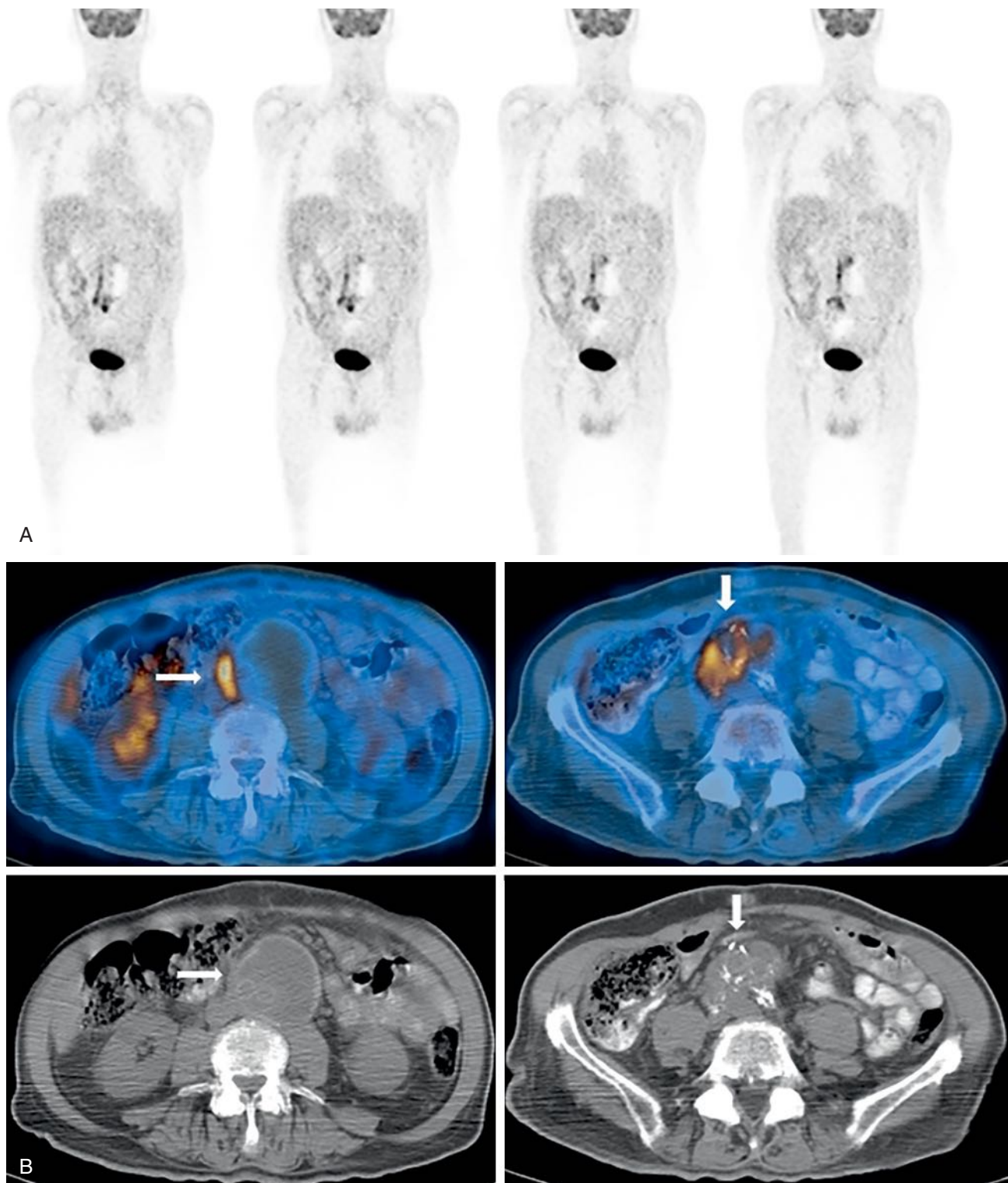


**Figure 31.2** Fluorodeoxyglucose (FDG) uptake in an infected aortic graft in a 79-year-old diabetic man who had undergone aorto-bi-iliac surgical repair of a dissecting AAA 10 years prior to the current examination. He presented with severe abdominal pain. Computed tomography (CT) angiography demonstrated a thickened posterior wall of the aneurysm. (A) Selected coronal positron emission tomography (PET) slices demonstrate a linear area of intense abnormal FDG uptake in the lower abdomen and upper pelvis. (B) The uptake is localized by PET/CT at its upper level to a thickened AAA wall (left column, arrows), consistent with active inflammation, and at the pelvic level to a soft tissue mass surrounding the right component of the graft and surgical clips (right column, arrows), consistent with an infected right vascular graft.

## Molecular Imaging of Large Vessel Vasculitis

In large vessel vasculitis, molecular imaging techniques can assist in the early diagnosis of inflammatory changes in the vascular walls, which are potentially reversible. This inflammatory process precedes anatomic changes; therefore, at the early stage, anatomic imaging modalities are unreliable. MRI is probably the best method to evaluate and reveal structural vascular abnormalities. However, in the early setting without anatomic changes, MRI cannot detect inflammation. FDG PET is able to identify vasculitis at an early stage, but because of the limited spatial resolution of the imaging device (4–5 mm), it is able to visualize only inflammation of the aorta and the large and medium-sized arteries. Based on which vessels are involved, FDG PET is able to diagnose giant cell arteritis (GCA) (involvement of the aorta and all large vessels), Takayasu arteritis (mainly involvement of the vessels in the thoracic region), and polyarteritis nodosa (involvement of the medium-sized arteries, which can be visible in the upper legs and arm (Fig. 31.3).<sup>67</sup> Moreover, FDG PET is able to diagnose associated diseases, such as polymyalgia rheumatica (PMR) or polychondritis (see Fig. 31.3). For these reasons, FDG PET is accepted as a major imaging technique for the early detection of vasculitis.<sup>68</sup> In addition, FDG PET has been shown to be superior to anatomic imaging modalities and is being increasingly used to assess response to therapy in documented cases of vasculitis.<sup>68,69</sup>

FDG PET has become increasingly important for the diagnosis of large vessel vasculitis, particularly in cases with non-specific presentation, such as fever of unknown origin, malaise, and weight loss. Vasculitis can be diagnosed early with FDG PET because the inflammatory process precedes morphologic changes.<sup>68</sup> Also, FDG PET detects more involved regions than MRI.<sup>68,70</sup> The overall reported sensitivity and specificity of

FDG imaging in untreated patients with large vessel vasculitis and increased inflammatory markers are in the range of 77% to 92% and 89% to 100%, respectively.<sup>69,71–74</sup> In the largest prospective study involving 35 patients with biopsy-proven GCA, the sensitivity of FDG imaging was 83%.<sup>75</sup> Increased FDG activity at the level of the aortic arch and subclavian arteries has been reported in 56% and in the lower limbs in 64% of cases.<sup>76–79</sup> In TA, increased FDG activity was noted in the aorta and brachiocephalic, carotid, and subclavian arteries and less frequently in the pulmonary arteries.<sup>80</sup> False-negative results have been reported in patients with temporal arteritis, caused either by high physiologic FDG uptake in the brain or the adjacent skin or by the small diameter of the involved vessel.<sup>73</sup> One study compared FDG PET, contrast-enhanced CT, MRI, and angiography in 18 patients with biopsy-proven TA. FDG PET had a sensitivity of 92%, a positive predictive value of 85%, and specificity and negative predictive value of 100% and was superior to morphologic imaging both in early diagnosis of inflammatory changes and for monitoring treatment effectiveness.<sup>73</sup> In another study, the role of FDG PET/CT was assessed in 39 patients with TA and 40 controls; it correlated with disease activity as defined by clinical and biochemical markers. Maximum SUV ( $SUV_{max}$ ) was significantly higher in patients with active disease than in those with inactive disease and controls. For an  $SUV_{max}$  cutoff of 2.1, active TA was detected with a sensitivity of 92.6%, specificity 91.7%, a positive predictive value of 96.2%, and a negative predictive value of 84.6%.  $SUV_{max}$  was also significantly higher in patients in whom relapse occurred during treatment than in patients with stable disease during treatment.<sup>80</sup>

A correlation between the intensity of vascular FDG activity and inflammatory markers has been found in GCA.<sup>81</sup> In TA, SUV measurements were found to be useful only for serial

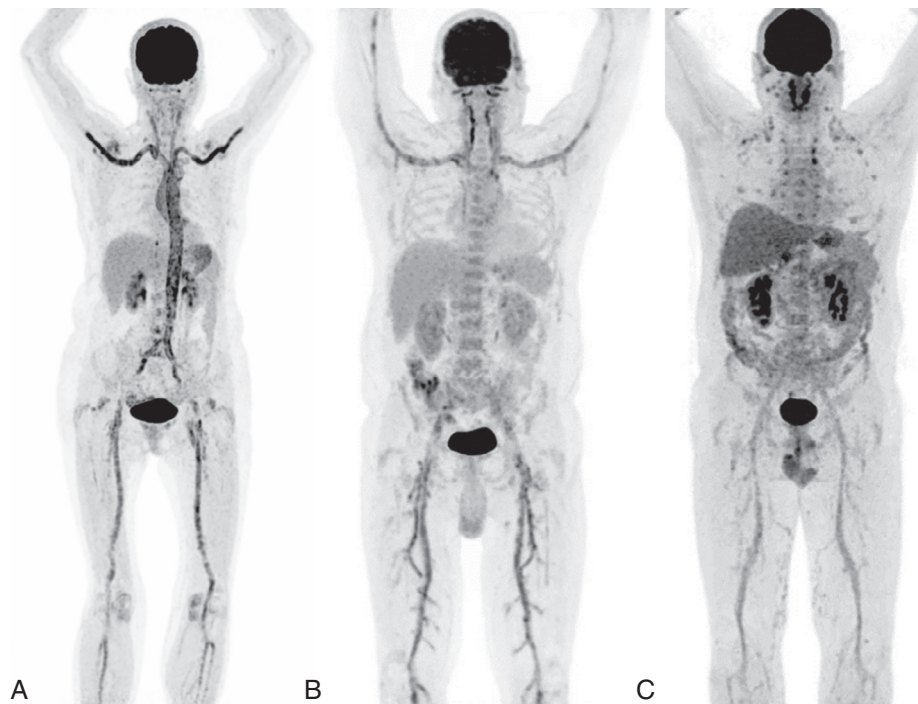


**Figure 31.3** Fluorodeoxyglucose uptake patterns in different vasculitis types and associated diseases. (A) Giant cell arteritis with intense uptake in the aorta and all the large vessels. This scan also shows increased uptake in the shoulders, hips, and knees, pointing to polymyalgia rheumatica. (B) Uptake in both large (subclavian and femoral arteries) and medium-sized arteries in the legs, pointing to polyarteritis nodosa. (C) Another example of polyarteritis nodosa, but also notice the uptake in the costochondral and costovertebral joints and the ears, indicating polychondritis.

follow-up studies, showing a decrease in patients whose disease responded to therapy.<sup>82</sup> FDG PET/CT was superior to MRI in monitoring GCA disease activity during immunosuppressive therapy. FDG imaging reliably detected the earliest improvement after treatment, in good correlation with inflammatory markers and clinical symptoms, whereas morphologic changes seen on MRI, such as wall thickening, resolved only later.<sup>66</sup> In a small number of patients with fever of unknown origin and negative workup results, FDG PET correctly diagnosed GCA, demonstrating findings that disappeared on follow-up studies after the administration of steroids (Fig. 31.4).<sup>83</sup> In patients who have previously received immunosuppressive therapy, FDG imaging is unreliable for assessment of inflammation.<sup>74,81</sup>

Recently, a joint procedural recommendation paper on FDG-PET/CT imaging in large vessel vasculitis and polymyalgia rheumatica was published. This extensive document was written by the Cardiovascular and Inflammation & Infection Committees of the European Association of Nuclear Medicine (EANM), the Cardiovascular Council of the Society of Nuclear Medicine and Molecular Imaging (SNMMI), the PET Interest Group (PIG, an expert group with rheumatologists and imagers interested in the field), and the American Society of Nuclear Cardiology (ASNC). This joint paper provides recommendations and statements, based on the available evidence in literature and consensus of experts in the field, for patient preparation, acquisition and interpretation for the diagnosis and follow-up of patients with suspected or diagnosed large vessel vasculitis and/or PMR. This position paper is now the internationally accepted standard for FDG-PET/CT imaging and reporting of LVV and PMR and should be followed by all nuclear centers.<sup>84</sup>

FDG PET/CT is a sensitive and specific imaging modality in the diagnosis of large vessel vasculitis. It can assist in

visualizing early inflammatory changes in patients with active disease, earlier than morphologic imaging techniques, thus enabling prompt treatment and possibly preventing occlusive complications. It can also be used as an index of disease activity and response to immunosuppressive therapy, but it appears to be unreliable in diagnosing vasculitis in patients receiving high doses of steroids.

## Molecular Imaging of Vascular Graft Infection

Molecular imaging modalities have a major role in the assessment of vascular graft infection; the basic principles already described for other vascular diseases apply also here.

Both labeled white blood cells (WBCs) and FDG PET have been used for the detection of infected vascular grafts, with FDG PET having several advantages over labeled WBC scintigraphy (higher target-to-background ratios, shorter study duration, no need for handling of the blood of potentially infected patients, and quantification possibilities).

Because of the relatively high incidence of nonspecific morphologic abnormalities in patients with infected vascular grafts, molecular imaging modalities have been used to assess the clinical and functional significance of anatomic findings with significant clinical consequences on optimized early diagnosis, defining the best therapeutic strategy. The major advantages of molecular imaging are related to its ability to define functional or metabolic alterations. However, it provides only scarce morphologic data. Therefore hybrid SPECT/CT and PET/CT are of particular value in patients with suspected infections of vascular prostheses.<sup>85,86</sup> Accurate spatial localization of abnormal radiotracer foci to a graft or only to the adjacent soft tissues may be impossible unless these highly specific functional or metabolic images with low background activity and therefore

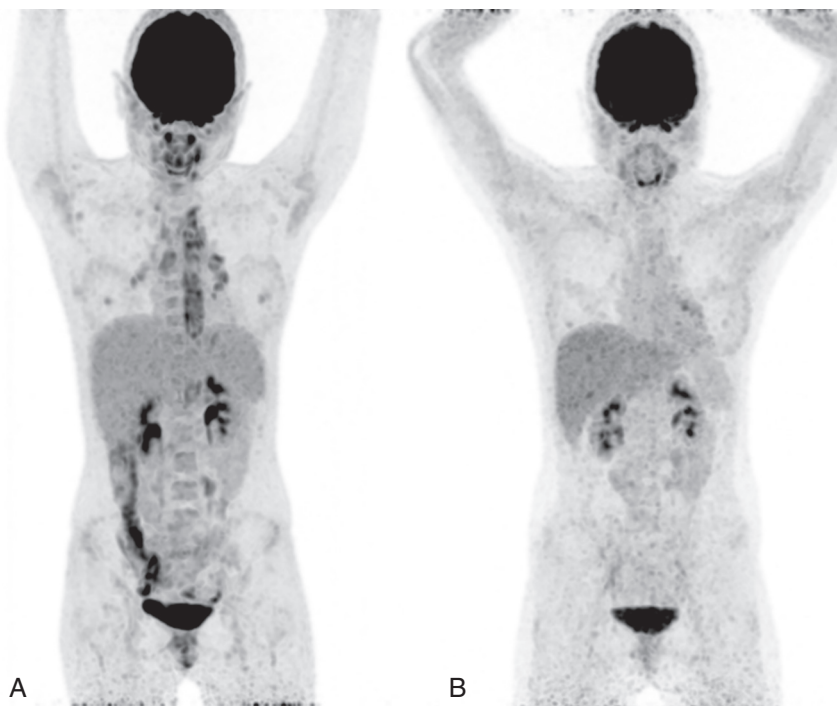


**Figure 31.4** Fluorodeoxyglucose (FDG) uptake in the diagnosis and follow-up of vasculitis. A 19-year-old woman presented with fever of unknown origin. Results of computed tomography, MRI and ultrasound (not shown) were negative. (A) Maximum intensity projection positron emission tomography image demonstrates intense abnormal FDG uptake along the thoracic aorta, and in mediastinal and hilar lymph nodes. Biopsy confirmed Takayasu arteritis. (B) Follow-up imaging 6 months after treatment shows significant improvement.

limited structural information are combined with an anatomic road map. Precise alignment of metabolic and anatomic images is crucial, particularly in the extremities and in regions prone to even involuntary patient motion between imaging sequences, which may harbor an infectious process in a structure located very close to several others (as is the case with vascular grafts).

### Radiolabeled White Blood Cell Imaging

Scintigraphy with radiolabeled WBCs has been used for assessment of suspected prosthetic graft infection. The overall sensitivity of WBCs for diagnosis of infected grafts ranges between 53% and 100%.<sup>87,88</sup> Although the circumstances have not been described in detail, false-negative results may be related to previous or concomitant antibiotic treatment or to the duration of symptoms.<sup>89</sup> The specificity of WBC scintigraphy ranges between 50% and 100% as well.<sup>87,88</sup> False-positive results have been reported in the presence of uptake in lymphocele, hematoma, thrombosis, bleeding, and pseudoaneurysms. Physiologic tracer uptake can be found in recently placed noninfected grafts within 1 month after surgery.<sup>89</sup> Many of the false-positive or false-negative studies can be overcome by using the correct acquisition criteria (at least dual time-point imaging) and the correct interpretation criteria (only uptake increasing over time is consistent with infection).

A study of 40 patients with suspected infection of abdominal aortic grafts compared the performance indices of <sup>111</sup>In-labeled WBCs and MRI. The positive predictive value of MRI was higher than that of WBC scintigraphy, although the negative predictive values were similar, around 80%.<sup>90</sup> SPECT studies performed with <sup>99m</sup>Tc-labeled WBCs are of better quality and therefore easier to interpret than studies using <sup>111</sup>In-labeled WBCs. <sup>99m</sup>Tc WBC imaging has reported sensitivity and specificity in the range of 82% to 100% and 75% to 100%, respectively.<sup>87,88</sup> The modality is of significant clinical value in cases where findings of other imaging modalities are inconclusive. False-positive results can be due to cross-labeling of red blood cells and platelets and by nonspecific perivascular accumulation of granulocytes early after surgery in healing wounds or graft anastomoses.<sup>87,88</sup>

In a study involving 82 patients with suspected infection, the use of labeled WBC SPECT/CT contributed significantly to the precise anatomic localization of suspicious foci of increased tracer uptake, thus confirming the diagnosis of infection and subsequently the precise localization and delineation of its extent in up to half of the patients.<sup>85</sup> This study included 24 patients with suspected vascular graft infection who were scanned with <sup>111</sup>In WBCs, with confirmed infected vascular implants in 10 patients. Overall, SPECT/CT provided more accurate data than planar imaging and contributory information in 67% of patients with suspected vascular graft infection. In one patient, SPECT/CT was falsely positive, showing focal vascular graft uptake that was unconfirmed by further follow-up and clinical outcome.<sup>85</sup> The role of <sup>99m</sup>Tc WBC SPECT/CT was also assessed retrospectively in 11 patients with suspected arterial graft infection. On the basis of clinical outcome, <sup>99m</sup>Tc WBC SPECT/CT identified six patients as having infection (true-positive results) and four as not having infection

(true-negative results). One false-positive result was seen in a patient imaged 2 years after implantation of a thoracoabdominal aortic endograft.<sup>91</sup>

### Fluorodeoxyglucose Positron Emission Tomography

FDG PET/CT has a high sensitivity for vascular graft infection, but specificity is somewhat lower than WBC SPECT/CT, especially in an early postoperative phase. Increased FDG uptake may also occur in native vessels. False-positive results can be due to increased radiotracer activity along implants, grafts, and stents or in healing postoperative scars as well as to the presence of known or unknown malignant disease.<sup>92</sup> A pattern of linear FDG uptake of mild to moderate intensity found along a vascular graft with no evidence or suspicion of infection can be attributed to a chronic aseptic inflammatory reaction to a synthetic graft that is mediated by macrophages, fibroblasts, and foreign-body giant cells (Fig. 31.5). This pattern is observed more frequently in recently implanted grafts but can persist for years after surgery.<sup>93</sup> Keidar et al. studied FDG uptake in 107 noninfected vascular graft prostheses in patients scanned for other, mainly oncologic reasons. Diffuse, homogeneous uptake was found in more than half of the grafts, more prevalent in Gore-Tex than in Dacron grafts. The FDG uptake in these synthetic grafts showed no change in intensity for a follow-up of up to 16 years.<sup>94</sup> Although a focal pattern of intense abnormal FDG uptake is indicative of infection, the use of PET alone is limited for diagnosis of an infected vascular graft mainly by its inability to precisely define the anatomic location of the increased radiotracer focus. Correlation of functional information provided by FDG PET with the anatomic data of CT or MRI in separately performed imaging procedures of the lower limbs is not accurate enough for localizing a focus of increased FDG uptake to the vascular prosthesis itself or to the surrounding soft tissues.

Hybrid PET/CT has improved the specificity of FDG imaging. The presence, intensity, and pattern (focal or diffuse) of increased radiotracer activity is defined on the PET component, and the precise localization of abnormal FDG foci to the graft or to adjacent soft tissues is determined by the CT component (Fig. 31.6). In patients with complicated regional anatomy after multiple surgical procedures, PET/CT can pinpoint to the infected implant and differentiate between various suspicious findings on CT. In patients with multiple grafts, PET/CT can diagnose or exclude infection involving one or more specific prostheses.

Keidar et al. studied 39 patients with suspected graft infections. FDG-avid foci were noted in 30 of 39 patients on PET/CT, allowing for the accurate localization of 16 foci to the grafts with a sensitivity of 93%, specificity of 91%, positive predictive value of 88%, and negative predictive value of 96% for the diagnosis of prosthetic involvement. This enabled accurate differentiation between graft and surrounding soft tissue infection.<sup>95</sup> In a prospective study of 96 suspected infected grafts in 76 patients, focal FDG uptake had a positive predictive value of 93% for the diagnosis of graft infection and a negative predictive value of 97%, compared with 89% and 67%, respectively, for a pattern of inhomogeneous tracer activity. Only focal FDG uptake and

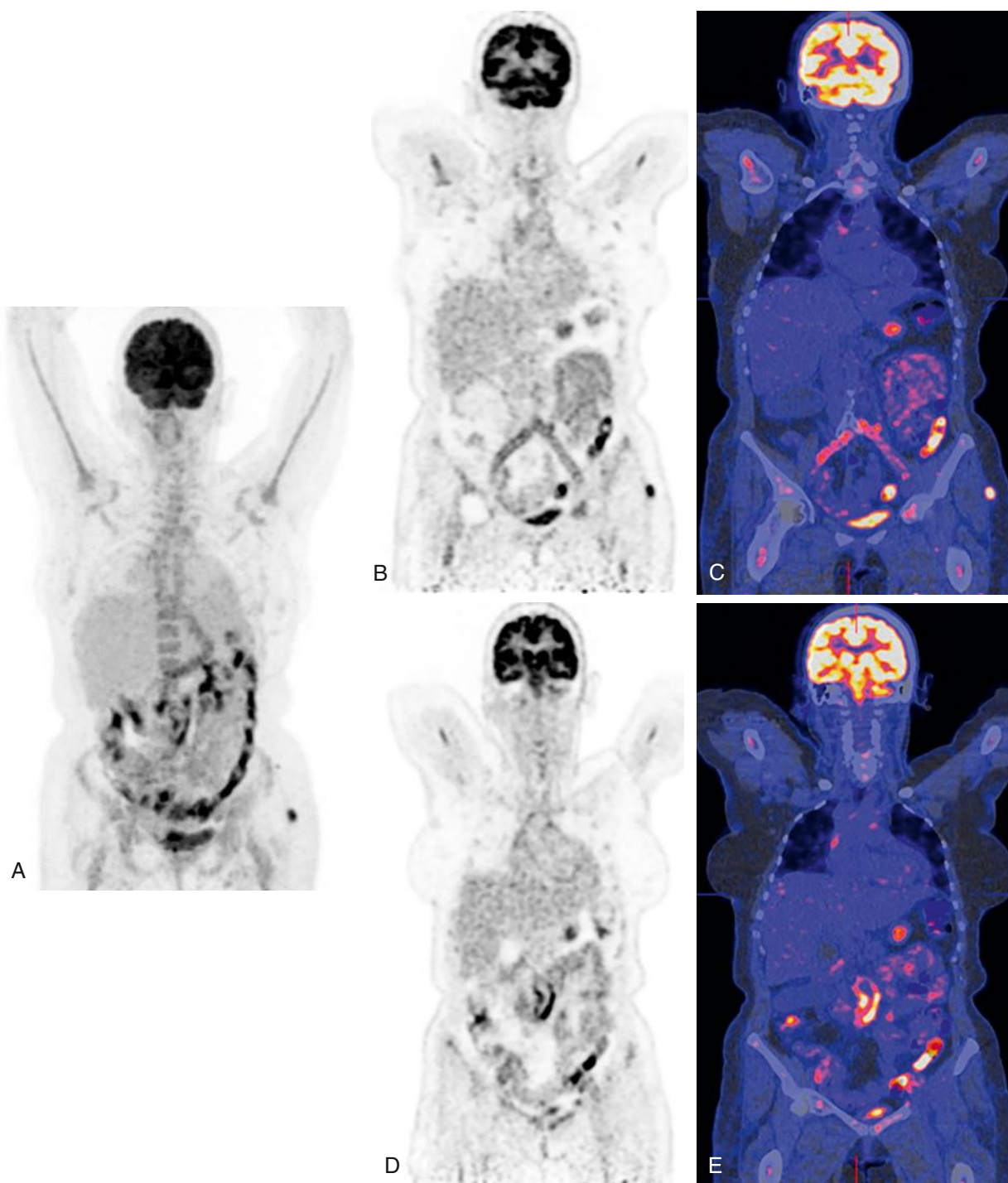


**Figure 31.5** Normal and abnormal fluorodeoxyglucose (FDG) uptake in an aortobifemoral vascular graft. (A) Coronal maximum intensity projection showing heterogeneous uptake at the graft and diffuse physiologic uptake in the colon. (B,C) Selected coronal FDG positron emission tomography (PET) and fused PET-computed tomography (CT) images of the iliac part of the prosthesis showing homogeneous uptake because of reactive inflammation. (D,E) Selected coronal FDG PET and fused PET-CT images of the aortic part of the prosthesis showing heterogeneous focal and intense uptake. This part of the prosthesis is infected.

irregular graft boundaries on CT were significant predictors of vascular graft infection, whereas smooth lesion boundaries with no focal FDG uptake had a positive predictive value of less than 5%. The overall diagnostic accuracy of FDG PET/CT was more than 95% in 75% of vascular grafts.<sup>96</sup> The incremental value of fused images of FDG PET and CT was assessed in 25 patients

with suspected vascular graft infections. In 15 patients, infection was proven by culture. FDG PET had a sensitivity of 93%, a specificity of 70%, a positive predictive value of 82%, and a negative predictive value of 88%; for CT, these values were significantly lower: 56%, 57%, 60%, and 58%, respectively. The results were improved when FDG and CT data were fused.<sup>97</sup>

Recently, a clinical practice guideline on the management of vascular graft and endograft infections was published by the European Society for Vascular Surgery (ESVS) and with endorsement of the EANM. This extensive guideline is aimed to assist physicians involved in the diagnosis and treatment of patients with vascular graft infections in selecting the best management strategy in different scenarios. Diagnostic imaging is part of this guideline and a nice image workflow shows which imaging technique can be used best. In both central and peripheral suspected vascular graft infection, CTA is the first imaging method performed. However, when results are equivocal, FDG-PET/CT can be used as second imaging technique in the case of a centrally located vascular graft. When the vascular graft is located in the limbs, both FDG-PET/CT or WBC scintigraphy can be used.<sup>98</sup>

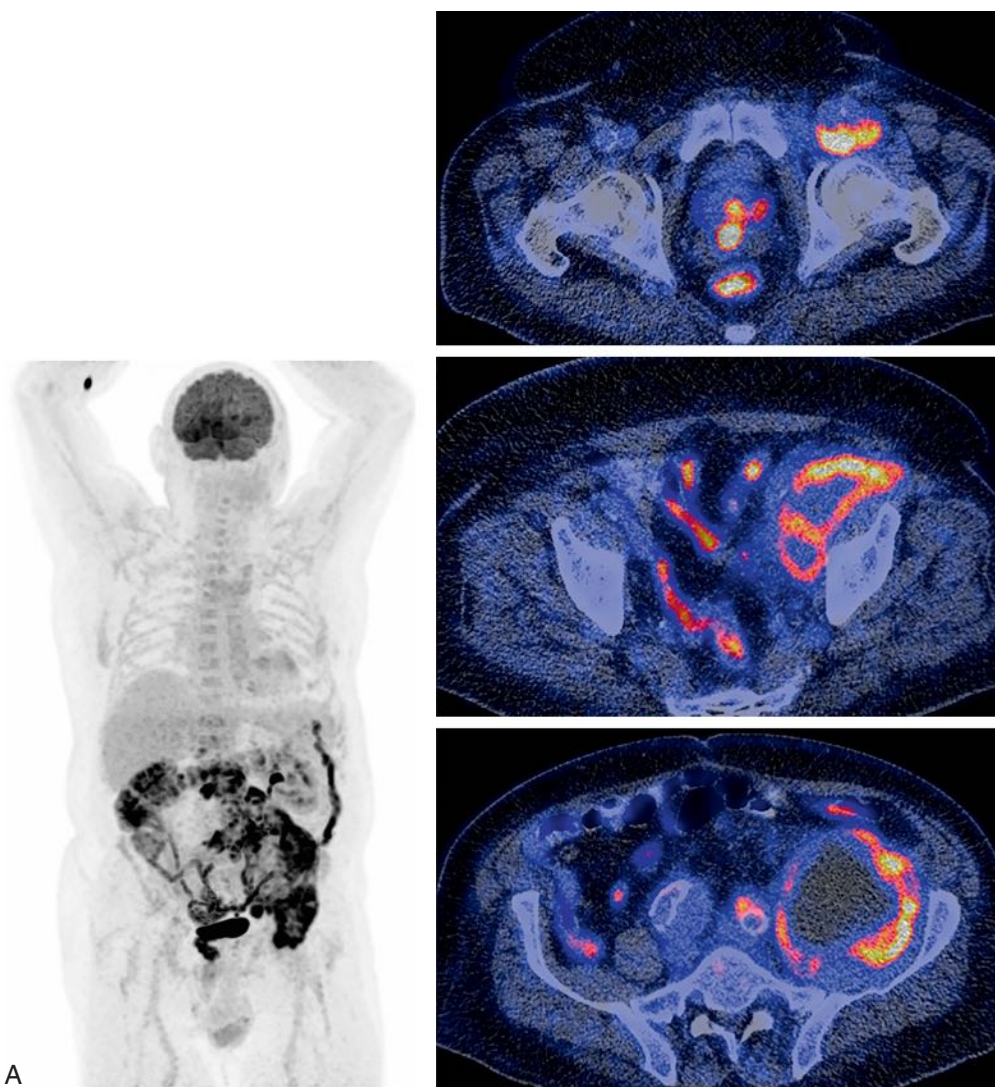
## LIMITATIONS AND RISKS

The limited resolution of the current technology of molecular imaging procedures, around 4–5 mm, is overcome by the unique information this technique offers on both function

and structure, which is often unattainable with morphologic imaging.

Another important limitation is the development of new molecular probes for imaging. There is significant difficulty in the radiolabeling of new substrates and in the development of new radiopharmaceuticals for clinical indications. Novel molecular probes for SPECT and PET are currently in the pipeline of basic and clinical research.

The combined modalities, SPECT/CT and PET/CT, offer greater detail and a higher level of accuracy. These studies, however, are associated with higher radiation exposure for the patient. For instance, most molecular imaging procedures result in radiation doses between 1 and 10 mSv and the effective dose for FDG PET/CT is around 4–5 mSv. With the use of hybrid devices, the burden of radiation derives from both the radiopharmaceuticals and the CT component. Advances in PET/CT scanner technology allow reduced injected activity of FDG and hence lead to a decrease in the effective dose. In addition, advances in CT technology, as well as careful planning of CT for either attenuation correction or diagnostic purposes can further lower the overall radiation dose.



*Continued*

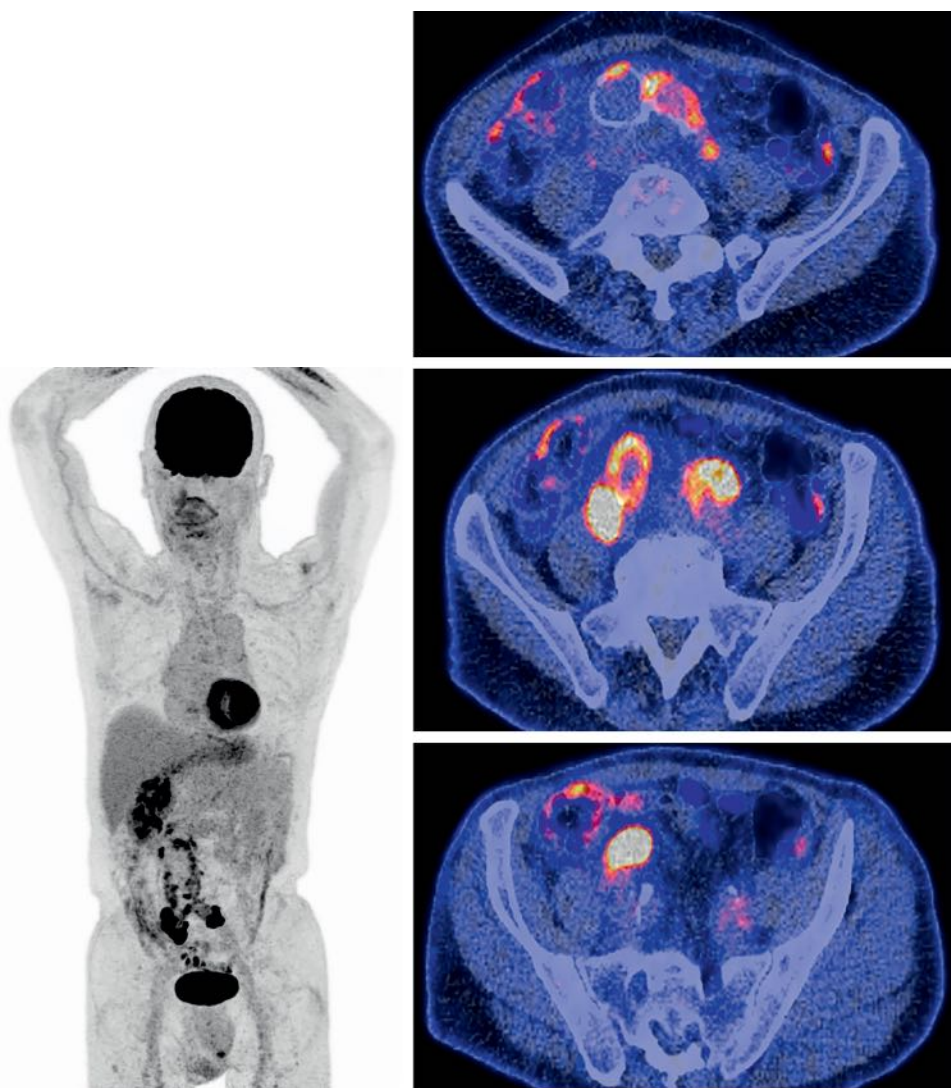


**Figure 31.6 (A,B)** Two FDG-PET/CT examples of infected vascular graft prosthesis with soft tissue involvement and abscess formation in the pelvis and groin.

## FUTURE ADVANCES

Vascular imaging is challenging to manage. It is therefore important to gather a wide expertise using a multidisciplinary team approach involving vascular medicine, vascular surgery and experienced nuclear (hybrid) imagers to perform the optimal diagnostics resulting in dedicated treatment and follow-up for each individual patient. It is also important to standardize the acquisition protocols and interpretation criteria throughout the world, not only to provide the nuclear medicine physicians with criteria indicating when to declare a scan positive but also to be able to better compare research results. Extensive efforts to provide this standardization have recently been taken.<sup>99</sup> Hybrid PET/MR technology has been developed and is now available for clinical use. The total radiation exposure in a combined PET/MR study is limited to that resulting from the administration of the PET tracer only. The combination of PET, with its sensitivity in the picomolar range, with the

high soft tissue contrast offered by MRI may play an important role in future imaging algorithms.<sup>100</sup> Bini et al. have compared PET/MR with PET/CT for carotid artery imaging and have also assessed various technical variables associated with the new technology (i.e., MR-based attenuation correction, carotid coil for PET/MR). Excellent correlations were reported, supporting the use of PET/MR for quantitative assessment of the inflammatory burden of the carotid arteries.<sup>101</sup> Recently, the first total body PET/CT camera systems were installed in clinical departments. Total body scanners are able to image the whole body (or a large part of the body) in one bed position, meaning that imaging only takes a few minutes. Total body PET/CT scanners will revolutionize and significantly expand the clinical potential. This new scanner can scan up to 15 times faster than a conventional PET/CT scanner; uses up to 15 times less radiation, makes imaging of radiotracers possible by more than three half-lives, and leads to an improved spatial resolution of about 2–3 mm.

## SELECTED KEY REFERENCES

- Ben-Haim S, Kupzov E, Tamir A, Israel O. Evaluation of 18F-FDG uptake and arterial wall calcifications using 18F-FDG PET/CT. *J Nucl Med.* 2004;45:1816–1821.
- Description and prevalence of the different patterns of vascular wall findings on PET and CT and of the relationship between FDG activity on PET and vascular wall calcifications on CT.*
- Chakfé N, et al. European Society for Vascular Surgery (ESVS) 2020 clinical practice guidelines on the management of vascular graft and endograft infections. *Eur J Vasc Endovasc Surg.* 2020;59:339–384.
- Practical guideline to assist physicians involved in the diagnosis and treatment of patients with vascular graft infections in selecting the best management strategy in different scenarios. This guideline also included a diagnostic imaging flowchart.*
- Cocker MS, Mc Ardle B, Spence JD, et al. Imaging atherosclerosis with hybrid [(18)F]fluorodeoxyglucose positron emission tomography/computed tomography imaging: what Leonardo da Vinci could not see. *J Nucl Cardiol.* 2012;19:1211–1225.
- A comprehensive review article discussing the role of FDG PET in the identification of high-risk plaques and in monitoring disease progression and response to therapy.*
- Elkhawad M, Rudd JH. Radiotracer imaging of atherosclerotic plaque biology. *Cardiol Clin.* 2009;27:345–354.
- Description of the principles of nuclear imaging in atherosclerosis and discussion of several radiotracers that can be used to assess high-risk plaques.*
- Figueroa AL, Subramanian SS, Cury RC, et al. Distribution of inflammation within carotid atherosclerotic plaques with high-risk morphological features: a comparison between positron emission tomography activity, plaque morphology, and histopathology. *Circ Cardiovasc Imaging.* 2012;5:69–77.
- A study assessing high-risk morphologic features of carotid artery plaques with CT and comparing them with inflammation as detected by F18 FDG PET and histologically in a subgroup of patients undergoing carotid endarterectomy inflammation. The results showed that multimodality imaging with CT and PET provides complementary information about high-risk morphologic features and inflammation.*
- Glaudemans AW, de Vrues EF, Galli F, Dierckx RA, Signore A. The use of 18F-FDG-PET/CT for diagnosis and treatment monitoring of inflammatory and infectious diseases. *Clin Dev Immunol.* 2013;2013:623036.
- Overview of, among others, diagnostic and therapeutic monitoring possibilities of FDG PET in vasculitis.*
- Glaudemans AW, Slart RH, Bozzao A, et al. Molecular imaging in atherosclerosis. *Eur J Nucl Med Mol Imaging.* 2010;37:2381–2397.
- Overview of the pathophysiology of atherosclerosis and all available radiopharmaceuticals.*
- Keidar Z, Engel A, Hoffman A, Israel O, Nitecki S. Prosthetic vascular graft infection: the role of 18F-FDG PET/CT. *J Nucl Med.* 2007;48:1230–1236.
- First and largest patient series assessing the role of FDG PET/CT for the diagnosis of vascular graft infection.*
- Keidar Z, Pirmisashvili N, Leiderman M, Nitecki S, Israel O. 18F-FDG uptake in noninfected prosthetic vascular grafts: incidence, patterns, and changes over time. *J Nucl Med.* 2014;55:392–395.
- Retrospective analysis of FDG uptake and pattern of uptake in a large series of noninfected vascular grafts.*
- Kotze CW, Groves AM, Menezes LJ, et al. What is the relationship between 18F-FDG aortic aneurysm uptake on PET/CT and future growth rate? *Eur J Nucl Med Mol Imaging.* 2011;38:1493–1499.
- Longitudinal study in patients with abdominal aortic aneurysms, showing an inverse trend between FDG uptake on PET and future aneurysm expansion and demonstrating that aortic aneurysms with lower metabolic activity may be more likely to expand.*
- Papathanasiou ND, Du Y, Menezes LJ, et al. 18F-fludeoxyglucose PET/CT in the evaluation of large-vessel vasculitis: diagnostic performance and correlation with clinical and laboratory parameters. *Br J Radiol.* 2012;85:e188–e194.
- Demonstrates the clinical role of FDG PET/CT in the assessment of patients with suspected large vessel vasculitis. FDG PET/CT can detect the extent and activity of large vessel vasculitis in untreated patients but is unreliable for the diagnosis in patients taking steroids.*
- Slart RH, Glaudemans AW, Chareonthaitawee P, et al. FDG-PET/CT(A) imaging in large vessel vasculitis and polymyalgia rheumatica: joint procedural recommendation of the EANM, SNMMI, and the PET Interest Group (PIG), and endorsed by the ASNC. *Eur J Nucl Med Mol Imaging.* 2018;45:1250–1269.
- Procedural recommendations for patient preparation, acquisition and interpretation for the diagnosis and follow-up of patients with suspected or diagnosed LVV and/or PMR; internationally accepted standard for FDG-PET/CT(A) imaging and reporting of LVV and PMR.*

A complete reference list can be found online at [www.expertconsult.com](http://www.expertconsult.com).

## REFERENCES

1. Boellaard R, et al. FDG PET/CT: EANM procedure guidelines for tumour imaging: version 2.0. *Eur J Nucl Med Mol Imaging*. 2015;42:328–354.
2. Cocker MS, et al. Imaging atherosclerosis with hybrid [(18)F]fluorodeoxyglucose positron emission tomography/computed tomography imaging: what Leonardo da Vinci could not see. *J Nucl Cardiol*. 2012;19:1211–1225.
3. Sheikine Y, et al. FDG-PET imaging of atherosclerosis: do we know what we see? *Atherosclerosis*. 2010;211:371–380.
4. Grant FD, et al. Skeletal PET with 18F-fluoride: applying new technology to an old tracer. *J Nucl Med*. 2008;49:68–78.
5. Glaudemans AW, et al. Molecular imaging of atherosclerosis. *Eur J Nucl Med Mol Imaging*. 2010;37:2381–2397.
6. Lees AM, et al. Imaging human atherosclerosis with 99mTc-labeled low density lipoproteins. *Arteriosclerosis*. 1988;8:461–470.
7. Tatsumi M, et al. Fluorodeoxyglucose uptake in the aortic wall at PET/CT: possible finding for active atherosclerosis. *Radiology*. 2003;229:831–837.
8. Ben-Haim S, et al. Evaluation of 18F-FDG uptake and arterial wall calcifications using 18F-FDG PET/CT. *J Nucl Med*. 2004;45:1816–1821.
9. Dunphy MP, et al. Association of vascular 18F-FDG uptake with vascular calcification. *J Nucl Med*. 2005;46:1278–1284.
10. Yun M, et al. 18F FDG uptake in the large arteries: a correlation study with the atherogenic risk factors. *Semin Nucl Med*. 2002;32:70–76.
11. Tahara N, et al. Vascular inflammation evaluated by [18F]-fluorodeoxyglucose positron emission tomography is associated with the metabolic syndrome. *J Am Coll Cardiol*. 2007;49:1533–1539.
12. Rudd JH, et al. Imaging atherosclerotic plaque inflammation with [18F]-fluorodeoxyglucose positron emission tomography. *Circulation*. 2002;105:2708–2711.
13. Davies JR, et al. Identification of culprit lesions after transient ischemic attack by combined 18F fluorodeoxyglucose positron-emission tomography and high-resolution magnetic resonance imaging. *Stroke*. 2005;36:2642–2647.
14. Silvera SS, et al. Multimodality imaging of atherosclerotic plaque activity and composition using FDG-PET/CT and MRI in carotid and femoral arteries. *Atherosclerosis*. 2009;207:139–143.
15. Kwee RM, et al. Reproducibility of fibrous cap status assessment of carotid artery plaques by contrast-enhanced MRI. *Stroke*. 2009;40:3017–3021.
16. Graebe M, et al. 18FDG PET and ultrasound echolucency in carotid artery plaques. *JACC Cardiovasc Imaging*. 2010;3:289–295.
17. Choi YS, et al. Uptake of F-18 FDG and ultrasound analysis of carotid plaque. *J Nucl Cardiol*. 2011;18:267–272.
18. Tawakol A, et al. In vivo 18F-fluorodeoxyglucose positron emission tomography imaging provides a noninvasive measure of carotid plaque inflammation in patients. *J Am Coll Cardiol*. 2006;48:1818–1824.
19. Figueroa AL, et al. Distribution of inflammation within carotid atherosclerotic plaques with high-risk morphological features: a comparison between positron emission tomography activity, plaque morphology, and histopathology. *Circ Cardiovasc Imaging*. 2012;5:69–77.
20. Masteling MG, et al. High-resolution imaging of human atherosclerotic carotid plaques with micro 18F-FDG PET scanning exploring plaque vulnerability. *J Nucl Cardiol*. 2011;18:1066–1075.
21. Grandpierre S, et al. Arterial foci of F-18 fluorodeoxyglucose are associated with an enhanced risk of subsequent ischemic stroke in cancer patients: a case-control pilot study. *Clin Nucl Med*. 2011;36:85–90.
22. Yoo HJ, et al. Vascular inflammation stratified by C-reactive protein and low-density lipoprotein cholesterol levels: analysis with 18F-FDG PET. *J Nucl Med*. 2011;52:10–17.
23. Rudd JH, et al. Relationships among regional arterial inflammation, calcification, risk factors, and biomarkers: a prospective fluorodeoxyglucose positron-emission tomography/computed tomography imaging study. *Circ Cardiovasc Imaging*. 2009;2:107–115.
24. Vallabhajosula S, et al. Atherosclerosis: imaging techniques and the evolving role of nuclear medicine. *J Nucl Med*. 1997;38:1788–1796.
25. Tahara N, et al. Vascular inflammation evaluated by [18F]-fluorodeoxyglucose positron emission tomography is associated with the metabolic syndrome. *J Am Coll Cardiol*. 2007;49:1533–1539.
26. Kim TN, et al. Vascular inflammation in patients with impaired glucose tolerance and type 2 diabetes: analysis with 18F-fluorodeoxyglucose positron emission tomography. *Circ Cardiovasc Imaging*. 2010;3:142–148.
27. Ogawa M, et al. Application of 18F-FDG PET for monitoring the therapeutic effect of antiinflammatory drugs on stabilization of vulnerable atherosclerotic plaques. *J Nucl Med*. 2006;47:1845–1850.
28. Corti R, et al. Effects of lipid-lowering by simvastatin on human atherosclerotic lesions: a longitudinal study by high-resolution, noninvasive magnetic resonance imaging. *Circulation*. 2001;104:249–252.
29. Corti R, et al. Lipid lowering by simvastatin induces regression of human atherosclerotic lesions: two years' follow-up by high-resolution noninvasive magnetic resonance imaging. *Circulation*. 2002;106:2884–2887.
30. Tahara N, et al. Simvastatin attenuates plaque inflammation: evaluation by fluorodeoxyglucose positron emission tomography. *J Am Coll Cardiol*. 2006;48:1825–1831.
31. Lee SJ, et al. Reversal of vascular 18F-FDG uptake with plasma high-density lipoprotein elevation by atherogenic risk reduction. *J Nucl Med*. 2008;49:1277–1282.
32. Ben-Haim S, et al. Changing patterns of abnormal vascular wall F-18 fluorodeoxyglucose uptake on follow-up PET/CT studies. *J Nucl Cardiol*. 2006;13:791–800.
33. Menezes IJ, et al. What is the natural history of 18F-FDG uptake in arterial atheroma on PET/CT? Implications for imaging the vulnerable plaque. *Atherosclerosis*. 2010;211:136–140.
34. Ehara S, et al. Spotty calcification typifies the culprit plaque in patients with acute myocardial infarction: an intravascular ultrasound study. *Circulation*. 2004;110:3424–3429.
35. Irkle A, et al. Identifying active vascular microcalcification by (18) F-sodium fluoride positron emission tomography. *Nat Commun*. 2015;6:7495.
36. Derlin T, et al. Correlation of inflammation assessed by 18F-FDG PET, active mineral deposition assessed by 18F-fluoride PET, and vascular calcification in atherosclerotic plaque: a dual-tracer PET/CT study. *J Nucl Med*. 2011;52:1020–1027.
37. Virgolini I, et al. Autologous low-density lipoprotein labeling allows characterization of human atherosclerotic lesions in vivo as to presence of foam cells and endothelial coverage. *Eur J Nucl Med*. 1991;18:948–951.
38. Iuliano L, et al. Preparation and biodistribution of 99m technetium labeled oxidized LDL in man. *Atherosclerosis*. 1996;126:131–141.
39. Vallabhajosula S. Technetium-99m-labeled chemotactic peptides: specific for imaging infection? *J Nucl Med*. 1997;38:1322–1326.
40. Demacker PN, et al. Evaluation of indium-111-polyclonal immunoglobulin G to quantitate atherosclerosis in Watanabe heritable hyperlipidemic rabbits with scintigraphy: effect of age and treatment with antioxidants or ethinylestradiol. *J Nucl Med*. 1993;34:1316–1321.
41. Sinzinger H, et al. Radioisotopic imaging of atheroma. In: Fuster V, ed. *Syndromes of Atherosclerosis: Correlations of Clinical Imaging and Pathology*. Armonk, NY: Futura Publishing Co. Inc.; 1996:369–383.
42. Moriwaki H, et al. Functional and anatomic evaluation of carotid atherothrombosis: a combined study of indium 111 platelet scintigraphy and B-mode ultrasonography. *Arterioscler Thromb Vasc Biol*. 1995;15:2234–2240.
43. Knight LC. Scintigraphic methods for detecting vascular thrombus. *J Nucl Med*. 1993;34(suppl):554–561.
44. Narula J, et al. Noninvasive localization of experimental atherosclerotic lesions with mouse/human chimeric Z2D3 F(ab)2 specific for the proliferating smooth muscle cells of human atheroma: imaging with conventional and negative charge-modified antibody fragments. *Circulation*. 1995;92:474–484.

45. Laufer EM, et al. Molecular imaging of macrophage cell death for the assessment of plaque vulnerability. *Arterioscler Thromb Vasc Biol.* 2009;29:1031–1038.
46. Kietelselaer BL, et al. Noninvasive detection of plaque instability with use of radiolabeled annexin A5 in patients with carotid-artery atherosclerosis. *N Engl J Med.* 2004;350:1472–1473.
47. Lees AM, et al. Imaging human atherosclerosis with 99mTc-labeled low density lipoproteins. *Arteriosclerosis.* 1988;8:461–470.
48. Glaudemans AW, et al. In vivo and in vitro evidence that 99mTc-HYNIC-interleukin-2 is able to detect T lymphocytes in vulnerable atherosclerotic plaques of the carotid artery. *Eur J Nucl Med Mol Imaging.* 2014;41:1710–1719.
49. Bird JL, et al. Evaluation of translocator protein quantification as a tool for characterising macrophage burden in human carotid atherosclerosis. *Atherosclerosis.* 2010;210:388–391.
50. Pugliese F, et al. Imaging of vascular inflammation with [11C]-PK11195 and positron emission tomography/computed tomography angiography. *J Am Coll Cardiol.* 2010;56:653–661.
51. Rominger A, et al. In vivo imaging of macrophage activity in the coronary arteries using 68Ga-DOTATATE PET/CT: correlation with coronary calcium burden and risk factors. *J Nucl Med.* 2010;51:193–197.
52. Kato K, et al. Evaluation and comparison of 11C-choline uptake and calcification in aortic and common carotid arterial walls with combined PET/CT. *Eur J Nucl Med Mol Imaging.* 2009;36:1622–1628.
53. Matter CM, et al. 18F-choline images murine atherosclerotic plaques ex vivo. *Arterioscler Thromb Vasc Biol.* 2006;26:584–589.
54. Kotze CW, et al. Increased metabolic activity in abdominal aortic aneurysm detected by 18F-fluorodeoxyglucose (18F-FDG) positron emission tomography/computed tomography (PET/CT). *Eur J Vasc Endovasc Surg.* 2009;38:93–99.
55. Truijers M, et al. In vivo imaging of abdominal aortic aneurysms: increased FDG uptake suggests inflammation in the aneurysm wall. *J Endovasc Ther.* 2008;15:462–467.
56. Sakalihasan N, et al. Positron emission tomography (PET) evaluation of abdominal aortic aneurysm (AAA). *Eur J Vasc Endovasc Surg.* 2002;23:431–436.
57. Xu XY, et al. High levels of 18F-FDG uptake in aortic aneurysm wall are associated with high wall stress. *Eur J Vasc Endovasc Surg.* 2010;39:295–301.
58. Reeps C, et al. Increased 18F-fluorodeoxyglucose uptake in abdominal aortic aneurysms in positron emission/computed tomography is associated with inflammation, aortic wall instability, and acute symptoms. *J Vasc Surg.* 2008;48:417–423.
59. Kotze CW, et al. What is the relationship between 18F-FDG aortic aneurysm uptake on PET/CT and future growth rate? *Eur J Nucl Med Mol Imaging.* 2011;38:1493–1499.
60. Tegler G, et al. Inflammation in the walls of asymptomatic abdominal aortic aneurysms is not associated with increased metabolic activity detectable by 18-fluorodeoxyglucose positron-emission tomography. *J Vasc Surg.* 2012;56:802–807.
61. Marini C, et al. Direct relationship between cell density and FDG uptake in asymptomatic aortic aneurysm close to surgical threshold: an in vivo and in vitro study. *Eur J Nucl Med Mol Imaging.* 2012;39:91–101.
62. Hagan PG, et al. The International Registry of Acute Aortic Dissection (IRAD): new insights into an old disease. *JAMA.* 2000;283:897–903.
63. Rudd JH. The role of 18F-FDG PET in aortic dissection. *J Nucl Med.* 2010;51:667–668.
64. He R, et al. Characterization of the inflammatory and apoptotic cells in the aortas of patients with ascending thoracic aortic aneurysms and dissections. *J Thorac Cardiovasc Surg.* 2006;131:671–678.
65. Kuehl H, et al. Detection of inflammation in patients with acute aortic syndrome: comparison of FDG-PET/CT imaging and serological markers of inflammation. *Heart.* 2008;94:1472–1477.
66. Kato K, et al. Uptake of 18F-FDG in acute aortic dissection: a determinant of unfavorable outcome. *J Nucl Med.* 2010;51:674–681.
67. Glaudemans AW, et al. The use of 18F-FDG-Pet/CT for diagnosis and treatment monitoring of inflammatory and infectious diseases. *Clin Dev Immunol.* 2013;2013:623036.
68. Meller J, et al. Early diagnosis and follow-up of aortitis with [(18)F] FDG PET and MRI. *Eur J Nucl Med Mol Imaging.* 2003;30:730–736.
69. Blockmans D, et al. Repetitive 18F-fluorodeoxyglucose positron emission tomography in giant cell arteritis: a prospective study of 35 patients. *Arthritis Rheum.* 2006;55:131–137.
70. Meller J, et al. Value of F-18 FDG hybrid camera PET and MRI in early Takayasu aortitis. *Eur Radiol.* 2003;13:400–405.
71. Meller J, et al. 18F-FDG PET and PET/CT in fever of unknown origin. *J Nucl Med.* 2007;48:35–45.
72. Bleeker-Rovers CP, et al. F-18-fluorodeoxyglucose positron emission tomography in diagnosis and follow-up of patients with different types of vasculitis. *Neth J Med.* 2003;61:323–329.
73. Webb M, et al. Molecular imaging of Takayasu's arteritis and other large-vessel vasculitis with 18F-FDG PET. *Nucl Med Commun.* 2006;27:547–549.
74. Papathanasiou ND, et al. 18F-Fludeoxyglucose PET/CT in the evaluation of large-vessel vasculitis: diagnostic performance and correlation with clinical and laboratory parameters. *Br J Radiol.* 2012;85:e188–e194.
75. Bleeker-Rovers CP, et al. F-18-fluorodeoxyglucose positron emission tomography in diagnosis and follow-up of patients with different types of vasculitis. *Neth J Med.* 2003;61:323–329.
76. Hooisma GA, et al. Parameters related to a positive test result for FDG PET(/CT) for large vessel vasculitis: a multicenter retrospective study. *Clin Rheumatol.* 2012;31:861–871.
77. Henes JC, et al. [18F] FDG-PET/CT as a new and sensitive imaging method for the diagnosis of large vessel vasculitis. *Clin Exp Rheumatol.* 2008;26(3 suppl 49):S47–S52.
78. Blockmans D, et al. Positron emission tomography in giant cell arteritis and polymyalgia rheumatica: evidence for inflammation of the aortic arch. *Am J Med.* 2000;108:246–249.
79. Ben-Haim S, et al. Cardiovascular infection and inflammation. *Semin Nucl Med.* 2009;39:103–114.
80. Tezuka D, et al. Role of FDG PET-CT in Takayasu arteritis: sensitive detection of recurrences. *JACC Cardiovasc Imaging.* 2012;5:422–429.
81. Walter MA, et al. The value of [18F]FDG-PET in the diagnosis of large-vessel vasculitis and the assessment of activity and extent of disease. *Eur J Nucl Med Mol Imaging.* 2005;32:674–681.
82. Kobayashi Y, et al. Aortic wall inflammation due to Takayasu arteritis imaged with 18F-FDG PET coregistered with enhanced CT. *J Nucl Med.* 2005;46:917–922.
83. Belhocine T, et al. [Horton's disease and extra-temporal vessel locations: role of 18FDG PET scan: report of 3 cases and review of the literature. *Rev Med Interne.* 2002;23:584–591.
84. Slart RH, et al. FDG-PET/CT(A) imaging in large vessel vasculitis and polymyalgia rheumatica: joint procedural recommendation of the EANM, SNMMI, and the PET Interest Group (PIG), and endorsed by the ASNC. *Eur J Nucl Med Mol Imaging.* 2018;45:1250–1269.
85. Bar-Shalom R, et al. SPECT/CT using 67Ga and 111In-labeled leukocyte scintigraphy for diagnosis of infection. *J Nucl Med.* 2006;47:587–594.
86. Keidar Z, et al. PET/CT using 2-deoxy-2-[18F]fluoro-d-glucose for the evaluation of suspected infected vascular graft. *Mol Imaging Biol.* 2003;5:23–25.
87. Palestro CJ, et al. Labeled leukocyte imaging: current status and future directions. *Q J Nucl Med Mol Imaging.* 2009;53:105–123.
88. Liberatore M, et al. Clinical usefulness of technetium-99m-HMPAO-labeled leukocyte scan in prosthetic vascular graft infection. *J Nucl Med.* 1998;39:875–879.
89. Seeger JM. Management of patients with prosthetic vascular graft infection. *Am Surg.* 2000;66:166–177.
90. Shahidi S, et al. Detection of abdominal aortic graft infection: comparison of magnetic resonance imaging and indium-labeled white blood cell scanning. *Ann Vasc Surg.* 2007;21:586–592.

91. Lou L, et al. 99mTc-WBC scintigraphy with SPECT/CT in the evaluation of arterial graft infection. *Nucl Med Commun.* 2010;31:411–416.
92. Wassélius J, et al. High 18F-FDG uptake in synthetic aortic vascular grafts on PET/CT in symptomatic and asymptomatic patients. *J Nucl Med.* 2008;49:1601–1605.
93. Cook GJ, et al. Normal physiological and benign pathological variants of 18-fluoro-2-deoxyglucose positron-emission tomography scanning: potential for error in interpretation. *Semin Nucl Med.* 1996;26:308–314.
94. Keidar Z, et al. 18F-FDG uptake in noninfected prosthetic vascular grafts: incidence, patterns, and changes over time. *J Nucl Med.* 2014;55:392–395.
95. Keidar Z, et al. Prosthetic vascular graft infection: the role of 18F-FDG PET/CT. *J Nucl Med.* 2007;48:1230–1236.
96. Spacek M, et al. Diagnostics of “non-acute” vascular prosthesis infection using 18F-FDG PET/CT: our experience with 96 prostheses. *Eur J Nucl Med Mol Imaging.* 2009;36:850–858.
97. Bruggink JL, et al. Accuracy of FDG-PET-CT in the diagnostic work-up of vascular prosthetic graft infection. *Eur J Vasc Endovasc Surg.* 2010;40:348–354.
98. Chakfé N, et al. European Society for Vascular Surgery (ESVS) 2020 clinical practice guidelines on the management of vascular graft and endograft infections. *Eur J Vasc Endovasc Surg.* 2020;59:339–384.
99. Bucerius J, et al. Position paper of the Cardiovascular Committee of the European Association of Nuclear Medicine (EANM) on PET imaging of atherosclerosis. *Eur J Nucl Med Mol Imaging.* 2016;43:780–792.
100. Ratib O, et al. Potential applications of PET/MR imaging in cardiology. *J Nucl Med.* 2014;55:40S–46S.
101. Bini J, et al. Quantitative carotid PET/MR imaging: clinical evaluation of MR-attenuation correction versus CT-attenuation correction in 18F-FDG PET/MR emission data and comparison to PET/CT. *Am J Nucl Med Mol Imaging.* 2015;5:293–304.

# Intravascular Ultrasound

HALIM YAMMINE, JOCELYN K. BALLAST, and FRANK R. ARKO III

## INTRODUCTION 405

### BASIC PRINCIPLES 405

#### Creating the Image 405

##### *Technology* 405

#### Interpreting the Image 407

##### *Gray Scale* 407

##### *Volumetric Three-Dimensional Intravascular Ultrasound* 407

##### *Color-Flow Intravascular Ultrasound* 407

##### *Virtual Histology Intravascular Ultrasound* 407

## CLINICAL APPLICATIONS 408

### Effectiveness of Intravascular Ultrasound 408

#### *Cost Versus Benefit* 408

#### *General Benefits of Intravascular Ultrasound* 409

### Arterial Applications: Carotid and Peripheral Arterial 409

#### *Peripheral Arterial Disease* 409

#### *Intravascular Ultrasound-Guided True Lumen Reentry* 410

#### *Carotid Applications* 410

### Endovascular Repair: Abdominal Aortic Aneurysms 410

#### *Preoperative Intravascular Ultrasound* 410

## *Intraoperative Intravascular Ultrasound* 410

### *After Repair* 410

### *Endovascular Repair: Thoracic Aortic Disease* 410

#### *Thoracic Aneurysms* 411

#### *Blunt Traumatic Aortic Injury* 411

#### *Coarctation* 412

## Dissection 412

### *Pre- and Intraoperative Intravascular Ultrasound* 412

### *After Deployment* 414

### *Penetrating Aortic Ulcers and Intramural Hematoma* 414

#### *Venous Imaging and Applications* 414

#### *Venous Thromboembolism* 414

#### *Chronic Cerebrospinal Venous Insufficiency* 414

#### *Venous Compression Syndromes* 414

## LIMITATIONS AND RISKS 415

### *Comparison of Intravascular Ultrasound with Other Imaging Modalities* 415

### *Limitations and Risks of Intravascular Ultrasound* 416

## FUTURE ADVANCES 416

## INTRODUCTION

Catheter-based endovascular techniques are increasingly being used in vascular surgery, with demand for detailed intraoperative imaging increasing accordingly. Intravascular ultrasound (IVUS) is a catheter-based endoluminal guidance system that was initially utilized in interventional cardiology in the 1980s.<sup>1–5</sup> Various trials and analyses of IVUS-guided versus angiographic-guided percutaneous coronary intervention (PCI) have concluded that IVUS-guided PCI results in similar or improved outcomes overall.<sup>6–15</sup> In fact, IVUS has been shown to be effective in improving procedural results and reducing restenosis and the need for reintervention in PCI. Since its initial clinical use in coronary artery interventions, IVUS has been shown to have a variety of applications in vascular intervention because of its ability to provide detailed pre-treatment diagnostic information on the extent and severity of

disease, to guide treatment intraoperatively, and to immediately assess the treatment's success.<sup>16</sup>

## BASIC PRINCIPLES

### Creating the Image

#### *Technology*

IVUS creates axial images perpendicular to the long axis of the catheter by transmitting sound waves covering 360 degrees around the tip of the catheter, which is delivered into the lumen of the vessel over a guidewire. This is achieved either mechanically or electronically. The mechanical system, produced by Boston Scientific Corporation, utilizes a flexible high-torque catheter with a quickly rotating ultrasound transducer located at the tip. Electronic systems, produced by Volcano Corporation, utilize 64 miniaturized transducer elements

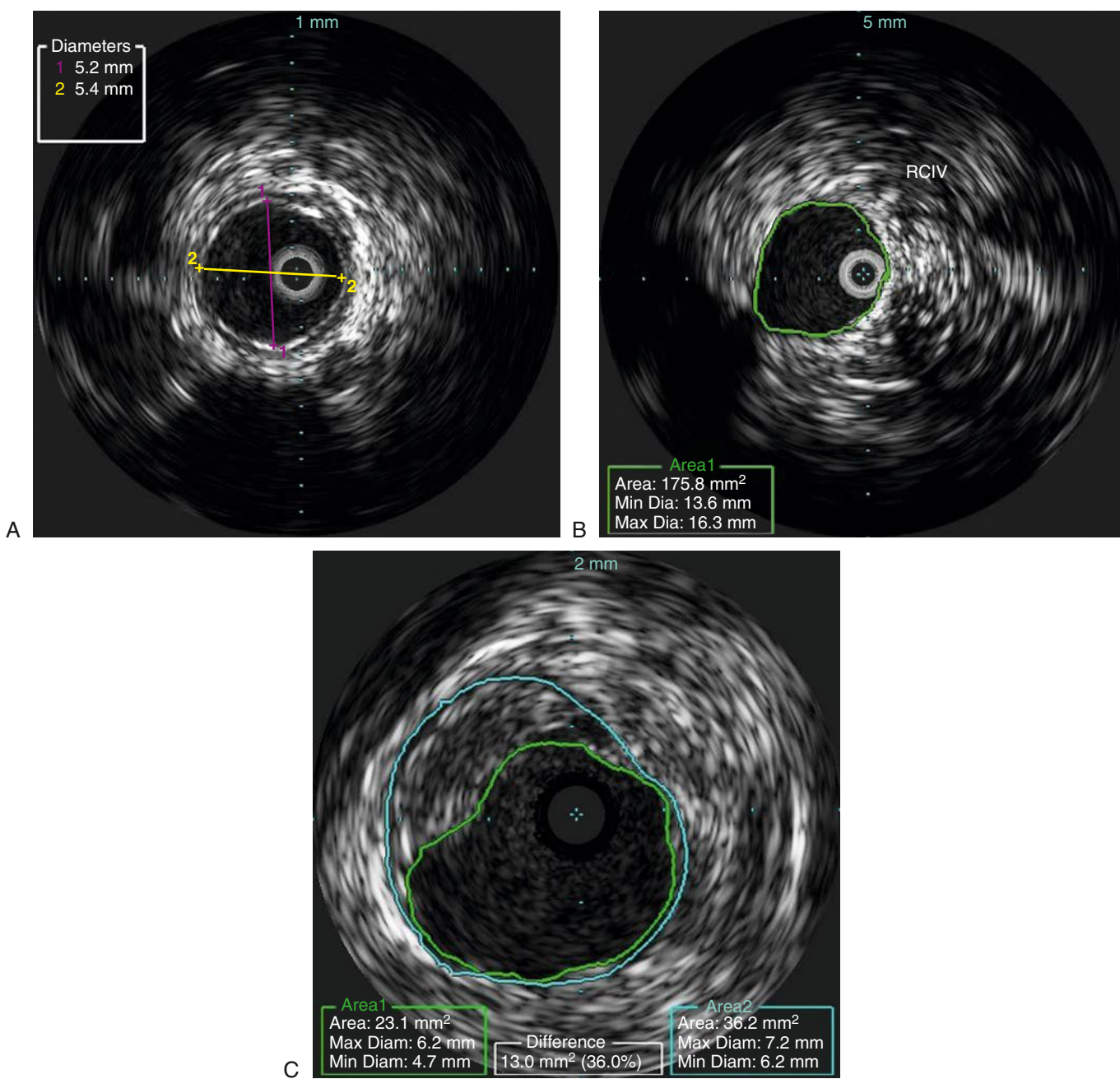


**Figure 32.1** It is possible to take a variety of measurements on the intravascular ultrasound console, including diameters (A) and area (B). It is also possible to find the amount of thrombus present in a vessel by measuring the area of the lumen and the area of the vessel (C). *RClV*, right common iliac vein.

located circumferentially around the tip of the catheter that are activated in sequence to produce an array of images. Information collected by IVUS transducers is reconstructed, displayed, and recorded visually on a separate console. This workstation facilitates the collection of measurements such as the diameter, circumference, and area of a vessel and allows for the capture of still images and video loops (Fig. 32.1).

In working with IVUS, it is important to choose the appropriate catheters and ultrasound frequencies to obtain the best possible imaging.<sup>17</sup> Higher frequencies improve image

resolution but decrease the depth of penetration. This makes them ideal for smaller vessels, as they provide more detail, with probes delivering 45 MHz being well suited to coronary vessels. Probes with frequencies around 20 MHz are ideal for larger peripheral vessels or occlusive branched vessels, whereas probes with lower frequencies around 10 MHz are well suited for imaging vessels such as the aorta, inferior vena cava, and iliacs (Table 32.1). These catheters must be delivered with larger sheaths and provide less detail, but they can scan the entire circumference of a vessel.

**TABLE 32.1** Table of Catheters for Noncoronary Vascular Imaging<sup>a</sup>

Catheter	Guidewire (in)	Frequency (MHz)	Sheath (F)	Working Length (cm)	Imaging Diameter (mm)	Manufacturer
Opticross	0.018	30	6	135	12	Boston Scientific
Eagle Eye Platinum	0.014	20	5	150	20	Volcano
Visions PV 014	0.014	20	5	150	20	Volcano
Visions PV 018	0.018	20	6	135	24	Volcano
Visions PV 035	0.035	10	8.5	90	60	Volcano

<sup>a</sup>In the United States, Boston Scientific Corporation and Volcano Corporation are the major manufacturers of FDA-cleared intravascular ultrasound (IVUS) systems.

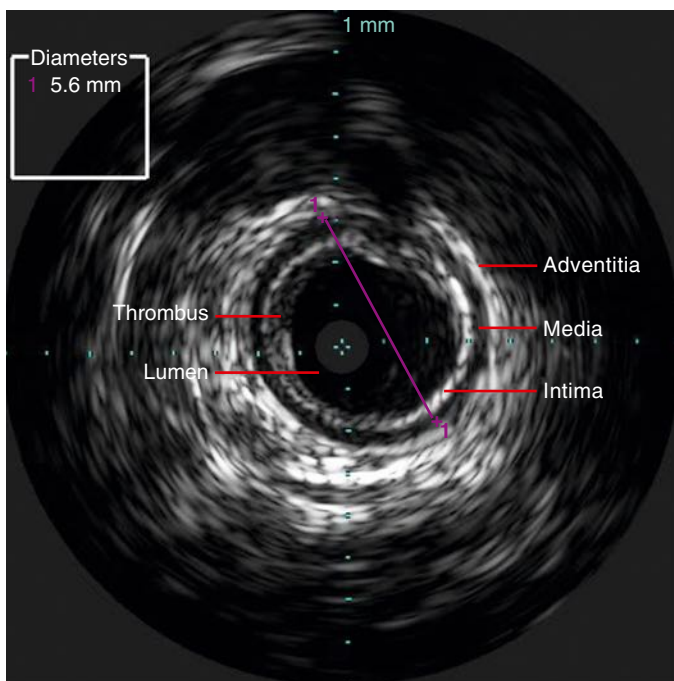


**Figure 32.2** In gray scale, the layers of the arterial wall are visualized clearly, with the intima and adventitia appearing bright and echogenic, while the media is darker and echolucent. The blood-filled lumen appears very dark, with the clear demarcation between the arterial wall and the lumen allowing measurements to be obtained.

## Interpreting the Image

### Gray Scale

As with other forms of ultrasound, IVUS displays two-dimensional images in gray scale. Ultrasound's ability to penetrate the material and the resultant amplitude of the returning signal determine the relative brightness or darkness of the vessel wall, reflecting its echogenicity or echolucency, respectively (Fig. 32.2).<sup>18,19</sup> It is also possible to visualize different types of plaques using IVUS. Heavily calcified plaques are highly echogenic and characterized by brightness and posterior shadowing. Fibrotic plaques are slightly less bright and lack the posterior shadowing of calcified plaques. Soft, lipid-filled plaques are echolucent and appear darker. Software allowing further characterization and analysis of vessels is also available with IVUS.

### Volumetric Three-Dimensional Intravascular Ultrasound

In order to overcome the limitations of two-dimensional visualization, three-dimensional IVUS has been developed to more accurately describe arterial morphology and atheroma distribution. Conventional methods have relied on a longitudinal reconstruction similar to an angiogram, created through an automated “pullback” of the IVUS probe and compiling a pixel-based two-dimensional longitudinal reconstruction. Because the catheter tip is not reliably in the center of the lumen, it is difficult to obtain accurate diameter and length measurements in longitudinal reconstructions.<sup>20</sup> However, in recent years more sophisticated three-dimensional reconstruction algorithms have been developed, such as a novel method allowing for simultaneous registration of two IVUS pullbacks of the same vessel.<sup>21</sup> This type of technology is likely to continue to improve, offering fewer errors in location and orientation registration.

### Color-Flow Intravascular Ultrasound

It is also possible to characterize blood flow with IVUS using color-flow software. This software, such as Volcano's Chroma-Flo, compares adjacent frames at 30 frames per second and identifies the movement of blood cells, coloring any normal blood flow red and faster blood flow yellow. Unlike Doppler, color-flow IVUS cannot measure flow velocities. However, it does provide more information about the interface between the vessel wall and the bloodstream, allowing for more accurate volumetric measurements and the ability to assess completeness of treatment (Fig. 32.3 and Video 32.1).<sup>22,23</sup>

### Virtual Histology Intravascular Ultrasound

Virtual histology (VH) IVUS utilizes the frequency of the returned signal as well as its amplitude to produce a color-coded map of a lesion based on the different frequencies at which various tissues reflect ultrasound. This allows histopathologic analysis of plaques based on their composition (Fig. 32.4). The Carotid Artery Plaque Virtual Histology Evaluation (CAPITAL) study, which compared 153 VH IVUS images with true histopathology sections from endarterectomies, found that VH IVUS was able to accurately diagnose 99.4% of thin-cap fibroatheromas, 96.1% of calcified thin-cap fibroatheromas,

**Video 32.1** Color flow IVUS.

85.9% of fibroatheromas, 85.5% of fibrocalcific plaques, 83.4% of pathologic intimal thickening, and 72.4% of calcified fibroatheromas.<sup>24</sup> A 2013 study analyzing 276 atherosclerotic

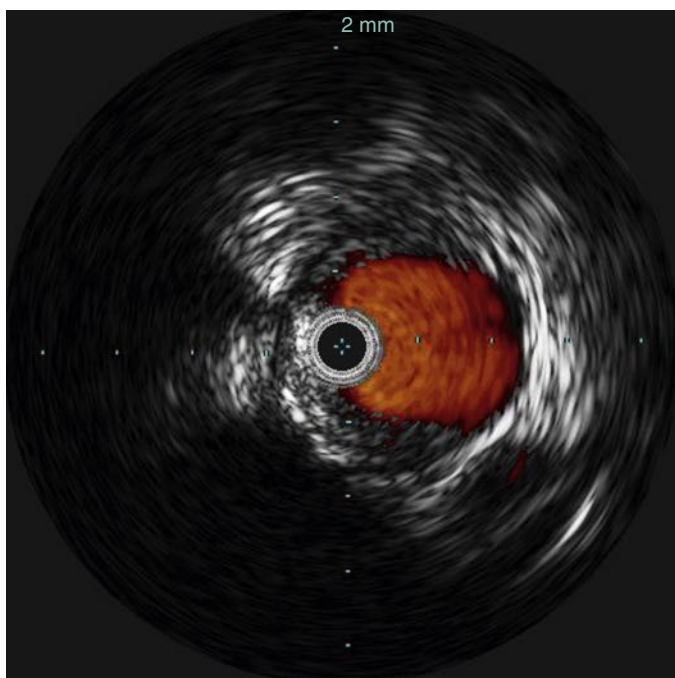


**Figure 32.3** Color-Flow Intravascular Ultrasound.

plaques also found that VH IVUS had high sensitivities for various types of plaques (87% for noncalcified thin-cap fibroatheromas, 92% for calcified thin-cap fibroatheromas, 85% for noncalcified fibroatheromas, 89% for calcified fibroatheromas, and 79% for pathologic intimal thickening).<sup>25</sup> Although the accuracy of VH IVUS varies in identifying different types of plaque, it is overall able to provide insight into the morphology of lesions. The information about plaque composition offered by VH IVUS may improve outcomes by allowing physicians to predict plaque behavior in response to treatment, determining whether plaques may resist treatment or embolize when grafts or balloons are expanded.<sup>26–31</sup> Histopathologic analysis using IVUS is currently available only for smaller vessels, since the maximum fields of display are less than 20 mm, but future advances in VH IVUS technology may improve plaque characterization in larger vessels.

## CLINICAL APPLICATIONS

### Effectiveness of Intravascular Ultrasound

#### Cost Versus Benefit

As of 2009, the cost of IVUS systems were listed at between \$100,000 and \$200,000, while the disposable IVUS catheters cost between \$600 and \$1000 each.<sup>32</sup> These can represent

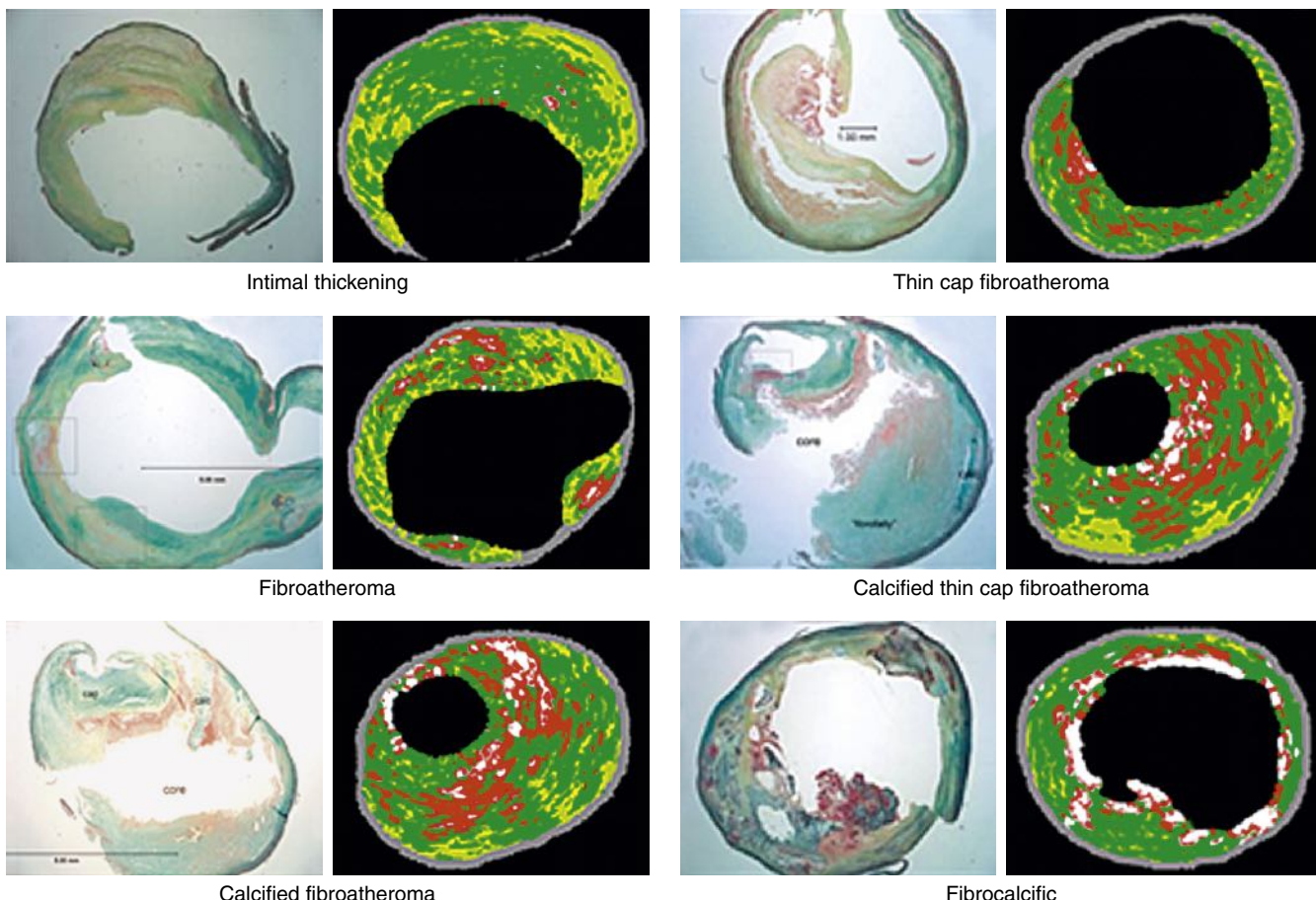


**Figure 32.4** Virtual histology intravascular ultrasound software color codes images of atherosclerotic plaques based on their histologic components: dark green = fibrous; yellow/green = fibrofatty; white = calcified; red = necrotic lipid core.

significant added costs to procedures. However, the benefits of using IVUS suggest that it is cost-effective, because increased effectiveness of treatment can prevent reintervention and improve morbidity/mortality rates, especially in complex cases.<sup>33</sup> In a study examining the cost-effectiveness of IVUS in PCI, results demonstrated that use of IVUS was cost-effective, especially in patients at greater risk of restenosis, who benefit from more accurate stent implantation.<sup>33</sup> Improved long-term clinical outcomes can certainly decrease costs, and IVUS has been shown to improve clinical outcomes in many studies. Studies of aortoiliac artery stenting found that clinical outcomes were improved with IVUS guidance.<sup>34,35</sup> Studies investigating peripheral and branch vessel stenting found that IVUS was able to detect unsatisfactory deployment of stents, allowing further measures to be taken immediately and preventing later reintervention.<sup>36</sup> Similarly, IVUS-guided treatment of lower limb endovascular interventions was found to be predictive of lower post-procedural complications and significantly improved limb salvage rates.<sup>37</sup> Overall, the benefits of IVUS use tend to outweigh additional procedural costs.

### General Benefits of Intravascular Ultrasound

IVUS is most often used because of its ability to provide additional diagnostic information to accurately assess vascular pathology, a benefit that has been well documented.<sup>38</sup> Intraoperatively, the dynamic imaging provided by IVUS allows for accurate deployment of grafts and assessment of successful therapy. The improved measurement ability of IVUS helps to determine proper stent graft sizing as well as in making last-minute adjustments based on intraoperative measurements.<sup>39</sup> Although measurements taken with IVUS have been found to be accurate overall, it is important to remember that because the catheter may not always be in the center of the lumen, it may provide a distorted oblique slice that does not reflect the true center-line diameter, especially in tortuous sections of the aorta.<sup>40</sup>

A significant benefit of IVUS is that it does not require the use of contrast. Because of this, patients with contrast allergies or renal impairment may benefit from preoperative imaging with IVUS instead of computed tomography angiography (CTA).<sup>41,42</sup> Intraoperatively, the use of IVUS is especially recommended as an alternative or adjunct to angiography because of its ability to decrease the volume of contrast injected as well as the radiation exposure.<sup>43</sup> It was shown in one comparison study that use of IVUS decreased fluoroscopy time from 39 to 19 minutes in comparable procedures.<sup>44</sup> In 2002, a study evaluating outcomes of endovascular aneurysm repair (EVAR) with IVUS as compared with angiography concluded that IVUS was accurate and reliable enough to be used for EVAR without additional angiographic assessment.<sup>45</sup> This ability to perform a procedure while eliminating or reducing contrast load and radiation exposure recommends the use of IVUS in patients with life-threatening contrast allergies or renal complications.<sup>46</sup> Because of its many benefits, IVUS has proven useful in a variety of vascular applications, including in the treatment of peripheral arterial disease, abdominal aortic aneurysm, thoracic aortic disease, dissection, and venous disease.

## Arterial Applications: Carotid and Peripheral Arterial

### Peripheral Arterial Disease

It has been shown that residual stenosis of greater than 60% after peripheral balloon angioplasty is associated with decreased patency rates.<sup>47</sup> Studies have also shown that more accurate sizing, especially with balloon-expandable stents, leads to better patency rates.<sup>48</sup> IVUS assessment of lumen diameter and degree of stenosis allows for accurate sizing of the vessel to be treated, thereby informing decisions regarding balloon and stent sizing.<sup>49</sup> One Japanese study found that 5-year overall patency rates were improved at 65% versus 35% when IVUS was used in the treatment of femoropopliteal lesions.<sup>50</sup> IVUS is also able to assess the initial results of balloon angioplasty and determine the need for further intervention, ensuring proper dilation of stents to improve apposition to vessel walls. In one study, 40% of patients had under-expanded stents after initial deployment and balloon expansion, but these were able to be further expanded with larger balloons because the lack of apposition was identified with IVUS.<sup>51</sup> Arteriography or angiography alone does not always visualize this type of problem, whereas IVUS is able to identify stent struts because of their echogenicity and assess the extent of stent expansion and apposition, allowing physicians to act to improve patency rates and overall success of treatment (Fig. 32.5).

In a study of popliteal aneurysms, researchers found that use of IVUS allowed accurate characterization of vessel morphology, including location and extent of thrombus burden. This improved outcomes in endovascular procedures because measurement of the diameter and location of desired

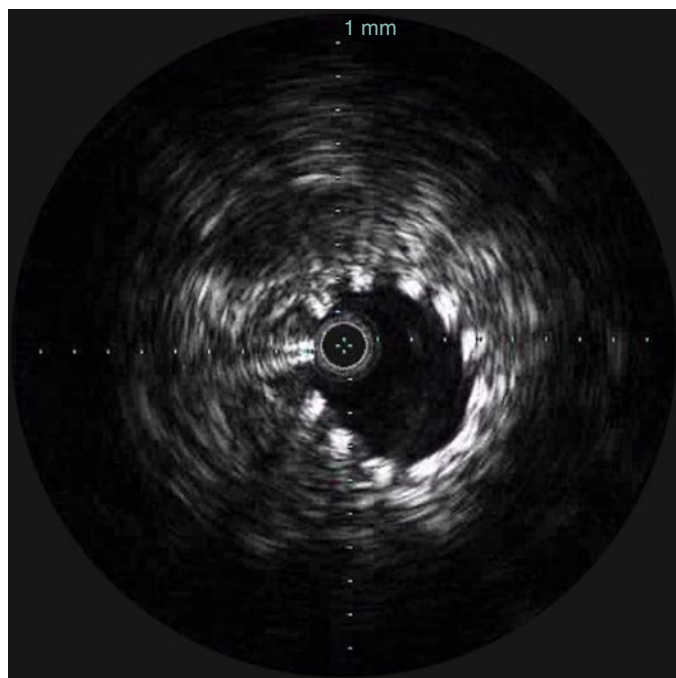


**Figure 32.5** The echolucency of stent grafts allows for evaluation of graft apposition.